

# Advancements in the heterogeneity of sex for tumors

**Edited by**

Jianbin Bi, Prem Prakash Kushwaha and  
Gongbo Fu

**Published in**

Frontiers in Pharmacology  
Frontiers in Oncology



## FRONTIERS EBOOK COPYRIGHT STATEMENT

The copyright in the text of individual articles in this ebook is the property of their respective authors or their respective institutions or funders. The copyright in graphics and images within each article may be subject to copyright of other parties. In both cases this is subject to a license granted to Frontiers.

The compilation of articles constituting this ebook is the property of Frontiers.

Each article within this ebook, and the ebook itself, are published under the most recent version of the Creative Commons CC-BY licence. The version current at the date of publication of this ebook is CC-BY 4.0. If the CC-BY licence is updated, the licence granted by Frontiers is automatically updated to the new version.

When exercising any right under the CC-BY licence, Frontiers must be attributed as the original publisher of the article or ebook, as applicable.

Authors have the responsibility of ensuring that any graphics or other materials which are the property of others may be included in the CC-BY licence, but this should be checked before relying on the CC-BY licence to reproduce those materials. Any copyright notices relating to those materials must be complied with.

Copyright and source acknowledgement notices may not be removed and must be displayed in any copy, derivative work or partial copy which includes the elements in question.

All copyright, and all rights therein, are protected by national and international copyright laws. The above represents a summary only. For further information please read Frontiers' Conditions for Website Use and Copyright Statement, and the applicable CC-BY licence.

ISSN 1664-8714  
ISBN 978-2-8325-6340-3  
DOI 10.3389/978-2-8325-6340-3

## About Frontiers

Frontiers is more than just an open access publisher of scholarly articles: it is a pioneering approach to the world of academia, radically improving the way scholarly research is managed. The grand vision of Frontiers is a world where all people have an equal opportunity to seek, share and generate knowledge. Frontiers provides immediate and permanent online open access to all its publications, but this alone is not enough to realize our grand goals.

## Frontiers journal series

The Frontiers journal series is a multi-tier and interdisciplinary set of open-access, online journals, promising a paradigm shift from the current review, selection and dissemination processes in academic publishing. All Frontiers journals are driven by researchers for researchers; therefore, they constitute a service to the scholarly community. At the same time, the *Frontiers journal series* operates on a revolutionary invention, the tiered publishing system, initially addressing specific communities of scholars, and gradually climbing up to broader public understanding, thus serving the interests of the lay society, too.

## Dedication to quality

Each Frontiers article is a landmark of the highest quality, thanks to genuinely collaborative interactions between authors and review editors, who include some of the world's best academicians. Research must be certified by peers before entering a stream of knowledge that may eventually reach the public - and shape society; therefore, Frontiers only applies the most rigorous and unbiased reviews. Frontiers revolutionizes research publishing by freely delivering the most outstanding research, evaluated with no bias from both the academic and social point of view. By applying the most advanced information technologies, Frontiers is catapulting scholarly publishing into a new generation.

## What are Frontiers Research Topics?

Frontiers Research Topics are very popular trademarks of the *Frontiers journals series*: they are collections of at least ten articles, all centered on a particular subject. With their unique mix of varied contributions from Original Research to Review Articles, Frontiers Research Topics unify the most influential researchers, the latest key findings and historical advances in a hot research area.

Find out more on how to host your own Frontiers Research Topic or contribute to one as an author by contacting the Frontiers editorial office: [frontiersin.org/about/contact](https://frontiersin.org/about/contact)



# Advancements in the heterogeneity of sex for tumors

## Topic editors

Jianbin Bi — The First Hospital of China Medical University, China

Prem Prakash Kushwaha — Case Western Reserve University, United States

Gongbo Fu — Department of Oncology, Nanjing General Hospital of Nanjing Military Command, China

## Citation

Bi, J., Kushwaha, P. P., Fu, G., eds. (2025). *Advancements in the heterogeneity of sex for tumors*. Lausanne: Frontiers Media SA. doi: 10.3389/978-2-8325-6340-3

# Table of contents

05	<b>Editorial: Recent advances in understanding sex-based tumor diversity</b> Swati Kushwaha, Radha Kushwaha and Prem Prakash Kushwaha
08	<b>Sexual dimorphism in bladder cancer: a review of etiology, biology, diagnosis, and outcomes</b> Sheng Zhu and Huasheng Zhao
22	<b>Integrated transcriptomic and immunological profiling reveals new diagnostic and prognostic models for cutaneous melanoma</b> Changchang Li, Nanhui Wu, Xiaoqiong Lin, Qiaochu Zhou and Mingyuan Xu
38	<b>Exploiting gender-based biomarkers and drug targets: advancing personalized therapeutic strategies in hepatocellular carcinoma</b> Lanqian Su, Huanyu Luo, Yalan Yan, Zhongqiu Yang, Jiaan Lu, Danqi Xu, Linjuan Du, Jie Liu, Guanhu Yang and Hao Chi
46	<b>PCAF acetylates AIB1 to form a transcriptional coactivator complex to promote glycolysis in endometrial cancer</b> Di Wu, Mingxia Li, Mingyang Wang, Zhifeng Yan and Yuanguang Meng
61	<b>Analysis of chromatin accessibility in peripheral blood mononuclear cells from patients with early-stage breast cancer</b> Longjie Xia, Jiamin Lu, Yixuan Qin, Runchun Huang, Fanbiao Kong and Yu Deng
73	<b>Effects of BYL-719 (alpelisib) on human breast cancer stem cells to overcome drug resistance in human breast cancer</b> Leinan Yu, Chuanbing Zang, Yuanchun Ye, Hongyu Liu and Jan Eucker
84	<b>ABCA1 promote tumor environment heterogeneity via epithelial mesenchymal transition in Huh7 and HepG2 liver cancer cell</b> Dinglai Yu, Fang Guo, Qiyu Zhang, Huajun Yu, Wenmin Wang and Yunzhi Chen
104	<b>CSNK1E is involved in TGF-<math>\beta</math>1 induced epithelial mesenchymal transformation and related to melanoma immune heterogeneity</b> Wangbing Hong, Xin Wang, Xinyu Huang, Pengfei Chen, Yifan Liu, Ziyang Zheng, Xin You, Yinghua Chen, Zengxin Xie, Gongnan Zhan and Heping Huang

- 122 **Transcriptome analysis of ovarian cancer uncovers association between tumor-related inflammation/immunity and patient outcome**  
Jingfang Wang, Wenrui Zhu, Xia Li, Yuanyuan Wu, Wenhui Ma, Yangzhou Wang, Weihong Zhao, Fang Wei and Wenhao Wang
- 141 **Exploring the genetic profiles linked to senescence in thyroid tumors: insights on predicting disease progression and immune responses**  
Baoliang Zhang and Yanping Pang



## OPEN ACCESS

## EDITED AND REVIEWED BY

Ying-Hong Feng,  
Uniformed Services University of the Health  
Sciences, United States

## \*CORRESPONDENCE

Prem Prakash Kushwaha,  
✉ prembiochembch@gmail.com

RECEIVED 23 March 2025

ACCEPTED 18 April 2025

PUBLISHED 28 April 2025

## CITATION

Kushwaha S, Kushwaha R and Kushwaha PP  
(2025) Editorial: Recent advances in  
understanding sex-based tumor diversity.  
*Front. Pharmacol.* 16:1598740.  
doi: 10.3389/fphar.2025.1598740

## COPYRIGHT

© 2025 Kushwaha, Kushwaha and Kushwaha.  
This is an open-access article distributed under  
the terms of the [Creative Commons Attribution  
License \(CC BY\)](#). The use, distribution or  
reproduction in other forums is permitted,  
provided the original author(s) and the  
copyright owner(s) are credited and that the  
original publication in this journal is cited, in  
accordance with accepted academic practice.  
No use, distribution or reproduction is  
permitted which does not comply with these  
terms.

# Editorial: Recent advances in understanding sex-based tumor diversity

Swati Kushwaha<sup>1</sup>, Radha Kushwaha<sup>2</sup> and  
Prem Prakash Kushwaha<sup>3\*</sup>

<sup>1</sup>Department of Botany, University of Allahabad, Allahabad, Uttar Pradesh, India, <sup>2</sup>Centre of Food Technology, University of Allahabad, Allahabad, Uttar Pradesh, India, <sup>3</sup>Department of Biological, Geological, and Environmental Sciences, Cleveland State University, Cleveland, OH, United States

## KEYWORDS

Sex specific tumor heterogeneity, cancer biology, tumor progression, precision oncology, therapeutic targets

## Editorial on the Research Topic

### Recent advances in understanding sex-based tumor diversity

## Introduction

Sex differences play a fundamental role in cancer incidence, progression, and treatment response; however, their influence remains underexplored in many aspects of oncology. Emerging research suggests that biological factors such as sex hormones, genetic variations, immune system differences, and metabolic pathways contribute to distinct tumor behavior and therapeutic outcomes between men and women. Understanding these differences is critical to advancing precision medicine and improving patient care. This Research Topic, *Recent advances in understanding sex-based tumor diversity*, brings together 10 cutting-edge studies that investigate the impact of sex on cancer biology across a range of malignancies. These investigations examine molecular mechanisms, prognostic markers, and therapeutic targets, revealing how sex affects tumor initiation, progression, immune responses, and treatment resistance, paving the way for personalized therapies.

## Article description

The first review, published by [Zhu and Zhao](#), explored the influence of sex on bladder cancer, from incidence to biology and outcomes. They assessed risk factors such as smoking, occupational exposures, and genetic mutations, along with sex differences in cancer development. They provided comprehensive insights into the role of hormones, chromosomes, metabolism, and the microbiome, while also highlighting gender gaps in diagnosis and prognosis. Their work underscores the need for further research and sex-specific treatments to improve care for all patients.

[Li et al.](#) analyzed cutaneous melanoma using TCGA and GEO data, integrating mutational, clinical, and single-cell sequencing to identify key genes. They developed a prognostic model using LASSO, linking genes to immune responses through functional and

immunological analyses. They demonstrated the role of GMR6 in melanoma cell proliferation, invasion, and migration. These findings identify potential therapeutic targets, offering new avenues to improve patient outcomes in cutaneous melanoma, particularly by targeting GMR6-mediated mechanisms.

A mini-review (Su et al.) explored sex differences in hepatocellular carcinoma, focusing on sex hormones, genetics, and environmental factors. The authors highlighted the sexual dimorphism of the liver and sex-specific risks such as alcohol and obesity in cancer development. The review explores molecular mechanisms, including androgen and estrogen signaling, that influence tumor biology and highlights the need for sex-specific research to improve diagnostics, treatment precision, and personalized therapies, aiming to enhance outcomes for liver cancer patients.

Wu et al. investigated the role of AIB1 in endometrial cancer, focusing on its impact on aerobic glycolysis and tumor progression. AIB1 is linked to poor prognosis and has been identified as a potential therapeutic target. Using cell lines and mouse models, researchers confirmed the high expression of AIB1 and its role in tumor proliferation and invasion. Mechanistically, AIB1 is acetylated by PCAF, binds to c-myc, and regulates glycolysis-related genes. These findings suggest that targeting AIB1-mediated glycolysis may offer a novel strategy for the treatment of estrogen-dependent endometrial cancer, thereby advancing personalized therapies.

Another study (Xia et al.) investigated the chromatin accessibility in peripheral blood mononuclear cells (PBMCs) from breast cancer patients to assess its diagnostic and prognostic potential. Using ATAC sequencing and bioinformatic analysis, they identified 1,906 differentially accessible regions and 1,632 differentially expressed genes. Nine key genes (e.g., JUN, CDC42, TRIB1) and five transcription factors (NFY, Sp2, ELK1) were linked to breast cancer progression. Their findings suggest that chromatin accessibility in PBMCs is a promising biomarker for early detection and therapeutic innovation in breast cancer.

Yu et al. investigated BYL-719, a PI3K p110 $\alpha$  inhibitor, to target breast cancer stem cells (BCSCs) and overcome drug resistance. Using a 3D mammosphere model, they found that BYL-719 inhibits BCSC proliferation, stemness, and epithelial-to-mesenchymal transition (EMT). The drug suppresses key pathways such as PI3K/AKT/mTOR, Notch, JAK-STAT, and MAPK/ERK that regulate the dynamics of the tumor microenvironment. The authors demonstrated that BYL-719 overcomes resistance in eribulin-resistant breast cancer cells. These results suggest that combining BYL-719 with other therapies may enhance breast cancer treatment strategies.

Yu et al. explored cell communication in hepatocellular carcinoma (HCC) using single-cell sequencing and clustering analysis. They identified malignant and cancer-associated fibroblast subpopulations, emphasizing SPP1-mediated interactions. Two clusters, C1 and C2, were distinguished, with C1 showing higher cytotoxicity and invasion. A gene risk model revealed increased immune pathway activity in C1, while high-risk scores correlated with poorer prognosis. They showed that ABCA1 promotes HCC progression by enhancing proliferation, invasion, and migration while reducing apoptosis. These findings provide critical insights into the pathogenesis and prognosis of HCC.

Hong et al. investigated WNT signaling genes in melanoma, identifying 19 prognostically relevant genes and developing a 13-gene model using LASSO regression. Key findings linked CSNK1E and RAC3 to epithelial-to-mesenchymal transition and immune evasion. They identified a role for CSNK1E in melanoma progression via the TGF- $\beta$  pathway. These results suggest that targeting CSNK1E and WNT/TGF- $\beta$  pathways could improve melanoma treatment and address therapy resistance.

Wang et al. investigated inflammatory gene expression in epithelial ovarian cancer and its role in immunotherapy resistance. Transcriptome analysis revealed two inflammatory gene patterns that differed in immune infiltration, prognosis, and treatment response. The high-risk group showed elevated M2 macrophage infiltration, increased tumor stemness, poorer prognosis, and reduced sensitivity to chemotherapy and immune checkpoint inhibitors. These findings underscore inflammation-related genes as potential targets for enhancing immunotherapy and prognostic evaluation, offering new strategies for early intervention and patient management.

Zhang and Pang studied cell senescence-associated genes in thyroid cancer, developing a prognostic model using differential expression, Cox regression, and LASSO analyses. Validated with Kaplan-Meier and ROC curves, the model predicts patient survival, tumor mutation burden, and response to immunotherapy across risk groups. Their findings offer new insights into thyroid cancer progression and immunotherapy, highlighting potential avenues for personalized treatment strategies.

Collectively, these studies advance our understanding of cancer biology by uncovering sex differences, molecular mechanisms, and therapeutic targets, paving the way for personalized treatments and improved patient outcomes across multiple malignancies.

## Author contributions

PK: Conceptualization, Writing – review and editing, Supervision, Writing – original draft, Formal Analysis. SK: Methodology, Writing – original draft. RK: Writing – review and editing, Formal Analysis, Writing – original draft, Conceptualization.

## Funding

The author(s) declare that no financial support was received for the research and/or publication of this article.

## Conflict of interest

The authors declare that the research was conducted in the absence of any commercial or financial relationships that could be construed as a potential conflict of interest.

## Generative AI statement

The authors declare that Generative AI was used in the creation of this manuscript. Used for grammatical editing.



## Publisher's note

All claims expressed in this article are solely those of the authors and do not necessarily represent those of their affiliated

organizations, or those of the publisher, the editors and the reviewers. Any product that may be evaluated in this article, or claim that may be made by its manufacturer, is not guaranteed or endorsed by the publisher.



## OPEN ACCESS

## EDITED BY

Jianbin Bi,  
The First Hospital of China Medical University,  
China

## REVIEWED BY

Chen Yang,  
German Cancer Research Center (DKFZ),  
Germany  
Maha Mohamed Saber-Ayad,  
University of Sharjah, United Arab Emirates  
Xun Fu,  
Wuhan University, China

## \*CORRESPONDENCE

Huasheng Zhao,  
✉ fhq2020@163.com

RECEIVED 23 October 2023

ACCEPTED 26 December 2023

PUBLISHED 12 January 2024

## CITATION

Zhu S and Zhao H (2024), Sexual dimorphism in bladder cancer: a review of etiology, biology, diagnosis, and outcomes.  
*Front. Pharmacol.* 14:1326627.  
doi: 10.3389/fphar.2023.1326627

## COPYRIGHT

© 2024 Zhu and Zhao. This is an open-access article distributed under the terms of the [Creative Commons Attribution License \(CC BY\)](https://creativecommons.org/licenses/by/4.0/). The use, distribution or reproduction in other forums is permitted, provided the original author(s) and the copyright owner(s) are credited and that the original publication in this journal is cited, in accordance with accepted academic practice. No use, distribution or reproduction is permitted which does not comply with these terms.

# Sexual dimorphism in bladder cancer: a review of etiology, biology, diagnosis, and outcomes

Sheng Zhu<sup>1</sup> and Huasheng Zhao<sup>2\*</sup>

<sup>1</sup>Department of Urology, Guilin Hospital of the Second Xiangya Hospital, Central South University, Guilin, China, <sup>2</sup>Department of Urology, ShaoYang Hospital, Affiliated to University of South China, ShaoYang, China

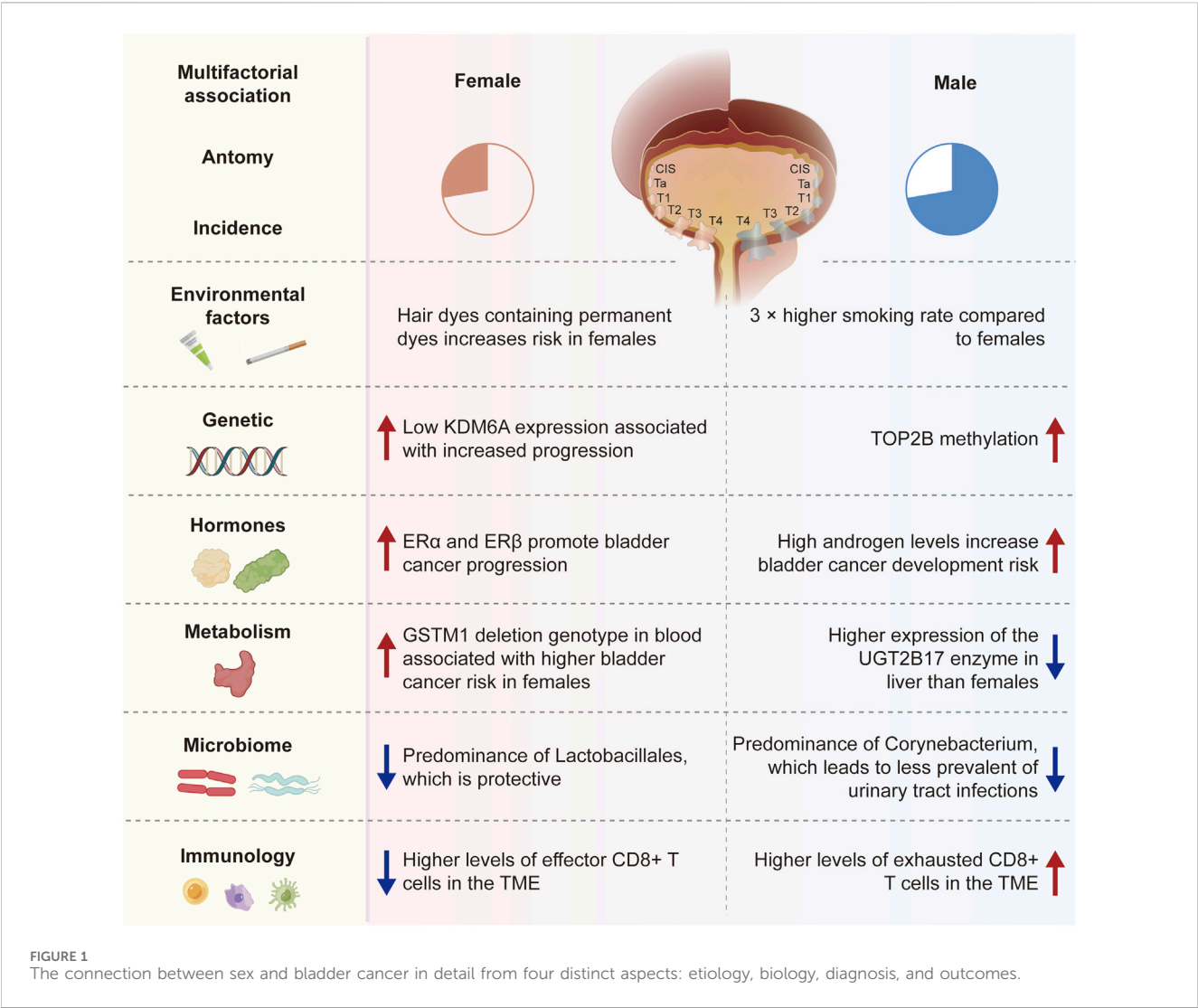
Bladder carcinoma represents a prevalent malignancy, wherein the influence of sex extends across its incidence, biological attributes, and clinical outcomes. This scholarly exposition meticulously examines pertinent investigations, elucidating the nuanced impact of sex on bladder cancer, and posits cogent avenues for future research and intervention modalities. In the initial discourse, an exhaustive scrutiny is undertaken of the etiological underpinnings of bladder cancer, encompassing variables such as tobacco consumption, occupational exposures, and genetic aberrations. Subsequently, a comprehensive dissection unfolds, delving into the intricate biological disparities inherent in sex vis-à-vis the initiation and progression of bladder cancer. This analytical framework embraces multifaceted considerations, spanning sex hormones, sex chromosomal dynamics, metabolic enzymatic cascades, and the intricate interplay with the microbiome. Lastly, a synthesized exposition encapsulates the ramifications of gender differentials on the diagnostic and prognostic landscapes of bladder cancer, underscoring the imperative for intensified investigative endeavors directed towards elucidating gender-specific variances and the formulation of tailored therapeutic strategies.

## KEYWORDS

bladder carcinoma, etiology, biology, diagnosis, sexual dimorphism

## 1 Introduction

One prevalent malignant tumor is bladder cancer (BC) (Richters et al., 2020). It has been widely reported that there are gender disparities in bladder cancer patients' epidemiology, diagnosis, and prognosis. Bladder cancer is more common in men than in women worldwide but a diagnosis of advanced bladder cancer is more common in females (Scosyrev et al., 2009). Extensive research has confirmed women's association with poorer oncological outcomes, including an elevated likelihood of mortality, disease recurrence and disease progression (Zeegers et al., 2000; Castela et al., 2001; Boffetta, 2008). Treatment disparities cannot fully explain these differences in survival rates between genders. Currently, various hypotheses, including physiological anatomical structures, disease phenotypes, hormone changes, sex epigenomics, diagnostic delays, and treatment strategies, are being used to explain sex-specific adverse outcomes. Therefore, this article will explore the connection between sex and bladder cancer in detail from four distinct aspects: etiology, biology, diagnosis, and outcomes (Figure 1).



2 Etiological difference in bladder cancer

2.1 Smoking

Smoking is widely recognized as one of the most significant risk factors for bladder cancer, as those who smoke have a notably higher chance of getting the disease than people who do not smoke (Strope and Montie, 2008). Smoking is linked to bladder cancer in one-third of women and at least 50% of men (Zeegers et al., 2000). Compared to female smokers, male smokers have a higher risk of developing bladder cancer (Castelao et al., 2001), which may be attributed to higher smoking rates and metabolic differences in men. Furthermore, studies have shown a linear correlation between smoking and the risk of bladder cancer, and quitting smoking can reduce the incidence of bladder cancer (Boffetta, 2008). In men and women, the incidence of bladder cancer is roughly 4:1 when smoking intensity is similar (Krabbe et al., 2015). The main cause of the gender difference in bladder cancer incidence is generally considered to be smoking. However, according to the study, there is a 3.31 relative risk of incidence of bladder cancer in

women when smoking rates are 70% for males and 10% for women, which is lower than the global average of 4.04. This implies that the variations in bladder cancer incidence across genders can only be partially explained by smoking (Hemelt et al., 2009).

2.2 Occupations

Chemical substances and carcinogens in certain occupational environments have different effects on the risk of bladder cancer in women and men, which may be related to gender differences in metabolic pathways and hormone levels. For example, occupations including driving, rubber manufacturing, hair styling, and petroleum product processing can expose workers to higher levels of aromatic amine chemicals, raising their risk of bladder cancer (Reulen et al., 2008; Samanic et al., 2008; Bevan et al., 2012). Additionally, studies have reported a higher risk of bladder cancer in women who use hair dyes containing permanent dyes, with women with a higher risk for the N-acetyltransferase-2 slow acetylation phenotype (Koutros et al., 2011). The statement indicating a higher risk of bladder cancer in women using hair dyes, especially those containing permanent dyes, in

association with the N-acetyltransferase-2 (NAT2) slow acetylation phenotype (Gago-Dominguez et al., 2001; Zhang et al., 2020). However, the evidence is not entirely consistent, and the relationship may be influenced by factors like dose, duration of exposure, and individual susceptibility. Long-term and frequent use of hair dyes has been suggested to be associated with an increased risk of bladder cancer, but findings across studies vary. To better understand the potential risks, assessing blood levels of carcinogenic compounds resulting from hair dye use is crucial, involving biomarkers of exposure or specific metabolite measurements. While references to such blood level measurements may require targeted literature searches, consulting systematic reviews or meta-analyses could offer a broader overview of the available evidence on the association between hair dye use, bladder cancer risk, and the role of dose, duration, and biomarkers. However, in terms of gender disparities, there is a lack of thorough research to assess the connection between bladder cancer and occupation.

## 2.3 Gene mutation

Some gene mutations associated with bladder cancer exhibit different frequencies and effects in men and women. Bladder cancer is typically believed to occur due to the entry of chemical substances in tobacco into the bloodstream, accumulating in the urine through filtration by the kidneys, and subsequently causing mutations in bladder cell genes. However, gene mutations are random events that may be influenced by the cellular microenvironment and can occur even without external stimuli (Wang et al., 2021; Lin et al., 2020). HRA, KRAS2, RB1, and FGFR3 are known somatic mutation genes associated with bladder cancer (Kiemenev et al., 1997; Cappellen et al., 1999). Gene changes such as STAG2, TERT, ESPL1, UTX, MLL, MLL3, CREBBP, EP300, NCOR1, and ARID1A are also linked to bladder cancer (Fliss et al., 2000; Solomon et al., 2013; Cha and Bochner, 2015). A higher risk of bladder cancer is associated with PTEN mutations in persons with breast cancer and thyroid cancer (Hemelt et al., 2009; Cordes et al., 2013). Studies have identified differences in gene mutation patterns between different genders in bladder cancer, particularly X chromosome-based genes (Gul et al., 2021). In a large clinical cohort study, 58 genes were found to undergo significant mutations in patients with muscle-invasive bladder cancer (MIBC), clustering into five subtypes (Cumberbatch and Catto, 2018). The basal-squamous subtype was more common in women. This suggests that next-generation sequencing technologies can provide a more comprehensive data foundation for exploring bladder cancer, which is of great significance for understanding the mechanisms of bladder cancer development and the reasons behind gender differences.

## 3 Biological differences in bladder cancer

### 3.1 Sex chromosome and epigenetics

Research has indicated that the loss of the Y chromosome in males raises the risk of cancer. In contrast, females with Turner syndrome (loss or partial loss of the X chromosome) have a significantly increased risk of bladder cancer, while males with Klinefelter

syndrome (extra copy of the X chromosome) have a significantly reduced risk of solid tumors (Ji et al., 2016; Theodorescu et al., 2022). Findings further show that sex hormones do not influence gender-biased effects of the X chromosome and that an extra copy of the X chromosome guards against bladder cancer (Kaneko and Li, 2018). Lysine-specific demethylase 6A is one of the most commonly mutated genes in bladder cancer (KDM6A), a tumor suppressor found on the X chromosome (Xp11.3) (Robertson et al., 2018; Koti et al., 2020). As a demethylase for trimethylation of histone H3 at lysine 27 (H3K27me3), KDM6A mutations result in the availability of H3K27 for acetylation. H3K27me3 modification is a transcriptionally repressive epigenetic mark that can form bivalent domains with the active transcription mark H3K4me3, keeping genes poised (Voigt et al., 2013). Additionally, studies have demonstrated the involvement of KDM6A in mediating the methyltransferase activity of H3K4me1 (Jang et al., 2017; Rickels et al., 2017). Cohort analysis has shown an association between reduced KDM6A expression and female bladder cancer progression (Kaneko and Li, 2018). The UTY (KDM6C) gene on the Y chromosome is a homologous gene of KDM6A (Lan et al., 2007). UTY can compensate for KDM6A mutation or deletion on the X chromosome on the Y chromosome (Lam et al., 2022). According to studies, deleting compensatory UTY on the Y chromosome may increase men's bladder cancer risk (Forsberg et al., 2014).

The interaction between sex hormones and their corresponding receptors plays a crucial role in the occurrence and development of bladder cancer, and the differences in hormone levels between genders may explain the variations in bladder cancer incidence. Research has shown that the presence of the androgen receptor (AR) gene, which is situated on the X chromosome (Xq11-12), could potentially explain the differences in bladder cancer occurrence across genders. Bladder cancer occurrence and development can be facilitated by AR mutations that affect ligand binding (Rahmani et al., 2013; Izumi et al., 2014a). According to multiple studies, androgens stimulate bladder cancer growth via classical and non-classical AR pathways (Izumi et al., 2014a; Deng et al., 2021). Based on the data, reducing bladder cancer invasion may be achieved by inhibiting AR, and anti-androgen Enzalutamide can reduce bladder cancer cell invasion (Deng et al., 2021). Targeting AR can also lower the expression of CD44, a gene linked to the invasion behavior of bladder tumors (Sottnik et al., 2021). Boorjian et al. have shown that more invasive tumor stage and AR expression are negatively correlated in bladder cancer, with lower levels of AR expression in female patients (Boorjian et al., 2004). However, several studies have not detected significant differences in tumor AR expression between genders (Mir et al., 2011; Tuygun et al., 2011; Mashhadi et al., 2014). A large body of research has shown that androgens and their downstream signaling pathways may not only be related to tumor progression in muscle-invasive bladder cancer (MIBC) but also have the potential to become therapeutic targets (Gakis and Stenzl, 2013; Xu et al., 2013; Izumi et al., 2014b; Mashhadi et al., 2014).

Estrogen binds to one of the two nuclear receptors, ER $\alpha$  and ER $\beta$ , structurally and functionally distinct. It has been found that ER $\alpha$  inhibits bladder cancer from occurrence, while ER $\beta$  has been shown to promote its development (Hsu et al., 2013). However, both ER subtypes have been found to promote bladder cancer progression. Both nuclear estrogen receptors (ER $\alpha$  and ER $\beta$ ) are responsible for transducing hormone signals into transcriptional responses (Xu et al.,

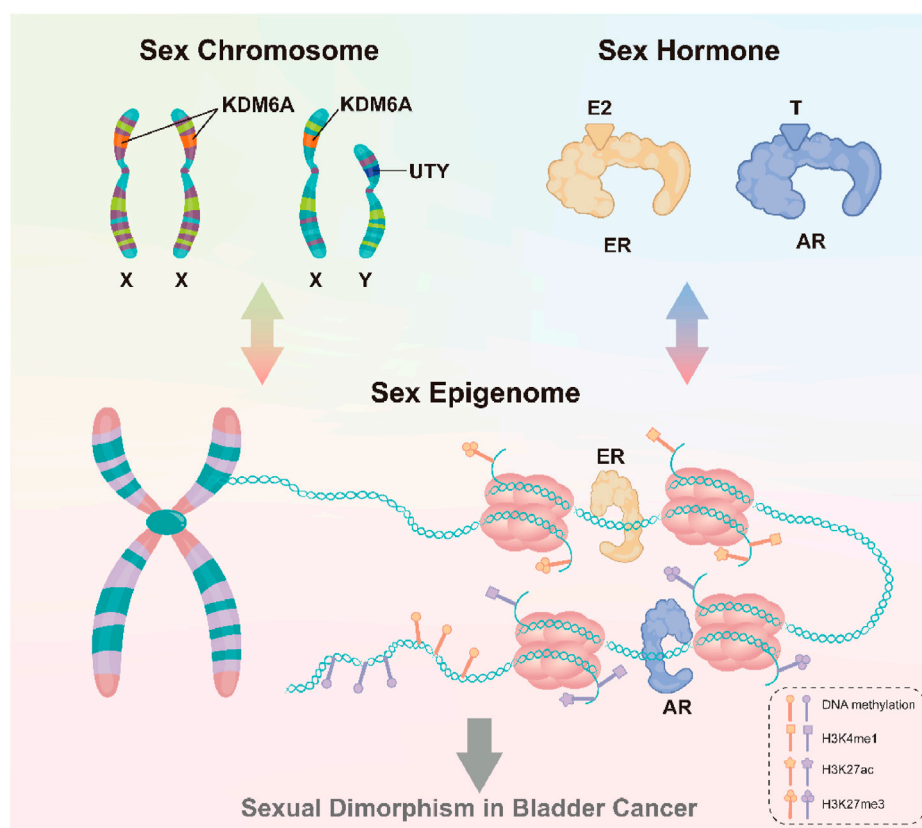


FIGURE 2

Sex chromosomes and sex hormones, through the sex epigenome, collectively influence gene expression and response to the environment, thus leading to the observed gender differences in bladder cancer.

2013). Shen et al. detected that ER $\beta$  is the predominant subtype expressed in UCB and that high levels of ER $\beta$  expression correlate with higher tumor grades (Shen et al., 2006; Tuygun et al., 2011). The team has also shown that exogenous estrogens promote bladder cancer cell growth *in vitro*, which can be inhibited by anti-estrogen drugs such as raloxifene (Shen et al., 2006). However, other studies have found that menopause raises the risk of bladder cancer (McGrath et al., 2006), and the use of combined estrogen and progesterone therapy can reduce this risk, which is not associated with estrogen use alone (Daugherty et al., 2013).

In summary, differences in bladder cancer incidence rates across genders are partly explained by the interaction of sex hormones and sex chromosomes (Figure 2). One type of cancer that has been connected to sex steroid hormones and the receptors on the surface of cells that they bind to is bladder cancer (Gakis and Stenzl, 2013; Xu et al., 2013), future research directions could focus on molecular mechanisms underlying gender-related incidence rate differences and develop potential therapies for bladder cancer targeting the androgen-AR signaling pathway or identifying patient populations that may benefit the most from preventive treatments.

### 3.2 Metabolic enzymes

Gender differences in metabolic detoxification may contribute to the varying incidence rates of bladder cancer (Zhang, 2013). The

ability of the liver pathway to degrade carcinogens differs between genders, leading to varying degrees of carcinogen accumulation in the urothelium (Buckley and Klaassen, 2007; Zhang, 2013). UDP-glucuronosyltransferases (UGTs), which are involved in the liver's process for breaking down aromatic amines, are responsible for eliminating exogenous and endogenous substances (Zhang, 2013; Hu et al., 2016; Meech et al., 2019), smoke from cigarettes contain carcinogens called aromatic amines that damage DNA. Therefore, the development of bladder cancer is significantly influenced by the detoxification of aromatic amines. Studies showed a noteworthy reduction in the UGT1A subtype enzyme expression in elevated bladder cancer compared to normal urothelium (Izumi et al., 2013). In liver tissue, males have higher expression of the UGT2B17 enzyme than females (Gallagher et al., 2010), indicating differences in enzyme activity between genders in metabolizing carcinogens. Additionally, it has been found that androgen receptor-mediated signaling inhibits UGT expression in bladder (Izumi et al., 2013; Zhang, 2013) and prostate cancer (Takayama et al., 2007), indicating a gender bias in the UGT detoxification pathway in bladder cancer. While several research studies have shown a connection between UGT and bladder cancer, there is still a need for large clinical cohort studies to definitively establish the significance of UGT in gender differences in bladder cancer (Hu et al., 2016).

Moreover, glutathione-S-transferase M1 (GSTM1), which binds to reduced glutathione to catalyze the detoxification of foreign



substances, is also considered a metabolic target for gender differences in bladder cancer incidence rates (Hengstler et al., 1998; Karagas et al., 2005; Yu et al., 2017). GST activity regulates exposure to carcinogens in the bladder urothelium and affects bladder cancer risk. A study found that females with the GSTM1 deletion genotype were more likely to develop bladder cancer, although this link was not found in males (Karagas et al., 2005; Salinas-Sánchez et al., 2011). Additionally, female smokers were shown to have a higher risk of bladder cancer when their blood samples had the GSTM1 deletion genotype, but not in non-smokers (Karagas et al., 2005), possibly due to females with the GSTM1 null genotype being unable to metabolize carcinogens in cigarette smoke. Additional clinical data is required to verify the relationship between GSTM1 and gender differences in bladder cancer.

According to the research findings on the comprehensive regulation of androgens on cell metabolism and detoxification, it can be hypothesized that the reason for the predominance of males in bladder cancer may be due to gender differences in enzymes responsible for carcinogen metabolism, resulting in varying degrees of exposure to environmental carcinogens (such as carcinogens in cigarette smoke), ultimately leading to differences in incidence rates. However, further research is needed to explore other potential metabolic targets contributing to differences in carcinogen processing and to conduct larger clinical cohort studies to determine the relationship between the expression of gender-related metabolic enzymes and the biology of bladder cancer.

### 3.3 Microbiome and microbiota

Data show that the microbiota may be associated with over one-fifth of malignant tumors (Garrett, 2015). The mechanisms of interaction between the microbiota and human cells involve at least one of the following: direct impacts on the host's innate immune system, interactions with their biochemistry, and host cell proliferation and death (Bhatt et al., 2017). The development and progression of bladder cancer involve a multifaceted interplay of sex hormones, chromosomes, liver enzymes, and the microbiome. Sex hormones, including estrogen and androgens, exert influence through receptors expressed in bladder cells, with androgens stimulating cancer growth. Alterations in sex chromosomes, such as Y chromosome loss in males and X chromosome anomalies in females, contribute to varying risks. Liver enzymes, notably metabolic detoxification enzymes like UDP-glucuronosyltransferases (UGTs) and glutathione-S-transferase M1 (GSTM1), exhibit gender-specific differences, affecting carcinogen detoxification and thus bladder cancer risk. The urinary microbiota, with variations between genders, has been linked to bladder cancer progression, suggesting that distinct microorganisms may create different local environments influencing tumor establishment. Understanding these factors in diverse pathological conditions, such as muscle-invasive or non-urothelial bladder cancer, is pivotal for personalized diagnostic and therapeutic strategies. Further research is essential to elucidate the nuanced mechanisms and interactions shaping bladder cancer development under different pathological contexts.

For example, *Salmonella typhi* may activate the Wnt/ $\beta$ -catenin pathway, which could lead to hepatobiliary and colorectal cancer

(Villaseñor et al., 2017). As urine can collect many disease-related changes, it can serve as a good source of biomarkers. According to recent research, bladder cancer and changes in the urine microbiome are related (Alfano et al., 2016; Bučević Popović et al., 2018). Because of the physiological variations between males and females, females are more prone to urinary tract infections. Wu et al. found that individuals with bladder cancer had a markedly elevated urinary microbiota bacterial abundance, with reductions in *Serratia*, *Proteus*, and *Roseomonas* and increases in *Acinetobacter*, *Anaerococcus*, and *Sphingobacterium* (Wu et al., 2018). A series of studies have also demonstrated that dysbiosis of the urinary microbiota may influence bladder cancer progression (Bi et al., 2019; Mai et al., 2019). These investigations suggest that distinct microorganisms in the urine of men and women may produce comparatively different local habitats, which may encourage or prevent the establishment of bladder tumors. Interactions between the immune system's sex hormones and the urine microbiome may be closely related (Curtiss et al., 2017). Sequencing results of urine samples showed that Lactobacillales and Corynebacterium dominate the urinary microbiota in females and males, respectively (Fouts et al., 2012). Lactobacillales have a protective effect against urinary tract infections (Kim and Park, 2018), and clinical trials have shown that oral administration of *Lactobacillus* preparations can slow down bladder cancer recurrence (Aso et al., 1995). Corynebacterium can influence the composition of the microbiota by hydrolyzing lipids and releasing free fatty acids with antimicrobial activity (Chen et al., 2018). Pederzoli et al. found a higher level of *Klebsiella* species in the urine of women with bladder cancer than in women with good health (Pederzoli et al., 2020). *Klebsiella* is linked to the development of bladder cancer (Mai et al., 2019), possibly due to the release of toxins by *Klebsiella* that cause DNA damage (Kaur et al., 2018). The aforementioned experimental results demonstrate that differences in urinary microbiota between different genders can be one of the reasons explaining the differences between biological genders in bladder cancer. The relationship between microbiota and cancer has been explained by various postulated processes, such as the induction of chronic inflammation, the promotion of cell proliferation, and the activation of procarcinogens (Xu et al., 2014). However, large-scale studies are still needed to clarify the precise connection between differences in the distribution of microbiota and the development of bladder cancer.

### 3.4 Immunobiology

Gender differences in immune responses may also impact the development and prognosis of bladder cancer. In patients with advanced bladder cancer, the microbiota's modulation affects how well they respond to systemic and adjuvant *Bacillus Calmette-Guérin* (BCG) immunotherapy (Killock, 2018; Routy et al., 2018; Stenehjem et al., 2018; Zitvogel et al., 2018). Studies suggest that *Lactobacillus* iners, which dominate the urinary microbiota in females, may preferentially bind to fibronectin, competing with BCG and weakening its efficacy (McMillan et al., 2013). When platinum-based chemotherapy fails to treat advanced bladder cancer patients, or they are not eligible for it, immune checkpoint inhibitors become the standard treatment. Studies

suggest that the gut microbiota composition may affect how well immune checkpoint blockade drugs work for metastatic melanoma (Matson et al., 2018). However, there is currently no research involving bladder cancer patients with metastases. A recent study found an association between Y chromosome loss and poorer prognosis (Abdel-Hafiz et al., 2023). Y chromosome loss in bladder cancer refers to the condition where cells, typically in males, experience a partial or complete loss of the Y chromosome. This genetic alteration is associated with more aggressive tumor characteristics, including increased invasiveness and the development of an immunosuppressive tumor microenvironment. Despite its negative impact on cancer aggressiveness, bladder cancers with Y chromosome loss paradoxically exhibit heightened sensitivity to immune checkpoint blockade therapy, suggesting a potential therapeutic vulnerability. The presence of Y chromosome loss in bladder cancer patients could serve as a prognostic marker, guiding clinical decision-making and personalized treatment strategies. Bladder cancers with Y chromosome loss exhibit more invasive and immunosuppressive tumor microenvironments but are also more sensitive to immune therapy. This study demonstrates an association between Y chromosome loss and increased response to immune checkpoint blockade therapy in humans and mice, suggesting a potential therapeutic avenue for this subset of bladder cancer. Additionally, data show a gender bias effect of CD8<sup>+</sup> T cells, leading to faster male tumor growth (Kwon et al., 2020). The study further indicates an increase in effector CD8<sup>+</sup> T cells in the tumor microenvironment (TME) of females, while males have higher levels of exhausted CD8<sup>+</sup> T cells in the TME (Kwon et al., 2020).

## 4 Sex-specific diagnostic differences

While males are more likely to have BC, females are frequently detected at an advanced stage (Mungan et al., 2000a; Lotan et al., 2005; Scosyrev et al., 2009; Fajkovic et al., 2011; Mallin et al., 2011; Rink et al., 2012; Kluth et al., 2014; Mitra et al., 2014; Soave et al., 2015). Over 23,000 MIBC patients were included in a study by Marieke J. Krimphove et al. (Fickenscher, 1999), which revealed that the proportion of female patients with non-urothelial bladder cancer was significantly higher (15.1% in females vs. 9.9% in males  $p < 0.001$ ). Among patients with histological variations, females exhibited poorer pathological features at diagnosis, with a higher prevalence of squamous cell carcinoma (46.9% in females vs. 28.7% in males;  $p < 0.001$ ), while males had a higher prevalence of neuroendocrine carcinoma (12.3% in females vs. 21.8% in males;  $p < 0.001$ ) or micropapillary differentiation carcinoma (3.8% in females vs. 9.0% in males;  $p < 0.001$ ). Although biological differences may contribute to this phenomenon, the timeliness and quality of the initial evaluation of hematuria, the most prevalent presenting symptom in both genders, maybe the main reason for the diagnostic stage differences (Fickenscher, 1999; Shephard et al., 2012). Several studies have demonstrated that compared to men, women with hematuria are less likely to see urologists for evaluation (Johnson et al., 2008; Nieder et al., 2010; Henning et al., 2013). Johnson et al. (Nieder et al., 2010) observed a 65% higher referral rate of urologists for male patients experiencing recurrent hematuria compared to

their female counterparts (median follow-up time of 26.5 months: 47% vs. 28%;  $p < 0.001$ ). Henning et al. (Henning et al., 2013) conducted a survey of 168 UCB patients (including 38 female patients) and found no gender differences in the initial symptoms ( $p > 0.05$ ). However, 78% of male patients directly consulted urologists, while only 55% of female patients did so ( $p < 0.05$ ). 49.2% of female patients and 19% of male patients were treated symptomatically without receiving a specific diagnosis ( $p < 0.04$ ), which did not result in any significant differences in tumor staging at the time of initial transurethral resection (Henning et al., 2013). Furthermore, a retrospective analysis of blood in urine patients in an institutional electronic medical record database found that only 8% of females were referred to urologists (Buteau et al., 2014). Similarly, an analysis of US and UK populations found that females had a significantly lower likelihood of receiving timely and complete blood in urine evaluation than males (Lyrtzopoulos et al., 2013; Garg et al., 2014; Bassett et al., 2015). Between 2000 and 2007, 35,646 people were diagnosed with UCB following blood in urine testing, based on an examination of the Surveillance, Epidemiology, and End Results (SEER) database. The average time from the first appearance of blood in urine to consulting a urologist was 27 days, significantly longer for female patients (Garg et al., 2014). The database comprised 100 health insurance plans from around 40 large US companies. According to the study, the average time it took for females to be diagnosed with bladder cancer was significantly longer than that of males. For example, the average diagnosis time for females was 85.5 days (95% confidence interval 81.3–89.4 days) compared to 73.6 days (71.2–76.1 days) for males ( $p < 0.001$ ). After receiving an initial diagnosis of hematuria, this difference still exists at 3 months, 6 months, and 9 months; females have a 26%, 16%, and 23% higher likelihood of experiencing delay, respectively. Additionally, a delay of more than 6 months between the onset of hematuria and diagnosis of bladder cancer is more common in females (17.3% vs. 14.1% in males;  $p < 0.001$ ).

Most bladder cancers originate in the urothelium, the bladder cavity's lining epithelium. Since the early signs and symptoms resemble urinary tract infections, female patients often receive antibiotic treatment before undergoing comprehensive urological evaluation. For example, Cohn et al. (Cohn et al., 2014) found in their survey that females undergo more urine analysis and urine culture and receive more urinary tract infection diagnoses before being diagnosed with bladder cancer, with a significantly higher proportion of females receiving antibiotics before diagnosis (40.1% in females vs. 35.4% in males;  $p < 0.001$ ), but fewer females undergo bladder imaging. This phenomenon was also observed by Aziz et al. (Aziz et al., 2015) in a smaller study group. In this study, 61.1% of female UCB patients received antibiotic treatment in the 12 months preceding diagnosis, while only 20% of male patients did ( $p = 0.005$ ). Moreover, voiding difficulties and stomach pain are linked to bladder cancer, and reports indicate that females with these complaints are more likely to receive empirical treatment without further evaluation, with 47% of females receiving treatment without further evaluation in the year before diagnosis, compared to only 19% of males ( $p < 0.05$ ) (Henning et al., 2013). According to Hollenbeck et al. (Bergman et al., 2013), patients who initially present with hematuria but are subsequently identified with bladder cancer (CSM) have a significant risk of cancer-specific mortality when their diagnosis is delayed.

These results show notable gender variations in the evaluation of hematuria, which may lead to an imbalance in the prompt identification of UCB. Females are more likely than males to present with lower urinary tract infection-related symptoms or hematuria. This delay could play a significant role in why females have worse survival rates and are more likely than males to suffer advanced-stage disease. Therefore, it is crucial to educate clinicians on standardized, guideline-based diagnostic and management approaches for all hematuria patients, irrespective of gender (Patel et al., 2008; Davis et al., 2012; Bergman et al., 2013).

## 5 Sex-specific differences in outcomes

### 5.1 Gender disparities in bladder cancer

Aside from the noted variations in the detection stage, female patients with bladder cancer also face an elevated likelihood of cancer-specific mortality compared to their male counterparts (Hashibe et al., 2003; Underwood et al., 2006; Tracey et al., 2009). Although males are diagnosed with bladder cancer at a rate approximately three times higher than females, their likelihood of dying from it is only about twice that of females, resulting in a lower CSM-to-incidence ratio for males (Shariat et al., 2010). Furthermore, female patients diagnosed with bladder cancer have a greater reduction in lifespan compared to males (6.5 years for females vs. 3.9 years for males) (Scosyrev et al., 2012). While some of the survival differences can be attributed to the higher incidence of late-stage disease in females, the differences in the presentation stage cannot fully explain the gender-related survival differences in bladder cancer patients, as studies show that female individuals have a lower prognosis across all disease stages. For example, the female patients' 5-year survival rate at stage I is 93.7%, a decrease of 2.8% compared to males; for stage II, it is 59.6%, a decrease of 5.9% compared to males; for stage III, it is 49.6%, a decrease of 9.2% compared to males; and for stage IV, it is 15.2%, a decrease of 11.9% compared to males (Mungan et al., 2000a). Some registry-based studies focusing on elderly populations have shown that female UCB patients have higher tumor staging and lower survival rates (Mungan et al., 2000a; Mungan et al., 2000b). A study by Kluth et al. (Moschini et al., 2019) used data from the Japanese Kanagawa cancer registry, which included 13,184 primary UCB patients from Japan between 1954 and 2010. After adjusting for patient age, treatment timing, and histological subtype, they found that CSM increased by approximately 40% in females. Another Japanese population-based registry study revealed that at the time of initial diagnosis, women's cancer staging was higher than men's, and the prognosis for women with bladder cancer that was localized or locally advanced was poorer than that of males.

Currently, in patients receiving radical cystectomy (RC) for bladder cancer, there is limited data supporting gender differences in survival rates. Some studies have suggested that female gender is an independent risk factor for CSM after RC (85, 112, 113). For example, Kluth et al. (Kluth et al., 2014) conducted a study analyzing 8,102 patients (including 1,605 females) who underwent RC and found that female gender was an independent predictor of bladder CSM (HR 1.17,  $p = 0.004$ ) after adjusting for various factors. Ingmar Wolff and colleagues

(Gago-Dominguez et al., 2001) analyzed studies published between 2012 and 2015 that focused on standardizing care for muscle-invasive bladder cancer (MIBC) and analyzing how gender affects prognosis. Among the 8 RC series studies, 5 reported higher CSM rates in female patients (Kiemeny et al., 1997; Cappellen et al., 1999; Fliss et al., 2000; Reulen et al., 2008; Zhang et al., 2020). Two studies specifically found gender-specific prognostic effects in early-stage disease (Kiemeny et al., 1997; Fliss et al., 2000). In these two studies, female patients also had lower survival rates, especially when it came to younger patients ( $\leq 55$  years and  $\leq 60$  years) and those who had lymphovascular invasion (LVI). However, no gender effect on prognosis was seen in two studies focusing on early invasive T1-high-grade UCB and TURB with intravesical treatment (Solomon et al., 2013; Cha and Bochner, 2015). Additionally, females were more likely to undergo RC (odds ratio [OR] 1.39; 95% CI 1.20–1.61) and had fewer complications ( $p < 0.05$ ).

Regarding a separate relationship between gender and survival following RC, there is, however, conflicting evidence. Using demographic, tumor, and therapeutic data to match 414 female and 2,153 male patients, Mitra et al. (Mallin et al., 2011) found no significant gender differences regarding recurrence-free, cancer-specific, and overall survival. After controlling for tumor stage and other factors, a different study including 398 male and 119 female RC patients found no relationship between postoperative survival and gender. Keck et al. (Cordes et al., 2013) conducted a study on patients undergoing adjuvant chemotherapy and found that female patients had higher CSM in a multivariate analysis (HR 2.40,  $p < 0.001$ ). Zhao et al. studied 233 eligible MIBC patients (177 males [76%] and 56 females [24%]) and 105 NMIBC patients (80 males [76.2%] and 25 females [23.8%]). According to this study, patients with bladder cancer who were female had a poorer prognosis than those who were male at particular stages, and obese females with higher BMI had poorer survival, while females with normal weight (BMI  $< 24$ ) had a higher likelihood of recurrence.

When analyzing gender differences in the prognosis of UCB, it is crucial to focus on patients with T4 bladder tumors. Gender-specific anatomical distinctions are present in the pT4 tumor stage, wherein pT4a tumors extend into the vagina or uterus in females and the prostate in males (Moschini et al., 2019). Women with pT4 bladder cancer had worse outcomes than men, according to a large study based on 583 occurrences of the disease among 4,257 patients (Tilki et al., 2010c). In an analysis by Matthias et al. (May et al., 2013), the 5-year cancer-specific survival rate for 245 pT4a UCB patients who did not receive chemotherapy before undergoing RC was 15% for females and 35% for males ( $p = 0.003$ ). Multivariate analysis showed that female patients had a poorer prognosis. Similarly, an analysis by Danielji et al. of 5,625 SEER database-based RC treatment for pT3–pT4 UCB patients also indicated that females had a higher independent risk of CSM compared to males (HR 1.20;  $p = 0.003$ ) (Lieberman et al., 2011a). However, analysis of a small sample ( $n = 128$ ) of pT4 tumor patients did not find a correlation between gender and survival rates (Kaushik et al., 2014), although this result may be due to the small sample size. Additionally, the results of these reports may be influenced by the heterogeneity of pT4 staging, especially in males. For example, the transmural infiltration of the primary bladder tumor is not considered when ductal and stromal invasion are categorized as pT4a. It is also possible for tumors

TABLE 1 Sex-specific differences in outcomes.

Aspect	Gender	Findings/Results
Bladder Cancer Incidence	Male	Diagnosed at a rate approximately three times higher than females (Shariat et al., 2010)
Bladder Cancer Mortality	Male	Likelihood of dying from bladder cancer is about twice that of females, resulting in a lower CSM-to-incidence ratio for males (Shariat et al., 2010)
Lifespan Reduction	Female	Female patients have a greater reduction in lifespan compared to males (6.5 years vs. 3.9 years) (Scosyrev et al., 2012)
Survival Differences	Female	Female individuals have a lower prognosis across all disease stages, including 5-year survival rates at different stages (Mungan et al., 2000a)
Registry Studies in Elderly Populations	Female	Female UCB patients in elderly populations have higher tumor staging and lower survival rates (Mungan et al., 2000a; Mungan et al., 2000b)
Japanese Kanagawa Cancer Registry Study	Female	CSM increased by approximately 40% in females, with higher cancer staging at initial diagnosis (Moschini et al., 2019)
Radical Cystectomy (RC)	Female	Limited data on gender differences in survival rates; some studies suggest female gender is an independent risk factor for CSM after RC (Tilki et al., 2010a; Tilki et al., 2010b; Kluth et al., 2014)
RC Series Studies on Muscle-Invasive BC	Female	5 out of 8 RC series studies reported higher CSM rates in female patients (Gago-Dominguez et al., 2001)
Early-Stage Prognostic Effects	Female	Some studies found gender-specific prognostic effects in early-stage disease, with lower survival rates in females (Kiemeny et al., 1997; Fliss et al., 2000)
Non-Metastatic Muscle-Invasive BC	Female	Female bladder CSM was poorer than that of males; females more likely to undergo RC with fewer complications (Cappellen et al., 1999)
Adjuvant Chemotherapy	Female	Female patients had higher CSM in a multivariate analysis (Cordes et al., 2013)
MIBC and NMIBC	Female	Female patients had poorer prognosis at particular stages, and obese females had poorer survival (Theodorescu et al., 2022)
T4 Bladder Tumors	Female	Female patients with pT4 bladder cancer had worse outcomes than males (Tilki et al., 2010c; Moschini et al., 2019)
SEER Database Analysis	Female	Higher independent risk of CSM in females with pT3–pT4 UCB (Lieberman et al., 2011a)
NMIBC Patient Registry Study	Female	Female NMIBC patients had significantly higher CSM than males (Alanee et al., 2015)
Post-Cystectomy Disparities	Female	Disparities in treatment for female cystectomy patients, with longer hospital stays and higher blood product costs (Cárdenas-Turanzas et al., 2008; Siegrist et al., 2010)
SEER Database Analysis (Post-RC)	Female	Female patients undergoing RC had a 20% higher risk of death within 90 days (Lieberman et al., 2011b).

designated as UCB to be poorly differentiated prostate cancer in cases of extremely undifferentiated tumors (Downes et al., 2013).

The relationship between gender and prognosis differences in NMIBC is also limited and sometimes contradictory. Fabiano et al. (Santos et al., 2015) found that similar to delayed diagnosis with hematuria, females also experienced delays in undergoing transurethral bladder resection compared to males. Additionally, studies have shown that the likelihood of receiving BCG therapy is similar for male and female NMIBC patients (Noon et al., 2013). For example, Jonathan et al. (Theodorescu et al., 2022) analyzed 472 (77.0%) male NMIBC patients and 141 (23.0%) female NMIBC patients who received BCG treatment and found no clear evidence of gender-based differences in treatment response, recurrence, and tolerability. Since these individuals did not have long-term BCG therapy or repeat transurethral resection, the generalizability of these findings is still questionable. It is worth noting that a population-based cancer registry study found that female NMIBC patients had significantly higher CSM than males (Noon et al., 2013). However, Alanee et al. (Alanee et al., 2015) analysis showed that females had a higher risk of CSM than carcinoma *in situ* (CIS) patients. In addition, female T1HG UCB patients had a greater chance of recurrence but not disease progression or death (Kluth

et al., 2013). Similarly, no association between gender and illness development or recurrence was discovered in an analysis conducted by Boorjian et al. (Boorjian et al., 2010) of 756 male and 265 female patients undergoing BCG treatment. After examining 15,215 high-grade T1 patients, Martin-Doyle et al. (Martin-Doyle et al., 2015) found that while there was no association between females and cancer-specific survival or tumor recurrence, they did have a notably increased risk of disease progression. Konrad Bilski et al. (Bilski et al., 2022) conducted a retrospective analysis of 388 male and 131 female patients with primary high-risk NMIBC treated with transurethral resection (TUR) and found that females were associated with an increased risk of disease recurrence, but there was no gender difference in disease progression.

Although the reasons for the gender disparities in post-cystectomy death rates have not been fully elucidated, several researchers have provided evidence of inequalities in the quality of treatment received by male and female cystectomy patients. A retrospective study by Cárdenas-Turanzas et al. (Cárdenas-Turanzas et al., 2008) showed that female patients undergoing RC had significantly longer hospital stays and higher blood product costs. According to Siegrist et al. (Siegrist et al., 2010), female patients undergoing cystectomies experienced increased



blood loss, longer operating times, more transfusion needs, and decreased pelvic lymph node dissection incidence. Additionally, an analysis of 12,722 UCB patients from the SEER database from 1988 to 2006 showed that female patients undergoing RC had a 20% higher risk of death within 90 days (Lieberman et al., 2011b). However, other research has demonstrated the absence of significant gender disparities in frequently employed surgical quality measures, such as lymph node counts and surgical margin status (Horstmann et al., 2008; Kluth et al., 2014; Messer et al., 2014; Mitra et al., 2014). As a result, it is unlikely that the marginal differences in overall survival rates between men and women can be attributed simply to unequal treatment between the sexes. Future studies should determine the fundamental causes of gender-specific variations in diagnostic features and pathological staging (Table 1).

## 5.2 Sex-specific responses in bladder cancer treatment

In addressing the efficacy of immune checkpoint inhibitors (ICIs) in bladder cancer treatment, it is imperative to explore potential sex-specific responses. Recent studies have suggested differential efficacy between male and female patients undergoing ICI treatment (Aragaki et al., 2022; Lindner et al., 2023). These investigations, characterized by variations in response rates and survival outcomes, underscore the importance of considering sex as a critical factor in immunotherapeutic interventions. Mechanisms underlying these sex-specific differences remain an active area of research, with hypotheses centered around hormonal, immunological, and genetic factors. Despite the promising strides made in systemic immunotherapy, challenges persist in the realm of bladder infusion chemotherapy, where localized drug delivery occurs directly into the bladder. Presently, bladder infusion chemotherapy lacks specific drug treatment options tailored to sex differences, necessitating further exploration and research. Ongoing initiatives are focused on identifying novel agents and optimizing drug delivery methods, urging future studies to delve into sex-specific responses to emerging treatments for a more personalized and effective approach.

Gender-related factors significantly influence various facets of bladder cancer drug therapy. Metabolic enzymes, particularly liver enzyme activity, exhibit gender-specific differences impacting chemotherapy drug metabolism and treatment outcomes. Hormonal influences, exemplified by estrogen and androgen receptor expression on bladder cancer cells, contribute to variations in hormone-targeted therapy responses. Studies indicate potential gender-related differences in immune checkpoint inhibitor responses, highlighting gender's crucial role in immunotherapy outcomes. Gender-specific variations in body composition and distribution influence drug pharmacokinetics, impacting treatment effectiveness and toxicity. Additionally, psychosocial factors and gender-specific side effects influence patient experiences and compliance with bladder cancer drug therapy. Ensuring adequate gender representation in clinical trials is crucial for generalizability, particularly understanding interactions with hormone replacement therapy in postmenopausal women. Exploring the reasons behind gender-

related survival disparities in bladder cancer guides efforts to tailor treatment strategies for improved outcomes.

Leveraging gender-specific characteristics for bladder cancer treatment involves a comprehensive approach to enhance therapeutic strategies and patient prognosis. Precision medicine, driven by genomic profiling, facilitates the development of targeted therapies tailored to individual profiles. Hormone-targeted therapies, modulating estrogen and androgen receptors based on expression patterns, offer gender-tailored interventions. Optimization of immunotherapy considers gender-related variations in immunological responses, ensuring enhanced treatment outcomes. Gender-specific pharmacokinetics in drug development ensure individualized dosing, optimizing drug exposure and efficacy. Inclusive clinical trial designs with adequate gender representation generate robust data to discern gender-specific responses to emerging therapies. Tailored psychosocial support programs address unique coping mechanisms and adherence challenges, contributing to overall wellbeing during treatment. Gender-tailored screening protocols, survivorship programs, and educational initiatives empower healthcare providers and communities to enhance early detection, survivorship care, and awareness of gender-related risk factors, advancing personalized, equitable, and effective bladder cancer therapies.

## 6 Conclusion

In conclusion, our comprehensive exploration of bladder cancer underscores the profound impact of sex on its multifaceted dimensions, illuminating crucial insights for future research and clinical interventions. The etiological panorama, encompassing factors such as smoking, occupational exposures, and genetic mutations, exhibits intriguing disparities in male and female populations. The nuanced biological differences, including the intricate interplay of sex hormones, sex chromosomes, metabolic enzymes, and the microbiome, provide a rich substrate for understanding the intricacies of bladder cancer initiation and progression.

Furthermore, our synthesis of gender-specific diagnostic and prognostic implications reveals substantial variations across all disease stages, transcending the detection phase and implicating fundamental disparities in disease outcomes. The dearth of conclusive evidence regarding gender-specific survival rates post-radical cystectomy calls for further exploration and validation. Addressing these disparities necessitates tailored research initiatives and the development of gender-specific treatment modalities.

In essence, this comprehensive review serves as a clarion call for heightened attention to sex-specific considerations in bladder cancer research and clinical practice. A more nuanced understanding of these gender-based disparities is essential for advancing personalized medicine and optimizing outcomes for all patients afflicted by this prevalent malignancy. Future investigations should delve deeper into the intricate interplay of sex-related factors, fostering a more precise and equitable approach to bladder cancer prevention, diagnosis, and treatment.



## Author contributions

SZ: Conceptualization, Data curation, Investigation, Methodology, Supervision, Writing—original draft, Writing—review and editing. HZ: Conceptualization, Data curation, Investigation, Methodology, Visualization, Writing—original draft, Writing—review and editing.

## Funding

The author(s) declare that no financial support was received for the research, authorship, and/or publication of this article.

## References

- Abdel-Hafiz, H. A., Schafer, J. M., Chen, X., Xiao, T., Gauntner, T. D., Li, Z., et al. (2023). Y chromosome loss in cancer drives growth by evasion of adaptive immunity. *Nature* 619 (7970), 624–631. doi:10.1038/s41586-023-06234-x
- Alanee, S., Bauman, J., Dynda, D., Frye, T., Konety, B., and Schwartz, B. (2015). Conservative management and female gender are associated with increased cancer-specific death in patients with isolated primary urothelial carcinoma *in situ*. *Eur. J. cancer care* 24 (3), 444–449. doi:10.1111/ecc.12217
- Alfano, M., Canducci, F., Nebuloni, M., Clementi, M., Montorsi, F., and Salonia, A. (2016). The interplay of extracellular matrix and microbiome in urothelial bladder cancer. *Nat. Rev. Urol.* 13 (2), 77–90. doi:10.1038/nrurol.2015.292
- Aragaki, A. K., Jing, Y., Hoffman-Censits, J., Choi, W., Hahn, N. M., Trock, B. J., et al. (2022). Gender-specific stratification of survival following immune checkpoint inhibitor therapy based on intratumoral expression of a B cell gene signature. *Eur. Urol. Oncol.* 5 (3), 338–346. doi:10.1016/j.euo.2021.07.003
- Aso, Y., Akaza, H., Kotake, T., Tsukamoto, T., Imai, K., and Naito, S. (1995). Preventive effect of a *Lactobacillus casei* preparation on the recurrence of superficial bladder cancer in a double-blind trial. The BLP Study Group. *Eur. Urol.* 27 (2), 104–109. doi:10.1159/000475138
- Aziz, A., Madersbacher, S., Otto, W., Mayr, R., Comploj, E., Pycha, A., et al. (2015). Comparative analysis of gender-related differences in symptoms and referral patterns prior to initial diagnosis of urothelial carcinoma of the bladder: a prospective cohort study. *Urol. Int.* 94 (1), 37–44. doi:10.1159/000363334
- Bassett, J. C., Alvarez, J., Koyama, T., Resnick, M., You, C., Ni, S., et al. (2015). Gender, race, and variation in the evaluation of microscopic hematuria among Medicare beneficiaries. *J. general Intern. Med.* 30 (4), 440–447. doi:10.1007/s11606-014-3116-2
- Bergman, J., Neuhausen, K., Chamie, K., Scales, C. D., Carter, S., Kwan, L., et al. (2013). Building a medical neighborhood in the safety net: an innovative technology improves hematuria workups. *Urology* 82 (6), 1277–1282. doi:10.1016/j.urology.2013.08.015
- Bevan, R., Young, C., Holmes, P., Fortunato, L., Slack, R., Rushton, LJB/C, et al. (2012). Occupational cancer in Britain. Gastrointestinal cancers: liver, oesophagus, pancreas and stomach. *Br. J. Cancer* 107 (1), S33–S40. doi:10.1038/bjc.2012.116
- Bhatt, A. P., Redinbo, M. R., and Bultman, S. J. (2017). The role of the microbiome in cancer development and therapy. *CA a cancer J. Clin.* 67 (4), 326–344. doi:10.3322/caac.21398
- Bi, H., Tian, Y., Song, C., Li, J., Liu, T., Chen, Z., et al. (2019). Urinary microbiota - a potential biomarker and therapeutic target for bladder cancer. *J. Med. Microbiol.* 68 (10), 1471–1478. doi:10.1099/jmm.0.001058
- Bilski, K., Kozikowski, M., Skrzypczyk, M. A., Dobruch, A., Hendricksen, K., D'Andrea, D., et al. (2022). Sex remains negative prognostic factor in contemporary cohort of high-risk non-muscle-invasive bladder cancer. *Cancers* 14 (24), 6110. doi:10.3390/cancers14246110
- Boffetta, P. (2008). Tobacco smoking and risk of bladder cancer. *Scand. J. urology Nephrol. Suppl.* 42 (218), 45–54. doi:10.1080/03008880802283664
- Boorjian, S., Ugras, S., Mongan, N. P., Gudas, L. J., You, X., Tickoo, S. K., et al. (2004). Androgen receptor expression is inversely correlated with pathologic tumor stage in bladder cancer. *Urology* 64 (2), 383–388. doi:10.1016/j.urology.2004.03.025
- Boorjian, S. A., Zhu, F., and Herr, H. W. (2010). The effect of gender on response to bacillus Calmette-Guérin therapy for patients with non-muscle-invasive urothelial carcinoma of the bladder. *BJU Int.* 106 (3), 357–361. doi:10.1111/j.1464-410X.2009.09137.x
- Bučević Popović, V., Šitum, M., Chow, C. T., Chan, L. S., Roje, B., and Terzić, J. (2018). The urinary microbiome associated with bladder cancer. *Sci. Rep.* 8 (1), 12157. doi:10.1038/s41598-018-29054-w
- Buckley, D. B., and Klaassen, C. D. (2007). Tissue- and gender-specific mRNA expression of UDP-glucuronosyltransferases (UGTs) in mice. *Drug metabolism Dispos. Biol. fate Chem.* 35 (1), 121–127. doi:10.1124/dmd.106.012070
- Buteau, A., Seideman, C. A., Svatek, R. S., Youssef, R. F., Chakrabarti, G., Reed, G., et al. (2014). What is evaluation of hematuria by primary care physicians? Use of electronic medical records to assess practice patterns with intermediate follow-up. *Urol. Oncol.* 32 (2), 128–134. doi:10.1016/j.urolonc.2012.07.001
- Cappellen, D., De Oliveira, C., Ricol, D., de Medina, S., Bourdin, J., Sastre-Garau, X., et al. (1999). Frequent activating mutations of FGFR3 in human bladder and cervix carcinomas. *Nat. Genet.* 23 (1), 18–20. doi:10.1038/12615
- Cárdenas-Turanzas, M., Cooksley, C., Kamat, A. M., Pettaway, C. A., and Elting, L. S. (2008). Gender and age differences in blood utilization and length of stay in radical cystectomy: a population-based study. *Int. urology Nephrol.* 40 (4), 893–899. doi:10.1007/s11255-008-9351-x
- Castelao, J. E., Yuan, J. M., Skipper, P. L., Tannenbaum, S. R., Gago-Dominguez, M., Crowder, J. S., et al. (2001). Gender- and smoking-related bladder cancer risk. *J. Natl. Cancer Inst.* 93 (7), 538–545. doi:10.1093/jnci/93.7.538
- Cha, E. K., and Bochner, B. H. (2015). Re: whole-genome and whole-exome sequencing of bladder cancer identifies frequent alterations in genes involved in sister chromatid cohesion and segregation. *Eur. Urol.* 67 (2), 350–351. doi:10.1016/j.eururo.2014.11.021
- Chen, Y. E., Fischbach, M. A., and Belkaid, Y. (2018). Skin microbiota-host interactions. *Nature* 553 (7689), 427–436. doi:10.1038/nature25177
- Cohn, J. A., Vekhter, B., Lyttle, C., Steinberg, G. D., and Large, M. C. (2014). Sex disparities in diagnosis of bladder cancer after initial presentation with hematuria: a nationwide claims-based investigation. *Cancer* 120 (4), 555–561. doi:10.1002/cncr.28416
- Cordes, I., Kluth, M., Zygis, D., Rink, M., Chun, F., Eichelberg, C., et al. (2013). PTEN deletions are related to disease progression and unfavourable prognosis in early bladder cancer. *Histopathology* 63 (5), 670–677. doi:10.1111/his.12209
- Cumberbatch, M. G., and Catto, J. W. F. (2018). Re: comprehensive molecular characterization of muscle invasive bladder cancer. *Eur. Urol.* 73 (3), 479–480. doi:10.1016/j.eururo.2017.11.022
- Curtiss, N., Balachandran, A., Krska, L., Peppiatt-Wildman, C., Wildman, S., and Duckett, J. (2017). A case controlled study examining the bladder microbiome in women with Overactive Bladder (OAB) and healthy controls. *Eur. J. obstetrics, Gynecol. reproductive Biol.* 214, 31–35. doi:10.1016/j.ejogrb.2017.04.040
- Daugherty, S. E., Lacey, J. V., Jr., Pfeiffer, R. M., Park, Y., Hoover, R. N., and Silverman, D. T. (2013). Reproductive factors and menopausal hormone therapy and bladder cancer risk in the NIH-AARP Diet and Health Study. *Int. J. cancer* 133 (2), 462–472. doi:10.1002/ijc.28022
- Davis, R., Jones, J. S., Barocas, D. A., Castle, E. P., Lang, E. K., Leveillee, R. J., et al. (2012). Diagnosis, evaluation and follow-up of asymptomatic microhematuria (AMH) in adults: AUA guideline. *J. urology* 188 (6), 2473–2481. doi:10.1016/j.juro.2012.09.078
- Deng, G., Wang, R., Sun, Y., Huang, C. P., Yeh, S., You, B., et al. (2021). Targeting androgen receptor (AR) with antiandrogen Enzalutamide increases prostate cancer cell invasion yet decreases bladder cancer cell invasion via differentially altering the AR/circRNA-ARC1/miR-125b-2-3p or miR-4736/PPARγ/MMP-9 signals. *Cell death Differ.* 28 (7), 2145–2159. doi:10.1038/s41418-021-00743-w
- Downes, M. R., Torlakovic, E. E., Aldaoud, N., Zlotta, A. R., Evans, A. J., and van der Kwast, T. H. (2013). Diagnostic utility of androgen receptor expression in discriminating poorly differentiated urothelial and prostate carcinoma. *J. Clin. pathology* 66 (9), 779–786. doi:10.1136/jclinpath-2013-201586

## Conflict of interest

The authors declare that the research was conducted in the absence of any commercial or financial relationships that could be construed as a potential conflict of interest.

## Publisher's note

All claims expressed in this article are solely those of the authors and do not necessarily represent those of their affiliated organizations, or those of the publisher, the editors and the reviewers. Any product that may be evaluated in this article, or claim that may be made by its manufacturer, is not guaranteed or endorsed by the publisher.

- Fajkovic, H., Halpern, J. A., Cha, E. K., Bahadori, A., Chromecki, T. F., Karakiewicz, P. I., et al. (2011). Impact of gender on bladder cancer incidence, staging, and prognosis. *World J. urology* 29 (4), 457–463. doi:10.1007/s00345-011-0709-9
- Fickenscher, L. (1999). Evaluating adult hematuria. *Nurse Pract.* 24 (9), 58–65. doi:10.1097/00006205-199909000-00005
- Fliss, M. S., Usadel, H., Caballero, O. L., Wu, L., Buta, M. R., Eleff, S. M., et al. (2000). Facile detection of mitochondrial DNA mutations in tumors and bodily fluids. *Sci. (New York, NY)* 287 (5460), 2017–2019. doi:10.1126/science.287.5460.2017
- Forsberg, L. A., Rasi, C., Malmqvist, N., Davies, H., Pasupulati, S., Pakalapati, G., et al. (2014). Mosaic loss of chromosome Y in peripheral blood is associated with shorter survival and higher risk of cancer. *Nat. Genet.* 46 (6), 624–628. doi:10.1038/ng.2966
- Fouts, D. E., Pieper, R., Szpakowski, S., Pohl, H., Knoblach, S., Suh, M. J., et al. (2012). Integrated next-generation sequencing of 16S rDNA and metaproteomics differentiate the healthy urine microbiome from asymptomatic bacteriuria in neuropathic bladder associated with spinal cord injury. *J. Transl. Med.* 10, 174. doi:10.1186/1479-5876-10-174
- Gago-Dominguez, M., Castela, J. E., Yuan, J. M., Yu, M. C., and Ross, R. K. (2001). Use of permanent hair dyes and bladder-cancer risk. *Int. J. Cancer* 91 (4), 575–579. doi:10.1002/1097-0215(200002)9999:9999<:aid-ijc1092>3.0.co;2-s
- Gakis, G., and Stenzl, A. (2013). Gender-specific differences in muscle-invasive bladder cancer: the concept of sex steroid sensitivity. *World J. urology* 31 (5), 1059–1064. doi:10.1007/s00345-013-1037-z
- Gallagher, C. J., Balliet, R. M., Sun, D., Chen, G., and Lazarus, P. (2010). Sex differences in UDP-glucuronosyltransferase 2B17 expression and activity. *Drug metabolism Dispos. Biol. fate Chem.* 38 (12), 2204–2209. doi:10.1124/dmd.110.035345
- Garg, T., Pinheiro, L. C., Atoria, C. L., Donat, S. M., Weissman, J. S., Herr, H. W., et al. (2014). Gender disparities in hematuria evaluation and bladder cancer diagnosis: a population based analysis. *J. urology* 192 (4), 1072–1077. doi:10.1016/j.juro.2014.04.101
- Garrett, W. S. (2015). Cancer and the microbiota. *Sci. (New York, NY)* 348 (6230), 80–86. doi:10.1126/science.aaa4972
- Gul, Z. G., Liaw, C. W., and Mehrazin, R. (2021). Gender differences in incidence, diagnosis, treatments, and outcomes in clinically localized bladder and renal cancer. *Urology* 151, 176–181. doi:10.1016/j.urology.2020.05.067
- Hashibe, M., Gao, T., Li, G., Dalbagni, G., and Zhang, Z. F. (2003). Comparison of bladder cancer survival among Japanese, Chinese, Filipino, Hawaiian and Caucasian populations in the United States. *Asian Pac. J. cancer Prev. APJCP.* 4 (3), 267–273.
- Hemelt, M., Yamamoto, H., Cheng, K. K., and Zeegers, M. P. (2009). The effect of smoking on the male excess of bladder cancer: a meta-analysis and geographical analyses. *Int. J. cancer* 124 (2), 412–419. doi:10.1002/ijc.23856
- Hengstler, J. G., Arand, M., Herrero, M. E., and Oesch, F. (1998). Polymorphisms of N-acetyltransferases, glutathione S-transferases, microsomal epoxide hydrolase and sulfotransferases: influence on cancer susceptibility. *Recent Results Cancer Res.* 154, 47–85. doi:10.1007/978-3-642-46870-4\_4
- Henning, A., Wehrberger, M., Madersbacher, S., Pycha, A., Martini, T., Comploj, E., et al. (2013). Do differences in clinical symptoms and referral patterns contribute to the gender gap in bladder cancer? *BJU Int.* 112 (1), 68–73. doi:10.1111/j.1464-410X.2012.11661.x
- Horstmann, M., Witthuhn, R., Falk, M., and Stenzl, A. (2008). Gender-specific differences in bladder cancer: a retrospective analysis. *Gen. Med.* 5 (4), 385–394. doi:10.1016/j.genm.2008.11.002
- Hsu, I., Vitkus, S., Da, J., and Yeh, S. (2013). Role of oestrogen receptors in bladder cancer development. *Nat. Rev. Urol.* 10 (6), 317–326. doi:10.1038/nrurol.2013.53
- Hu, D. G., Mackenzie, P. I., McKinnon, R. A., and Meech, R. (2016). Genetic polymorphisms of human UDP-glucuronosyltransferase (UGT) genes and cancer risk. *Drug metab. Rev.* 48 (1), 47–69. doi:10.3109/03602532.2015.1131292
- Izumi, K., Li, Y., Ishiguro, H., Zheng, Y., Yao, J. L., Netto, G. J., et al. (2014b). Expression of UDP-glucuronosyltransferase 1A in bladder cancer: association with prognosis and regulation by estrogen. *Mol. Carcinog.* 53 (4), 314–324. doi:10.1002/mc.21978
- Izumi, K., Taguri, M., Miyamoto, H., Hara, Y., Kishida, T., Chiba, K., et al. (2014a). Androgen deprivation therapy prevents bladder cancer recurrence. *Oncotarget* 5 (24), 12665–12674. doi:10.18632/oncotarget.2851
- Izumi, K., Zheng, Y., Hsu, J. W., Chang, C., and Miyamoto, H. (2013). Androgen receptor signals regulate UDP-glucuronosyltransferases in the urinary bladder: a potential mechanism of androgen-induced bladder carcinogenesis. *Mol. Carcinog.* 52 (2), 94–102. doi:10.1002/mc.21833
- Jang, Y., Wang, C., Zhuang, L., Liu, C., and Ge, K. (2017). H3K4 methyltransferase activity is required for MLL4 protein stability. *J. Mol. Biol.* 429 (13), 2046–2054. doi:10.1016/j.jmb.2016.12.016
- Ji, J., Zöller, B., Sundquist, J., and Sundquist, K. (2016). Risk of solid tumors and hematological malignancy in persons with Turner and Klinefelter syndromes: a national cohort study. *Int. J. cancer* 139 (4), 754–758. doi:10.1002/ijc.30126
- Johnson, E. K., Daignault, S., Zhang, Y., and Lee, C. T. (2008). Patterns of hematuria referral to urologists: does a gender disparity exist? *Urology* 72 (3), 498–502. doi:10.1016/j.urology.2008.01.086
- Kaneko, S., and Li, X. (2018). X chromosome protects against bladder cancer in females via a KDM6A-dependent epigenetic mechanism. *Sci. Adv.* 4 (6), eaar5598. doi:10.1126/sciadv.aar5598
- Karagas, M. R., Park, S., Warren, A., Hamilton, J., Nelson, H. H., Mott, L. A., et al. (2005). Gender, smoking, glutathione-S-transferase variants and bladder cancer incidence: a population-based study. *Cancer Lett.* 219 (1), 63–69. doi:10.1016/j.canlet.2004.10.006
- Kaur, C. P., Vadivelu, J., and Chandramathi, S. (2018). Impact of *Klebsiella pneumoniae* in lower gastrointestinal tract diseases. *J. Dig. Dis.* 19 (5), 262–271. doi:10.1111/1751-2980.12595
- Kaushik, D., Frank, I., Eisenberg, M. S., Cheville, J. C., Tarrell, R., Thapa, P., et al. (2014). Gender-specific survival following radical cystectomy for pT4 bladder cancer. *World J. urology* 32 (6), 1433–1439. doi:10.1007/s00345-013-1232-y
- Kiemeny, L. A., Moret, N. C., Witjes, J. A., Schoenberg, M. P., and Tulinius, H. (1997). Familial transitional cell carcinoma among the population of Iceland. *J. urology* 157 (5), 1649–1651. doi:10.1016/s0022-5347(01)64821-3
- Killock, D. (2018). Immunotherapy: gut bacteria modulate responses to PD-1 blockade. *Nat. Rev. Clin. Oncol.* 15 (1), 6–7. doi:10.1038/nrclinonc.2017.182
- Kim, J.-M., and Park, Y.-JJUT (2018). Lactobacillus and urine microbiome in association with urinary tract infections and bacterial vaginosis. *Urogenit. Tract. Infect.* 13 (1), 7–13. doi:10.14777/uti.2018.13.1.7
- Kluth, L. A., Fajkovic, H., Xylinas, E., Crivelli, J. J., Passoni, N., Rouprêt, M., et al. (2013). Female gender is associated with higher risk of disease recurrence in patients with primary T1 high-grade urothelial carcinoma of the bladder. *World J. urology* 31 (5), 1029–1036. doi:10.1007/s00345-012-0996-9
- Kluth, L. A., Rieken, M., Xylinas, E., Kent, M., Rink, M., Rouprêt, M., et al. (2014). Gender-specific differences in clinicopathologic outcomes following radical cystectomy: an international multi-institutional study of more than 8000 patients. *Eur. Urol.* 66 (5), 913–919. doi:10.1016/j.eururo.2013.11.040
- Koti, M., Ingersoll, M. A., Gupta, S., Lam, C. M., Li, X., Kamat, A. M., et al. (2020). Sex differences in bladder cancer immunobiology and outcomes: a collaborative review with implications for treatment. *Eur. Urol. Oncol.* 3 (5), 622–630. doi:10.1016/j.euo.2020.08.013
- Koutros, S., Silverman, D. T., Baris, D., Zahm, S. H., Morton, L. M., Colt, J. S., et al. (2011). Hair dye use and risk of bladder cancer in the New England bladder cancer study. *Int. J. cancer* 129 (12), 2894–2904. doi:10.1002/ijc.26245
- Krabbe, L. M., Svatek, R. S., Shariat, S. F., Messing, E., and Lotan, Y. (2015). Bladder cancer risk: use of the PLCO and NLST to identify a suitable screening cohort. *Urol. Oncol.* 33 (2), 65.e19–e25. doi:10.1016/j.urolonc.2014.06.009
- Kwon, H., Chung, D., Kaneko, S., Li, A., Zhou, L., Riesenberger, B., et al. (2020). Distinct CD8+ T cell programming in the tumor microenvironment contributes to sex bias in bladder cancer outcome. Available at: <https://doi.org/10.1101/2020.04.13.039735>.
- Lam, C. M., Li, Z., Theodorescu, D., and Li, X. (2022). Mechanism of sex differences in bladder cancer: evident and elusive sex-biasing factors. *Bladder cancer (Amsterdam, Neth.)* 8 (3), 241–254. doi:10.3233/BLC-211658
- Lan, F., Bayliss, P. E., Rinn, J. L., Whetstone, J. R., Wang, J. K., Chen, S., et al. (2007). A histone H3 lysine 27 demethylase regulates animal posterior development. *Nature* 449 (7163), 689–694. doi:10.1038/nature06192
- Liberman, D., Alasker, A., Sun, M., Ismail, S., Lughezzani, G., Jeldres, C., et al. (2011a). Radical cystectomy for patients with pT4 urothelial carcinoma in a large population-based study. *BJU Int.* 107 (6), 905–911. doi:10.1111/j.1464-410X.2010.09590.x
- Liberman, D., Lughezzani, G., Sun, M., Alasker, A., Thuret, R., Abdollah, F., et al. (2011b). Perioperative mortality is significantly greater in septuagenarian and octogenarian patients treated with radical cystectomy for urothelial carcinoma of the bladder. *Urology* 77 (3), 660–666. doi:10.1016/j.urology.2010.07.537
- Lin, J., Yang, J., Xu, X., Wang, Y., Yu, M., and Zhu, Y. (2020). A robust 11-genes prognostic model can predict overall survival in bladder cancer patients based on five cohorts. *Cancer Cell Int.* 20, 402. doi:10.1186/s12935-020-01491-6
- Lindner, A. K., Lackner, F., Tymoszyk, P., Barth, D. A., Seeber, A., Kocher, F., et al. (2023). Sex hormones influence survival of patients with metastatic urothelial carcinoma undergoing immune checkpoint therapy. *Biol. Sex. Differ.* 14 (1), 38. doi:10.1186/s13293-023-00522-x
- Lotan, Y., Gupta, A., Shariat, S. F., Palapattu, G. S., Vazina, A., Karakiewicz, P. I., et al. (2005). Lymphovascular invasion is independently associated with overall survival, cause-specific survival, and local and distant recurrence in patients with negative lymph nodes at radical cystectomy. *J. Clin. Oncol.* 23 (27), 6533–6539. doi:10.1200/JCO.2005.05.516
- Lyratzopoulos, G., Abel, G. A., McPhail, S., Neal, R. D., and Rubin, G. P. (2013). Gender inequalities in the promptness of diagnosis of bladder and renal cancer after symptomatic presentation: evidence from secondary analysis of an English primary care audit survey. *BMJ open* 3 (6), e002861. doi:10.1136/bmjopen-2013-002861
- Mai, G., Chen, L., Li, R., Liu, Q., Zhang, H., and Ma, Y. (2019). Common core bacterial biomarkers of bladder cancer based on multiple datasets. *BioMed Res. Int.* 2019, 4824909. doi:10.1155/2019/4824909

- Mallin, K., David, K. A., Carroll, P. R., Milowsky, M. I., and Nanus, D. M. (2011). Transitional cell carcinoma of the bladder: racial and gender disparities in survival (1993 to 2002), stage and grade (1993 to 2007). *J. urology* 185 (5), 1631–1636. doi:10.1016/j.juro.2010.12.049
- Martin-Doyle, W., Leow, J. J., Orsola, A., Chang, S. L., and Bellmunt, J. (2015). Improving selection criteria for early cystectomy in high-grade T1 bladder cancer: a meta-analysis of 15,215 patients. *J. Clin. Oncol.* 33 (6), 643–650. doi:10.1200/JCO.2014.57.6967
- Mashhadi, R., Pourmand, G., Kosari, F., Mehrsai, A., Salem, S., Pourmand, M. R., et al. (2014). Role of steroid hormone receptors in formation and progression of bladder carcinoma: a case-control study. *Urology J.* 11 (6), 1968–1973.
- Matson, V., Fessler, J., Bao, R., Chongsawat, T., Zha, Y., Alegre, M. L., et al. (2018). The commensal microbiome is associated with anti-PD-1 efficacy in metastatic melanoma patients. *Sci. (New York, NY)* 359 (6371), 104–108. doi:10.1126/science.aao3290
- May, M., Bastian, P. J., Brookman-May, S., Fritsche, H. M., Tilki, D., Otto, W., et al. (2013). Gender-specific differences in cancer-specific survival after radical cystectomy for patients with urothelial carcinoma of the urinary bladder in pathologic tumor stage T4a. *Urol. Oncol.* 31 (7), 1141–1147. doi:10.1016/j.urolonc.2011.09.011
- McGrath, M., Michaud, D. S., and De Vivo, I. (2006). Hormonal and reproductive factors and the risk of bladder cancer in women. *Am. J. Epidemiol.* 163 (3), 236–244. doi:10.1093/aje/kwj028
- McMillan, A., Macklaim, J. M., Burton, J. P., and Reid, G. (2013). Adhesion of *Lactobacillus iners* AB-1 to human fibronectin: a key mediator for persistence in the vagina? *Reprod. Sci. (Thousand Oaks, Calif.)* 20 (7), 791–796. doi:10.1177/1933719112466306
- Meech, R., Hu, D. G., McKinnon, R. A., Mubarakah, S. N., Haines, A. Z., Nair, P. C., et al. (2019). The UDP-glycosyltransferase (UGT) superfamily: new members, new functions, and novel paradigms. *Physiol. Rev.* 99 (2), 1153–1222. doi:10.1152/physrev.00058.2017
- Messer, J. C., Shariat, S. F., Dinney, C. P., Novara, G., Fradet, Y., Kassouf, W., et al. (2014). Female gender is associated with a worse survival after radical cystectomy for urothelial carcinoma of the bladder: a competing risk analysis. *Urology* 83 (4), 863–867. doi:10.1016/j.urology.2013.10.060
- Mir, C., Shariat, S. F., Van Der Kwast, T. H., Ashfaq, R., Lotan, Y., Evans, A., et al. (2011). Loss of androgen receptor expression is not associated with pathological stage, grade, gender or outcome in bladder cancer: a large multi-institutional study. *BJU Int.* 108 (1), 24–30. doi:10.1111/j.1464-410X.2010.09834.x
- Mitra, A. P., Skinner, E. C., Schuckman, A. K., Quinn, D. I., Dorff, T. B., and Daneshmand, S. (2014). Effect of gender on outcomes following radical cystectomy for urothelial carcinoma of the bladder: a critical analysis of 1,994 patients. *Urol. Oncol.* 32 (1), 52.e1–e9. doi:10.1016/j.urolonc.2013.08.007
- Moschini, M., Zamboni, S., Mattei, A., Baumeister, P., Di Bona, C., Cornelius, J., et al. (2019). Radical cystectomy in pathological T4a and T4b bladder cancer patients: is there any space for sub stratification? *Urol. Int.* 102 (3), 269–276. doi:10.1159/000493899
- Mungan, N. A., Aben, K. K., Schoenberg, M. P., Visser, O., Coebergh, J. W., Witjes, J. A., et al. (2000b). Gender differences in stage-adjusted bladder cancer survival. *Urology* 55 (6), 876–880. doi:10.1016/s0090-4295(00)00523-9
- Mungan, N. A., Kiemeny, L. A., van Dijk, J. A., van der Poel, H. G., and Witjes, J. A. (2000a). Gender differences in stage distribution of bladder cancer. *Urology* 55 (3), 368–371. doi:10.1016/s0090-4295(99)00481-1
- Nieder, A. M., Lotan, Y., Nuss, G. R., Langston, J. P., Vyas, S., Manoharan, M., et al. (2010). Are patients with hematuria appropriately referred to Urology? A multi-institutional questionnaire based survey. *Urol. Oncol.* 28 (5), 500–503. doi:10.1016/j.urolonc.2008.10.018
- Noon, A. P., Albertsen, P. C., Thomas, F., Rosario, D. J., and Catto, J. W. (2013). Competing mortality in patients diagnosed with bladder cancer: evidence of undertreatment in the elderly and female patients. *Br. J. cancer* 108 (7), 1534–1540. doi:10.1038/bjc.2013.106
- Patel, J. V., Chambers, C. V., and Gomella, L. G. (2008). Hematuria: etiology and evaluation for the primary care physician. *Can. J. urology* 15 (1), 54–61. discussion 2.
- Pederzoli, F., Ferraresi, R., Amato, V., Locatelli, I., Alchera, E., Lucianò, R., et al. (2020). Sex-specific alterations in the urinary and tissue microbiome in therapy-naïve urothelial bladder cancer patients. *Eur. Urol. Oncol.* 3 (6), 784–788. doi:10.1016/j.euo.2020.04.002
- Rahmani, A. H., Alzohairy, M., Babiker, A. Y., Khan, A. A., Aly, S. M., and Rizvi, M. A. (2013). Implication of androgen receptor in urinary bladder cancer: a critical mini review. *Int. J. Mol. Epidemiol. Genet.* 4 (3), 150–155.
- Reulen, R. C., Kellen, E., Buntinx, F., Brinkman, M., and Zeegers, M. P. (2008). A meta-analysis on the association between bladder cancer and occupation. *Scand. J. urology Nephrol. Suppl.* 42 (218), 64–78. doi:10.1080/03008880802325192
- Richters, A., Aben, K. K. H., and Kiemeny, L. (2020). The global burden of urinary bladder cancer: an update. *World J. Urol.* 38 (8), 1895–1904. doi:10.1007/s00345-019-02984-4
- Rickels, R., Herz, H. M., Sze, C. C., Cao, K., Morgan, M. A., Collings, C. K., et al. (2017). Histone H3K4 monomethylation catalyzed by Trp and mammalian COMPASS-like proteins at enhancers is dispensable for development and viability. *Nat. Genet.* 49 (11), 1647–1653. doi:10.1038/ng.3965
- Rink, M., Ehdaie, B., Cha, E. K., Green, D. A., Karakiewicz, P. I., Babjuk, M., et al. (2012). Stage-specific impact of tumor location on oncologic outcomes in patients with upper and lower tract urothelial carcinoma following radical surgery. *Eur. Urol.* 62 (4), 677–684. doi:10.1016/j.eururo.2012.02.018
- Robertson, A. G., Kim, J., Al-Ahmadie, H., Bellmunt, J., Guo, G., Cherniack, A. D., et al. (2018). Comprehensive molecular characterization of muscle-invasive bladder cancer. *Cell.* 174 (4), 1033. doi:10.1016/j.cell.2018.07.036
- Routy, B., Le Chatelier, E., Derosa, L., Duong, C. P. M., Alou, M. T., Daillère, R., et al. (2018). Gut microbiome influences efficacy of PD-1-based immunotherapy against epithelial tumors. *Sci. (New York, NY)* 359 (6371), 91–97. doi:10.1126/science.aan3706
- Salinas-Sánchez, A. S., Sánchez-Sánchez, F., Donate-Moreno, M. J., Rubio-del-Campo, A., Gimenez-Bachs, J. M., Lorenzo-Romero, J. G., et al. (2011). Polymorphic deletions of the GSTT1 and GSTM1 genes and susceptibility to bladder cancer. *BJU Int.* 107 (11), 1825–1832. doi:10.1111/j.1464-410X.2010.09683.x
- Samanic, C. M., Kogevinas, M., Silverman, D. T., Tardón, A., Serra, C., Malats, N., et al. (2008). Occupation and bladder cancer in a hospital-based case-control study in Spain. *Occup. Environ. Med.* 65 (5), 347–353. doi:10.1136/oem.2007.035816
- Santos, F., Dragomir, A., Kassouf, W., Franco, E. L., and Aprikian, A. (2015). Predictors of preoperative delays before radical cystectomy for bladder cancer in Quebec, Canada: a population-based study. *BJU Int.* 115 (3), 389–396. doi:10.1111/bju.12742
- Scosyrev, E., Golijanin, D., Wu, G., and Messing, E. (2012). The burden of bladder cancer in men and women: analysis of the years of life lost. *BJU Int.* 109 (1), 57–62. doi:10.1111/j.1464-410X.2011.10318.x
- Scosyrev, E., Noyes, K., Feng, C., and Messing, E. (2009). Sex and racial differences in bladder cancer presentation and mortality in the US. *Cancer* 115 (1), 68–74. doi:10.1002/cncr.23986
- Shariat, S. F., Sfakianos, J. P., Droller, M. J., Karakiewicz, P. I., Meryn, S., and Bochner, B. H. (2010). The effect of age and gender on bladder cancer: a critical review of the literature. *BJU Int.* 105 (3), 300–308. doi:10.1111/j.1464-410X.2009.09076.x
- Shen, S. S., Smith, C. L., Hsieh, J. T., Yu, J., Kim, I. Y., Jian, W., et al. (2006). Expression of estrogen receptors-alpha and -beta in bladder cancer cell lines and human bladder tumor tissue. *Cancer* 106 (12), 2610–2616. doi:10.1002/cncr.21945
- Shepherd, E. A., Stapley, S., Neal, R. D., Rose, P., Walter, F. M., and Hamilton, W. T. (2012). Clinical features of bladder cancer in primary care. *Br. J. general Pract.* 62 (602), e598–e604. doi:10.3399/bjgp12X654560
- Siegrist, T., Savage, C., Shabsigh, A., Cronin, A., and Donat, S. M. (2010). Analysis of gender differences in early perioperative complications following radical cystectomy at a tertiary cancer center using a standardized reporting methodology. *Urol. Oncol.* 28 (1), 112–117. doi:10.1016/j.urolonc.2009.04.012
- Soave, A., Dahlem, R., Hansen, J., Weisbach, L., Minner, S., Engel, O., et al. (2015). Gender-specific outcomes of bladder cancer patients: a stage-specific analysis in a contemporary, homogenous radical cystectomy cohort. *Eur. J. Surg. Oncol.* 41 (3), 368–377. doi:10.1016/j.ejso.2014.03.003
- Solomon, D. A., Kim, J. S., Bondaruk, J., Shariat, S. F., Wang, Z. F., Elkahoul, A. G., et al. (2013). Frequent truncating mutations of STAG2 in bladder cancer. *Nat. Genet.* 45 (12), 1428–1430. doi:10.1038/ng.2800
- Sottnik, J. L., Vanderlinden, L., Joshi, M., Chauca-Diaz, A., Owens, C., Hansel, D. E., et al. (2021). Androgen receptor regulates CD44 expression in bladder cancer. *Cancer Res.* 81 (11), 2833–2846. doi:10.1158/0008-5472.CAN-20-3095
- Stenehjem, D. D., Tran, D., Nkrumah, M. A., and Gupta, S. (2018). PD1/PDL1 inhibitors for the treatment of advanced urothelial bladder cancer. *OncoTargets Ther.* 11, 5973–5989. doi:10.2147/OTT.S135157
- Strope, S. A., and Montie, J. E. (2008). The causal role of cigarette smoking in bladder cancer initiation and progression, and the role of urologists in smoking cessation. *J. urology* 180 (1), 31–37. discussion 7. doi:10.1016/j.juro.2008.03.045
- Takayama, K., Kaneshiro, K., Tsutsumi, S., Horie-Inoue, K., Ikeda, K., Urano, T., et al. (2007). Identification of novel androgen response genes in prostate cancer cells by coupling chromatin immunoprecipitation and genomic microarray analysis. *Oncogene* 26 (30), 4453–4463. doi:10.1038/sj.onc.1210229
- Theodorescu, D., Li, Z., and Li, X. (2022). Sex differences in bladder cancer: emerging data and call to action. *Nat. Rev. Urol.* 19 (8), 447–449. doi:10.1038/s41585-022-00591-4
- Tilki, D., Reich, O., Svatek, R. S., Karakiewicz, P. I., Kassouf, W., Novara, G., et al. (2010a). Characteristics and outcomes of patients with clinical carcinoma *in situ* only treated with radical cystectomy: an international study of 243 patients. *J. urology* 183 (5), 1757–1763. doi:10.1016/j.juro.2010.01.025
- Tilki, D., Svatek, R. S., Karakiewicz, P. I., Isbarn, H., Reich, O., Kassouf, W., et al. (2010b). Characteristics and outcomes of patients with pT4 urothelial carcinoma at radical cystectomy: a retrospective international study of 583 patients. *J. urology* 183 (1), 87–93. doi:10.1016/j.juro.2009.08.145
- Tilki, D., Svatek, R. S., Novara, G., Seitz, M., Godoy, G., Karakiewicz, P. I., et al. (2010b). Stage pT0 at radical cystectomy confers improved survival: an international study of 4,430 patients. *J. urology* 184 (3), 888–894. doi:10.1016/j.juro.2010.04.081

- Tracey, E., Roder, D., Luke, C., and Bishop, J. (2009). Bladder cancer survivals in New South Wales, Australia: why do women have poorer survival than men? *BJU Int.* 104 (4), 498–504. doi:10.1111/j.1464-410X.2009.08527.x
- Tuygun, C., Kankaya, D., Imamoglu, A., Sertcelik, A., Zengin, K., Oktay, M., et al. (2011). Sex-specific hormone receptors in urothelial carcinomas of the human urinary bladder: a comparative analysis of clinicopathological features and survival outcomes according to receptor expression. *Urol. Oncol.* 29 (1), 43–51. doi:10.1016/j.urolonc.2009.01.033
- Underwood, W., 3rd, Dunn, R. L., Williams, C., and Lee, C. T. (2006). Gender and geographic influence on the racial disparity in bladder cancer mortality in the US. *J. Am. Coll. Surg.* 202 (2), 284–290. doi:10.1016/j.jamcollsurg.2005.09.009
- Villaseñor, T., Madrid-Paulino, E., Maldonado-Bravo, R., Urbán-Aragón, A., Pérez-Martínez, L., and Pedraza-Alva, G. (2017). Activation of the Wnt pathway by *Mycobacterium tuberculosis*: a wnt-wnt situation. *Front. Immunol.* 8, 50. doi:10.3389/fimmu.2017.00050
- Voigt, P., Tee, W. W., and Reinberg, D. (2013). A double take on bivalent promoters. *Genes & Dev.* 27 (12), 1318–1338. doi:10.1101/gad.219626.113
- Wang, L., Wang, Y., Wang, J., Li, L., and Bi, J. (2021). Identification of a prognosis-related risk signature for bladder cancer to predict survival and immune landscapes. *J. Immunol. Res.* 2021, 3236384. doi:10.1155/2021/3236384
- Wu, P., Zhang, G., Zhao, J., Chen, J., Chen, Y., Huang, W., et al. (2018). Profiling the urinary microbiota in male patients with bladder cancer in China. *Front. Cell. Infect. Microbiol.* 8, 167. doi:10.3389/fcimb.2018.00167
- Xu, W., Yang, L., Lee, P., Huang, W. C., Nossa, C., Ma, Y., et al. (2014). Mini-review: perspective of the microbiome in the pathogenesis of urothelial carcinoma. *Am. J. Clin. Exp. urology* 2 (1), 57–61.
- Xu, Y., Zhang, N. Z., Chen, J., and Yuan, H. Q. (2013). Biomarkers in urothelial carcinoma of the bladder: the potential cross-talk between transforming growth factor- $\beta$ 1 and estrogen receptor  $\beta$ /androgen receptor pathways. *Med. hypotheses* 80 (6), 716–718. doi:10.1016/j.mehy.2013.02.018
- Yu, C., Hequn, C., Longfei, L., Long, W., Zhi, C., Feng, Z., et al. (2017). GSTM1 and GSTT1 polymorphisms are associated with increased bladder cancer risk: evidence from updated meta-analysis. *Oncotarget* 8 (2), 3246–3258. doi:10.18632/oncotarget.13702
- Zeegers, M. P., Tan, F. E., Dorant, E., and van Den Brandt, P. A. (2000). The impact of characteristics of cigarette smoking on urinary tract cancer risk: a meta-analysis of epidemiologic studies. *Cancer* 89 (3), 630–639. doi:10.1002/1097-0142(20000801)89:3<630::aid-cnrcr19>3.3.co;2-h
- Zhang, Y. (2013). Understanding the gender disparity in bladder cancer risk: the impact of sex hormones and liver on bladder susceptibility to carcinogens. *J. Environ. Sci. health* 31 (4), 287–304. doi:10.1080/10590501.2013.844755
- Zhang, Y., Birmann, B. M., Han, J., Giovannucci, E. L., Speizer, F. E., Stampfer, M. J., et al. (2020). Personal use of permanent hair dyes and cancer risk and mortality in US women: prospective cohort study. *Bmj* 370, m2942. doi:10.1136/bmj.m2942
- Zitvogel, L., Ma, Y., Raoult, D., Kroemer, G., and Gajewski, T. F. (2018). The microbiome in cancer immunotherapy: diagnostic tools and therapeutic strategies. *Sci. (New York, NY)* 359 (6382), 1366–1370. doi:10.1126/science.aar6918



## Glossary

<b>BC</b>	Bladder Cancer
<b>HRA</b>	High-Risk HPV (Human Papillomavirus)-Associated
<b>KRAS2</b>	Kirsten Rat Sarcoma Viral Oncogene Homolog 2
<b>RB1</b>	Retinoblastoma 1
<b>FGFR3</b>	Fibroblast Growth Factor Receptor 3
<b>STAG2</b>	Stromal Antigen 2
<b>TERT</b>	Telomerase Reverse Transcriptase
<b>ESPL1</b>	Extra Spindle Pole Bodies Like 1
<b>UTX</b>	Ubiquitously Transcribed Tetratricopeptide Repeat X-Linked
<b>MLL</b>	Mixed-Lineage Leukemia
<b>CREBBP</b>	CREB-Binding Protein
<b>EP300</b>	E1A Binding Protein P300
<b>NCOR1</b>	Nuclear Receptor Corepressor 1
<b>ARID1A</b>	AT-Rich Interaction Domain 1A
<b>PTEN</b>	Phosphatase and Tensin Homolog
<b>MIBC</b>	Muscle-Invasive Bladder Cancer
<b>AR</b>	Androgen Receptor
<b>BCG</b>	Bacillus Calmette-Guérin
<b>CD</b>	Cluster of Differentiation
<b>ER</b>	Estrogen Receptor
<b>GSTM1</b>	Glutathione-S-transferase M1
<b>H3K27me3</b>	Histone H3 Lysine 27 Trimethylation
<b>KDM6A</b>	Lysine-specific Demethylase 6A
<b>MIBC</b>	Muscle-Invasive Bladder Cancer
<b>UCB</b>	Urothelial Carcinoma of the Bladder
<b>UGT</b>	UDP-glucuronosyltransferase
<b>MIBC</b>	Muscle-Invasive Bladder Cancer
<b>UCB</b>	Urothelial Carcinoma of the Bladder
<b>SEER</b>	Surveillance, Epidemiology, and End Results
<b>CSM</b>	Cancer-Specific Mortality
<b>HR</b>	Hazard Ratio
<b>NMIBC</b>	Non-Muscle-Invasive Bladder Cancer
<b>CIS</b>	Carcinoma <i>In Situ</i>
<b>TUR</b>	Transurethral Resection





## OPEN ACCESS

## EDITED BY

Jianbin Bi,  
The First Hospital of China Medical University,  
China

## REVIEWED BY

Xusheng Tu,  
Third Affiliated Hospital of Sun Yat-sen  
University, China  
Hualin Chen,  
Peking Union Medical College Hospital (CAMS),  
China

## \*CORRESPONDENCE

Changchang Li,  
✉ lichangchang\_88@163.com

RECEIVED 21 February 2024

ACCEPTED 13 May 2024

PUBLISHED 28 May 2024

## CITATION

Li C, Wu N, Lin X, Zhou Q and Xu M (2024),  
Integrated transcriptomic and immunological  
profiling reveals new diagnostic and prognostic  
models for cutaneous melanoma.  
*Front. Pharmacol.* 15:1389550.  
doi: 10.3389/fphar.2024.1389550

## COPYRIGHT

© 2024 Li, Wu, Lin, Zhou and Xu. This is an  
open-access article distributed under the terms  
of the [Creative Commons Attribution License  
\(CC BY\)](https://creativecommons.org/licenses/by/4.0/). The use, distribution or reproduction in  
other forums is permitted, provided the original  
author(s) and the copyright owner(s) are  
credited and that the original publication in this  
journal is cited, in accordance with accepted  
academic practice. No use, distribution or  
reproduction is permitted which does not  
comply with these terms.

# Integrated transcriptomic and immunological profiling reveals new diagnostic and prognostic models for cutaneous melanoma

Changchang Li<sup>1\*</sup>, Nanhui Wu<sup>2</sup>, Xiaoqiong Lin<sup>1</sup>, Qiaochu Zhou<sup>1</sup>  
and Mingyuan Xu<sup>2</sup>

<sup>1</sup>Department of Dermatology, Wenzhou Hospital of Integrated Traditional Chinese and Western Medicine, Wenzhou, China, <sup>2</sup>Department of Dermatopathology, Shanghai Skin Disease Hospital, Tongji University School of Medicine, Shanghai, China

The mortality rate associated with cutaneous melanoma (SKCM) remains alarmingly high, highlighting the urgent need for a deeper understanding of its molecular underpinnings. In our study, we leveraged bulk transcriptome sequencing data from the SKCM cohort available in public databases such as TCGA and GEO. We utilized distinct datasets for training and validation purposes and also incorporated mutation and clinical data from TCGA, along with single-cell sequencing data from GEO. Through dimensionality reduction, we annotated cell subtypes within the single-cell data and analyzed the expression of tumor-related pathways across these subtypes. We identified differentially expressed genes (DEGs) in the training set, which were further refined using the Least Absolute Shrinkage and Selection Operator (LASSO) machine learning algorithm, employing tenfold cross-validation. This enabled the construction of a prognostic model, whose diagnostic efficacy we subsequently validated. We conducted Gene Ontology (GO) and Kyoto Encyclopedia of Genes and Genomes (KEGG) analyses on the DEGs, and performed immunological profiling on two risk groups to elucidate the relationship between model genes and the immune responses relevant to SKCM diagnosis, treatment, and prognosis. We also knocked down the GMR6 expression level in the melanoma cells and verified its effect on cancer through multiple experiments. The results indicate that the GMR6 gene plays a role in promoting the proliferation, invasion, and migration of cancer cells in human melanoma. Our findings offer novel insights and a theoretical framework that could enhance prognosis, treatment, and drug development strategies for SKCM, potentially leading to more precise therapeutic interventions.

## KEYWORDS

SKCM, melanoma, LASSO machine learning algorithm, differential gene expression, immune infiltration analysis

## 1 Introduction

SKCM is globally recognized as the third most prevalent type of skin cancer and the 19th most common cancer overall (Davey et al., 2021). Despite constituting only about 1% of all skin cancers, SKCM is the most invasive and perilous type, responsible for 90% of skin cancer-related deaths (Eddy and Chen, 2020). In the United States in 2023, approximately 97,610 new cases of SKCM were projected, accompanied by an estimated mortality of 7,990

(Siegel et al., 2023). *In situ* SKCM represents the precursor stage to malignant SKCM, with its incidence rising even faster than that of malignant SKCM (Wei et al., 2016; Sacchetto et al., 2018). The 5-year survival rate for localized SKCM is 99%, but it drops to 63% for regional metastatic SKCM and further plummets to 20% for distant metastatic cases (Fakhoury et al., 2024). Major risk factors for SKCM include environmental factors like excessive UV exposure, genetic factors, gender, age, race, and immune factors (Hawkes et al., 2016; Davey et al., 2021). Females have a lower risk of SKCM, and their prognosis is better than males (El Sharouni et al., 2019). Socioeconomic status is closely linked to SKCM incidence, with higher socioeconomic status correlating to higher malignant SKCM rates, though tumors are thinner, and prognosis is relatively better compared to lower socioeconomic status patients (Gibson et al., 2020). Despite advancements in surgery, radiation therapy, chemotherapy, and targeted treatments such as KIT inhibitors, SKCM poses challenges due to difficulties in early non-invasive identification, high invasiveness, and early occurrence of local or distant metastases, leading to an overall poor prognosis (Lo and Fisher, 2014; Slipicevic and Herlyn, 2015; Davis et al., 2019). Therefore, in-depth research into the mechanisms of SKCM occurrence and development, especially those leading to metastasis and recurrence, is crucial. Identifying key biomarkers and exploring crucial target genes are essential for the diagnosis, treatment, and prognosis of SKCM.

Numerous studies have investigated the role of specific gene families in SKCM and constructed prognostic models (Luo et al., 2023; Yue et al., 2023). However, these studies have primarily focused on subsequent analyses based on specific functional gene sets. Analyzing the intrinsic correlations and potential therapeutic targets of gene expression from a holistic transcriptomic perspective can provide a more comprehensive understanding of the disease. Additionally, the analysis paradigm has expanded from simple prognostic model construction and molecular mechanism analysis to drug prediction. This “treatment-prognosis” comprehensive analysis offers a theoretical basis for improving cancer treatment. However, existing studies are based on the “pRRophetic” R package (Li et al., 2022; Zhao et al., 2023). Considering the early release year of the “pRRophetic” R package (Geeleher et al., 2014), it is necessary to perform drug prediction for SKCM based on the new “oncopredict” package (Maeser et al., 2021).

In this study, we performed a comprehensive analysis of both bulk transcriptomic and single-cell sequencing data for SKCM, sourced from the public databases of The Cancer Genome Atlas (TCGA) and The Gene Expression Omnibus (GEO). Initially, we applied dimensionality reduction techniques to the single-cell dataset, annotating cellular subtypes and examining the expression of tumor-related pathways across these subtypes. We then leveraged the bulk transcriptomic data to construct predictive models, which were rigorously validated using designated training and validation sets. Differential expression analysis identified a set of genes (DEGs) from the training dataset. These DEGs were further scrutinized using the Least Absolute Shrinkage and Selection Operator (LASSO) machine learning algorithm, enhanced with tenfold cross-validation, to refine the model development and perform validation tests. In addition, we conducted Gene Ontology (GO) and Kyoto Encyclopedia of Genes and Genomes

(KEGG) enrichment analyses, as well as mutation analysis on these DEGs. Furthermore, we utilized three immune infiltration algorithms to explore immune-related dynamics within two defined risk groups, uncovering potential links between the prognostic model and tumor immunity. Sensitivity analysis was also employed to guide targeted drug selection. Our findings provide significant new insights and a solid theoretical foundation for advancing the prognosis and therapeutic strategies for SKCM.

## 2 Materials and methods

### 2.1 Data acquisition and preprocessing

We acquired bulk transcriptome sequencing data, mutation data, and clinical information for a melanoma cohort of 457 patients from The Cancer Genome Atlas (TCGA, <https://portal.gdc.cancer.gov/>), designated as TCGA-SKCM. Additionally, we downloaded bulk transcriptome sequencing data (GSE65904) for 208 melanoma patients and single-cell sequencing data (GSE72056) from The Gene Expression Omnibus (GEO, <https://www.ncbi.nlm.nih.gov/geo/>). All data utilized in this study are freely available through these public databases, which ensures compliance with ethical standards and eliminates the need for additional ethical approval. Our data acquisition and analysis processes conformed to all relevant guidelines and regulations.

### 2.2 Single-cell sequencing analysis

We analyzed single-cell sequencing data using the “Seurat” package. Our initial steps included stringent quality control and data cleaning to ensure the integrity and accuracy of our analyses. The quality thresholds set were: mitochondrial gene content (percent.mt) less than 10%, a minimum of 1000 RNA counts (nCount\_RNA), and RNA feature numbers (nFeature\_RNA) between 100 and 5000. Following data preprocessing, we utilized Uniform Manifold Approximation and Projection (UMAP) for dimensionality reduction of the single-cell data. Cell subtypes were then annotated using specific markers for each subtype, with expression distributions visualized through dot plots, violin plots, and feature plots. Additionally, the “cellchat” package facilitated the analysis of intercellular communication, visualizing interactions and quantifying proportions of each cell subtype. To assess pathway activity, the “PROGENy” package calculated pathway scores for each tumor-related pathway in individual cells, averaging these scores to determine the overall pathway activity level for each cell subtype. A heatmap was then generated to display and compare pathway activity levels across 14 tumor-related pathways among different cell subtypes, aiming to elucidate variations in pathway engagement.

### 2.3 Construction and validation of a machine learning prognostic model

The analysis is based on a cohort of 457 melanoma patients from TCGA-SKCM dataset. Differential gene expression analysis was

conducted using the “tinyarray” package, with the criteria for selecting DEGs set at  $p < 0.05$  and  $|\log^2(\text{FoldChange})| > 1$ . Subsequently, DEGs underwent univariate COX regression analysis with a significance threshold of  $p < 0.05$  to identify genes influencing prognosis. The identified prognostic genes were subjected to LASSO machine learning algorithm using the “glmnet” and “survival” packages, with ten-fold cross-validation. The LASSO algorithm, along with cross-validation, was employed for further gene selection, and coefficients were calculated to construct the prognostic model. The computation of the risk score for each patient involved multiplying the expression value of each gene by its corresponding coefficient and summing the outcomes. The formula for the risk score is as follows:

$$\text{Risk Score} = \sum_{i=1}^n [\text{Expression value}_{\text{gene}_i} * \text{Coefficient}_{\text{gene}_i}]$$

In the context provided, the term “Expression value” represents the expression level obtained from the sequencing or chip data of the model genes, while “Coefficient” represents the coefficient corresponding to the model genes when the error is minimized during cross-validation calculations. Individual patient risk scores are calculated, and depending on whether the score exceeds or falls below the median value of all patient risk scores, individuals are categorized into either the high-risk group or the low-risk group. To validate the universality of the model, we selected GSE65904 as an external validation cohort. Risk scores were calculated based on the above formula and method, and patients were grouped accordingly. Validation was performed alongside the training cohort. Risk cumulative factor plots were visually represented for both the training and validation cohorts. Survival curves were also plotted to verify the overall survival (OS) differences between high-risk and low-risk patient groups. Following this, the training cohort underwent univariate COX regression analysis for the selected model genes to ascertain their potential as prognostic factors. Forest plots were generated for visualization. Furthermore, age, gender, and risk score were collectively subjected to univariate COX regression analysis to evaluate their potential as prognostic factors and to compare the magnitude of risk associated with each. We further analyzed the differential expression of model genes between the two risk groups. The expression correlation among model genes was also analyzed and presented using a heatmap. Following this, gender, age, risk score, and metastasis status were incorporated to construct a nomogram prognostic model.

## 2.4 Functional enrichment and mutation analysis

Prior to constructing the LASSO machine learning model, we conducted univariate COX regression analysis on DEGs. Subsequently, we performed Gene Ontology (GO) and Kyoto Encyclopedia of Genes and Genomes (KEGG) analyses to observe the enrichment of these genes in specific functional pathways, visualizing the results through bubble plots. The GO and KEGG analyses were executed using the R package

“clusterProfiler” (version 4.0.5), with a significance threshold set at a False Discovery Rate (FDR)  $< 0.05$ .

Utilizing the R package “maftools” (version 2.12.0), we analyzed and visualized the differential mutation profiles of DEGs in two risk groups. The waterfall plot presented the top 6 genes in each group, accompanied by statistics on the proportion of nucleotide transitions and transversions. Moreover, our emphasis was on scrutinizing the mutation sites and types of genes exhibiting the highest mutation frequencies among the two risk groups. Employing the “RCircos” package, we generated a circular chromosome plot to annotate the positions of model genes on the chromosomes.

## 2.5 Immune-related analysis

We employed the Spearman correlation method to analyze the relationship between the risk score and 43 immune checkpoint genes, presenting the results in a bar chart. Furthermore, correlations between model genes and the immune checkpoint genes were visualized using a heatmap. To assess immune cell infiltration in two risk groups, we utilized three algorithms: Microenvironment Cell Populations-counter (MCPcounter), Single-sample Gene Set Enrichment Analysis (ssGSEA), and Estimation of Cell Types in Bulk Expression Data (xCell). These algorithms analyzed transcriptome-wide gene expression data to estimate immune cell infiltration scores. Initially, ssGSEA assigned scores to 23 immune cell types for individual patients, with variations depicted in box plots. We then used Spearman correlation to evaluate the relationships between the risk score, model genes, and immune cell levels, visualizing these relationships through scatter plots and heatmaps. The MCPcounter algorithm identified differences in 10 immune cell types between high-risk and low-risk groups, with results shown in box plots and correlations with model genes and risk score illustrated via scatter plots and heatmaps. Utilizing the xCell package, the xCell algorithm computed infiltration scores for 67 immune cell types, with differences between risk groups depicted in box plots and correlations presented in a heatmap.

## 2.6 Drug sensitivity analysis

We accessed drug-related data from the Genomics of Drug Sensitivity in Cancer (GDSC, <https://www.cancerrxgene.org/>) database using the “oncoPredict” R package. Initial analyses explored differences in drug sensitivity between the two risk groups, visualized through a volcano plot. Spearman correlation was then applied to ascertain the relationships between model genes and 61 drugs, with the findings displayed in a heatmap. Finally, we assessed the variations in drug sensitivity between the risk groups, presenting these findings through box plots.

## 2.7 Cell culture and transfection

In this study, the malignant melanoma cell line of human(A375) was procured from the Cell Bank of the

Chinese Academy of Sciences. We cultured the cell line in high-glucose Dulbecco's Modified Eagle Medium (DMEM, Sigma, Darmstadt, Germany) supplemented with 10% Fetal Bovine Serum (FBS Premium, BI, Israel). Cell culture flasks were maintained in a humidified incubator with 5% CO<sub>2</sub> at 37°C to promote exponential growth of the cells.

For transfection experiments with the A375 cell line, two primer sequences and one siRNA sequence targeting GRM6 were custom-designed and manufactured by GIMA Corporation, China. Initially, A375 cells were dissociated from culture flasks and resuspended in complete growth medium. Cells were evenly seeded onto 6-well plates at a density of  $1 \times 10^4$  cells per well, with each well supplemented to a final volume of 2 mL with complete medium. Upon cell adherence, siRNA and the transfection reagent PolyFast (catalog number HY-K1014, MCE, United States) were pre-mixed according to the instructions of manufacturer and incubated at 23°C for 15 min. Then, the mixture was then evenly distributed into the respective wells using a pipette. We replaced culture medium after 6 h of transfection, and subsequent experiments were performed 48 h post-transfection. Primer sequences: GRM6: Forward: 5'- ACTGATCTGCAGTGGCTCAT - 3', Reverse: 5'- GCCCAGCTTTGTGATCTTGT - 3';  $\beta$ -actin: Forward: 5'- CCTGGCACCCAGCACAAT - 3', Reverse: 5'- GGGCCGGAC TCGTCATAC- 3'. siRNA: siGRM6: Sense: 5'- ACUGUUUAA GAUCAGUAUA - 3', Antisense: 5' -CAAGTATATCGCCTT CACAA - 3'; siNC: Sense: 5'- UUCUCCGAACGUGUCACG UTT- 3', Antisense: 5' -ACGUGACUCGUUCGGAGAATT - 3'.

## 2.8 Total RNA extraction and RT-qPCR

In this study, the RT-qPCR technology was employed to assess the knockdown efficiency of siGRM6. Cells were digested using trypsin (HyClone, United States), followed by three washes with PBS and centrifugation at 4°C to remove the supernatant. Subsequently, 700  $\mu$ L of Trizol (Takara, Japan) was added to operate lysing procedure on cells according to the manufacturer's instructions. After incubating on ice for 5 min, 200  $\mu$ L of chloroform (SINOPHARM, China), 500  $\mu$ L of isopropanol (SINOPHARM, China), and 1 mL of ethanol (SINOPHARM, China) were added. Before new chemicals were added, full mixing was guaranteed, followed by centrifugation at 4°C and incubation on ice for 15 min. After discarding all organic solvents and air-drying for 20 min, RNA precipitate was obtained.

Then, we added 20  $\mu$ L of DEPC-treated water to dissolve the precipitate, and we measuring concentration through a Nanodrop 2000 instrument (Thermo, United States). Based on the manufacturer's instructions, we reverse-transcribed RNA into cDNA using the PrimeScript RT kit (TaKaRa, Japan). Subsequently, we mixed cDNA samples with SYBR GreenER Supermix kit (TaKaRa, Japan). We operated real-time fluorescence quantitative PCR analysis at 7500 Real-Time PCR System (Thermo Fisher Scientific, United States). The parameters of PCR were set according to the SYBR GreenER Supermix kit instructions. Based on the Ct values, the relative expression level on GRM6 was calculated through the method of  $2^{-\Delta\Delta CT}$  normalized to  $\beta$ -actin.

## 2.9 CCK8 assay

After transfection for 48 h, GMR6-NC and GRM6-si cell lines were transferred to a 96-well plate (6000 cells/well) and returned to the incubator for attachment. Three replicate wells were set up for each group. Following the manufacturer's instructions, CCK8 reagent (KeyGEN, China) was mixed with complete culture medium to ensure a total volume of 200  $\mu$ L per well, which was swiftly added to the 96-well plate using a pipette. The plate was completely wrapped in aluminum foil to avoid light exposure, and the absorbance at 450 nm for each well was measured on the instrument after 2 h. This process was repeated at 24, 48, 72, and 96-h time points.

## 2.10 EdU staining for DNA replication

"GMR6-NC" and "GRM6-si" cells were seeded at a density of  $5 \times 10^4$  cells/mL in a 48-well plate and incubated at 37°C for 24 h. Then, 200  $\mu$ L of EdU culture medium was added to each well, and cells were incubated for 2 h before collection. The 2 cell groups were observed under a fluorescence microscope, and images were taken to record DAPI staining, EdU staining, and merged staining.

## 2.11 Transwell assay

During the study, a layer of matrix gel was coated on the inner surface of the chamber (Thermo, United States) diluted at a ratio of 1:9, with 30  $\mu$ L added to each chamber. Next, 600  $\mu$ L of complete culture medium was added to each well of a 24-well plate. After 48 h of transfection, cells were digested and suspended in culture medium without FBS. To ensure the accuracy of the experiment, cells were diluted to a concentration of 30,000 cells per well, with 200  $\mu$ L of liquid added to each chamber. The chambers were then incubated in the incubator for 24 h. During this period, the liquid in the chambers was removed, and a moist cotton swab was used to wipe off the non-invading cells.

To further analyze the experimental results, the chambers were immersed in polyformaldehyde for 20 min. Subsequently, they were washed three times with PBS and stained with 0.1% crystal violet staining solution for 20 min. After washing again with PBS, the chambers were dried, and images were captured under a microscope for further analysis and discussion.

## 2.12 Wound healing assay

In cell culture experiments, transfected cells were first removed from the culture medium after 48 h, followed by three washes with PBS to clean residual substances. Next, using a 200  $\mu$ L pipette tip assisted by a ruler, a vertical line was slowly and evenly scratched in each well. To avoid cross-contamination between different wells, the pipette tip was changed with each well. Subsequently, basic culture medium without FBS was added to each well, and the area of the scratch wound at time 0 was observed and photographed under a microscope. The plate was then placed in the cell culture incubator for cultivation, and photographs were taken again after 48 h to



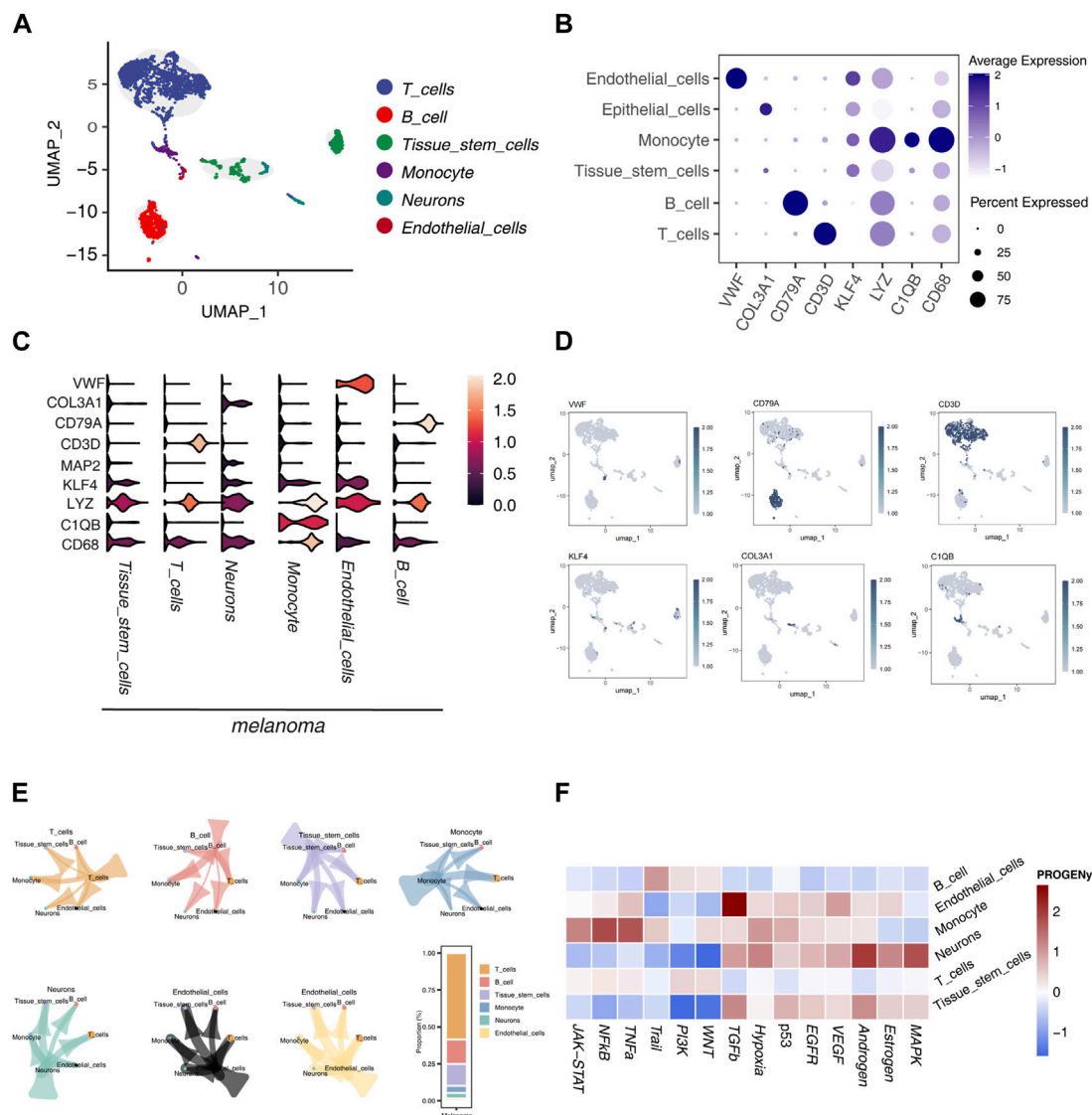


FIGURE 1

Single-Cell Sequencing Data Analysis (A) UMAP dimensionality reduction and annotation of single-cell sequencing data GSE72056, categorizing cell subgroups into 6 classes. (B) Dot plot illustrating the differential expression of marker genes in different subgroups. (C) Violin plot displaying the differential expression of marker genes in different subgroups. (D) Coloring and marking marker gene expression distribution in UMAP visualization. (E) Analysis of communication relationships between cell subgroups using the "cellchat" package, visualized. (F) Heatmap displaying the score differences of each tumor-related pathway calculated by the "PROGENy" package in each cell.

record the area of the healed wound. Finally, the percentage of scratch closure was calculated to evaluate the growth and repair ability of the cells.

## 2.13 Statistical analysis

All statistical analyses were conducted using R software (version 4.1.3). COX regression analysis was performed with the "survival" and "survminer" packages. Differential expression analysis utilized the "limma" package, and visualization tasks were predominantly carried out using "ggplot2". Statistical significance was established at a threshold of  $p < 0.05$ , with significance levels marked as  $*p < 0.05$ ,  $**p < 0.01$ ,  $***p < 0.001$ , and  $****p < 0.0001$ .

## 3 Results

### 3.1 Single-cell sequencing analysis

UMAP dimensionality reduction was applied to single-cell sequencing data (GSE72056), resulting in the classification of cells into six distinct subtypes: T cells, B cells, tissue stem cells, monocytes, neurons, and endothelial cells (Figure 1A). Among these, endothelial cells exhibited the highest expression of von Willebrand factor (VWF), with significant levels of KLF4 and LYZ also noted. In monocytes, LYZ, C1QB, and CD68 demonstrated elevated expression compared to other subtypes and markers. CD79A was the most expressed gene in B cells, whereas CD3D was predominant in T cells (Figure 1B).

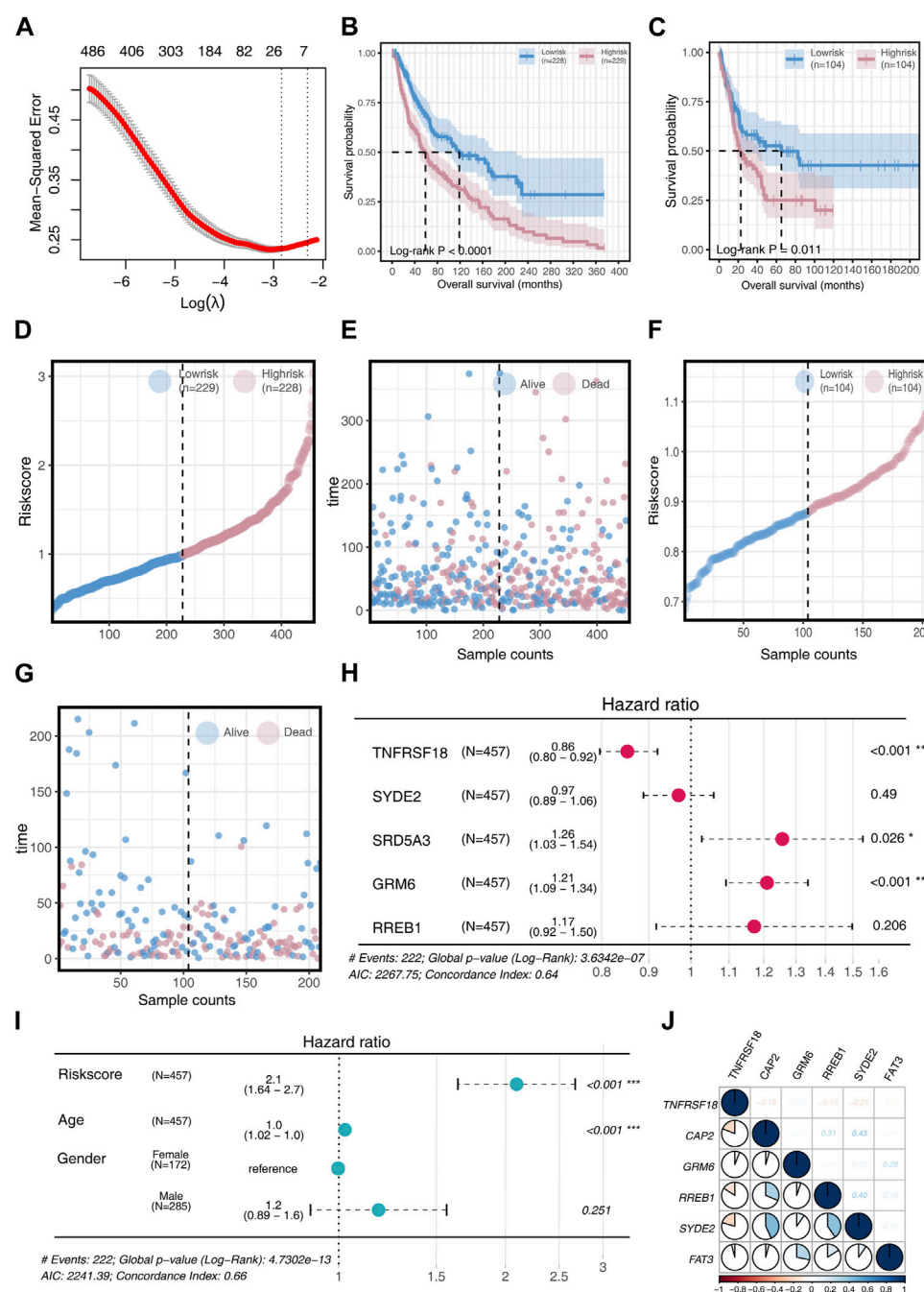


FIGURE 2

Model Construction and Validation (A) Acquisition of DEGs for univariate COX regression analysis and implementation of LASSO machine learning to construct a prognostic model. (B) Survival differences in two risk groups in the training set. (C) Survival differences in two risk groups in the validation set. (D) Risk score changes in two risk groups in the training set. (E) Survival time comparison in two risk groups in the training set. (F) Risk score changes in two risk groups in the validation set. (G) Survival time comparison in two risk groups in the validation set. (H) Univariate COX regression analysis to determine if model genes can serve as prognostic factors, visualized through a forest plot. (I) Univariate COX regression analysis to determine if Risk score, Age, and Gender can serve as prognostic factors, visualized through a forest plot. (J) Analysis of inter-gene correlations in the model.

Violin plots further illustrated these gene expression variations across subtypes.

Notably, CD68 not only showed the highest expression in monocytes but also exceeded the expression of other markers in different cell subtypes. Similarly, LYZ exhibited a widespread expression pattern. KLF4 was more prominently expressed in neurons and monocytes. The neuron subtype showed higher

expression of MAP2 and COL3A1 (Figure 1C). Each marker gene's expression was color-coded in the UMAP visualization to enhance the clarity of their distribution across subtypes (Figure 1D).

We also explored the communication relationships between cell subtypes, revealing extensive signaling interactions. T cells were the most communicative, particularly with other immune cells, followed by B cells (Figure 1E). An analysis of 14 tumor-related pathways

indicated differential activation across cell subtypes. B cells showed higher activity levels in the WNT, PI3K, and Trail pathways, although other pathways exhibited lower activity, suggesting a restricted role in tumor-related functions. Endothelial cells displayed the highest activity in the TGF- $\beta$  pathway, with notable activity in the Estrogen and VEGF pathways, indicating their dynamic involvement in tumorigenesis. Monocytes had elevated activity in the TNF- $\alpha$ , NF- $\kappa$ B, and JAK-STAT pathways, reflecting significant pathway activation. Neurons showed elevated activity in the MAPK, Estrogen, and Androgen pathways but lower activity in the WNT and PI3K pathways, highlighting a selective pathway engagement. T cells exhibited low activity across all pathways examined. Tissue stem cells showed notable activity in the Androgen and TGF- $\beta$  pathways, with reduced activity in the WNT and PI3K pathways, suggesting a selective activation pattern (Figure 1F).

## 3.2 Constructing and validating of a machine learning prognostic model

In our study, the SKCM patient cohort served as the training set, while the GSE65904 patient cohort was used for validation. Initial analysis identified differentially expressed genes (DEGs), and a univariate COX regression analysis was conducted. These DEGs were further refined using a LASSO machine learning algorithm, resulting in a prognostic model comprising six key genes: TNFRSF18, CAP2, GRM6, RREB1, SYDE2, and FAT3, as depicted in Figure 2A. The risk score was computed for each patient using the formula:

$$\text{Risk score} = \text{TNFRSF18}^* - 0.585 + \text{CAP2} * 0.328 + \text{GRM6} * 0.305 \\ + \text{RREB1} * 1.986 + \text{SYDE2}^* - 0.223 + \text{FAT3}^* - 0.006$$

Patients were categorized into high-risk and low-risk groups based on the median risk score. The high-risk group demonstrated significantly poorer overall survival (OS) than the low-risk group ( $p < 0.05$ , Figures 2B,C). A cumulative risk factor plot showed an increasing trend of deceased patients and a decline in extended OS with rising risk scores (Figures 2D–G).

Further univariate COX regression analysis highlighted TNFRSF18, SRD5A3, and GRM6 as significant prognostic factors. TNFRSF18 was associated with a protective effect (HR = 0.86), while SRD5A3 (HR = 1.26) and GRM6 (HR = 1.21) were linked to poorer prognosis (Figure 2H). The risk score and age were both significant prognostic factors ( $p < 0.001$ ), with the risk score providing more substantial prognostic information (HR = 2.1) compared to age (HR = 1.0) (Figure 2I).

Correlation analysis among model genes revealed that TNFRSF18 mostly exhibited negative correlations with other genes. Conversely, positive correlations were observed among the remaining model genes, with CAP2 showing strong positive associations with RREB1 ( $R = 0.31$ ) and SYED2 ( $R = 0.31$ ), GRM6 with FAT3 ( $R = 0.28$ ), and RREB1 with SYED2 ( $R = 0.40$ ) (Figure 2J).

Gene expression analyses between the two risk groups showed higher expression levels of all model genes, except for TNFRSF18, in

the high-risk group ( $p < 0.01$ , Figure 3A). Chromosome circle plots highlighted the genomic locations of the model genes (Figure 3B).

A nomogram integrating risk score, age, and type was constructed to enhance the prognostic model's accuracy (Figure 3C). Spearman correlation analysis identified mostly negative correlations between the risk score and most immune checkpoint genes, except for positive correlations with EDRNB, VTCN1, and VEGFB (Figure 3D). Most model genes also displayed significant negative correlations with immune checkpoint genes, with the notable exception of TNFRSF18, which showed significant positive correlations (Figure 3E).

## 3.3 Enrichment analysis and mutation analysis

Prior to constructing the LASSO machine learning model, we conducted univariate COX regression analysis of DEGs (Differentially Expressed Genes). Following this, GO and KEGG analyses were conducted on the DEGs. The GO analysis revealed that DEGs are predominantly enriched in the number of pathways related to Cell Component (CC). In general, DEGs exhibit predominant enrichment in biological pathways and processes, encompassing energy metabolism, substance metabolism, cell signal transduction, cell structure and dynamics, and protein processing (Figure 4A).

The KEGG analysis results indicated that DEGs are primarily enriched in biological processes such as cell signal transduction, cell metabolism, cell growth and death, and endocytosis (Figure 4B).

Additionally, we conducted mutation analysis on the training dataset. The results showed that FAT3, GRM6, CAP2, RREB1, SYDE2, and TNFRSF18 exhibit higher mutation frequencies in both risk groups. FAT3 has the highest mutation rate in both risk groups, followed by GRM6. Other gene mutation rates are significantly lower compared to these two. In the analysis of mutation types, Missense Mutation appeared most frequently, followed by Multi Hit. FAT3 exhibited various mutation forms, with Missense Mutation and Multi Hit being the most prevalent (Figures 4C,D).

Regarding the analysis of mutation frequencies, the transition (Ti) frequency was higher than the transversion (Tv) frequency in both risk groups. Among them, the nucleotide substitution rate of C>T was the highest (Figures 4E,F).

Moreover, mutation sites and types of GRM6 were analyzed in the two risk groups. Within the high-risk group, GRM6 demonstrated an elevated mutation rate, a wider spectrum of mutation locations, and a greater diversity of mutation types (Figures 4G,H).

## 3.4 Immune-related analysis

In this study, we employed the ssGSEA algorithm to perform an immune-related analysis, evaluating the infiltration of immune cells in two distinct risk groups. For each patient in the two risk groups, we calculated scores for 23 immune cells. Statistically significant distinctions were noted in the scores of the 23 immune cells between the two risk groups ( $p < 0.05$ ). Remarkably, the scores of all immune

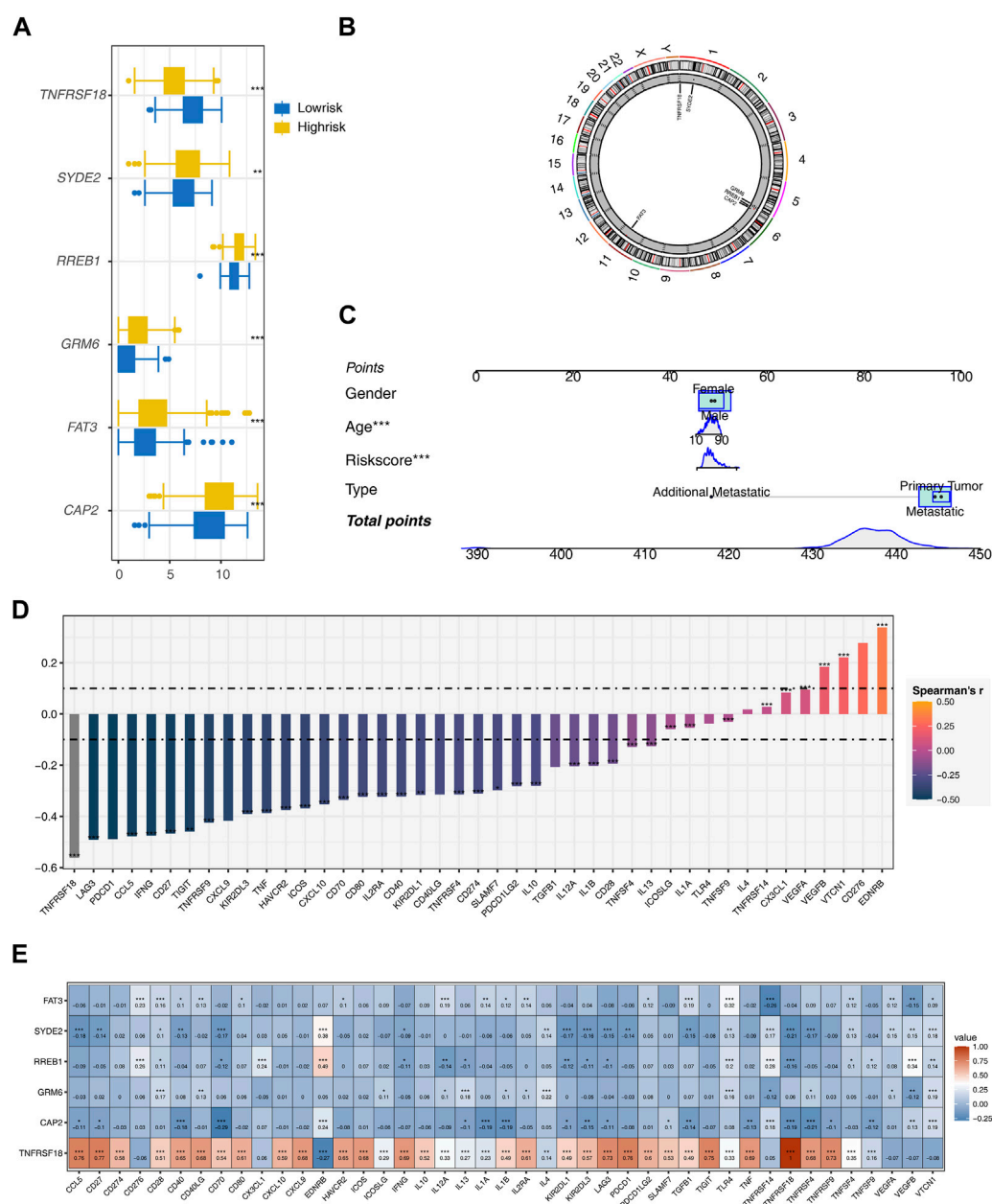


FIGURE 3

Further Analysis of the Model (A) Expression differences of model genes between two risk groups. (B) Chromosome circular plot displaying the genomic locations of model genes. (C) Construction of a nomogram prognostic model incorporating Risk score, Age, Gender, and Type. (D) Calculation of the correlation between model genes and 43 immune checkpoint genes using Spearman's correlation method. (E) Heatmap displaying the expression correlations between model genes and immune checkpoint genes.

cells in the low-risk group surpassed those in the high-risk group, signifying a heightened immune infiltration activity in the low-risk group (Figure 5A).

Subsequent analysis employing Spearman correlation unveiled noteworthy negative associations between the risk score and Macrophage, Activated CD8 T cell, Monocyte, CD56dim natural killer cell, Gamma delta cell, and Immature dendritic cell ( $p < 0.001$ ,  $R < -0.2$ , Figures 5B–G). TNFRSF18 demonstrated a marked positive correlation with Monocyte ( $p < 0.001$ ,  $R = 0.64$ ), whereas CAP2, SYDE2, and FAT3 displayed substantial negative correlations with Monocyte ( $p < 0.001$ ,  $R < -0.1$ , Figures 5H–K).

Heatmap results further demonstrated a significant negative correlation between the risk score and all immune cells ( $p < 0.05$ ), with the highest negative correlation observed between the risk score and Activated CD8 T cell ( $R = -0.55$ ), and the lowest negative correlation with Type 2 T helper cell ( $R = -0.1$ , Figure 5L).

Employing the MCPcounter algorithm, we computed variations in scores for 10 immune cells between the high-risk and low-risk groups. The findings suggested elevated infiltration levels of the majority of immune cells in the low-risk group, with the exception of Endothelial cells and Fibroblasts (Figure 6A). Spearman correlation analysis suggested positive correlations between most model genes,



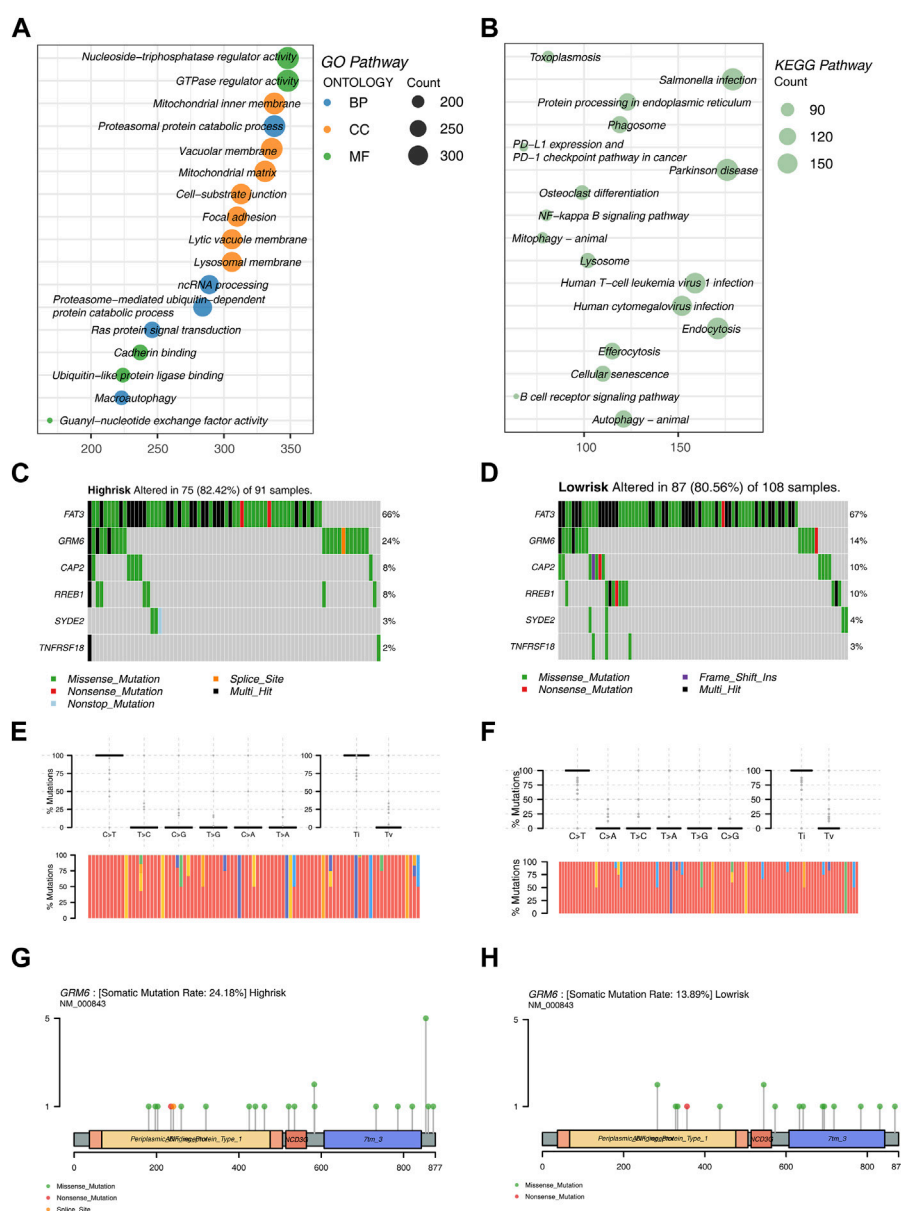


FIGURE 4

Enrichment Analysis and Mutation Analysis (A) Bubble plot illustrating enriched functional pathways in GO analysis of DEGs. (B) Bubble plot illustrating enriched functional pathways in KEGG analysis of DEGs. (C) Mutation analysis in the high-risk group of the training set. (D) Mutation analysis in the low-risk group of the training set. (E) Top 6 genes and the proportion of nucleotide transitions and transversions in the high-risk group. (F) Top 6 genes and the proportion of nucleotide transitions and transversions in the low-risk group. (G) Mutation sites and types of GRM6 in the high-risk group. (H) Mutation sites and types of GRM6 in the low-risk group.

especially TNFRSF18, and immune cells ( $p < 0.05$ ,  $R > 0.1$ , Figures 6B–H). The risk score exhibited a noteworthy positive correlation with Endothelial cells ( $p < 0.001$ ,  $R = 0.17$ ) and marked negative correlations with Cytotoxic lymphocytes, Myeloid dendritic cells, and B lineage ( $p < 0.001$ ,  $R < -0.3$ , Figures 6I–L). The heatmap indicated that, except for TNFRSF18, most model genes were negatively correlated with immune cells, while FAT3 exhibited a highly positive correlation with Endothelial cells and Fibroblasts ( $p < 0.001$ ,  $R > 0.5$ , Figure 6M). The risk score demonstrated a significant positive correlation exclusively with Endothelial cells and exhibited negative correlations with the majority of other cells (Figure 6N). The high-risk group shows significantly higher levels

of infiltration for several immune cell types compared to the low-risk group (Figure 7A). Additionally, the risk score is negatively correlated with specific immune cells, such as Activated CD8 T cells (Figure 7B).

### 3.5 Drug sensitivity analysis

We initially performed an analysis of divergent drug sensitivity between the two risk groups and illustrated the outcomes through a volcano plot (Figure 8A). TNFRSF18, GRM6, and FAT3 exhibited a negative correlation with most drugs, while CAP2, RREB1, and

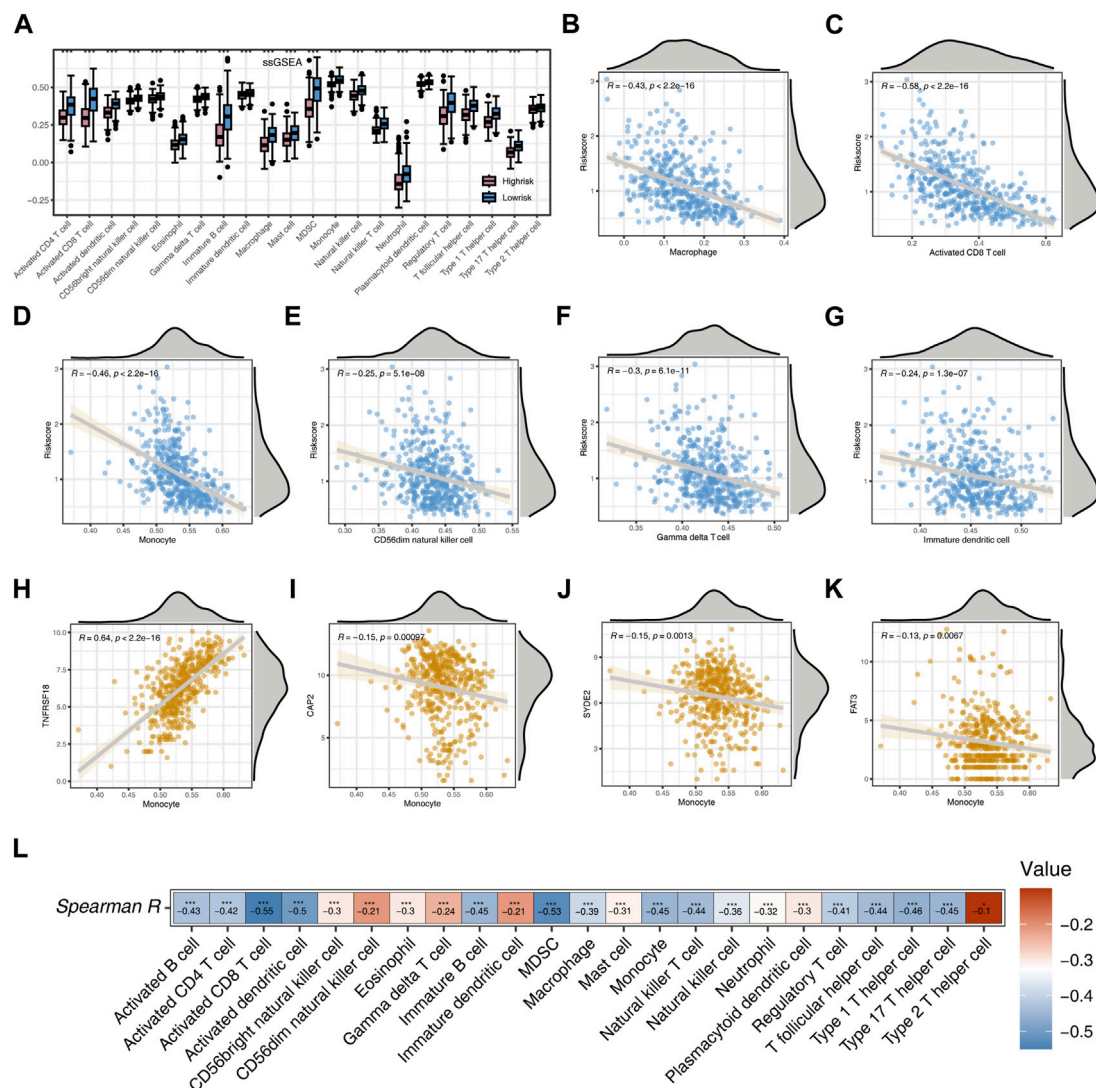


FIGURE 5

Analysis Based on ssGSEA Immune Algorithm (A) Immunocell scoring using the ssGSEA algorithm for two risk groups. (B) Correlation between Risk score and Macrophage. (C) Correlation between Risk score and Activated CD8 T cell. (D) Correlation between Risk score and Monocyte. (E) Correlation between Risk score and CD56dim natural killer cell. (F) Correlation between Risk score and Gamma delta cell. (G) Correlation between Risk score and Immature dendritic cell. (H) Correlation between TNFRSF18 and Monocyte. (I) Correlation between CAP2 and Monocyte. (J) Correlation between SYDE2 and Monocyte. (K) Correlation between FAT3 and Monocyte. (L) Heatmap of the correlation between risk score and immune cells. Significance levels are denoted as follows: \* $p < 0.05$ , \*\* $p < 0.01$ , and \*\*\* $p < 0.001$ .

SYDE2 showed a positive correlation with most drugs (Figure 8B). RO-3306\_1052 and BI-25361086 demonstrated higher drug scores in the low-risk group (Figures 8C,D), whereas AZ960\_1250, Entospletinib\_1630, Navitoclax1011, XAV939\_1268, WEHI-5391997, and 5-Fluorouracil1073 exhibited higher drug scores in the high-risk group (Figures 8E–J). Personalized drug selection for treatment based on individual patient groups may result in improved therapeutic outcomes.

### 3.6 Impact of GRM6 knockdown on A375 melanoma cell functions

Through RT-qPCR experiments, we thoroughly investigated the expression of the “GRM6-NC” control group and the “GRM6-si”

knockdown group in the A375 cell line. It was accurately determined that GRM6-si had a good knockdown effect (Figure 9A). CCK8 assays confirmed that the proliferation ability of the A375 cell line significantly decreased when the GRM6 gene was knocked down (Figure 9B). Transwell assays confirmed that after knocking down the GRM6 gene, the number of invasive cells in the si-GRM6 group decreased, which means the invasion ability correspondingly weakened (Figure 9C). We also found that the wound healing assay showed that the migration ability of the si-GRM6 group was significantly reduced (Figure 9D). EdU experiments also confirmed a significant decrease in the proliferation ability of the A375 cell line when the GRM6 gene was knocked down (Figure 9E). Overall, our research results revealed the role of the GRM6 gene in promoting cancer in human melanoma, achieved by promoting the proliferation, invasion, and migration ability of melanoma cells.



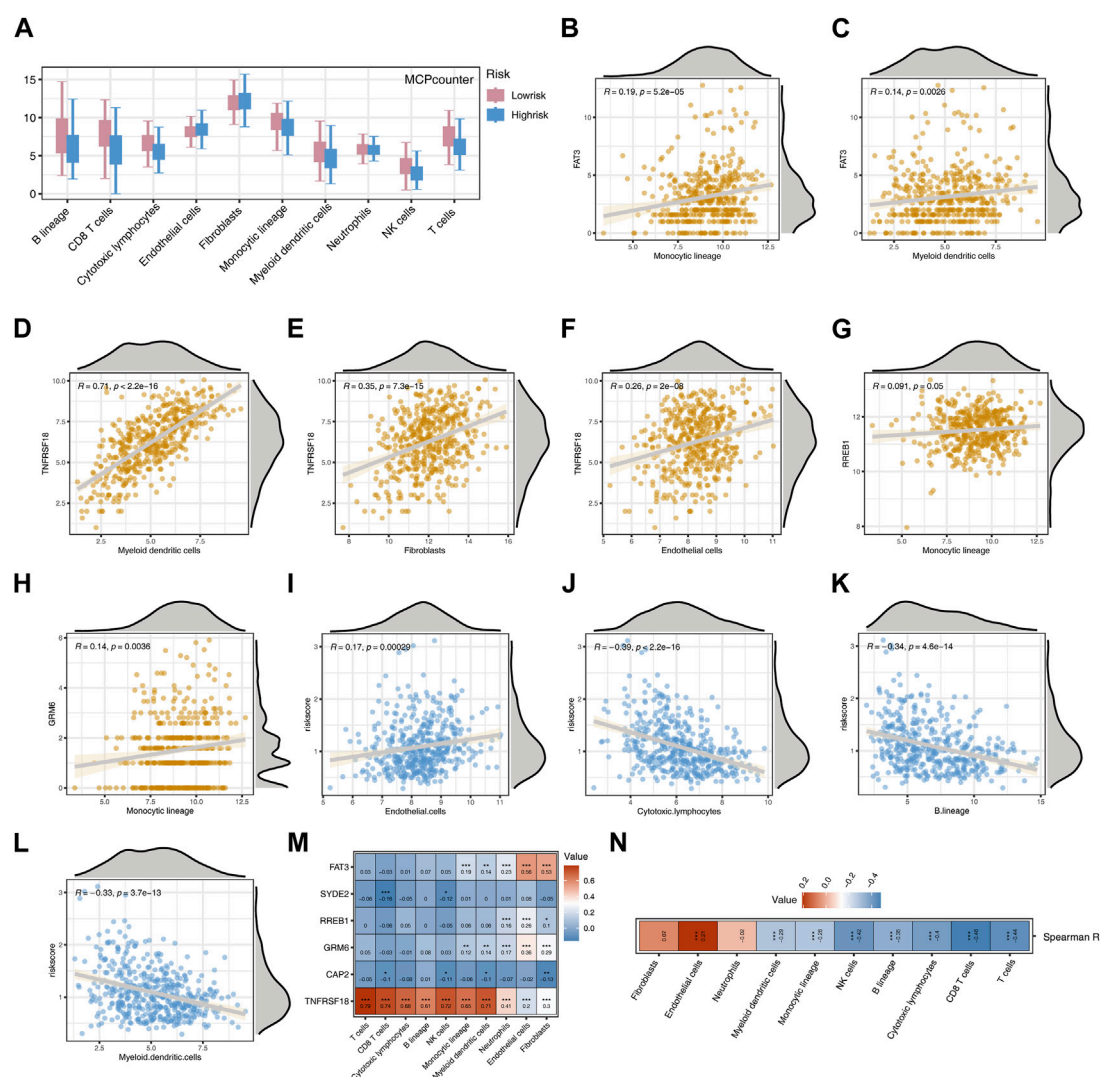


**FIGURE 6** Analysis Based on MCPcounter Immune Algorithm (A) Boxplot showing differences in the scores of 10 immune cell types between two risk groups. (B) Correlation between FAT3 and Monocyte lineage. (C) Correlation between FAT3 and Myeloid dendritic cells. (D) Correlation between TNFRSF18 and Myeloid dendritic cells. (E) Correlation between TNFRSF18 and Fibroblasts. (F) Correlation between TNFRSF18 and Endothelial cells. (G) Correlation between RREB1 and Monocyte lineage. (H) Correlation between ERM6 and Monocyte lineage. (I) Correlation between Endothelial cells and Risk score. (J) Correlation between Cytotoxic lymphocytes and Risk score. (K) Correlation between B lineage and Risk score. (L) Correlation between Myeloid dendritic cells and Risk score. (M) Heatmap representing the correlation between model genes and immune cells. (N) Heatmap representing the correlation between Risk score and immune cells.

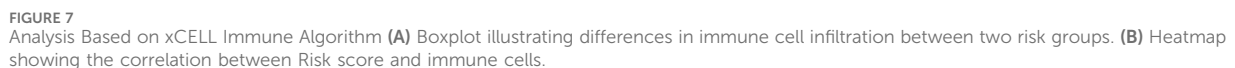
## 4 Discussion

Cutaneous melanoma (SKCM) is a type of skin cancer that initially impacts patient quality of life minimally. However, its non-invasive discrimination during early diagnosis is challenging, often resulting in missed opportunities for optimal treatment when patients first seek medical attention. Malignant SKCM is highly invasive, with about 20% of patients experiencing metastasis at the time of initial diagnosis. Advanced-stage malignant SKCM often responds poorly to radiation and chemotherapy, resulting in severe side effects and a grim prognosis. The lack of specific treatments for SKCM, other than early surgical excision, highlights the critical need for research into the mechanistic roles of SKCM-related genes, the construction of prognostic models, and the prediction of drug

responses to improve early diagnosis, precise treatment, and patient outcomes.

To investigate the genetic landscape of SKCM, we accessed bulk transcriptome sequencing data from the public databases TCGA and GEO, partitioning these into training and validation sets for robust model construction and validation. Additionally, we collected mutation data and clinical information from TCGA and acquired single-cell sequencing data for SKCM from GEO. These datasets hold significant potential for enhancing patient diagnosis, treatment, and prognosis assessment.

Using the single-cell dataset GSE72056, we applied UMAP dimensionality reduction and annotated cells into six subtypes using specific marker genes for each subgroup. Communication analysis among cell subtypes highlighted active immune cell



Utilizing multiple independent datasets from diverse platforms for model construction and validation enhances the

model's generalization capability, leading to more compelling conclusions. This strategy is currently widely employed in the analysis of various diseases (Li J. et al., 2022; Guan et al., 2022). We conducted differential gene expression analysis on patient data from the training set to identify DEGs. Subsequently, we performed univariate COX regression analysis on DEGs to filter out genes that significantly impact prognosis. The selected genes underwent LASSO machine learning algorithm, applying L1 regularization to enhance the model's simplicity and accuracy by imposing a penalty on the absolute sum of regression coefficients. Ultimately, a prognostic model comprising six genes (TNFRSF18, CAP2, GRM6, RREB1, SYDE2, FAT3) was constructed. TNFRSF18, also known as GITR, is a co-stimulatory T-cell receptor and a member of the TNF receptor superfamily (Nocentini and Riccardi, 2009). Some cancer patients have shown therapeutic efficacy in checkpoint inhibition of TNFRSF18, particularly in preclinical models. However, TNFRSF18 involvement is ineffective in controlling late-stage, immunogenically poor tumors such as B16 SKCM

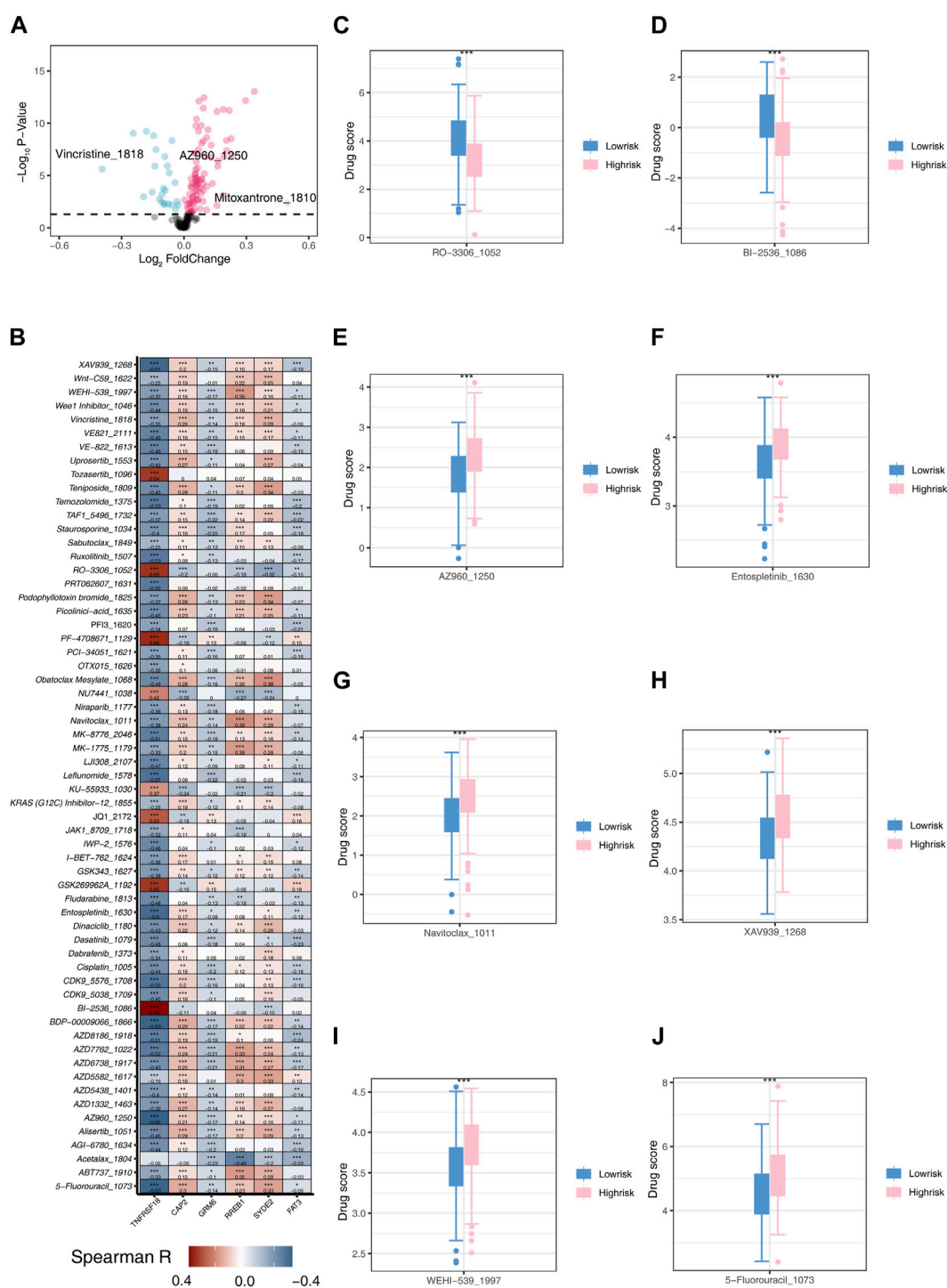


FIGURE 8

Drug Sensitivity Analysis (A) Volcano plot illustrating differences in drug sensitivity between two risk groups. (B) Heatmap depicting the correlation between model genes and 61 different drugs. (C) Boxplot showing the sensitivity difference of RO-3306\_1052 between two risk groups. (D) Boxplot showing the sensitivity difference of BI-2536\_1086 between two risk groups. (E) Boxplot showing the sensitivity difference of AZ960\_1250 between two risk groups. (F) Boxplot showing the sensitivity difference of Entospletinib\_1630 between two risk groups. (G) Boxplot showing the sensitivity difference of Navitoclax\_1011 between two risk groups. (H) Boxplot showing the sensitivity difference of XAV939\_1268 between two risk groups. (I) Boxplot showing the sensitivity difference of WEHI-539\_1997 between two risk groups. (J) Boxplot showing the sensitivity difference of 5-Fluorouracil\_1073 between two risk groups.

(Hirschhorn et al., 2021). CAP2, a muscle actin-binding protein, regulates cell processes by controlling the dynamics of the cell cytoskeleton (Pelucchi et al., 2023). Its expression in cancerous

tissues significantly surpasses that in non-tumor tissues, rendering it a plausible diagnostic and prognostic marker for individuals with cancer (Li et al., 2020). GRM6, also known as

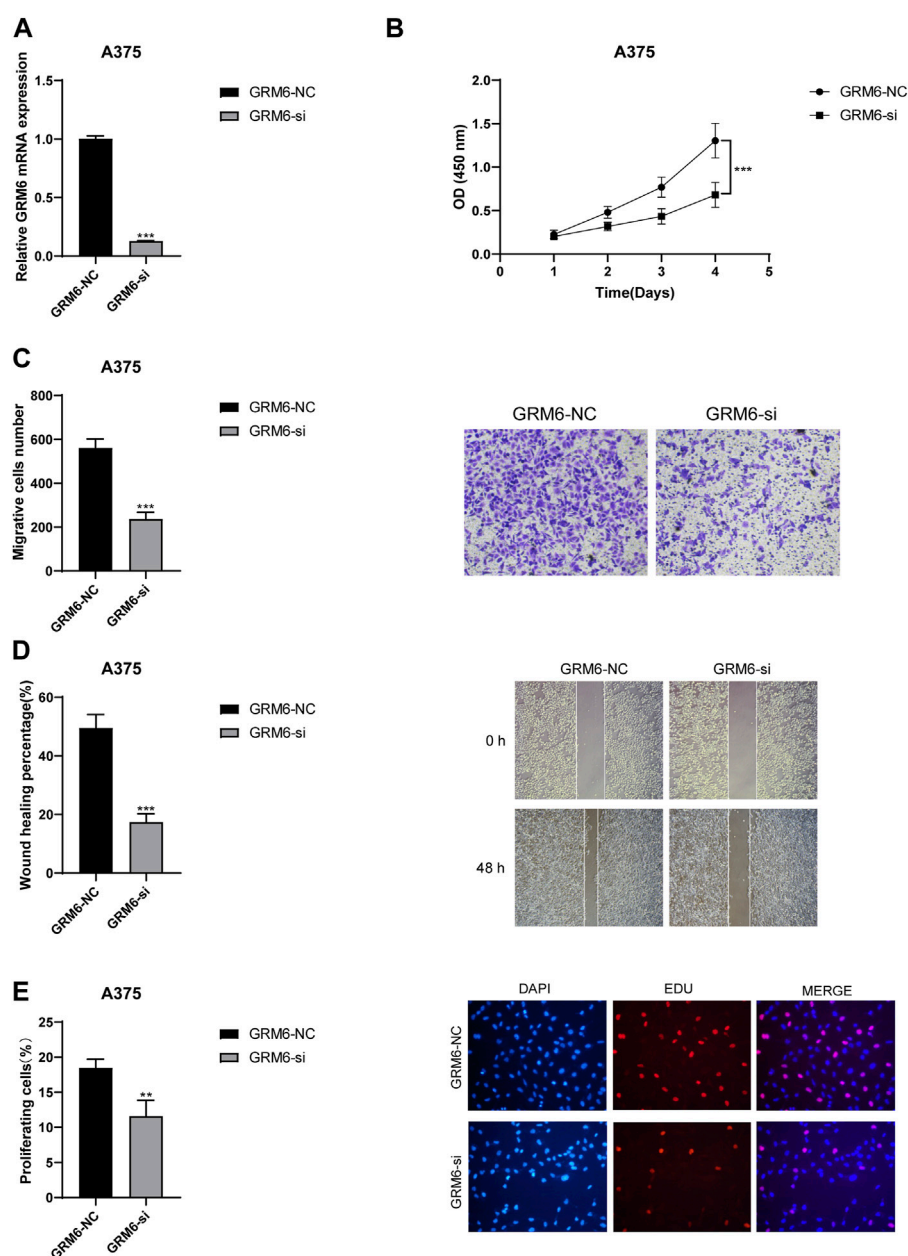


FIGURE 9

Functional consequences of GRM6 knockdown in A375 melanoma cells. **(A)** RT-qPCR results showing effective knockdown of GRM6 expression in the "GRM6-si" group compared to the control "GRM6-NC" group. **(B)** CCK8 assay results indicating a significant reduction in cell proliferation ability following GRM6 gene silencing. **(C)** Transwell assay results demonstrating decreased invasion ability in A375 cells after GRM6 knockdown. **(D)** Wound healing assay data revealing reduced migration ability of cells in the si-GRM6 group. **(E)** EdU assay results confirming a significant decrease in proliferation rates in GRM6-silenced A375 cells.

mGluR6, is a major excitatory neurotransmitter in the central nervous system. It activates ionotropic and metabotropic glutamate receptors, mediating glutamate synaptic transmission between photoreceptors and ON bipolar cells (Varin et al., 2021). SKCM may lead to SKCM-related retinal lesions, as evidenced in GRM6 (Dhingra et al., 2011). RREB1, a transcription factor that specifically binds to RAS response elements (RRE) on gene promoters, is associated with scrotal SKCM (Thiagalingam et al., 1996; Fujimoto-Nishiyama et al., 1997; Zhang et al., 1999; Date et al., 2004; Mukhopadhyay et al.,

2007). SYDE2, an activator of Rho GTPase, has unclear functional implications in tumorigenesis. Studies suggest a potential tumor-suppressive role of SYDE2 in advanced clear cell renal cell carcinoma (Cui et al., 2022). FAT3, a member of the cadherin-related family, has been previously correlated with adverse prognosis in cancer patients (Jiang et al., 2023).

In the training and validation sets, we categorized patients into high-risk and low-risk groups. The survival prognosis of patients in the high-risk group was significantly lower than that in the low-risk group, indicating substantial potential for our



model to predict patient outcomes. Among the six genes in the prognosis model, we identified TNFRSF18 as having a protective effect on prognosis. Expression differences were observed for all model genes between the two risk groups, with TNFRSF18 showing higher expression in the low-risk group. In the examination of the correlation with immune checkpoint genes, TNFRSF18 exhibited a significant positive correlation with most immune checkpoint genes. This suggests that TNFRSF18 may serve as an immunotherapeutic target for SKCM, and therapeutic approaches aimed at activating TNFRSF18 expression while inhibiting negative immune regulatory activity may enhance the efficacy of SKCM immunotherapy. Further experimental validation is needed to confirm our hypotheses.

To explore the functional implications of differentially expressed genes (DEGs), we conducted Gene Ontology (GO) and Kyoto Encyclopedia of Genes and Genomes (KEGG) analyses. These DEGs were predominantly enriched in biological processes such as cell signaling, metabolism, growth and death, and endocytosis. We hypothesize that the high activity across these biological pathways contributes to SKCM's malignancy, highlighting potential avenues for therapeutic intervention.

A mutational analysis performed on the training set identified FAT3 as having the highest mutation rate, closely followed by GRM6. Notably, GRM6 mutations were particularly prevalent within the high-risk group, characterized by a variety of mutation types and locations. These findings underline the need for further comprehensive studies to understand the impact of GRM6 mutations and aberrant expression on melanoma progression.

Immunological correlation analysis, utilizing three distinct immune cell infiltration algorithms, assessed the differences in immune cell infiltration between the two risk groups. The analysis revealed that the low-risk group displayed more active immune infiltration than the high-risk group. Scoring differences between these groups showed that most model genes, particularly TNFRSF18, positively correlated with immune cell activity. Conversely, the risk score exhibited a negative correlation with most immune cells, reinforcing our previous findings that high-risk SKCM correlates with poorer prognosis. This analysis also emphasizes the critical role of TNFRSF18 in the context of SKCM treatment. Additionally, drug sensitivity analysis conducted on the two risk groups highlighted significant differences in their response to various drugs. Based on these findings, we advocate for personalized drug selection strategies tailored to distinct patient subgroups to optimize therapeutic outcomes.

## 5 Conclusion

In conclusion, this study successfully delineated the complex molecular landscape of SKCM, revealing significant findings through the analysis of DEGs, mutation profiles, and immunological correlations. Our comprehensive examination of transcriptomic and mutational data enabled the identification of key genes that are enriched in crucial biological processes and exhibit high mutation rates, such as

GRM6 and FAT3, suggesting their pivotal roles in SKCM pathogenesis. The construction and validation of a prognostic model highlighted the differential risk and survival outcomes between patient subgroups, underscoring the importance of early and accurate risk stratification in clinical practice. Moreover, our findings on immune cell infiltration and drug sensitivity emphasize the potential of personalized medicine in treating SKCM, advocating for tailored therapeutic approaches based on individual genetic and immunological profiles. Ultimately, this study provides valuable insights into the underlying mechanisms of SKCM, proposes new therapeutic targets, and supports the advancement of personalized treatment strategies that could significantly improve patient outcomes.

## Data availability statement

The datasets analyzed during this study are available on the GEO website (<https://www.ncbi.nlm.nih.gov/geo/>) and the TCGA website (<https://portal.gdc.cancer.gov/>). Furthermore, we have uploaded the complete raw data to Nutstore, accessible via this link: <https://www.jianguoyun.com/p/DauTKoYQ64nLDBjhys4FIAA>.

## Ethics statement

The studies involving humans were approved by the Department of Dermatology, Wenzhou Hospital of Integrated Chinese and Western Medicine. The studies were conducted in accordance with the local legislation and institutional requirements. The participants provided their written informed consent to participate in this study.

## Author contributions

CL: Conceptualization, Data curation, Writing—original draft, Writing—review and editing. NW: Data curation, Writing—review and editing. XL: Data curation, Writing—review and editing. QZ: Data curation, Writing—review and editing. MX: Data curation, Writing—review and editing.

## Conflict of interest

The authors declare that the research was conducted in the absence of any commercial or financial relationships that could be construed as a potential conflict of interest.

## Publisher's note

All claims expressed in this article are solely those of the authors and do not necessarily represent those of their affiliated organizations, or those of the publisher, the editors and the reviewers. Any product that may be evaluated in this article, or claim that may be made by its manufacturer, is not guaranteed or endorsed by the publisher.



## References

- Cui, Y., Wu, J., Zhou, Z., Ma, J., and Dong, L. (2022). Two novel lncRNAs AF111167.2 and AL162377.1 targeting miR-21-5p mediated down expression of SYDE2 correlates with poor prognosis and tumor immune infiltration of ccRCC. *Heliyon* 8 (10), e11079. doi:10.1016/j.heliyon.2022.e11079
- Date, S., Nibu, Y., Yanai, K., Hirata, J., Yagami, K., and Fukamizu, A. (2004). Finb, a multiple zinc finger protein, represses transcription of the human angiotensinogen gene. *Int. J. Mol. Med.* 13 (5), 637–642. doi:10.3892/ijmm.13.5.637
- Davey, M. G., Miller, N., and McNerney, N. M. (2021). A review of epidemiology and cancer biology of malignant melanoma. *Cureus* 13 (5), e15087. doi:10.7759/cureus.15087
- Davis, L. E., Shalin, S. C., and Tackett, A. J. (2019). Current state of melanoma diagnosis and treatment. *Cancer Biol. Ther.* 20 (11), 1366–1379. doi:10.1080/15384047.2019.1640032
- Dhingra, A., Fina, M. E., Neinstein, A., Ramsey, D. J., Xu, Y., Fishman, G. A., et al. (2011). Autoantibodies in melanoma-associated retinopathy target TRPM1 cation channels of retinal ON bipolar cells. *J. Neurosci. official J. Soc. Neurosci.* 31 (11), 3962–3967. doi:10.1523/JNEUROSCI.6007-10.2011
- Eddy, K., and Chen, S. (2020). Overcoming immune evasion in melanoma. *Int. J. Mol. Sci.* 21 (23), 8984. doi:10.3390/ijms21238984
- El Sharouni, M. A., Witkamp, A. J., Sigurdsson, V., van Diest, P. J., Louwman, M. W. J., and Kukutsch, N. A. (2019). Sex matters: men with melanoma have a worse prognosis than women. *J. Eur. Acad. Dermatology Venereol. JEADV* 33 (11), 2062–2067. doi:10.1111/jdv.15760
- Fakhoury, J. W., Lara, J. B., Manwar, R., Zafar, M., Xu, Q., Engel, R., et al. (2024). Photoacoustic imaging for cutaneous melanoma assessment: a comprehensive review. *J. Biomed. Opt.* 29 (1), S11518. doi:10.1117/1.JBO.29.S1.S11518
- Fujimoto-Nishiyama, A., Ishii, S., Matsuda, S., Inoue, J., and Yamamoto, T. (1997). A novel zinc finger protein, Finb, is a transcriptional activator and localized in nuclear bodies. *Gene* 195 (2), 267–275. doi:10.1016/s0378-1119(97)00172-8
- Geleher, P., Cox, N., and Huang, R. S. (2014). pRRophetic: an R package for prediction of clinical chemotherapeutic response from tumor gene expression levels. *PLoS one* 9 (9), e107468. doi:10.1371/journal.pone.0107468
- Gibson, J. A. G., Dobbs, T. D., Griffiths, R., Song, J., Akbari, A., Whitaker, S., et al. (2020). The association of smoking and socioeconomic status on cutaneous melanoma: a population-based, data-linkage, case-control study. *Br. J. dermatology* 182 (5), 1136–1147. doi:10.1111/bjd.18526
- Guan, R., Zou, J., Mei, J., Deng, M., and Guo, R. (2022). Four-gene signature predicting overall survival and immune infiltration in hepatocellular carcinoma by bioinformatics analysis with RT-qPCR validation. *BMC cancer* 22 (1), 830. doi:10.1186/s12885-022-09934-1
- Hawkes, J. E., Truong, A., and Meyer, L. J. (2016). Genetic predisposition to melanoma. *Seminars Oncol.* 43 (5), 591–597. doi:10.1053/j.seminoncol.2016.08.003
- Hirschhorn, D., Betof Warner, A., Maniyar, R., Chow, A., Mangarin, L. M., Cohen, A. D., et al. (2021). Cyclophosphamide enhances the antitumor potency of GITR engagement by increasing oligoclonal cytotoxic T cell fitness. *JCI insight* 6 (20), e151035. doi:10.1172/jci.insight.151035
- Jiang, Y., Wu, Y., Zhang, L., Wang, Y., Xu, G., Deng, Y., et al. (2023). Loss of chromosome 9p21 is associated with a poor prognosis in adenocarcinoma of the pancreas. *Precis. Clin. Med.* 6 (4), pbad030. doi:10.1093/pcmedi/pbad030
- Li, A. A., Zhang, Y., Tong, W. L., Chen, J. W., Huang, S. H., Liu, J. M., et al. (2022a). Identification of a novel pyroptosis-related gene signature indicative of disease prognosis and treatment response in skin cutaneous melanoma. *Int. J. general Med.* 15, 6145–6163. doi:10.2147/IJGM.S367693
- Li, J., Han, T., Wang, X., Wang, Y., Chen, X., Chen, W., et al. (2022b). Construction of a novel immune-related mRNA signature to predict the prognosis and immune characteristics of human colorectal cancer. *Front. Genet.* 13, 851373. doi:10.3389/fgenet.2022.851373
- Li, L., Fu, L. Q., Wang, H. J., and Wang, Y. Y. (2020). CAP2 is a valuable biomarker for diagnosis and prognostic in patients with gastric cancer. *Pathology Oncol. Res. POR* 26 (1), 273–279. doi:10.1007/s12253-018-0450-4
- Lo, J. A., and Fisher, D. E. (2014). The melanoma revolution: from UV carcinogenesis to a new era in therapeutics. *Sci. (New York, NY)* 346 (6212), 945–949. doi:10.1126/science.1253735
- Luo, Y., Ni, R., Jin, X., Feng, P., Dai, C., Jiang, L., et al. (2023). FOXD1 expression-based prognostic model for uveal melanoma. *Heliyon* 9 (11), e21333. doi:10.1016/j.heliyon.2023.e21333
- Maeser, D., Gruener, R. F., and Huang, R. S. (2021). oncoPredict: an R package for predicting *in vivo* or cancer patient drug response and biomarkers from cell line screening data. *Briefings Bioinforma.* 22 (6), bbab260. doi:10.1093/bib/bbab260
- Mukhopadhyay, N. K., Cinar, B., Mukhopadhyay, L., Lutchman, M., Ferdinand, A. S., Kim, J., et al. (2007). The zinc finger protein ras-responsive element binding protein-1 is a coregulator of the androgen receptor: implications for the role of the Ras pathway in enhancing androgenic signaling in prostate cancer. *Mol. Endocrinol. Baltim. Md* 21 (9), 2056–2070. doi:10.1210/me.2006-0503
- Nocentini, G., and Riccardi, C. (2009). GITR: a modulator of immune response and inflammation. *Adv. Exp. Med. Biol.* 647, 156–173. doi:10.1007/978-0-387-89520-8\_11
- Pelucchi, S., Macchi, C., D'Andrea, L., Rossi, P. D., Speciani, M. C., Stringhi, R., et al. (2023). An association study of cyclase-associated protein 2 and frailty. *Aging Cell* 22 (9), e13918. doi:10.1111/accel.13918
- Sacchetto, L., Zanetti, R., Comber, H., Bouchardy, C., Brewster, D. H., Broganelli, P., et al. (2018). Trends in incidence of thick, thin and *in situ* melanoma in Europe. *Eur. J. cancer (Oxford, Engl. 1990)* 92, 108–118. doi:10.1016/j.ejca.2017.12.024
- Siegel, R. L., Miller, K. D., Wagle, N. S., and Jemal, A. (2023). Cancer statistics. *CA a cancer J. Clin.* 73 (1), 17–30. doi:10.3322/caac.21332
- Slipicevic, A., and Herlyn, M. (2015). KIT in melanoma: many shades of gray. *J. investigative dermatology* 135 (2), 337–338. doi:10.1038/jid.2014.417
- Thiagalangam, A., De Bustros, A., Borges, M., Jasti, R., Compton, D., Diamond, L., et al. (1996). RREB-1, a novel zinc finger protein, is involved in the differentiation response to Ras in human medullary thyroid carcinomas. *Mol. Cell. Biol.* 16 (10), 5335–5345. doi:10.1128/mcb.16.10.5335
- Varin, J., Bouzidi, N., Dias, M. M. S., Pugliese, T., Michiels, C., Robert, C., et al. (2021). Restoration of mGluR6 localization following AAV-mediated delivery in a mouse model of congenital stationary night blindness. *Investigative Ophthalmol. Vis. Sci.* 62 (3), 24. doi:10.1167/iovs.62.3.24
- Wei, E. X., Qureshi, A. A., Han, J., Li, T. Y., Cho, E., Lin, J. Y., et al. (2016). Trends in the diagnosis and clinical features of melanoma *in situ* (MIS) in US men and women: a prospective, observational study. *J. Am. Acad. Dermatology* 75 (4), 698–705. doi:10.1016/j.jaad.2016.05.011
- Yue, C., Lian, W., Duan, M., Xia, D., Cao, X., and Peng, J. (2023). The predictive efficacy of programmed cell death in immunotherapy of melanoma: a comprehensive analysis of gene expression data for programmed cell death biomarker and therapeutic target discovery. *Environ. Toxicol.* 2023.
- Zhang, L., Zhao, J., and Edenberg, H. J. (1999). A human Raf-responsive zinc-finger protein that binds to divergent sequences. *Nucleic acids Res.* 27 (14), 2947–2956. doi:10.1093/nar/27.14.2947
- Zhao, S., Zhu, Y., Liu, H., He, X., and Xie, J. (2023). System analysis based on the pyroptosis-related genes identifies GSDMD as a novel therapy target for skin cutaneous melanoma. *J. Transl. Med.* 21 (1), 801. doi:10.1186/s12967-023-04513-9



## OPEN ACCESS

## EDITED BY

Gongbo Fu,  
Nanjing General Hospital of Nanjing Military  
Command, China

## REVIEWED BY

Yuquan Chen,  
Monash University, Australia

## \*CORRESPONDENCE

Jie Liu,  
✉ 123574514@qq.com  
Guanhu Yang,  
✉ gy182915@ohio.edu  
Hao Chi,  
✉ chihao7511@163.com

<sup>†</sup>These authors have contributed equally to  
this work

RECEIVED 16 May 2024

ACCEPTED 04 June 2024

PUBLISHED 20 June 2024

## CITATION

Su L, Luo H, Yan Y, Yang Z, Lu J, Xu D, Du L, Liu J,  
Yang G and Chi H (2024), Exploiting gender-  
based biomarkers and drug targets: advancing  
personalized therapeutic strategies in  
hepatocellular carcinoma.  
*Front. Pharmacol.* 15:1433540.  
doi: 10.3389/fphar.2024.1433540

## COPYRIGHT

© 2024 Su, Luo, Yan, Yang, Lu, Xu, Du, Liu, Yang  
and Chi. This is an open-access article  
distributed under the terms of the [Creative  
Commons Attribution License \(CC BY\)](#). The use,  
distribution or reproduction in other forums is  
permitted, provided the original author(s) and  
the copyright owner(s) are credited and that the  
original publication in this journal is cited, in  
accordance with accepted academic practice.  
No use, distribution or reproduction is  
permitted which does not comply with these  
terms.

# Exploiting gender-based biomarkers and drug targets: advancing personalized therapeutic strategies in hepatocellular carcinoma

Lanqian Su<sup>1†</sup>, Huanyu Luo<sup>1†</sup>, Yalan Yan<sup>1†</sup>, Zhongqiu Yang<sup>2†</sup>,  
Jiaan Lu<sup>1</sup>, Danqi Xu<sup>1</sup>, Linjuan Du<sup>3</sup>, Jie Liu<sup>2\*</sup>, Guanhu Yang<sup>4\*</sup> and  
Hao Chi<sup>1\*</sup>

<sup>1</sup>Clinical Medical College, Southwest Medical University, Luzhou, China, <sup>2</sup>Department of General Surgery, Dazhou Central Hospital, Dazhou, China, <sup>3</sup>Department of Oncology, Dazhou Central Hospital, Dazhou, China, <sup>4</sup>Department of Specialty Medicine, Ohio University, Athens, OH, United States

This review systematically examines gender differences in hepatocellular carcinoma (HCC), identifying the influence of sex hormones, genetic variance, and environmental factors on the disease's epidemiology and treatment outcomes. Recognizing the liver as a sexually dimorphic organ, we highlight how gender-specific risk factors, such as alcohol consumption and obesity, contribute differently to hepatocarcinogenesis in men and women. We explore molecular mechanisms, including the differential expression of androgen and estrogen receptors, which mediate diverse pathways in tumor biology such as cell proliferation, apoptosis, and DNA repair. Our analysis underscores the critical need for gender-specific research in liver cancer, from molecular studies to clinical trials, to improve diagnostic accuracy and therapeutic effectiveness. By incorporating a gender perspective into all facets of liver cancer research, we advocate for a more precise and personalized approach to cancer treatment that acknowledges gender as a significant factor in both the progression of HCC and its response to treatment. This review aims to foster a deeper understanding of the biological and molecular bases of gender differences in HCC and to promote the development of tailored interventions that enhance outcomes for all patients.

## KEYWORDS

hepatocellular carcinoma, gender heterogeneity, gender-specific therapies, cancer immunotherapy, sex hormone, molecular pathways, drug targets, treatment strategies

## 1 Introduction

Globally, liver cancer constitutes the third-highest cancer mortality, with approximately 90% through Hepatocellular carcinoma (HCC) (Kuwano et al., 2022). According to the GLOBOCAN 2020 database survey, it was estimated that about 9.5 and 8.7 ratios of age-standardized new cases and deaths in the world accounted for liver cancer, respectively, which has been increasing (Wei et al., 2014). Currently, the tumor has been treated with surgical resection, liver transplantation, chemotherapy, radiotherapy, and targeted therapies such as sorafenib (Jiang et al., 2019; Qi et al., 2020; Li et al., 2023a; Su et al.,

2023a; Zhang S. et al., 2023). While surgery and transplantation can be done in the early stage of the disease, however, most of the patients are diagnosed at a later age of the tumor, where the tumor has advanced and cannot be amenable to surgery and transplantation (Pan et al., 2014; Chaoul et al., 2020; Su et al., 2022a). Chemotherapy and radiotherapy treatments are characterized by systemic toxicity and side effects, but the so-called targeted treatment is emerging and in advanced stages, it is already very promising, although it still encounters the problem of drug resistance and a high relapse rate (Kamimura et al., 2020; Su et al., 2022b; Li et al., 2023b; Su et al., 2023b; Gao et al., 2023). This really highlights the urgent need for advances in early detection and more effective systemic therapies that are individualized and take into account patient differences at all levels, including gender (Chi et al., 2023; Grani et al., 2023).

The liver is highly sexually dimorphic, and a combination of hormonal, genetic, and environmental factors greatly influence the gender differences observed in hepatocarcinogenesis, treatment, and incidence (Marker et al., 2023; Huillet et al., 2024). For instance, the liver is very sensitive to sex hormones that include androgens and estrogens, and differences in molecular pathways have been noticed during the hepatocarcinogenesis phase, such as gene expression associated with the regulation of the cell cycle, apoptosis, and DNA repair (Singhal and Schlondorff, 1987; LoMauro and Aliverti, 2021). The liver is a tissue that bears additional sex-specific risk factors, one being alcohol consumption and obesity for the development of HCC. Some sex-specific risk factors, including alcohol intake, obesity, and insulin resistance, have been implicated in hepatocarcinogenesis, likely due to sex differences in alcohol metabolism and fat distribution impacting susceptibility to HCC (D'Souza et al., 2020; Izquierdo et al., 2022; Kardashian et al., 2023). That highlights the pressing need for a transition to a gender perspective in the entire flow of liver cancer research, from epidemiological inquiry to molecular analysis.

Here, we have presented a systematic review of several dimensions of the impact of gender differences on HCC, including the genetic background of the disease, pathogenesis, treatment response, and prognosis. The aim is to promote a more precise medical approach, leading to better outcomes for all patients with liver cancer (Nan et al., 2021).

## 2 Factors affecting gender differences in HCC

The proposed mechanisms for gender differences in HCC are thought to be complex and multifactorial (Pok et al., 2016). They are currently attributed to gender differences in environmental objective factors, behavioral risk factors, immune responses, metabolic risk factors, tumor biology and hormonal factors (Bashir Hamidu et al., 2021).

### 2.1 Environmental and lifestyle factors

Geographical differences in HCC and its etiology are clear; in general, they are due to the distribution of risk factors and different development between regions (Mousavi et al., 2013;

Yan et al., 2020; Enomoto et al., 2021). Indeed, the highest age-standardized incidence rates (ASRs) of HCC are estimated in East Asia, North Africa, and South-East Asia (Jiang et al., 2012; Okoronkwo et al., 2017). Sex differences are also reflected in the risk factors of HCC: Studies in recent years demonstrate that HBV and HCV are the major infectious agents associated with liver cancer (Zhang et al., 2020; Wang et al., 2021). The prevalence of HBV infection is greater among males than females (Poorolajal and Majdzadeh, 2009). However, the incidence of HCV is higher among females at 20.36 cases per 100 person-years than among males at 15.20 cases per 100 person-years (Puri et al., 2014). These days, the impact of viral hepatitis on liver cancer is waning, due to effective therapies (HBV, HCV) and vaccines (Nasr et al., 2023).

Non-viral causes (especially heavy consumption of alcohol) appear to have partially replaced the role of diseases caused virally in the case of HCC (Lee et al., 2021; Zhang J. et al., 2023). Effects of alcohol and its metabolites vary with age, race, and gender, with gender being marked mostly by differences. In terms of alcohol metabolism and in the context of heavy drinking, the relationship with HCC in women is stronger than in men, perhaps due to higher activities of alcohol dehydrogenases in women or a more prominent link of alcohol intake with cirrhosis risk in women (Bell et al., 2004; KASL, 2012). In meta-analyses, heavy drinking ( $\geq 4$  drinks/day) was associated with about a fourfold risk for women but only about a 59% increase for men (McGlynn et al., 2021). However, a higher intake of alcohol by men is experienced than women (Milman and Kirchhoff, 1996). Although heavy alcohol drinking has been established as one of the risk factors for liver cancer, most data indicated a weak negative association with light or moderate alcohol drinking and a reduced risk of HCC (Gao et al., 2020; Liu et al., 2022; Singh et al., 2023).

### 2.2 Inheritance and gene expression

Males and females present an active difference in gene expression. Figure 1 For example, studies have demonstrated that in male hepatocytes derived from individuals with HCC, the androgen receptor (AR) significantly enhances the expression of Enhancer of zeste homolog 2 (EZH2) at the transcriptional level. This enhancement facilitates an increase in the trimethylation level at lysine 27 of histone H3 (H3K27me3), effectively repressing the inhibitors of Wnt signaling pathways. This event activates Wnt/ $\beta$ -cyclin signaling and promotes the proliferation and transformation of liver tumor cells (Tsang et al., 2016; Baliou et al., 2020). On the other hand, estrogen in females, acting through the ER $\alpha$  receptor, can upregulate the protein tyrosine phosphatase receptor type O (PTPRO), which serves as a wide spectrum of cancer types (HCC, colorectal carcinoma, etc.) tumor suppressor protein (Asbagh et al., 2014; Xu et al., 2014).  $\alpha$  binds to the estrogen response element (ERE) of the PTPRO gene promoter, inducing dephosphorylation of Janus kinase 2 (JAK2) and phosphatidylinositol 3-kinase (PI3K), which in turn causes a decrease of the activity of the transcription factor STAT3, thus leading to inhibition of the HCC cell proliferation (Wu and Lou, 2023; Su et al., 2024).

Moreover, Era binds directly to the ERE of the peroxisome proliferator-activated receptor alpha (PPAR $\alpha$ ) gene, which is a

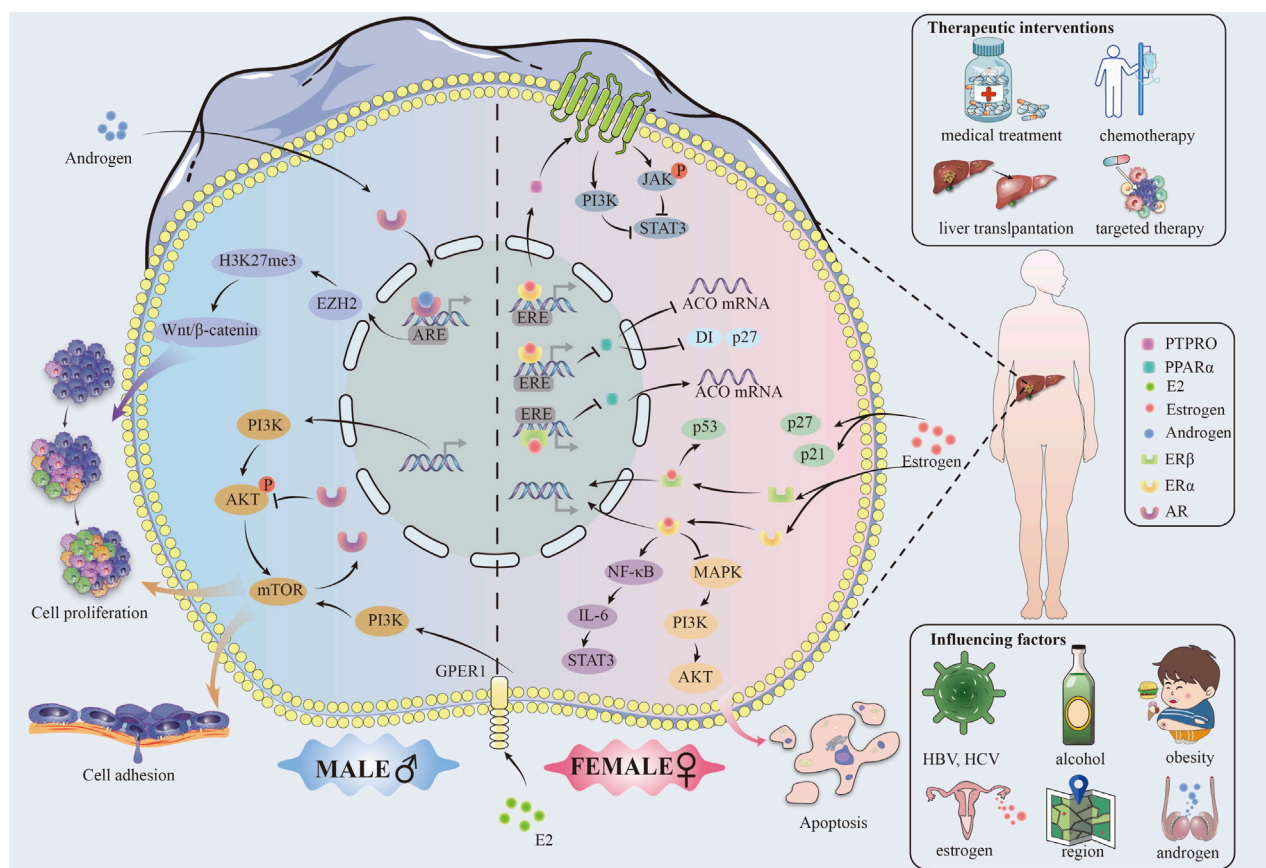


FIGURE 1  
Gender differences in hepatocellular cancer.

nuclear receptor protein with the function of a transcription factor, crucial for the oxidative processes in the hepatocytes (Memaj et al., 2023). Together, they decrease transcription of the PPAR $\alpha$  gene and further regulate PPAR $\alpha$  target acyl-coenzyme A oxidase (ACO), cell cycle proteins D1 and P27, blocking the proliferation of cancer cells and promoting apoptosis (Meng and Liu, 2022).

ER $\beta$  can downregulate PPAR $\alpha$  and its downstream genes through interaction with the EREs of the PPAR $\alpha$  gene to inhibit HCC development (Meng and Liu, 2022). In addition, it is through the action of ER $\beta$  that the translocation of PPAR $\alpha$  from the cytoplasm to the nucleus is prevented, and the transcription activity of PPAR $\alpha$  consequently decreases. This hormone-receptor complex subsequently induces homodimerization or heterodimerization of ER, translocation to the nucleus, binding to EREs on promoters of target genes, and induction of genomic effects of gene activation and epigenetic changes (Krolick and Shi, 2022).

In order to gain a comprehensive understanding of the factors influencing sex differences, it is essential to consider the regulatory networks downstream of hormones, in addition to genetic factors and the direct role of sex hormones. Estrogens can indirectly bring about the expression of genes by interaction with specific transcription factors through non-genomic effects, which can influence signaling pathways for the development of HCC

(Mandalà, 2020). For example, ER $\alpha$  interacts with the repressor NF- $\kappa$ B by inhibiting the IL-6/STAT3 activation pathway (Meng and Liu, 2022).

## 2.3 Influence of sex hormone

Estrogen and androgen have a key role in the molecular mechanisms of HCC (Liu et al., 2020). Estrogen can block the production of IL-6, a pro-inflammatory tumor growth and metastasis-promoting factor, through the JAK/STAT signaling pathway. At the same time, estrogen decreases the expression of TNF- $\alpha$ , another pro-inflammatory cytokine able to activate cancer cells through the NF- $\kappa$ B signaling pathway (Miller, 2018). On the other side, androgens could further enhance the development of HCC through increased expression of the above pro-inflammatory cytokines, exaggerating the inflammatory response (Wu et al., 2015). Androgens also have been demonstrated to upregulate the proliferation of HCC cells by activating their receptor AR, which in turn promotes the expression of c-Myc, an important regulator of cell proliferation and survival (Bao et al., 2020; Cho et al., 2020; Cui et al., 2020; Zhu et al., 2020; Gao et al., 2021) (Supplementary Table S1).



## 3 Molecular mechanisms and gender differences in HCC

### 3.1 Mechanisms of proliferation, invasion and metastasis

In HCC, gender differences have profound effects on tumor cell proliferation, invasion, and metastasis, where mechanistic target of rapamycin (mTOR) signaling is associated with many features of cancer (Ferrín et al., 2020). On the one hand, AR negatively regulates the feedback activation of AKT-mTOR signaling (Zhang et al., 2018). On the other hand, mTOR promotes the expression of nuclear AR protein by inhibiting ubiquitin-dependent AR degradation and enhancing its nuclear localization through enhancing the nuclear localization of AR, consequently mechanistically explaining AR overexpression in the nucleus of HCC cells (Zhang et al., 2018). AR overexpression was strongly associated with advanced tumor stage and low survival (29220539). Approximately a third of HCC tumors showed overexpressed nuclear AR protein in a series of 142 paired HCC tumors and their neighboring non-cancerous liver tissues (Zhang et al., 2018).

Furthermore, research has demonstrated that the estrogen receptor complex inhibits the mTOR signaling pathway, thereby impeding tumor growth (Ke et al., 2022). The activation of the PI3K-Akt (~70%) and mechanistic target of rapamycin complex 1 (mTORC1) (~45%) pathways was observed in HCC and demonstrated a positive correlation with tumor metastasis, recurrence and poor prognosis (Chaturantabut et al., 2019). A study using the HCC zebrafish model suggested that G protein-coupled estrogen receptor 1 (GPER1) could be a factor in the progress of hepatocarcinogenesis by inducing proliferation of hepatocytes and regulating organ growth via GPER1-PI3K-mTOR signaling transduction (Wojnarowski et al., 2022). E2-The pro-proliferative consequences of PI3K-mTOR signaling activation by GPER1 and the strong response to the presence of GPER1 antagonist therapy during cancer development and progression, as evidenced by *in vivo* human data (Ferrín et al., 2020; Tian et al., 2023). All these experimental results point to the fact that drugs targeted at E2-GPER1 should offer a new promising application for therapeutic use in liver cancer prevention and treatment (Chaturantabut et al., 2019).

Activation of the PI3K/AKT signaling pathway promotes hepatocyte proliferation and increases the capability of epithelial mesenchymal transition (EMT) through increasing HCC cell growth, migration, and invasion (Cantile et al., 2019). AR upregulates integrin  $\beta$ 1 expression through the PI3K/AKT/mTOR signal pathway, consequently, increasing in cellular adhesion, which could be a potential characteristic of advanced hepatocellular cancer with high metastasis (Carlos-Reyes et al., 2021). However, it was found that mice lacking hepatic AR developed more undifferentiated tumors and larger tumor sizes at the late metastatic stage compared to mouse models expressing AR, and these mice also died earlier due to increased lung metastasis. This suggests that hepatic AR may play a dual but opposing role in promoting HCC development and inhibiting HCC metastasis (Ma et al., 2012; Wen et al., 2014).

Studies have indicated that there should be gender specificity of p53 gene mutations in the development process of HCC (Shi et al., 1995). In addition, mutations in p53, a key oncogene for cell cycle regulation and apoptosis, were seen to hasten tumor progression (Chuery et al., 2017). Men suffering from liver cancer were more

associated with the frequency of p53 mutations than women (Finch and Tower, 2014). Besides, p53 is a vital regulator for the cellular response to DNA damage (Li and Wong, 2018). The ER $\beta$  complex in estrogen (ER $\beta$ ) partially contributes to the stabilization and activation of p53 in HCC cells, thus prohibiting the delivery of damaged DNA through aberrant cell cycle arrest and apoptosis.

### 3.2 Cell cycle regulation and apoptosis

Sex differences exert their influence on cell cycle regulation through the alteration of key regulatory proteins such as cyclins, cyclin-dependent kinases (CDKs), and CDK inhibitors, including p21 and p27 (Lim and Kaldis, 2013). Estrogens can upregulate the expression of p21 and p27, which will lead to cell arrest in phase G1 by stopping the activity of CDK, blocking the tumor cell cycle (Eto, 2010; Madhu Krishna et al., 2018). On the other hand, androgens downregulate the expression of these inhibitory proteins, thereby bringing the cell cycle on and causing tumor proliferation (Yu et al., 2017).

Apoptosis is programmed cell death, a process that assumes huge importance as a self-regulatory mechanism in the organism (Li et al., 2019). The identified Bcl-2 family proteins to date have an anti-apoptotic function, for example, Bcl-2, and pro-apoptotic action, for example, Bax (Chen et al., 2016). Estrogens will increase the expression of pro-apoptotic proteins, including Bax, to promote programmed cell death in damaged cells, whereas androgens may support the intensification of survival signaling, for example, by increasing the expression of Bcl-2 proteins that inhibit apoptosis (Arunkumar et al., 2012; Herson et al., 2013; Sanaei et al., 2022).

## 4 Medical treatment in HCC

Studies carried out in the tumor microenvironment (TME), immune response, Liver Transplant (LT) acceptance rate, and hormone therapy have alluded to a significant effect of gender differences on the outcomes of cancer treatment and survival. This fact propounds that future treatment strategies can incorporate gender-specific immune response and hormone modulation for more precise and effective anti-cancer strategies.

Sexual dimorphism exists in the immune response (Rehman and Masson, 2005; Wu et al., 2009; Mitchell et al., 2020). Women generate both adaptive and innate immunity responses much stronger than men, but at the same time, they suffer from systemic autoimmune diseases much more highly than men (Murgia et al., 2022; Zhang et al., 2022). In the case of non-small cell lung cancer (NSCLC) at an early stage, males present with a cold TME in which there is a defect in T-cell rejection. Contrary to that, female patients have a hotter TME, greater infiltration of dendritic cells (DCs), CD8 T cells and CD4 T cells, and greater upregulation of immune checkpoint molecules in T cells (Conforti et al., 2021).

In advanced HCC, liver transplantation is the standard treatment for end-stage liver disease (ESLD) (Hill et al., 2023). Studies have shown that women are less likely than men to receive LT because the hypothesis responsible for the gender-based variation in radical treatment is limited by the ability of Model for End-Stage Liver Disease (MELD) scores based on cr measurements in females (Mindikoglu et al., 2013; Karnam et al., 2021). In one study, females



received 1–2.4 fewer cr-derived MELD scores compared to males with similar renal function (Allen et al., 2018). However, researchers came up with a new multivariate model, MELD 3.0, meant to account for the factor of gender difference on waiting lists (Kim et al., 2021).

Sex differences in treatments that antagonize sex hormones and sex hormone receptors. Anti-ER therapy was found to promote tumor development in a mouse model, however, several studies have demonstrated that anti-AR therapy inhibits liver tumorigenesis (Ahotupa et al., 1994; Williams et al., 1997; Ma et al., 2012; Tang et al., 2021). Anti-hormonal therapy primarily disrupts the interaction between hormones and hormone receptors, thereby modulating downstream targets. However, the effect of anti-hormone therapy on HCC has been controversial. Very few clinical studies or randomized control trials demonstrate increased survival or survival in patients with advanced HCC. Most of the studies concluded that patients with HCC do not benefit from antihormonal drug therapy, mainly from side effects from the drugs and variability of the estrogen receptor. Survival outcomes in patients with HCC are affected by gender differences (Farinati et al., 1990; Martínez Cerezo et al., 1994; Grimaldi et al., 1998; Li Z. et al., 2023).

Gender differences affect survival outcomes in patients with HCC. HBV-infected male patients have an increased incidence of HCC compared to women, while men have higher serum HBV DNA titres. These data suggest that the overall survival among men is significantly shortened in comparison to women among patients with HCC (Chen et al., 2009; Sayaf et al., 2022). Female HBV patients have a decreased risk for HCC and improved survival with hormone replacement therapy (HRT) (Hassan et al., 2017; Wang et al., 2022). Ten thousand four hundred seventy-four women in the cohort study were postmenopausal and infected with HBV. Incidence rate in the HRT group of HCC and all-cause mortality of the HRT group decreased, compared with those in the no HRT group. Indeed, parallel research has concluded that an association exists between HRT and reduced HCC risk and better survival outcomes (Wang et al., 2022).

## 5 Discussion

The liver is a highly sexually dimorphic organ, possessing at least 72% of sexually differentiated genes (Yang et al., 2006). Sex hormones play a central role in gender preference in HCC, and thus multiple anti-sex hormone therapies or anti-sex hormone receptor therapies have been tried. Tamoxifen (TMX) therapy and hormone replacement therapy (HRT) are the two core regimens for hormone therapy in HCC (Meng and Liu, 2022). Although the efficacy of TMX in HCC remains controversial, there are still relevant studies reporting a positive relationship between the cancer inhibitory effect of TMX and ER $\alpha$  expression levels. In the work of Villa et al., 50 HCC patients were differentiated by wild-type ER $\alpha$  and ER $\alpha$  mRNA variant lacking exon 5 (ER $\Delta$ 5) phenotypes and the therapeutic efficacy of TMX was confirmed in patients with wild-type phenotype (Villa et al., 1996). Thereby the use of hormone therapy may largely dependent on the classification of ER $\alpha$  and screen or amplification of HCC patients with higher ER $\alpha$  expression may be beneficial to improve the sensitivity of hormone therapy. The effectiveness of estrogen replacement therapy in HCC has been demonstrated to some extent, however, estrogen may increase the risk of breast, ovarian and endometrial cancer in female patients and may have an unfavorable effects (American Medical Association, 2002; Meng and Liu, 2022; Wang et al., 2022). Exploring HCC hormone

therapy in combination with first-line drugs may be an option to improve efficacy.

AR is a crucial player in male dominant hepatocarcinogenesis. On one hand, abundant evidence shows that androgens exert tumor-promoting effects. On the other hand, AR blockade has been proved to do little benefit for HCC patients. It may be a fact that differences in sex hormone profiles are important not only in the initiation but also at the different stages of hepatocarcinogenesis, for example, the anti-tumor functions of AR in metastatic HCC (Ma et al., 2012). In addition, AR overexpression might also be used as an independent factor to predict the prognosis of patients with HCC. However, a portion of HCC was detected with the expression of C-terminal truncated AR-SVs. AR-SVs have been identified to play an important role in the acquired resistance to AR inhibitors (Dauki et al., 2020; Qiao et al., 2021; Katleba et al., 2023). Therefore, we imply that AR-SVs might also be involved in the occurrence of acquired resistance to AR inhibitors in HCC.

## Author contributions

LS: Data curation, Writing–original draft. HL: Conceptualization, Data curation, Writing–original draft. YY: Writing–original draft. ZY: Writing–original draft. JLu: Writing–original draft. DX: Writing–original draft. LD: Writing–original draft. JLi: Writing–original draft, Writing–review and editing. GY: Writing–original draft, Writing–review and editing. HC: Conceptualization, Writing–original draft, Writing–review and editing.

## Funding

The author(s) declare that financial support was received for the research, authorship, and/or publication of this article. The study was approved by Dazhou Science and Technology Bureau project (21ZDYF0025), Sichuan Medical Association Project (S21048, Q23095) and chen xiao-ping foundation for the development of science and technology of hubei province (CXPJH123003-008).

## Conflict of interest

The authors declare that the research was conducted in the absence of any commercial or financial relationships that could be construed as a potential conflict of interest.

## Publisher's note

All claims expressed in this article are solely those of the authors and do not necessarily represent those of their affiliated organizations, or those of the publisher, the editors and the reviewers. Any product that may be evaluated in this article, or claim that may be made by its manufacturer, is not guaranteed or endorsed by the publisher.

## Supplementary material

The Supplementary Material for this article can be found online at: <https://www.frontiersin.org/articles/10.3389/fphar.2024.1433540/full#supplementary-material>

## References

- Ahotupa, M., Hirsimäki, P., Pärssinen, R., and Mäntylä, E. (1994). Alterations of drug metabolizing and antioxidant enzyme activities during tamoxifen-induced hepatocarcinogenesis in the rat. *Carcinogenesis* 15, 863–868. doi:10.1093/carcin/15.5.863
- Allen, A. M., Heimbach, J. K., Larson, J. J., Mara, K. C., Kim, W. R., Kamath, P. S., et al. (2018). Reduced access to liver transplantation in women: role of height, MELD exception scores, and renal function underestimation. *Transplantation* 102, 1710–1716. doi:10.1097/TP.0000000000002196
- American Medical Association (2002). Long-term use of estrogen-only hormone replacement therapy (HRT) linked with increased risk of ovarian cancer. *Gynecol. Obstet. Mex.* 70, 409–410.
- Arunkumar, R., Sharmila, G., Elumalai, P., Senthilkumar, K., Banudevi, S., Gunadharini, D. N., et al. (2012). Effect of diallyl disulfide on insulin-like growth factor signaling molecules involved in cell survival and proliferation of human prostate cancer cells *in vitro* and *in silico* approach through docking analysis. *Phytomedicine* 19, 912–923. doi:10.1016/j.phymed.2012.04.009
- Asbagh, L. A., Vazquez, I., Vecchione, L., Budinska, E., De Vriendt, V., Baietti, M. F., et al. (2014). The tyrosine phosphatase PTPRO sensitizes colon cancer cells to anti-EGFR therapy through activation of SRC-mediated EGFR signaling. *Oncotarget* 5, 10070–10083. doi:10.18632/oncotarget.2458
- Baliou, S., Kyriakopoulos, A. M., Spandidos, D. A., and Zoumpouris, V. (2020). Role of taurine, its haloamines and its lncRNA TUG1 in both inflammation and cancer progression. On the road to therapeutics? (Review). *Int. J. Oncol.* 57, 631–664. doi:10.3892/ijo.2020.5100
- Bao, S. X., Wang, C. H., Jin, S., Hu, K. W., and Lu, J. T. (2020). miR-135b-5p suppresses androgen receptor-enhanced hepatocellular carcinoma cell proliferation via regulating the HIF-2 $\alpha$ /c-Myc/P27 signals *in vitro*. *Onco Targets Ther.* 13, 9991–10000. doi:10.2147/OTT.S268214
- Bashir Hamidu, R., Chalikonda, D. M., and Hann, H. W. (2021). Gender disparity in host responses to hepatitis B-related hepatocellular carcinoma: a case series. *Vaccines (Basel)* 9, 838. doi:10.3390/vaccines9080838
- Bell, B. P., Mast, E. E., Terrault, N., and Hutin, Y. J. (2004). Prevention of hepatitis C in women. *Emerg. Infect. Dis.* 10, 2035–2036. doi:10.3201/eid1011.040624\_04
- Cantile, M., Palmieri, G., and Botti, G. (2019). Developmental gene markers in tumor pathogenesis and progression. *Dis. Markers* 2019, 5462562. doi:10.1155/2019/5462562
- Carlos-Reyes, A., Muñoz-Lino, M. A., Romero-Garcia, S., López-Camarillo, C., and Hernández-de la Cruz, O. N. (2021). Biological adaptations of tumor cells to radiation therapy. *Front. Oncol.* 11, 718636. doi:10.3389/fonc.2021.718636
- Chang-Lee, S. N., Hsu, H. H., Shibu, M. A., Ho, T. J., Tsai, C. H., Chen, M. C., et al. (2017). E2/ER $\beta$  inhibits PPAR $\alpha$  to regulate cell-proliferation and enhance apoptosis in Hep3B-hepatocellular carcinoma. *Pathol. Oncol. Res.* 23, 477–485. doi:10.1007/s12253-016-0136-8
- Chaoul, N., Mancarella, S., Lupo, L., Giannelli, G., and Dituri, F. (2020). Impaired anti-tumor T cell response in hepatocellular carcinoma. *Cancers (Basel)* 12, 627. doi:10.3390/cancers12030627
- Chaturantabut, S., Schwartz, A., Evason, K. J., Cox, A. G., Labella, K., Schepers, A. G., et al. (2019). Estrogen activation of G-protein-coupled estrogen receptor 1 regulates phosphoinositide 3-kinase and mTOR signaling to promote liver growth in zebrafish and proliferation of human hepatocytes. *Gastroenterology* 156, 1788–1804. doi:10.1053/j.gastro.2019.01.010
- Chen, C. J., Yang, H. I., and Iloeje, U. H. (2009). Hepatitis B virus DNA levels and outcomes in chronic hepatitis B. *Hepatology* 49, S72–S84. doi:10.1002/hep.22884
- Chen, M., Wu, J., Luo, Q., Mo, S., Lyu, Y., Wei, Y., et al. (2016). The anticancer properties of herba epimedii and its main bioactive components icaritin and icaridin II. *Nutrients* 8, 563. doi:10.3390/nu8090563
- Chi, H., Zhao, S., Yang, J., Gao, X., Peng, G., Zhang, J., et al. (2023). T-cell exhaustion signatures characterize the immune landscape and predict HCC prognosis via integrating single-cell RNA-seq and bulk RNA-sequencing. *Front. Immunol.* 14, 1137025. doi:10.3389/fimmu.2023.1137025
- Cho, Y., Park, M. J., Kim, K., Kim, S. W., Kim, W., Oh, S., et al. (2020). Reactive oxygen species-induced activation of Yes-associated protein-1 through the c-Myc pathway is a therapeutic target in hepatocellular carcinoma. *World J. Gastroenterol.* 26, 6599–6613. doi:10.3748/wjg.v26.i24.6599
- Chuery, A. C. S., Silva, I., Ribalta, J. C. L., and Speck, N. M. G. (2017). Association between the p53 arginine/arginine homozygous genotype at codon 72 and human papillomavirus E6/E7 mRNA expression. *Braz J. Infect. Dis.* 21, 248–254. doi:10.1016/j.bjid.2017.03.002
- Conforti, F., Pala, L., Pagan, E., Bagnardi, V., De Pas, T., Queirolo, P., et al. (2021). Sex-based dimorphism of anticancer immune response and molecular mechanisms of immune evasion. *Clin. Cancer Res.* 27, 4311–4324. doi:10.1158/1078-0432.CCR-21-0136
- Cui, S. Z., Lei, Z. Y., Guan, T. P., Fan, L. L., Li, Y. Q., Geng, X. Y., et al. (2020). Targeting USP1-dependent KDM4A protein stability as a potential prostate cancer therapy. *Cancer Sci.* 111, 1567–1581. doi:10.1111/cas.14375
- Dauki, A. M., Blachly, J. S., Kautto, E. A., Ezzat, S., Abdel-Rahman, M. H., and Coss, C. C. (2020). Transcriptionally active androgen receptor splice variants promote hepatocellular carcinoma progression. *Cancer Res.* 80, 561–575. doi:10.1158/0008-5472.CAN-19-1117
- D'Souza, S., Lau, K. C., Coffin, C. S., and Patel, T. R. (2020). Molecular mechanisms of viral hepatitis induced hepatocellular carcinoma. *World J. Gastroenterol.* 26, 5759–5783. doi:10.3748/wjg.v26.i38.5759
- Enomoto, H., Ueno, Y., Hiasa, Y., Nishikawa, H., Hige, S., Takikawa, Y., et al. (2021). The transition in the etiologies of hepatocellular carcinoma-complicated liver cirrhosis in a nationwide survey of Japan. *J. Gastroenterol.* 56, 158–167. doi:10.1007/s00535-020-01748-x
- Eto, I. (2010). Upstream molecular signaling pathways of p27(Kip1) expression: effects of 4-hydroxytamoxifen, dexamethasone, and retinoic acids. *Cancer Cell Int.* 10, 3. doi:10.1186/1475-2867-10-3
- Farinati, F., Salvagnini, M., de Maria, N., Fornasiero, A., Chiamonte, M., Rossaro, L., et al. (1990). Unresectable hepatocellular carcinoma: a prospective controlled trial with tamoxifen. *J. Hepatol.* 11, 297–301. doi:10.1016/0168-8278(90)90211-9
- Ferrín, G., Guerrero, M., Amado, V., Rodríguez-Perálvarez, M., and De la Mata, M. (2020). Activation of mTOR signaling pathway in hepatocellular carcinoma. *Int. J. Mol. Sci.* 21, 1266. doi:10.3390/ijms21041266
- Finch, C. E., and Tower, J. (2014). Sex-specific aging in flies, worms, and missing great-granddads. *Cell* 156, 398–399. doi:10.1016/j.cell.2014.01.028
- Gao, C., Fang, L., Zhang, H., Zhang, W. S., Li, X. O., and Du, S. Y. (2020). Metformin induces autophagy via the AMPK-mTOR signaling pathway in human hepatocellular carcinoma cells. *Cancer Manag. Res.* 12, 5803–5811. doi:10.2147/CMAR.S257966
- Gao, D., Asghar, S., Hu, R., Chen, S., Niu, R., Liu, J., et al. (2023). Recent advances in diverse nanosystems for nitric oxide delivery in cancer therapy. *Acta Pharm. Sin. B* 13, 1498–1521. doi:10.1016/j.apsb.2022.11.016
- Gao, Y., Yu, X. F., and Chen, T. (2021). Human endogenous retroviruses in cancer: expression, regulation and function (Review). *Oncol. Lett.* 21, 121. doi:10.3892/ol.2020.12382
- Grani, G., Ciotti, L., Del Gatto, V., Montesano, T., Biffoni, M., Giacomelli, L., et al. (2023). The legacy of the COVID-19 pandemics for thyroid cancer patients: towards the application of clinical practice recommendations. *Endocrine* 79, 45–48. doi:10.1007/s12020-022-03132-6
- Grimaldi, C., Bleiberg, H., Gay, F., Messner, M., Rougier, P., Kok, T. C., et al. (1998). Evaluation of antiandrogen therapy in unresectable hepatocellular carcinoma: results of a European Organization for Research and Treatment of Cancer multicentric double-blind trial. *J. Clin. Oncol.* 16, 411–417. doi:10.1200/JCO.1998.16.2.411
- Guo, Y., Wu, G., Yi, J., Yang, Q., Jiang, W., Lin, S., et al. (2021). Anti-hepatocellular carcinoma effect and molecular mechanism of the estrogen signaling pathway. *Front. Oncol.* 11, 763539. doi:10.3389/fonc.2021.763539
- Hassan, M. M., Botrus, G., Abdel-Wahab, R., Wolff, R. A., Li, D., Twardy, D., et al. (2017). Estrogen replacement reduces risk and increases survival times of women with hepatocellular carcinoma. *Clin. Gastroenterol. Hepatol.* 15, 1791–1799. doi:10.1016/j.cgh.2017.05.036
- Herson, P. S., Bombardier, C. G., Parker, S. M., Shimizu, T., Klawitter, J., Klawitter, J., et al. (2013). Experimental pediatric arterial ischemic stroke model reveals sex-specific estrogen signaling. *Stroke* 44, 759–763. doi:10.1161/STROKEAHA.112.675124
- Hill, A. L., Khan, M., Kiani, A. Z., Lindemann, J. D., Vachharajani, N., Doyle, M. B., et al. (2023). Global liver transplantation: emerging trends and ethical challenges. *Langenbecks Arch. Surg.* 408, 418. doi:10.1007/s00423-023-03144-4
- Hou, J., Xu, J., Jiang, R., Wang, Y., Chen, C., Deng, L., et al. (2013). Estrogen-sensitive PTPRO expression represses hepatocellular carcinoma progression by control of STAT3. *Hepatology* 57, 678–688. doi:10.1002/hep.25980
- Huillet, M., Lasserre, F., Gratacap, M. P., Engelmann, B., Bruse, J., Polizzi, A., et al. (2024). Pharmacological activation of constitutive androstane receptor induces female-specific modulation of hepatic metabolism. *JHEP Rep.* 6, 100930. doi:10.1016/j.jhepr.2023.100930
- Izquierdo, A. G., Carreira, M. C., Rodríguez-Carnero, G., Perez-Lois, R., Seoane, L. M., Casanueva, F. F., et al. (2022). Gender dimorphism in hepatic carcinogenesis-related gene expression associated with obesity as a low-grade chronic inflammatory disease. *Int. J. Mol. Sci.* 23, 15002. doi:10.3390/ijms232315002
- Jiang, X. B., Ke, C., Zhang, G. H., Zhang, X. H., Sai, K., Chen, Z. P., et al. (2012). Brain metastases from hepatocellular carcinoma: clinical features and prognostic factors. *BMC Cancer* 12, 49. doi:10.1186/1471-2407-12-49
- Jiang, Y., Han, Q. J., and Zhang, J. (2019). Hepatocellular carcinoma: mechanisms of progression and immunotherapy. *World J. Gastroenterol.* 25, 3151–3167. doi:10.3748/wjg.v25.i25.3151
- KASL (2012). KASL clinical practice Guidelines: management of chronic hepatitis B. *Clin. Mol. Hepatol.* 18, 109–162. doi:10.3350/cmh.2012.18.2.109

- Kamimura, K., Yokoo, T., Abe, H., Sakai, N., Nagoya, T., Kobayashi, Y., et al. (2020). Effect of diphtheria toxin-based gene therapy for hepatocellular carcinoma. *Cancers (Basel)* 12, 472. doi:10.3390/cancers12020472
- Kardashian, A., Serper, M., Terrault, N., and Nephew, L. D. (2023). Health disparities in chronic liver disease. *Hepatology* 77, 1382–1403. doi:10.1002/hep.32743
- Karnam, R. S., Chen, S., Xu, W., Chen, C., Elangainesan, P., Ghanekar, A., et al. (2021). Sex disparity in liver transplant and access to living donation. *JAMA Surg.* 156, 1010–1017. doi:10.1001/jamasurg.2021.3586
- Katleba, K. D., Ghosh, P. M., and Mudryj, M. (2023). Beyond prostate cancer: an androgen receptor splice variant expression in multiple malignancies, non-cancer pathologies, and development. *Biomedicine* 11, 2215. doi:10.3390/biomedicine11082215
- Ke, Y., Zu, S., Chen, L., Liu, M., Yang, H., Wang, F., et al. (2022). Combination of estrogen receptor alpha and histological type helps to predict lymph node metastasis in patients with stage IA2 to IIA2 cervical cancer. *Cancer Manag. Res.* 14, 317–325. doi:10.2147/CMAR.S343518
- Kim, W. R., Mannalithara, A., Heimbach, J. K., Kamath, P. S., Asrani, S. K., Biggins, S. W., et al. (2021). MELD 3.0: the model for end-stage liver disease updated for the modern era. *Gastroenterology* 161, 1887–1895.e4. doi:10.1053/j.gastro.2021.08.050
- Krolick, K. N., and Shi, H. (2022). Estrogenic action in stress-induced neuroendocrine regulation of energy homeostasis. *Cells* 11, 879. doi:10.3390/cells11050879
- Kuwano, A., Yada, M., Narutomi, F., Nagasawa, S., Tanaka, K., Kurosaka, K., et al. (2022). Therapeutic efficacy of atezolizumab plus bevacizumab for hepatocellular carcinoma with WNT/ $\beta$ -catenin signal activation. *Oncol. Lett.* 24, 216. doi:10.3892/ol.2022.13337
- Lee, C. W., Yu, M. C., Wang, C. C., Lee, W. C., Tsai, H. I., Kuan, F. C., et al. (2021). Liver resection for hepatocellular carcinoma larger than 10 cm: a multi-institution long-term observational study. *World J. Gastrointest. Surg.* 13, 476–492. doi:10.4240/wjgs.v13.i5.476
- Li, H., Guo, L., Su, K., Li, C., Jiang, Y., Wang, P., et al. (2023b). Construction and validation of tace therapeutic efficacy by alr score and nomogram: a large, multicenter study. *J. Hepatocell. Carcinoma* 10, 1009–1017. doi:10.2147/JHC.S414926
- Li, H., Wu, Z., Chen, J., Su, K., Guo, L., Xu, K., et al. (2023a). External radiotherapy combined with sorafenib has better efficacy in unresectable hepatocellular carcinoma: a systematic review and meta-analysis. *Clin. Exp. Med.* 23, 1537–1549. doi:10.1007/s10238-022-00972-4
- Li, Y., Yang, D., Wang, Y., Li, Z., and Zhu, C. (2019). Co-delivery doxorubicin and silybin for anti-hepatoma via enhanced oral hepatic-targeted efficiency. *Int. J. Nanomedicine* 14, 301–315. doi:10.2147/IJN.S187888
- Li, Y. Q., and Wong, C. S. (2018). Effects of p21 on adult hippocampal neuronal development after irradiation. *Cell Death Discov.* 4, 15. doi:10.1038/s41420-018-0081-2
- Li, Z., Lan, L., Zhou, Y., Li, R., Chavin, K. D., Xu, H., et al. (2023c). Developing deep learning-based strategies to predict the risk of hepatocellular carcinoma among patients with nonalcoholic fatty liver disease from electronic health records. medRxiv.
- Lim, S., and Kaldis, P. (2013). Cdks, cyclins and CKIs: roles beyond cell cycle regulation. *Development* 140, 3079–3093. doi:10.1242/dev.091744
- Liu, S., Wang, R., Lou, Y., and Liu, J. (2020). Uncovering the mechanism of the effects of pien-tze-huang on liver cancer using network Pharmacology and molecular docking. *Evid. Based Complement. Altern. Med.* 2020, 4863015. doi:10.1155/2020/4863015
- Liu, Z., Song, C., Suo, C., Fan, H., Zhang, T., Jin, L., et al. (2022). Alcohol consumption and hepatocellular carcinoma: novel insights from a prospective cohort study and nonlinear Mendelian randomization analysis. *BMC Med.* 20, 413. doi:10.1186/s12916-022-02622-8
- LoMauro, A., and Aliverti, A. (2021). Sex and gender in respiratory physiology. *Eur. Respir. Rev.* 30, 210038. doi:10.1183/16000617.0038-2021
- Ma, W. L., Hsu, C. L., Yeh, C. C., Wu, M. H., Huang, C. K., Jeng, L. B., et al. (2012). Hepatic androgen receptor suppresses hepatocellular carcinoma metastasis through modulation of cell migration and anoikis. *Hepatology* 56, 176–185. doi:10.1002/hep.25644
- Madhu Krishna, B., Chaudhary, S., Mishra, D. R., Naik, S. K., Suklabaidya, S., Adhya, A. K., et al. (2018). Estrogen receptor  $\alpha$  dependent regulation of estrogen related receptor  $\beta$  and its role in cell cycle in breast cancer. *BMC Cancer* 18, 607. doi:10.1186/s12885-018-4528-x
- Mandalá, M. (2020). Influence of estrogens on uterine vascular adaptation in normal and preeclamptic pregnancies. *Int. J. Mol. Sci.* 21, 2592. doi:10.3390/ijms21072592
- Marker, P. C., Unterberger, C. J., and Swanson, S. M. (2023). GH-dependent growth of experimentally induced carcinomas *in vivo*. *Endocr. Relat. Cancer* 30, e220403. doi:10.1530/ERC-22-0403
- Martínez Cerezo, F. J., Tomás, A., Donoso, L., Enríquez, J., Guarnier, C., Balanzó, J., et al. (1994). Controlled trial of tamoxifen in patients with advanced hepatocellular carcinoma. *J. Hepatol.* 20, 702–706. doi:10.1016/s0168-8278(05)80138-2
- McGlynn, K. A., Petrick, J. L., and El-Serag, H. B. (2021). Epidemiology of hepatocellular carcinoma. *Hepatology* 73 (Suppl. 1), 4–13. doi:10.1002/hep.31288
- Memaj, P., Ouzerara, Z., and Jornayvaz, F. R. (2023). Role of oxidative stress and carcinoembryonic antigen-related cell adhesion molecule 1 in nonalcoholic fatty liver disease. *Int. J. Mol. Sci.* 24, 11271. doi:10.3390/ijms24111271
- Meng, X., and Liu, X. (2022). Therapeutic value of estrogen receptor  $\alpha$  in hepatocellular carcinoma based on molecular mechanisms. *J. Clin. Transl. Hepatol.* 10, 140–146. doi:10.14218/JCTH.2021.00224
- Miller, L. E. (2018). Methylsulfonylmethane decreases inflammatory response to tumor necrosis factor- $\alpha$  in cardiac cells. *Am. J. Cardiovasc. Dis.* 8, 31–38.
- Milman, N., and Kirchhoff, M. (1996). Relationship between serum ferritin, alcohol intake, and social status in 2235 Danish men and women. *Ann. Hematol.* 72, 145–151. doi:10.1007/s002770050153
- Mindikoglu, A. L., Emre, S. H., and Magder, L. S. (2013). Impact of estimated liver volume and liver weight on gender disparity in liver transplantation. *Liver Transpl.* 19, 89–95. doi:10.1002/lt.23553
- Mitchell, T., De Miguel, C., and Gohar, E. Y. (2020). Sex differences in redox homeostasis in renal disease. *Redox Biol.* 31, 101489. doi:10.1016/j.redox.2020.101489
- Mousavi, S. F., Moosavy, S. H., Alavian, S. M., Eghbali, H., and Mahboobi, H. (2013). Distribution of hepatitis C virus genotypes among patients with hepatitis C virus infection in hormozgan, Iran. *Hepat. Mon.* 13, e14324. doi:10.5812/hepatmon.14324
- Murgia, F., Giagnoni, F., Lorefice, L., Caria, P., Dettori, T., D'Alterio, M. N., et al. (2022). Sex hormones as key modulators of the immune response in multiple sclerosis: a review. *Biomedicine* 10, 3107. doi:10.3390/biomedicine10123107
- Nan, Y., Xu, X., Gao, Y., Wang, R., Li, W., Yang, M., et al. (2021). Consensus on the secondary prevention of primary liver cancer. *Hepatol. Int.* 15, 1289–1300. doi:10.1007/s12072-021-10259-7
- Nasr, P., von Seth, E., Mayerhofer, R., Ndegwa, N., Ludvigsson, J. F., and Hagström, H. (2023). Incidence, prevalence and mortality of chronic liver diseases in Sweden between 2005 and 2019. *Eur. J. Epidemiol.* 38, 973–984. doi:10.1007/s10654-023-01028-x
- Okoronkwo, N., Wang, Y., Pitchumoni, C., Koneru, B., and Pyrsopoulos, N. (2017). Improved outcomes following hepatocellular carcinoma (HCC) diagnosis in patients screened for HCC in a large academic liver center versus patients identified in the community. *J. Clin. Transl. Hepatol.* 5, 31–34. doi:10.14218/JCTH.2016.00051
- Pan, Y., Sun, C., Huang, M., Liu, Y., Qi, F., Liu, L., et al. (2014). A genetic variant in pseudogene E2F3P1 contributes to prognosis of hepatocellular carcinoma. *J. Biomed. Res.* 28, 194–200. doi:10.7555/JBR.28.20140052
- Pok, S., Barn, V. A., Wong, H. J., Blackburn, A. C., Board, P., Farrell, G. C., et al. (2016). Testosterone regulation of cyclin E kinase: a key factor in determining gender differences in hepatocarcinogenesis. *J. Gastroenterol. Hepatol.* 31, 1210–1219. doi:10.1111/jgh.13232
- Poorolajal, J., and Majdzadeh, R. (2009). Prevalence of chronic hepatitis B infection in Iran: a review article. *J. Res. Med. Sci.* 14, 249–258.
- Puri, N., DeBeck, K., Feng, C., Kerr, T., Rieb, L., and Wood, E. (2014). Gender influences on hepatitis C incidence among street youth in a Canadian setting. *J. Adolesc. Health* 55, 830–834. doi:10.1016/j.jadohealth.2014.07.006
- Qi, Y., Liu, Y., Yu, B., Hu, Y., Zhang, N., Zheng, Y., et al. (2020). A lactose-derived CRISPR/Cas9 delivery system for efficient genome editing *in vivo* to treat orthotopic hepatocellular carcinoma. *Adv. Sci. (Weinh)* 7, 2001424. doi:10.1002/adv.202001424
- Qiao, Y., Wang, X. M., Mannan, R., Pitchaiya, S., Zhang, Y., Wotring, J. W., et al. (2021). Targeting transcriptional regulation of SARS-CoV-2 entry factors ACE2 and TMPRSS2. *Proc. Natl. Acad. Sci. U. S. A.* 118, e2021450118. doi:10.1073/pnas.2021450118
- Rehman, H. U., and Masson, E. A. (2005). Neuroendocrinology of female aging. *Gend. Med.* 2, 41–56. doi:10.1016/s1550-8579(05)80008-7
- Sanaei, M. J., Razi, S., Pourbagheri-Sigaroodi, A., and Bashash, D. (2022). The PI3K/Akt/mTOR pathway in lung cancer; oncogenic alterations, therapeutic opportunities, challenges, and a glance at the application of nanoparticles. *Transl. Oncol.* 18, 101364. doi:10.1016/j.tranon.2022.101364
- Sayaf, K., Gabbia, D., Russo, F. P., and De Martin, S. (2022). The role of sex in acute and chronic liver damage. *Int. J. Mol. Sci.* 23, 10654. doi:10.3390/ijms231810654
- Shi, C. Y., Phang, T. W., Wee, A., Ngoi, S. S., Lin, Y., Li, B., et al. (1995). Mutations of the tumour suppressor gene p53 in colorectal and hepatocellular carcinomas. *Ann. Acad. Med. Singap.* 24, 204–210.
- Singh, S., Hoque, S., Zekry, A., and Sowmya, A. (2023). Radiological diagnosis of chronic liver disease and hepatocellular carcinoma: a review. *J. Med. Syst.* 47, 73. doi:10.1007/s10916-023-01968-7
- Singhal, P. C., and Schlondorff, D. (1987). Hyperosmolar state associated with rhabdomyolysis. *Nephron* 47, 202–204. doi:10.1159/000184492
- Song, H., Yu, Z., Sun, X., Feng, J., Yu, Q., Khan, H., et al. (2018). Androgen receptor drives hepatocellular carcinogenesis by activating enhancer of zeste homolog 2-mediated Wnt/ $\beta$ -catenin signaling. *EBioMedicine* 35, 155–166. doi:10.1016/j.ebiom.2018.08.043
- Su, J., Liu, X., Zhao, X., Ma, H., Jiang, Y., Wang, X., et al. (2024). Curcumin inhibits the growth of hepatocellular carcinoma via the MARCH1-mediated modulation of JAK2/



- STAT3 signaling. *Recent Pat. Anticancer Drug Discov.* 19. doi:10.2174/0115748928261490231124055059
- Su, K., Guo, L., Ma, W., Wang, J., Xie, Y., Rao, M., et al. (2022b). PD-1 inhibitors plus anti-angiogenic therapy with or without intensity-modulated radiotherapy for advanced hepatocellular carcinoma: a propensity score matching study. *Front. Immunol.* 13, 972503. doi:10.3389/fimmu.2022.972503
- Su, K., Liu, Y., Wang, P., He, K., Wang, F., Chi, H., et al. (2022a). Heat-shock protein 90 $\alpha$  is a potential prognostic and predictive biomarker in hepatocellular carcinoma: a large-scale and multicenter study. *Hepatol. Int.* 16, 1208–1219. doi:10.1007/s12072-022-10391-y
- Su, K., Shen, Q., Tong, J., Gu, T., Xu, K., Li, H., et al. (2023b). Construction and validation of a nomogram for HBV-related hepatocellular carcinoma: a large, multicenter study. *Ann. Hepatol.* 28, 101109. doi:10.1016/j.aohep.2023.101109
- Su, K., Wang, F., Li, X., Chi, H., Zhang, J., He, K., et al. (2023a). Effect of external beam radiation therapy versus transcatheter arterial chemoembolization for non-diffuse hepatocellular carcinoma ( $\geq 5$  cm): a multicenter experience over a ten-year period. *Front. Immunol.* 14, 1265959. doi:10.3389/fimmu.2023.1265959
- Sun, E. J., Wankell, M., Palamuthusingam, P., McFarlane, C., and Hebbard, L. (2021). Targeting the PI3K/Akt/mTOR pathway in hepatocellular carcinoma. *Biomedicines* 9, 1639. doi:10.3390/biomedicines9111639
- Tang, N., Dou, X., You, X., Li, Y., Li, X., and Liu, G. (2021). Androgen receptors act as a tumor suppressor gene to suppress hepatocellular carcinoma cells progression via miR-122-5p/RAB16 signaling. *Front. Oncol.* 11, 756779. doi:10.3389/fonc.2021.756779
- Tian, L. Y., Smit, D. J., and Jücker, M. (2023). The role of PI3K/AKT/mTOR signaling in hepatocellular carcinoma metabolism. *Int. J. Mol. Sci.* 24, 2652. doi:10.3390/ijms24032652
- Tsang, D. P., Wu, W. K., Kang, W., Lee, Y. Y., Wu, F., Yu, Z., et al. (2016). Yin Yang 1-mediated epigenetic silencing of tumour-suppressive microRNAs activates nuclear factor- $\kappa$ B in hepatocellular carcinoma. *J. Pathol.* 238, 651–664. doi:10.1002/path.4688
- Villa, E., Dugani, A., Fantoni, E., Camellini, L., Buttafoco, P., Grottola, A., et al. (1996). Type of estrogen receptor determines response to antiestrogen therapy. *Cancer Res.* 56, 3883–3885.
- Wang, C. H., Lin, R. C., Hsu, H. Y., and Tseng, Y. T. (2022). Hormone replacement therapy is associated with reduced hepatocellular carcinoma risk and improved survival in postmenopausal women with hepatitis B: a nationwide long-term population-based cohort study. *PLoS One* 17, e0271790. doi:10.1371/journal.pone.0271790
- Wang, H., Zheng, Y., Huang, J., and Li, J. (2021). Mitophagy in antiviral immunity. *Front. Cell Dev. Biol.* 9, 723108. doi:10.3389/fcell.2021.723108
- Wei, K. R., Yu, X., Zheng, R. S., Peng, X. B., Zhang, S. W., Ji, M. F., et al. (2014). Incidence and mortality of liver cancer in China, 2010. *Chin. J. Cancer* 33, 388–394. doi:10.5732/cjc.014.10088
- Wen, S., Niu, Y., Lee, S. O., and Chang, C. (2014). Androgen receptor (AR) positive vs negative roles in prostate cancer cell deaths including apoptosis, anoikis, entosis, necrosis and autophagic cell death. *Cancer Treat. Rev.* 40, 31–40. doi:10.1016/j.ctrv.2013.07.008
- Williams, G. M., Iatropoulos, M. J., and Karlsson, S. (1997). Initiating activity of the anti-estrogen tamoxifen, but not toremifene in rat liver. *Carcinogenesis* 18, 2247–2253. doi:10.1093/carcin/18.11.2247
- Wojnarowski, K., Cholewińska, P., Palić, D., Bednarska, M., Jarosz, M., and Wiśniewska, I. (2022). Estrogen receptors mediated negative effects of estrogens and xenoestrogens in teleost fishes-review. *Int. J. Mol. Sci.* 23, 2605. doi:10.3390/ijms23052605
- Wu, C. T., Chen, W. C., Lin, P. Y., Liao, S. K., and Chen, M. F. (2009). Androgen deprivation modulates the inflammatory response induced by irradiation. *BMC Cancer* 9, 92. doi:10.1186/1471-2407-9-92
- Wu, J., Zhang, J., Shen, B., Yin, K., Xu, J., Gao, W., et al. (2015). Long noncoding RNA lncTCF7, induced by IL-6/STAT3 transactivation, promotes hepatocellular carcinoma aggressiveness through epithelial-mesenchymal transition. *J. Exp. Clin. Cancer Res.* 34, 116. doi:10.1186/s13046-015-0229-3
- Wu, M., and Lou, S. (2023). Deciphering the influence of estradiol and estrogen receptors on cognitive function: a bibliometric analysis and emerging research trends. *Med. Sci. Monit.* 29, e939676. doi:10.12659/MSM.939676
- Xu, D., Wang, X., Yan, S., Yin, Y., Hou, J., Wang, X., et al. (2014). Interaction of PTPRO and TLR4 signaling in hepatocellular carcinoma. *Tumour Biol.* 35, 10267–10273. doi:10.1007/s13277-014-2302-5
- Yan, W., Cheng, L., and Zhang, D. (2020). Ultrasound-targeted microbubble destruction mediated si-CyclinD1 inhibits the development of hepatocellular carcinoma via suppression of PI3K/AKT signaling pathway. *Cancer Manag. Res.* 12, 10829–10839. doi:10.2147/CMAR.S263590
- Yang, X., Schadt, E. E., Wang, S., Wang, H., Arnold, A. P., Ingram-Drake, L., et al. (2006). Tissue-specific expression and regulation of sexually dimorphic genes in mice. *Genome Res.* 16, 995–1004. doi:10.1101/gr.5217506
- Yu, P., Duan, X., Cheng, Y., Liu, C., Chen, Y., Liu, W., et al. (2017). Androgen-independent LNCaP cells are a subline of LNCaP cells with a more aggressive phenotype and androgen suppresses their growth by inducing cell cycle arrest at the G1 phase. *Int. J. Mol. Med.* 40, 1426–1434. doi:10.3892/ijmm.2017.3125
- Zhang, H., Li, X. X., Yang, Y., Zhang, Y., Wang, H. Y., and Zheng, X. F. S. (2018). Significance and mechanism of androgen receptor overexpression and androgen receptor/mechanistic target of rapamycin cross-talk in hepatocellular carcinoma. *Hepatology* 67, 2271–2286. doi:10.1002/hep.29715
- Zhang, J., Dong, K., Zhang, X., Li, C., Yu, J., and Wang, W. (2023b). Characteristics of lactate metabolism phenotype in hepatocellular carcinoma. *Sci. Rep.* 13, 19674. doi:10.1038/s41598-023-47065-0
- Zhang, S., Jiang, C., Jiang, L., Chen, H., Huang, J., Gao, X., et al. (2023a). Construction of a diagnostic model for hepatitis B-related hepatocellular carcinoma using machine learning and artificial neural networks and revealing the correlation by immunoassay. *Tumour Virus Res.* 16, 200271. doi:10.1016/j.tvr.2023.200271
- Zhang, W., Liu, F., Huang, J., Guo, X., Dong, W., Wei, S., et al. (2020). Effect of menopausal status on the survival and recurrence of sex-classified hepatocellular carcinoma after liver resection: a case-matched study with propensity score matching. *Aging (Albany NY)* 12, 25895–25915. doi:10.18632/aging.202155
- Zhang, Y., Zhang, X., Li, W., Du, Y., Hu, W., and Zhao, J. (2022). Biomarkers and risk factors for the early prediction of immune-related adverse events: a review. *Hum. Vaccin Immunother.* 18, 2018894. doi:10.1080/21645515.2021.2018894
- Zhao, P., Malik, S., and Xing, S. (2021). Epigenetic mechanisms involved in HCV-induced hepatocellular carcinoma (HCC). *Front. Oncol.* 11, 677926. doi:10.3389/fonc.2021.677926
- Zhu, H., Chen, Y., Zhang, J., Qian, C., Qiu, W., Shen, H., et al. (2020). Knockdown of TRIM37 promotes apoptosis and suppresses tumor growth in gastric cancer by inactivation of the ERK1/2 pathway. *Oncotargets Ther.* 13, 5479–5491. doi:10.2147/OTT.S233906



## OPEN ACCESS

## EDITED BY

Jianbin Bi,  
The First Hospital of China Medical  
University, China

## REVIEWED BY

Peng Xu,  
Northern Theater Command, China  
Xuebo Qin,  
Hebei Chest Hospital, China

## \*CORRESPONDENCE

Zhifeng Yan

✉ yanzhifeng2002@163.com

Yuanguang Meng

✉ meng6512@vip.sina

RECEIVED 03 June 2024

ACCEPTED 14 August 2024

PUBLISHED 05 September 2024

## CITATION

Wu D, Li M, Wang M, Yan Z and Meng Y  
(2024) PCAF acetylates AIB1 to form a  
transcriptional coactivator complex to  
promote glycolysis in endometrial cancer.  
*Front. Oncol.* 14:1442965.  
doi: 10.3389/fonc.2024.1442965

## COPYRIGHT

© 2024 Wu, Li, Wang, Yan and Meng. This is an  
open-access article distributed under the terms  
of the [Creative Commons Attribution License](#)  
(CC BY). The use, distribution or reproduction  
in other forums is permitted, provided the  
original author(s) and the copyright owner(s)  
are credited and that the original publication  
in this journal is cited, in accordance with  
accepted academic practice. No use,  
distribution or reproduction is permitted  
which does not comply with these terms.

# PCAF acetylates AIB1 to form a transcriptional coactivator complex to promote glycolysis in endometrial cancer

Di Wu<sup>1</sup>, Mingxia Li<sup>2</sup>, Mingyang Wang<sup>2</sup>, Zhifeng Yan<sup>2\*</sup>  
and Yuanguang Meng<sup>1,2,3\*</sup>

<sup>1</sup>School of Medicine, Nankai University, Tianjin, China, <sup>2</sup>Department of Obstetrics and Gynecology, The First Affiliated Center of Chinese People's Liberation Army (PLA) General Hospital, Beijing, China, <sup>3</sup>Department of Obstetrics and Gynecology, The Seventh Medical Center of Chinese PLA General Hospital, Beijing, China

**Introduction:** Despite rapid advances in molecular biology, personalized molecular therapy remains a clinical challenge for endometrial cancer due to its complex and heterogeneous tumor microenvironment. Based on clinical findings, AIB1 is a marker molecule for poor prognosis in endometrial cancer and may serve as a potential therapeutic target. Moreover, it is well known that aerobic glycolysis plays an important role in tumor energy metabolism. It has been previously reported in various hormone-related tumor studies that AIB1 affects glycolysis and promotes tumor development. However, the link between AIB1 and aerobic glycolysis in estrogen-dependent endometrial cancer remains unclear.

**Methods:** We used two endometrial cancer cell lines to validate the high expression of target genes and the effect on the proliferative and invasive capacity of the tumors and verified the pattern of interactions and epigenetic modifications by CHIP and CO-IP techniques. Finally, the conclusions were validated on homozygous mice

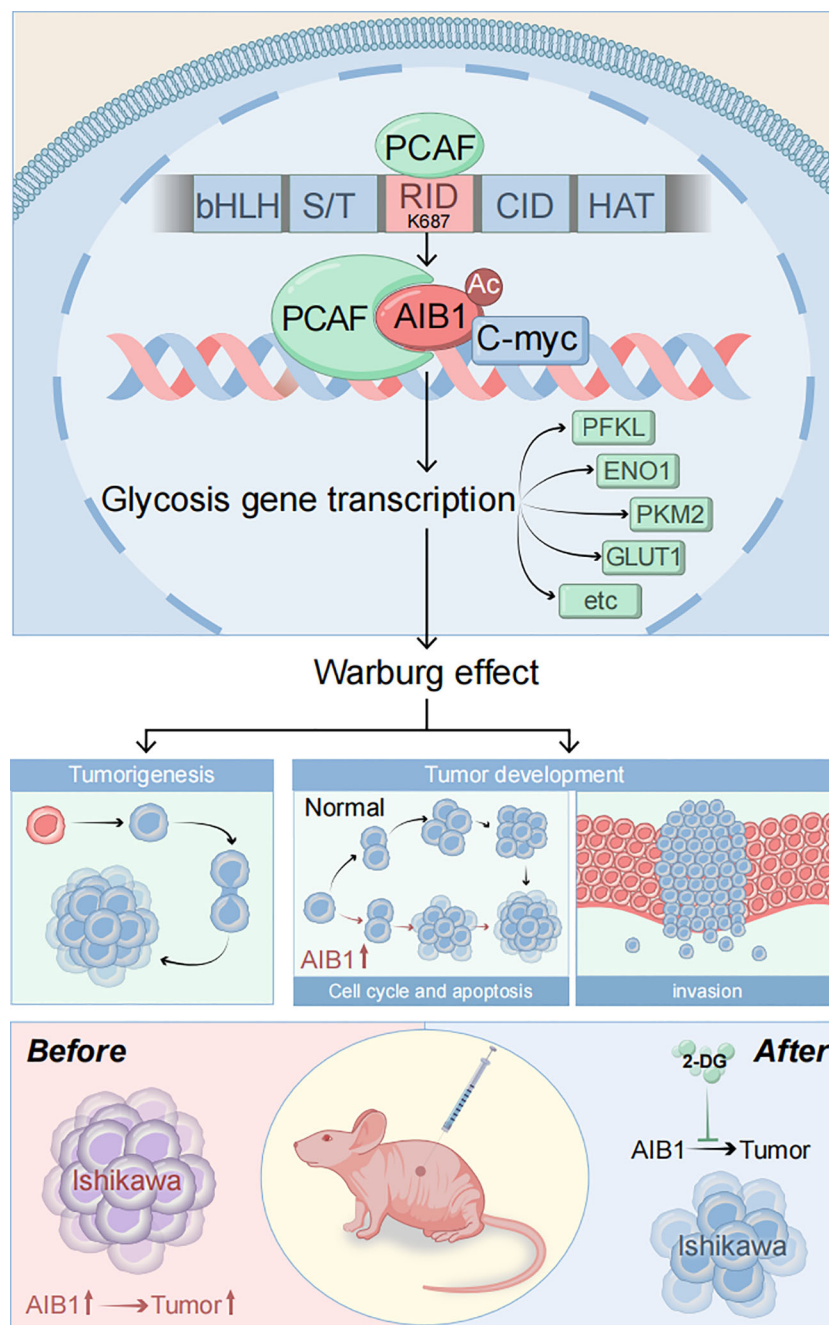
**Results:** In this study, we investigated the transcriptional co-activation functions of AIB1, including its acetylation by PCAF, binding to the c-myc transcription factor, and recruitment of glycolysis-related gene promoters.

**Discussion:** Our findings provide new clues that perturbation of normal homeostatic levels of AIB1 is linked with endometrial cancer. These findings suggest that targeting AIB1-mediated regulation of aerobic glycolysis may offer a novel therapeutic approach for endometrial cancer with high AIB1 expression, opening new avenues for personalized diagnostics and treatment strategies in this disease.

## KEYWORDS

endometrial cancer, aerobic glycolysis, amplified in breast cancer 1, P300/CBP-associated factor, molecular target





GRAPHICAL ABSTRACT

## 1 Introduction

Endometrial cancer is one of the most common gynecological malignancies worldwide, and it ranks sixth in incidence among female malignant tumors globally in global cancer statistics 2020 (1). Furthermore, 66,200 new cases of EC and 13,030 EC-related deaths in the US were estimated for 2023 (2). However, in emerging economies like China, the incidence of endometrial cancer has been rising significantly in recent years and trending toward a younger patient population (3). For example, a 2022

study found that the incidence of endometrial cancer in China has been increasing by approximately 3% annually. This calls for an active search for optimized cancer control strategies, especially in developing countries experiencing rapid social and economic changes. Early diagnosis and precise prognostic assessment are particularly effective ways to control endometrial cancer. In conjunction with current developments in molecular biology, individualized diagnosis and treatment based on molecular markers need to be integrated into existing health plans in order to cope with complex endometrial cancers that are

increasingly exposed globally or for which treatment options are still limited.

Therefore, studying the mechanisms underlying endometrial cancer development and identifying key regulatory molecules are crucial for promoting early diagnosis, understanding individualized differences, and achieving precise treatment to improve prognosis. Energy metabolism disorder is an important mechanism for tumor occurrence and development. German biochemist Otto Warburg discovered that tumor cells primarily obtain energy through glycolysis, even under conditions of sufficient oxygen supply—a phenomenon known as “aerobic glycolysis” or the “Warburg effect”. (4). Glycolysis plays a vital role in various pathological processes associated with cancer (5). Active glycolysis improves the tolerance of tumor cells to ischemia and hypoxia conditions and avoids apoptosis caused by the inhibition of oxidative phosphorylation; secondly, tumor cells can utilize the intermediates of glycolysis or provide raw materials for anabolism through upregulation of the pentose phosphate pathway to satisfy the rapid proliferation of tumor cells. Thirdly, abnormal alterations in the function of key enzymes involved in gluconeogenesis can often lead to tumorigenesis. Additionally, the accumulation of lactic acid, the end product of aberrant glucose metabolism in tumors, can create an acidic local environment that disrupts the cellular matrix and promotes tumor invasion.

Emerging evidence indicates that the glycolytic processes of tumor cells, and the key regulatory factors, represent promising targets for cancer diagnosis and treatment. (6–8). Amplified in breast cancer 1 (AIB1), as a member of the steroid hormone receptor co activator family (SRC), interacts with multiple transcription factors to enhance their transcriptional activity. Studies have shown that the overexpression of AIB1 can affect various signaling pathways by promoting glycolysis, thereby initiating the development of diverse cancers, including breast, colorectal, and liver. (9–11). The posttranslational modification of AIB1, such as acetylation by the histone acetyltransferase PCAF, is crucial for regulating its protein expression and activity. PCAF can acetylate non-histone substrates, including AIB1, p53, and NF- $\kappa$ B, and participate in various cellular processes like proliferation, differentiation, apoptosis, and DNA damage repair. (12–14).

However, the interaction site of PCAF and AIB1 and the molecular mechanism of whether they can affect tumorigenesis and development through regulation of glycolytic metabolism remain unclear. Therefore, this study aims to elucidate how acetylation of AIB1 by PCAF promotes aerobic glycolysis and proliferation in endometrial cancer.

## 2 Materials and methods

### 2.1 Cell lines and cell culture

HEC-1A and Ishikawa cells were cultured in DMEM. The HEC-1A cell was obtained from the Academy of Military Medical Sciences and was free of mycoplasma contamination. Ishikawa was obtained from Cellverse Company (article number: iCell-h113) in Shanghai. Cell lines were validated using the short tandem repeat (STR)

method. All media were supplemented with 10% fetal bovine serum and 1% penicillin–streptomycin. All cells were cultured at 37°C in an atmosphere containing 5% CO<sub>2</sub> and 70%–80% humidity.

### 2.2 Clinical samples

A total of 112 patients suffering from endometrial cancer who have accepted standard surgery were obtained from the First Affiliated Hospital of PLA General Hospital prior to the study. All of the samples were embedded in paraffin. These patients did not undergo any therapeutic intervention before surgery. Two senior pathologists from the hospital's pathology department examined all pathological tissue in accordance with World Health Organization standards.

### 2.3 siRNAs and plasmids

Oligonucleotides of siRNA targeting NCOA3 and PCAF respectively, and control siRNA were produced by JTS Scientific (Wuhan, China). The sequences are presented in [Supplementary Table 1](#). Cells were transfected with the siRNAs at a final siRNA concentration of 50 nM using Lipofectamine 2000 (Invitrogen), according to the manufacturer's instructions. The human pcDNA3.1-Myc-NCOA3 plasmid was purchased from Gene-bio (Henan, China). The human pcDNA3.1-Flag-PCAF plasmid was a gift from Professor Xiaojie Xu at Academy of Military Medical Sciences. DNA sequencing and enzyme digestion identification were performed to confirm plasmids integrity and accuracy.

### 2.4 Construction of stable knockdown and overexpression cell lines

Firstly, overexpression and knockdown constructs were generated using the lentiviral backbone vector pLVX-CMV-puro and the shRNA vector SHC201-u6-puro, respectively. Secondly, pspax2 and pMD2G were selected as auxiliary plasmids to form the lentiviral packaging system. Thirdly, 293t adherent cells were prepared with a convergence rate of 70% and the plasmids transfected in a 4:3:1 ratio. After 72 h, the lentiviral supernatant was collected, the viral titer was determined by fluorescence microscopy, and the virus was stored at –80°C for future use. Finally, the Ishikawa and HEC-1A cell lines were infected with the lentivirus, and stable knockdown cell lines were selected using puromycin.

### 2.5 RNA extraction and quantitative reverse transcription polymerase chain reaction

The TRIzol reagent (Invitrogen) was used to extract total RNA from cells in accordance with manufacturer instructions, and PrimeScript RT reagent kit (Vazyme, Nanjing, China) was used to transform RNA to cDNA. Quantitative RT-PCR (qRT-PCR) was performed on a CFX96 Dice<sup>TM</sup> real-time PCR system (Bio-Rad

Laboratories, Inc., CA) using Taq Pro Universal SYBR qPCR Master Mix (Vazyme, Nanjing, China). Each sample was run in triplicates. The sequence of primers used in the study are presented in [Supplementary Table 2](#).

## 2.6 Western blotting

Proteins were extracted from cells with the addition of protease inhibitors to prevent degradation during the lysis process. Protein concentrations were then quantified using the BCA method to ensure accurate results. Target proteins were separated via SDS-PAGE electrophoresis, followed by incubation with primary and secondary antibodies. The specific protein antibodies involved in this study include DYKDDDDK Tag Monoclonal Antibody (FG4R) (Invitrogen, MA1-91878); Myc Tag Antibody (PA1-981); c-Myc Antibody (MA1-980); PCAF Antibody (703379); and AIB1 Antibody (MA5-15898).

## 2.7 Cell proliferation

The CCK-8 and colony formation assays were utilized to assess cell viability and proliferation. For the CCK-8 assay, cells were seeded in six-well plates and incubated with the experimental conditions. After the desired timepoint, the CCK-8 reagent was added and the absorbance at 450 nm was measured using a spectrophotometer, which correlates with the number of viable cells. For the colony formation assay, cells were seeded, treated with experimental conditions, and then incubated to allow colony formation. The colonies were then fixed, stained with methylene blue, and quantified.

## 2.8 Cell cycle and apoptosis

Cells were synchronized, fixed, and permeabilized to preserve cellular structures and DNA integrity. The cells were then stained with propidium iodide (PI) and subjected to flow cytometry analysis to assess cell cycle distribution. Annexin V staining was also performed to detect apoptosis.

## 2.9 Migration and invasion assays

For the Transwell migration assay, cells are seeded in the top chamber of a Transwell insert with a porous membrane, whereas the bottom chamber contained serum-containing medium. After incubation, the cells on the top or bottom of the membrane were fixed, stained, and quantified using image analysis. The invasion assay was similar, but the membrane was coated with Matrigel to assess the cells' invasive capacity.

## 2.10 Coimmunoprecipitation assay

Starting by lysing the cells to obtain the supernatant, the indicated antibody was added for incubation overnight with

shaking at 4°C. The next morning, washed Protein A/G magnetic beads were added to the antigen-antibody complex system for continued incubation. Sediment was centrifuged and retained. After washing three times with IP washing buffer, loading buffer was added to the complex system and denatured at 100°C for 10 min. Then, the samples were subjected to immunoblot analysis.

## 2.11 Chromatin immunoprecipitation

The first step was to fix  $2 \times 10^6$  cells/ml with 1% formaldehyde for 10 min at room temperature. Glycine (0.125 M) was added immediately to quench for 8 min at 37°C and wash three times with PBS. Next, the nuclei were extracted after ultrasonic disruption. The third step was to incubate overnight at 4°C with an anti-c-Myc antibody or IgG, along with Protein A/G magnetic beads. Afterward, washing complexes with high-salt solutions, purified DNA was obtained for subsequent quantitative PCR (qPCR) analysis. The primer sequences for the glucose metabolism related gene promoter are provided in [Supplementary Table](#).

## 2.12 Immunoblotting

Endometrial cancer tissue chips containing 37 patients were purchased from Ximin Trading company (Qingdao, China), and Jiankun Herun Technology Company (Beijing, China) was commissioned to provide immunohistochemical testing services.

## 2.13 Cellular energy metabolism assays

Mammalian cells have two key energy metabolism pathways, aerobic respiration and glycolysis. Aerobic respiration takes place in the cytoplasm and mitochondria, and the process of consuming oxygen drives the cell to oxidize and break down the nutrient substrates (sugars, lipids, proteins) and release energy to synthesize large amounts of ATP, so the mitochondria are also known as the “energy factory” of the cell. Glycolysis occurs in the cytoplasm of cells and is an anaerobic decomposition process that mainly breaks down glucose into lactic acid and produces small amounts of ATP. Glycolysis and oxidative phosphorylation are two key energy-producing pathways in cells. Most cells have the ability to switch between these two pathways, adapting to changes in their environment.

Extracellular acidification rate (ECAR) and oxygen consumption rate (OCR) were measured with a XFe96 Analyzer. Briefly, cells digested to a density of  $1 \times 10^4$ /well were seeded in XFe96 assay plates (Agilent Technologies, Santa Clara, CA, USA) and were then placed in an incubator of 37°C and 5% CO<sub>2</sub> for 24 h. Simultaneously, an XFe96 cartridge was hydrated the day prior to the XF assay. Then, XF Real Time ATP Rate Assay Medium was prepared and warmed to 37°C at the day of assay. Next, the cell culture plate was retrieved from the CO<sub>2</sub> incubator and the cells' state was viewed. Around 1 h before detection,

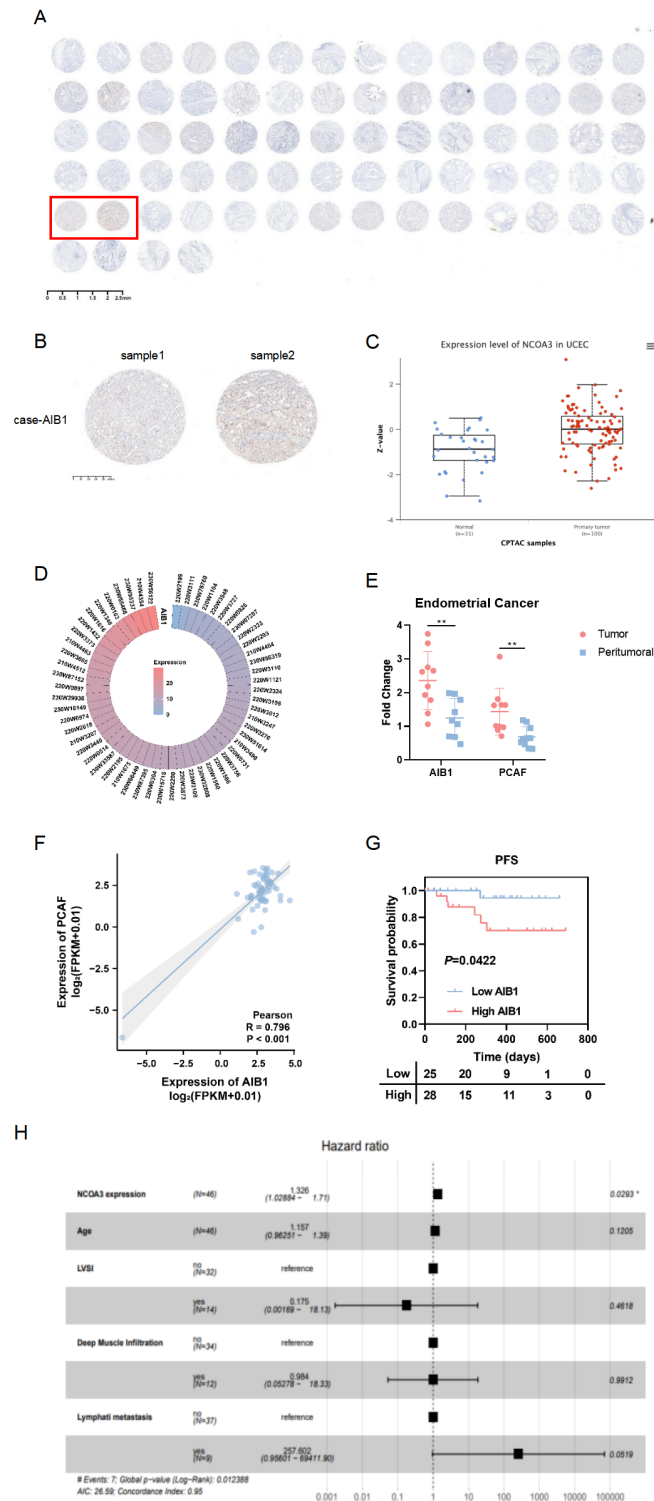


**FIGURE 1**  
AIB1 is enriched and predicts outcome in endometrial cancer. **(A)** Tumor tissue microarrays containing 74 loci from 37 endometrial cancer patients. Also, immunohistochemistry (IHC) protein analysis of AIB1 was completed in the above samples. **(B)** Results of applying IHC to detect AIB1 expression at different sites of tumor tissues of the same patient. **(C)** High AIB1 expression is associated with poor prognosis in tumor patients according to CPTAC database information. **(D)** Heat map of AIB1 expression in clinical endometrial cancer patients detected by application of second-generation gene sequencing technology. **(E)** There were 10 endometrial cancer patients with good concordance selected to compare the expression of AIB1 and PCAF in tumor and paracancerous tissues using RT-PCR assays. **(F)** Positive correlation between PCAF and AIB1 expression based on genetic testing of clinical patients. **(G)** Kaplan–Meier analysis of progression-free survival (PFS) according to mRNA expression of AIB1 in clinical patients (n = 112). Blue dots represent patients with low AIB1 expression, and red dots represent patient with high AIB1 expression. **(H)** Multifactorial survival analysis of 112 endometrial cancer tissues from clinical samples using PFS as the primary outcome indicator. High AIB1 expression is an independent prognostic influencer in endometrial cancer patients (P=0.0293). (\*P<.05, \*\*P<.01, \*\*\*P<.001).

culture medium was replaced by XF Real-Time ATP Rate Assay Medium (Agilent Technologies). Subsequently, the cells were treated sequentially with 1  $\mu$ M of glucose, 1  $\mu$ M of oligomycin (ATP synthase inhibitor), and 0.5  $\mu$ M of 2-DG (the glycolytic inhibitor) at time points for measurement of ECAR. For OCR, once all required ports were filled with drugs, the cartridge and utility plate were transferred to the XFe96/XF96 instrument and cartridge calibration was started using the assay template created before.

## 2.14 Animal studies

We purchased 30 BALB/c nude mice (female, 4–5 weeks old, 16–18 g in body weight) from Vital River Company (Beijing, China) and randomly assigned them to six groups ( $n = 5$  per group). Each group of mice was placed in a cage for feeding. The mice were housed at the specific pathogen-free (SPF) facility following the principles of animal welfare strictly. The animal experiment was divided into six groups: the control group compared with

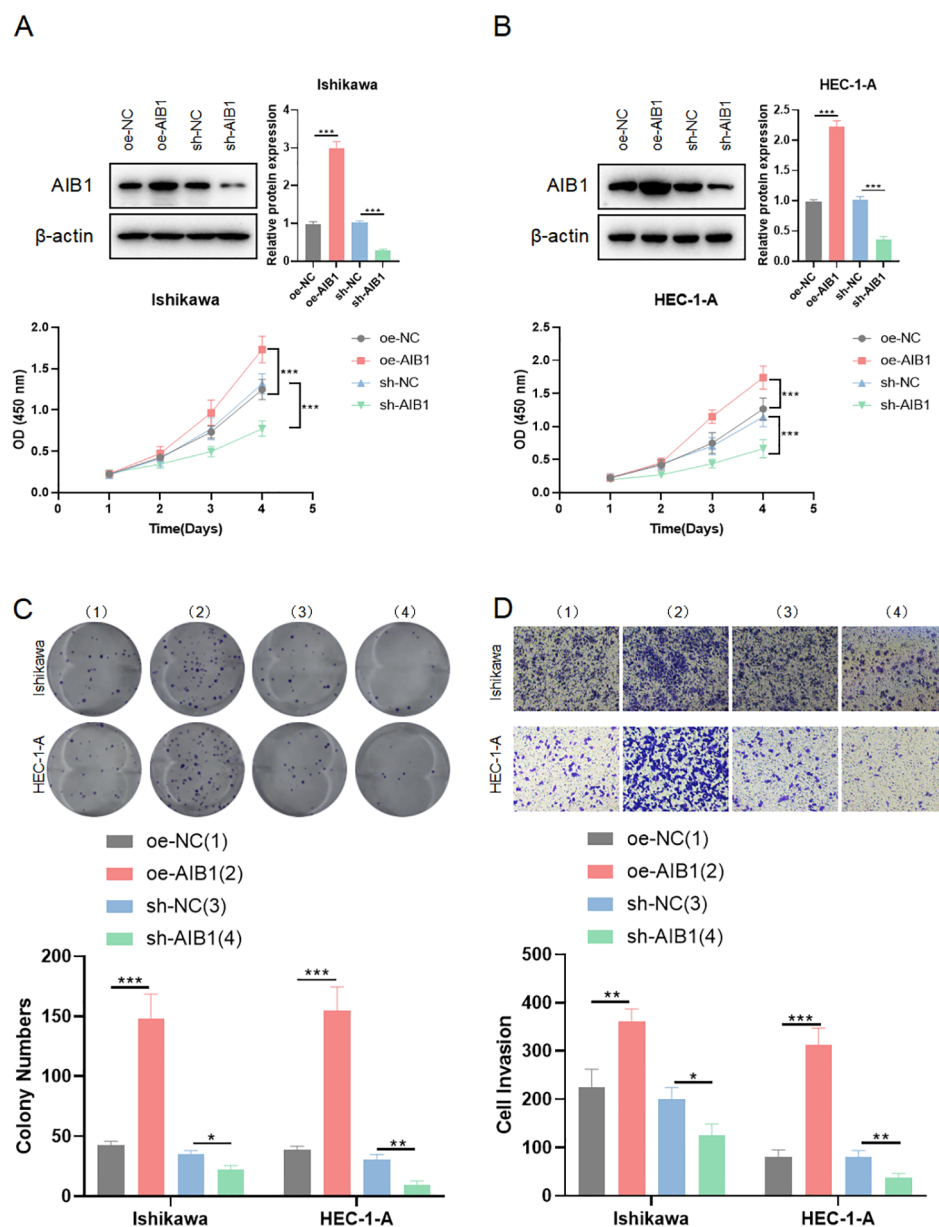


FIGURE 2

AIB1 affects endometrial cancer cell proliferation and infiltration. (A, B) Cells were transfected with either sh-NC and oe-NC or sh-AIB1 and oe-AIB1. Cell proliferation was measured after 5 days. Graphs display absorbance measured at 450 nm using an enzyme meter in Ishikawa (A) and HEC-1-A (B). (C) Colony forming assay was carried out with cells treated with either sh-NC and oe-NC or sh-AIB1 and oe-AIB1 for a total of 14 days. Representative images of the cells stained with crystal violet at day 14. Graph displays colony numbers in different conditions in two cell lines. All experiments are representative of three biologically independent replicates. Two-sided t-tests were used to calculate P values (\*\*\* $P \leq 0.001$ , \*\* $P \leq 0.01$ , \* $P \leq 0.05$ ). (D) Transwell assay was performed to assess the migration ability of Ishikawa and HEC-1-A cells. The grouping and replications were the same as in the colony forming assay.



overexpression, the AIB1 overexpression group, the AIB1 overexpression and administration of 2-DG group, the control group compared with knockdown, the AIB1 knockdown group, and the AIB1 knockdown and administration of 2-DG group. The administration method of 2-DG is intraperitoneal injection of 500 mg/kg. A tumor-bearing mouse model was established by

subcutaneously injecting 100  $\mu$ l of the transfected cells into the mice. Tumor volume was measured using a vernier caliper every 4 days and quantified using the following formula: Volume ( $\text{mm}^3$ ) = length  $\times$  width<sup>2</sup>/2. After 28 days' measurement or humane end point, the mice were sacrificed. Subsequently, the tumors were isolated from all mice.

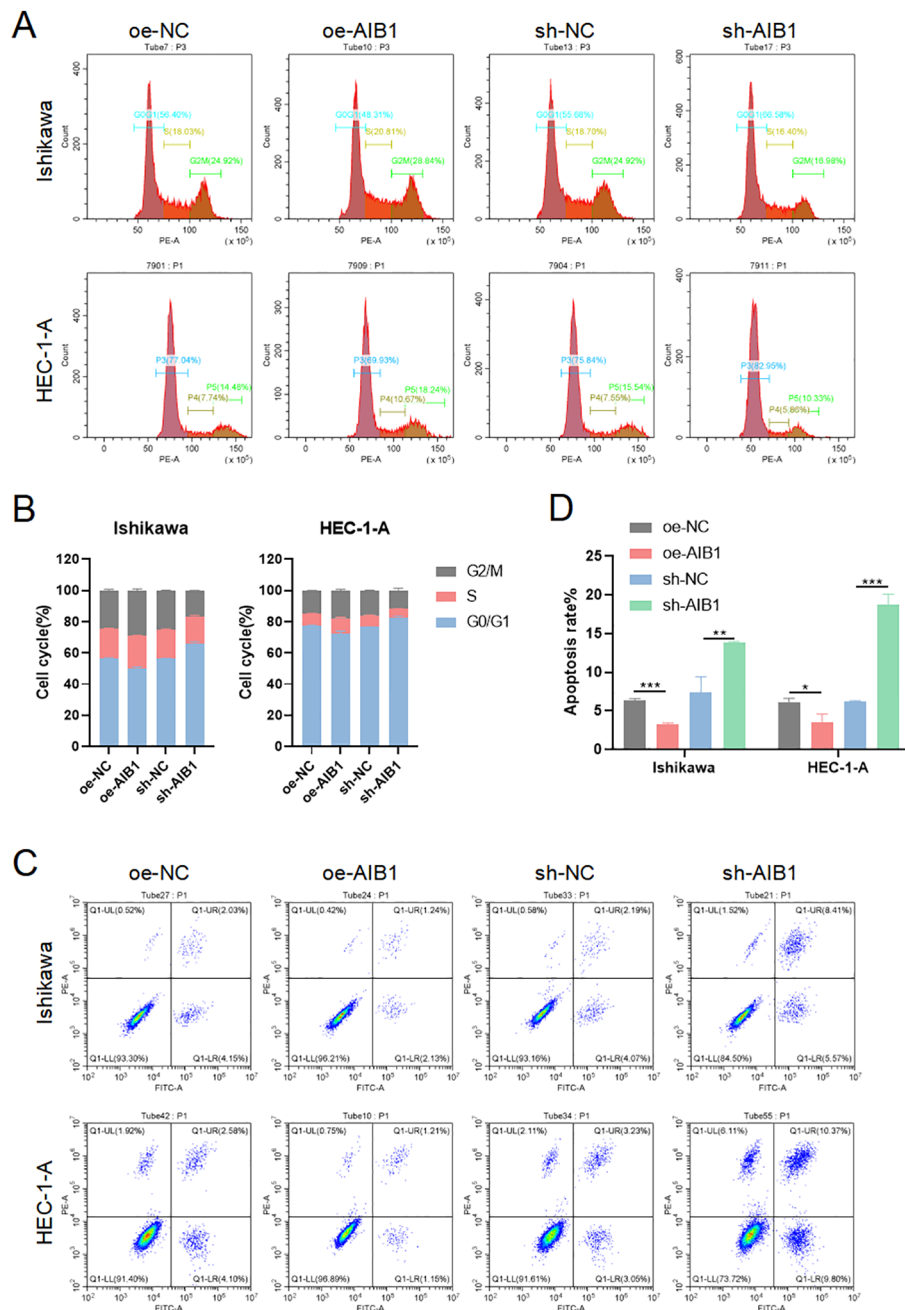


FIGURE 3

AIB1 induces cell cycle and disrupts apoptosis. (A) The effect of AIB1 knockdown and overexpression on the EC cell cycle. (B) AIB1 knockdown increased the proportion of cells in the G1 phase in both EC cell lines. (\* $P < .05$ , \*\* $P < .01$ , \*\*\* $P < .001$ ). (C) Endometrial cancer cell apoptosis was detected by flow cytometry analysis. (D) The graph displays the apoptosis rate of both Ishikawa and HEC-1-A cell lines. Compared with the NC control group, cells treated with the AIB1 knockdown apoptotic index were significantly higher. In opposite, high AIB1 expression disrupts regular programmed cell death.

## 2.15 Bioinformatics analysis

We retrieved expression data and clinical information from the Department of Obstetrics and Gynecology of the First Medical Center of the General Hospital of the Chinese People's Liberation Army. The LIMMA package was used to identify DEGs between good and poor prognosis endometrial cancer tissue samples. An adjusted  $P < 0.05$  and an absolute  $\log_2 FC > 1$  were considered statistically significant. To determine the potential biological processes and pathways of the overlapping DEGs, ingenuity pathway analysis (IPA, [www.qiagen.com/ingenuity](http://www.qiagen.com/ingenuity)) (accessed on 03 July 2020) and protein interaction network was performed, with  $P < 0.01$  and absolute  $\log_2 FC > 1$  as the threshold values.

## 2.16 Statistical analyses

GraphPad Prism 8.4.2 was used for data analysis. Data were expressed as mean  $\pm$  SD. Comparisons between two groups were performed by T-test, comparisons among multiple groups were performed by one-way ANOVA. P-values  $< 0.05$  indicate statistical significance. \* represents  $0.01 < P \leq 0.05$ , \*\* represents  $0.001 < P \leq 0.01$ , \*\*\* represents  $P < 0.001$ .

## 3 Results

### 3.1 AIB1 is a novel oncogene and associated with poor prognosis

Consistent with the Clinical Proteomic Tumor Analysis Consortium (CPTAC) analysis (Figure 1C), tissue microarray (Ximin Trading Company) results from 37 patients with endometrial cancer showed that AIB1 was highly expressed in tumor tissue, as well as in the nucleoplasm and cytoplasm (Figures 1A, B). AIB1 gene expression was detected correspondingly in 57 clinical samples sourced from the General Hospital of the People's Liberation Army (PLA), as shown in Figure 1D. Tissue samples from 10 of these patients were randomly selected and tested for central and paracancerous AIB1 and PCAF expression. It was found that both molecules were significantly more highly expressed in the tumor compared with the paraneoplastic tissue, and the difference was statistically significant ( $P < 0.01$ ) (Figure 1E). Moreover, a positive correlation was found between AIB1 and PCAF expression in Figure 1F ( $R = 0.796$ ,  $P < 0.001$ ). Subsequently, long-term follow-up of 112 endometrial cancer patients with complete genomic and transcriptomic molecular information in our institution showed that high AIB1 expression predicted poor prognosis ( $P = 0.042$ ) (Figure 1G). In addition, high AIB1 expression was also confirmed to be an independent risk factor for shorter progression-free survival by a multifactorial prognostic analysis ( $P = 0.029$ ) (Figure 1H).

### 3.2 AIB1 promotes tumor proliferation and invasion

To investigate the impact of AIB1 on EC cell line growth and proliferation, AIB1 overexpression and knockdown efficiency were confirmed by immunoblotting experiments. Next, the effects of AIB1 overexpression and knockdown status on cell proliferation viability were verified using two cell lines, HEC-1A and Ishikawa, respectively. The results showed that AIB1 overexpression significantly increased tumor proliferation capacity. Conversely, the effect was significantly weakened in knockdown (Figures 2A, B). Then, plate cloning experiments again verified the proto-oncogene function of AIB1, confirming that tumor cells highly express the gene and promote tumor growth ( $P < 0.001$ ). Conversely, knocking down the gene inhibits tumor growth ( $P < 0.05$ ) (Figure 2C). In addition, the results of the invasion assay showed that overexpression of AIB1 significantly enhanced the migratory infiltration ability of tumor cells ( $P < 0.01$ ) and vice versa ( $P < 0.05$ ) (Figure 2D). The differences were all statistically significant.

### 3.3 AIB1 affects cell cycle and programmed death processes

The cell cycle is a highly regulated process that controls the growth and division of cells at the appropriate times and in the correct manner. It is divided into distinct phases to perform a series of events, each with specific functions and checkpoints to ensure accurate replication and division (15). Cells in G1 phase grow in size, synthesize proteins, and prepare for DNA replication. Immediately following the replication of the cell's genetic material occurs in the S phase. The G2 phase is a period of growth and preparation for cell division (16). The mitosis phase encompasses the process of dividing the duplicated DNA and cellular contents into two daughter cells. To investigate whether growth inhibition upon AIB1 depletion is related to alterations in the cell-cycle profile of EC cells, we analyzed cellular DNA content with flow cytometry. As shown in Figures 3A, B, AIB1 knockdown in Ishikawa and HEC-1A cells induced G1 arrest. Overexpression of the proto-oncogene AIB1 affects cell cycle regulation, thereby disrupting the normal regulation of cell growth and division, leading to uncontrolled cell division and cancer development. Consistently, we also observed that the percentage of cells in the G1 phase decreased concurrently with an increased percentage in the S phase.

Apoptosis, the best-known form of programmed cell death, is a key physiological mechanism for limiting the expansion of cell populations, both to maintain tissue homeostasis and to remove potentially deleterious cells, such as those with persistent DNA damage (17). Loss of apoptosis can allow the survival and accumulation of abnormal cells, promoting tumor initiation. Impaired apoptosis can also contribute to tumor progression and metastasis. Cancer cells often acquire resistance to apoptosis, which enables them to evade cell death signals and survive in adverse conditions. The results of the present study show that AIB1-

overexpressing endometrial cancer cell lines disrupt a regulated and evolutionarily conserved cell death program. However, when knocking down the AIB1 gene, cells activate apoptosis as an important tumor suppression strategy (Figures 3C, D).

### 3.4 AIB1 influences tumor occurrence and development by glycolysis

Given the crucial role of energy metabolism in cancer, we investigated whether AIB1 could influence tumorigenesis and progression through its impact on glycolysis, a key metabolic pathway in cancer cells. We previously successfully identified AIB1 as a prognostic differentially expressed gene using second-generation sequencing based on a grouping of endometrial cancer clinical samples with follow-up prognosis. Next, we analyzed the two groups of differentially expressed genes to form a volcano map based on the level of AIB1 expression (Figure 4A). Meanwhile, genes involved in glucose metabolism were screened to be closely related to AIB1 (Figure 4B). Moreover, the key proteins in the glycolysis process related to AIB1 were associated through a PPI network (Figure 4C). Immediately afterward, the differential gene enrichment analysis revealed that the high expression of AIB1 was associated with glucose metabolism and cell proliferation pathway (Figure 4D).

To determine the functional relevance of AIB1-mediated glycolysis, we performed rescue experiments by inhibiting glycolysis using a specific inhibitor, such as 2-deoxyglucose (2-DG). We found that the inhibition of glycolysis significantly attenuated the proliferative advantage conferred by AIB1 overexpression in two EC cell lines ( $P < 0.001$ ), suggesting that AIB1 promotes tumorigenesis and progression, at least in part, through enhanced glycolytic metabolism. In Figures 4E, F, it was shown that 2-DG can significantly reverse AIB1 promotion of abnormal cell proliferation. Correspondingly, knockdown of AIB1 significantly attenuated the effect of glycolysis on cell viability. The results of the EDU assay were consistent between the two cell lines (Figures 4G, H). In addition, the results of the extracellular acidification assay (ECAR) and oxidative phosphorylation assay (OCR) confirmed that high expression of AIB1 promotes tumor glycolysis (Figures 4I, J).

### 3.5 PCAF acetylates AIB1 at K687 and binds as a transcriptional coactivator complex

AIB1 (amplified in breast cancer 1), also known as SRC-3 (steroid receptor coactivator 3), is a transcriptional coactivator protein that plays a crucial role in regulating gene expression. It consists of several distinct structural components including the following. N-terminal basic helix-loop-helix-Per/ARNT/Sim (bHLH-PAS) domain involved in DNA binding and heterodimerization between proteins containing these motifs is the most conserved region among SRC family members (18). The nuclear receptor interacting domain (RID) immediately following the serine/threonine-rich region (S/T) contains the LXXLL (where L is leucine and X is any amino acid) motif that is important for nuclear receptor binding. The intrinsic transcriptional

activation domain (AD), which is responsible for interacting with the general transcriptional coactivator CBP/p300, is located at the c-terminus of the SRC molecule receptor interaction domain (19). Furthermore, the AIB1 C-terminal HAT structural domain may be involved in chromatin remodeling and assembly of the peripromoter transcription machinery during nuclear receptor-directed transcription initiation. The five functional domains of AIB1 are shown in Figure 5A. However, its importance in AIB1 transcriptional activation when considering activity remains to be clarified.

Previous studies have shown that posttranslational modifications of the AIB1 protein are pivotal in the regulation of gene processes (20). Our studies revealed that PCAF co-precipitated with AIB1 in extracts prepared in Ishikawa and HEC-1A cells and that overexpression of PCAF and AIB1 led to acetylation of AIB1 and formation of transcriptional co-activation complexes, which enhanced its transcriptional activity. In order to clarify the specific binding sites, we constructed plasmids with five separate structural domains of AIB1 with a Myc tag and full-length plasmids, respectively, and co-transfected them with Flag-PCAF plasmid in endometrial cancer cell lines, which not only proved the protein interactions but also identified the specific roles of PCAF and AIB1 in the region of amino acids 580–840 by immunoprecipitation (Figure 5B).

Next, based on the fact that PCAF has an acetyltransferase role, we further determined whether PCAF and AIB1 protein interactions are achieved through an acetylated form. We performed co-immunoprecipitation assay and acetylation antibody to confirm that PCAF greatly catalyzes the acetylation of AIB1 (especially in the 580–840 amino acid region) in endometrial cancer cells (Figure 5C). To further validate the acetylation active site of AIB1, we mutated the lysines at positions 616, 619, 620, and 687 to arginine to mimic deacetylation, resulting in an AIB1 acetylase inactivation mutant.

We subsequently found that the acetylation ability of K616, K619, and K620 mutants was similar to that of wild-type AIB1, but the acetylation level of K687 was significantly attenuated in the precipitates of PCAF and AIB1 interaction. These results suggest that PCAF acetylates AIB1 at K687 (Figure 5D).

### 3.6 Co-activation complex regulate downstream glycolysis through c-myc

c-Myc is a transcription factor that plays a critical role in regulating cellular metabolism and promoting tumor growth. It is one of the most commonly deregulated oncogenes in human cancers, and its overexpression or constitutive activation is observed in a wide range of cancer types. (21–23). Therefore, we speculate that AIB1 may induce the glucose metabolism reprogramming by c-myc in the endometrial cancer. In order to further explore the mode and extent of action of AIB1 affecting tumor glycolytic metabolism, we tried to compare the expression of transcription factor c-myc in the transcriptional co-activation complex after overexpression of AIB1 alone versus co-transfection of AIB1 and PCAF plasmid. Fortunately, the results showed that the ability of the transcriptional co-activation complex to bind transcription factors was significantly stronger than the recruitment of AIB1 alone (Figure 6A).

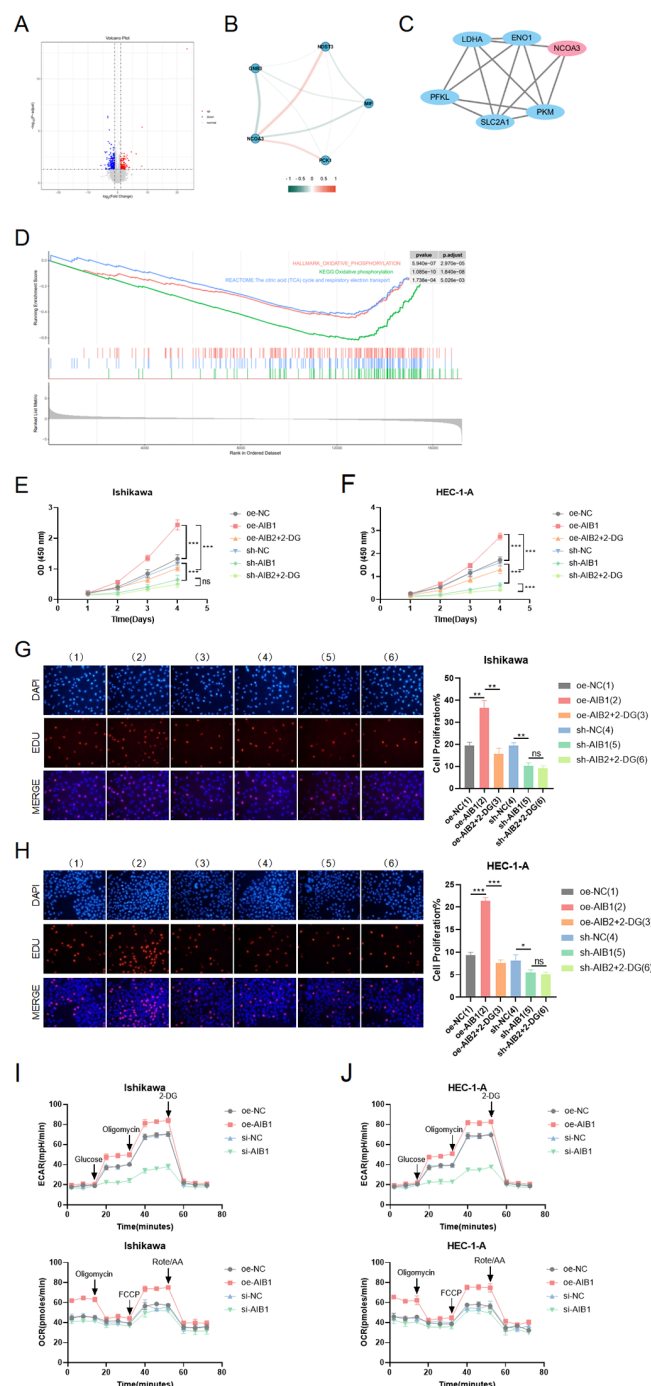
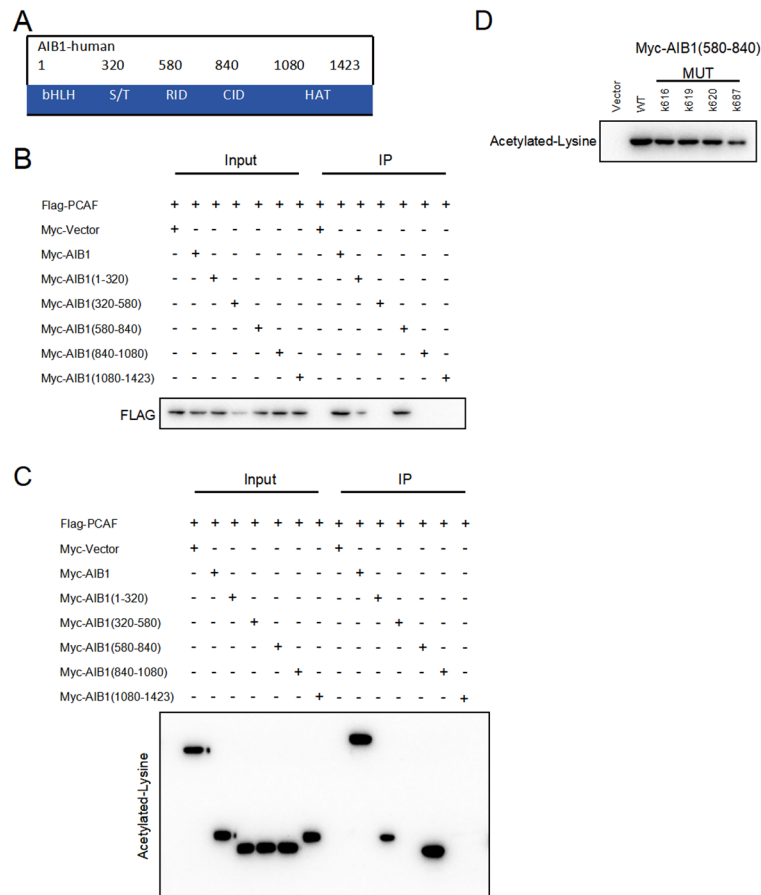


FIGURE 4

Role of AIB1 in tumor glucose metabolism. **(A)** Transcriptomics data from 112 clinical endometrial cancer patients were grouped according to AIB1 expression level, and volcano plots were drawn to compare the two groups of differential genes. Red dots and blue dots represent differential expression (absolute  $\log_2$  fold change  $>1$  and adjusted  $P$ -value  $<0.05$ ), and gray sections are non-significant differential expression. **(B)** The graph shows the interrelationship of differential genes with AIB1 in the volcano map. **(C)** In protein-protein interaction (PPI) network analysis, it was found that AIB1 can directly or indirectly interact with several other glucose metabolism-related genes. Larger nodes represent stronger gene connectivity, and thicker lines indicate more reliable interconnections between genes and higher combined score values. **(D)** GSEA enrichment analysis showed that DEGs were significantly enriched in two glucose metabolism-related pathways, namely, oxidative phosphorylation and the citric acid (TCA) cycle and respiratory electron transport. These two pathways were significantly downregulated in the AIB1 high-expression group compared with the AIB1 low-expression group. In addition, differentially expressed genes were also significantly enriched in pathways mediating cell proliferation, such as the mTOR signaling pathway (KEGG enrichment analysis), the PI3K-Akt signaling pathway (GSEA enrichment analysis), and the PI3K-Akt signaling pathway (GSEA enrichment analysis). **(E, F)** The graphs demonstrate the effect on cell proliferation viability after addition of the glycolysis inhibitor (2-DG). The results were validated simultaneously in two cell lines, respectively. **(G, H)** EdU staining was used to show the effect of 2-DG drugs on cell proliferation in different treatment groups in two cell lines. The results further evaluate that the AIB1 gene affects tumors through glycolysis processes. **(I, J)** The extracellular acidification rate analyses of Ishikawa and HEC-1-A cells stably expressing knockdown control, shAIB1, 2-DG adding to shAIB1 and overexpression control, oeAIB1, 2-DG adding to oeAIB1. The oxygen consumption rate analysis as the above. ns  $P>0.05$ , \* $P<0.05$ , \*\* $P<0.01$ , \*\*\* $P<0.001$ .



**FIGURE 5** PCAF and AIB1 interact and acetylate at K687. **(A)** The AIB1 protein consists of several functional structural domains, including the N-terminal bHLH, the serine/threonine-rich region, and C-terminal transcriptionally active structural domains. **(B)** Co-IP analysis of the interaction of Myc-AIB1 and Flag-PCAF in Ishikawa cells. Flag antibody expression is detected by pulling with Myc-tagged magnetic beads. Results indicate that AIB1 interacts with PCAF through its RID domain (580 aa–840 aa). **(C)** PCAF acetylates the RID functional structural domain of AIB1. The interaction of AIB1 with PCAF was confirmed by the Co-IP assay. **(D)** PCAF acetylation AIB1 at k687.

To next investigate how the transcription activation complex binds to the glycolytic enzymes promoter, which spans –2,000 to –1 (the translation initial site is 0), we performed chromatin immunoprecipitation (ChIP) and qPCR as shown in Figure 6B. The results showed that PCAF/AIB1/c-Myc could pull down the DNA fragment of the PFKL, ENO1, LDHA, PKM2, and GLUT1 promoter region but not PGK1 and HK2 (Figure 6C).

### 3.7 AIB1/glycolysis axis regulates endometrial cancer growth *in vivo*

On the basis of AIB1 regulating tumor proliferation and invasion in EC cells *in vitro*, we constructed the *in vivo* phenotype of the AIB1/glycolysis axis to perform subsequent verification. We examined the effect of the axis on tumor growth by subcutaneously injecting EC cells carrying the construct described in Figure 7 into BALB/c nude mice. There was no significant difference in initial mouse body weight among groups. After the mice developed palpable tumors, they were randomly assigned into 2-DG or PBS in nude mice injected with Ishikawa cells overexpressing or knocking down the AIB1 gene.

Unsurprisingly, overexpression of AIB1 significantly promoted endometrial tumor growth. Moreover, the tumor-promoting effect of AIB1 was significantly attenuated after pharmacological intervention with the glycolysis inhibitor 2-DG (Figures 7A, C). In contrast, when AIB1 was knocked down, tumor growth was inhibited and the effect of 2-DG intervention on tumor growth was not significant (Figures 7B, D).

## 4 Discussion

Endometrial carcinoma (EC) is a highly heterogeneous disease, with diverse etiologies, pathogenesises, clinical features, and molecular characteristics. Recent advancements, spearheaded by the landmark Cancer Genome Atlas (TCGA) project, have ushered in a shift from traditional morphology-based classification to a more nuanced molecular taxonomy of endometrial cancer. This four-subtype system, defined by POLE mutations, microsatellite instability, copy number alterations, and copy-number high tumors, has important prognostic and therapeutic implications (24–27).



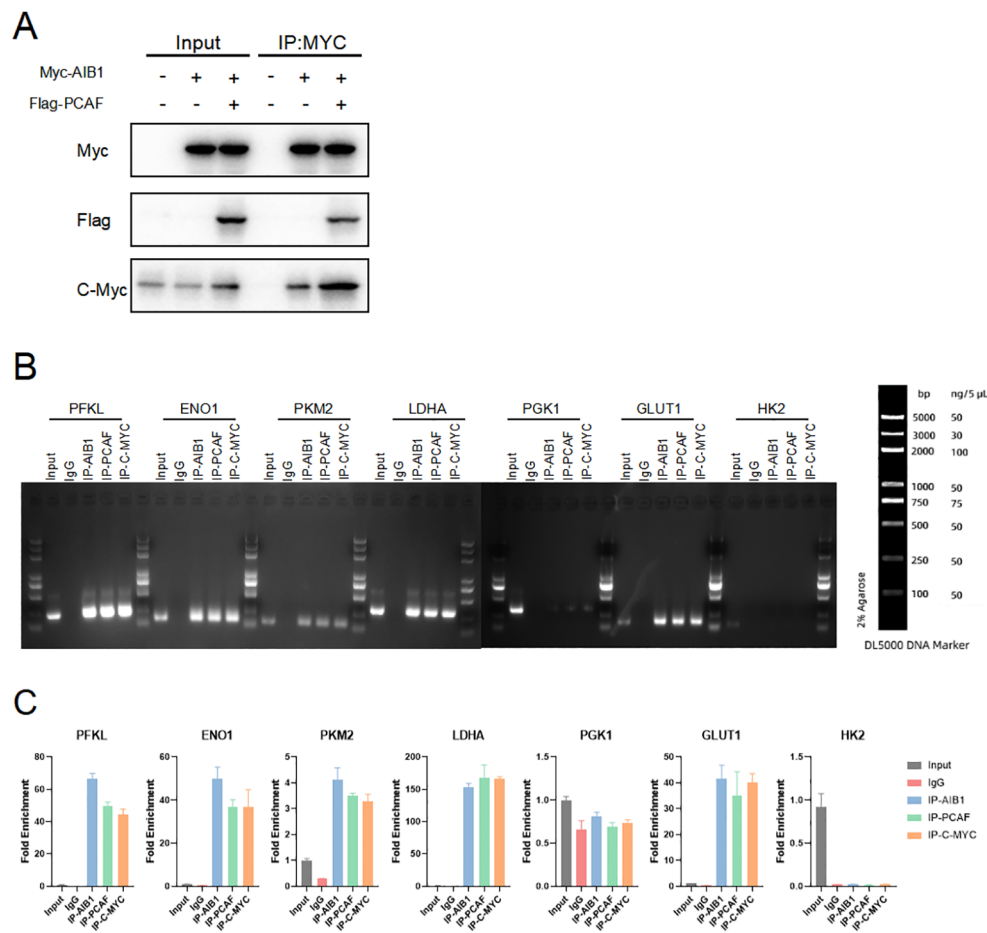


**FIGURE 6** Glycolysis gene expression is regulated by AIB1 and PCAF complex by mediating c-myc transcriptional activity. **(A)** COIP analysis showed that both PCAF and AIB1 could bind to native c-myc alone, but complex formation bound c-myc more pronouncedly. **(B, C)** ChIP analysis of the AIB1 complex and transcription factor occupancy on the indicated glycolytic gene promoters in Ishikawa cells. The graph shows the enrichment of genes relative to input. All data shown are mean  $\pm$  SD of triplicate measurements that have been repeated three times with similar results.

Although there is no precise and effective means to screen and prevent endometrial cancer, endometrial cancer research has transitioned into the molecular era, with a growing focus on understanding the underlying molecular mechanisms driving its development and progression. This shift has allowed for the identification of molecular markers with prognostic significance, providing insights into the heterogeneous nature of the disease and potential therapeutic targets.

The molecule AIB1 (amplified in breast cancer 1), also known as SRC-3 (steroid receptor coactivator 3), has emerged as a promising prognostic marker in endometrial cancer. The AIB1 gene is located on chromosome 20q12 and consists of multiple exons. Previous studies have shown that AIB1 plays a crucial role in hormone signaling and glucose metabolic pathways and is associated with tumor progression, metastasis, and resistance to hormone-based therapies (28, 29). Building upon this molecular framework, our study aimed to elucidate the role of the transcriptional coactivator AIB1 (also known as SRC-3) in endometrial cancer progression and its potential as a clinically relevant biomarker.

Consistent with findings from public databases, our analysis of 66 endometrial cancer patients demonstrated that high AIB1 expression was an independent predictor of poor clinical outcomes. Mechanistically, we found that AIB1 plays a crucial role in promoting aberrant tumor metabolism, specifically by enhancing glycolysis. The acetylation of AIB1 at k687 by the acetyltransferase PCAF forms a transcriptional activation complex that binds to c-Myc, a master regulator of the glycolytic program. This metabolic reprogramming was functionally validated through cell-based assays, wherein the inhibition of glycolysis significantly attenuated the proliferative and invasive capacities of endometrial cancer cells. Notably, knockdown of AIB1 diminished the effects of glycolysis inhibitors, underscoring the central role of this coactivator in regulating these metabolic pathways. In addition, in combination with immunoprecipitation experiments, it was verified that the formation of a transcriptional activation complex between AIB1 and PCAF activates the glycolytic process to a greater extent than AIB1 alone to affect tumor progression.

These findings suggest that AIB1 may serve as a promising prognostic biomarker and a potential therapeutic target in endometrial cancer. Pharmacological strategies aimed at

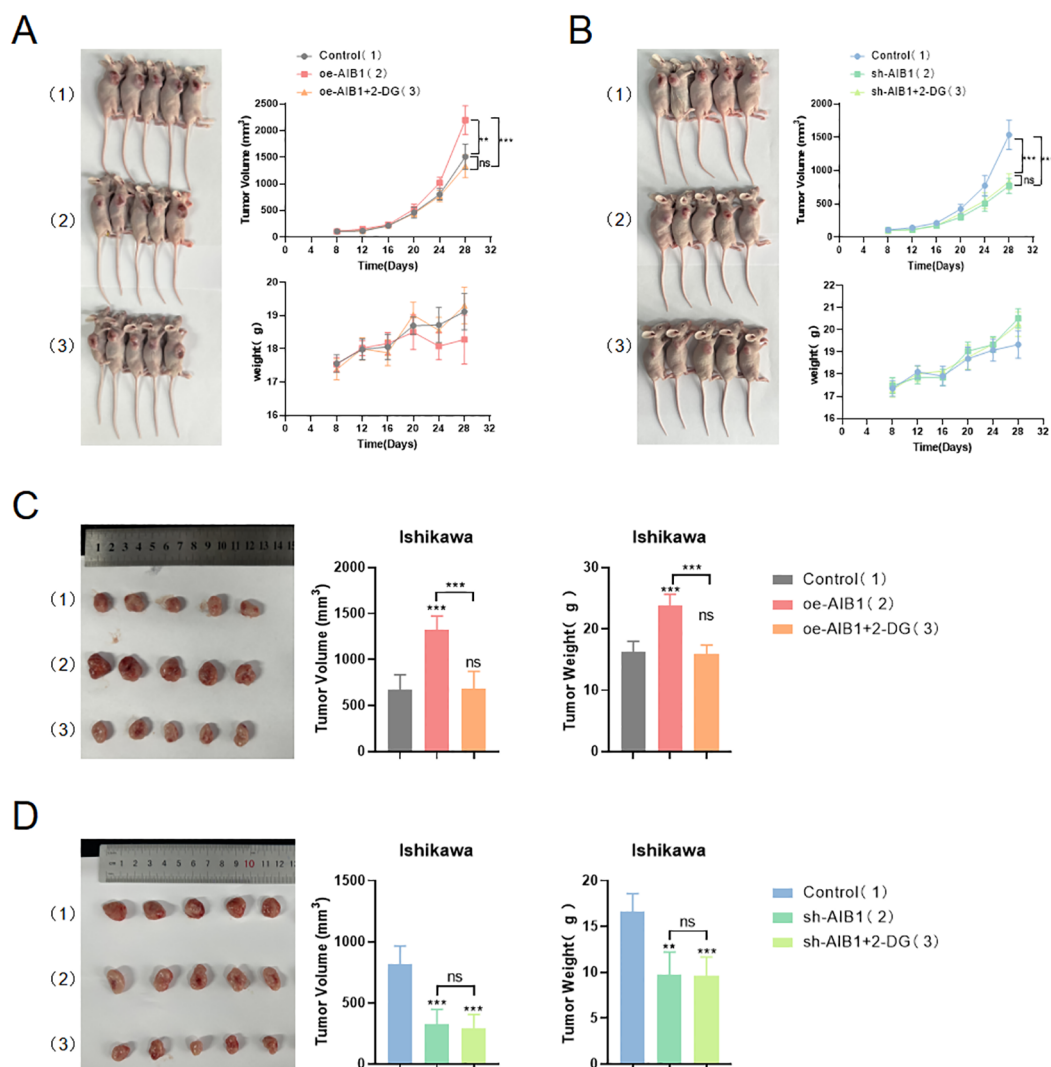


FIGURE 7

AIB1 regulates glycolysis and promotes tumor growth *in vivo*. Mice were randomly assigned to six groups ( $n = 5$  per group) and were injected with vehicle (Control) or overexpression and knockdown AIB1 Ishikawa cells. Then immediately afterward, nude mice were treated with deoxy-d-glucose (2-DG) or equal volume of PBS. The effects of the drug on mouse weight and body tumor measurements are shown by the growth curve (A, B). In addition, the excised tumors, tumor size, and tumor weight are shown (C, D). Data are presented as the means  $\pm$  SEM. ns, No significance.

disrupting the AIB1-driven glycolytic network could hold clinical promise in curtailing disease progression. Whereas our findings provide valuable mechanistic insights into the role of AIB1 in endometrial cancer metabolism and progression, the current study has several limitations that should be acknowledged. The interconnected nature of cancer metabolism involves complex crosstalk between various pathways and interactions with the tumor microenvironment, which were not fully explored in this study (30). The focus on AIB1 and glycolysis may overlook immune microenvironment changing with metabolic reprogramming in endometrial cancer (31, 32). Additionally, our analysis was based on a relatively small patient cohort, and broader validation in larger, more diverse patient populations will be necessary to firmly establish the clinical utility of AIB1 as a prognostic biomarker. Future research should investigate the broader metabolic dependencies and vulnerabilities associated with AIB1

overexpression, as well as evaluate potential combinatorial therapeutic strategies targeting these metabolic alterations.

Despite these limitations, our study lays an important foundation for further exploration of AIB1 as a therapeutic target in endometrial cancer. Key next steps should include the development of specific AIB1 inhibitors and the evaluation of their efficacy in preclinical models and clinical trials. Deeper mechanistic understanding of how AIB1 coordinates transcriptional regulation of glycolytic and other metabolic pathways may also uncover additional druggable vulnerabilities. Integrating AIB1 assessment with comprehensive molecular profiling of endometrial tumors could also help refine patient stratification and guide the selection of tailored treatment approaches. Ultimately, a multifaceted approach combining biomarker development, metabolic targeting, and personalized therapy will be crucial to improving clinical outcomes for endometrial cancer patients.

## Data availability statement

The datasets presented in this study can be found in online repositories. The names of the repository/repositories and accession number(s) can be found in the article/Supplementary Material.

## Ethics statement

The manuscript presents research on animals that do not require ethical approval for their study.

## Author contributions

DW: Data curation, Formal analysis, Methodology, Visualization, Writing – original draft. ML: Methodology, Resources, Writing – review & editing. MW: Data curation, Formal analysis, Methodology, Writing – review & editing. ZY: Conceptualization, Project administration, Resources, Writing – review & editing. YM: Conceptualization, Project administration, Supervision, Writing – review & editing.

## Funding

The author(s) declare financial support was received for the research, authorship, and/or publication of this article. The

project was funded by the Beijing Natural Science Foundation of China (ID:7222163), and the project leader is ZY, who is one of the co-corresponding authors of this article, and whose main contribution is to guide the technical line of the article and the translation of its clinical significance.

## Conflict of interest

The authors declare that the research was conducted in the absence of any commercial or financial relationships that could be construed as a potential conflict of interest.

## Publisher's note

All claims expressed in this article are solely those of the authors and do not necessarily represent those of their affiliated organizations, or those of the publisher, the editors and the reviewers. Any product that may be evaluated in this article, or claim that may be made by its manufacturer, is not guaranteed or endorsed by the publisher.

## Supplementary material

The Supplementary Material for this article can be found online at: <https://www.frontiersin.org/articles/10.3389/fonc.2024.1442965/full#supplementary-material>

## References

- Sung H, Ferlay J, Siegel RL, Laversanne M, Soerjomataram I, Jemal A, et al. Global cancer statistics 2020: GLOBOCAN estimates of incidence and mortality worldwide for 36 cancers in 185 countries. *CA Cancer J Clin.* (2021) 71(3):209–49. doi: 10.3322/caac.21660
- Che WQ, Li YJ, Tsang CK, Wang YJ, Chen Z, Wang XY, et al. How to use the Surveillance, Epidemiology, and End Results (SEER) data: research design and methodology. *Mil Med Res.* (2023) 0(1):50. doi: 10.1186/s40779-023-00488-2.
- Jing CY, Li SN, Shan BE, et al. Hysteroscopic curettage followed by megestrol acetate plus metformin as a fertility-sparing treatment for women with atypical endometrial hyperplasia or well-differentiated endometrioid endometrial carcinoma. *Clin Med Insights Oncol.* (2022) 16:11795549221110522. doi: 10.1177/11795549221110522
- Warburg O. Über das Verhalten von Aszites-Tumorzellen zu Sauerstoff von höheren Drucken [The reaction of ascites tumor cells to oxygen under high pressure]. *Arch Geschwulstforsch.* (1953) 6(1):7–11.
- Yang X, Min A, Gegen T, et al. PHLPP1 inhibits the growth and aerobic glycolysis activity of human ovarian granular cells through inactivating AKT pathway. *BMC Women's Health.* (2024) 24:25. doi: 10.1186/s12905-023-02872-5
- Meng Z, Bian X, Ma L, et al. UBC9 stabilizes PFKFB3 to promote aerobic glycolysis and proliferation of glioblastoma cells. *Int J Biochem Cell Biol.* (2023) 165:106491. doi: 10.1016/j.biocel.2023.106491
- Qiu Z, Wang C, Huang P, et al. RFX6 facilitates aerobic glycolysis-mediated growth and metastasis of hepatocellular carcinoma through targeting PGAM1. *Clin Transl Med.* (2023) 13:e1511. doi: 10.1002/ctm2.1511
- Han J, Li S, Cao J, et al. SLC9A2, suppressing by the transcription suppressor ETS1, restrains growth and invasion of osteosarcoma via inhibition of aerobic glycolysis. *Environ Toxicol.* (2024) 39:238–51. doi: 10.1002/tox.23963
- Li Y, Liang J, Dang H, Zhang R, Chen P, Shao Y. NCOA3 is a critical oncogene in thyroid cancer via the modulation of major signaling pathways. *Endocrine.* (2022) 75:149–58. doi: 10.1007/s12020-021-02819-6
- Kiliti AJ, Sharif GM, Martin MB, Wellstein A, Riegel AT. AIB1/SRC-3/NCOA3 function in estrogen receptor alpha positive breast cancer. *Front Endocrinol (Lausanne).* (2023) 14:1250218. doi: 10.3389/fendo.2023.1250218
- Miller J, Dakic A, Spurgeon M, et al. AIB1 is a novel target of the high-risk HPV E6 protein and a biomarker of cervical cancer progression. *J Med Virol.* (2022) 94:3962–77. doi: 10.1002/jmv.27795
- Liu T, Wang X, Hu W, et al. Epigenetically down-regulated acetyltransferase PCAF increases the resistance of colorectal cancer to 5-fluorouracil. *Neoplasia.* (2019) 21:557–70. doi: 10.1016/j.neo.2019.03.011
- Infante P, Canetti G, Gulino A, Di Marcotullio L. Yin-Yang strands of PCAF/Hedgehog axis in cancer control. *Trends Mol Med.* (2014) 20:416–8. doi: 10.1016/j.molmed.2014.05.003
- Rajendran R, Garva R, Ashour H, et al. Acetylation mediated by the p300/CBP-associated factor determines cellular energy metabolic pathways in cancer. *Int J Oncol.* (2013) 42:1961–72. doi: 10.3892/ijo.2013.1907
- Jamasbi E, Hamelian M, Hossain MA, Varmira K. The cell cycle, cancer development and therapy. *Mol Biol Rep.* (2022) 49:10875–83. doi: 10.1007/s11033-022-07788-1
- Almalki SG. The pathophysiology of the cell cycle in cancer and treatment strategies using various cell cycle checkpoint inhibitors. *Pathol Res Pract.* (2023) 251:154854. doi: 10.1016/j.prp.2023.154854
- Morana O, Wood W, Gregory CD. The apoptosis paradox in cancer. *Int J Mol Sci.* (2022) 23:1328. doi: 10.3390/ijms23031328
- Liao L, Kuang SQ, Yuan Y, Gonzalez SM, O'Malley BW, Xu J. Molecular structure and biological function of the cancer-amplified nuclear receptor coactivator SRC-3/AIB1. *J Steroid Biochem Mol Biol.* (2002) 83:3–14. doi: 10.1016/s0960-0760(02)00254-6
- Koh SS, Chen D, Lee YH, Stallcup MR. Synergistic enhancement of nuclear receptor function by p160 coactivators and two coactivators with protein methyltransferase activities. *J Biol Chem.* (2001) 276:1089–98. doi: 10.1074/jbc.M004228200

20. Wu H, Sun L, Zhang Y, et al. Coordinated regulation of AIB1 transcriptional activity by sumoylation and phosphorylation. *J Biol Chem.* (2006) 281:21848–56. doi: 10.1074/jbc.M603772200
21. Li S, Yu J, Zhang J, Li X, Yu J. LSD1 interacting with HSP90 promotes skin wound healing by inducing metabolic reprogramming of hair follicle stem cells through the c-MYC/LDHA axis. *FASEB J.* (2023) 37:e23031. doi: 10.1096/fj.202202001RR
22. Han J, Xie C, Liu B, et al. Tetraspanin 1 regulates papillary thyroid tumor growth and metastasis through c-Myc-mediated glycolysis. *Cancer Sci.* (2023) 114:4535–47. doi: 10.1111/cas.15970
23. Zhao L, Yu N, Zhai Y, et al. The ubiquitin-like protein UBTD1 promotes colorectal cancer progression by stabilizing c-Myc to upregulate glycolysis. *Cell Death Dis.* (2024) 15:502. doi: 10.1038/s41419-024-06890-5
24. Cancer Genome Atlas Research Network, Kandoth C, Schultz N, et al. Integrated genomic characterization of endometrial carcinoma. *Nature.* (2013) 497:67–73. doi: 10.1038/nature12113
25. Goulder A, Gaillard SL. Molecular classification of endometrial cancer: entering an era of precision medicine. *J Gynecol Oncol.* (2022) 33:e47. doi: 10.3802/jgo.2022.33.e47
26. Dagher C, Liu YL, Mueller JJ, Weigelt B. Moving into the modern era of molecular classification for endometrial cancer. *J Surg Oncol.* (2024) 129:120–5. doi: 10.1002/jso.27552
27. Karpel H, Slomovitz B, Coleman RL, Pothuri B. Biomarker-driven therapy in endometrial cancer. *Int J Gynecol Cancer.* (2023) 33:343–50. doi: 10.1136/ijgc-2022-003676
28. Liu N, Meng QX, Wang GS. [The relationship between the expression of amplified in breast cancer 1, androgen receptor and tamoxifen resistance in breast cancer]. *Zhonghua Yi Xue Za Zhi.* (2023) 103(20):1553–9. doi: 10.3760/cma.j.cn112137-20230115-00081
29. Li L, Liang Y, Kang L, et al. Transcriptional regulation of the warburg effect in cancer by SIX1. *Cancer Cell.* (2018) 33:368–385.e7. doi: 10.1016/j.ccell.2018.01.010
30. Jiang H, Wei H, Wang H, et al. Zeb1-induced metabolic reprogramming of glycolysis is essential for macrophage polarization in breast cancer. *Cell Death Dis.* (2022) 13:206. doi: 10.1038/s41419-022-04632-z
31. Li Z, Wang Q, Huang X, et al. Lactate in the tumor microenvironment: A rising star for targeted tumor therapy. *Front Nutr.* (2023) 10:1113739. doi: 10.3389/fnut.2023.1113739
32. Chetta P, Sriram R, Zadra G. Lactate as key metabolite in prostate cancer progression: what are the clinical implications? *Cancers (Basel).* (2023) 15:3473. doi: 10.3390/cancers15133473



## OPEN ACCESS

## EDITED BY

Jianbin Bi,  
The First Hospital of China Medical University,  
China

## REVIEWED BY

Dong Wei,  
Hebei General Hospital, China  
Haijun Peng,  
Hebei Chest Hospital, China  
Adil Maqbool,  
Health and Disease Research Center for Rural  
Peoples, Dhaka, Bangladesh

## \*CORRESPONDENCE

Longjie Xia,  
✉ longjiexia1988@126.com  
Fanbiao Kong,  
✉ surgeonkong2020@stu.jnu.edu.cn  
Yu Deng,  
✉ dengyu68@sysu.edu.cn

<sup>†</sup>These authors have contributed equally to  
this work

RECEIVED 16 July 2024

ACCEPTED 27 August 2024

PUBLISHED 23 September 2024

## CITATION

Xia L, Lu J, Qin Y, Huang R, Kong F and Deng Y  
(2024) Analysis of chromatin accessibility in  
peripheral blood mononuclear cells from  
patients with early-stage breast cancer.  
*Front. Pharmacol.* 15:1465586.  
doi: 10.3389/fphar.2024.1465586

## COPYRIGHT

© 2024 Xia, Lu, Qin, Huang, Kong and Deng.  
This is an open-access article distributed under  
the terms of the [Creative Commons Attribution  
License \(CC BY\)](#). The use, distribution or  
reproduction in other forums is permitted,  
provided the original author(s) and the  
copyright owner(s) are credited and that the  
original publication in this journal is cited, in  
accordance with accepted academic practice.  
No use, distribution or reproduction is  
permitted which does not comply with these  
terms.

# Analysis of chromatin accessibility in peripheral blood mononuclear cells from patients with early-stage breast cancer

Longjie Xia<sup>1,2\*†</sup>, Jiamin Lu<sup>3†</sup>, Yixuan Qin<sup>1†</sup>, Runchun Huang<sup>1†</sup>,  
Fanbiao Kong<sup>4\*</sup> and Yu Deng<sup>3\*</sup>

<sup>1</sup>Department of Cosmetology and Plastic Surgery Center, The People's Hospital of Guangxi Zhuang  
Autonomous Region, Guangxi Academy of Medical Sciences, Nanning, China, <sup>2</sup>Department of General  
Surgery, Guangzhou First People's Hospital, Guangzhou, China, <sup>3</sup>Department of Plastic Surgery, The First  
Affiliated Hospital of Sun Yat-Sen University, Guangzhou, China, <sup>4</sup>Department of Colorectal and Anal  
Surgery, The People's Hospital of Guangxi Zhuang Autonomous Region, Guangxi Academy of Medical  
Sciences, Nanning, China

**Objective:** This study was aimed at exploring a specific open region of chromatin  
in the peripheral blood mononuclear cells (PBMCs) of patients with breast cancer  
and evaluating its feasibility as a biomarker for diagnosing and predicting breast  
cancer prognosis.

**Methods:** We obtained PBMCs from breast cancer patients and healthy people  
for the assay for transposase-accessible chromatin (ATAC) sequencing (n = 3) and  
obtained the GSE27562 chip sequencing data for secondary analyses. Through  
bioinformatics analysis, we mined the pattern changes for chromatin accessibility  
in the PBMCs of breast cancer patients.

**Results:** A total of 1,906 differentially accessible regions (DARs) and  
1,632 differentially expressed genes (DEGs) were identified via ATAC  
sequencing. The upregulated DEGs in the disease group were mainly  
distributed in the cells, organelles, and cell-intima-related structures and were  
mainly responsible for biological functions such as cell nitrogen complex  
metabolism, macromolecular metabolism, and cell communication, in  
addition to functions such as nucleic acid binding, enzyme binding, hydrolase  
reaction, and transferase activity. Combined with microarray data analysis, the  
following set of nine DEGs showed intersection between the ATAC and  
microarray data: JUN, MSL2, CDC42, TRIB1, SERTAD3, RAB14, RHOB, RAB40B,  
and PRKDC. HOMER predicted and identified five transcription factors that could  
potentially bind to these peak sites, namely NFY, Sp 2, GFY, NRF, and ELK 1.

**Conclusion:** Chromatin accessibility analysis of the PBMCs from patients with  
early-stage breast cancer underscores its potential as a significant avenue for  
biomarker discovery in breast cancer diagnostics and treatment. By screening the  
transcription factors and DEGs related to breast cancer, this study provides a  
comprehensive theoretical foundation that is expected to guide future clinical  
applications and therapeutic developments.

## KEYWORDS

breast cancer, peripheral blood mononuclear cells, chromatin transposase sequencing,  
transcription factor, ATAC-seq



# 1 Introduction

Breast cancer is the first among the major malignancies that threaten the lives of female patients. Early diagnosis and treatment are key to improving the prognosis of breast cancer, so an increasing number of tumor predictive markers are being widely studied and applied in clinical practice.

The detection of peripheral blood mononuclear cells (PBMCs) and chromatin transposase sequencing such as the high-throughput assay for transposase-accessible chromatin sequencing (ATAC-seq) can provide more sensitive and specific guidance in the diagnosis and treatment of cancer patients (Ding et al., 2020). PBMC testing can be used to detect and analyze circulating tumor cells (CTCs), which are highly relevant to breast-cancer-metastasis-related studies. CTCs are the means by which tumor cells spread to other parts of the body through the blood or lymphatic fluid and constitute one of the important links in breast cancer metastasis. CTC testing can help physicians and researchers detect metastasis risks early, thereby guiding individualized treatment; it can also be used to explore the heterogeneity of gene expressions between individual tumor cells, providing insights into the molecular mechanisms of tumor development (Ding et al., 2020). ATAC-seq technology can be combined with other methods, such as RNA chip data and ChIP-seq, to further explore the mechanisms of initiation and development of breast cancer (Wang et al., 2021).

In recent years, given the rapid development of multiple omics, researchers have attempted to understand the mechanisms of various organisms. Therefore, we also adopted the multi-omics method combined with ATAC-seq and RNA chip data to explore the gene expressions of PBMCs; we also investigated the relationships between chromatin accessibility from the level of transcriptomics and epigenetic omics to explore the molecular mechanism and genetic bases of early-stage breast cancer to enable prediction of the potential therapeutic targets of breast cancer.

# 2 Materials and methods

## 2.1 Acquisition of the specimens

The blood samples required for the study were obtained through the Breast Surgery Department of Guangzhou First People's Hospital from three early-stage breast cancer patients and three healthy adult volunteers. This study was approved by the Ethics Committee of Guangzhou First People's Hospital (approval no. K-2023-019-01). All clinical studies were conducted in accordance with the principles of the Declaration of Helsinki.

## 2.2 Acquisition, processing, and purification of PBMC specimens

Three women with early-stage breast cancer were selected as the experimental group, while three women without breast diseases were chosen as the control group. Blood samples were extracted from these subjects from the forearm; we obtained 5 mL of whole blood from each subject, which was placed in appropriate tubes (BD Vacutainer™)

containing ethylenediamine tetraacetic acid, mixed for 8–10 times, and marked with the patient name and outpatient/hospital number before being stored at 4°C and transported to the laboratory for cell treatment within 2 h. During processing the tubes were centrifuged for 30 min at 2,500 rpm using a centrifuge with a swing bucket rotor. The plasma layer was removed, and the remaining sample was poured into a 15-mL conical tube. Next, 5 mL of frozen phosphate-buffered saline (PBS) containing 2% fetal calf serum (FBS) was added to a separate tube, capped, and mixed in an inverted position. The contents were then poured into the 15-mL conical tube and centrifuged at 1,200 rpm for 10 min at room temperature; the supernatant was then discarded for ATAC detection.

## 2.3 ATAC sequencing

The sample used for sequencing contained approximately  $5 \times 10^4$  cells in 100–200  $\mu$ L, and the cell survival was controlled above 90% as much as possible. Then, 1 M of DNase was added in the ratio of 1:50 and mixed at 37°C for 30 min; this sample was centrifuged at 500g for 5 min, and the supernatant was carefully discarded. Next, 1 mL of precooled EPITM ATAC lysis buffer was added to the sample and mixed in an ice bath for 3 min before being centrifuged at 500g for 10 min; during centrifugation, the 50  $\mu$ L transposase reaction system was configured with 35  $\mu$ L of ddH<sub>2</sub>O, 10  $\mu$ L of 5 $\times$  TT buffer, and 5  $\mu$ L of Tn5 mix. The supernatant was then removed, and the nuclei were collected and added to the reaction system before mixing thoroughly 20 times. Following this, the samples were incubated for 30 min at 37°C and agitation at 1,000 rpm; lastly, the DNA was extracted from the incubated samples.

The raw data were obtained in the fastq format using fastp software (<https://github.com/OpenGene/fastp>); this procedure controls the raw data, including IP samples and input samples, and performs adaptor removal, repetitive sequence, and low quality sequences to yield clean data in the fastq format. Then, FastQC (<https://github.com/s-andrews/FastQC>) was applied to this clean data for quality control analysis. The clean reads data were then aligned with the reference genome using BWA software (version 0.7.17-r1188).

The data were further processed after comparing the bam files. The mitochondrial genome and duplicates were removed, where the duplicate refers to the sequence of reads to the genome at exactly the base and alignment with the reference genome. To avoid the impacts of these replications on subsequent analyses, we used Picard to remove the duplicates. Next, we used bedtools to remove the blacklist region. For reads on the positive strand, the starting position of alignment was +4, and for reads on the negative strand that are 5 bp to the left, the starting position of the alignment was -5 bp. We used the deeptools-alignmentSieve software (version: 3.5.1) to remove the offset reads, and HOMER was used to predict the motif sequences in the possible peak binding data.

## 2.4 GSE27562 chip data download and standardization

We downloaded the GSE27562 dataset from the NCBI gene expression omnibus (GEO) database (<http://www.ncbi.nlm.nih>.

gov/geo) to obtain the chip data. This dataset mainly includes information from female patients diagnosed with breast cancer, patients with benign breast masses, patients with negative molybdenum targets, and patients after breast cancer surgery. We extracted the data of 57 female patients diagnosed with breast cancer and 31 patients without abnormalities as the control groups, including their Affymetrix cel and probe annotation files for the subsequent analyses. The platform used for the chip data is the GPL570 [HG-U133\_Plus\_2] Affymetrix Human Genome U133 Plus 2.0 Array (Affymetrix Company, United States).

After successfully downloading the data from BRAINARRAY and the GeneChip custom chip description file (CDF) from GENCODE, the data were background corrected and normalized using Affymetrix power tools software. Then, the gene-level probe set was mapped to the human GENCODE annotation (version 28) using a custom perl script. Only the RNA in the GENCODE database with probe-set annotation was retained as “PROTEIN-CODING,” while the other genes were filtered out. The rationality of line data normalization in the boxplot was assessed with log2PM. The differentially expressed genes (DEGs) were defined as genes with  $|\log_2FC| > 0.5$  and adjusted  $p < 0.05$ . DEGs from the breast cancer and normal populations from the ATAC-seq and microarray reanalysis were retrieved for intersection analysis using the Venn diagram.

## 2.5 Data normalization and batch effect correction

To ensure comparability and reliability of our data analyses, we implemented robust normalization and batch effect correction. For the ATAC-seq data, we used the fragments per kilobase of transcripts per million mapped reads (FPKM) method to normalize the sequencing depth across samples, which mitigated the impacts of varying sequencing depths. The GSE27562 microarray data were processed for background correction, normalization, and probe-level signal summarization using the robust multiarray average (RMA) method. To address potential batch effects, we applied the “ComBat” method to the ATAC-seq data and used the “sva” R package for the GSE27562 data. These procedures effectively reduced the technical variability and enhanced the consistency and accuracy of the downstream analyses.

## 3 Results

### 3.1 Baseline and ATAC data quality inspections

We selected three women with early-stage breast cancer as the experimental group and three healthy adult women as the control group. The experimental group did not receive any treatment for early breast cancer, while the women in the control group had no breast masses until presentation (Table 1).

The ATAC-seq quality control results are presented in Table 2, for which we observed the accessible regions and found that all specimens had 99% match with the genome (Table 3).

### 3.2 Analyses of association degree and accessible region data for breast cancer PBMC ATAC-seq samples

The correlations among the samples are shown in Figure 1A, and a total of 1,906 differentially accessible regions (DARs) and 1,632 DEGs were identified by ATAC-seq. From Figure 1B, it is seen that the DARs are mainly distributed in the promoter regions of the DEGs, followed by distal intergenic as well as other intronic regions. The ATAC-seq signals were enriched in the open chromatin regions and were positively correlated with the gene transcription activities. Heatmap analysis shows the enrichment distribution of the base sequence between the start positions (TSS) of the transcription factors (TFs) and the 3 kb upstream as well as downstream region of all genes: the signals of the two groups of cells are mostly located within  $\pm 3$  kb. The overall trend of the control group is slightly higher than that of the experimental group. These results suggest intergroup differences, and the heatmaps of the distances between the DARs and transcription initiation regions of the samples are shown in Figure 1C.

Based on the Kyoto encyclopedia of genes and genomes (KEGG) and gene ontology (GO) enrichment analyses of the DEGs corresponding to the DARs, the differential genes were found to be enriched for N-glycan biosynthesis, T receptor signaling, peroxisome, GnRH signaling pathway, protein processing in the endoplasmic reticulum, and other pathways (Figure 1D). In the GO enrichment analysis, the DEGs of the experimental group were mainly distributed in the cells, organelles, and cell-membrane-related structures and were mainly responsible for biological functions like cell nitrogen complex metabolism, macromolecular metabolism, and cell communication, in addition to other functions like nucleic acid binding, enzyme binding, hydrolase enzyme reaction, and transferase activity (Figure 1E).

### 3.3 GEO online database for breast cancer PBMC microarray analysis

We searched the GEO database for chip data related to the PBMCs of breast cancer and finally selected the GSE27562 dataset, which mainly includes information from female patients diagnosed with breast cancer, patients with benign breast masses, patients with negative molybdenum targets, and patients after breast cancer surgery. We extracted the population data for 57 female patients with breast cancers and 31 mammography cases for secondary analyses (Figure 2A). By setting  $|\log_2FC| > 0.5$  and  $p < 0.05$  in these data, we found that 86 genes were upregulated and 55 genes were downregulated in the PBMCs of the experimental group. The GO and KEGG enrichment analyses of the DEGs revealed that the upregulated genes were primarily clustered in the GO hematopoiesis as well as hemoglobin-related subterms. The

TABLE 1 Clinical patient information.

Group	Sample number	Age	Sex	Diagnosis	Surgical operation	Pathological type	Clinical stage
Experimental group	CSW	42	Female	Breast cancer	Denied	HR-/HER2+	cTisN0M0
	CXH	52	Female	Breast cancer	Denied	HR-/HER2-	cT1N0M0
	QXL	63	Female	Breast cancer	Denied	HR+/HER2-	cT2N0M0
Control group	CYZ	64	Female	Normal	Denied	None	0
	S13	48	Female	Normal	Denied	None	0
	S8	48	Female	Normal	Denied	None	0

TABLE 2 ATAC quality controlled results.

Sample name	Number of original sequences	Total base numbers	Total number of sequences controlled and paired	Total number of bases that are quality-controlled and paired	GC ratio
CSW	118,518,974	1.78e+10	94,544,598	1.12e+10	0.445
CXH	146,227,086	2.19e+10	113,165,584	1.31e+10	0.443
CYZ	191,688,422	2.88e+10	140,223,270	1.58e+10	0.45
QXL	122,565,338	1.84e+10	89,271,816	8.85e+09	0.451
S13	218,332,778	3.27e+10	176,448,968	2.27e+10	0.437
S8	238,892,846	3.58e+10	198,617,718	2.53e+10	0.443

TABLE 3 Analysis of the sequence alignment results.

Sample name	Total number of sequences	Number of sequences in the alignment	Comparison rate
CXH	113,165,584	113,056,514	99.9
QXL	89,271,816	89,195,666	99.91
CSW	94,544,598	94,466,193	99.92
S8	198,617,718	198,465,443	99.92
CYZ	140,223,270	140,107,764	99.92
S13	176,448,968	176,351,915	99.94

KEGG analysis showed that the upregulated genes were mainly enriched for MAPK signaling, TNF signaling, IL-17 post-absorption, GnRH signaling, and NOD-like receptor signaling (Figure 2E; Table 4), while the downregulated genes were mainly enriched for hematopoietic cell lines, cytokine receptors and their interactions with cellular proteins, sulfur metabolism, nitrogen metabolism, and protein outputs (Table 5).

### 3.4 Association analysis between ATAC-seq and gene microarray data

Intersection analysis of the peripheral blood ATAC sequencing and mRNA chip data from public databases revealed nine differentially expressed genes, namely JUN, MSL2, CDC42, TRIB1, SERTAD3, RAB14, RHOB, RAB40B, and PRKDC.

Among these, seven DEGs were noted to be regulated by both mRNA data and ATAC sequencing, namely JUN, MSL2, CDC42, TRIB1, SERTAD3, RAB14, and RHOB (Figure 3A). The RAB40B gene showed ATAC upregulation and mRNA downregulation (Figure 3B), while the PRKDC gene showed ATAC downregulation and mRNA upregulation (Figure 3C); there were no intersecting genes between both downregulations (Figure 3D).

### 3.5 Motif predictions

The open regions of the chromatin may be bound by TFs to regulate gene expressions, and specific base sequences with high affinities to certain TFs are called as motifs. In the motif analysis, five specific TFs were identified: NFY, Sp 2, GFY, NRF, and ELK 1 (Table 6).

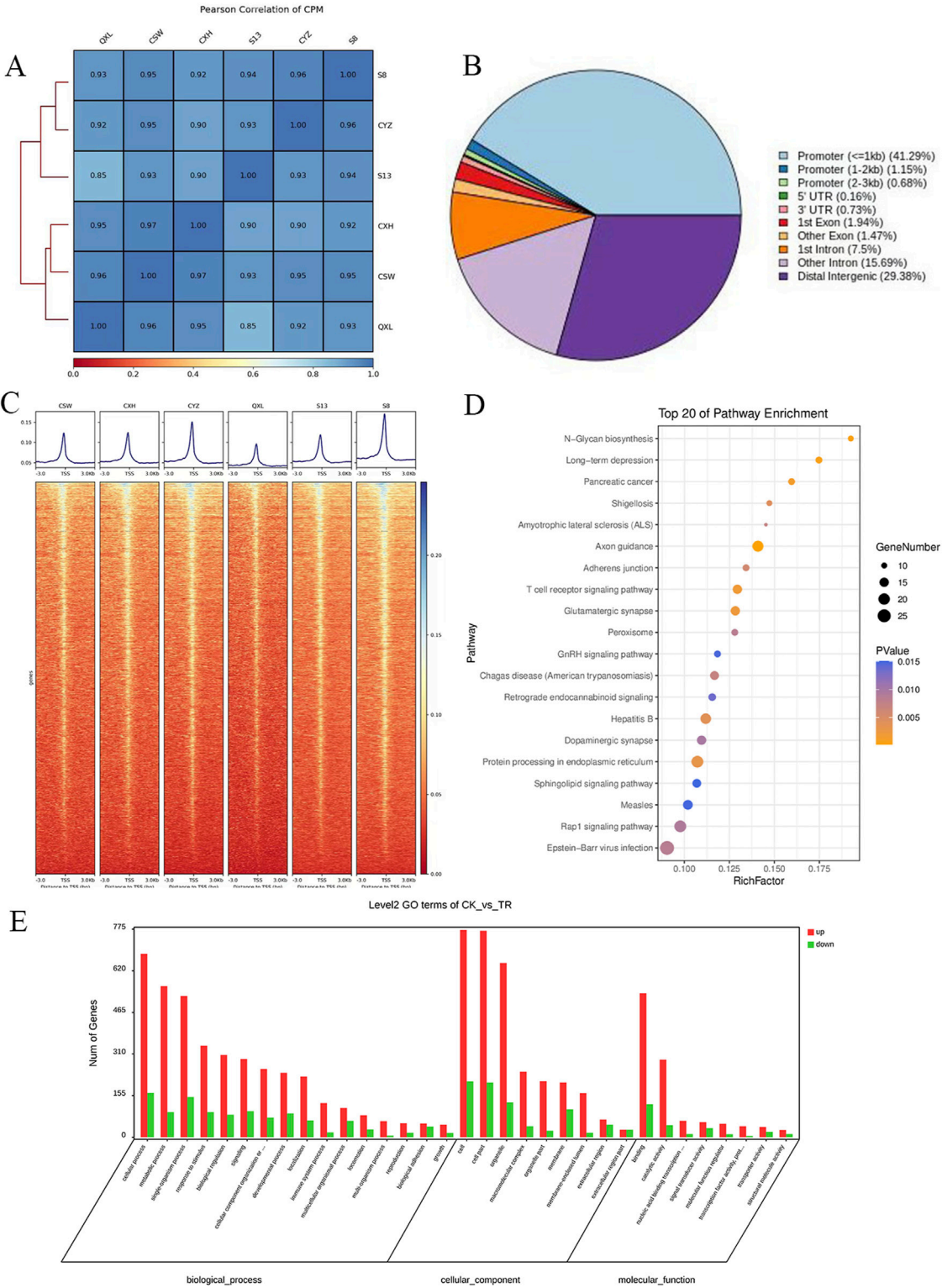


**FIGURE 1** Analysis of the degree of correlation and accessible region data from ATAC-seq samples: **(A)** Pearson association analysis between the samples; **(B)** distribution of the accessible regions of the differential genes; **(C)** heatmap of the distance of the differentially accessible region (DAR) from the transcription start region (TSS) for each sample. **(D)** KEGG enrichment analysis of the top 20 pathways enriched by the differentially expressed genes (DEGs), where the dot sizes indicate the numbers of differential genes in each of the channels; the larger the dot size, the more are the number of genes. The colors indicate the *p*-values, where blue indicates *p* > 0.01, purple indicates *p* > 0.005 and *p* < 0.01, and yellow indicates *p* < 0.005. **(E)** Bar graph of the GO enrichment analysis of the DEGs, where red indicates that the DEG enriched subterms are upregulated in the disease group and green indicates the subterms that downregulate DEG enrichment in the disease group.



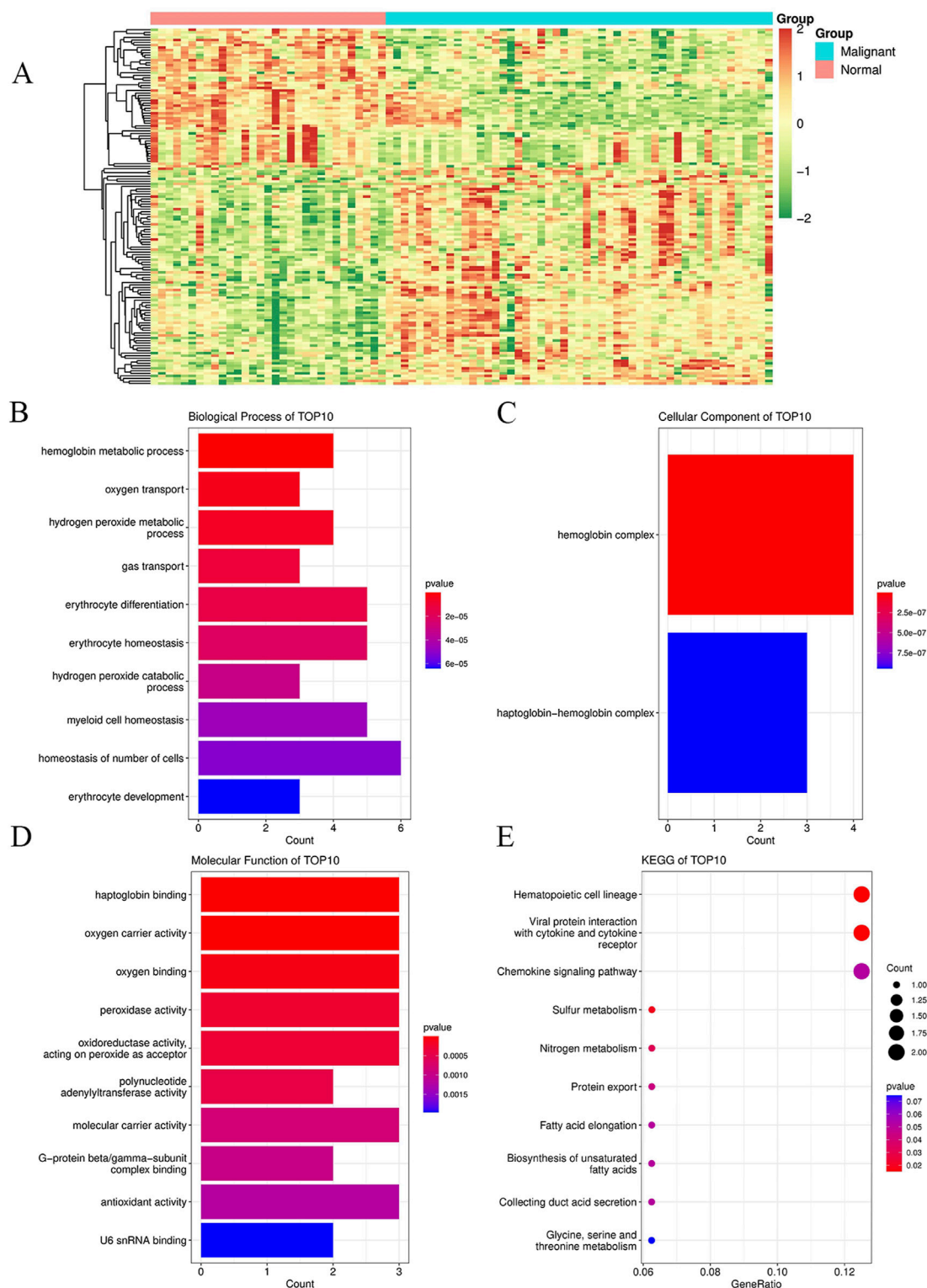


**FIGURE 2** Enrichment analyses of DEGs and their functions in peripheral blood mononuclear cells between breast cancer patients and healthy controls for the GSE27562 dataset from the GEO database. **(A)** Heatmaps of all the genes in the GSE27562 dataset, where blue represents the tumor group and orange represents the normal group; the red data indicate increased expressions, green data indicate decreased expressions, and darker colors indicate higher gene expression value changes from the two extremes. **(B)** GO enrichment analysis of the DEGs for biological processes. **(C)** GO enrichment analysis of the DEGs for cellular components. **(D)** GO enrichment analysis of the DEGs for molecular functions. **(E)** KEGG enrichment analysis of the DEGs. In **(B–E)**, the dot sizes indicate the numbers of differential genes in each channel, with larger sizes implying more numbers and colors indicating the *p*-values.



TABLE 4 KEGG enrichment analysis of the top 10 upregulated differentially expressed genes in breast cancer patients and normal population.

ID	Description	Gene ratio	Q-value
hsa04010	MAPK signaling pathway	0.14	0.010452
hsa04668	TNF signaling pathway	0.12	0.001096
hsa05167	Kaposi-sarcoma-associated herpesvirus infection	0.12	0.00689
hsa05417	Lipid and atherosclerosis	0.12	0.008378
hsa05120	Epithelial cell signaling in <i>Helicobacter pylori</i> infection	0.10	0.001096
hsa04657	IL-17 signaling pathway	0.10	0.002538
hsa04933	AGE-RAGE signaling pathway in diabetic complications	0.10	0.002698
hsa04928	Parathyroid hormone synthesis, secretion, and action	0.10	0.002989
hsa04380	Osteoclast differentiation	0.10	0.006025
hsa04932	Non-alcoholic fatty liver disease	0.10	0.008378

TABLE 5 KEGG enrichment analysis of the top 10 downregulated differentially expressed genes in breast cancer patients and normal population.

ID	Description	Gene ratio	Q-value
hsa04640	Hematopoietic cell lineage	0.05	0.190316
hsa04061	Viral protein interactions with cytokines and cytokine receptors	0.05	0.190316
hsa04062	Chemokine signaling pathway	0.05	0.190316
hsa04060	Cytokine-to-cytokine-receptor interactions	0.05	0.257848
hsa04080	Neuroactive ligand–receptor interactions	0.05	0.282966
hsa00920	Sulfur metabolism	0.02	0.190316
hsa00910	Nitrogen metabolism	0.02	0.190316
hsa03060	Protein export	0.02	0.190316
hsa00062	Fatty-acid elongation	0.02	0.190316
hsa01040	Biosynthesis of unsaturated fatty acids	0.02	0.190316

Other functional analysis results are shown in [Figures 2B–D](#).

## 4 Discussion

The determination of transposase-accessible chromatin involves the use of the hyperactive Tn5 transposase to cut the accessible genomic DNA and attach sequencing adaptor primers to the DNA ends to measure the openness of certain DNA regions as well as obtain important information about the open chromatin state of the entire genome of a certain cell type (Buenrostro et al., 2013; Gross and Garrard, 1988; Adey et al., 2010). This transposase preferentially inserts sequencing junctions at the unprotected regions of the DNA, thus serving as a probe to measure the genome-wide accessibility of the chromatin (Buenrostro et al., 2015). ATAC-seq technology explores how the open regions in the genome may be gene regulatory elements, such as enhancers, promoters, and TF-binding regions often enriched for TF-specific binding sites, which share similar DNA sequence patterns (motifs).

By collecting PBMC suspensions from breast cancer patients and normal controls, we identified five TFs that were highly expressed in breast cancer patients: NFY, Sp 2, GFY, NRF, and

ELK 1. Four of these TFs have already been reported in breast cancer. The nuclear transcription factor Y (NFY) is a cancer-promoting gene that enhances the value-added invasion and metastasis of breast cancer by promoting the expression of proline-rich 11 (PRR 11) (Wang et al., 2019). The Sp 2 TF regulates the biological functions in breast cancer by modulating the mitochondrially related differentially expressed genes (mrDEGs) (Yan et al., 2021). Inhibition of the NFKB (NRF) TF along with non-coding the RNA TROJAN has been shown to abolish CDK2 activity and reverse the resistances of breast cancer cells to CDK4/6 inhibitors (Jin et al., 2020). The ELK 1 TF inhibits cell proliferation in breast cancer along with the tumor suppressor small non-coding RNA 135a (miR-135a) (Ahmad et al., 2018). As a new discovery in this work, the olfactory signaling factor (GFY regulator) has not been evaluated for its role in breast cancer and may therefore be used as a prediction target for the diagnosis, treatment, or prognosis of breast cancer in the future.

The combined use of ATAC-seq and RNA microarray data reveal differences in the gene expressions and regulations between

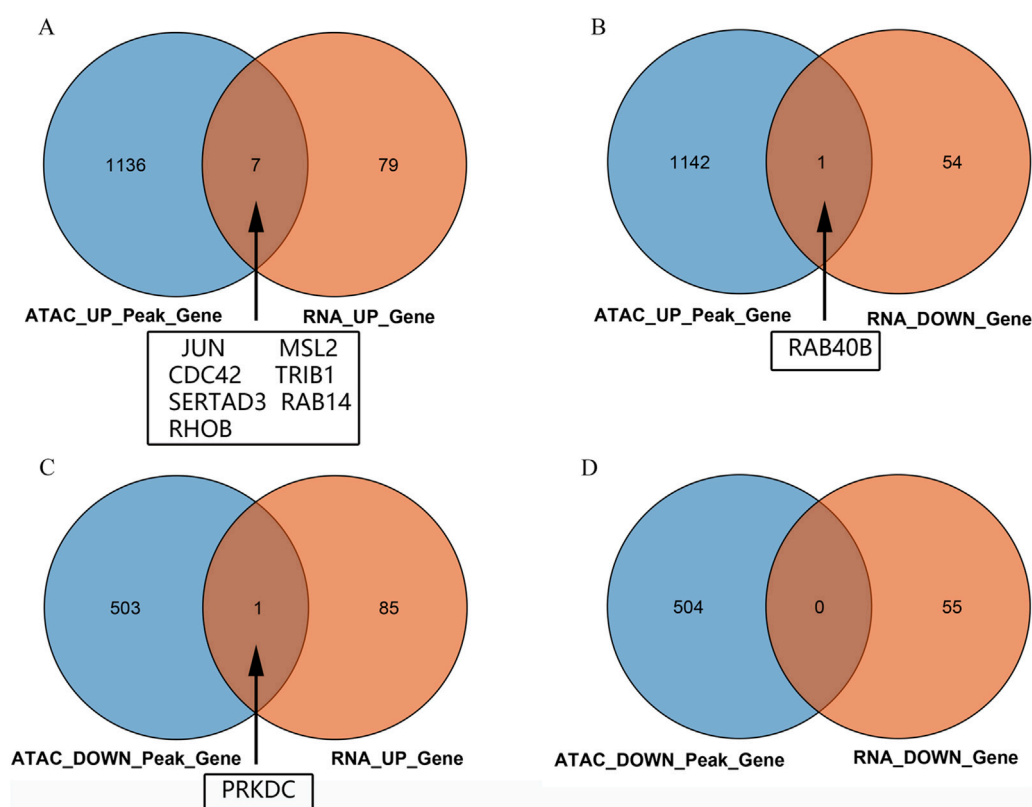


FIGURE 3

Venn diagrams of the intersections between the ATAC peaks of the peripheral blood mononuclear cells and chip data: (A) intersection of upregulated genes between ATAC and mRNA; (B) intersection of genes between upregulated ATAC and downregulated mRNA; (C) intersection of genes between downregulated ATAC and upregulated mRNA; (D) intersection of downregulated genes between ATAC and mRNA.

tumor and normal cells. In our experiments, we used the ATAC-seq data of human peripheral blood samples from a public database RNA chip and found nine DEGs, namely JUN, MSL2, CDC42, TRIB1, SERTAD3, RAB14, RHOB, RAB40B, and PRKDC. Eight of these genes have already been reported in breast cancer. JUN can be divided into cellular JUN (c-JUN) and viral JUN (v-JUN). c-JUN is a member of the activated protein-1 (AP-1) TF family that is stimulated by upstream signals and can be transmitted by the JUN N-terminal kinase (JNK) to regulate gene expressions at the transcriptional level, thereby inducing cancer (Vogt, 2001). c-JUN is a potential regulator that stimulates the transformation of breast cells into HR+/HER2-type breast cancers (Zhu et al., 2022). The cell division control protein 42 homolog (CDC42) is frequently upregulated by several cell surface receptors and breast cancer oncogenes, as noted by Cruz-Collazo et al. (2021); the CDC42 inhibitor inhibits infiltration and metastasis of triple-negative breast cancer cells while also inducing cell cycle arrest and apoptosis of HER2-overexpression-type breast cancer cells. It reduces tumor growth and metastasis while inhibiting the migration and invasion of HR+/HER2-type breast cancer cells (Khan et al., 2020). SERTAD3 is a pro-cancer gene located within the 19q13 amplicon that has been shown to inhibit the growth of breast cancer cells and enhance tumor sensitivity to treatment with the drug tamoxifen (Li et al., 2021a). The RAS homolog family member B (RHOB) gene acts as a tumor suppressor and is the guanosine triphosphate enzyme of the RHO family; some







researchers have found that RHOB plays an important role in inhibiting breast cancer invasion and metastasis (Wieland et al., 2021), and reducing RHOB expression can increase the migration and invasion capacities of triple-negative breast cancer cell lines. Restoration of the breast cancer 1 (BRCA 1) gene expressions in BRCA1-mutant triple-negative breast cancer cell lines can increase the expression of RHOB, resulting in reduced migration capacity. These results suggest that RHOB protein and BRCA1 mutations are potential therapeutic targets for breast cancer (Privat et al., 2020). RHOB alters the hormonal responses of breast cancer cells by affecting the expressions of the estrogen receptors (ERs) and progesterone receptors (PRs). We have shown that RHOB regulates the expressions of ERs and controls their protein and mRNA levels; furthermore, RHOB regulates the expressions of PRs by enhancing the recruitment of ERs and other major coregulatory factors to PR gene promoters. A major consequence of RHOB regulation is that it differentially affects the proliferation of breast cancer cell lines. It was earlier demonstrated that RHOB promotes the expressions of ERs and PRs in a manner related to cell proliferation in human breast cancer (Médale-Giamarchi et al., 2013). Some investigators found that RHOB expression was upregulated after treatment with atorvastatin, implying the potential application of RHOB as a target for tumor suppressor gene therapy in breast cancer (Ma et al., 2019). The recombination process of cellular programs in malignant cells is a stage where the tumor is very vulnerable. The male-specific lethal 2 homolog (MSL

TABLE 6 HOMER predicts the top 20 transcription factors motifs with high binding probabilities in ATAC sequencing.

Rank	Motif/Name	Q-value	% of Targets Sequences with Motif	% of Background Sequences with Motif
1	 Sp1(Zf)/Promoter/Homer	<0.001	21.56%	7.24%
2	 NFY(CCAAT)/Promoter/Homer	<0.001	21.20%	7.15%
3	 Ronin(THAP)/ES-Thap11-ChIP-Seq(GSE51522)/Homer	<0.001	4.93%	0.33%
4	 GFY-Staf(?,Zf)/Promoter/Homer	<0.001	5.35%	0.63%
5	 KLF3(Zf)/MEF-Klf3-ChIP-Seq(GSE44748)/Homer	<0.001	22.82%	10.29%
6	 KLF1(Zf)/HUDEP2-KLF1-CutnRun(GSE136251)/Homer	<0.001	33.89%	18.61%
7	 Sp5(Zf)/mES-Sp5.Flag-ChIP-Seq(GSE72989)/Homer	<0.001	35.10%	20.15%
8	 GFY(?)/Promoter/Homer	<0.001	4.93%	0.77%
9	 Elk4(ETS)/Hela-Elk4-ChIP-Seq(GSE31477)/Homer	<0.001	16.05%	7.18%
10	 Fli1(ETS)/CD8-FLI-ChIP-Seq(GSE20898)/Homer	<0.001	24.34%	13.38%
11	 NRF1(NRF)/MCF7-NRF1-ChIP-Seq(Unpublished)/Homer	<0.001	9.50%	3.17%
12	 Elf4(ETS)/BMDM-Elf4-ChIP-Seq(GSE88699)/Homer	<0.001	20.83%	10.92%
13	 KLF6(Zf)/PDAC-KLF6-ChIP-Seq(GSE64557)/Homer	<0.001	32.90%	20.65%
14	 Elk1(ETS)/Hela-Elk1-ChIP-Seq(GSE31477)/Homer	<0.001	15.95%	7.52%

(Continued on following page)

TABLE 6 (Continued) HOMER predicts the top 20 transcription factors motifs with high binding probabilities in ATAC sequencing.

Rank	Motif/Name	Q-value	% of Targets Sequences with Motif	% of Background Sequences with Motif
15	 NRF(NRF)/Promoter/Homer	<0.001	9.86%	3.68%
16	 ELF1(ETS)/Jurkat-ELF1-ChIP-Seq(SRA014231)/Homer	<0.001	14.74%	6.87%
17	 KLF5(Zf)/LoVo-KLF5-ChIP-Seq(GSE49402)/Homer	<0.001	37.88%	25.79%
18	 Sp2(Zf)/HEK293-Sp2.eGFP-ChIP-Seq(Encode)/Homer	<0.001	41.82%	29.46%
19	 ETS(ETS)/Promoter/Homer	<0.001	9.86%	3.92%
20	 ETV4(ETS)/HepG2-ETV4-ChIP-Seq(ENCODE)/Homer	<0.001	24.29%	14.73%

2) gene suppresses tumor proliferation through disruption-induced excessive chromosomal instability (CIN) (Valsecchi et al., 2021). Hence, targeting MSL may be a valuable approach to treating tumors by increasing the CINs beyond the levels tolerated by cancer cells without inducing serious side effects (Monserrat et al., 2021) in normal tissues. For example, in hepatocellular carcinoma (HCC), MSL 2 overexpression has been found to partially block the inhibitory effects of the miRNA-296-3p tumor suppressor gene mode for proliferation and migration of the HCC cells, which could be used as a target for HCC therapy (Li et al., 2021b). It was also shown that MSL 2 plays a role in maintaining a normal histone modification profile that contributes to the repair of DNA damage (Lai et al., 2013). However, the role of MSL 2 in breast cancer has not been reported in other studies; hence, it may be used as a future therapeutic target in breast cancer. Tribbles pseudokinase 1 (TRIB1) is a pro-cancer gene involved in cancer initiation and progression, which could be used as a biomarker for the diagnosis and prognosis of diseases. Studies have shown that both overexpression and knockdown of TRIB1 in myeloid cells promote the growth of breast tumors in mice; myeloid TRIB1 is a negative regulator of the antitumor cytokine IL-15. Increased expression of myeloid TRIB2 reduces IL-15 levels in breast tumors, resulting in reduced numbers of T cells that are key to the antitumor immune responses. Thus, the roles of TRIB1 in chemotherapeutic responses in human breast cancer are critical and provide mechanistic insights into the importance of controlling myeloid TRIB 1 expression in breast cancer development (Kim et al., 2022). TRIB1 can also be developed as a biomarker for direct targeted therapy and predicting treatment responses (McMillan et al., 2021). RAB14 inhibition mediated by miR-320a suppresses cell

proliferation, migration, and invasion in breast cancers. It has also been shown that RAB14 is a miR-320a target in breast cancer; thus, silencing RAB14 inhibits proliferation, migration, and invasion of breast cancer cell lines (Yu et al., 2016). However, RAB14 actively interacts with Nischarin by regulating the production of exosomes in breast cancer cells, subsequently affecting tumor cell adhesion, cell migration, tumor growth, and metastasis (Maziveyi et al., 2019). RAB40B is also a member of the RAS family of oncogenes and plays an important role in breast cancer cell formation, invasion, and metastasis (Jacob et al., 2013). DNA-dependent protein kinase (PRKDC) has been shown to modulate tumor sensitivity to chemotherapy and is a potential prognostic and predictive indicator of the efficacy of adjuvant chemotherapy in cancer patients. Some studies have shown that PRKDC expression is significantly higher in breast cancer tissue samples; high expression of PRKDC is also associated with a higher tumor grade, positive lymph node metastasis, and chemoresistance. Furthermore, PRKDC downregulates the sensitivity of the HR+/HER2-type breast cancer cells (MCF-7 line) to chemotherapeutic agents *in vitro* and in xenograft mouse models, indicating that PRKDC is a prognostic biomarker of chemoresistance in breast cancer patients (Sun et al., 2017). High expression of PRKDC is also a prognostic marker of poor survival in breast cancer patients (Zhang et al., 2019).

## 5 Conclusion

The use of ATAC-seq technology to identify motifs has important roles in gene regulation and disease; it provides an

important basis for greater understanding of the mechanisms of TF-specific binding sites as well as new ideas for the study of TFs, enhancers, and promoters and development of new drugs. The present study identifies several key genes and TFs associated with breast cancer, providing a macroscopic theoretical basis for further research in this area. Future studies should focus on the functional validation of these identified genes and their interactions with the TFs to enhance our mechanistic understanding of their roles in breast cancer progression. Such validation could offer critical insights into their potential as therapeutic targets and contribute to the development of more effective treatment strategies. The combined application of ATAC-seq and RNA-seq can provide complementary results in tumor genomics research, help researchers better understand the regulatory mechanisms and expression profile changes during the occurrence and development of tumors, and improve the understanding and treatability of tumors. However, the present study is limited by its relatively small sample size. To strengthen the clinical relevance and utility of the identified biomarkers, future studies should focus on validating these biomarkers in larger cohorts. This would not only confirm their potential as diagnostic and prognostic tools but also enhance their applicability in personalized medicine for breast cancer treatment.

The TFs and differential genes identified and discovered in this study provide a macroscopic theoretical basis for breast cancer research and can be potential targets for future breast cancer treatments.

## Data availability statement

The original contributions presented in the study are included in the article/supplementary material; further inquiries can be directed to the corresponding authors.

## Ethics statement

The studies involving humans were approved by the Ethics and Human Subject Committee of Guangzhou First People's Hospital. The studies were conducted in accordance with the local legislations

and institutional requirements. All participants provided written informed consent to participate in this study.

## Author contributions

LX: conceptualization, methodology, project administration, resources, writing–original draft, and writing–review and editing. JL: software, supervision, and writing–original draft. YQ: data curation, formal analysis, and writing–original draft. RH: data curation, visualization, and writing–original draft. FK: funding acquisition, formal analysis, investigation, and writing–original draft. YD: resources, and writing–review and editing.

## Funding

The authors declare that financial support was received for the research, authorship, and/or publication of this article. This work was supported by the Scientific Research Project of Guangxi Health Commission (no. z20180739), Youth Foundation of People's Hospital of Guangxi Zhuang Autonomous Region (no. QN2018-22), and the Natural Science Foundation of Guangxi (no. 2022JJA141179).

## Conflict of interest

The authors declare that the research was conducted in the absence of any commercial or financial relationships that could be construed as a potential conflict of interest.

## Publisher's note

All claims expressed in this article are solely those of the authors and do not necessarily represent those of their affiliated organizations, or those of the publisher, the editors, and the reviewers. Any product that may be evaluated in this article, or claim that may be made by its manufacturer, is not guaranteed or endorsed by the publisher.

## References

- Adey, A., Morrison, Asan, H. G., Xun, X., Kitzman, J. O., Turner, E. H., Stackhouse, B., et al. (2010). Rapid, low-input, low-bias construction of shotgun fragment libraries by high-density *in vitro* transposition. *Genome Biol.* 11, R119. doi:10.1186/gb-2010-11-12-r119
- Ahmad, A., Zhang, W., Wu, M., Tan, S., and Zhu, T. (2018). Tumor-suppressive miRNA-135a inhibits breast cancer cell proliferation by targeting ELK1 and ELK3 oncogenes. *Genes and genomics* 40, 243–251. doi:10.1007/s13258-017-0624-6
- Buenrostro, J. D., Giresi, P. G., Zaba, L. C., Chang, H. Y., and Greenleaf, W. J. (2013). Transposition of native chromatin for fast and sensitive epigenomic profiling of open chromatin, DNA-binding proteins and nucleosome position. *Nat. methods* 10, 1213–1218. doi:10.1038/nmeth.2688
- Buenrostro, J. D., Wu, B., Chang, H. Y., and Greenleaf, W. J. (2015). ATAC-seq: a method for Assaying chromatin accessibility genome-wide. *Curr. Protoc. Mol. Biol.* 109, 21.29.21–21. doi:10.1002/0471142727.mb2129s109
- Cruz-Collazo, A., Ruiz-Calderon, J. F., Picon, H., Borrero-Garcia, L. D., Lopez, I., Castillo-Pichardo, L., et al. (2021). Efficacy of rac and Cdc42 inhibitor MBQ-167 in triple-negative breast cancer. *Mol. cancer Ther.* 20, 2420–2432. doi:10.1158/1535-7163.MCT-21-0348
- Ding, S., Chen, X., and Shen, K. (2020). Single-cell RNA sequencing in breast cancer: understanding tumor heterogeneity and paving roads to individualized therapy. *Cancer Commun. lond. Engl.* 40, 329–344. doi:10.1002/cac2.12078
- Gross, D. S., and Garrard, W. T. (1988). Nuclease hypersensitive sites in chromatin. *Annu. Rev. Biochem.* 57, 159–197. doi:10.1146/annurev.bi.57.070188.001111
- Jacob, A., Jing, J., Lee, J., Schedin, P., Gilbert, S. M., Peden, A. A., et al. (2013). Rab40b regulates trafficking of MMP2 and MMP9 during invadopodia formation and invasion of breast cancer cells. *J. cell Sci.* 126, 4647–4658. doi:10.1242/jcs.126573
- Jin, X., Ge, L. P., Li, D. Q., Shao, Z. M., Di, G. H., Xu, X. E., et al. (2020). LncRNA TROJAN promotes proliferation and resistance to CDK4/6 inhibitor via CDK2 transcriptional activation in ER+ breast cancer. *Mol. cancer* 19, 87. doi:10.1186/s12943-020-01210-9
- Khan, S., Shukla, S., Farhan, M., Sinha, S., Lakra, A. D., Penta, D., et al. (2020). Centchroman prevents metastatic colonization of breast cancer cells and disrupts



- angiogenesis via inhibition of RAC1/PAK1/ $\beta$ -catenin signaling axis. *Life Sci.* 256, 117976. doi:10.1016/j.lfs.2020.117976
- Kim, T., Johnston, J., Castillo-Lluva, S., Cimas, F. J., Hamby, S., Gonzalez-Moreno, S., et al. (2022). TRIB1 regulates tumor growth via controlling tumor-associated macrophage phenotypes and is associated with breast cancer survival and treatment response. *Theranostics* 12, 3584–3600. doi:10.7150/thno.72192
- Lai, Z., Moravcová, S., Canitrot, Y., Andrzejewski, L. P., Walshe, D. M., and Rea, S. (2013). Msl2 is a novel component of the vertebrate DNA damage response. *PLoS one* 8, e68549. doi:10.1371/journal.pone.0068549
- Li, X., An, M., and Gao, Z. (2021b). In hepatocellular carcinoma, miRNA-296-3p targets MSL2 and suppresses cell proliferation and invasion. *J. Oncol.* 2021, 7430468. doi:10.1155/2021/7430468
- Li, Y., Liu, L., Lv, Y., Zhang, Y., Zhang, L., Yu, H., et al. (2021a). Silencing long non-coding RNA HNF1A-AS1 inhibits growth and resistance to TAM of breast cancer cells via the microRNA-363/SERTAD3 axis. *J. Drug Target.* 29, 742–753. doi:10.1080/1061186x.2021.1878362
- Ma, Q., Gao, Y., Xu, P., Li, K., Xu, X., Gao, J., et al. (2019). Atorvastatin inhibits breast cancer cells by downregulating PTEN/AKT pathway via promoting Ras homolog family member B (RhoB). *Biomed. Res. Int.* 2019, 3235021. doi:10.1155/2019/3235021
- Maziveyi, M., Dong, S., Baranwal, S., Mehrmezhad, A., Rathinam, R., Huckaba, T. M., et al. (2019). Exosomes from Nischarin-Expressing cells reduce breast cancer cell Motility and tumor growth. *Cancer Res.* 79, 2152–2166. doi:10.1158/0008-5472.CAN-18-0842
- McMillan, H. D., Keeshan, K., Dunbier, A. K., and Mace, P. D. (2021). Structure vs. Function of TRIB1-myeloid neoplasms and beyond. *Cancers* 13, 3060. doi:10.3390/cancers13123060
- Médale-Giamarchi, C., Lajoie-Mazenc, I., Malissein, E., Meunier, E., Couderc, B., Bergé, Y., et al. (2013). RhoB modifies estrogen responses in breast cancer cells by influencing expression of the estrogen receptor. *Breast cancer Res. BCR* 15, R6. doi:10.1186/bcr3377
- Montserrat, J., Morales Torres, C., Richardson, L., Wilson, T. S., Patel, H., Domart, M. C., et al. (2021). Disruption of the MSL complex inhibits tumour maintenance by exacerbating chromosomal instability. *Nat. cell Biol.* 23, 401–412. doi:10.1038/s41556-021-00657-2
- Privat, M., Cavard, A., Zekri, Y., Ponelle-Chachuat, F., Molnar, I., Sonnier, N., et al. (2020). A high expression ratio of RhoA/RhoB is associated with the migratory and invasive properties of basal-like Breast Tumors. *Int. J. Med. Sci.* 17, 2799–2808. doi:10.7150/ijms.43101
- Sun, G., Yang, L., Dong, C., Ma, B., Shan, M., and Ma, B. (2017). PRKDC regulates chemosensitivity and is a potential prognostic and predictive marker of response to adjuvant chemotherapy in breast cancer patients. *Oncol. Rep.* 37, 3536–3542. doi:10.3892/or.2017.5634
- Valsecchi, C. I. K., Basilicata, M. F., Georgiev, P., Gaub, A., Seyfferth, J., Kulkarni, T., et al. (2021). RNA nucleation by MSL2 induces selective X chromosome compartmentalization. *Nature* 589, 137–142. doi:10.1038/s41586-020-2935-z
- Vogt, P. K. (2001). Jun, the oncoprotein. *Oncogene* 20, 2365–2377. doi:10.1038/sj.onc.1204443
- Wang, X., Yan, J., Shen, B., and Wei, G. (2021). Integrated chromatin accessibility and transcriptome landscapes of doxorubicin-resistant breast cancer cells. *Front. cell Dev. Biol.* 9, 708066. doi:10.3389/fcell.2021.708066
- Wang, Y., Zhang, C., Mai, L., Niu, Y., Wang, Y., and Bu, Y. (2019). PRR11 and SKA2 gene pair is overexpressed and regulated by p53 in breast cancer. *BMB Rep.* 52, 157–162. doi:10.5483/bmbrep.2019.52.2.207
- Wieland, A., Strissel, P. L., Schorle, H., Bakirci, E., Janzen, D., Beckmann, M. W., et al. (2021). Brain and breast cancer cells with PTEN loss of function reveal enhanced durotaxis and RHOB dependent amoeboid migration utilizing 3D scaffolds and aligned microfiber tracts. *Cancers* 13, 5144. doi:10.3390/cancers13205144
- Yan, L. R., Wang, A., Lv, Z., Yuan, Y., and Xu, Q. (2021). Mitochondria-related core genes and TF-miRNA-hub mrDEGs network in breast cancer. *Biosci. Rep.* 41. doi:10.1042/BSR20203481
- Yu, J., Wang, L., Yang, H., Ding, D., Zhang, L., Wang, J., et al. (2016). Rab14 suppression mediated by MiR-320a inhibits cell proliferation, migration and invasion in breast cancer. *J. Cancer* 7, 2317–2326. doi:10.7150/jca.15737
- Zhang, Y., Yang, W. K., Wen, G. M., Tang, H., Wu, C. A., Wu, Y. X., et al. (2019). High expression of PRKDC promotes breast cancer cell growth via p38 MAPK signaling and is associated with poor survival. *Mol. Genet. Genomic Med.* 7, e908. doi:10.1002/mgg3.908
- Zhu, P., Liu, G., Wang, X., Lu, J., Zhou, Y., Chen, S., et al. (2022). Transcription factor c-Jun modulates GLUT1 in glycolysis and breast cancer metastasis. *BMC cancer* 22, 1283. doi:10.1186/s12885-022-10393-x



## OPEN ACCESS

## EDITED BY

Jianbin Bi,  
The First Hospital of China Medical University,  
China

## REVIEWED BY

Hashem Obaid Alsaab,  
Taif University, Saudi Arabia  
Jianguo Gao,  
Hebei Chest Hospital, China  
Yongjin Luo,  
People's Hospital of Guangxi Zhuang  
Autonomous Region, China

## \*CORRESPONDENCE

Jan Eucker,  
✉ jan1653@163.com

RECEIVED 04 June 2024

ACCEPTED 06 September 2024

PUBLISHED 14 October 2024

## CITATION

Yu L, Zang C, Ye Y, Liu H and Eucker J (2024)  
Effects of BYL-719 (alpelisib) on human breast  
cancer stem cells to overcome drug resistance  
in human breast cancer.  
*Front. Pharmacol.* 15:1443422.  
doi: 10.3389/fphar.2024.1443422

## COPYRIGHT

© 2024 Yu, Zang, Ye, Liu and Eucker. This is an  
open-access article distributed under the terms  
of the [Creative Commons Attribution License](#)  
(CC BY). The use, distribution or reproduction in  
other forums is permitted, provided the original  
author(s) and the copyright owner(s) are  
credited and that the original publication in this  
journal is cited, in accordance with accepted  
academic practice. No use, distribution or  
reproduction is permitted which does not  
comply with these terms.

# Effects of BYL-719 (alpelisib) on human breast cancer stem cells to overcome drug resistance in human breast cancer

Leinan Yu<sup>1</sup>, Chuanbing Zang<sup>1</sup>, Yuanchun Ye<sup>2</sup>, Hongyu Liu<sup>1</sup> and Jan Eucker<sup>1,3\*</sup>

<sup>1</sup>Department of Hematology, Oncology and Cancer Immunology, Campus Benjamin Franklin Charité - Universitätsmedizin Berlin, Corporate Member of Freie Universität Berlin and Humboldt-Universität zu Berlin, Berlin, Germany, <sup>2</sup>School of Science, Shenzhen Campus of Sun Yat-Sen University, Shenzhen, Guangdong, China, <sup>3</sup>Department of Oncology, Rheumatology and Gastroenterology, Vivantes Klinikum Spandau, Berlin, Germany

**Introduction:** Breast cancer continues to be a major health concern and is currently the most commonly diagnosed cancer worldwide. Relapse, metastasis, and therapy resistance are major clinical issues that doctors need to address. We believe BYL-719, which is PI3 kinase p110a inhibitor, could also inhibit the breast cancer stem cell phenotype and epithelial-to-mesenchymal transition (EMT). In addition to the PI3K/AKT signaling pathway, BYL-719 can also inhibit essential cancer-related signaling pathways, all of which would ultimately act on the microenvironment of cancer stem cells, which is quite complicated and regulates the characteristics of tumors. These include the stemness and resistance of malignant tumors, plasticity of cancer stem cells, and anti-apoptotic features.

**Materials and methods:** A three-dimensional (3D) mammosphere culture method was used *in vitro* to culture and collect breast cancer stem cells (BCSCs). MTT, clonogenic, and cell apoptosis assays were used to detect cell viability, self-renewal, and differentiation abilities. A sphere formation assay under 3D conditions was used to detect the mammosphere inhibition rate of BYL-719. The subpopulation of CD44<sup>+</sup>CD24<sup>-</sup> was detected using flow cytometry analysis while EMT biomarkers and essential signaling pathways were detected using western blotting. All the data were analyzed using GraphPad Prism 9 software.

**Results:** BCSC-like cells were obtained by using the 3D cell culture method *in vitro*. We confirmed that BYL-719 could inhibit BCSC-like cell proliferation in 3D cultures and that the stemness characteristics of BCSC-like cells were inhibited. The PI3K/AKT/mTOR signaling pathway could be inhibited by BYL-719, and the Notch, JAK-STAT and MAPK/ERK signaling pathways which have crosstalk in the tumor microenvironment (TME) are also inhibited. By comparing eribulin-resistant breast cancer cell lines, we confirmed that BYL-719 could effectively overcome drug resistance.

**Summary/conclusion:** The 3D cell culture is a novel and highly effective method for enriching BCSCs *in vitro*. Furthermore, the stemness and EMT of BCSCs were inhibited by BYL-719 by acting on various signaling pathways. Finally, we believe that drug resistance can be overcome by targeting the BCSCs. Conjugation of BYL-719 with other anti-neoplastic agents may be a promising treatment for this in clinic.

## KEYWORDS

breast cancer, breast cancer stem cell, BYL-719 (alpelisib), PI3K/Akt signaling pathway, stemness, resistance

# 1 Introduction

Breast cancer continues to be a serious global public health issue, with an unprecedented impact on human lifespan and health (Sung et al., 2021; Wilkinson and Gathani, 2022). Over the last few decades, thousands of scientists have focused on the mechanisms and comprehensive therapies of breast cancer, and their research has made substantial progress in our understanding of the disease (Wang Z. et al., 2024). They have revealed that the main factors contributing to breast cancer include aging, family history, reproductive factors, estrogen, progesterone, and lifestyles (Sun et al., 2017). The conventional treatments for breast cancer comprise surgery, radiotherapy, chemotherapy, endocrine therapy, neoadjuvant therapy, and adjuvant therapy (Wang and Wu, 2023; Zhang et al., 2023). Although different treatment methods are available, metastasis, relapse, and resistance are the usual problems that patients and doctors face after several years of treatment. These problems lead to a lowered 5-year survival rate and reduced quality of life later on (Taskindoust et al., 2021). As research continues to evolve, scientists have found that one of the most important reasons for these problems is the presence of breast cancer stem cells (BCSCs) (De Angelis et al., 2019). They have elucidated the concept and function of BCSCs, emphasizing their existence in humans for long periods and their high plasticity along with self-renewal properties (Zhang et al., 2020). In 2006, the American Association for Cancer Research defined a CSC as a cell within a tumor that possesses the capacity to self-renew and cause heterogeneous lineages of cancer cells that comprise a tumor (Najafi et al., 2019). It is well known that special proteins that determine the key phenotype can be used as markers for specific cells (Luo et al., 2024). Currently, BCSCs are usually identified by expression of specific phenotypes; CD44<sup>+</sup>/CD24<sup>-</sup>/low and/or CD133<sup>+</sup> are most frequently used (Li et al., 2017), and it is identified as a small subpopulation of heterogeneous breast cancer cells with strong self-renewal and proliferation properties (Zhang et al., 2020). The major putative mechanisms underlying the properties of BCSCs include the tumor microenvironment (TME), stem cell-related signaling pathways, enhancement of epithelial-to-mesenchymal transition (EMT) cellular programming, DNA damage and repair pathways, as well as miRNA and epigenetic alterations (Nilendu et al., 2018; Zhang et al., 2022). Although highly proliferative, BCSCs predominantly remain in a quiescent state or cycle slowly, shielding them from chemotherapy and radiation damage. Collectively, these factors contribute to the survival of BCSCs during treatment and their ability to re-establish tumor masses post-therapy.

Commercially available inhibitors target both membrane proteins and BCSC-related signaling pathways. BYL-719 (alpelisib) is an inhibitor of phosphatidylinositol 3-kinase (PI3K) that has substantial anticancer action (Markham, 2019). It functions by specifically inhibiting class I PI3K p110 $\alpha$ , the catalytic subunit of PI3K, a lipid kinase involved in numerous biological processes, including proliferation, survival, differentiation, and metabolism. Patients treated with alpelisib have shown better tolerance and longer progression-free survival (PFS) (Markham, 2019). Alpelisib also possesses favorable pharmacokinetic properties, characterized by rapid and significant absorption (Marbury et al., 2023). Currently, there are no data on the effects of PI3K inhibitors on BCSC-like cells (Chang et al., 2021). In our research, alpelisib was

established as a highly effective PI3K $\alpha$  inhibitor which could also affect the BCSCs and interrupt the crosstalk between signaling pathways including Notch, JAK/STAT and MAPK/ERK signaling pathways and studies have already showed there exits cross-talks in TME of BCSC, which is a complicated microenvironment includes intrinsic and extrinsic factors. This suggests that between these important signaling pathways and all these molecules have inter-linkages and interactions. As previously described, these intricate signal transduction pathways are not linear. The PI3K/AKT/mTOR signaling pathway is responsible for the promotion of cell proliferation, survival, and cell cycle progression (Glaviano et al., 2023). Notch inhibits the proliferation and differentiation of CSCs, thus maintains the CSC phenotype and contributes to the transformation process (Martínez-Pérez et al., 2024). The JAK-STAT pathway is always considered to have a role which could regulate the survival and proliferation of BCSCs. It is also believed to be associated with metastasis and drug resistance. The signal transducer and activator of transcription (STAT) protein family plays a major role in cancer (Liongue et al., 2024). Mitogen-activated protein kinase (MAPK) cascades is important to the cellular processes, including differentiation, apoptosis, proliferation, and responses to stress. It is one of the most critical cancer related signaling pathways (Guo et al., 2020). Furthermore, it is now confirmed that the activation of extracellular signal-regulated kinase (ERK) leads to the formation of spheres and the CSC-like properties (Choi et al., 2018). Additionally, it can block the TME to disrupt stem cell characteristics, such as self-renewal therapeutic resistance, tumor recurrence, and metastasis (Fruman et al., 2017). Now it is confirmed that Notch signaling is related with self-renewal ability, activating of PI3K signaling leads to enhanced antiapoptotic ability, JAK-STAT signaling leads to tumor progression and drug resistance (Butti et al., 2019). Together with tumor microenvironment-sustaining effects (exosomes or chemokines), these factors could contribute to a therapy-resistant phenotype of BCSC, highlighting the importance of precision treatment approaches in managing complex cancers (Yang et al., 2024).

It has already been shown in much cancer research that the three-dimensional (3D) cell culture models could provide an overview of cell-to-cell communication and interactions (Habanjar et al., 2021). Moreover, 3D cell culture models can reproduce important aspects of tumor structure and microenvironment, and also help to reduce the use of laboratory animals in drug trials (Barbosa et al., 2021). Using the 3D cell culture method, we confirmed that BYL-719 could effectively overcome drug resistance by inhibiting BCSCs, which may be a prominent clinical tool in the future. Our experimental methods and research ideas were innovative. However, there is still a need for in-depth studies on BYL-719 and the mechanisms of overcoming breast cancer resistance, as there is not much similar research currently available.

## 2 Materials and methods

### 2.1 Cell culture

Human breast cancer cell lines, MCF-7 and T47D, were purchased from the American Type Culture Collection (Rockville, MD, United States). The cells were grown in RPMI

1640 (Gibco) containing 10% fetal bovine serum (Gibco), with penicillin (100 U/mL), and streptomycin B (100 mg/mL). All cells were cultured in a 5% CO<sub>2</sub> incubator at 37°C with 5% relative humidity (Zhao et al., 2024).

## 2.2 Three-dimensional (3D) mammosphere culture method

Cells (1,000/cm<sup>2</sup> cells per well) were added to a low attachment six-well plate in serum free DMED/F12 medium (Corning, United States) supplemented with 2 mM L-glutamine, 100 U/mL penicillin/streptomycin, 20 ng/mL EGF (90201, BPS Bioscience), 10 ng/mL FGF (3718-FB-100, Biotechne), 2.5% Matrigel (Corning, United States) and 1× B27 supplement (17504044, Gibco). The plates were incubated for 5–7 days until the mammospheres (>40 µm) were formed. The mammospheres from each well were then collected. After slow centrifugation, the spheres were trypsinized for 2–3 min to separate them into single-cell suspensions. After at least five repetitions, we collected the enriched BCSC-like cells for the experiments by the 3D culture method (Lee et al., 2023).

## 2.3 Cells viability via 3-(4,5-dimethylthiazol-2-yl)-2,5-diphenyltetrazolium bromide (MTT) assay

To determine the dose response to BYL-719 (S2814, Selleck, United States), cells were seeded in a 96-well plate in six replicates at the density of  $2 \times 10^3$ /well and incubated overnight, then treated with serial dilutions of BYL-719 at 37°C for 96 h. After 96 h treatment, cells were incubated with 10 µL yellow MTT solution (Cell Proliferation Kit I (MTT), Roche) for 2–3 h in the incubator (Zhao et al., 2020). The 100 µL solubilization solution was then added and the plate was placed overnight in the incubator in a humidified atmosphere. Absorbance of the formazan product was measured at 490 nm using a microplate reader.

## 2.4 Clonogenic assay (2D)

One thousand cells per well in were added to a 12-well plate with 1 mL DMED/F12 medium supplemented with 2 mM L-glutamine, 100 U/mL penicillin/streptomycin, 20 ng/mL EGF, 10 ng/mL FGF, and 1× B27 supplement containing different concentrations of BYL-719. After 7 days, the medium was replaced with 1 mL fresh medium with appropriate concentrations of BYL-719 and incubated for another 7 days. After 2 weeks of incubation, cell colonies (Brix et al., 2021) were visualized using Quick staining (Merck, Darmstadt, Germany) and photographed.

## 2.5 Mammospheres forming assay

Five hundred cells per well were added to a 24-well low attachment plate in 500 µL mammosphere media are added to each well and incubated with different concentrations of BYL-719

for 5 days. The mammospheres (diameter >40 µm) were counted and mammosphere forming efficiency (Lombardo et al., 2015) were calculated as percentage of cells seeded and recorded.

## 2.6 Sphere-formation assay (3D condition)

Two thousand cells/well in with 100 µL mammosphere media with appropriate concentrations of BYL-719 were added to a 96-well U bottom low attachment plate. The cells were cultured for 10 days. After incubation, the diameters of the spheres in each well were measured and compared with those in control wells.

## 2.7 Flow cytometry analysis to detect biomarkers of BCSCs

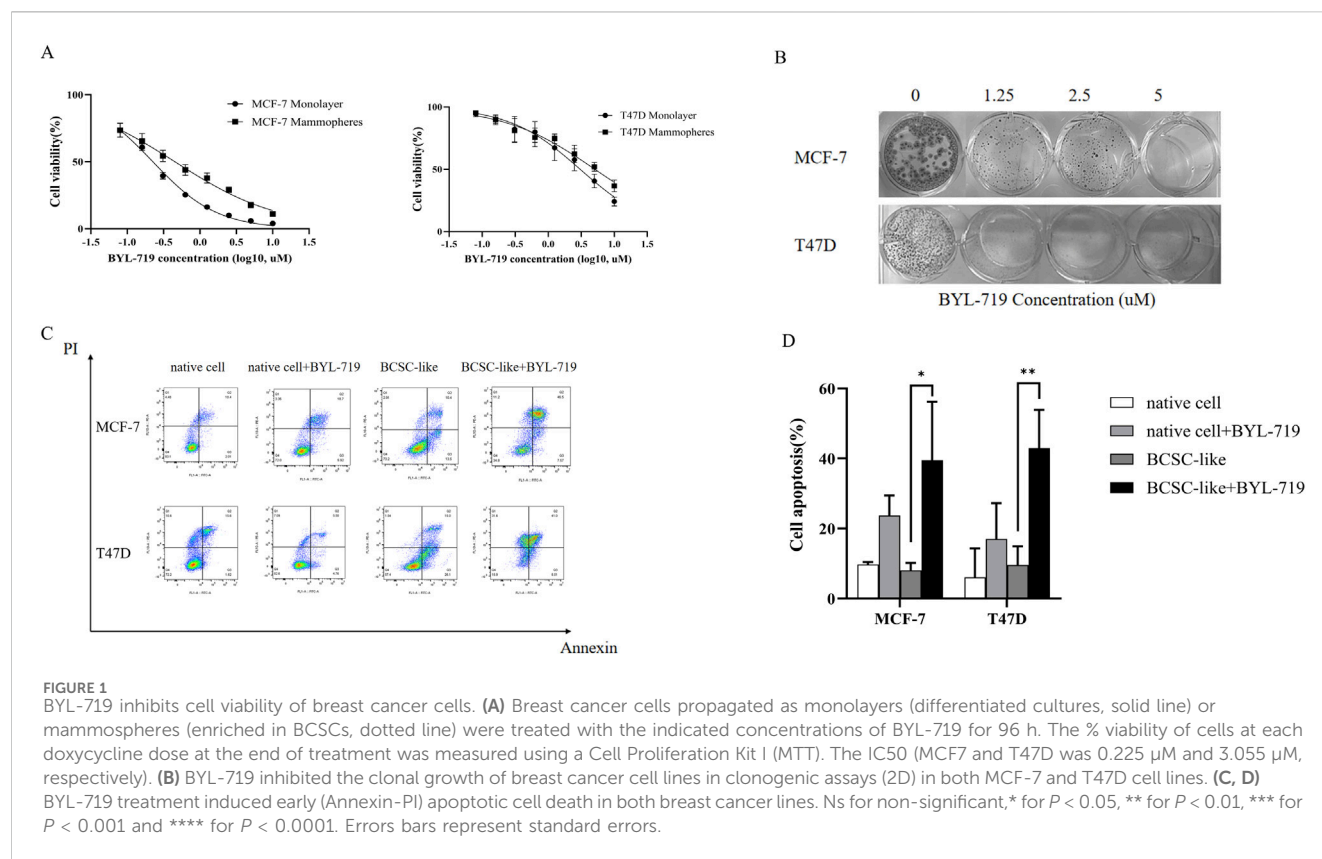
The reversed cells were digested by Accutase. Cells were washed, blocked with FC block (1:50), centrifuged and resuspended in 100 µL fluorescence-activated cell sorting (FACS) buffer (PBS containing 0.5% BSA and 0.1% sodium azide), containing fluorochrome-conjugated monoclonal antibodies against human CD44 (FITC, 555478, BD Biosciences) at 1:80 dilution and CD24 (PE, 555428, BD Biosciences) at 1:20 dilution. The cells were then washed again with cold PBS, suspended, filtered through 40-µm nylon mesh before analysis and measured with a CytoFlex flow cytometer (Beckman, United States).

## 2.8 Cell apoptosis via annexin V/PI assay

Cells were seeded overnight and treated with 1 µM concentration of BYL-719. After 24 h drug treatment, cells were detached by 0.25% trypsin, washed and resuspend in 1× binding Buffer at a concentration of  $1 \times 10^6$  cells/mL. The solution was then transferred to a 5 mL FACS tube. 1 µL of FITC (Annexin V PE Annexin V Apoptosis Detection Kit I) was added, and the cells were gently vortexed and incubated at RT (25°C) for 15 min in the dark. The 1× Binding Buffer (400 µL) and 2 µL PI were added to each tube. Apoptosis was analyzed using flow cytometry and the FlowJo software (V10).

## 2.9 Western blotting

The extracted proteins were separated using 10% SDS-PAGE gels. Blots were incubated at 4°C overnight with the primary antibodies against NANOG (#4903, 1:2,000, Cell Signaling Technology), OCT3/4 (#365509, 1:1,000, Santa Cruz), Sox2 (#3579, 1:1,000, Cell Signaling Technology), EMT (#9782, 1:500, Cell Signaling Technology), p-4ebp1 (#2855, 1:500, Cell Signaling Technology), p-P70S6k (#9205, 1:500, Cell Signaling Technology), p-AKT (#9271, 1:500, Cell Signaling Technology), and pARF (#9542, 1:500, Cell Signaling Technology), the Notch Activated Targets Antibody Sample Kit (#68309, 1:1,000, Cell Signaling Technology). Secondary antibodies (Santa Cruz) were then used and detected using ECL Prime Western Blotting Detection Reagent (GE Healthcare). Images were obtained using the ImageJ software (Wang J. et al., 2024).



## 2.10 Statistics

Statistical analyses were performed using the GraphPad Prism 9 software (GraphPad Software, La Jolla, United States). Shapiro-Wilk and Kolmogorov-Smirnov tests were used for normal distribution analysis. Unpaired t-tests (with Welch's correction in data without equal variances) were used for two independent data sets. One-way ANOVA (with Welch's correction in data without equal variances) and Tukey's multiple comparisons test were used for more than two independent samples. Half-maximal IC<sub>50</sub> values were calculated using non-linear regression analysis. Statistical significance was set at  $P < 0.05$ . The following symbols were used: ns, non-significant; \* $P < 0.05$ , \*\* $p < 0.01$ , \*\*\* $p < 0.001$ , and \*\*\*\* $p < 0.0001$ . Error bars represent the standard error. The 95% confidence interval (CI) were calculated.

## 3 Results

### 3.1 BYL-719 inhibits cell viability of breast cancer cells and mammospheres

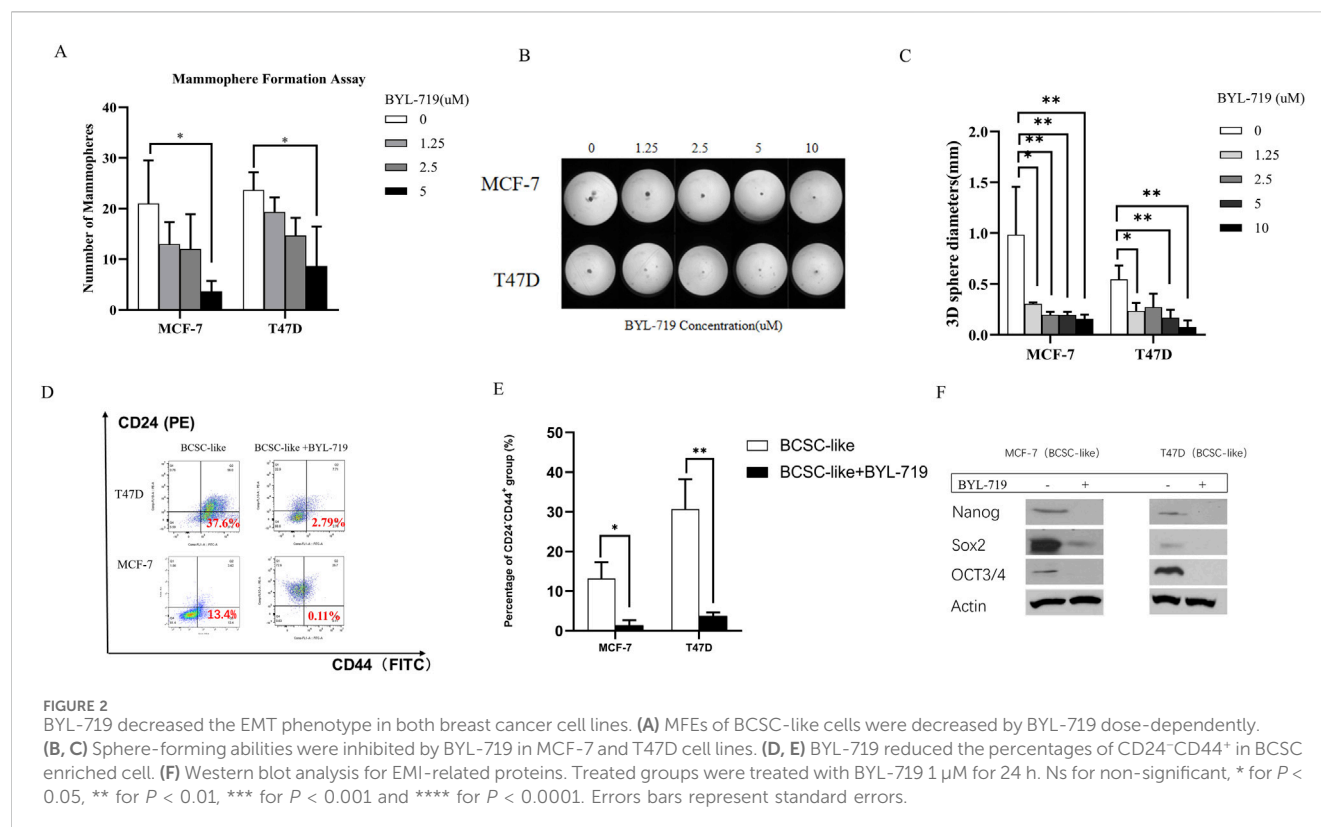
MCF-7 and T47D human breast cancer cells were treated with increasing concentrations of BYL-719 for 96 h, and the effect of BYL-719 on cell viability was measured. BYL-719 inhibited viability of breast cancer cells in a dose-dependent manner with IC<sub>50</sub> values (concentration of drug that inhibits 50% of cell viability relative to untreated cells) for MCF-7 and T47D of 0.225  $\mu$ M and 3.055  $\mu$ M, respectively (Figure 1A). In addition, treatment with BYL-719 significantly inhibited proliferation

of BCSC-enriched mammosphere cultures 96 h after a single treatment (Figure 1A). However, in agreement with other studies demonstrating that BCSCs are in general more resistant to anticancer drugs, the IC<sub>50</sub> values for BCSC-enriched mammosphere cultures increased approximately two-fold for both lines (0.453  $\mu$ M and 5.105  $\mu$ M for MCF-7 and T47D, respectively) (Figure 1A). We further confirmed the toxic effects of BYL-719 via clonogenic assays and assessed its impact on the cellular self-renewal capacity. The number of colonies formed with different concentrations of BYL-719 was significantly reduced compared to that of the controls in MCF-7 and T47D cells (Figure 1B). Colonies were fixed and visualized using quick stain. Finally, by using Annexin-PI straining and FACS analysis to detect the apoptosis, we showed that BYL-719 of the concentration of 1  $\mu$ M induced apoptosis especially in BCSC-like cell populations (Figure 1C). Apoptotic cells in the BYL-719 treated group of BCSC-like cell populations were significantly increased compared to those in the BCSC-like cell groups in both cell lines (MCF-7:  $p = 0.00107$ , 95% CI, 8.246 to 54.77; T47d:  $p = 0.0079$ , 95% CI, 9.976–56.72) (Figure 1C). These results suggest that BYL-719 can activate and promote cell death signaling pathways, including autophagy, apoptosis, ferroptosis, and necroptosis, through crosstalk among the BCSC signaling pathways.

### 3.2 BYL-719 inhibits stem cell marker expression and self-renewal in breast cancer stem cells

The self-renewal capacity of BCSCs in both breast cancer lines was measured using a mammosphere-forming efficiency (MFE)





assay. The MFE assay with BCSC-enriched cell populations showed a strong dose-dependent reduction in MFEs by BYL-719 in both cell lines. By the concentration of 5  $\mu$ M, MFE decreased in both cell lines (MFE for MCF-7,  $p = 0.047$ , 95% CI, 1.627–33.04; MFE for T47D,  $p = 0.0262$ , 95% CI, 2.370–27.63) (Figure 2A). Next, we performed a 3D sphere-forming assay using different concentrations of BYL-719 to determine its effects of BYL-719 in 3D condition. After incubation, the spheres formed in each well were photographed, and their diameters were calculated using GraphPad Prism 9 software (Figure 2B). In both cell lines, BYL-719 significantly reduced sphere diameter, indicating that stemness and resistance could be inhibited by BYL-719 (Figure 2C). We also investigated the effect of BYL-719 on the BCSC population using a combination of surface markers for BCSCs. The CD44<sup>+</sup>CD24<sup>−</sup> cell population has been shown to identify a subpopulation of cells in breast cancer enriched for BCSCs. This is illustrated in Figure 2D. Before the FACS analysis, each group was treated with BYL-719 at a concentration of 1  $\mu$ M for 24 h. After treatment with BYL-719, the CD44<sup>+</sup>CD24<sup>−</sup> cell populations present in BCSCs significantly decreased compared to those in untreated cells (MCF-7,  $p = 0.0088$ , 95% CI, 4.941–18.64; T47D,  $p = 0.0237$ , 95% CI, 8.631–45.32) (Figure 2E). Inhibition of stem cell factors at the gene level was accompanied by lower protein levels after treatment with 1  $\mu$ M BYL-719 for 24 h compared to that in untreated controls (Figure 2F). Nanog, Sox2, and OCT3/4 levels were significantly decreased in both MCF-7 and T47D cell lines; for the MCF-7 cell line, Nanog ( $p < 0.001$ ; 95% CI, 0.9908–1.045); Sox2 ( $p = 0.0069$ , 95% CI, 0.5014–1.062); OCT3/4 ( $p = 0.0014$ , 95% CI, 0.5370–0.7396), and for T47D cell line, Nanog ( $p = 0.0007$ , 95% CI, 0.6007–0.7528); Sox2

( $p = 0.0047$ , 95% CI, 0.5294–0.9732); and OCT3/4 ( $p = 0.0026$ , 95% CI, 0.7925–1.239).

### 3.3 BYL-719 inhibits various important signaling pathways

Western blot analysis demonstrated that the PI3K/AKT/mTOR inhibitor alpelisib (BYL-719) was highly effective. By comparing BCSC-like group and BYL-719 treated group (1  $\mu$ M, 24 h), the downstream proteins changed significantly (Figure 3A). We detected a significant rise in BCSC-like group than native cell, in MCF-7 cell line, p-P70S6K ( $p = 0.0059$ , 95% CI, 0.5835–1.167); p-4EBP1 ( $p = 0.0296$ ; 95% CI, 0.1505–1.093); p-AKT ( $p = 0.0457$ ; 95% CI, 0.0316–1.304); p-ARF ( $p = 0.0437$ ; 95% CI, 0.04852–1.334). And in T47D cell line, p-P70S6K ( $p = 0.0498$ ; 95% CI, 0.0020–2.362); p-4EBP1 ( $p = 0.0447$ ; 95% CI, 0.05451–1.797); p-AKT ( $p = 0.0371$ ; 95% CI, 0.1561–1.965); and p-ARF ( $p = 0.0463$ ; 95% CI, 0.0556–2.654). After treatment with BYL-719, the levels of all the downstream protein markers decreased. The decrease in p-P70S6K; p-4EBP1 and p-AKT enables us to demonstrate that the PI3K/AKT/mTOR signaling pathway is active in BCSC and is susceptible to efficient inhibition by BYL-719. p-ARF regulates several activities that are crucial to the functioning of cells, including transcription, apoptosis, and the response to DNA damage.

Other signaling pathways that crosstalk with the PI3K/AKT/mTOR signaling pathway in the TME of BCSCs and act as PI3K inhibitors include the MAPK/ERK, Notch, and STAT signaling pathways. BYL-719 can affect these signaling pathways as well as

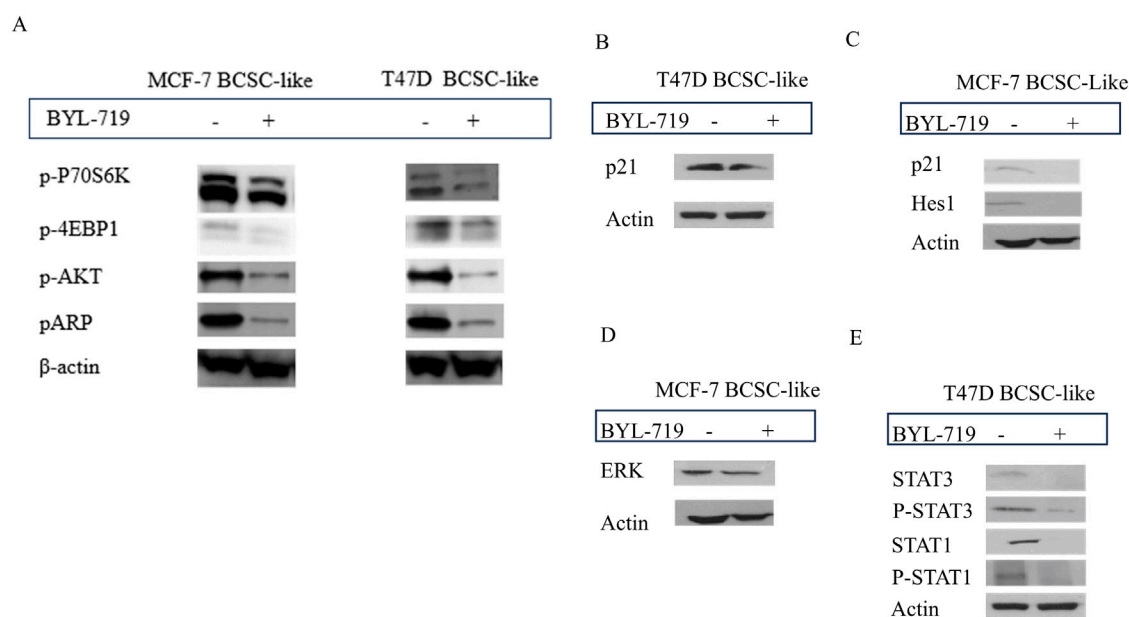


FIGURE 3

The inhibition of BYL-719 in PI3K/AKT/mTOR; Notch; MAPK/ERK; JAK/STAT signaling pathways. All the treated groups were treated with BYL-719 of the concentration of 1  $\mu$ M for 24 h. **(A)** BYL-719 inhibited PI3K/AKT/mTOR signaling pathway in MCF-7 BCSC-like treated group and T47D BCSC-like treated group. **(B, C)** Notch signaling pathway and p21 protein were inhibited by BYL-719 in MCF-7 BCSC-like treated group and T47D BCSC-like treated group. **(D)** ERK was decreased in MCF-7 BCSC-like treated group. **(E)** JAK/STAT signaling pathway was inhibited by BYL-719 in T47D BCSC-like treated group. Image **(B)** and Image **(E)** are from the same cells in a same experiment, with the same loading control. Image **(C)** and Image **(D)** are from the same cells in a same experiment, with the same loading control. We separate these images in order to explain the changes in different signaling pathways more clearly.

some intrinsic and extrinsic pathways. The levels of some important proteins in these signaling pathways significantly changed ( $P < 0.05$ ).

In the MAPK/ERK pathway, we detected the ERK protein which has been proved to be associated with the sphere-formation and maintainance of CSC-like characteristics. More importantly, ERK inhibitors are able to overcome the acquired drug resistance induced by upstream kinases inhibitors. In addition, ERK inhibition is the most effective target in MAPK/ERK signaling pathway (Liu et al., 2018). We detected a significant decrease of ERK protein treated with 1  $\mu$ M BYL-719 for 24 h ( $p = 0.0256$ ; 95% CI, 0.5083–2.904) (Figure 3D). The ERK/MAPK signaling pathway was thought to be inhibited by BYL-719, a widely known PI3K inhibitor. Notably, altered proteins can be found in a variety of cell types. Hes1 have an important function in the maintenance of cancer stem cells self-renewal, cancer metastasis, and epithelial-mesenchymal transition (EMT) process induction, as well as chemotherapy resistance (Liu et al., 2015). In BC, CDKN1A/p21 is induced by the Akt pathway, particularly in HER-2/neu-overexpressing cells, results in cytoplasmic localization in breast cancer cell lines. This is particularly noteworthy. This event is essential for the survival of cancer cells and their resistance to apoptosis. Moreover, the recent research indicate the p21 protein may lead to the chemoresistance. After treatment with the same dose of BYL-719, p21 decreased in both cell lines, and we detected a decrease in Hes1 expression in MCF-7 cells (Figures 3B, C). Although the targeted molecules were different, the trends were the same in both groups, suggesting that the Notch signaling pathway was activated in BCSC-like cells and could be effectively inhibited by the PI3K inhibitor BYL-719. Quantification of p21 ( $p = 0.0340$ ; 95% CI, 0.03491–0.3408) and HES1 ( $p = 0.0418$ ; 95%

CI, 0.01394–0.2904) levels significantly reduced after treatment with BYL-719.

In the T47D cell line, p21 was also decreased in the BYL-719 treated group (1  $\mu$ M, 24 h) ( $p = 0.0237$ ; 95% CI, 0.1697–1.378) and the STAT signaling pathway, which were associated with breast cancer and the stem cells (Figure 3E). STAT3 ( $p = 0.0350$ ; 95% CI, 0.06291–0.6618), P-STAT3 ( $p = 0.0375$ ; 95% CI, 0.04564–0.5930), STAT1 ( $p = 0.0466$ ; 95% CI, 0.03697–1.955), and P-STAT1 ( $p = 0.0481$ ; 95% CI, 0.02025–1.905) were all significantly decreased, corroborating our hypothesis that BYL-719 effectively suppresses the JAK/STAT signaling pathway activity.

### 3.4 Roles of BCSC-like cells in eribulin resistance and effects of BYL-719 in overcoming eribulin resistance in breast cancer cells

We analyzed whether the addition of BYL-719 to the culture increased the sensitivity of the cells to eribulin. MTT assays were performed to determine the effects of the combination of the two drugs. All the cell lines were proved to be resistant to eribulin via the MTT assays. Even extremely high concentration of eribulin had poor effects on the cell lines as shown in Figures 4A–C, while the combination groups of the BYL-719 and eribulin led to stronger cytotoxicity in ER cells compared to that with each drug alone, indicating that BYL-719 has the potential to increase the sensitivity of ER cells to eribulin.

Under 3D conditions, BYL-719 inhibited the growth and proliferation of ER-resistant cells in most cell lines by calculating

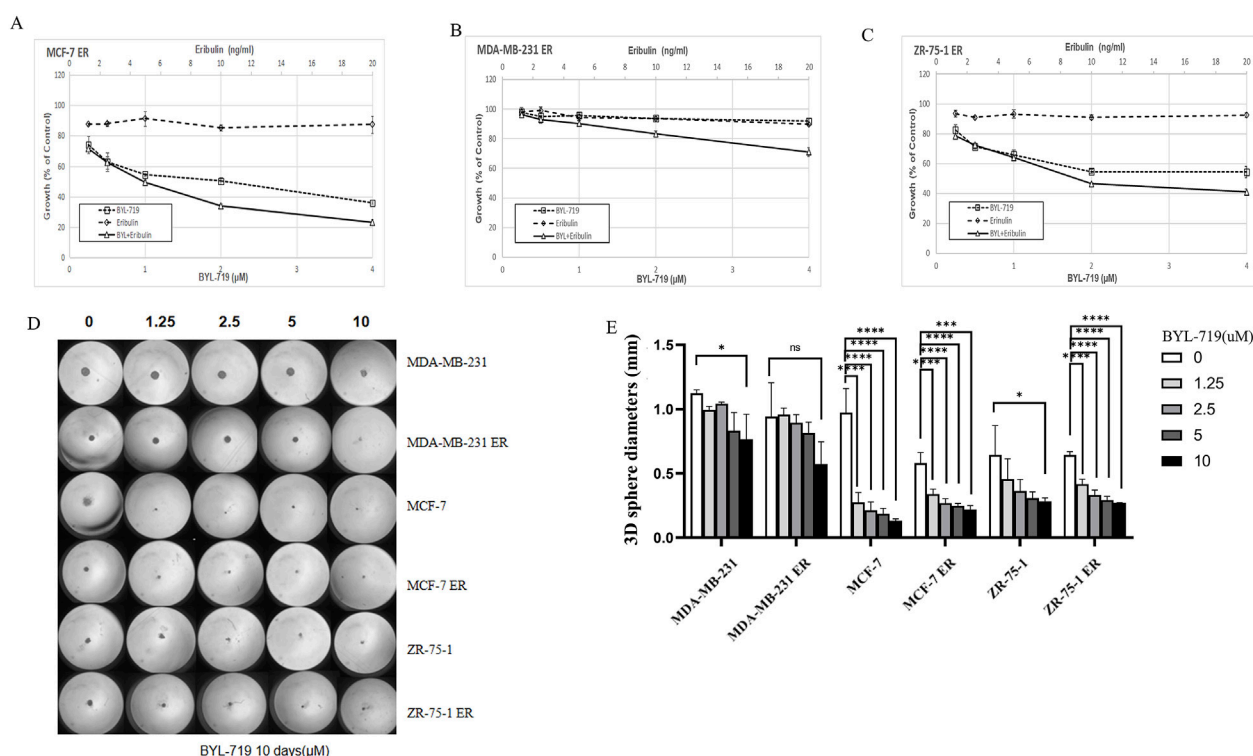


**FIGURE 4** (A–C) BYL-719 could inhibit the cell viability of ER vells (D, E) Sphere-forming abilities of ER cells were all inhibited by BYL-719. Ns for non-significant, \* for  $P < 0.05$ , \*\* for  $P < 0.01$ , \*\*\* for  $P < 0.001$  and \*\*\*\* for  $P < 0.0001$ . Errors bars represent standard errors.

the diameters of the spheres, except for the MDA-MB-231 ER cell group, which showed a high level of resistance (Figures 4D, E). These data indicated that there was no cross-resistance to BYL-719 in eribulin-resistant cells.

In the clonogenic assay, all six groups were inhibited by BYL-719, indicating that BCSC self-renewal and stemness were inhibited by BYL-719 (Figure 5A). Inhibition was more apparent in native breast cancer cell lines than in ER cells. These findings were attributed to the increased percentage of BCSC in the ER cells.

The mammosphere formation assay under 3D conditions (Figure 5C) showed that the number of mammospheres in ER cells significantly decreased after treatment with different doses of BYL-719 for 5 days. However, a significant reduction in the number of mammospheres was observed. Both the stemness of ER cells and their capacity to produce mammospheres decreased.

For further confirmation, we performed FACS sorting and western blotting to analyze the expression of surface and cytoplasmic BCSC markers in BCSC enriched ER cells under treatment with BYL-719. As shown in Figure 5B, we found that the subpopulation of cells with CD44<sup>+</sup>/CD24<sup>-</sup> surface markers in BCSC enriched in ER cells were reduced after treated by 1 μM BYL-719 for 24 h, indicating that even small dose of BYL-719 could have a direct effect on BCSCs. These differences were considered statistically significant, Nanog ( $p = 0.0152$ ; 95% CI, 0.5036–2.662), SOX2 ( $p = 0.0116$ ; 95% CI, 0.4989–2.200), and OCT3/4 ( $p = 0.0320$ ; 95% CI, 0.05508–0.7305). These findings were confirmed using western blotting, which demonstrated that BYL-719 substantially reduced BCSC-related protein levels in BCSC-enriched MCF-7 ER cells (Figure 5D).

In MCF-7 ER cells, important signaling pathways, including Notch and STAT, which crosstalk with the PI3K/AKT/mTOR signaling pathway in the TME, showed significant changes ( $p < 0.05$ ). Some changes were even more significant than those observed in native cells.

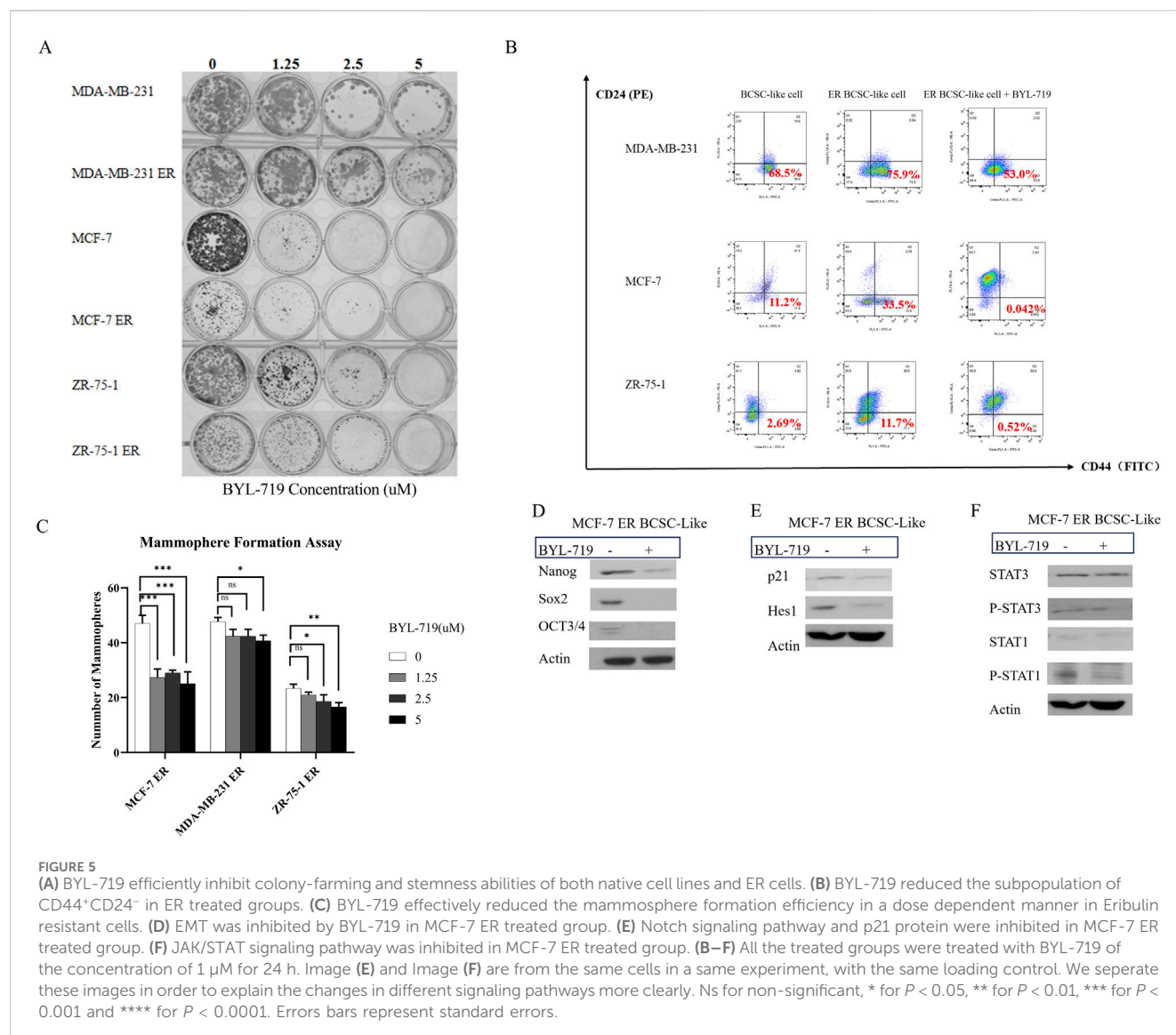
As shown in Figure 5E, by analyzing the Notch signaling pathway, p21 ( $p = 0.0361$ ; 95% CI, 0.02892–0.3332) and Hes1 ( $p = 0.0372$ ; 95% CI, 0.05508–0.7305) notably decreased in the MCF-7 ER BCSC-like group. These results confirmed our hypothesis that the Notch signaling pathway is active in BCSC and inhibited by BYL-719.

The results in Figure 5F showed P-STAT3 ( $p = 0.0466$ ; 95% CI, 0.0090–0.4803) and P-STAT1 ( $p = 0.0459$ ; 95% CI, 0.06989–3.057) were inhibited by BYL-719. However, we did not detect significant changes in STAT1 and STAT3. We still confirm that the STAT/JAK signaling pathway could also be inhibited by adding BYL-719 because phosphorylation in the Notch signaling pathway is closely associated with stem cells.

## 4 Discussion

### 4.1 The 3D-cell culture method is a novel and highly effective method to enrich BCSCs *in vitro*

While two-dimensional (2D) cell culture systems *in vitro* are widely used, they often fall short in accurately replicating physiological conditions relevant to clinical research. To address this limitation, in this experiment, we employed a three-dimensional



(3D) mammosphere culture method, through which BCSC-like cells were harvested *in vitro*. These BCSC-like cells were harvested using a 3D cell culture method, whereby spheroids were derived from primary breast cancer cell lines and collected from differentiated cells (Habbanjar et al., 2021). They are also referred to as “tumoroids” (Idrisova et al., 2022). The cell population is a subset of cells capable of dictating invasion, metastasis, heterogeneity, and therapeutic resistance in tumors (Jaggupilli and Elkord, 2012). CD44 and CD24 are important and widely recognized BCSC surface markers (Cataldo et al., 2024) which are found in many tumor types and are often used together or in combination with other putative markers to isolate stem cells from solid tumors (Jaggupilli and Elkord, 2012). This subpopulation of breast cancer cells (CD44<sup>+</sup>/CD24<sup>+</sup>) has stem/progenitor cell properties (Alvarez-Elizondo and Weihs, 2022). To quantify the ratio of CD44<sup>+</sup>/CD24<sup>+</sup> subpopulation of cells, FACS was performed in this experiment. Moreover, BCSC-like cells are known to express higher levels of EMT, a phenomenon in which epithelial cells acquire mesenchymal properties, a process that has been observed in tumor progression and invasion (Savagner, 2010).

Therefore, protein markers, including Nanog, OCT3/4, and SOX2, were detected, as they promote the emergence of CSCs with mesenchymal properties necessary for proliferation and self-renewal, which are required for secondary tumor formation (Vuoriluoto et al., 2011).

## 4.2 The stemness are inhibited by BYL-719 in both cell lines

Treatment with BYL-719 significantly inhibited the proliferation of BCSC-enriched mammosphere cultures 96 h after a single treatment (Figure 1A) and the IC<sub>50</sub> values for BCSC-enriched mammosphere cultures increased by approximately two-fold for both cell lines. This indicates that stemness is indeed inhibited by BYL-719.

Furthermore, by performing an *in vitro* clonogenic assay, we detected cell survival. This is significant because clonogenic ability indicates the stemness of cancer cells, which is crucial in tumors where the capacity for unlimited proliferation can lead to tumor



recurrences. As demonstrated in Figure 1B, both breast cancer cell lines exhibited an evident decrease in the number of colonies. Additionally, apoptosis was detected in both the control and treatment groups (Figure 1C). These findings suggest that BYL-719 is highly effective, as it promoted apoptosis in BCSC-like cells. This implies that BYL-719 could active and promote the cell death signaling pathways, which include autophagy, apoptosis, ferroptosis, and necroptosis through crosstalk among BCSC signaling pathways. Moreover, it inhibited anti-apoptotic mechanisms via survivin, Mcl-1, Bcl-2, IAPs, and DNA-repairing proteins (Kist and Vucic, 2021).

In the mammosphere formation assay, the volume of mammospheres decreased by the enhancing concentration of BYL-719, as shown in Figure 2A. Under the 3D condition, the diameters of spheres were inhibited, as shown in Figure 2B. Additionally, the stem cell surface marker CD44 and CD24 were detected, and the proportion of the subpopulation (CD44<sup>+</sup>/CD24<sup>−</sup>) were then calculated by FACS analysis (Figure 2C). In both cell lines, the proportion of CD44<sup>+</sup>/CD24<sup>−</sup> cells significantly decreased after treatment with 1  $\mu$ M BYL-719 for 24 h (Figure 2D). By comparing the western blot of MCF-7 BCSC-like and MCF-7 BCSC-like cells in 1  $\mu$ M BYL-719 for 48 h, the decrease of Nanog, SOX2 and OCT3/4 were statistically significant (Figure 2E).

### 4.3 BYL-719 inhibited the stemness by acting on various signaling pathways which play essential roles in the TME of BCSCs

The PI3K/mTOR signaling pathway is essential for cell survival and proliferation (Glaviano et al., 2023). In fact, some malignancies, such as non-small-cell lung, breast, prostate, and colorectal cancer, exhibit an abnormal activation of PI3K/AKT/mTOR signaling (Jiang et al., 2020; Yu et al., 2022). Although the PI3K/AKT/mTOR pathway has been extensively investigated in cancer, few studies have been conducted on CSCs (Yoon et al., 2024). Blocking the PI3K signaling pathway to stop tumor growth is not a new concept; many inhibitors, such as two rapalogues, everolimus, and temsirolimus, have been used for many years with good efficacy (Bai et al., 2018). In our study, we confirmed the inhibition of PI3K by decreasing p-P70S6K; p-4EBP1, p-AKT, and p-ARP (Figure 3A).

Moreover, other major signaling pathways are also involved in CSC self-renewal and differentiation, including the Notch, MAPK/ERK, JAK-STAT, Wnt/ $\beta$ -catenin, and Hedgehog (Hh) signaling pathways (Bhal and Kundu, 2023). Additionally, other important signaling pathways in CSCs include TNF- $\alpha$ /NF- $\kappa$ B, transforming growth factor- $\beta$  (TGF- $\beta$ ), and receptor tyrosine kinase (RTK) signaling pathways (Chia et al., 2024; Borlongan and Wang, 2023). These signaling pathways are related to self-renewal and differentiation (Xu et al., 2018). Western blotting was performed to detect changes in important proteins in the MAPK/ERK, Notch, and JAK-STAT signaling pathways, which were confirmed to be important in BCSCs (Figures 3B–E). The mitogen-activated protein kinase/extracellular signal-regulated kinase (MAPK/ERK) pathway is associated with cell proliferation, differentiation, migration, aging, and apoptosis (Sun et al., 2015). Similarly, the Notch signaling pathway also plays an important role in cell development and differentiation (Shi et al., 2024). Furthermore, the JAK-STAT signaling pathway is also activated in BCSCs, and persistent

activation of STAT3 can stimulate cell survival and maintain stem cell properties in BCSCs (Zhou et al., 2007). Interestingly, the PI3K/mTOR pathway regulates STAT3 expression and promotes the survival and proliferation of BCSCs (Zhou et al., 2007). In our study, important downstream proteins were detected, and we confirmed the significant inhibition of all these signaling pathways.

### 4.4 BYL-719 could help overcome the drug resistance of breast cancer cells by acting on BCSCs

In the final phase of our experiment, the function and influence of BYL-719 to the resistance of tumor cells were the focus. To explore this, several drug-resistant cell lines were also cultured. Specifically, three eribulin-resistant cell lines, including-MCF-7 ER, MDA-MB-231 ER, and ZR-75-1 ER—were used in this study. These cell lines were cultured, collected, and confirmed to be highly resistant to eribulin, a non-taxane microtubule dynamics inhibitor with tubulin-based anti-mitotic activity and chemotherapeutic effects (Perry, 2011).

As is well-documented, CSCs can easily adapt to environmental changes and are inherently more resistant to conventional therapies compared to other cells in the tumor (Najafi et al., 2019). This drug resistance in CSCs could be secondary to radiotherapy or chemotherapy or may even be induced after isolation from chemotherapy (Prieto-Vila et al., 2017). The combination of intrinsic and extrinsic factors significantly contributes to the CSC-mediated resistance to treatment (Najafi et al., 2019). Intrinsic factors include EMT, oxidative regulators, stem cells, and signaling effects, whereas extrinsic factors include cellular plasticity and some signaling factors (Najafi et al., 2019). To overcome clinical resistance to treatment, scientists have focused on novel insights into CSCs. While standard therapies act on rapidly dividing cells and are generally effective in reducing the size of the primary tumor, complete eradication remains challenging due to the presence of CSCs. Despite their high proliferative capacity, CSCs, such as BCSCs, spend most of their time in a resting state (cell cycle phase G0), which allows them to protect themselves from chemotherapy and radiation (Zou et al., 2011). Moreover, the relative resistance of BCSCs to radiation and cytotoxic agents may be due to a more efficient DNA damage response mechanism, which can result in less cell death than that in other breast cell types (Saha and Lukong, 2022; Chang et al., 2015). Furthermore, BCSCs are more resistant to radiotherapy and chemotherapy due to their abundance in hypoxic regions (Chang et al., 2015). The fact that BCSCs are resistant to standard therapies highlights the need for novel therapies targeting BCSC populations. These distinct characteristics, markers, and resistance mechanisms suggest that targeting BCSCs is an essential breakthrough for developing more effective therapies for patients with breast cancer, either alone or in combination with currently used therapies.

Currently, BCSCs are suggested to be novel and essential targets for clinical BCSC therapy to overcome drug resistance and relapse. Emerging findings regarding surface markers and signaling networks support the development of therapeutic approaches using BCSCs (Conde et al., 2022) as a target. In future, we will do more experiments at the gene level and *in vivo* animal



experiments will be performed. Additionally, we intend to explore the combination of BYL-719 with other chemotherapeutic agents. Our hope is to identify the related genes of BCSCs in future.

## 5 Conclusion

Our research demonstrated that BYL-719 has a significant effect on BCSCs, and that the combination of BYL-719 with eribulin further overcomes drug resistance. We are optimistic that these findings will contribute to the development of therapies that can directly target BCSCs, thereby reducing metastasis and relapse in breast cancer. We believe that drug-resistant patients will benefit from the combination of BYL-719 with other chemotherapeutic agents in future studies.

## Data availability statement

The raw data supporting the conclusions of this article will be made available by the authors, without undue reservation.

## Ethics statement

Ethical approval was not required for the studies on humans in accordance with the local legislation and institutional requirements because only commercially available established cell lines were used.

## Author contributions

LY: Data curation, Formal Analysis, Investigation, Methodology, Software, Supervision, Validation, Visualization,

Writing–original draft, Writing–review and editing. CZ: Supervision, Writing–review and editing, Resources, Project administration, Conceptualization, Investigation, Funding acquisition. YY: Writing–review and editing, Software, Methodology. HL: Supervision, Conceptualization, Resources, Writing–review and editing. JE: Resources, Conceptualization, Supervision, Project administration, Writing–review and editing, Funding acquisition.

## Funding

The authors declare that financial support was received for the research, authorship, and/or publication of this article.

## Conflict of interest

The authors declare that the research was conducted in the absence of any commercial or financial relationships that could be construed as a potential conflict of interest.

The authors declare that this study received funding from Novartis Pharma GmbH (Funding Number: “SLAP-004”). The funder had the following involvement with the study: study design.

## Publisher's note

All claims expressed in this article are solely those of the authors and do not necessarily represent those of their affiliated organizations, or those of the publisher, the editors and the reviewers. Any product that may be evaluated in this article, or claim that may be made by its manufacturer, is not guaranteed or endorsed by the publisher.

## References

- Alvarez-Elizondo, M. B., and Weihs, D. (2022). Breast cancer stem cells: mechanobiology reveals highly invasive cancer cell subpopulations. *Cell. Mol. Life Sci.* 79 (3), 134. doi:10.1007/s00018-022-04181-w
- Bai, X., Ni, J., Beretov, J., Graham, P., and Li, Y. (2018). Cancer stem cell in breast cancer therapeutic resistance. *Cancer Treat. Rev.* 69, 152–163. doi:10.1016/j.ctrv.2018.07.004
- Barbos, M. A. G., Xavier, C. P. R., Pereira, R. F., Petrikaitė, V., and Vasconcelos, M. H. (2021). 3D 467 cell culture models as recapitulators of the tumor microenvironment for the screening of anti- 468 cancer drugs. *Cancers*.
- Bhal, S., and Kundu, C. N. (2023). Targeting crosstalk of signaling pathways in cancer stem cells: a promising approach for development of novel anti-cancer therapeutics. *Med. Oncol.* 40 (2), 82. doi:10.1007/s12032-022-01905-7
- Borlongan, M. C., and Wang, H. (2023). Profiling and targeting cancer stem cell signaling pathways for cancer therapeutics. *Front. Cell. Dev. Biol.* 11, 1125174. doi:10.3389/fcell.2023.1125174
- Brix, N., Samaga, D., Belka, C., Zitzelsberger, H., and Lauber, K. (2021). Analysis of clonogenic growth *in vitro*. *Nat. Protoc.* 16 (11), 4963–4991. doi:10.1038/s41596-021-00615-0
- Butti, R., Gunasekaran, V. P., Kumar, T. V. S., Banerjee, P., and Kundu, G. C. (2019). Breast cancer stem cells: biology and therapeutic implications. *Int. J. Biochem. Cell. Biol.* 107, 38–52. doi:10.1016/j.biocel.2018.12.001
- Cataldo, D., Aravena, G., Escobar, A., Tapia, J. C., Peralta, O. A., and Torres, C. G. (2024). Effect of melatonin on chemoresistance exhibited by spheres derived from canine mammary carcinoma cells. *Anim. (Basel)* 14 (8), 1229. doi:10.3390/ani14081229
- Chang, C. H., Zhang, M., Rajapakshe, K., Coarfa, C., Edwards, D., Huang, S., et al. (2015). Mammary stem cells and tumor-initiating cells are more resistant to apoptosis and exhibit increased DNA repair activity in response to DNA damage. *Stem Cell. Rep.* 5 (3), 378–391. doi:10.1016/j.stemcr.2015.07.009
- Chang, D. Y., Ma, W. L., and Lu, Y. S. (2021). Role of alpelisib in the treatment of PIK3CA-mutated breast cancer: patient selection and clinical perspectives. *Ther. Clin. Risk Manag.* 17, 193–207. doi:10.2147/TCRM.S251668
- Chia, Z. J., Cao, Y. N., Little, P. J., and Kamato, D. (2024). Transforming growth factor-β receptors: versatile mechanisms of ligand activation. *Acta Pharmacol. Sin.* 45, 1337–1348. doi:10.1038/s41401-024-01235-6
- Choi, C., Thi Thao Tran, N., Van Ngu, T., Park, S. W., Song, M. S., Kim, S. H., et al. (2018). Promotion of tumor progression and cancer stemness by MUC15 in thyroid cancer via the GPCR/ERK and integrin-FAK signaling pathways. *Oncogenesis* 7 (11), 85. doi:10.1038/s41389-018-0094-y
- Conde, I., Ribeiro, A. S., and Paredes, J. (2022). Breast cancer stem cell membrane biomarkers: therapy targeting and clinical implications. *Cells* 11 (6), 934. doi:10.3390/cells11060934
- De Angelis, M. L., Francescangeli, F., and Zeuner, A. (2019). Breast cancer stem cells as drivers of tumor chemoresistance, dormancy and relapse: new challenges and therapeutic opportunities. *Cancers (Basel)* 11 (10), 1569. doi:10.3390/cancers11101569
- Fruman, D. A., Chiu, H., Hopkins, B. D., Bagrodia, S., Cantley, L. C., and Abraham, R. T. (2017). The PI3K pathway in human disease. *Cell.* 170 (4), 605–635. doi:10.1016/j.cell.2017.07.029
- Glaviano, A., Foo, A. S. C., Lam, H. Y., Yap, K. C. H., Jacot, W., Jones, R. H., et al. (2023). PI3K/AKT/mTOR signaling transduction pathway and targeted therapies in cancer. *Mol. Cancer* 22 (1), 138. doi:10.1186/s12943-023-01827-6

- Guo, Y. J., Pan, W. W., Liu, S. B., Shen, Z. F., Xu, Y., and Hu, L. L. (2020). ERK/MAPK signalling pathway and tumorigenesis. *Exp. Ther. Med.* 19 (3), 1997–2007. doi:10.3892/etm.2020.8454
- Habanjar, O., Diab-Assaf, M., Caldefie-Chezet, F., and Delort, L. (2021). 3D cell culture systems: tumor application, advantages, and disadvantages. *Int. J. Mol. Sci.* 22 (22), 12200. doi:10.3390/ijms222212200
- Idrisova, K. F., Simon, H. U., and Gomzikova, M. O. (2022). Role of patient-derived models of cancer in translational oncology. *Cancers (Basel)* 15 (1), 139. doi:10.3390/cancers15010139
- Jaggupilli, A., and Elkord, E. (2012). Significance of CD44 and CD24 as cancer stem cell markers: an enduring ambiguity. *Clin. Dev. Immunol.* 2012, 708036. doi:10.1155/2012/708036
- Jiang, N., Dai, Q., Su, X., Fu, J., Feng, X., and Peng, J. (2020). Role of PI3K/AKT pathway in cancer: the framework of malignant behavior. *Mol. Biol. Rep.* 47 (6), 4587–4629. doi:10.1007/s11033-020-05435-1
- Kist, M., and Vucic, D. (2021). Cell death pathways: intricate connections and disease implications. *Embo J.* 40 (5), e106700. doi:10.15252/embj.2020106700
- Lee, S. Y., Koo, I. S., Hwang, H. J., and Lee, D. W. (2023). *In vitro* three-dimensional (3D) cell culture tools for spheroid and organoid models. *SLAS Discov.* 28 (4), 119–137. doi:10.1016/j.slasd.2023.03.006
- Li, W., Ma, H., Zhang, J., Zhu, L., Wang, C., and Yang, Y. (2017). Unraveling the roles of CD44/CD24 and ALDH1 as cancer stem cell markers in tumorigenesis and metastasis. *Sci. Rep.* 7 (1), 13856. doi:10.1038/s41598-017-14364-2
- Liongue, C., Sobah, M. L., and Ward, A. C. (2024). Signal transducer and activator of transcription proteins at the nexus of immunodeficiency, autoimmunity and cancer. *Biomedicines* 12 (1), 45. doi:10.3390/biomedicines12010045
- Liu, F., Yang, X., Geng, M., and Huang, M. (2018). Targeting ERK, an Achilles' Heel of the MAPK pathway, in cancer therapy. *Acta Pharm. Sin. B* 8 (4), 552–562. doi:10.1016/j.apsb.2018.01.008
- Liu, Z. H., Dai, X. M., and Du, B. (2015). Hes1: a key role in stemness, metastasis and multidrug resistance. *Cancer Biol. Ther.* 16 (3), 353–359. doi:10.1080/15384047.2015.1016662
- Lombardo, Y., de Giorgio, A., Coombes, C. R., Stebbing, J., and Castellano, L. (2015). Mammosphere formation assay from human breast cancer tissues and cell lines. *J. Vis. Exp.* 97, 52671. doi:10.3791/52671
- Luo, H., Li, Y., Song, H., Zhao, K., Li, W., Hong, H., et al. (2024). Role of EZH2-mediated epigenetic modification on vascular smooth muscle in cardiovascular diseases: a mini-review. *Front. Pharmacol.* 15, 1416992. doi:10.3389/fphar.2024.1416992
- Marbury, T., El-Hashimy, M., Blumenstein, L., Letellier, F., Sengupta, T., Lorenzo, S., et al. (2023). Pharmacokinetics and safety of multiple-dose alpelisib in participants with moderate or severe hepatic impairment: a phase 1, open-label, parallel group study. *J. Cancer* 14 (9), 1571–1578. doi:10.7150/jca.82736
- Markham, A. (2019). Alpelisib: first global approval. *Drugs* 79 (11), 1249–1253. doi:10.1007/s40265-019-01161-6
- Martínez-Pérez, J., Torrado, C., Domínguez-Cejudo, M. A., and Valladares-Ayerbes, M. (2024). Targeted treatment against cancer stem cells in colorectal cancer. *Int. J. Mol. Sci.* 25 (11), 6220. doi:10.3390/ijms25116220
- Najafi, M., Mortezaee, K., and Majidpoor, J. (2019). Cancer stem cell (CSC) resistance drivers. *Life Sci.* 234, 116781. doi:10.1016/j.lfs.2019.116781
- Nilendu, P., Kumar, A., Kumar, A., Pal, J. K., and Sharma, N. K. (2018). Breast cancer stem cells as last soldiers eluding therapeutic burn: a hard nut to crack. *Int. J. Cancer* 142 (1), 7–17. doi:10.1002/ijc.30898
- Perry, C. M. (2011). Eribulin. *Drugs* 71 (10), 1321–1331. doi:10.2165/11207520-000000000-00000
- Prieto-Vila, M., Takahashi, R. U., Usuba, W., Kohama, I., and Ochiya, T. (2017). Drug resistance driven by cancer stem cells and their niche. *Int. J. Mol. Sci.* 18 (12), 2574. doi:10.3390/ijms18122574
- Saha, T., and Lukong, K. E. (2022). Breast cancer stem-like cells in drug resistance: a review of mechanisms and novel therapeutic strategies to overcome drug resistance. *Front. Oncol.* 12, 856974. doi:10.3389/fonc.2022.856974
- Savagner, P. (2010). The epithelial-mesenchymal transition (EMT) phenomenon. *Ann. Oncol.* 21 (Suppl. 7), vii89–92. doi:10.1093/annonc/mdq292
- Shi, Q., Xue, C., Zeng, Y., Yuan, X., Chu, Q., Jiang, S., et al. (2024). Notch signaling pathway in cancer: from mechanistic insights to targeted therapies. *Signal Transduct. Target. Ther.* 9 (1), 128. doi:10.1038/s41392-024-01828-x
- Sun, Y., Liu, W. Z., Liu, T., Feng, X., Yang, N., and Zhou, H. F. (2015). Signaling pathway of MAPK/ERK in cell proliferation, differentiation, migration, senescence and apoptosis. *J. Recept. Signal Transduct. Res.* 35 (6), 600–604. doi:10.3109/10799893.2015.1030412
- Sun, Y. S., Zhao, Z., Yang, Z. N., Xu, F., Lu, H. J., Zhu, Z. Y., et al. (2017). Risk factors and preventions of breast cancer. *Int. J. Biol. Sci.* 13 (11), 1387–1397. doi:10.7150/ijbs.21635
- Sung, H., Ferlay, J., Siegel, R. L., Laversanne, M., Soerjomataram, I., Jemal, A., et al. (2021). Global cancer statistics 2020: GLOBOCAN estimates of incidence and mortality worldwide for 36 cancers in 185 countries. *CA Cancer J. Clin.* 71 (3), 209–249. doi:10.3322/caac.21660
- Taskindoust, M., Thomas, S. M., Sammons, S. L., Fayanju, O. M., DiLalla, G., Hwang, E. S., et al. (2021). Survival outcomes among patients with metastatic breast cancer: review of 47,000 patients. *Ann. Surg. Oncol.* 28 (12), 7441–7449. doi:10.1245/s10434-021-10227-3
- Vuoriluoto, K., Haugen, H., Kiviluoto, S., Mpindi, J. P., Nevo, J., Gjerdrum, C., et al. (2011). Vimentin regulates EMT induction by Slug and oncogenic H-Ras and migration by governing Axl expression in breast cancer. *Oncogene* 30 (12), 1436–1448. doi:10.1038/ncr.2010.509
- Wang, J., An, G., Peng, X., Zhong, F., Zhao, K., Qi, L., et al. (2024). Effects of three Huanglian-derived polysaccharides on the gut microbiome and fecal metabolome of high-fat diet/streptozocin-induced type 2 diabetes mice. *Int. J. Biol. Macromol.* 273 (Pt 1), 133060. doi:10.1016/j.ijbiomac.2024.133060
- Wang, J., and Wu, S. G. (2023). Breast cancer: an overview of current therapeutic strategies, challenge, and perspectives. *Breast Cancer (Dove Med. Press)* 15, 721–730. doi:10.2147/bctt.s432526
- Wang, Z., Che, S., and Yu, Z. (2024). PROTAC: novel degradable approach for different targets to treat breast cancer. *Eur. J. Pharm. Sci.* 198, 106793. doi:10.1016/j.ejps.2024.106793
- Wilkinson, L., and Gathani, T. (2022). Understanding breast cancer as a global health concern. *Br. J. Radiol.* 95 (1130), 20211033. doi:10.1259/bjr.20211033
- Xu, X., Zheng, L., Yuan, Q., Zhen, G., Crane, J. L., Zhou, X., et al. (2018). Transforming growth factor- $\beta$  in stem cells and tissue homeostasis. *Bone Res.* 6 (1), 2. doi:10.1038/s41413-017-0005-4
- Yang, X., Yang, C., Zhang, S., Geng, H., Zhu, A. X., Bernards, R., et al. (2024). Precision treatment in advanced hepatocellular carcinoma. *Cancer Cell.* 42 (2), 180–197. doi:10.1016/j.ccell.2024.01.007
- Yoon, C., Lu, J., Ryeom, S. W., Simon, M. C., and Yoon, S. S. (2024). Retraction Note: PIK3R3, part of the regulatory domain of PI3K, is upregulated in sarcoma stem-like cells and promotes invasion, migration, and chemotherapy resistance. *Cell. Death Dis.* 15 (3), 226. doi:10.1038/s41419-024-06609-6
- Yu, L., Wei, J., and Liu, P. (2022). Attacking the PI3K/Akt/mTOR signaling pathway for targeted therapeutic treatment in human cancer. *Seminars Cancer Biol.* 85, 69–94. doi:10.1016/j.semcancer.2021.06.019
- Zhang, J., Zhang, B., Pu, C., Cui, J., Huang, K., Wang, H., et al. (2023). Nanoliposomal Bcl-xL proteolysis-targeting chimera enhances anti-cancer effects on cervical and breast cancer without on-target toxicities. *Adv. Compos. Hybrid Mater.* 6 (2), 78. doi:10.1007/s42114-023-00649-w
- Zhang, T., Zhou, H., Wang, K., Wang, X., Wang, M., Zhao, W., et al. (2022). Role, molecular mechanism and the potential target of breast cancer stem cells in breast cancer development. *Biomed. Pharmacother.* 147, 112616. doi:10.1016/j.biopha.2022.112616
- Zhang, X., Powell, K., and Li, L. (2020). Breast cancer stem cells: biomarkers, identification and isolation methods, regulating mechanisms, cellular origin, and beyond. *Cancers (Basel)* 12 (12), 3765. doi:10.3390/cancers12123765
- Zhao, K., Li, B., He, D., Zhao, C., Shi, Z., Dong, B., et al. (2020). Chemical characteristic and bioactivity of hemicellulose-based polysaccharides isolated from *Salvia miltiorrhiza*. *Int. J. Biol. Macromol.* 165 (Pt B), 2475–2483. doi:10.1016/j.ijbiomac.2020.10.113
- Zhao, K., Qian, C., Qi, L., Li, Q., Zhao, C., Zhang, J., et al. (2024). Modified acid polysaccharide derived from *Salvia przewalskii* with excellent wound healing and enhanced bioactivity. *Int. J. Biol. Macromol.* 263 (Pt 2), 129803. doi:10.1016/j.ijbiomac.2024.129803
- Zhou, J., Wulfschle, J., Zhang, H., Gu, P., Yang, Y., Deng, J., et al. (2007). Activation of the PTEN/mTOR/STAT3 pathway in breast cancer stem-like cells is required for viability and maintenance. *Proc. Natl. Acad. Sci. U. S. A.* 104 (41), 16158–16163. doi:10.1073/pnas.0702596104
- Zou, P., Yoshihara, H., Hosokawa, K., Tai, I., Shinmyozu, K., Tsukahara, F., et al. (2011). p57(Kip2) and p27(Kip1) cooperate to maintain hematopoietic stem cell quiescence through interactions with Hsc70. *Cell. Stem Cell.* 9 (3), 247–261. doi:10.1016/j.stem.2011.07.003



## OPEN ACCESS

## EDITED BY

Jianbin Bi,  
The First Hospital of China Medical University,  
China

## REVIEWED BY

Igotz Delgado,  
University of the Basque Country, Spain  
Zijia Tao,  
The First Affiliated Hospital of China Medical  
University, China  
Jianyang Ao,  
Tongji University, China

## \*CORRESPONDENCE

Yunzhi Chen,  
✉ fyydwk@163.com

<sup>†</sup>These authors have contributed equally to  
this work

RECEIVED 19 September 2024

ACCEPTED 03 December 2024

PUBLISHED 19 December 2024

## CITATION

Yu D, Guo F, Zhang Q, Yu H, Wang W and  
Chen Y (2024) ABCA1 promote tumor  
environment heterogeneity via epithelial  
mesenchymal transition in Huh7 and  
HepG2 liver cancer cell.  
*Front. Pharmacol.* 15:1498528.  
doi: 10.3389/fphar.2024.1498528

## COPYRIGHT

© 2024 Yu, Guo, Zhang, Yu, Wang and Chen.  
This is an open-access article distributed under  
the terms of the [Creative Commons Attribution  
License \(CC BY\)](#). The use, distribution or  
reproduction in other forums is permitted,  
provided the original author(s) and the  
copyright owner(s) are credited and that the  
original publication in this journal is cited, in  
accordance with accepted academic practice.  
No use, distribution or reproduction is  
permitted which does not comply with these  
terms.

# ABCA1 promote tumor environment heterogeneity via epithelial mesenchymal transition in Huh7 and HepG2 liver cancer cell

Dinglai Yu<sup>1†</sup>, Fang Guo<sup>2†</sup>, Qiyu Zhang<sup>1</sup>, Huajun Yu<sup>1</sup>,  
Wenmin Wang<sup>3</sup> and Yunzhi Chen<sup>1\*</sup>

<sup>1</sup>Department of Hepatobiliary Pancreatic Surgery, First Affiliated Hospital of Wenzhou Medical University, Wenzhou, China, <sup>2</sup>Department of Gynecology, Wenzhou People's Hospital, Wenzhou, China, <sup>3</sup>The Yangtze River Delta Biological Medicine Research and Development Center of Zhejiang Province (Yangtze Delta Region Institution of Tsinghua University), Hangzhou, Zhejiang, China

In this study, we delve into the intrinsic mechanisms of cell communication in hepatocellular carcinoma (HCC). Initially, employing single-cell sequencing, we analyze multiple malignant cell subpopulations and cancer-associated fibroblast (CAF) subpopulations, revealing their interplay through receptor-ligand interactions, with a particular focus on SPP1. Subsequently, employing unsupervised clustering analysis, we delineate two clusters, C1 and C2, and compare their infiltration characteristics using various tools and metrics, uncovering heightened cytotoxicity and overall invasion abundance in C1. Furthermore, our gene risk scoring model indicates heightened activity of the immune therapeutic pathway in C1. Lastly, employing a formulated scoring system, we stratify patients into high and low-risk groups, revealing notably poorer outcomes in the high-risk cohort on Kaplan-Meier curves. Risk scores exhibit a negative correlation with model genes and immune cell infiltration scores, indicating poor prognosis in the high-risk group. Further characterization elucidates the regulatory landscape of the high and low-risk groups across various signaling pathways. In addition, we used wet lab experiments to prove that ABCA1 plays a pro-oncogenic role in hepatocellular carcinoma cells by promoting proliferation, invasion, migration, and reducing apoptosis. In summary, these findings provide crucial insights, offering valuable clues and references for understanding HCC pathogenesis and patient prognosis.

## KEYWORDS

hepatocellular carcinoma, single-cell sequencing, tumor microenvironment, risk stratification, immune therapeutic pathway

## 1 Introduction

While hepatocellular carcinoma (HCC) ranks as the fifth most common malignancy globally, it stands as the second leading cause of cancer-related mortality worldwide (Chen K. et al., 2023). In 2020, there were approximately 906,000 new cases and 830,000 deaths attributed to HCC, with an incidence of 4.7% and a mortality rate of 8.3% (Sung et al., 2021). In China, there were an estimated 431,383 new cases and 412,216 deaths from HCC in 2022, representing roughly half of the global increase in HCC cases and deaths (Fu et al., 2023).

The incidence of HCC is rapidly increasing among both males and females (Islami et al., 2017; Jeong et al., 2018), notably serving as a primary cause of cancer-related mortality in transitional countries such as Mongolia, Thailand, Cambodia, Egypt, and Guatemala (Sung et al., 2021; Tong et al., 2020). HCC constitutes 80%–90% of primary liver cancers, with cholangiocarcinoma (CCA) accounting for 10%–15%, while vascular sarcomas and hepatoblastomas represent a smaller proportion (Li et al., 2021). Chronic inflammatory etiologies, including hepatitis B virus (HBV), hepatitis C virus (HCV) infections, alcoholic steatohepatitis (ASH), non-alcoholic steatohepatitis (NASH), aflatoxin exposure, cirrhosis, smoking, obesity, diabetes, iron overload, various dietary habits, and sedentary lifestyle, are major risk factors for HCC (Li et al., 2021; Anwanwan et al., 2020; Li and Wang, 2016; Duan et al., 2014). HCC may present without evident signs or symptoms, with nonspecific manifestations including right upper quadrant pain, abdominal distension, jaundice, poor appetite, persistent fatigue, and weight loss (Mokdad et al., 2015). Histologically, HCCs are classified by the World Health Organization (WHO) into well-differentiated, moderately differentiated, poorly differentiated, and undifferentiated subtypes, with growth patterns including capsule invasion, infiltration into adjacent liver parenchyma, satellite nodule formation, tumor thrombus formation, and intrahepatic metastasis (Li and Wang, 2016). The incidence of metastatic liver cancer is 18–40 times higher than that of primary hepatic malignancies, owing to the unique anatomical microenvironment of the liver facilitating colonization by extrahepatic cancer cells (including colorectal, pancreatic, breast, melanoma, and lung cancers) (Liu et al., 2023). Liver metastasis significantly impacts both the 5-year survival rate and quality of life (Li et al., 2021), with only approximately 20% of patients with extrahepatic metastases being suitable for surgery (Zhou et al., 2016). Early-stage HCC may benefit from partial hepatectomy, ablation therapy, or liver transplantation, with varying prognostic outcomes. However, the local failure rate of ablation therapy is significantly higher than that of surgical resection, and percutaneous ablation in the pre-transplant setting carries a risk of tumor dissemination, potentially rendering initially transplant-eligible patients ineligible (Bruix et al., 2015). Liver transplantation is limited by donor scarcity and delays between transplant indications and surgery (Soulen and García-Mónaco, 2021), with a median 5-year survival rate of approximately 70%. Nevertheless, 15% of liver transplant recipients experience recurrence post-treatment, with a median 5-year survival rate ranging from 20% to 35%, complicated by the anatomical challenges of early cancer detection (Li and Wang, 2016; Gao et al., 2021; Cheng et al., 2016). For nearly half of HCC patients diagnosed in advanced stages, conventional treatments such as curative resection and ablation therapy may be precluded, although options such as targeted drug therapy or immunotherapy remain available (Zhou et al., 2016; Chen Y. et al., 2023). Sorafenib, an orally administered kinase inhibitor targeting tumor cells, represents a relatively novel therapeutic option for HCC patients with advanced or metastatic disease. However, fewer than one-third of eligible patients benefit from sorafenib, with associated adverse events and a median time to resistance of less than 6 months from initiation of treatment (Anwanwan et al., 2020; Hao et al., 2023). Therefore, comprehensive research into the mechanisms underlying HCC

development and progression is imperative, particularly for identifying more effective treatment modalities and elucidating the role of key genetic factors, which are crucial for the diagnosis, treatment, and prognosis of HCC.

As the culmination of our introduction, this study aims to unravel the intricate mechanisms of cell communication within HCC. Utilizing single-cell sequencing, we dissect the interplay between multiple malignant cell subpopulations and cancer-associated fibroblasts (CAFs), with a special emphasis on SPP1-mediated receptor-ligand interactions. Through unsupervised clustering, we identify two distinct clusters, C1 and C2, and characterize their infiltration patterns, revealing elevated cytotoxicity and invasion in C1. Our gene risk scoring model further highlights heightened immune therapeutic pathway activity in C1. Moreover, patient stratification based on a formulated scoring system demonstrates poorer outcomes in the high-risk group. Wet lab experiments validate the oncogenic role of ABCA1 in promoting HCC cell proliferation, invasion, migration, and reducing apoptosis. Collectively, our findings offer novel insights into HCC pathogenesis and patient prognosis, laying the groundwork for future research and therapeutic strategies.

## 2 Material and methods

### 2.1 Data collection and preprocessing

Firstly, we retrieved bulk transcriptomic data and corresponding clinical information for HCC from The Cancer Genome Atlas (TCGA, <https://portal.gdc.cancer.gov/>) database. Additionally, we obtained two bulk RNA-seq datasets, GSE14520 and GSE76427, from The Gene Expression Omnibus (GEO, <https://www.ncbi.nlm.nih.gov/geo/>) database. Furthermore, we downloaded the ICGC-JP dataset from the International Cancer Genome Consortium (ICGC, <https://dcc.icgc.org/>) database. Finally, three single-cell sequencing datasets for HCC, namely, GSE146115, GSE146409, and GSE166635, were obtained from TISCH2 (<http://tisch.comp-genomics.org/home/>) database. All publicly available databases utilized in this study permit unrestricted access and utilization without additional ethical approval. Our data retrieval and analysis procedures adhere to relevant guidelines. We standardized all sequencing data into Transcripts per million (TPM) format. Records with missing information were excluded, and in cases where a gene had multiple entries, the mean value was calculated across all entries.

### 2.2 Single-cell sequencing data analysis

Utilizing the “Seurat” package and the SCP pipeline (<https://github.com/zhanghao-njmu/SCP>), we conducted analysis on the single-cell sequencing data. To ensure the accuracy and reliability of subsequent research, we initially performed quality control on the acquired data. Our criteria were as follows: percent. mt <25, nFeature\_RNA <9,000. Additionally, we employed the “harmony” package to integrate and batch-correct the quality-controlled single-cell data. Subsequently, we employed Uniform Manifold Approximation and Projection (UMAP) for



dimensionality reduction and clustering of the single-cell data. We annotated and visualized several major cell types based on relevant information provided by the TISCH database. Concurrent with cell annotation, we validated the subclasses by cross-referencing the gene expression profiles with established cell type annotations.

To investigate the interaction and communication between malignant cell clusters and Cancer-Associated Fibroblasts (CAFs) clusters, we performed UMAP dimensionality reduction again for both cell types based on the EPCAM expression levels of malignant cell clusters ( $n = 7,186$ ) and the expression levels of COL1A1 and COL1A2 for CAFs clusters ( $n = 698$ ). We further subdivided them into several cell subclusters and visualized the results. Next, we utilized RunSlingshot to construct developmental trajectories of malignant and CAFs cell subclusters and predicted their developmental paths.

Subsequently, we conducted Differentially Expressed Genes (DEGs) analysis for each cell subcluster, with parameters set as follows:  $fc.threshold = 1$ ,  $only.pos = FALSE$ . Finally, we performed Gene Ontology Biological Process (GO\_BP) enrichment analysis for each cell subcluster and selected the top six statistically significant GO\_BP enrichment terms for visualization. Parameters were set as follows:  $db = "GO\_BP"$ ,  $species = "Homo\_sapiens"$ ,  $DE\_threshold = "avg\_log_2FC > \log_2(1.5) \ \& \ p\_val\_adj < 0.05."$

## 2.3 Analysis of cell communication

We conducted an analysis of cell communication by using the CellChat and NicheNet algorithms on various cell subpopulations. Firstly, we presented an interaction network in the form of a chord diagram, demonstrating the frequency and strength of interactions among different subpopulations of malignant and CAFs cells. Subsequently, we visualized the ligand-receptor relationships and pairings between different cell pathways within each subpopulation. Additionally, we focused on the expression patterns of SPP1 as a ligand and its various receptors in the malignant and CAFs subpopulations, using a violin plot. Furthermore, we analyzed the significance of different subpopulations in the SPP1 signaling pathway. To explore the interaction network within each cell subpopulation, we created scatter plots to display the outward and inward interaction strengths of each subpopulation. Finally, by using certain genes in the CAFs subpopulation as ligands and genes in the malignant subpopulation as receptors, we analyzed the binding potential and biological effects of these ligand-receptor interactions, which were visualized using a heat map.

## 2.4 Constructing gene regulatory networks

We utilized the “SCENIC” R package to construct GRNs for HCC. Leveraging the single-cell dataset of HCC and relevant algorithms, we particularly focused on the distribution and expression patterns of five regulatory factors associated with HCC (BRF1\_extended\_29g, ARNTL\_extended\_39g, ARNTL\_24g, BCLAF1\_extended\_22g, ATF3\_extended\_16g) across various cell subpopulations, visualized using UMAP. Additionally, we generated a heatmap illustrating the differential activity levels of these five regulatory factors between malignant and CAFs cells. Subsequently,

we amalgamated all target genes regulated by these five factors into a signature and proceeded with further analysis based on this signature.

## 2.5 Unsupervised clustering and correlation analysis

Utilizing the aforementioned signature, we conducted unsupervised clustering analysis using the “ConsensusClusterPlus” R package with the following parameters:  $maxK = 9$ ,  $reps = 1,000$ ,  $pItem = 0.8$ ,  $pFeature = 1$ ,  $tmyPal = color$ ,  $title = "ConsensusCluster/"$ ,  $clusterAlg = "km"$ ,  $distance = "euclidean"$ ,  $seed = 123,456$ . By subjecting tumor tissue samples to hierarchical clustering, we attempted sample grouping. Subsequently, leveraging Cumulative Distribution Function (CDF) curves and Proportion of Ambiguous Clustering (PAC) scores, we selected the most appropriate  $k$  value for grouping, resulting in two distinct clusters (C1 and C2). Furthermore, we employed the TCGA-LIHC dataset and conducted log-rank testing to plot Kaplan-Meier (KM) curves, demonstrating survival disparities between the different clusters.

## 2.6 Differential analysis of HCC tumor microenvironment

To gain insight into the disparities within the HCC TME across distinct clusters, we leveraged the clustering results to conduct comparative analyses of the TME in clusters C1 and C2. Initially, employing Single-sample Gene Set Enrichment Analysis (ssGSEA), we evaluated the relative infiltration abundance of diverse immune cell subtypes within the two clusters. Subsequently, we depicted the disparities in the activity levels of CYT (cytotoxic activity), GFP (T cell inflamed gene expression profile), IFNG (INF- $\gamma$ ), and TMB (tumor mutation burden) between the two clusters using box plots. Additionally, we assessed the infiltration abundance of immune cell subtypes in both clusters using five TME deconvolution algorithms (CIBERSORT, MCP-counter, quanTIseq, EPIC, and TIMER) from the “IOBR” R package (<https://github.com/IOBR/IOBR>), scoring the results accordingly. Furthermore, we downloaded 150 immunomodulators and chemokines from the TISIDB database (<http://cis.hku.hk/TISIDB/>), including 41 chemokines, 24 immunoinhibitors, 46 immunostimulators, 21 Major Histocompatibility Complex (MHC), and 18 receptors. Based on this data, we constructed a heatmap illustrating the expression profiles of relevant immune regulatory molecules across different clusters. Finally, employing Gene Set Variation Analysis (GSVA), we enriched scores for the anti-cancer immunity cycle and immunotherapy-predicted pathways in the two clusters, followed by an analysis of the disparities between the clusters.

## 2.7 Gene set enrichment analysis

Initially, we utilized the “limma” package to identify differentially expressed genes between clusters C1 and C2. Subsequently, employing the “clusterprofiler” R package, we



conducted GSEA to delineate the signaling pathways enriched and discovered the upregulated cancer signatures within both clusters. Concurrently, data visualization was performed using the “GseaVis” R package to generate bubble plots illustrating the results. Additionally, GSEA was employed to identify both upregulated and downregulated signaling pathways within the C1 cluster.

## 2.8 Construction of prognostic models

Based on the communication signature between malignant and CAFs cellular subgroups, we employed the Least Absolute Shrinkage and Selection Operator (LASSO) method to screen prognostic marker genes within the TCGA-LIHC dataset. Subsequently, utilizing the multiCOX analysis approach, we constructed a prognostic model for HCC. Employing the model formula, each patient was assigned a score, yielding a RiskScore for every sample. The RiskScore is defined by summing the product of gene expression levels and their corresponding coefficients, as demonstrated below:

$$\text{Risk score} = \sum_{i=1}^n [\text{Exp}_{\text{gene}_i} * \beta_i]$$

Here,  $\text{Exp}_{\text{gene}_i}$  represents the expression level of the model gene, and  $\beta_i$  represents the corresponding coefficient of the model gene. Additionally, we visualized the coefficients of the prognostic model through a lollipop plot of feature gene coefficients. Based on the median score, patients were divided into high-risk and low-risk groups. Using the TCGA dataset ( $n = 329$ ), we plotted KM curves to analyze the prognosis of the two risk groups and constructed Receiver Operating Characteristic (ROC) curves to analyze the model's performance at 1, 3, and 5 years. We define a model as having good diagnostic performance in this dataset when the area under the curve (AUC) exceeds 0.6. Subsequently, we validated the prognostic model in external validation sets GSE76427 ( $n = 115$ ), GSE14520 ( $n = 242$ ), and ICGC-JP ( $n = 240$ ). We utilized KM curves and ROC curves to validate the predictive ability of the model in different datasets. Next, we conducted correlation analysis, demonstrating the correlation between RiskScore and various immune checkpoint levels and immune cell infiltration levels through a correlation heatmap. Using the “limma” package, we performed DEGs analysis between the high-risk and low-risk groups, identifying differentially expressed genes between the two groups. Finally, through GSEA, we analyzed the abnormal signaling pathways that were upregulated and downregulated in the high-risk group.

## 2.9 Cell culture and transfection

We used human liver cancer cell lines HepG2 and Huh7 (Cell Bank of the Chinese Academy of Sciences). Huh7 cells were cultured in DMEM (HyClone, United States), and HepG2 cells in MEM (HyClone, United States), both supplemented with 10% FBS (BI, Israel) and 100 U/mL penicillin/100 µg/mL streptomycin (HyClone, United States). Cells were maintained in a humidified CO2 incubator at 37°C.

For transfection, Huh7 cells were treated with ABCA1 shRNA (Sangon, China) to knock down expression, while HepG2 cells were transfected with an ABCA1 overexpression plasmid (with a negative control). Cells were resuspended in complete medium and seeded into 6-well plates at  $1 \times 10^4$  cells/well with 2 mL of medium. Transfection was performed using PolyFast reagent (MCE, United States, catalog number HY-K1014) according to the manufacturer's instructions. After a 15-min incubation at room temperature, the cells were re-incubated. The medium was refreshed 6 h post-transfection, and subsequent experiments were conducted 48 h later.

## 2.10 RT-qPCR and total RNA extraction

We used RT-qPCR to measure ABCA1 mRNA expression in different cell groups. Cells in 6-well plates were trypsinized (KeyGEN, China), washed with PBS, and centrifuged at 4°C (800–2,000 rpm). RNA was extracted using 800–1,000 µL Trizol (Takara, Japan), followed by chloroform precipitation and ethanol/isopropanol purification (SINOPHARM, China). The RNA was resuspended in 20 µL DEPC-treated water and quantified using a Nanodrop 2000 spectrophotometer (Thermo, United States). Reverse transcription was performed with the PrimeScript RT reagent kit (TaKaRa, Japan), and RT-qPCR was conducted using SYBR GreenER Supermix (TaKaRa, Japan) on a 7,500 Real-Time PCR System (Thermo Fisher Scientific, United States) according to the manufacturer's protocols. ABCA1 expression was quantified using the  $2^{-\Delta\Delta CT}$  method, normalized to  $\beta$ -actin.

## 2.11 Colony formation assay

Colony Formation Assay was employed to determine differences in colony numbers among different cell lines. Cells were initially seeded at a density of  $1 \times 10^3$  cells per well in a 6-well plate, gently agitated, and subsequently cultured in a cell culture incubator for approximately 14 days. Following removal of the culture medium, the cells underwent three washes with PBS. Colonies underwent fixation using formaldehyde for 15 min, followed by staining with 1 mL of 0.5% crystal violet (Solarbio, China), three subsequent PBS washes, air-drying, and subsequent imaging and quantification.

## 2.12 CCK8 assay

After 48 h post-transfection, Huh7 and HepG2 cell lines were plated into 96-well plates at a density of 6,000 cells per well and returned to the incubator for adherence. Each experimental group was replicated three times. The CCK-8 reagent (KeyGEN, China) was reconstituted as per the manufacturer's instructions by diluting it with complete culture medium to achieve a final volume of 200 µL per well. Using a pipette, the prepared solution was swiftly aliquoted into the wells of the 96-well plates. The plates were shielded from light exposure by covering them with aluminum foil, and absorbance readings at 450 nm were taken using a spectrophotometer following a 2-h incubation period. Subsequent

measurements were taken at 24, 48, 72, and 96-h time points, repeating the aforementioned steps.

## 2.13 EDU assay

We used the EdU assay to assess proliferation level differences among different groups of Huh7 and HepG2 cells. Following a 48-h transfection period, the culture medium was removed, and cells were washed three times with PBS. As per the protocol, cells were permeabilized with 0.3% Triton X-100 (Beyotime, China) for 25 min at room temperature. After permeabilization, cells were incubated with EdU reaction mixture to allow EdU incorporation into newly synthesized DNA. Subsequently, cells were washed again with PBS and fixed with a fixing solution. Following fixation, cells were stained with a fluorescent azide to visualize EdU incorporation. After washing to remove excess stain, cells were counterstained with DAPI for 10 min to visualize nuclei. Finally, each well was washed with PBS, and anti-fluorescence quenching reagent (Beyotime, China) was added to preserve the fluorescence signal. The plates were then examined, and images were captured using a fluorescent microscope.

## 2.14 Wound healing assay

Following 48 h of transfection, the medium was aspirated, and PBS was introduced. Using a precise ruler for guidance, a deliberate single straight scratch was introduced into each well using a 200  $\mu$ L pipette. The pipette tip was substituted after each well, and cells underwent three PBS washes. Subsequently, each well received basic culture medium lacking FBS. At this point, microscopic images were captured to document the initial scratch, measure the wound area, and define this moment as time point zero. After incubating the cells in a cell culture incubator for 48 h, images were taken again to measure the healed wound area and calculate the percentage of scratch closure.

## 2.15 Total protein extraction and Western blot analysis

Western blotting was used to assess protein expression of ZO-1, E-cadherin, Vimentin, Slug, ABCA1, and  $\beta$ -actin in Huh7 and HepG2 cells. Cells were lysed using RIPA buffer with protease inhibitors (100:1), sonicated (40% amplitude, 1s pulses, 3 cycles), and incubated on ice for 30 min with shaking. Lysates were centrifuged (10,000 rpm, 15 min, 4°C), and supernatants were collected for protein quantification. Samples were prepared with loading buffer, heated (95°C, 5 min), and subjected to electrophoresis (20  $\mu$ g/lane, 10% SDS-PAGE, 100V). Proteins were transferred to a PVDF membrane (0.45  $\mu$ m), blocked (10 min), and incubated with primary antibodies overnight at low temperature. After washing, membranes were incubated with HRP-conjugated secondary antibodies (1.5 h, RT) and visualized using an ECL kit. Antibodies were sourced from Proteintech.

## 2.16 Transwell assay

Transwell chambers (Thermo, United States) were coated with extracellular matrix gel (1:8 dilution, 40  $\mu$ L/chamber) and dried for 24 h. Cells (20,000/chamber) were seeded in serum-free medium (200  $\mu$ L/chamber) on a 24-well plate with 500  $\mu$ L complete medium per well. After 20-h incubation in a CO<sub>2</sub> incubator, non-invading cells were removed, and chambers were fixed with 4% paraformaldehyde, washed, and stained with 0.1% crystal violet. Microscopic images were then captured.

## 2.17 Flow cytometry for detecting cell apoptosis

Flow cytometry was employed to assess apoptosis in Huh7 and HepG2 cells. Following reagent centrifugation, cells were washed, digested with trypsin (without EDTA, with 3-min interval checks), and centrifuged at 2,000 rpm for 5 min. After two additional PBS washes, cells were suspended in 400  $\mu$ L of binding buffer. Annexin V FITC/PI staining solution was added, followed by a 15-min incubation at 37°C. Cells were then transferred to flow cytometry tubes and filtered through a nylon mesh. The FL1 channel (for FITC green fluorescence) and FL3 channel (for PI red fluorescence, Ex = 488 nm, Em  $\geq$  630 nm) were used for analysis. Voltage and compensation settings on the flow cytometer were adjusted to ensure that 99% of cells occupied the lower left quadrant.

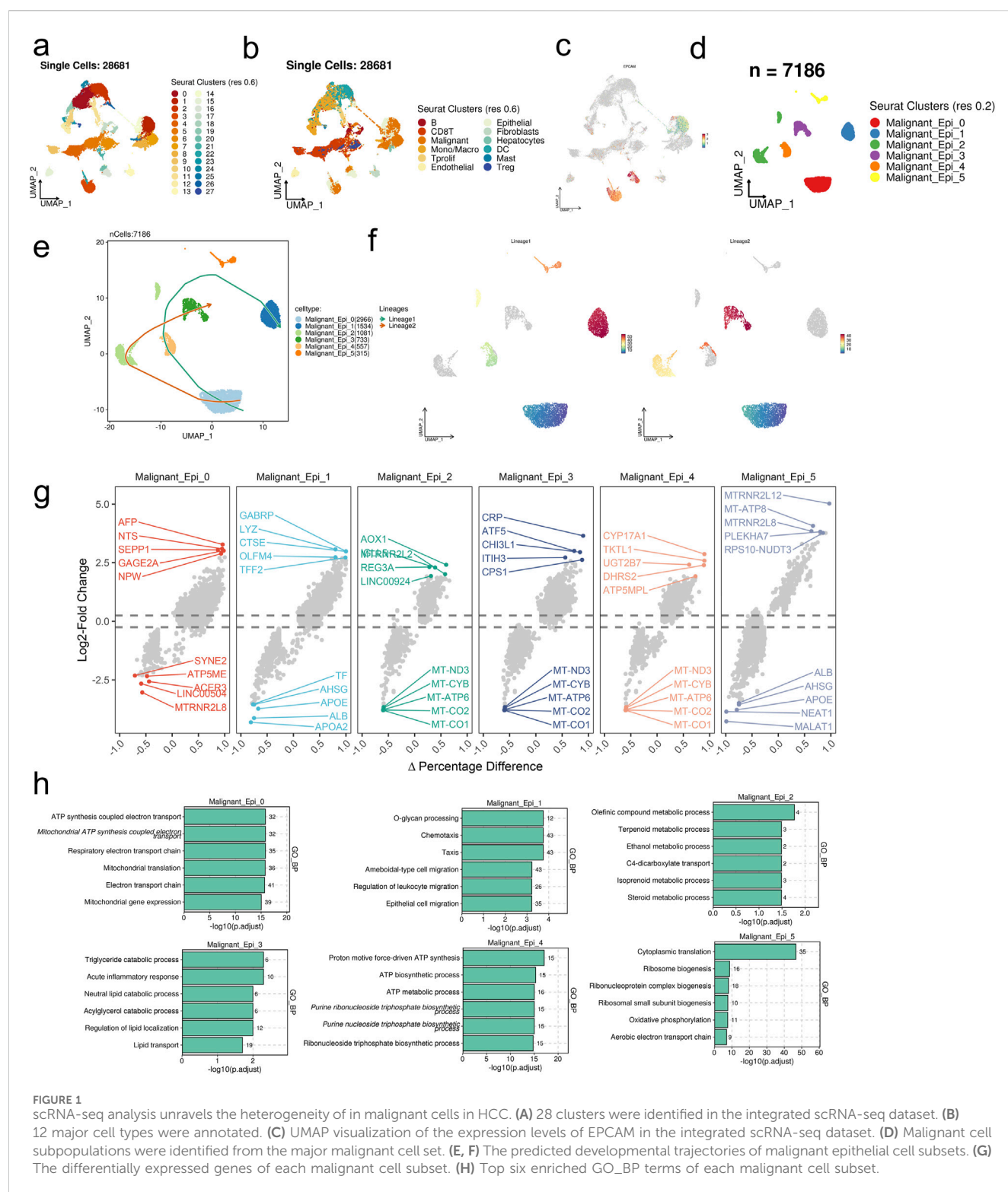
## 2.18 Statistical analysis

All statistical analyses were conducted using R software (version 4.1.3). Differential gene expression analysis was performed using the “limma” package. The “ggplot2” package was employed as the primary tool for visualization. A threshold of  $p < 0.05$  was considered statistically significant (\* $p < 0.05$ ; \*\* $p < 0.01$ ; \*\*\* $p < 0.001$ ; \*\*\*\* $p < 0.0001$ ).

# 3 Results

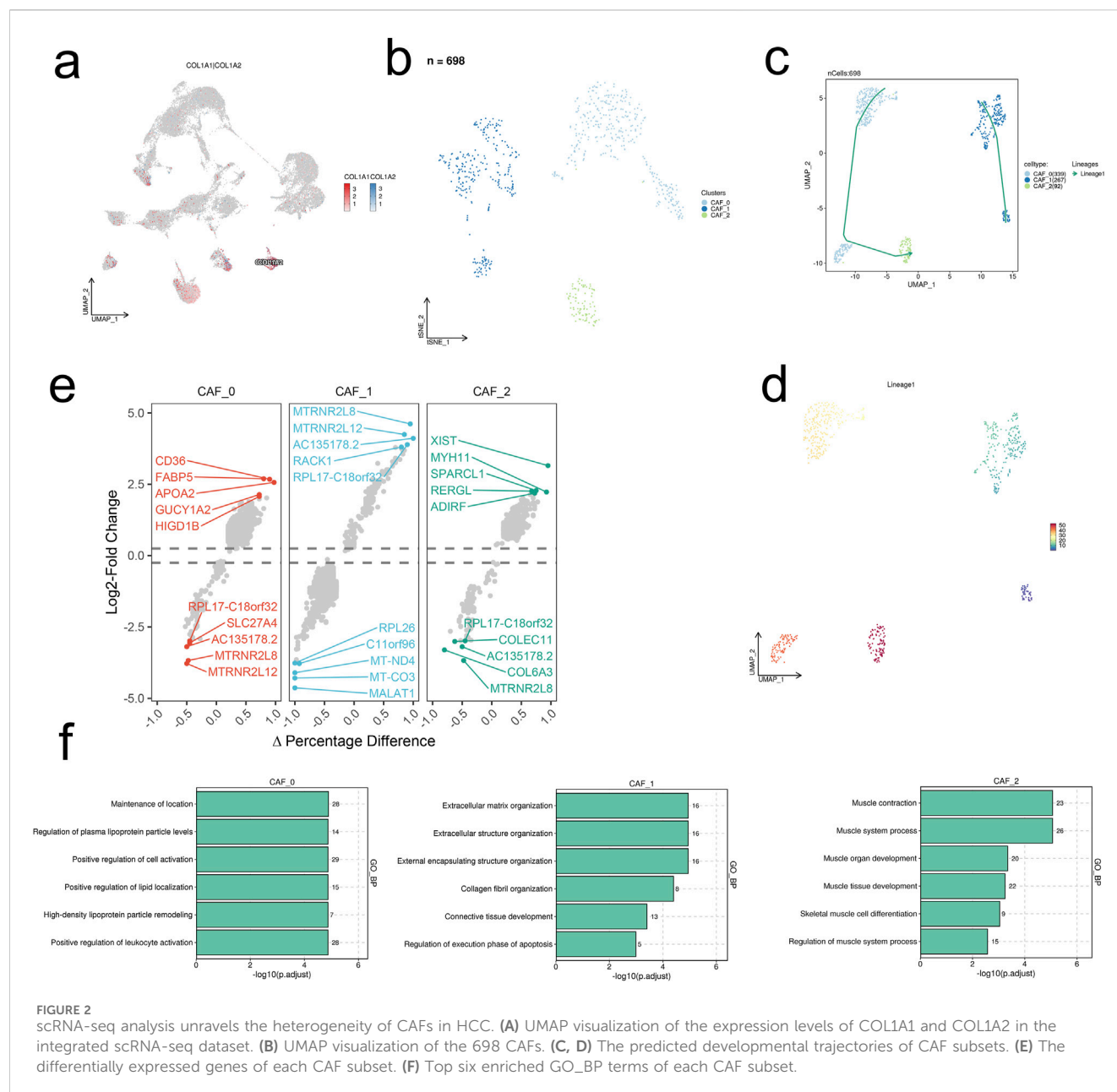
## 3.1 Single-cell data analysis of malignant cell populations

Utilizing integrated single-cell sequencing data, UMAP dimensionality reduction clustering identified 28 clusters, subsequently annotated into 12 major cell types based on information provided by the TISCH database (Figures 1A, B). Further analysis of the target malignant cell population delineated it into 6 cellular subgroups: Malignant\_Epi\_0, Malignant\_Epi\_1, Malignant\_Epi\_2, Malignant\_Epi\_3, Malignant\_Epi\_4, and Malignant\_Epi\_5 (Figures 1C, D). Developmental trajectory prediction revealed two trajectories: Lineages1 (Malignant\_Epi\_0- Malignant\_Epi\_4- Malignant\_Epi\_1) and Lineages2 (Malignant\_Epi\_0- Malignant\_Epi\_2- Malignant\_Epi\_3), all originating from Malignant\_Epi\_0 (Figures 1E, F).



In differential gene expression analysis, genes associated with metabolism, immune inflammation, neuroregulation, and cell signaling pathways were upregulated across the 6 cellular subgroups, while genes related to mitochondria, ribosomes, long non-coding RNA, lipoproteins, and plasma proteins were downregulated (Figure 1G). GO\_BP enrichment analysis

revealed statistically significant enrichment of the top 6 pathways across the 6 cellular subgroups, including cellular mitochondrial functions, mobility and migration, metabolic processes, lipid metabolism regulation and transport processes, ATP synthesis and metabolism, protein synthesis, and energy metabolism (Figure 1H).



### 3.2 Single-cell data analysis of CAF cell population

Furthermore, we conducted a detailed analysis of the CAF cell population, reducing its dimensionality into 3 groups using UMAP: CAF\_0, CAF\_1, and CAF\_2 (Figures 2A, B). Predicted developmental trajectories revealed a single trajectory: Lineages1 (CAF\_1, CAF\_0, CAF\_2) (Figures 2C, D). In the analysis of Differentially Expressed Genes (DEGs), genes related to cell structure and signaling transduction, protein synthesis, and nucleic acid metabolism were found to be upregulated across the 3 cellular subgroups, while genes associated with mitochondria, ribosomes, mitochondrial and nuclear-encoded RNA, extracellular matrix proteins, and receptors were downregulated (Figure 2E). GO\_BP enrichment analysis indicated statistically significant enrichment of the top 6 pathways across the 3 cellular

subgroups, including maintenance of normal biological functions and homeostasis, extracellular matrix, and the muscular system (Figure 2F).

### 3.3 Cellular communication analysis and construction of gene regulatory networks

The figure demonstrates that the interactions and strengths among Malignant\_Epi\_0, Malignant\_Epi\_1, Malignant\_Epi\_4, CAF\_0, and other cellular subgroups are relatively strong, while Malignant\_Epi\_2, Malignant\_Epi\_3, Malignant\_Epi\_5, CAF\_1, and CAF\_2 exhibit weaker interactions (Figure 3A). We investigated the receptor communication relationships within different cellular subgroups, focusing particularly on the SPP1 receptor relationships. SPP1 expression levels are notably higher in CAF\_0,



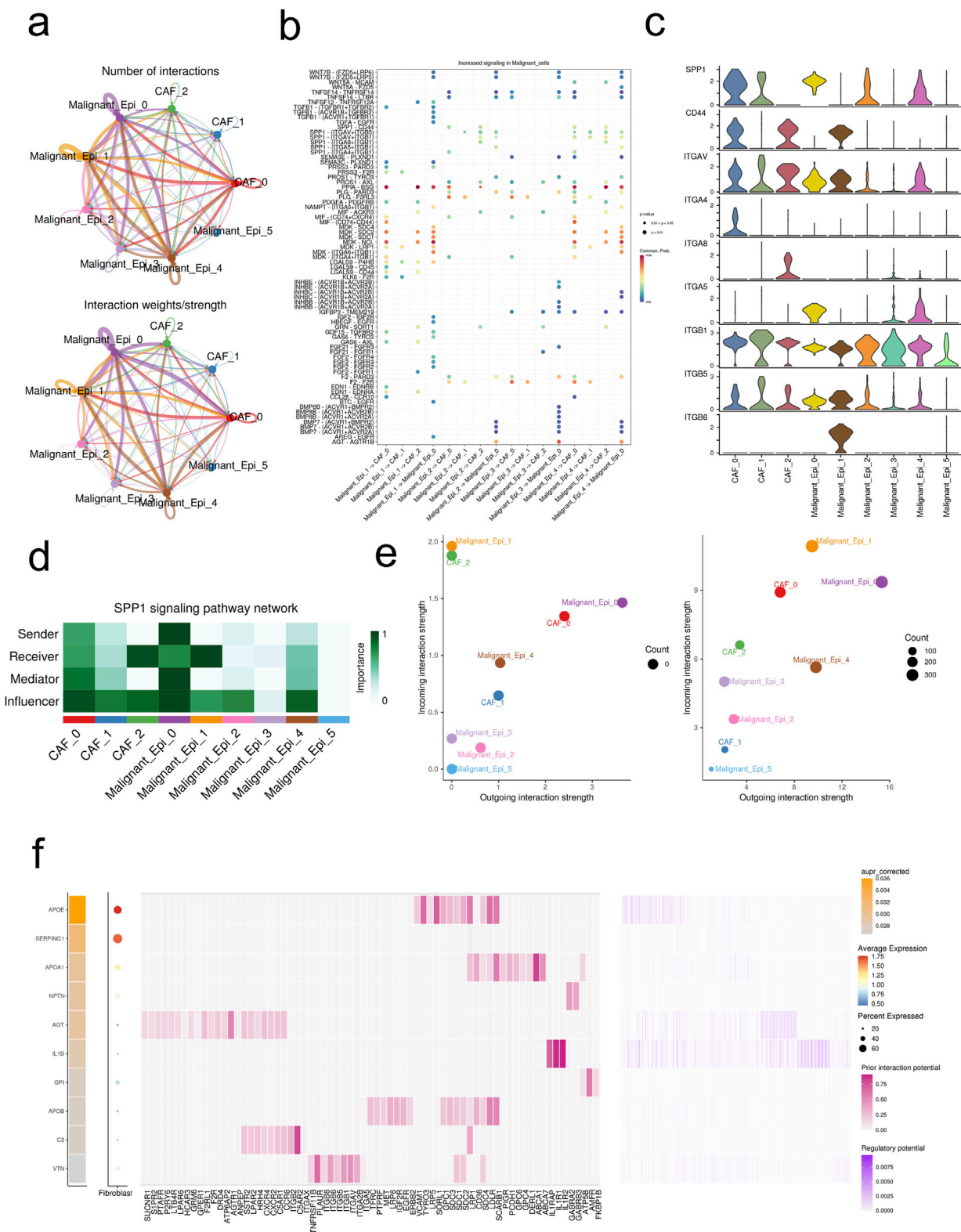
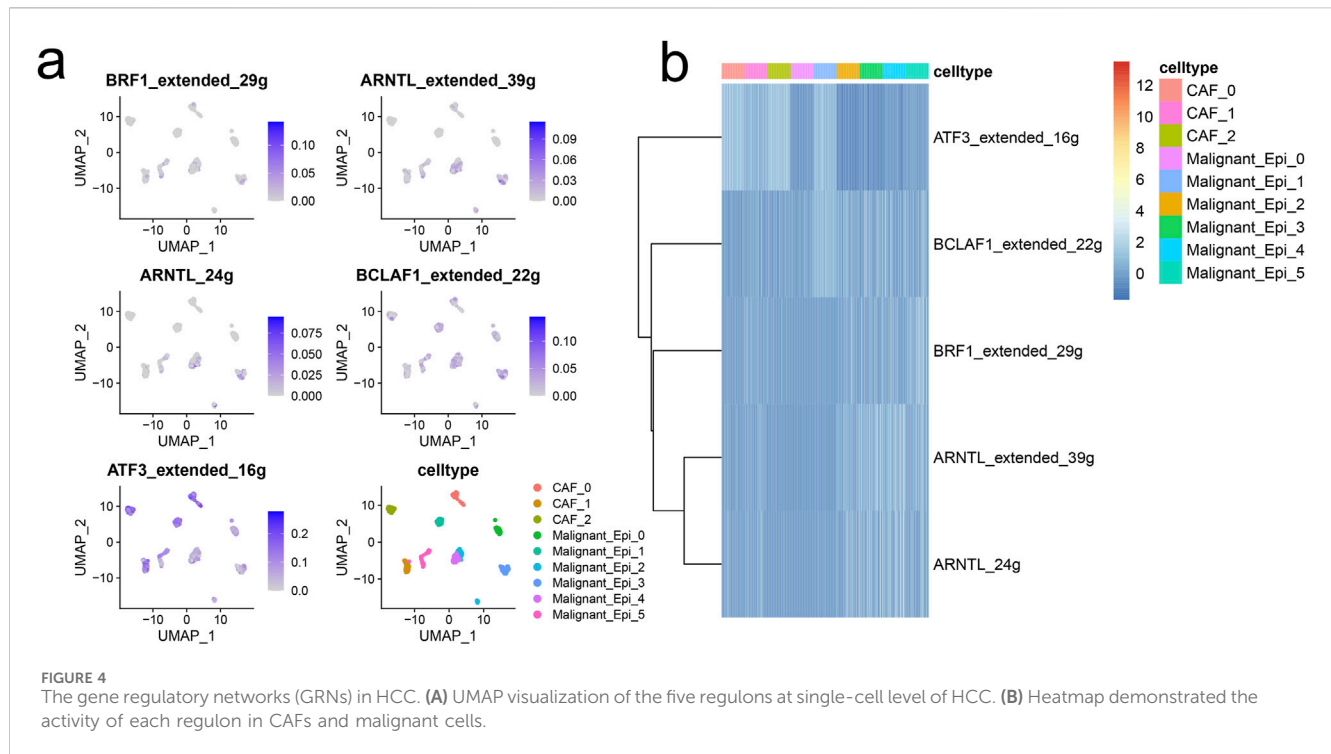


**FIGURE 3** Intercellular communications between CAFs and malignant cells. **(A)** The intercellular interactions between subsets of CAFs and malignant cells. **(B)** The ligand-receptor pairs between CAFs and malignant cells. **(C)** Expression profiles of SPP1 signaling pathway in CAFs and malignant cells. **(D)** The importance of each subset of CAFs and malignant cells in the SPP1 signaling pathway. **(E)** The incoming/outgoing strength of each subset of CAFs and malignant cells in the SPP1 signaling pathway (left) and the whole signaling pathways (right). **(F)** Top ligands in the communication network. Ligand-target gene matrix denoting the potential regulatory relationships between ligands and target genes among CAFs and malignant cells. The color intensity represented the regulatory potentials.





CAF\_1, Malignant Epi 0, Malignant Epi 2, and Malignant Epi 4 subgroups. Among the potential targets of SPP1, ITGB1 is actively expressed in all cellular subgroups, whereas ITGA4, ITGA8, and ITGB6 are inactive in most cellular subgroups (Figures 3B, C). Analysis of the SPP1 signaling pathway network reveals that Malignant\_Epi\_0 exhibits higher importance in Sender, Receiver, Mediator, and Influencer aspects, while Malignant\_Epi\_3 demonstrates lower importance (Figure 3D). Both CAF cellular subgroups and malignant cell populations exhibit weaker outward and inward interaction strengths in the SPP1 pathway compared to the entire signaling pathway (Figure 3E). The ligand-receptor gene matrix indicates binding potential and biological effects only when IL1B serves as the ligand and IL1RAP, IL1R1, IL1R2 serve as receptors (Figure 3F). Additionally, using the “SCENIC” package, we focused on five regulatory factors at the single-cell level in HCC (BRF1 \_extended \_29g, ARNTL\_extended \_39g, ARNTL \_24g, BCLAF1\_extended \_22g, ATF3\_extended \_16g). We found that ATF3\_extended \_16g is expressed at higher levels in three CAF cellular subgroups and six Malignant cellular subgroups compared to the other four factors (Figure 4A). Heatmap results indicate that, except for ATF3\_extended \_16g, the remaining regulatory factors exhibit high expression in the Malignant\_Epi\_5, Malignant\_Epi\_4, Malignant\_Epi\_3, and Malignant\_Epi\_2 cellular subgroups (Figure 4B).

### 3.4 Unsupervised clustering and survival disparity analysis

In this section, we explore unsupervised clustering of tumor tissue samples and investigate survival disparities. Utilizing hierarchical clustering, we identified  $k = 2$  as the optimal grouping based on

CDF curve analysis and PAC scores. Notably, the consensus matrix plot exhibited robust intra-cluster cohesion and inter-cluster distinctiveness (Figures 5A–C). Kaplan-Meier survival curves unveiled significant survival discrepancies between the two clusters, with cluster 1(C1) displaying inferior prognosis ( $p = 0.031$ , Figure 5D).

### 3.5 Analysis of HCC tumor microenvironment disparities

We commenced our investigation by analyzing the relative infiltration of immune cell subtypes within C1 and Cluster 2(C2). C1 exhibited higher relative infiltration rates in Activated CD4 T cells, Central memory CD4 T cells, Central memory CD8 T cells, and Effector memory CD4 T cells compared to C2, while C2 demonstrated higher relative infiltration rates in CD56bright natural killer cells, eosinophils, Regulatory T cells, and T follicular helper cells compared to C1 (Figure 5E). Moreover, C1 surpassed C2 in CYT indicators, indicating heightened cytotoxic activity within C1, which may confer a favorable anti-tumor response (Figure 5F). In the analysis of immune cell infiltration, C1 showed elevated levels compared to C2 in Activated CD4 T cells, Central memory CD4 T cells, Central memory CD8 T cells, Effector memory CD4 T cells, Regulatory T cells, T follicular helper cells, and Type 2 T helper cells, while C2 exhibited higher levels in CD56bright natural killer cells and eosinophils. Overall, C1 displayed higher infiltration levels compared to C2 in the MCPcounter, quanTlseq, EPIC, and TIMER analyses, except for the “Other” category, where C2 was higher (Figure 6A). Furthermore, in the immune modulator expression profile, we categorized 150 factors into 5 classes (chemokine, Immunoinhibitor, Immunostimulator, MHC,

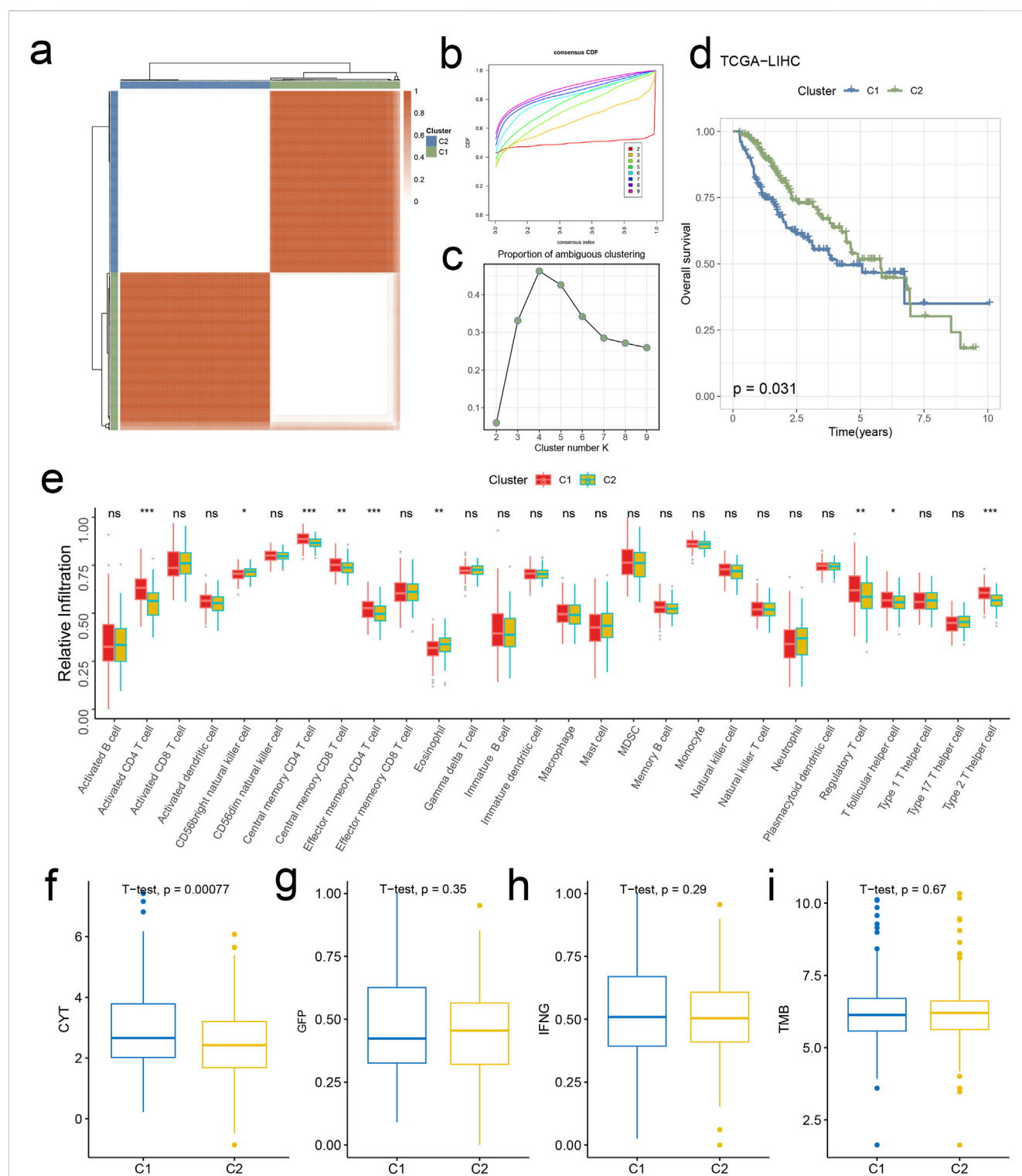
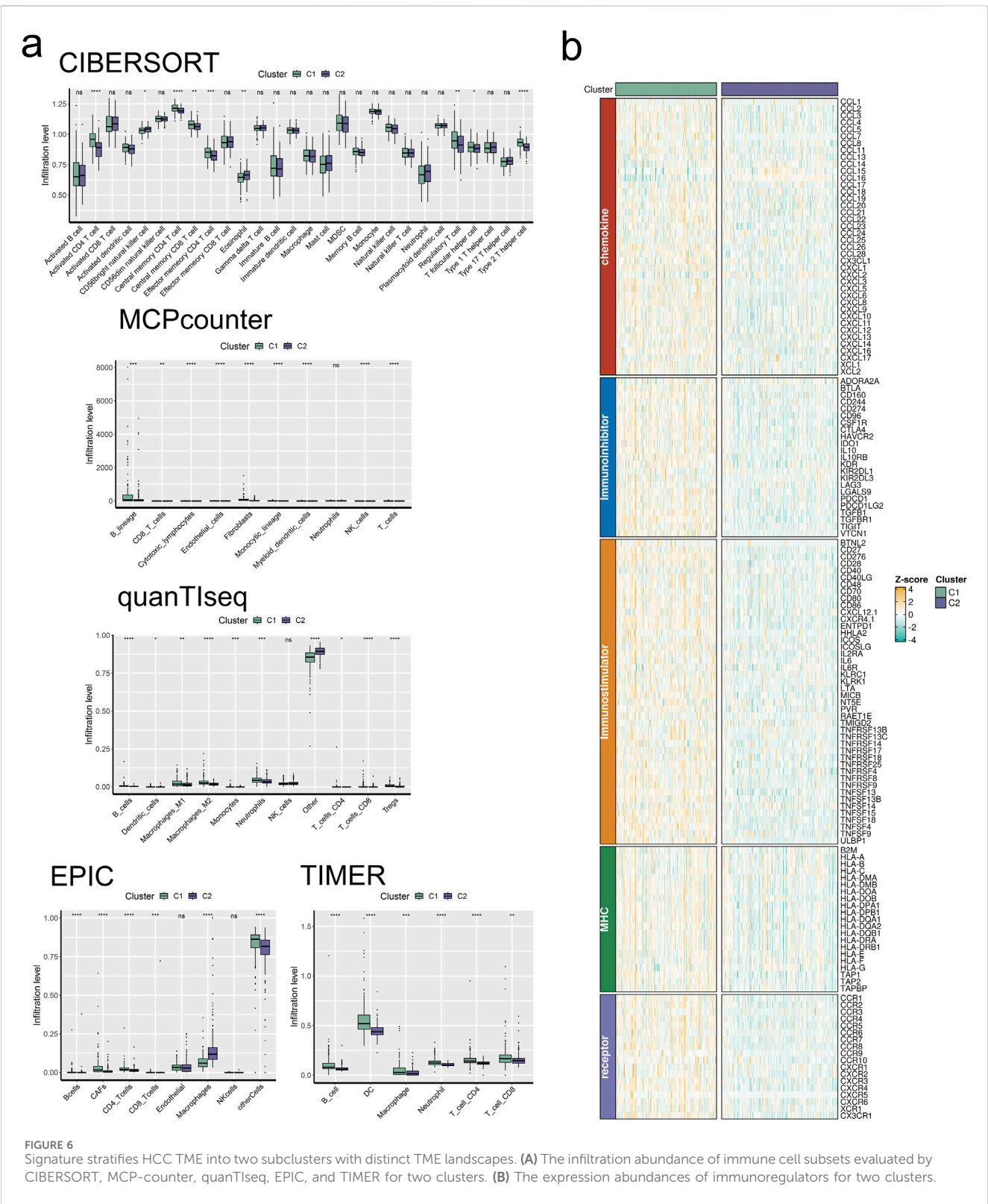


FIGURE 5

Signature stratifies HCC TME into two subclusters with distinct prognosis and biological features. (A) The consensus score matrix of all samples when  $k = 2$ . A higher consensus score denotes higher similarity. (B) The CDF curves of the consensus matrix for each  $k$  (indicated by colors). (C) The PAC score for each  $k$ . (D) KM survival curves with log-rank test demonstrate survival discrepancies between two clusters. (E) Relative infiltration abundances of 28 immune cell subsets in two clusters.  $p$  values are determined by the Wilcoxon test. ns: non-significant; \* $p < 0.05$ ; \*\*\* $p < 0.001$ . The activities of CYT (F), GFP (G), IFNG (H), and TMB (I) between two clusters.

receptor). Notably, C1 and C2 exhibited significant disparities in immune infiltration, with C1 displaying markedly higher overall abundance than C2 (Figure 6B). In the anti-cancer immunity cycle,

Enrichment Scores (ES) of C1 consistently exceeded those of C2, with the majority of pathways in the immunotherapy-predicted pathway graph favoring C1 (Figures 7A, B).

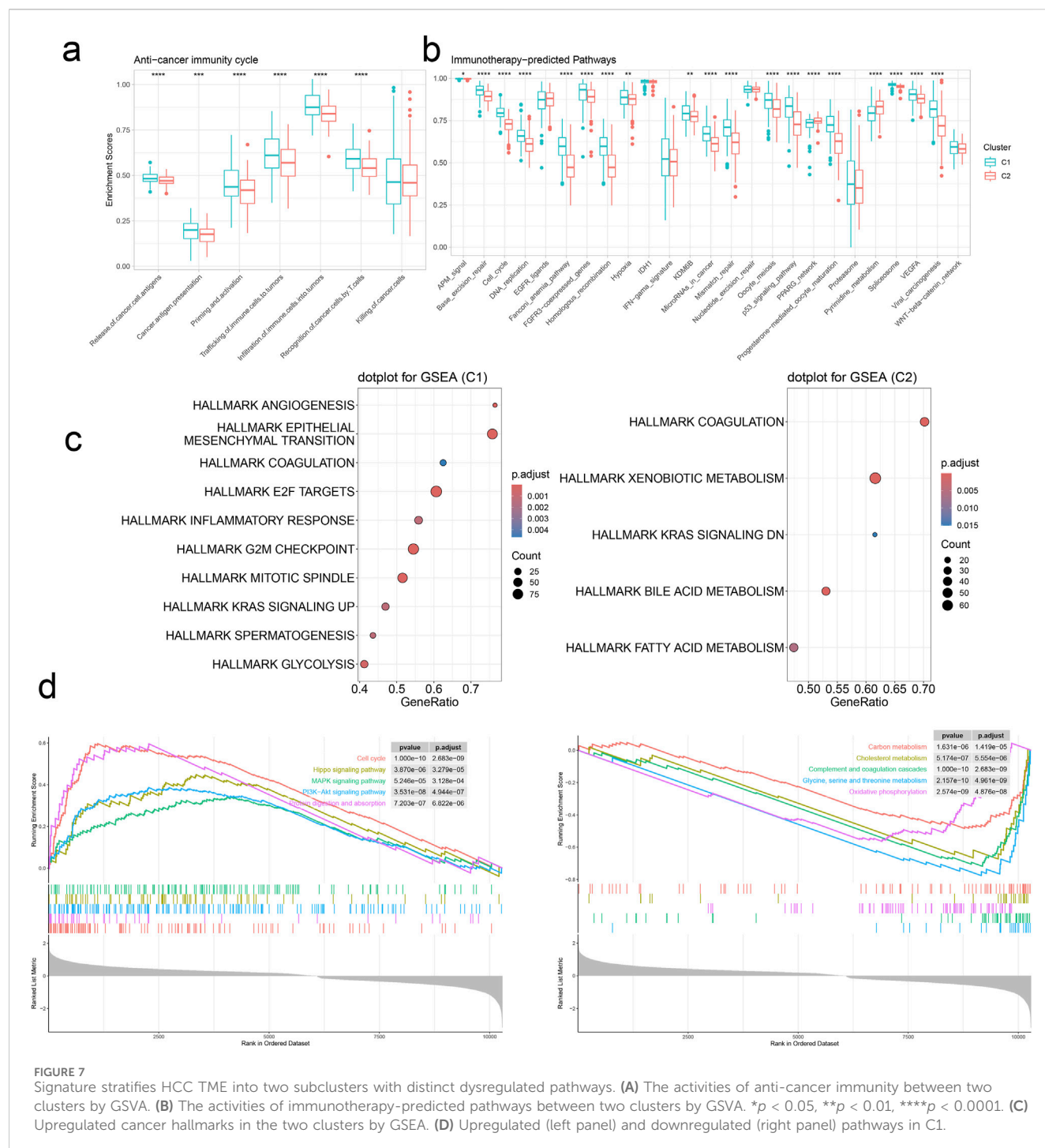


**FIGURE 6** Signature stratifies HCC TME into two subclusters with distinct TME landscapes. **(A)** The infiltration abundance of immune cell subsets evaluated by CIBERSORT, MCP-counter, quanTlseq, EPIC, and TIMER for two clusters. **(B)** The expression abundances of immunoregulators for two clusters.

### 3.6 Gene set enrichment analysis enrichment analysis

We conducted Gene Set Enrichment Analysis (GSEA) to identify the pathways enriched in C1 and C2. Notably, C1 exhibited significant enrichment in HALLMARK EPITHELIAL-MESENCHYMAL

TRANSITION, HALLMARK E2F TARGETS, and HALLMARK G2M CHECKPOINT, while C2 showed prominent enrichment in HALLMARK XENOBIOTIC METABOLISM. Additionally, we observed that C1 cluster harmoniously upregulated pathways related to Cell cycle, Hippo signaling pathway, MAPK signaling pathway, PI3K-Akt signaling pathway, and Protein digestion and

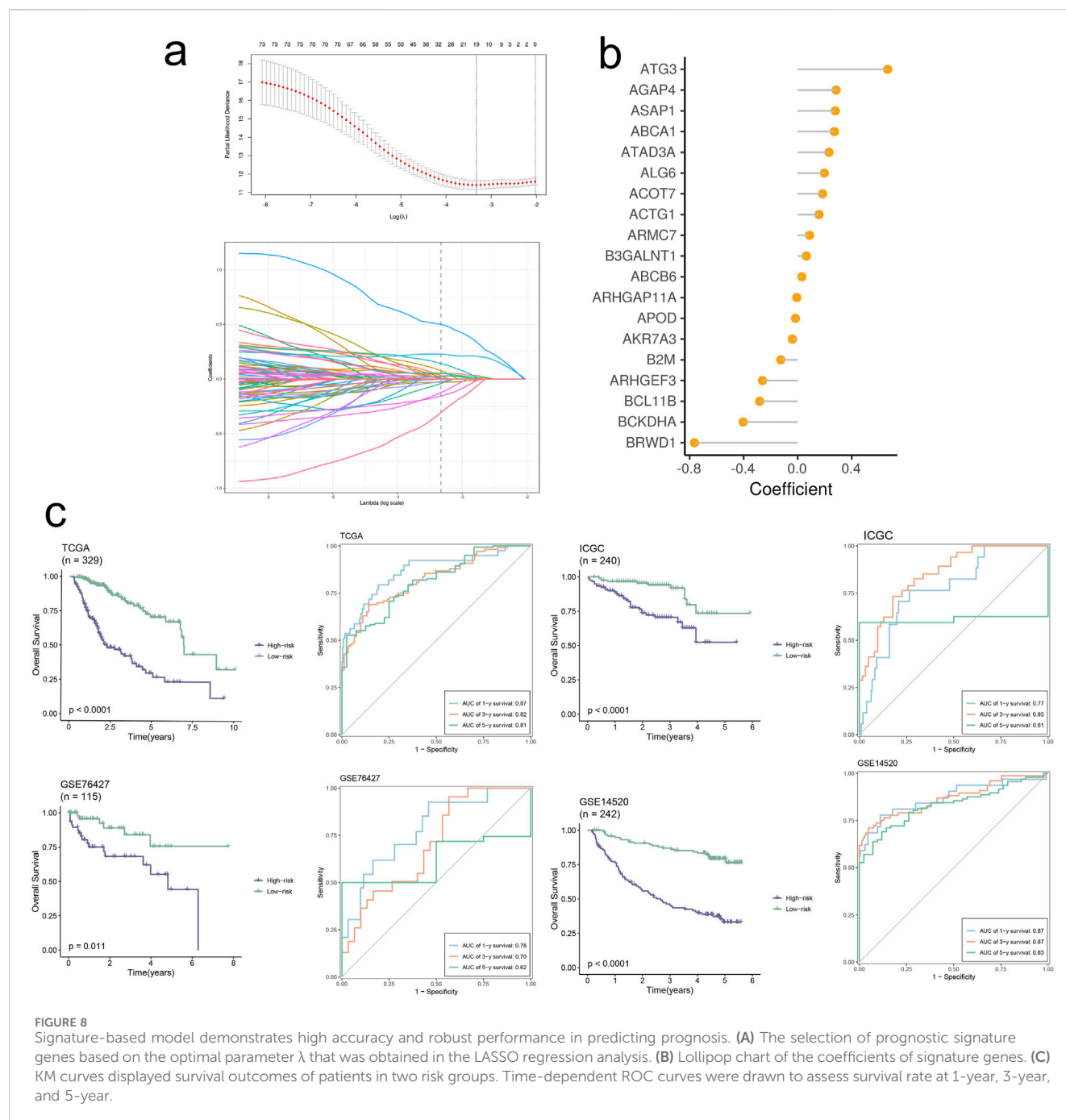


absorption, while concurrently downregulating pathways associated with Carbon metabolism, Cholesterol metabolism, Complement and coagulation cascades, Glycine, serine, and threonine metabolism, and Oxidative phosphorylation (Figures 7C, D). Our findings are similar to those obtained from the differential gene enrichment pathway analysis of malignant tumor cell subpopulations and CAF-related subpopulations in single-cell sequencing. Our analytical results demonstrate certain enriched pathway characteristics of tumors from different data dimensions, indicating a degree of universality.

### 3.7 Construction and validation of prognostic model

The final set of 19 genes was obtained through stepwise Cox proportional hazards regression, with nonzero coefficients (Figures 8A, B). Subsequently, patients were scored using the model formula to derive individual RiskScores. Based on the median of RiskScore calculations, patients were stratified into high-risk and low-risk groups. As depicted in Figure 8C, patients in the high-risk group exhibited significantly poorer overall performance compared to





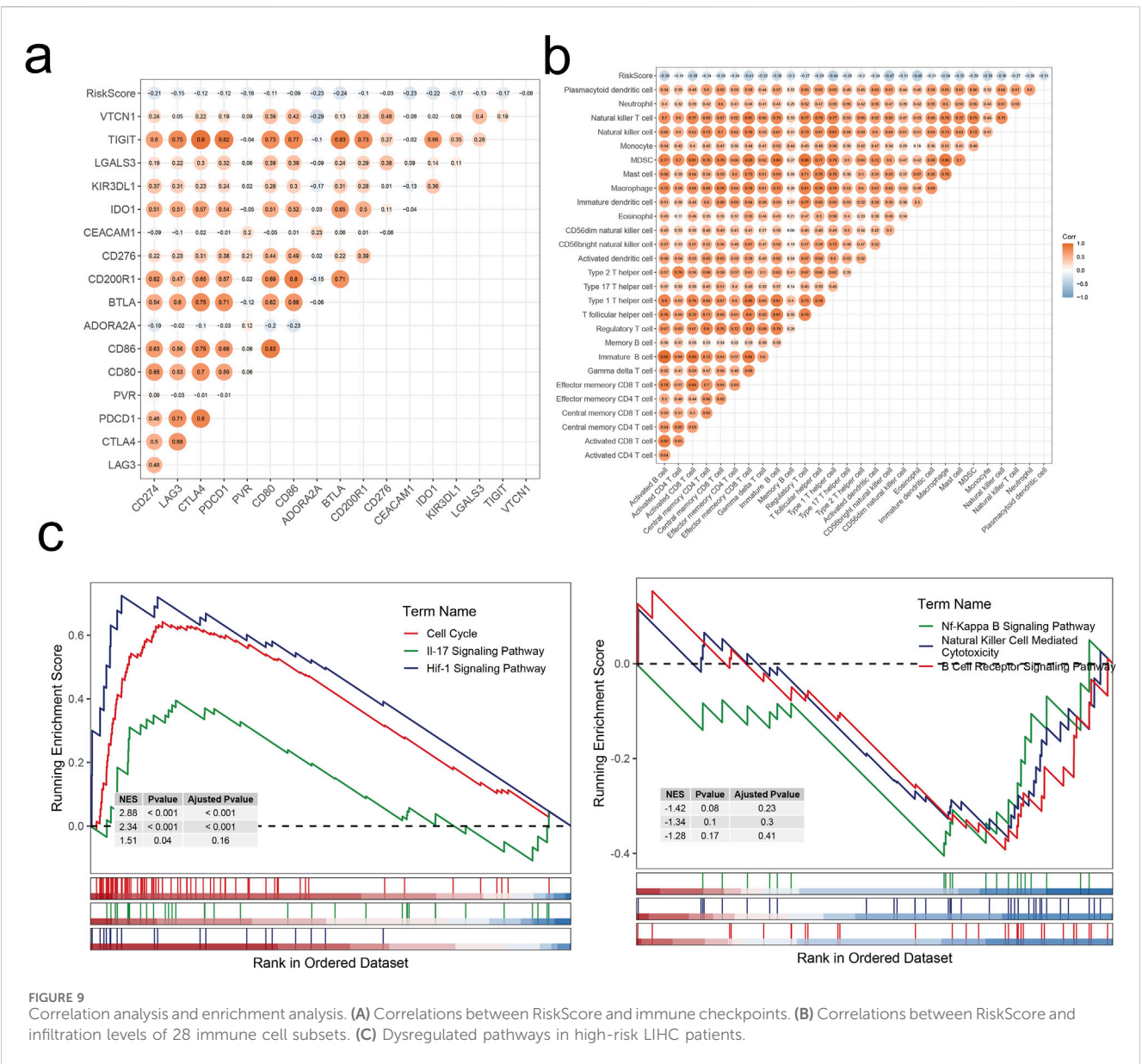
those in the low-risk group across all four datasets ( $p < 0.01$ ) according to the Kaplan-Meier curves. Our model demonstrated robust validation performance across the four datasets ( $AUC > 0.6$ ). A multiple correlation analysis was conducted, revealing mostly negative correlations between Riskscore and model genes (Figure 9A). Additionally, Riskscore exhibited negative correlations with immune cell infiltration scores (Figure 9B). Differential expression gene analysis was performed using the “limma” package to compare high- and low-risk groups, followed by Gene Set Enrichment Analysis (GSEA) on the selected differentially expressed genes. Finally, GSEA was employed to identify pathways upregulated (three on the left) and downregulated (three on the right) in the high-risk group

(Figure 9C). The above results are analogous to those obtained from the enrichment analysis of single-cell subpopulations.

### 3.8 ABCA1 plays a pro-oncogenic role in HCC cells

RT-qPCR analysis revealed that knockdown of ABCA1 significantly reduced ABCA1 mRNA expression in Huh7 cells compared to controls. Conversely, overexpression of ABCA1 markedly increased ABCA1 mRNA expression in HepG2 cells ( $p < 0.001$ , Figures 10A, B). Colony formation assays demonstrated fewer colonies in the ABCA1 knockdown





group of Huh7 cells and more colonies in the ABCA1-overexpressing group of HepG2 cells, indicating a role for ABCA1 in promoting HCC cell proliferation ( $p < 0.001$ , Figures 10C, D). CCK8 assays showed decreased cell viability in Huh7 cells following ABCA1 knockdown, whereas increased viability was observed in HepG2 cells upon ABCA1 overexpression ( $p < 0.001$ , Figures 10E, F). EDU assays indicated reduced proliferation in Huh7 cells with ABCA1 knockdown compared to controls ( $p < 0.001$ ), and increased proliferation in HepG2 cells with ABCA1 overexpression ( $p < 0.01$ , Figure 10G). Wound healing assays demonstrated reduced cell migration capability following ABCA1 knockdown ( $p < 0.001$ ), and enhanced migration upon ABCA1 overexpression in HepG2 cells ( $p < 0.01$ , Figure 11A). Western blot analysis revealed significant expression differences of ZO-1, E-cadherin, Vimentin, and Slug proteins between normal and overexpressing ABCA1 conditions in both Huh7 and HepG2 cells (Figure 11B). Transwell assays showed increased

invasive cell counts in both control groups, with significantly higher invasion in cells expressing higher levels of ABCA1 ( $p < 0.001$ , Figure 11C). Flow cytometry analysis indicated a higher apoptotic percentage in cells with lower ABCA1 expression, suggesting a role for ABCA1 in reducing apoptosis in HCC cells ( $p < 0.001$ , Figure 11D). In summary, ABCA1 plays a pro-oncogenic role in HCC cells by promoting proliferation, invasion, migration, and reducing apoptosis.

## 4 Discussion

HCC represents a major histological subtype of liver cancer and ranks among the deadliest malignancies. According to relevant data, the global number of new HCC cases reached 905,677 in 2020, with 830,180 new deaths reported (Foerster et al., 2022). Despite advancements in therapeutic strategies, the mortality rate of HCC

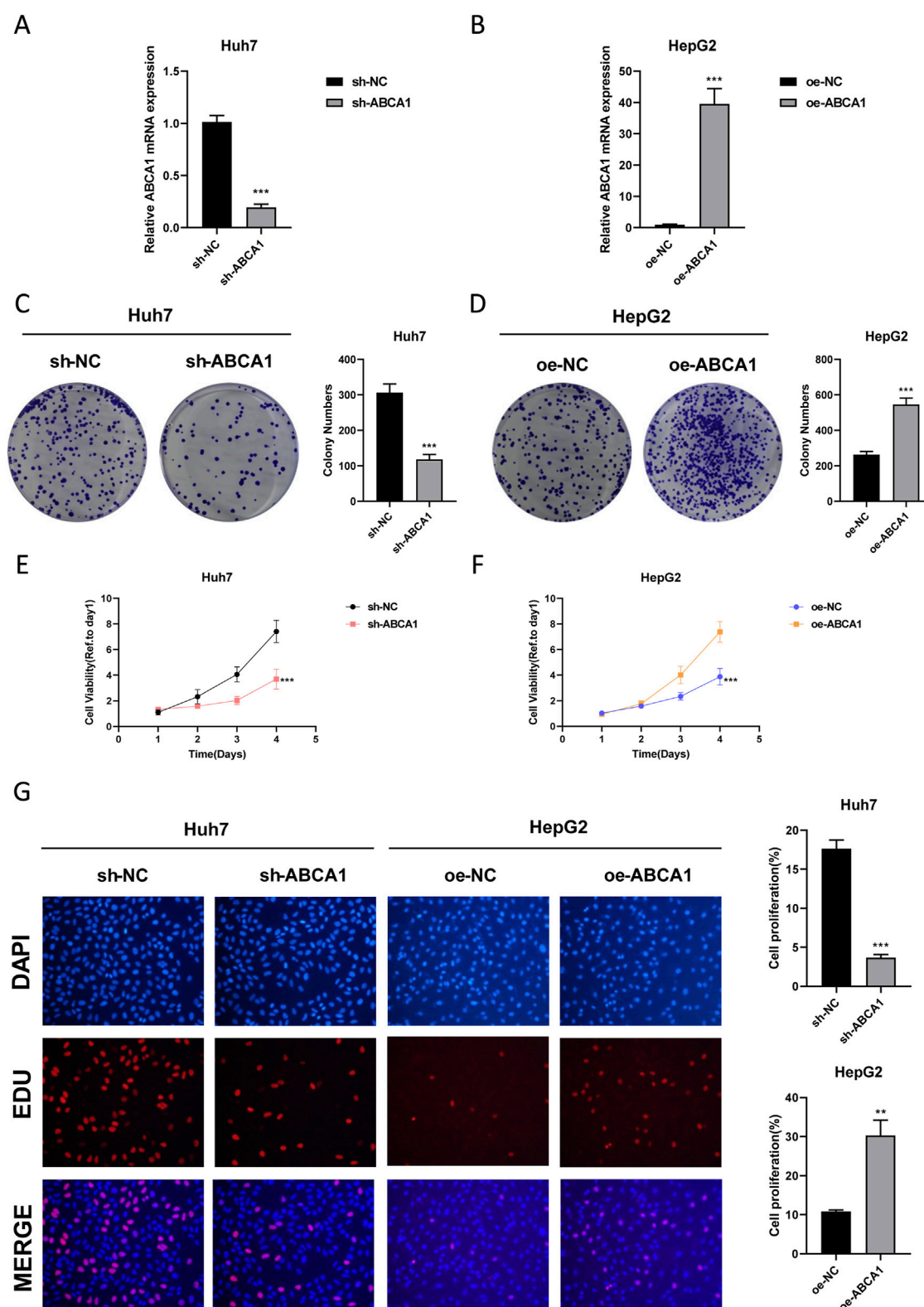
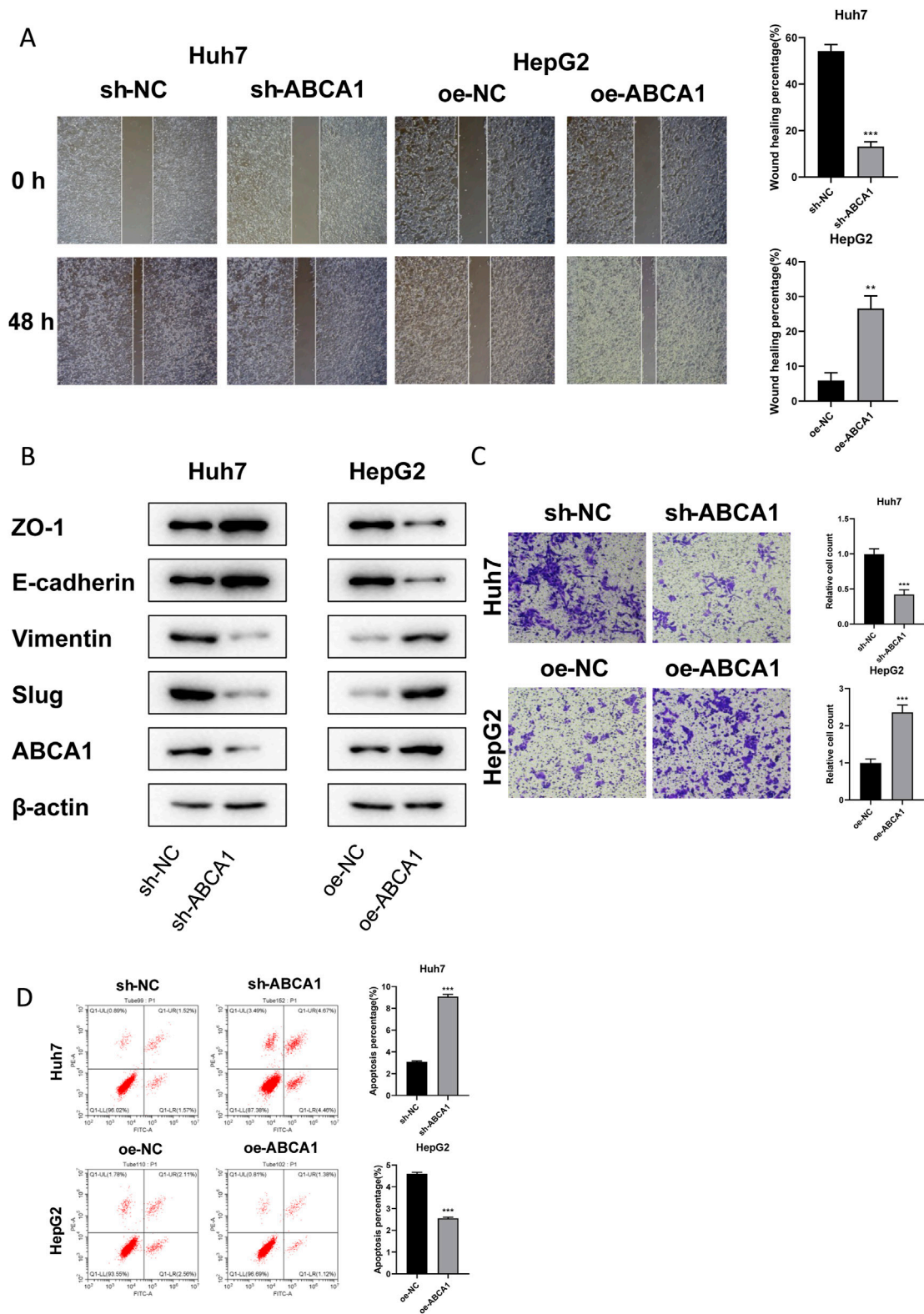


FIGURE 10

Efficiency validation of ABCA1 knockdown and overexpression and their impact on cancer cell proliferation. (A) RT-qPCR experiment validating the knockdown efficiency of sh-ABCA1 in Huh7 cell line. (B) RT-qPCR experiment validating the overexpression efficiency of oe-ABCA1 in HepG2 cell line. (C) Colony formation assay reflecting differences in proliferation levels between ABCA1 knockdown group and control group cells. (D) Colony formation assay reflecting differences in proliferation levels between ABCA1 overexpression group and control group cells. (E) CCK8 assay reflecting differences in proliferation levels between ABCA1 knockdown group and control group cells. (F) CCK8 assay reflecting differences in proliferation levels between ABCA1 overexpression group and control group cells. (G) EDU assay reflecting differences in proliferation levels between ABCA1 knockdown group, ABCA1 overexpression group, and control group cells.



**FIGURE 11**  
Effects of ABCA1 knockdown and overexpression on cell migration, invasion, and apoptosis capabilities. **(A)** Wound healing assay validating differences in migration levels between ABCA1 knockdown group, ABCA1 overexpression group, and control group cells. **(B)** Western blot validating differences in migration-related protein expression levels between ABCA1 knockdown group, ABCA1 overexpression group, and control group cells. **(C)** Transwell assay validating differences in invasion levels between ABCA1 knockdown group, ABCA1 overexpression group, and control group cells. **(D)** Flow cytometry validating differences in apoptosis levels between ABCA1 knockdown group, ABCA1 overexpression group, and control group cells.



remains high, primarily due to its late-stage diagnosis. Once HCC progresses to an advanced stage, it becomes highly invasive with a dismal prognosis, resulting in a 5-year survival rate of around 20% for patients (Chen et al., 2022).

The optimal treatment for HCC is liver resection or transplantation, yet the surgical cure rate is only about 20%, and surgical indications are stringent, leaving most patients with conservative treatment options (Llovet et al., 2024). Concurrently, CAFs have been implicated in HCC's tumor proliferation, angiogenesis, metastasis, and chemotherapy resistance (Biffi and Tuveson, 2021). Therefore, investigating the correlation between malignant cells in HCC and CAFs using bioinformatics techniques, analyzing the role of HCC-related genes and signaling pathways in the TME, and constructing prognostic models are of significant importance. Furthermore, the screening and analysis of differentially expressed genes contribute to early diagnosis and precision treatment of HCC.

We downloaded bulk transcriptomic data and corresponding clinical data of HCC from the public database TCGA, datasets GSE14520 and GSE76427 from the GEO database, ICGC-JP dataset from the ICGC database, and three single-cell sequencing datasets GSE146115, GSE146409, and GSE166635 from the TISCH2 database. These datasets hold immense research and application potential in the diagnosis, treatment, and prognostic assessment of patients.

After quality control, we performed UMAP dimensionality reduction on the single-cell sequencing data, resulting in 28 clusters, annotated into 12 major cell types. Further UMAP dimensionality reduction was conducted on 2 cell types—malignant cell clusters based on EPCAM expression levels and CAFs cell clusters based on COL1A1 and COL1A2 expression levels—yielding 6 malignant cell subgroups and 3 CAFs cell subgroups. By constructing developmental lineages and trajectories for each cell subgroup, we observed that each malignant cell subgroup generally exhibited two developmental trajectories, with the Malignant\_Epi\_0 cell subgroup likely being their common developmental origin. In contrast, each CAFs cell subgroup had only one developmental trajectory, with an unknown developmental origin. We conducted DEGs analysis for each cell subgroup. Among the 6 malignant cell subgroups, MT-ND3, MT-CYB, MT-ATP6, MT-CO2, and MT-CO1 were identified as differentially expressed genes in the Malignant\_Epi\_2, Malignant\_Epi\_3, and Malignant\_Epi\_4 cell subgroups, while ALB, AHSG, and APOE were also identified as differentially expressed genes in the Malignant\_Epi\_1 and Malignant\_Epi\_5 subgroups, exhibiting a consistent downregulation trend across all subgroups. We infer that the downregulation of these genes may promote tumor proliferation and metastasis, leading to unfavorable prognosis. Among the 3 CAFs cell subgroups, RPL17-C18orf32, AC135178.2, and MTRNR2L8 were identified as differentially downregulated genes in CAF\_0 and CAF\_2, but exhibited an upregulation trend in CAF\_1. Finally, we conducted GO\_BP enrichment analysis and extracted the top six statistically significant signaling pathways for each cell subgroup.

To delve deeper into the correlation between malignant cells and CAFs, we conducted cell communication analysis on various cell subpopulations using the CellChat and NicheNet algorithms. Beyond examining the frequency and strength of interactions

between each cell subpopulation, we also investigated the receptor relationships of different pathways within these subpopulations. Specifically, we focused on the SPP1 signaling pathway to elucidate the ligand-receptor pairing status. Through detailed analysis of various components of the SPP1 signaling pathway, we observed that the Malignant\_Epi\_0 cell subpopulation is crucial in all four aspects—Sender, Receiver, Mediator, and Influencer—while the Malignant\_Epi\_3 subpopulation exhibits the opposite pattern, indicating divergent modes of action concerning SPP1. We also studied the outward and inward interaction strengths of each cell subpopulation. Finally, by pairing genes expressed by CAFs as ligands with genes expressed by malignant cells as receptors, we analyzed their binding potential and biological efficacy. We found that only when IL1B acts as the ligand and IL1RAP, IL1R1, and IL1R2 act as receptors, both binding potential and biological effects are evident. Furthermore, we constructed GRNs based on single-cell data from HCC. During this process, we focused on the distribution and expression of five regulatory factors associated with HCC across different cell subpopulations: BRF1\_extended\_29g, ARNTL\_extended\_39g, ARNTL\_24g, BCLAF1\_extended\_22g, and ATF3\_extended\_16g. BRF1 encodes one of the three subunits of RNA polymerase III transcription factor complex, which plays a core role in initiating transcription of genes encoding tRNA, 5S rRNA, and other small structural RNAs. Studies have shown that BRF1 is highly expressed in human tumor tissues of HCC patients, and inhibiting its expression can suppress HCC development (Lin et al., 2020). ARNTL encodes a protein with a basic helix-loop-helix structure and has been shown to exert anti-tumor effects in many human cancers. Downregulation of ARNTL in HCC patients promotes growth and metastasis of HCC cells both *in vitro* and *in vivo*, significantly correlating with low survival rates (Yang et al., 2022). BCLAF1 interacts with members of the Bcl2 family of anti-apoptotic proteins and enhances HIF1 $\alpha$  expression in HCC tissues under hypoxic conditions, thereby promoting HCC-related angiogenesis and disease progression. Therefore, BCLAF1 is likely to be a therapeutic target for anti-proliferation and anti-angiogenesis treatment in HCC (Wen et al., 2019). ATF3, a member of the cAMP responsive element-binding protein (CREB) family, has been found to be a tumor suppressor that inhibits proliferation and metastasis of HCC cells. It also significantly correlates with intrahepatic metastasis and overall survival (OS) of HCC patients (Chen et al., 2018). For these five regulatory factors, we also explored differences in their activity levels between malignant and CAF cells. Subsequently, we merged the target genes of these five regulatory factors to obtain a signature for unsupervised clustering analysis.

We applied unsupervised clustering analysis to hierarchically cluster tumor tissue samples, aiming to categorize the samples. By selecting the most suitable value for (k) [where (k = 2)], we partitioned the samples into two distinct clusters, denoted as C1 and C2. Subsequently, we performed KM survival analysis on each cluster, which showed that the survival rates for both clusters decreased over time. Following this, we compared the TMEs of the two clusters.

First, we utilized ssGSEA to score 28 immune cell subsets to measure their relative infiltration abundance. Comparing the statistically significant data, we found that in cluster C1, there were higher levels of immune cell infiltration for Activated

CD4 T cells, Effector Memory CD4 T cells, Regulatory T cells, and Type 2 T helper cells. Conversely, in cluster C2, Eosinophils exhibited higher levels of infiltration compared to cluster C1. These findings suggest that each cluster may play distinct and significant roles in different immune response regulations.

Next, we analyzed the expression levels of CYT, GFP, IFNG, and TMB between clusters C1 and C2, finding that only CYT showed statistically significant differences, with cluster C1 exhibiting significantly higher activity than cluster C2. To further understand the TMEs, we used five different algorithms—CIBERSORT, MCP-counter, quanTIseq, EPIC, and TIMER—to assess the infiltration levels of immune cell subsets in the two clusters. The results aligned with our earlier findings.

We then extracted data for 150 immunomodulators and chemokines from the TISIDB database, including chemokines, Immunoinhibitors, Immunostimulators, MHC, and receptors. We analyzed their expression patterns in both clusters. The results indicated that these five types of substances were generally highly expressed in cluster C1 and under-expressed in cluster C2. This could suggest that cluster C1 is more closely associated with immune regulation and immune response, while cluster C2 might be involved in the inhibition and regulation of immune activity.

Finally, we used GSVA to measure the enrichment scores for the anti-cancer immunity cycle and immunotherapy-predicted pathways in the two clusters. Upon observation, we noted that the C1 cluster exhibited higher Enrichment Scores in both the anti-cancer immunity cycle and immunotherapy-predicted pathway. Therefore, we reasonably infer that target genes within the C1 cluster play a pivotal role in the regulation and treatment of anti-cancer immunity. This finding contributes to a better understanding of the mechanisms underlying different cell clusters in immunotherapy, while also providing significant guidance for the formulation of cancer treatment strategies.

We utilized the “limma” package to identify differential genes between the C1 and C2 clusters and performed GSEA. This revealed upregulated cancer signatures in both clusters. Specifically, in the C1 cluster, upregulated cancer signatures were closely associated with various aspects of tumor initiation, progression, immune microenvironment, metastasis, and cell cycle regulation. Conversely, upregulated cancer signatures in the C2 cluster implicated multiple metabolic pathways, suggesting that modulating aberrant metabolic pathways might be a crucial therapeutic strategy in HCC treatment. Additionally, GSEA helped identify upregulated and downregulated signaling pathways in the C1 cluster. Analysis revealed that upregulated signaling pathways were linked to tumor cell proliferation and signal transduction, while downregulated pathways involved fundamental metabolic processes such as the complement and coagulation cascade, energy metabolism, and protein synthesis. Overall, the abnormal proliferation of cells in the C1 cluster, coupled with suppressed metabolic processes, exacerbates tumor growth, dissemination, and metastasis. Furthermore, the downregulation of the complement and coagulation cascade pathway may be associated with the abnormal coagulation status observed in HCC patients.

Utilizing the TCGA-LIHC dataset, we employed LASSO and multiCOX analysis methods to construct a HCC prognostic model and assigned scores to model factors, yielding a RiskScore for each

sample. Based on the median score, we stratified samples into high and low-risk groups. Subsequently, KM curves were plotted to predict prognosis for both high and low-risk groups, revealing a progressive decrease in survival rates over time for both groups, with notably poorer prognosis observed in the high-risk group. We assessed the model’s diagnostic performance at 1, 3, and 5-year time points through ROC curve analysis, demonstrating good performance. Furthermore, we validated the prognostic model in three external datasets (GSE76427, GSE14520, ICGC-JP) using KM and ROC curve analyses, showing excellent accuracy and predictive ability across different datasets.

We then examined the correlation between RiskScore and various immune checkpoint levels and immune cell infiltration levels. Differential gene expression analysis was performed to identify DEGs between high and low-risk groups. Subsequently, GSEA revealed dysregulated signaling pathways in high-risk group patients. Analysis indicated that upregulated signaling pathways in the high-risk group were associated with tumor cell proliferation and cell cycle regulation, promoting malignant tumor growth and development. Conversely, downregulated signaling pathways were linked to anti-tumor immune responses and immune regulation, likely facilitating tumor immune evasion and affecting the regulation of the TME, thus exerting significant adverse effects on HCC prognosis. These inferences also corroborated the accuracy of our prognostic model.

Single-cell sequencing, with its outstanding resolution, demonstrates significant advantages over bulk sequencing in elucidating disease mechanisms. However, considering cost-effectiveness and the convenience of large-scale application, bulk sequencing still holds its ground. Therefore, combining these two technologies for comparative analysis can fully leverage their respective strengths. In this study, we conducted in-depth differential expression and enrichment analyses on malignant cell subpopulations and CAF subpopulations at the single-cell level, while exploring differential gene enrichment among different clusters and model risk groups at the bulk sequencing level.

The comparative analysis revealed that both single-cell sequencing and bulk sequencing identified the universal upregulation of metabolic pathways in the tumor microenvironment, suggesting that metabolic reprogramming may be a common feature in tumor development. Furthermore, both technologies observed the activation of cell signaling transduction-related pathways, which are closely related to the proliferation and migration of tumor cells. Notably, single-cell sequencing uniquely captured the upregulation of immune inflammation and neuroregulatory-related pathways in malignant cell subpopulations, which were not explicitly identified in bulk sequencing, highlighting the powerful ability of single-cell sequencing in resolving cell subpopulation-specific characteristics. On the other hand, bulk sequencing detected the upregulation of pathways related to epithelial-mesenchymal transition (EMT), a finding not directly reflected in single-cell sequencing. Given that EMT is a complex process involving multiple cell subpopulations and pathway interactions, it may be implicitly manifested in single-cell sequencing as differential expression patterns among different subpopulations. Furthermore, we speculate that the upregulation of metabolic and signal transduction pathways observed in single-cell sequencing may be intrinsically linked to the activation of cell cycle



regulation, Hippo signaling pathway, MAPK signaling pathway, and PI3K-Akt signaling pathway observed in bulk sequencing, all of which jointly contribute to the proliferation and survival of tumor cells.

Despite the differences in pathway analysis between single-cell sequencing and bulk sequencing, they both emphasize the complexity and heterogeneity of the tumor microenvironment. This heterogeneity may arise from interactions among different cell subpopulations and the diversity of pathway regulation. By integrating the results of these two sequencing technologies, we hope to gain a deeper understanding of the molecular mechanisms underlying tumor development and progression, and provide new perspectives and ideas for the formulation of future therapeutic strategies.

We conducted knockdown and overexpression experiments of ABCA1 in two HCC cell lines. Subsequent phenotypic assays confirmed that ABCA1 exerts a pro-oncogenic effect in HCC cells by promoting proliferation, invasion, migration, and reducing apoptosis. Our wet lab experiments corroborate the bioinformatic findings, providing robust evidence for the role of ABCA1 in liver cancer. This study not only reinforces the computational results but also lays a foundation for future research.

However, our study still has certain limitations. We are acutely aware that relying solely on *in vitro* experimental results poses significant constraints when directly translating to clinical applications. To bridge the gap in clinical translation, we plan to initially utilize animal models, particularly patient-derived xenograft (PDX) models and humanized mouse models that closely mimic the tumor characteristics of patients, to simulate a more authentic *in vivo* environment and further explore the functions and mechanisms of ABCA1. This will include, but is not limited to, assessing the specific effects of ABCA1 on tumor growth, metastasis, and the tumor immune microenvironment *in vivo*. Subsequently, we will employ high-throughput screening and precision medicine strategies to identify potential therapeutic targets for ABCA1 and develop corresponding therapeutic interventions. Furthermore, we will closely monitor changes in relevant biomarkers, with the aim of establishing a biomarker system that can predict treatment efficacy and patient prognosis. Our objective is to build a solid evidence base through advanced preclinical research to guide future clinical trials and facilitate the clinical translation of ABCA1-related research.

## 5 Conclusion

Through comprehensive integration of TCGA, GEO, ICGC, and TISCH2 databases, we conducted single-cell sequencing analysis and cell communication analysis on multiple malignant and CAFs cell subpopulations, revealing the functional characteristics and receptor relationships of each cell subgroup. Additionally, we constructed GRNs, delving into the regulatory factors associated with HCC and their target genes. Utilizing an unsupervised clustering analysis based on target genes, we identified two clusters, C1 and C2, and analyzed their TME differences. Furthermore, through GSEA, we identified upregulated cancer features in two clusters and signaling pathways that were both upregulated and downregulated in the C1 cluster.

We constructed a prognostic model and assigned scores, grouping patients based on RiskScore and predicting their

prognosis accordingly. The results demonstrated the excellent accuracy and clinical utility of our model. Additionally, we discovered a correlation between RiskScore, immune checkpoint expression, and immune cell infiltration levels. GSEA analysis revealed dysregulated signaling pathways in the high-risk group, adversely affecting HCC prognosis. Our study provides important insights for the prognostic evaluation and formulation of treatment strategies for HCC.

## Data availability statement

The raw data supporting the conclusions of this article will be made available by the authors, without undue reservation.

## Ethics statement

Ethical approval was not required for the studies on humans in accordance with the local legislation and institutional requirements because only commercially available established cell lines were used.

## Author contributions

DY: Conceptualization, Data curation, Methodology, Writing—original draft, Writing—review and editing. FG: Data curation, Formal Analysis, Methodology, Writing—review and editing. QZ: Conceptualization, Formal Analysis, Supervision, Validation, Writing—original draft. HY: Data curation, Methodology, Software, Writing—review and editing. WW: Conceptualization, Investigation, Methodology, Validation, Writing—review and editing. YC: Conceptualization, Data curation, Methodology, Supervision, Writing—original draft, Writing—review and editing.

## Funding

The author(s) declare that financial support was received for the research, authorship, and/or publication of this article. This work was supported by the Zhejiang Provincial Top Key Discipline in Surgery (Grant No. 2008-255).

## Acknowledgments

The authors would like to thank the biological Science Department of Peking Core Stone for the helpful in the copy editing work of this article.

## Conflict of interest

The authors declare that the research was conducted in the absence of any commercial or financial relationships that could be construed as a potential conflict of interest.

## Publisher's note

All claims expressed in this article are solely those of the authors and do not necessarily represent those of their affiliated

organizations, or those of the publisher, the editors and the reviewers. Any product that may be evaluated in this article, or claim that may be made by its manufacturer, is not guaranteed or endorsed by the publisher.

## References

- Anwanwan, D., Singh, S. K., Singh, S., Saikam, V., and Singh, R. (2020). Challenges in liver cancer and possible treatment approaches. *Biochim. Biophys. Acta Rev. Cancer* 1873 (1), 188314. doi:10.1016/j.bbcan.2019.188314
- Biffi, G., and Tuveson, D. A. (2021). Diversity and biology of cancer-associated fibroblasts. *Physiol. Rev.* 101 (1), 147–176. doi:10.1152/physrev.00048.2019
- Bruix, J., Han, K. H., Gores, G., Llovet, J. M., and Mazzaferro, V. (2015). Liver cancer: approaching a personalized care. *J. Hepatol.* 62 (1 Suppl. 1), S144–S156. doi:10.1016/j.jhep.2015.02.007
- Chen, C., Ge, C., Liu, Z., Li, L., Zhao, F., Tian, H., et al. (2018). ATF3 inhibits the tumorigenesis and progression of hepatocellular carcinoma cells via upregulation of CYR61 expression. *J. Exp. Clin. Cancer Res.* 37 (1), 263. doi:10.1186/s13046-018-0919-8
- Chen, D., Liu, J., Zang, L., Xiao, T., Zhang, X., Li, Z., et al. (2022). Integrated machine learning and bioinformatic analyses constructed a novel stemness-related classifier to predict prognosis and immunotherapy responses for hepatocellular carcinoma patients. *Int. J. Biol. Sci.* 18 (1), 360–373. doi:10.7150/ijbs.66913
- Chen, K., Li, Y., Wang, B., Yan, X., Tao, Y., Song, W., et al. (2023). Patient-derived models facilitate precision medicine in liver cancer by remodeling cell-matrix interaction. *Front. Immunol.* 14, 1101324. doi:10.3389/fimmu.2023.1101324
- Chen, Y., Liu, Y., Chen, S., Zhang, L., Rao, J., Lu, X., et al. (2023). Liver organoids: a promising three-dimensional model for insights and innovations in tumor progression and precision medicine of liver cancer. *Front. Immunol.* 14, 1180184. doi:10.3389/fimmu.2023.1180184
- Cheng, Z., Li, X., and Ding, J. (2016). Characteristics of liver cancer stem cells and clinical correlations. *Cancer Lett.* 379 (2), 230–238. doi:10.1016/j.canlet.2015.07.041
- Duan, X. Y., Zhang, L., Fan, J. G., and Qiao, L. (2014). NAFLD leads to liver cancer: do we have sufficient evidence? *Cancer Lett.* 345 (2), 230–234. doi:10.1016/j.canlet.2013.07.033
- Foerster, F., Gairing, S. J., Müller, L., and Galle, P. R. (2022). NAFLD-driven HCC: safety and efficacy of current and emerging treatment options. *J. Hepatol.* 76 (2), 446–457. doi:10.1016/j.jhep.2021.09.007
- Fu, X., Zhang, Y., Luo, Q., Ju, Y., and Song, G. (2023). Targeting the mechano-microenvironment and liver cancer stem cells: a promising therapeutic strategy for liver cancer. *Cancer Biol. Med.* 20 (11), 816–829. doi:10.20892/j.issn.2095-3941.2023.0229
- Gao, S., Gang, J., Yu, M., Xin, G., and Tan, H. (2021). Computational analysis for identification of early diagnostic biomarkers and prognostic biomarkers of liver cancer based on GEO and TCGA databases and studies on pathways and biological functions affecting the survival time of liver cancer. *BMC Cancer* 21 (1), 791. doi:10.1186/s12885-021-08520-1
- Hao, L., Li, S., Deng, J., Li, N., Yu, F., Jiang, Z., et al. (2023). The current status and future of PD-L1 in liver cancer. *Front. Immunol.* 14, 1323581. doi:10.3389/fimmu.2023.1323581
- Islami, F., Miller, K. D., Siegel, R. L., Fedewa, S. A., Ward, E. M., and Jemal, A. (2017). Disparities in liver cancer occurrence in the United States by race/ethnicity and state. *CA Cancer J. Clin.* 67 (4), 273–289. doi:10.3322/caac.21402
- Jeong, S., Zheng, B., Wang, H., Xia, Q., and Chen, L. (2018). Nervous system and primary liver cancer. *Biochim. Biophys. Acta Rev. Cancer* 1869 (2), 286–292. doi:10.1016/j.bbcan.2018.04.002
- Li, L., and Wang, H. (2016). Heterogeneity of liver cancer and personalized therapy. *Cancer Lett.* 379 (2), 191–197. doi:10.1016/j.canlet.2015.07.018
- Li, X., Ramadori, P., Pfister, D., Seehawer, M., Zender, L., and Heikenwalder, M. (2021). The immunological and metabolic landscape in primary and metastatic liver cancer. *Nat. Rev. Cancer* 21 (9), 541–557. doi:10.1038/s41568-021-00383-9
- Lin, M., Huang, C., Ren, W., Chen, J., Xia, N., and Zhong, S. (2020). Mitogen- and stress-activated protein kinase 1 mediates alcohol-upregulated transcription of Brf1 and tRNA genes to cause phenotypic alteration. *Oxid. Med. Cell Longev.* 2020, 2067959. doi:10.1155/2020/2067959
- Liu, W., Zhou, X., Yao, Q., Chen, C., Zhang, Q., Ding, K., et al. (2023). *In situ* expansion and reprogramming of Kupffer cells elicit potent tumoricidal immunity against liver metastasis. *J. Clin. Invest.* 133 (8), e157937. doi:10.1172/JCI157937
- Llovet, J. M., Kelley, R. K., Villanueva, A., Singal, A. G., Pikarsky, E., Roayaie, S., et al. (2024). Author correction: hepatocellular carcinoma. *Nat. Rev. Dis. Prim.* 10 (1), 10. doi:10.1038/s41572-024-00500-6
- Mokdad, A. A., Singal, A. G., and Yopp, A. C. (2015). JAMA PATIENT PAGE. Liver cancer. *Jama.* 314 (24), 2701. doi:10.1001/jama.2015.15425
- Soulen, M. C., and García-Mónaco, R. (2021). Closing the gap in curative ablation of liver cancer. *Radiology* 301 (1), 237–238. doi:10.1148/radiol.2021211204
- Sung, H., Ferlay, J., Siegel, R. L., Laversanne, M., Soerjomataram, I., Jemal, A., et al. (2021). Global cancer statistics 2020: GLOBOCAN estimates of incidence and mortality worldwide for 36 cancers in 185 countries. *CA Cancer J. Clin.* 71 (3), 209–249. doi:10.3322/caac.21660
- Tong, A. K., Tham, W. Y., Too, C. W., Tai, D. W., Chow, P. K., and Ng, D. C. (2020). Molecular imaging and therapy of liver tumors. *Semin. Nucl. Med.* 50 (5), 419–433. doi:10.1053/j.semnuclmed.2020.04.004
- Wen, Y., Zhou, X., Lu, M., He, M., Tian, Y., Liu, L., et al. (2019). Bclaf1 promotes angiogenesis by regulating HIF-1 $\alpha$  transcription in hepatocellular carcinoma. *Oncogene* 38 (11), 1845–1859. doi:10.1038/s41388-018-0552-1
- Yang, Y., Yang, T., Zhao, Z., Zhang, H., Yuan, P., Wang, G., et al. (2022). Down-regulation of BMAL1 by MiR-494-3p promotes hepatocellular carcinoma growth and metastasis by increasing GPAM-mediated lipid biosynthesis. *Int. J. Biol. Sci.* 18 (16), 6129–6144. doi:10.7150/ijbs.74951
- Zhou, Y., Li, Y., Zhou, T., Zheng, J., Li, S., and Li, H. B. (2016). Dietary natural products for prevention and treatment of liver cancer. *Nutrients* 8 (3), 156. doi:10.3390/nu8030156



## OPEN ACCESS

## EDITED BY

Jianbin Bi,  
The First Hospital of China Medical University,  
China

## REVIEWED BY

WenQin Lian,  
Xiamen University, China  
Danyang Li,  
Harbin Medical University, China  
Xiang Huang,  
Wenzhou Medical University, China

## \*CORRESPONDENCE

Xin You,  
✉ youxin1206@hotmail.com  
Heping Huang,  
✉ hpjxfb@163.com

<sup>†</sup>These authors have contributed equally to  
this work

RECEIVED 25 September 2024

ACCEPTED 28 November 2024

PUBLISHED 13 January 2025

## CITATION

Hong W, Wang X, Huang X, Chen P, Liu Y,  
Zheng Z, You X, Chen Y, Xie Z, Zhan G and  
Huang H (2025) CSNK1E is involved in TGF- $\beta$ 1  
induced epithelial mesenchymal  
transformation and related to melanoma  
immune heterogeneity.  
*Front. Pharmacol.* 15:1501849.  
doi: 10.3389/fphar.2024.1501849

## COPYRIGHT

© 2025 Hong, Wang, Huang, Chen, Liu, Zheng,  
You, Chen, Xie, Zhan and Huang. This is an  
open-access article distributed under the terms  
of the [Creative Commons Attribution License](https://creativecommons.org/licenses/by/4.0/)  
(CC BY). The use, distribution or reproduction in  
other forums is permitted, provided the original  
author(s) and the copyright owner(s) are  
credited and that the original publication in this  
journal is cited, in accordance with accepted  
academic practice. No use, distribution or  
reproduction is permitted which does not  
comply with these terms.

# CSNK1E is involved in TGF- $\beta$ 1 induced epithelial mesenchymal transformation and related to melanoma immune heterogeneity

Wangbing Hong<sup>1†</sup>, Xin Wang<sup>2†</sup>, Xinyu Huang<sup>3†</sup>, Pengfei Chen<sup>1</sup>,  
Yifan Liu<sup>1</sup>, Ziyang Zheng<sup>1</sup>, Xin You<sup>1\*</sup>, Yinghua Chen<sup>1</sup>, Zengxin Xie<sup>1</sup>,  
Gongnan Zhan<sup>1</sup> and Heping Huang<sup>1\*</sup>

<sup>1</sup>Department of Plastic and Cosmetic Surgery, Jiangxi Maternal and Child Health Hospital, Nanchang, Jiangxi, China, <sup>2</sup>Medical Center of Burn Plastic and Wound Repair, The First Affiliated Hospital of Nanchang University, Nanchang, Jiangxi, China, <sup>3</sup>Department of Plastic and Aesthetic Surgery, Nanfang Hospital of Southern Medical University, Guangzhou, Guangdong, China

**Introduction:** Melanoma (MM), the deadliest form of skin cancer, originates from melanocytes. Despite advances in immunotherapy that have somewhat improved the prognosis for MM patients, high levels of resistance to treatment continue to result in poor clinical outcomes. Identifying novel biomarkers and therapeutic targets is critical for improving the prognosis and treatment of MM.

**Methods:** In this study, we analyzed the expression patterns of WNT signaling pathway genes in MM and explored their potential mechanisms. Using Cox regression analysis, we identified 19 prognostic-related genes. Consistency clustering was performed to evaluate the potential of these genes as classifiers for prognosis. The Least Absolute Shrinkage and Selection Operator (LASSO) algorithm was then applied to refine the gene set and construct a 13-gene prognostic model. We validated the model at multiple time points to assess its predictive performance. Additionally, correlation analyses were performed to investigate the relationships between key genes and processes, including epithelial-to-mesenchymal transition (EMT) and immune responses.

**Results:** We identified that CSNK1E and RAC3 were significantly positively correlated with the EMT process, with CSNK1E showing a similar expression trend to EMT-related genes. Both genes were also negatively correlated with multiple immune cell types and immune checkpoint genes. The 13-gene prognostic model demonstrated excellent predictive performance in MM prognosis. Pan-cancer analysis further revealed heterogeneous expression patterns and prognostic potential of CSNK1E across various cancers. Wet experiments confirmed that CSNK1E promotes MM cell proliferation, invasion, and migration, and enhances malignant progression through the TGF- $\beta$  signaling pathway.

**Discussion:** Our findings suggest that CSNK1E plays a crucial role in MM progression and could serve as a potential therapeutic target. The WNT and TGF- $\beta$  pathways may work synergistically in regulating the EMT process in MM,

highlighting their potential as novel therapeutic targets. These insights may contribute to the development of more effective treatments for MM, particularly for overcoming resistance to current therapies.

#### KEYWORDS

CSNK1E, TGF- $\beta$  1, epithelial mesenchymal transformation, melanoma, LASSO

## 1 Introduction

Melanoma (MM) is the deadliest form of skin cancer (Guo et al., 2021), accounting for over 75% of skin cancer-related deaths (Rebecca et al., 2020) and approximately 0.7% of all cancer mortality (Schadendorf et al., 2018). Moreover, MM is among the few cancers whose incidence is currently on the rise (Poklepovic and Luke, 2020).

Melanoma incidence and mortality are higher in men than in women, and the underlying biological mechanisms responsible for the sex differences in cutaneous melanoma are unknown and complicated by clinical variables such as anatomical site, skin light type, body mass index, and variability in immune response. Therefore, we sought to investigate prognostic and immunological differences in melanoma by sex.

Melanocytes originate from neural crest stem cells (NCSC), and their malignant transformation leads to MM. Typically, MM arises from nevus and/or intermediate lesions, undergoing progressive dysplasia before becoming invasive and ultimately metastatic (Lin and Fisher, 2007). The transformation of melanocytes into MM is primarily driven by carcinogenic signaling pathways, which are triggered by a combination of environmental and genetic factors. Common environmental factors include ultraviolet (UV) exposure in Caucasians, whereas in individuals of Asian and African descent, trauma, chronic inflammation, and infections are more prevalent triggers (Liu et al., 2016; Splendiani et al., 2024). Genetic factors often involve a relevant family history (Splendiani et al., 2024). Phenotypic heterogeneity exists within MM, which can significantly affect diagnosis and prognosis (Grafanaki et al., 2023). Studies have classified MM into four subtypes based on driving mutations: BRAF-mutant, RAS-mutant, NF1-mutant, and wild-type BRAF/RAS/NF1, with common mutations also including KIT or GNAQ/GNA11 (Kiuru and Busam, 2017). Additionally, transcriptomic analyses have categorized MM into: undifferentiated (AXL-high, SOX10/NGFR/MITF-low), neural crest-like (SOX10-high, NGFR-high, MITF-low), transitory (SOX10-high, NGFR-medium, MITF-medium), and melanocytic (SOX10-high, NGFR-low, MITF-high) (Comandante-Lou et al., 2022). Histopathologically, MM is generally classified into superficial spreading, nodular, malignant lentigo, and acral lentiginous types, which may correspond to distinct pathogenic mechanisms, thus influencing treatment approaches. For instance, UV exposure may drive BRAF mutations, often resulting in superficial spreading MM (Armstrong and Cust, 2017), while trauma and inflammation can elevate cytokines and reactive oxygen species, significantly correlating with acral MM (Zhang et al., 2014). A comprehensive grasp of the molecular mechanisms driving MM has advanced the creation of targeted therapies. Research indicates that immune checkpoint inhibitors are effective in approximately one-third of patients (Sharma et al.,

2017). BRAF inhibitors (BRAFi), as well as combinations of BRAFi and MEK inhibitors (MEKi), can benefit up to 50% of BRAF-mutant patients with advanced MM (Flaherty et al., 2012). Furthermore, combined checkpoint inhibitors, such as anti-PD-1 and anti-CTLA-4 antibodies, can improve overall survival in advanced patients (Rogiers et al., 2019). Talimogene laherparepvec, as the first approved oncolytic virus therapy, has also shown survival benefits. However, over 80% of patients experience recurrence after BRAF/MEK inhibitor treatment, and the efficacy of targeted therapies in wild-type BRAF patients is limited (Johnpulle et al., 2016), with 60%–70% of patients not responding to checkpoint inhibitor therapy (Jerby-Arnon et al., 2018). Therefore, it is essential to further explore the molecular mechanisms involved in MM development and to identify key target genes to enhance treatment and prognostic evaluation.

The WNT signaling pathway comprises 19 glycoproteins, including  $\beta$ -catenin, Disheveled (DVL), Lrp6, and Axin (Bryja et al., 2017). This pathway is involved in regulating the cell cycle and embryonic development, and it plays significant roles in inflammation and cancer progression (Clevers, 2006). Recent studies suggest that the WNT pathway could serve as a biomarker and a potential therapeutic target in cancer (Miete et al., 2022). There are two main classes into which the WNT pathway is categorized: the canonical pathway and the non-canonical pathway (Akoumianakis et al., 2022; Liu et al., 2022; Zhao et al., 2022). The canonical WNT/ $\beta$ -catenin pathway is linked to the nuclear translocation of  $\beta$ -catenin and usually plays a role in the proliferation and maintenance of stem and progenitor cells (Tai et al., 2015). In contrast, the non-canonical WNT pathways may relate to  $\beta$ -catenin-independent mechanisms (Zimmerman et al., 2012) and participate in regulating planar cell polarity (PCP) signaling and WNT/ $\text{Ca}^{2+}$  signaling pathways (Anastas and Moon, 2013). The PCP signaling pathway modulates cytoskeletal remodeling, cell polarity regulation, and cell migration (Logan and Nusse, 2004; Semenov et al., 2007), whereas the WNT/ $\text{Ca}^{2+}$  signaling pathway influences cancer progression and intercellular communication (Liang et al., 2003; Vargas et al., 2019). Alterations in the WNT signaling pathway are observed in many cancers. Studies suggest that in breast cancer, the composition of WNT signaling proteins is modified, with alterations observed at the DNA level, in mRNA post-transcriptional modifications, and in protein post-translational modifications. Nevertheless, the activation of WNT signaling is mainly driven by epigenetic changes (Xu et al., 2020). In colorectal cancer (CRC), the WNT/ $\beta$ -catenin pathway is crucial for both the initiation and sustenance of the disease, with suppression of WNT pathway expression demonstrating therapeutic potential against CRC (Zhao et al., 2022). Additionally, the abnormal activation of WNT/ $\beta$ -catenin signaling may be associated with the development of prostate, breast, ovarian, and pancreatic cancers (Jung and Park, 2020). Many surface markers of cancer stem cells serve as targets for the WNT pathway, and when this pathway is dysregulated, it can result in



resistance to tumor treatment (Ring et al., 2014). These factors suggest that the WNT pathway significantly influences the occurrence, development, and prognosis of various tumors. Currently, multiple studies have elucidated the role of the WNT/ $\beta$ -catenin pathway in malignant melanoma (MM), but consensus has not been reached. Activated canonical WNT/ $\beta$ -catenin signaling has been associated with reduced melanoma proliferation, acting as a negative regulator of tumor growth in both patient-derived tissues and mouse models of melanoma (Kim et al., 2020). However, other studies have shown that WNT signaling is reactivated during the malignant transformation of melanoma (Sinnberg et al., 2018). Aberrant activation of the WNT/ $\beta$ -catenin pathway has been observed in nearly one-third of human melanoma cases (Vaid et al., 2016). Despite the conflicting findings regarding the WNT pathway in MM, its diverse roles in cancer underscore the necessity for further investigation into its specific functions in MM. Such research could provide valuable insights for developing novel therapeutic strategies.

In this study, we aimed to explore potential therapeutic targets of the WNT pathway in MM through bioinformatics analysis. Initially, we performed a Cox regression analysis on the WNT pathway gene set, identifying 19 genes. Subsequently, we conducted consistent clustering analysis on these 19 genes, resulting in the identification of two subtypes. We then constructed a model using these genes and selected 13 that were prognostically relevant. Using the model, we predicted risk scores for high-risk and low-risk groups and analyzed the expression levels of the 13 genes within both groups, leading to the identification of two epithelial-mesenchymal transition (EMT)-related genes, CSNK1E and RAC3. We conducted a further analysis of the relationship between these genes and immune cells, particularly noting the relationship between CSNK1E and immune checkpoints. Finally, we performed a pan-cancer analysis of the CSNK1E gene, investigating its expression across various cancers and its prognostic implications, as well as its co-expression with EMT-related genes. Our work offers new targets for MM research and provides robust support for both scientific and clinical studies. What's more, We conducted three phenotypic experiments following the knockdown of CSNK1E in human melanoma cell lines to enhance the credibility of our bioinformatics conclusions.

## 2 Materials and methods

### 2.1 Data acquisition and preprocessing

We downloaded the dataset GSE91061 from the Gene Expression Omnibus (GEO, <https://www.ncbi.nlm.nih.gov/geo/>) website. After integrating the data, we converted it into Transcripts Per Million (TPM) format and applied  $\log_2$  transformation to mitigate excessive data dispersion. GEO is an open-access database that does not require additional ethical approval. We adhered to relevant guidelines for data collection and utilization.

### 2.2 Gene screening and consistency clustering

We conducted a Cox regression analysis on 5,917 genes related to the WNT pathway in MM. Genes were deemed significant if they met the criteria of  $p < 0.05$  and a hazard ratio (HR) not equal to 1,

indicating their impact on survival in MM patients. A forest plot was generated using the “forestplot” package to visualize these results, allowing us to identify genes influencing prognosis based on their HR. For comparative analysis, we performed consistency clustering on the selected genes using the R package “ConsensusClusterPlus”. The optimal number of clusters (k) was established by identifying the value where the cumulative distribution function (CDF) curve levels off, signifying maximum stability without any significant increases. We further validated this k value using a Delta Area Plot, typically choosing the last inflection point as the optimal cluster number. Visualization of the results was accomplished with “ggplot2,” revealing a consistency heatmap that illustrated the “high cohesion, low coupling” characteristics of the clusters. Finally, we utilized the R package “survival” to conduct survival analyses on the identified clusters, employing the “ggsurvplot” function from the “survminer” package to visualize survival outcomes between different clusters.

### 2.3 Model construction and risk assessment

To further identify Wnt pathway genes associated with prognosis, we employed the Least Absolute Shrinkage and Selection Operator (LASSO) method to screen and construct a relevant prognostic model. The optimal model fit is established by identifying the minimum likelihood deviation on the y-axis of the cross-validation curve, which signifies the best  $\log(\lambda)$  value. Following this, we included the variables related to this optimal  $\log(\lambda)$  value in the equation. The risk score for each patient was calculated by summing the products of the coefficients and expression levels of the respective variables (genes). The GSE91061 cohort data was divided into high-risk and low-risk groups based on the median score for risk assessment. Utilizing the R package “ggrisk”, we demonstrate how patients' survival times and the expression levels of the model genes change as the risk score increases. Following that, survival analysis was performed on both risk groups, utilizing the “ggsurvplot” package to visualize the survival curves. Additionally, we assessed the prognostic prediction efficacy of the model for two risk groups using receiver operating characteristic curve (ROC), where an area under the curve (AUC) value greater than 0.6 indicates better performance. Finally, we visualized the correlation between the model genes and EMT-related physiological processes using the “ggplot2” package.

### 2.4 Survival analysis and immune-related analysis

Firstly, we conducted survival analyses on the model genes. The “ggsurvplot” function from the R package “survminer” was employed to visualize the survival curves. To explore the connection between gene expression levels and immune cell infiltration, we utilized “ggplot2,” creating lollipop plots that demonstrated the correlation between the two selected genes and immune cells. A significant and strong correlation between the two variables is considered when  $p < 0.05$  and the  $|R| > 0.2$ . A positive R value indicated a positive regulatory relationship between the gene

and immune cells, while a negative R value suggested a negative regulatory relationship.

Subsequently, we selected the four types of immune cells most strongly correlated with these two genes and visualized the relationships using scatter plots. The statistical significance was established at  $p < 0.05$ , with the magnitude of R reflecting the strength of correlation. Based on the outcomes of these correlation analyses, we further explored immune checkpoint genes related to CSNK1E using the “IOBR” package for correlation analysis of gene expression data. This yielded several immune checkpoint genes significantly correlated with CSNK1E expression, which were visualized as boxplots using the “ggpubr” package.

## 2.5 Pan-cancer analysis

We analyzed the expression levels of CSNK1E across 33 cancer types and compared them with normal control groups, utilizing the “ggpubr” package for visualization to elucidate the potential role of CSNK1E in cancer development. We then investigated the effect of the CSNK1E gene on overall survival (OS) in these cancers, treating results as statistically significant when  $p < 0.05$ . Prognostic relevance was assessed based on the  $\log_{10}$  (HR) values: a  $\log_{10}$  (HR)  $> 0$  indicated that abnormal CSNK1E expression may correlate with poorer survival rates, while  $\log_{10}$ (HR)  $< 0$  suggested a potential association with better survival rates. Further, we analyzed the co-expression of CSNK1E with nine genes related to EMT to investigate the relationship between CSNK1E and EMT, hypothesizing potential functions of CSNK1E that could accelerate the discovery and functional analysis of new genes. Finally, we conducted a dry analysis on 37 different cancer types, identifying statistical significance at  $p < 0.05$ . To assess the strength of the association with stem cells, the Pearson correlation coefficient was used, where higher coefficients reflect stronger correlations. This was visualized using “ggplot2” to examine the similarities between tumor cells and stem cells.

## 2.6 Tissue acquisition from patients

We selected melanoma and normal tissue samples from six patients diagnosed with melanoma at Southern Hospital. All selected patients received a definitive diagnosis of melanoma, with other diseases excluded, and none had undergone any treatment prior to sampling. Informed consent was secured from all patients to safeguard their privacy and rights. The ethics committee of Southern Hospital approved our experimental ethics documents.

## 2.7 Cell culture and transfection

For the wet lab validation of our results, we utilized human melanoma cell lines COLO 792, COLO 829, SK-MEL-3, Hs 939, T, and A-375, along with the normal human skin cell line TE353. sk, all sourced from the Chinese Academy of Sciences Cell Bank. COLO 792 and COLO 829 were cultured in Roswell Park Memorial Institute 1,640 (RPMI-1640, HyClone, United States), while SK-

MEL-3, Hs 939, T, A-375, and TE353.sk were cultured in Dulbecco's Modified Eagle Medium (DMEM, HyClone, United States). All media contained 10% fetal bovine serum (FBS, KeyGEN, China) and 1% penicillin-streptomycin mix (Procell, China), with cell culture flasks incubated at 37°C in 5% CO<sub>2</sub>. The medium was replaced every 36 h to maintain the cells in a good logarithmic growth phase.

We conducted transfection experiments for the cell lines COLO 792 and COLO 829. To inhibit the expression of the gene CSNK1E in the cell lines, we commissioned a biotech company to design and produce siRNA and shRNA (Sangon Biotech, China) for knocking down CSNK1E, using a negative control (NC) as a comparison. Trypsin (KeyGEN, China) was used to digest the cells, which were then thoroughly resuspended in the culture medium. Following this, the cells were evenly distributed into a 6-well plate at a density of  $3 \times 10^4$  cells per well, with each well adjusted to a total volume of 2 mL using the medium. After observing cell adhesion under the microscope, siRNA was mixed with the transfection reagent Lipofectamine™ 3,000 (Thermo, United States) in a specified ratio and allowed to sit at room temperature for 10 min as per the instructions. The mixture was then added to the wells using a micropipette. During transfection, the medium was replaced every 5 h, and experiments were carried out 48 h after the transfection was completed. The sequences of the shRNAs used in our study are as follows (5'-3'):

sh-Negative control: UUCUCCGAACGUGUCACGU

sh- CSNK1E-1: CUUAGUGUCUUAUGUAU

sh- CSNK1E-2: AGCGGGUCCUUCGGAGAU.

## 2.8 Western blot assay

First, we extracted protein from both tissue and cell samples. For patient and normal control tissues, we added protein lysis buffer (Beyotime, China, RIPA lysis buffer: protease inhibitor = 100:1) to the pre-weighed tissues, minced them on ice, and subjected them to ultrasonic disruption. For the cell lines, the cells in the 6-well plate were digested and transferred to centrifuge tubes, centrifuged at 800 rpm for 5 min, and the supernatant was discarded. The protein lysis buffer was added to the cell pellet, and the mixture was thoroughly mixed using a pipette. Both the disrupted tissue and cell mixtures were lysed on ice for 30 min, with gentle mixing every 10 min. Subsequently, they were centrifuged at 12,000 rpm at 4°C for 15 min, and the supernatant was retained. Next, we determined the protein concentration using the BCA method, performed in a 96-well plate with three replicates for each sample group. Each well received 2 µL of the protein sample, 18 µL of PBS, varying concentrations of protein standard solutions, and 200 µL of BCA working solution (Beyotime, China), followed by incubation at 37°C for 30 min. Absorbance at 562 nm was then measured using a microplate reader to determine the concentrations of the protein samples and to estimate the loading amounts for electrophoresis. Each lane was prepared by mixing the sample with loading buffer (Beyotime, China) and PBS in a specified ratio, heated in a 95°C water bath for 5 min to denature the proteins, and then cooled on ice. The sample proteins were subjected to SDS-PAGE electrophoresis at 150V, which was stopped after approximately 1 h. The membrane transfer was subsequently carried out by

assembling the apparatus and adding the transfer buffer, followed by setting a current of 200 mA to transfer the proteins onto a PVDF membrane. The PVDF membrane was placed in an incubation box, where blocking solution was added and the membrane was incubated on a shaker at room temperature for 15 min. Dilute the primary antibody (Polyclonal antibody, Proteintech, United States) and add it to the incubation box, then shake overnight at 4°C. Subsequently, introduce the diluted secondary antibody (HRP-conjugated Goat Anti-Rabbit IgG (H + L), Cat No: SA00001-2, Proteintech, United States) and incubate at room temperature for 1.5 h. Prior to the addition of the blocking solution, primary antibody, and secondary antibody, as well as after the incubation, wash the PVDF membrane three times with TBST (KeyGEN, China), allowing 5 min between each wash. Finally, apply chemiluminescent substrate to the PVDF membrane, expose it using a luminescence imaging system, and quantify the protein band intensity using ImageJ software.

## 2.9 Colony formation assay

After 48 h of transfection, we performed a colony formation assay on the cell lines COLO 792 and COLO 829. The cells from the original six-well plate were digested with trypsin and seeded into a new six-well plate, with 700 cells per well. The new six-well plate was placed in a 37°C incubator with 5% CO<sub>2</sub> to continue cell culture, with media changes and cell observations every 72 h. Cultivation was stopped and images were taken when it was observed under a microscope that the majority of individual clones contained more than 50 cells. After washing with PBS, 1 mL of paraformaldehyde (Solarbio, China) was added to each well to fix the cells for 30 min, followed by the addition of 1 mL of crystal violet staining solution (Solarbio, China) to each well for cell staining. After 40 min, the cells were rinsed multiple times with PBS and then left to dry. Finally, photographs were taken of the entire six-well plate and each individual well, and the cells were counted.

## 2.10 Wound healing assay

We conducted a scratch assay on the COLO 792 and COLO 829 cell lines 48 h post-transfection. Cells were placed in a 24-well plate, with the culture medium being changed every 6 h. A 200 µL pipette tip was used to gently and uniformly create a linear scratch in each well, assisted by a ruler, followed by PBS washing to remove floating cells. Images of the wells were captured at this point (designated as time zero) to record the wound area. A basic medium without FBS was then added, and the plate was incubated at 37°C. After an additional 48 h, we captured images again to assess wound healing and document the wound area at the 48-h mark. Furthermore, for the COLO 792 cell line, we also investigated the effects of varying concentrations of TGF-β1 (0 ng/mL, 10 ng/mL, and 20 ng/mL) on cell migration capabilities, as well as the impact of knocking down CSNK1E on high-concentration TGF-β1 (20 ng/mL) induced cell migration.

## 2.11 Transwell assay

To assess the invasion and migration capabilities of the cells before and after CSNK1E knockdown, we conducted a transwell assay on the COLO 792 and COLO 829 cell lines, 48 h following transfection. The cells were digested with trypsin and resuspended in serum-free medium. Chambers (Corning, United States) were placed in each well of a 24-well plate, and the cells were evenly seeded into the chambers at a density of  $4 \times 10^4$  cells per well. Each chamber was filled with a total volume of 200 µL of serum-free medium, while 600 µL of FBS-rich medium was added outside the chambers. The 24-well plate was then incubated at 37°C for 24 h. Following this, the media inside and outside the chambers were discarded, and the chambers were washed with PBS. After adding paraformaldehyde to the wells, the chambers were fixed at room temperature for 20 min. Crystal violet staining was performed in the dark for 20 min, followed by PBS washing, and any remaining cells inside the chambers were scraped off using moist cotton swabs. High-power fields (200× magnification) of the chambers and wells were captured under a microscope, and cell counts were facilitated using ImageJ software. We evaluated the cells' migration and invasion capabilities in succession through the transwell assay. In preparation for the invasion assay, the chambers were pre-coated with Matrigel (Corning, United States) before seeding the cells; however, this step was omitted for the migration assay. Additionally, for the COLO 792 cell line, we investigated the effects of different concentrations (0 ng/mL, 10 ng/mL, and 20 ng/mL) of TGF-β1 on cell invasion and migration, as well as the impact of high-concentration TGF-β1 (20 ng/mL) following CSNK1E knockdown.

## 2.12 Immunofluorescence assay

To examine the alterations in protein levels of CSNK1E, Vimentin, and ZO1 after CSNK1E knockdown, we conducted an immunofluorescence assay on the COLO 792 cell line. After 48 h of transfection, the cells were digested with trypsin and seeded into a 12-well plate, replenishing the well volume with culture medium to allow for adhesion. Following a wash with PBS, the cells were fixed with formaldehyde for 30 min and then washed three times with PBS. Subsequently, 0.2% Triton X-100 (Gibco, United States) was added to permeabilize the cell membrane at room temperature for 5 min. Afterward, a blocking solution (Gibco, United States) was added, which was removed after 60 min using a pipette. The diluted primary antibody (Proteintech, United States) was then introduced to the wells, and the 12-well plate was incubated overnight at 4°C on a shaker. After washing with PBS to remove unbound primary antibody, the diluted secondary antibody (CoraLite488-conjugated Goat Anti-Rabbit IgG (H + L), Cat No: SA00013-2, Proteintech, United States) was added and incubated at room temperature for 40 min, with unbound secondary antibody also washed away with PBS. Finally, DAPI fluorescent dye (SINOPHARM, China) was applied to the wells and incubated in the dark for 5 min to label the cell nuclei. The results were examined, and images were taken with a fluorescence microscope.

## 2.13 Statistical analysis

All statistical analyses were conducted using R software (version 4.1.3). Unless otherwise specified, our figures were generated using the “ggplot2” package. A  $p$ -value less than 0.05 was considered statistically significant (\* $p < 0.05$ ; \*\* $p < 0.01$ ; \*\*\* $p < 0.001$ ; \*\*\*\* $p < 0.0001$ ).

## 3 Result

### 3.1 Gene screening and consistency clustering

We initially conducted a Cox analysis on 5,917 genes involved in the WNT pathway, identifying 19 genes including PRKCG and WNT1. Among these, 10 genes, such as PRKCG and WNT1, exhibited HR less than 1, indicating they may serve as protective factors against MM, suggesting their expression is associated with a lower risk of disease or better prognosis. Conversely, 9 genes, including RAC3 and VANGL1, had HR values greater than 1, categorizing them as risk factors for MM, where their expression could indicate a higher risk of disease or poorer prognosis ( $p < 0.05$ , HR  $\neq 1$ , Figure 1A). Subsequently, we performed consistency clustering on the selected 19 genes. The CDF curve plateaued when  $k$  reached the optimal number of clusters, verified by the Delta area, resulting in  $k = 2$  (Figure 1B). Thus, we categorized all samples into two subtypes: C1 and C2, which exhibited characteristics of “high cohesion, low coupling” in the consistency heatmap (Figures 1C, D). We then conducted survival analysis on subtypes C1 and C2. The OS prediction for C1 was significantly higher than that for C2 ( $p < 0.05$ , Figure 1E).

### 3.2 Model construction and risk assessment

We constructed a LASSO regression model using 19 selected genes. The cross-validation curve indicated that the optimal fitting effect was achieved when the variable corresponding to  $\log(\lambda)$  was 13, as evidenced by the lowest point on the  $y$ -axis (Figure 2A). Basing on the median risk score, we stratified the GSE91061 dataset into high-risk and low-risk groups. Over time, both groups exhibited a significant decline in survival counts and an increase in mortality; however, the survival count in the high-risk group was markedly lower than that in the low-risk group. In the low-risk group, there's an increase in the expression levels of SFRP1, FZD6, RAC2, PLCB2, PRKACB, CAMK2B, WNT1, and PRKCG, while in the high-risk group, PPP2R1A, CSNK1E, WNT11, VANGL1, and RAC3 showed higher expression levels (Figure 2B). Subsequently, we conducted survival analysis for both risk groups. As time progressed, the OS predictions for both groups declined, while cumulative risk increased. It is important to highlight that the overall survival predictions for the high-risk group were markedly lower than those for the low-risk group, which also showed a significantly lower cumulative risk. In order to evaluate the model's predictive performance, we employed ROC curves, which revealed AUC values exceeding 0.6 for 1-year, 3-year, and 5-year predictions, indicating satisfactory predictive performance (Figure 2C). Furthermore, we

analyzed the correlation between the model genes and physiological processes associated with EMT. Our findings demonstrated a negative correlation between the physiological process of positive regulation of epithelial cell migration and the genes CSNK1E and RAC3, while a positive correlation was observed between the epithelial-to-mesenchymal transition process and CSNK1E and RAC3 ( $p < 0.01$ , Figure 2D).

### 3.3 Survival analysis and immune correlation analysis

We conducted survival analyses on the 13 genes identified in our model, assessing the variations in survival rates associated with high versus low expression levels. Among these, the high expression group of CAMK2B, FZD6, PLCB2, PRKACB, RAC2, SFRP1, and WNT1 exhibited significantly better survival rates than the low expression group. In contrast, the low expression group of PLAAT1, RAC3, PPP2R1A, CSNK1E, VANGL1, and WNT11 was associated with significantly better survival rates ( $p < 0.05$ , Figure 3). Additionally, we conducted an analysis of the correlation between CSNK1E and RAC3 across 24 different immune cell types. CSNK1E demonstrated negative regulatory relationships with 21 immune cells, notably the strongest with T cells, while RAC3 showed similar negative correlations with 18 immune cells, particularly with Macrophages and activated dendritic cells ( $p < 0.05$ ,  $R < 0$ , Figures 4A, B). We chose the four immune cell types that exhibited the strongest correlations with these genes for scatter plot analysis. This analysis revealed a negative correlation between CSNK1E expression and T cells, cytotoxic cells, activated dendritic cells, and dendritic cells ( $p < 0.001$ ,  $R < -0.3$ , Figure 4C), as well as a similar relationship for RAC3 with Macrophages, activated dendritic cells, TFH, and T cells ( $p < 0.001$ ,  $R < -0.3$ , Figure 4D). Notably, both genes exhibit a significant negative correlation with T cells. Subsequently, the relationship between CSNK1E expression and ten immune checkpoint genes was analyzed. Fluctuations in CSNK1E expression correlated with elevated levels of six immune checkpoints: CD274, CTLA4, HAVCR2, LAG3, PDCD1, and TIGIT, particularly pronounced in CSNK1E low expression group. In contrast, IGSF8, ITIPRIPL1, and SIGLEC15 showed no significant differences between the high and low expression groups of CSNK1E; however, the expression levels in both groups were higher than those in the normal group. Elevated immune checkpoint expression suggests a stronger suppression of immune function, potentially linked to poorer prognoses in MM ( $p < 0.05$ , Figure 4E).

### 3.4 Pan-cancer analysis

We conducted a pan-cancer analysis of CSNK1E across 33 different cancer types, comparing its expression levels in tumor versus normal groups. Notably, in 15 cancers, including bladder cancer (BLCA), cholangiocarcinoma (CHOL), colorectal cancer (COAD), esophageal cancer (ESCA), head and neck squamous cell carcinoma (HNSC), kidney renal clear cell carcinoma (KIRC), kidney renal papillary cell carcinoma (KIRP), liver hepatocellular carcinoma (LIHC), lung adenocarcinoma (LUAD), lung squamous cell carcinoma (LUSC), pan-cancer



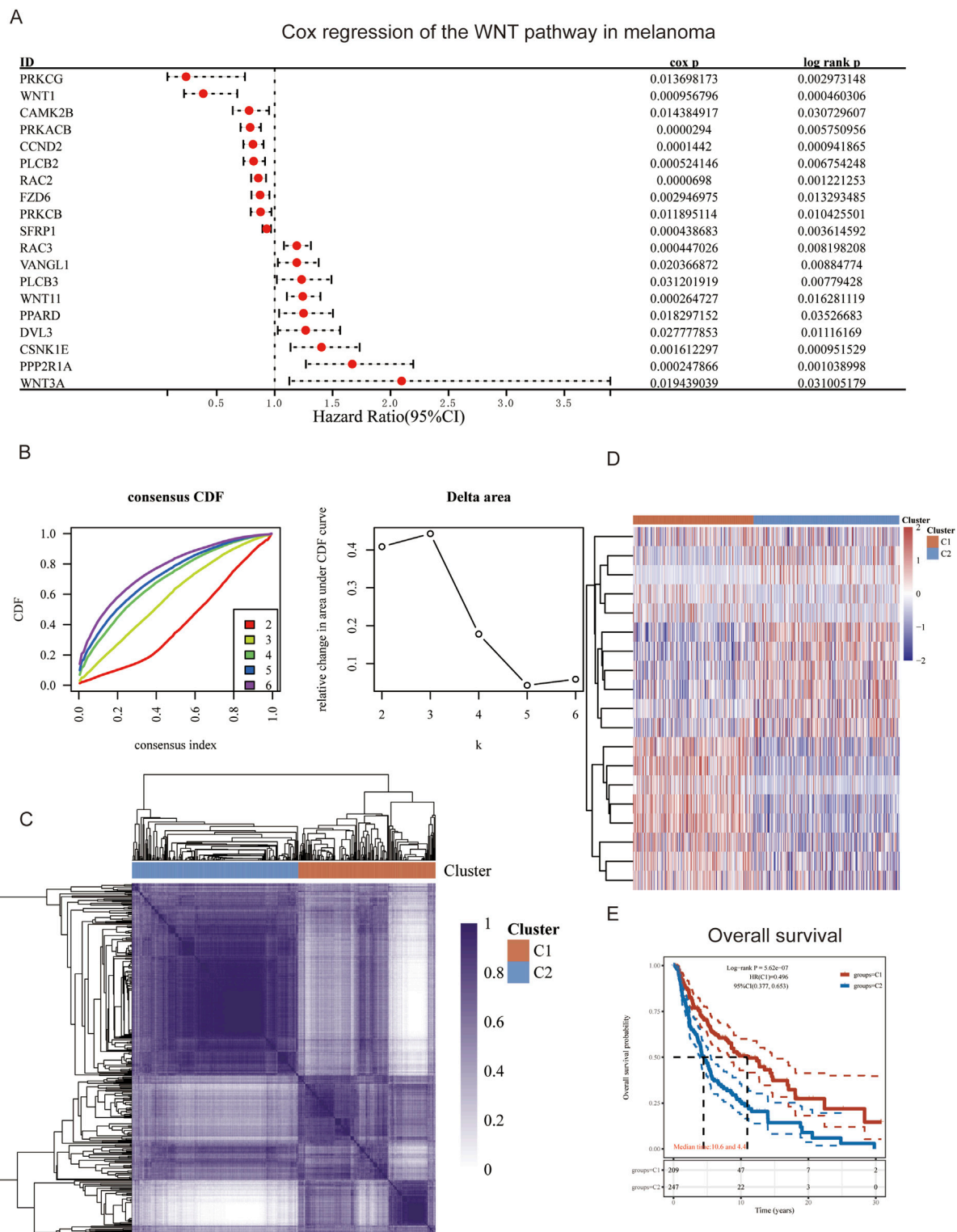


**FIGURE 1** Gene Screening and Consistency Clustering. **(A)** Forest plot of Cox regression analysis for WNT pathway gene set; **(B)** Consistency cumulative distribution function and Delta area plot; **(C)** Consistency heatmap with two clusters; **(D)** Heatmap of differentially expressed genes; **(E)** Survival curves for patient groups C1 and C2.

(PCPG), prostate cancer (PRAD), rectum adenocarcinoma (READ), stomach adenocarcinoma (STAD), and thyroid carcinoma (THCA), the tumor group exhibited significantly higher expression levels compared to the normal group ( $p < 0.05$ , Figure 5A). Subsequently, we performed a prognostic analysis across these 33 cancers, identifying CSNK1E as a risk factor in 12 cancer types, including

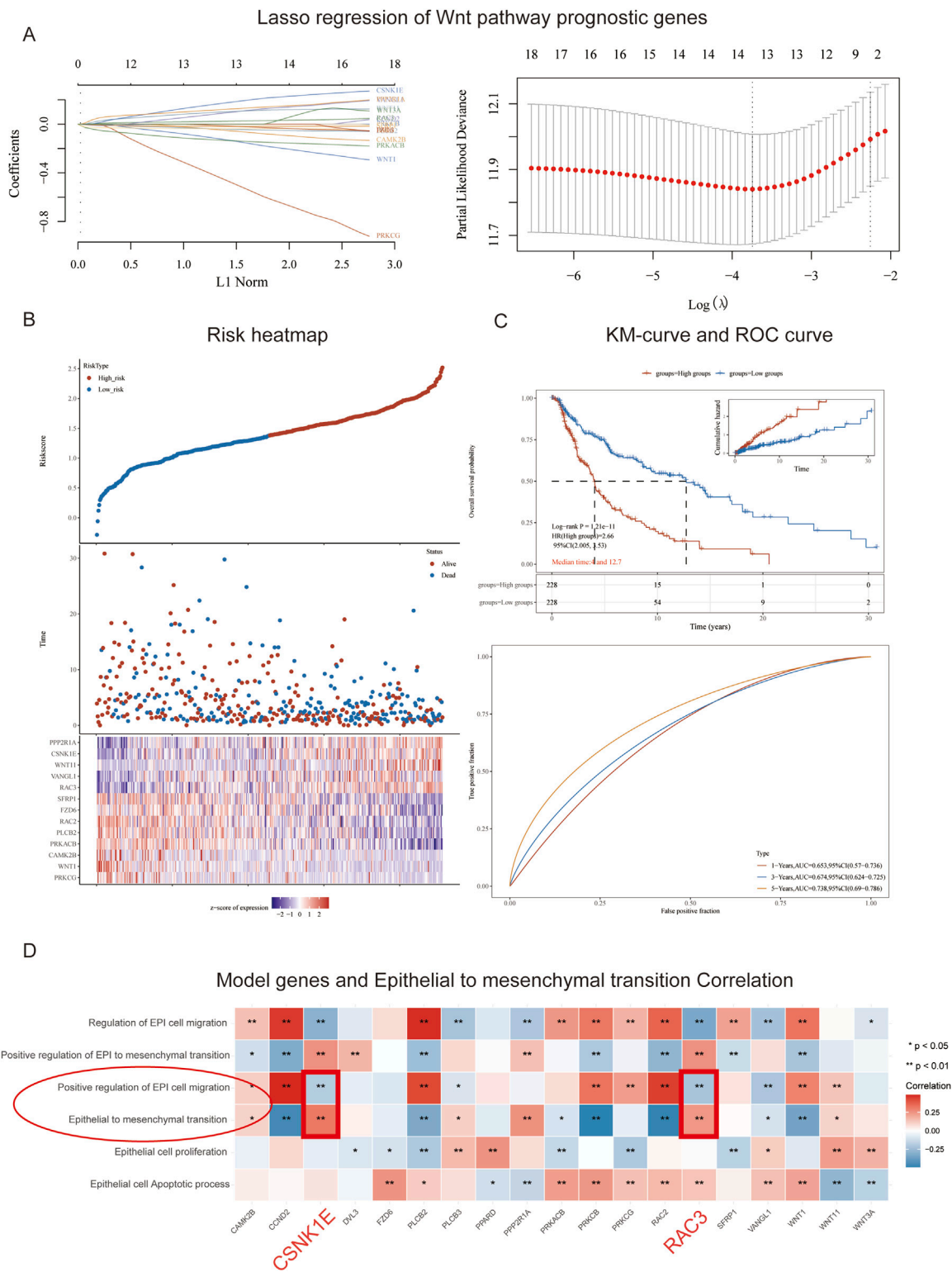
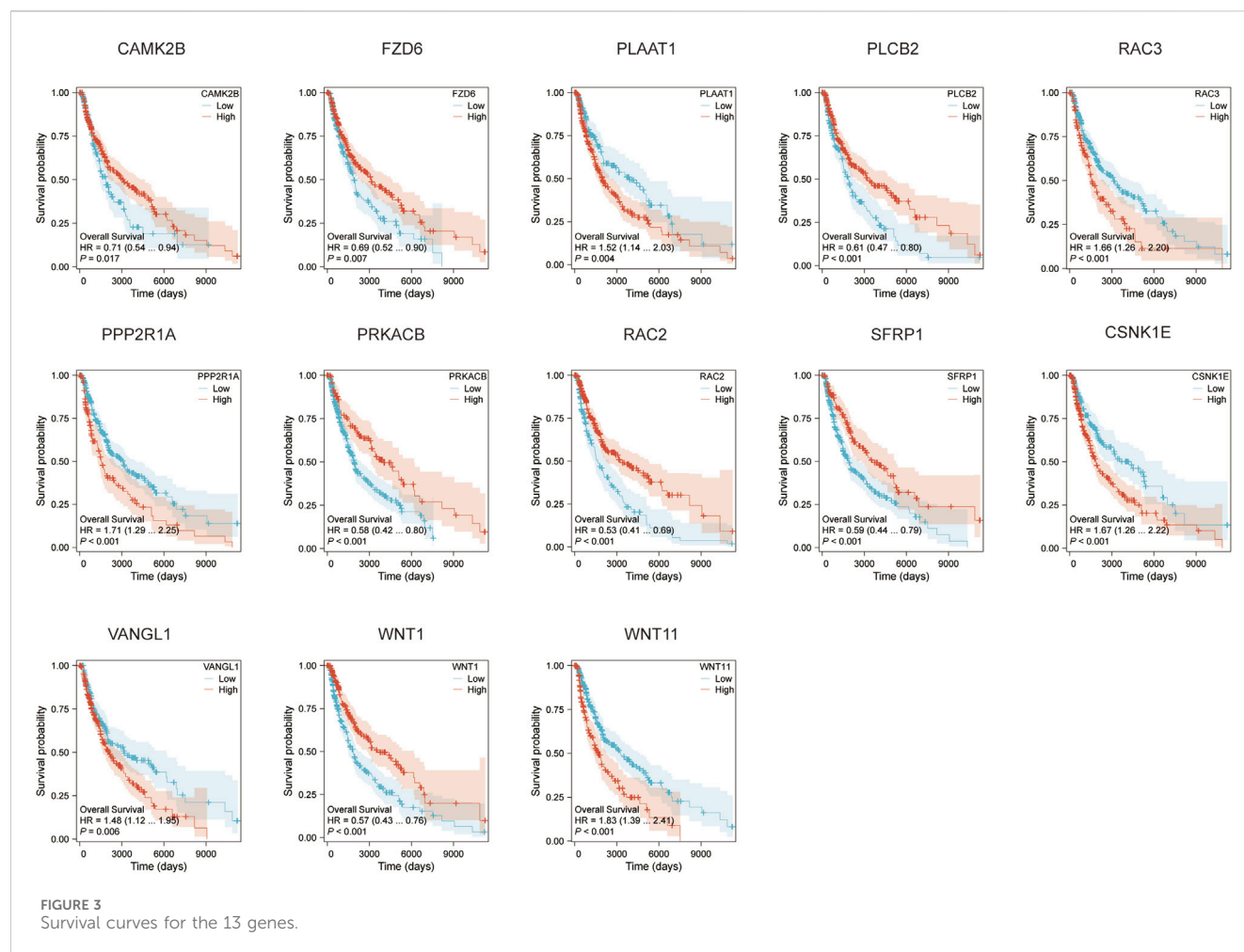


**FIGURE 2** Model Construction and Risk Assessment. **(A)** Path plot of regression coefficients and cross-validation curve; **(B)** Triplet plot of risk scores for high and low-risk groups in the GSE91061 cohort; **(C)** Survival curves and ROC curves for high and low-risk groups in the GSE91061 cohort; **(D)** Heatmap showing the correlation between 13 genes and EMT.

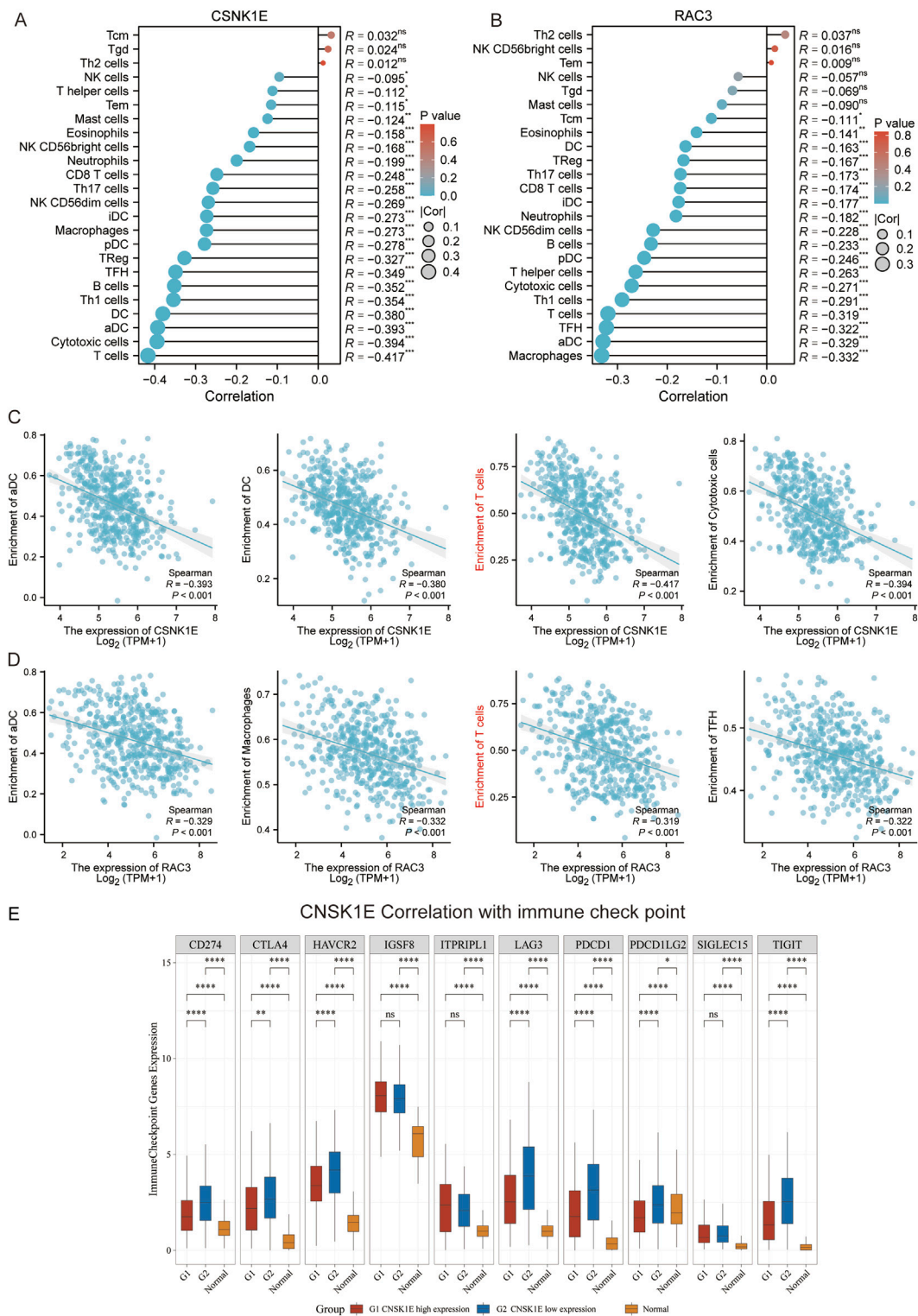


adrenocortical carcinoma (ACC), BLCA, HNSC, KIRC, lower grade glioma (LGG), LIHC, LUAD, mesothelioma (MESO), ovarian cancer (OV), sarcoma (SARC), skin cutaneous melanoma (SKCM), and uveal melanoma (UVM), with a correlation to poorer prognosis ( $p < 0.05$ ,  $\log_{10}(\text{HR}) > 0$ , Figure 5B). We further analyzed the co-expression of CSNK1E with genes related to EMT. In the low expression group, the levels of nine EMT-regulating genes—TRIM28, GSK3B, NOTCH1, SMAD4, CUL7, SNAI1, TGFBR1, CTNNB1, and HIF1A—were significantly diminished compared to those in the high expression group. This finding suggests a potential association between increased CSNK1E expression and enhanced EMT activity (Figure 5C). Finally, we assessed gene stemness across 37 cancers, observing a significant negative correlation in brain cancer (GBMLGG), acute myeloid leukemia (AML), and LGG, while a noteworthy positive correlation was found in both testicular cancer (TGCT) and thymoma ( $p < 0.05$ , Figure 5D).

### 3.5 CSNK1E plays a pro-cancer role in melanoma

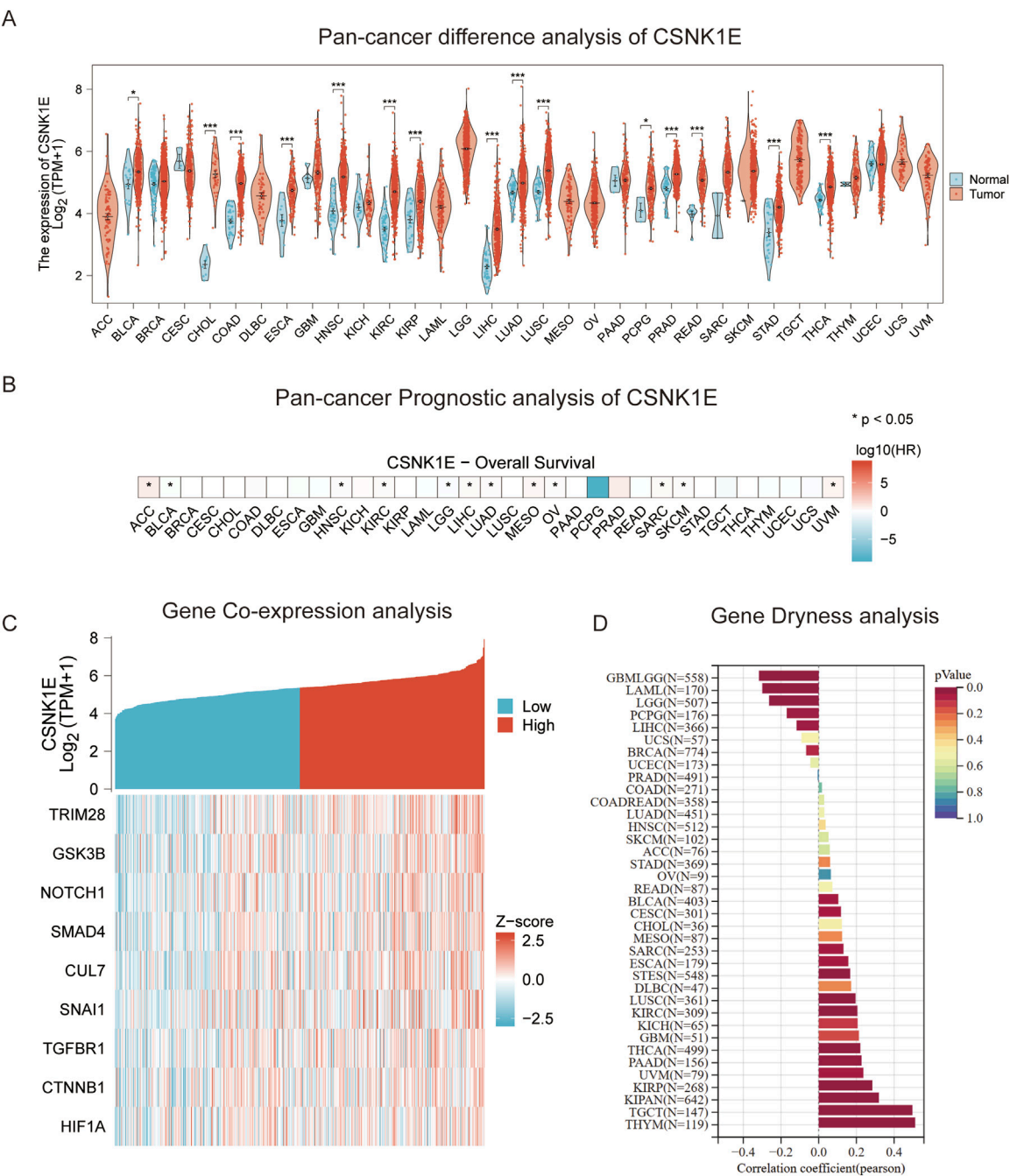
According to the results from Western blot assays, CSNK1E is expressed in both normal and tumor tissues, with significantly

higher levels in tumor samples. In six cell lines—COLO 792, COLO 829, TE353, SK-MEL-3, Hs 939, T, and A-375—CSNK1E expression was notably greater in cancer cell lines in comparison to normal skin cells. The bar graph depicting the relative expression levels of proteins indicates that the silencing of CSNK1E resulted in a marked decrease in protein levels, dropping below 50% of the NC group, indicating effective transfection ( $p < 0.001$ , Figure 6A). Images and corresponding bar graphs from the colony formation assays for COLO 792 and COLO 829 reveal that silencing CSNK1E significantly decreased the number of colonies formed, indicating reduced cell proliferation ( $p < 0.001$ , Figure 6B). Results from wound healing assays demonstrated a significant decrease in wound healing percentage after CSNK1E silencing, reflecting diminished cell migration capabilities ( $p < 0.001$ , Figure 6C). Transwell assays demonstrated that the number of invasive and migratory cells in the CSNK1E knockdown groups was significantly reduced compared to the NC group. Further indicating reduced invasive and migratory abilities ( $p < 0.01$ , Figure 7A). After silencing CSNK1E, there was a notable rise in the protein levels of E-Cadherin and ZO1, while levels of N-Cadherin, Vimentin, and MMP9 significantly decreased ( $p < 0.001$ , Figure 7B). Immunofluorescence results indicated that following shRNA-mediated CSNK1E knockdown, intracellular levels of CSNK1E and Vimentin decreased, while ZO1 levels



**FIGURE 4** Immune-Related Analysis. **(A)** Lollipop plot depicting the correlation between CSNK1E and 24 immune cell types; **(B)** Lollipop plot depicting the correlation between RAC3 and 24 immune cell types; **(C)** Scatter plot illustrating the correlation between CSNK1E and four immune cell types; **(D)** Scatter plot illustrating the correlation between RAC3 and four immune cell types; **(E)** Boxplot of expression differences for 10 immune checkpoint genes associated with CSNK1E across high, low, and normal expression groups.

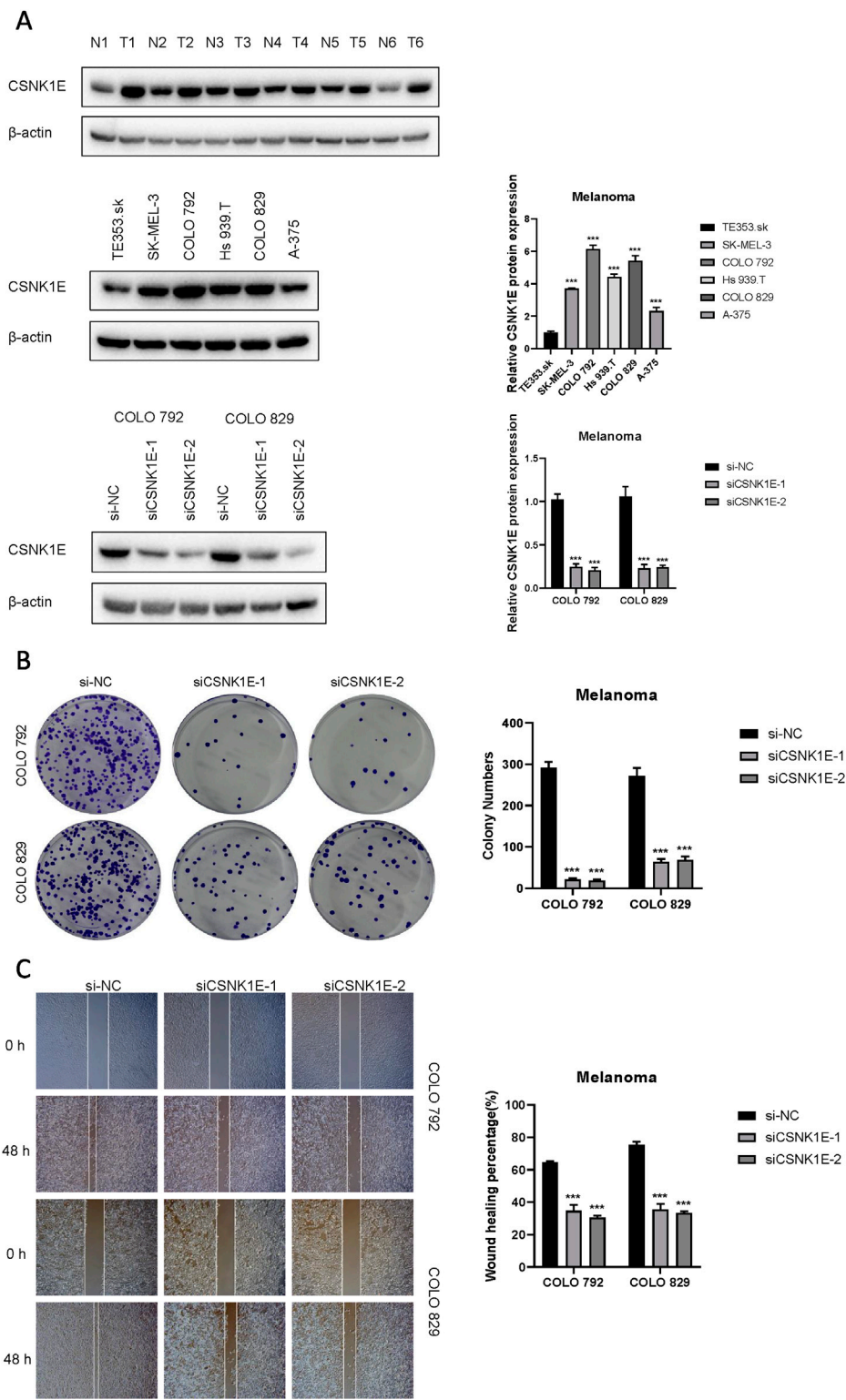




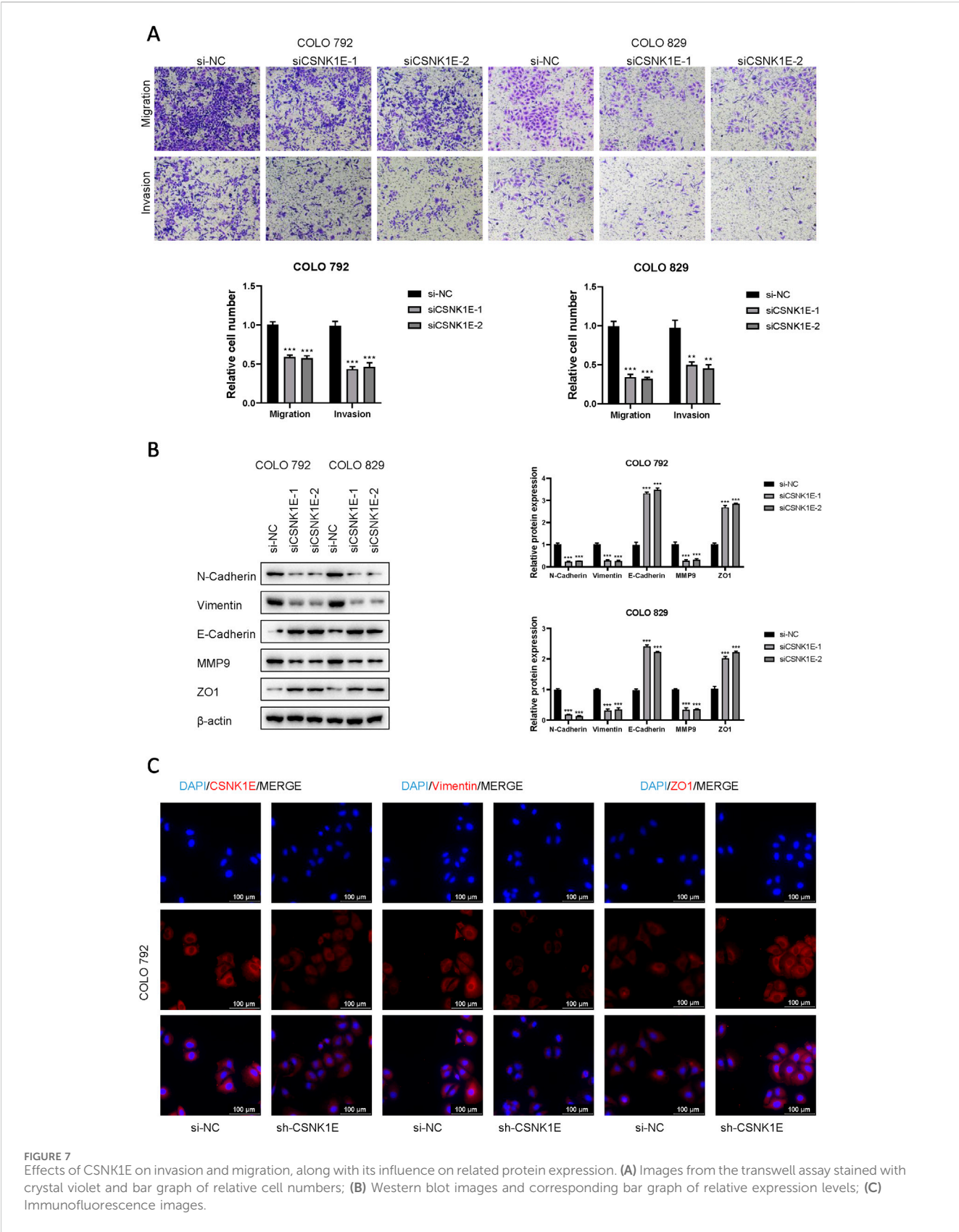
**FIGURE 5** Pan-Cancer Analysis. (A) Violin plot of differential expression of CSNK1E across 33 cancer types; (B) Heatmap of survival analysis for CSNK1E in 33 cancer types; (C) Co-expression heatmap of CSNK1E with EMT-related genes across high and low expression groups; (D) Graphical representation of stemness analysis across 37 cancer types.

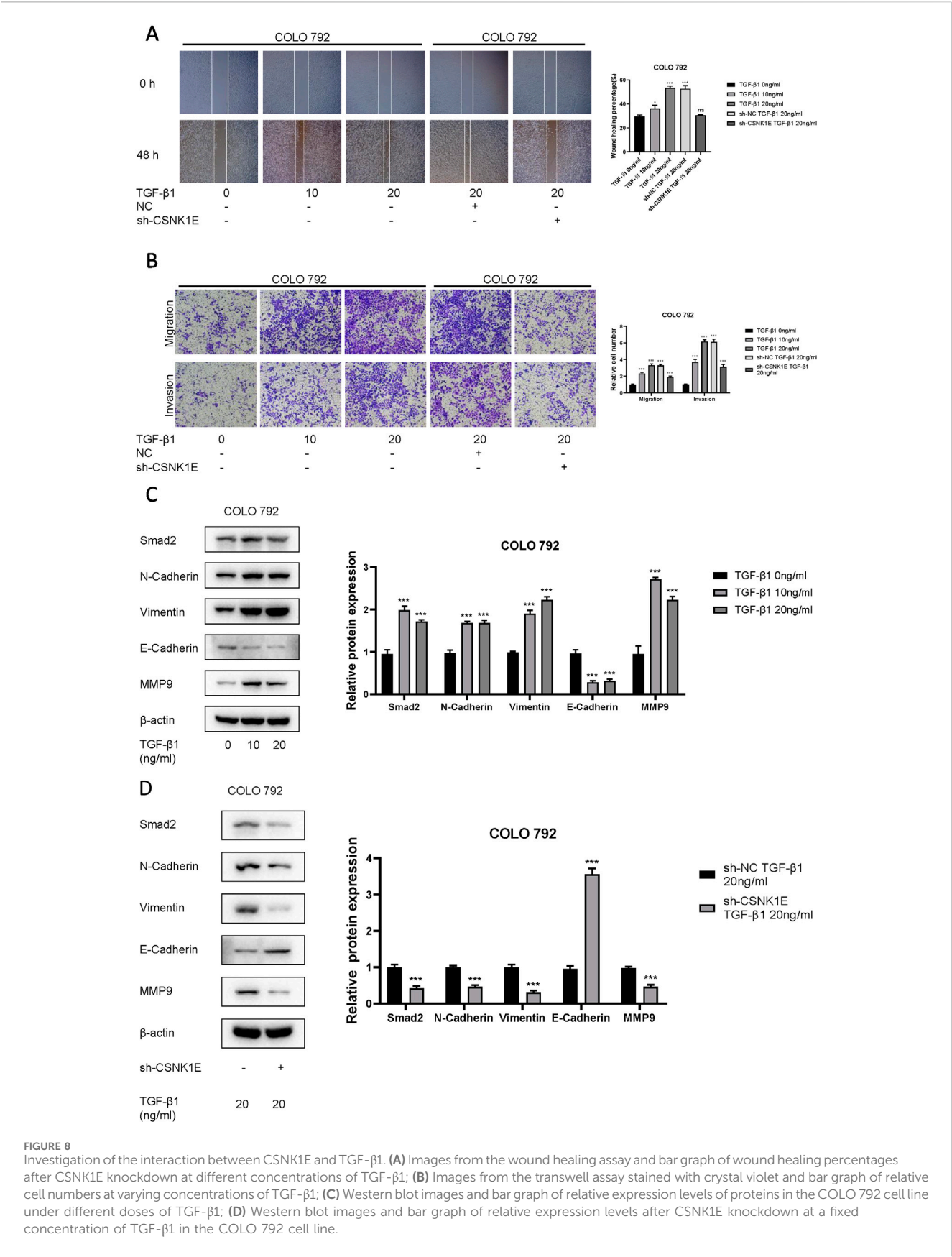
increased (Figure 7C). Additionally, TGF- $\beta$ 1 was found to enhance cell migration, with varying effects at different doses. Specifically, as TGF- $\beta$ 1 concentration increased from 0 ng/mL to 10 ng/mL and 20 ng/mL, wound healing percentage significantly improved ( $p < 0.05$ ). However, following CSNK1E knockdown, the migratory enhancement effect of TGF- $\beta$ 1 was diminished, showing no statistical difference in wound healing percentage at 20 ng/mL

TGF- $\beta$ 1 compared to controls. This suggests that silencing CSNK1E can reverse the TGF- $\beta$ 1-induced migration in cancer cells, implying a potential synergistic role of CSNK1E in TGF- $\beta$ 1-related pathways (Figure 8A). Transwell experiments yielded similar results: increased TGF- $\beta$ 1 concentrations significantly enhanced cell invasion and migration, but the effects were attenuated following CSNK1E silencing, although the number of



**FIGURE 6** Expression of CSNK1E in various tissues and cell lines, and its impact on proliferation and migration. **(A)** Western blot images and corresponding bar graphs of relative protein expression levels of CSNK1E in different tissues and cell lines, as well as following knockdown; **(B)** Images from the colony formation assay along with the corresponding bar graph of colony numbers; **(C)** Images from the wound healing assay and bar graph showing the percentage of wound healing.







invasive and migratory cells at 20 ng/mL TGF- $\beta$ 1 remained higher than controls, indicating partial reversal of TGF- $\beta$ 1's effects by CSNK1E knockdown ( $p < 0.001$ , Figure 8B). Finally, protein band and expression level bar graphs indicated that following TGF- $\beta$ 1 addition, E-Cadherin levels significantly decreased, while Smad2, N-Cadherin, Vimentin, and MMP9 levels increased. Notably, when TGF- $\beta$ 1 concentration increased from 10 ng/mL to 20 ng/mL, the levels of Smad2 and MMP9 decreased. Post-CSNK1E knockdown, only E-Cadherin levels significantly increased compared to controls, while the other four proteins showed significant reductions, further supporting the notion of CSNK1E's synergistic role in TGF- $\beta$ 1-related pathways at the molecular level ( $p < 0.001$ , Figure 8C).

## 4 Discussion

Melanoma (MM) is the most lethal type of skin cancer and presents significant treatment challenges among solid tumors (Wolchok and Saenger, 2007). Its onset is linked to the malignant transformation of melanocytes (Lo and Fisher, 2014), and it exhibits a high level of immunogenicity, making immunotherapy a significant treatment modality. However, early immunotherapy approaches have shown substantial cytotoxicity (Ozbay Kurt et al., 2023). Data indicate that 40%–80% of patients may possess innate resistance to immune checkpoint inhibitors (ICIs), and the therapy combining CTLA-4 and PD-1 has been associated with severe adverse effects (Ballotti et al., 2020). Consequently, investigating the mechanisms underlying resistance in MM, identifying key biomarkers and exploring pivotal target genes are of great importance, as these factors are essential for diagnosis, treatment, and prognosis. There's a close association between the WNT signaling pathway's abnormal activation and the development and progression of several cancers (Zhang et al., 2018), including its role in promoting tumor dissemination and the development of resistance. Several proteins within the WNT pathway have been identified as potential therapeutic targets and biomarkers. However, research on the WNT pathway in MM remains limited. This study investigates the potential roles of WNT-related genes in MM and develops a prognostic model, thereby offering constructive insights and directions for discovering new therapeutic targets and enhancing prognosis in MM.

We conducted a Cox regression analysis on the gene set associated with the WNT pathway, identifying 19 genes linked to the occurrence and prognosis of malignant melanoma. Subsequently, these 19 genes underwent consistent clustering, resulting in two distinct subtypes. The consistency heatmap demonstrated characteristics of "high cohesion and low coupling". The survival differences between clusters C1 and C2 were statistically significant, indicating the reliability of the classification and establishing that  $k = 2$  is the optimal number of clusters. Next, we developed a LASSO regression model incorporating 13 of the identified genes, including PPR2R1A, CSNK1E, and WNT11. Using the risk scores generated by this model, we classified the samples into high-risk and low-risk groups. The high-risk group exhibited poorer survival outcomes, characterized by elevated expression of five genes, including

CSNK1E and RAC3, suggesting their potential influence on prognosis. There was a statistically significant difference in survival between the high- and low-risk groups, with the low-risk group exhibiting a substantially higher survival rate. The ROC curve analysis revealed that the model demonstrated strong predictive performance, indicating that the results might be widely applicable. Additionally, we examined the relationship between the 13 genes and the EMT process. Notably, CSNK1E and RAC3 demonstrated a significant correlation with EMT, indicating their potential involvement in mediating the metastatic process of MM cells, as EMT facilitates tumor cell invasion through the basement membrane into the bloodstream. Survival analysis of the 13 genes revealed that high expression levels of CAMK2B, FZD6, PLCB2, PRKACB, RAC2, SFRP1, and WNT1 were associated with improved survival rates, suggesting that the activation of these genes may positively influence MM prognosis. Conversely, the activation of PLAAT1, RAC3, PPP2R1A, CSNK1E, VANGL1, and WNT11 correlated with poorer prognostic outcomes.

We assessed the relationship between CSNK1E and RAC3 across 24 immune cell types, discovering that CSNK1E had the strongest correlation with T cells, whereas RAC3 was most closely linked to macrophages and also showed a notable association with T cells. Considering the crucial impact of immune checkpoint expression on T cell functionality, we further explored the connection between CSNK1E and ten immune checkpoints.

We then performed a pan-cancer analysis of CSNK1E across 33 different cancer types. Remarkably, in 15 of these cancers, including BLCA, CSNK1E expression levels in tumor samples were significantly elevated compared to normal tissues. This finding implies that CSNK1E might have a comparable role in various cancers, leading us to propose that it could act as a potential biomarker for early diagnosis and treatment across multiple cancer types. Additionally, we investigated the relationship between CSNK1E expression and prognosis across the 33 cancer types, identifying it as a risk factor in 12 of them, including ACC and BLCA. Following this, we analyzed the co-expression patterns of CSNK1E with genes linked to EMT. The high-expression group of CSNK1E exhibited more active expression of EMT-related genes, leading us to speculate that CSNK1E may influence the invasiveness and metastatic capabilities of MM cells through its regulatory role in EMT. This could potentially provide new therapeutic targets for MM treatment and prognosis assessment. Finally, we explored the relationship between stem cells and 37 cancer types. Our findings may offer a novel target for MM therapy and provide theoretical support for advancements in biotechnology.

Using the LASSO machine learning algorithm, we identified 19 genes associated with the WNT signaling pathway and constructed a regression model comprising 13 genes, including PRR2R1A, CSNK1E, WNT11, VANGL1, and RAC3. The CSNK1E gene encodes casein kinase 1 epsilon (CK1 $\epsilon$ ), which primarily regulates circadian rhythms by phosphorylating clock gene products (Knippschild et al., 2005). Additionally, CK1 $\epsilon$  influences cell differentiation and proliferation through protein phosphorylation (Meng et al., 2010). Moreover, CK1 $\epsilon$  is capable of phosphorylating other critical proteins within the WNT signaling pathway, so that it can regulate cell division and tumor growth in pancreatic cancer, salivary gland cancer, and colorectal adenocarcinoma (Brockschmidt

et al., 2008; Frierson et al., 2002). For example, CK1 $\epsilon$  is involved in phosphorylating low-density lipoprotein receptor-related proteins 5 and 6 (LRP5/6) as well as Dvl (Price, 2006), which subsequently promotes the recognition of the Axin and glycogen synthase kinase 3 beta (GSK-3 $\beta$ ) complex (Mao et al., 2001). The phosphorylation of  $\beta$ -catenin by GSK-3 $\beta$  is inhibited by the LRP5/6 complex subsequently (Piao et al., 2008), thereby extending the half-life of  $\beta$ -catenin (Del Valle-Pérez et al., 2011). Additionally, CK1 $\epsilon$  collaborates with GSK3 $\beta$  to phosphorylate adenomatous polyposis coli (APC), thereby facilitating the binding of  $\beta$ -catenin to APC (Rubinfeld et al., 2001). In the p53 signaling pathway, DNA damage facilitates the interaction between CK1 $\epsilon$  and its binding partner, MDM2, resulting in multivalent phosphorylation of MDM2 and enhancing p53 activity (Schitteck and Sinnberg, 2014). Nonetheless, there is a notable absence of literature on the role of CSNK1E in MM at present, highlighting the need for further research into its functions in tumor biology. RAC, belonging to the Rho GTPase subfamily (Hodge and Ridley, 2016), encompasses three isoforms: RAC1, RAC2, and RAC3 (Haataja et al., 1997). These proteins, along with their closely related homolog Cdc42, play multifaceted roles in cellular processes such as cytoskeletal regulation, EMT, transcription, proliferation, cell polarity, apoptosis, phagocytosis, and vesicular transport. They serve as central regulatory factors in the metastasis and invasion of cancer cells (Maldonado et al., 2020). Notably, overexpression of RAC3 has been implicated in the development of various cancers. In typical circumstances, RAC3 is mainly found in brain tissue and neuronal cells (Corbetta et al., 2009), yet its expression is upregulated in breast cancer, prostate cancer, and brain tumors. In aggressive breast cancer, RAC3's specific binding partner CIB1 facilitates the recruitment of RAC3, promoting integrin activation at invasive pseudopodia, thereby regulating adhesion and degradation of the extracellular matrix (ECM) (Wang et al., 2022). With its ectopic expression allowing cells to avoid excessive autophagy and cell death caused by the inhibition of isoprenylcysteine carboxyl methyltransferase (Icmt) (Zhu et al., 2011). Nevertheless, the precise function of RAC3 in MM is still not well defined, highlighting the necessity for further research into its roles.

## 5 Conclusion

In this study, we first conducted Cox regression analysis on a gene set associated with the WNT signaling pathway, followed by consistent clustering. We then employed the LASSO algorithm to construct a model and assessed risk within the GSE91061 cohort. Additionally, we examined the relationship between 13 genes and EMT, conducting immune analysis on the two genes that showed the strongest correlations. Finally, a pan-cancer analysis of CSNK1E was conducted, and we explored the co-expression of EMT-related genes. Our findings offer new targets for MM research, providing theoretical support for both scientific inquiry and clinical investigation.

## Data availability statement

Publicly available datasets were analyzed in this study. This data can be found here: Raw data and WB original images: <https://www.jianguoyun.com/p/DSolhzMQ9rv3DBiSieQFIAA>.

## Ethics statement

The studies involving humans were approved by [Department of Plastic and Aesthetic Surgery, The First Affiliated Hospital of Nanchang University (2023)CDYFYLYK(08-029)]. The studies were conducted in accordance with the local legislation and institutional requirements. The participants provided their written informed consent to participate in this study. Ethical approval was not required for the studies on animals in accordance with the local legislation and institutional requirements because only commercially available established cell lines were used.

## Author contributions

WH: Data curation, Formal Analysis, Writing—original draft, Writing—review and editing. XW: Conceptualization, Data curation, Writing—original draft, Writing—review and editing. XH: Conceptualization, Data curation, Writing—original draft, Writing—review and editing. PC: Conceptualization, Data curation, Writing—original draft, Writing—review and editing. YL: Conceptualization, Data curation, Writing—original draft, Writing—review and editing. ZZ: Writing—original draft, Writing—review and editing. XY: Conceptualization, Data curation, Writing—original draft, Writing—review and editing. YC: Conceptualization, Data curation, Writing—original draft, Writing—review and editing. ZX: Conceptualization, Data curation, Writing—original draft, Writing—review and editing. GZ: Conceptualization, Writing—original draft, Writing—review and editing. HH: Conceptualization, Data curation, Writing—original draft, Writing—review and editing.

## Funding

The author(s) declare that no financial support was received for the research, authorship, and/or publication of this article.

## Conflict of interest

The authors declare that the research was conducted in the absence of any commercial or financial relationships that could be construed as a potential conflict of interest.

## Publisher's note

All claims expressed in this article are solely those of the authors and do not necessarily represent those of their affiliated organizations, or those of the publisher, the editors and the reviewers. Any product that may be evaluated in this article, or claim that may be made by its manufacturer, is not guaranteed or endorsed by the publisher.

## References

- Akoumianakis, I., Polkinghorne, M., and Antoniadis, C. (2022). Non-canonical WNT signalling in cardiovascular disease: mechanisms and therapeutic implications. *Nat. Rev. Cardiol.* 19 (12), 783–797. doi:10.1038/s41569-022-00718-5
- Anastas, J. N., and Moon, R. T. (2013). WNT signalling pathways as therapeutic targets in cancer. *Nat. Rev. Cancer* 13 (1), 11–26. doi:10.1038/nrc3419
- Armstrong, B. K., and Cust, A. E. (2017). Sun exposure and skin cancer, and the puzzle of cutaneous melanoma: A perspective on Fears et al. Mathematical models of age and ultraviolet effects on the incidence of skin cancer among whites in the United States. *American Journal of Epidemiology* 177, 105: 420–427. *Cancer Epidemiol.* 48, 147–156. doi:10.1016/j.canep.2017.04.004
- Ballotti, R., Cheli, Y., and Bertolotto, C. (2020). The complex relationship between MITF and the immune system: a Melanoma ImmunoTherapy (response) Factor? *Mol. Cancer* 19 (1), 170. doi:10.1186/s12943-020-01290-7
- Brockschmidt, C., Hirner, H., Huber, N., Eismann, T., Hillenbrand, A., Giamas, G., et al. (2008). Anti-apoptotic and growth-stimulatory functions of CK1 delta and epsilon in ductal adenocarcinoma of the pancreas are inhibited by IC261 *in vitro* and *in vivo*. *Gut* 57 (6), 799–806. doi:10.1136/gut.2007.123695
- Bryja, V., Červenka, I., and Čájanek, L. (2017). The connections of Wnt pathway components with cell cycle and centrosome: side effects or a hidden logic? *Crit. Rev. Biochem. Mol. Biol.* 52 (6), 614–637. doi:10.1080/10409238.2017.1350135
- Clevers, H. (2006). Wnt/beta-catenin signaling in development and disease. *Cell* 127 (3), 469–480. doi:10.1016/j.cell.2006.10.018
- Comandante-Lou, N., Baumann, D. G., and Fallahi-Sichani, M. (2022). AP-1 transcription factor network explains diverse patterns of cellular plasticity in melanoma cells. *Cell Rep.* 40 (5), 111147. doi:10.1016/j.celrep.2022.111147
- Corbetta, S., Gualdoni, S., Ciceri, G., Monari, M., Zuccaro, E., Tybulewicz, V. L. J., et al. (2009). Essential role of Rac1 and Rac3 GTPases in neuronal development. *Faseb J.* 23 (5), 1347–1357. doi:10.1096/fj.08-121574
- Del Valle-Pérez, B., Arqués, O., Vinyoles, M., de Herrerros, A. G., and Duñach, M. (2011). Coordinated action of CK1 isoforms in canonical Wnt signaling. *Mol. Cell Biol.* 31 (14), 2877–2888. doi:10.1128/MCB.01466-10
- Flaherty, K. T., Infante, J. R., Daud, A., Gonzalez, R., Kefford, R. F., Sosman, J., et al. (2012). Combined BRAF and MEK inhibition in melanoma with BRAF V600 mutations. *N. Engl. J. Med.* 367 (18), 1694–1703. doi:10.1056/NEJMoa1210093
- Frierson, H. F., Jr., El-Naggar, A. K., Welsh, J. B., Sapinoso, L. M., Su, A. I., Cheng, J., et al. (2002). Large scale molecular analysis identifies genes with altered expression in salivary adenoid cystic carcinoma. *Am. J. Pathol.* 161 (4), 1315–1323. doi:10.1016/S0002-9440(10)64408-2
- Grafanaki, K., Grammatikakis, I., Ghosh, A., Gopalan, V., Olgun, G., Liu, H., et al. (2023). Noncoding RNA circuitry in melanoma onset, plasticity, and therapeutic response. *Pharmacol. Ther.* 248, 108466. doi:10.1016/j.pharmthera.2023.108466
- Guo, W., Wang, H., and Li, C. (2021). Signal pathways of melanoma and targeted therapy. *Signal Transduct. Target Ther.* 6 (1), 424. doi:10.1038/s41392-021-00827-6
- Haataja, L., Groffen, J., and Heisterkamp, N. (1997). Characterization of RAC3, a novel member of the Rho family. *J. Biol. Chem.* 272 (33), 20384–20388. doi:10.1074/jbc.272.33.20384
- Hodge, R. G., and Ridley, A. J. (2016). Regulating Rho GTPases and their regulators. *Nat. Rev. Mol. Cell Biol.* 17 (8), 496–510. doi:10.1038/nrm.2016.67
- Jerby-Arnon, L., Shah, P., Cuoco, M. S., Rodman, C., Su, M. J., Melms, J. C., et al. (2018). A cancer cell program promotes T cell exclusion and resistance to checkpoint blockade. *Cell* 175 (4), 984–997.e24. doi:10.1016/j.cell.2018.09.006
- Johnpulle, R. A., Johnson, D. B., and Sosman, J. A. (2016). Molecular targeted therapy approaches for BRAF wild-type melanoma. *Curr. Oncol. Rep.* 18 (1), 6. doi:10.1007/s11912-015-0485-6
- Jung, Y. S., and Park, J. I. (2020). Wnt signaling in cancer: therapeutic targeting of Wnt signaling beyond  $\beta$ -catenin and the destruction complex. *Exp. Mol. Med.* 52 (2), 183–191. doi:10.1038/s12276-020-0380-6
- Kim, G. H., Fang, X. Q., Lim, W. J., Park, J., Kang, T. B., Kim, J. H., et al. (2020). Cinobufagin suppresses melanoma cell growth by inhibiting LEF1. *Int. J. Mol. Sci.* 21 (18), 6706. doi:10.3390/ijms21186706
- Kiuru, M., and Busam, K. J. (2017). The NF1 gene in tumor syndromes and melanoma. *Lab. Invest.* 97 (2), 146–157. doi:10.1038/labinvest.2016.142
- Knipschild, U., Gocht, A., Wolff, S., Huber, N., Löhler, J., and Stöter, M. (2005). The casein kinase 1 family: participation in multiple cellular processes in eukaryotes. *Cell Signal* 17 (6), 675–689. doi:10.1016/j.cellsig.2004.12.011
- Liang, H., Chen, Q., Coles, A. H., Anderson, S. J., Pihan, G., Bradley, A., et al. (2003). Wnt5a inhibits B cell proliferation and functions as a tumor suppressor in hematopoietic tissue. *Cancer Cell* 4 (5), 349–360. doi:10.1016/s1535-6108(03)00268-x
- Lin, J. Y., and Fisher, D. E. (2007). Melanocyte biology and skin pigmentation. *Nature* 445 (7130), 843–850. doi:10.1038/nature05660
- Liu, J., Xiao, Q., Xiao, J., Niu, C., Li, Y., Zhang, X., et al. (2022). Wnt/ $\beta$ -catenin signalling: function, biological mechanisms, and therapeutic opportunities. *Signal Transduct. Target Ther.* 7 (1), 3. doi:10.1038/s41392-021-00762-6
- Liu, L., Zhang, W., Gao, T., and Li, C. (2016). Is UV an etiological factor of acral melanoma? *J. Expo. Sci. Environ. Epidemiol.* 26 (6), 539–545. doi:10.1038/jes.2015.60
- Lo, J. A., and Fisher, D. E. (2014). The melanoma revolution: from UV carcinogenesis to a new era in therapeutics. *Science* 346 (6212), 945–949. doi:10.1126/science.1253735
- Logan, C. Y., and Nusse, R. (2004). The Wnt signaling pathway in development and disease. *Annu. Rev. Cell Dev. Biol.* 20, 781–810. doi:10.1146/annurev.cellbio.20.010403.113126
- Maldonado, M. D. M., Medina, J. I., Velazquez, L., and Dharmawardhane, S. (2020). Targeting rac and Cdc42 GEFs in metastatic cancer. *Front. Cell Dev. Biol.* 8, 201. doi:10.3389/fcell.2020.00201
- Mao, J., Wang, J., Liu, B., Pan, W., Farr, G. H., 3rd, Flynn, C., et al. (2001). Low-density lipoprotein receptor-related protein-5 binds to Axin and regulates the canonical Wnt signaling pathway. *Mol. Cell* 7 (4), 801–809. doi:10.1016/s1097-2765(01)00224-6
- Meng, Q. J., Maywood, E. S., Bechtold, D. A., Lu, W. Q., Li, J., Gibbs, J. E., et al. (2010). Entrainment of disrupted circadian behavior through inhibition of casein kinase 1 (CK1) enzymes. *Proc. Natl. Acad. Sci. U. S. A.* 107 (34), 15240–15245. doi:10.1073/pnas.1005101107
- Miete, C., Solis, G. P., Koval, A., Brückner, M., Katanaev, V. L., Behrens, J., et al. (2022). Gai2-induced conductin/axin2 condensates inhibit Wnt/ $\beta$ -catenin signaling and suppress cancer growth. *Nat. Commun.* 13 (1), 674. doi:10.1038/s41467-022-28286-9
- Ozbay Kurt, F. G., Lasser, S., Arkhypov, I., Utikal, J., and Umansky, V. (2023). Enhancing immunotherapy response in melanoma: myeloid-derived suppressor cells as a therapeutic target. *J. Clin. Invest.* 133 (13), e170762. doi:10.1172/JCI170762
- Piao, S., Lee, S. H., Kim, H., Yum, S., Stamos, J. L., Xu, Y., et al. (2008). Direct inhibition of GSK3 $\beta$  by the phosphorylated cytoplasmic domain of LRP6 in Wnt/ $\beta$ -catenin signaling. *PLoS One* 3 (12), e4046. doi:10.1371/journal.pone.0004046
- Poklepovic, A. S., and Luke, J. J. (2020). Considering adjuvant therapy for stage II melanoma. *Cancer* 126 (6), 1166–1174. doi:10.1002/cncr.32585
- Price, M. A. (2006). CKI, there's more than one: casein kinase I family members in Wnt and Hedgehog signaling. *Genes Dev.* 20 (4), 399–410. doi:10.1101/gad.1394306
- Rebecca, V. W., Somasundaram, R., and Herlyn, M. (2020). Pre-clinical modeling of cutaneous melanoma. *Nat. Commun.* 11 (1), 2858. doi:10.1038/s41467-020-15546-9
- Ring, A., Kim, Y. M., and Kahn, M. (2014). Wnt/catenin signaling in adult stem cell physiology and disease. *Stem Cell Rev. Rep.* 10 (4), 512–525. doi:10.1007/s12015-014-9515-2
- Rogiers, A., Boekhout, A., Schwarze, J. K., Awada, G., Blank, C. U., and Neyns, B. (2019). Long-term survival, quality of life, and psychosocial outcomes in advanced melanoma patients treated with immune checkpoint inhibitors. *J. Oncol.* 2019, 5269062. doi:10.1155/2019/5269062
- Rubinfeld, B., Tice, D. A., and Polakis, P. (2001). Axin-dependent phosphorylation of the adenomatous polyposis coli protein mediated by casein kinase I epsilon. *J. Biol. Chem.* 276 (42), 39037–39045. doi:10.1074/jbc.M105148200
- Schadendorf, D., van Akkooi, A. C. J., Berking, C., Griewank, K. G., Gutzmer, R., Hauschild, A., et al. (2018). Melanoma. *Lancet* 392 (10151), 971–984. doi:10.1016/S0140-6736(18)31559-9
- Schitteck, B., and Sinnberg, T. (2014). Biological functions of casein kinase 1 isoforms and putative roles in tumorigenesis. *Mol. Cancer* 13, 231. doi:10.1186/1476-4598-13-231
- Semenov, M. V., Habas, R., Macdonald, B. T., and He, X. (2007). SnapShot: noncanonical Wnt signaling pathways. *Cell* 131 (7), 1378. doi:10.1016/j.cell.2007.12.011
- Sharma, P., Hu-Lieskovan, S., Wargo, J. A., and Ribas, A. (2017). Primary, adaptive, and acquired resistance to cancer immunotherapy. *Cell* 168 (4), 707–723. doi:10.1016/j.cell.2017.01.017
- Sinnberg, T., Levesque, M. P., Krochmann, J., Cheng, P. F., Ikenberg, K., Meraz-Torres, F., et al. (2018). Wnt-signaling enhances neural crest migration of melanoma cells and induces an invasive phenotype. *Mol. Cancer* 17 (1), 59. doi:10.1186/s12943-018-0773-5
- Splendiani, E., Besharat, Z. M., Covre, A., Maio, M., Di Giacomo, A. M., and Ferretti, E. (2024). Immunotherapy in melanoma: can we predict response to treatment with circulating biomarkers? *Pharmacol. Ther.* 256, 108613. doi:10.1016/j.pharmthera.2024.108613
- Tai, D., Wells, K., Arcaroli, J., Vanderbilt, C., Aisner, D. L., Messersmith, W. A., et al. (2015). Targeting the WNT signaling pathway in cancer therapeutics. *Oncologist* 20 (10), 1189–1198. doi:10.1634/theoncologist.2015-0057
- Vaid, M., Singh, T., Prasad, R., and Katiyar, S. K. (2016). Bioactive proanthocyanidins inhibit growth and induce apoptosis in human melanoma cells by decreasing the accumulation of  $\beta$ -catenin. *Int. J. Oncol.* 48 (2), 624–634. doi:10.3892/ijo.2015.3286

- Vargas, J. Y., Loria, F., Wu, Y. J., Córdova, G., Nonaka, T., Bellow, S., et al. (2019). The Wnt/Ca(2+) pathway is involved in interneuronal communication mediated by tunneling nanotubes. *Embo J.* 38 (23), e101230. doi:10.15252/embj.2018101230
- Wang, L., Shi, J., Liu, S., Huang, Y., Ding, H., Zhao, B., et al. (2022). RAC3 inhibition induces autophagy to impair metastasis in bladder cancer cells via the PI3K/AKT/mTOR pathway. *Front. Oncol.* 12, 915240. doi:10.3389/fonc.2022.915240
- Wolchok, J. D., and Saenger, Y. M. (2007). Current topics in melanoma. *Curr. Opin. Oncol.* 19 (2), 116–120. doi:10.1097/CCO.0b013e32801497c6
- Xu, X., Zhang, M., Xu, F., and Jiang, S. (2020). Wnt signaling in breast cancer: biological mechanisms, challenges and opportunities. *Mol. Cancer* 19 (1), 165. doi:10.1186/s12943-020-01276-5
- Zhang, M., Weng, W., Zhang, Q., Wu, Y., Ni, S., Tan, C., et al. (2018). The lncRNA NEAT1 activates Wnt/ $\beta$ -catenin signaling and promotes colorectal cancer progression via interacting with DDX5. *J. Hematol. Oncol.* 11 (1), 113. doi:10.1186/s13045-018-0656-7
- Zhang, N., Wang, L., Zhu, G. N., Sun, D. J., He, H., Luan, Q., et al. (2014). The association between trauma and melanoma in the Chinese population: a retrospective study. *J. Eur. Acad. Dermatol. Venereol.* 28 (5), 597–603. doi:10.1111/jdv.12141
- Zhao, H., Ming, T., Tang, S., Ren, S., Yang, H., Liu, M., et al. (2022). Wnt signaling in colorectal cancer: pathogenic role and therapeutic target. *Mol. Cancer* 21 (1), 144. doi:10.1186/s12943-022-01616-7
- Zhu, W. L., Hossain, M. S., Guo, D. Y., Liu, S., Tong, H., Khakpoor, A., et al. (2011). A role for Rac3 GTPase in the regulation of autophagy. *J. Biol. Chem.* 286 (40), 35291–35298. doi:10.1074/jbc.M111.280990
- Zimmerman, Z. F., Moon, R. T., and Chien, A. J. (2012). Targeting Wnt pathways in disease. *Cold Spring Harb. Perspect. Biol.* 4 (11), a008086. doi:10.1101/cshperspect.a008086





## OPEN ACCESS

## EDITED BY

Jianbin Bi,  
The First Hospital of China Medical University,  
China

## REVIEWED BY

Yutao Wang,  
Chinese Academy of Medical Sciences and  
Peking Union Medical College, China  
Yu Tian,  
Benedictine University, United States  
Anne Krogsdam,  
Innsbruck Medical University, Austria

## \*CORRESPONDENCE

Wenhao Wang,  
✉ [wwh199459@sxmu.edu.cn](mailto:wwh199459@sxmu.edu.cn)  
Jingfang Wang,  
✉ [wangjingfang740401@163.com](mailto:wangjingfang740401@163.com)

RECEIVED 23 September 2024

ACCEPTED 20 January 2025

PUBLISHED 06 February 2025

## CITATION

Wang J, Zhu W, Li X, Wu Y, Ma W, Wang Y,  
Zhao W, Wei F and Wang W (2025)  
Transcriptome analysis of ovarian cancer  
uncovers association between tumor-related  
inflammation/immunity and patient outcome.  
*Front. Pharmacol.* 16:1500251.  
doi: 10.3389/fphar.2025.1500251

## COPYRIGHT

© 2025 Wang, Zhu, Li, Wu, Ma, Wang, Zhao, Wei  
and Wang. This is an open-access article  
distributed under the terms of the [Creative Commons Attribution License \(CC BY\)](https://creativecommons.org/licenses/by/4.0/). The use,  
distribution or reproduction in other forums is  
permitted, provided the original author(s) and  
the copyright owner(s) are credited and that the  
original publication in this journal is cited, in  
accordance with accepted academic practice.  
No use, distribution or reproduction is  
permitted which does not comply with these  
terms.

# Transcriptome analysis of ovarian cancer uncovers association between tumor-related inflammation/immunity and patient outcome

Jingfang Wang<sup>1\*</sup>, Wenrui Zhu<sup>1</sup>, Xia Li<sup>1</sup>, Yuanyuan Wu<sup>1</sup>,  
Wenhui Ma<sup>1</sup>, Yangzhou Wang<sup>2</sup>, Weihong Zhao<sup>1</sup>, Fang Wei<sup>1</sup> and  
Wenhao Wang<sup>1\*</sup>

<sup>1</sup>Department of Obstetrics and Gynecology, Second Hospital of Shanxi Medical University, Taiyuan, Shanxi, China, <sup>2</sup>Department of Stomatology, Changzhi Medical College, Changzhi, Shanxi, China

**Background:** Epithelial ovarian cancer (EOC) is a cancer that affects the female reproductive system and is highly lethal. It poses significant challenges in terms of treatment and often has a poor prognosis. In recent years, with the advent of PARPi, the treatment of ovarian cancer has entered a new stage of full-process management. Although more and more drugs have been approved, the therapeutic effect of PARPi is still very limited. With the rapid development of PD-1/PD-L1, CTLA-4, oncolytic viruses, cancer vaccines, adoptive cell therapy, etc., tumor immunotherapy has provided new opportunities for the treatment of ovarian cancer.

**Methods:** This study used comprehensive transcriptome analysis across multiple databases to gather gene transcripts and clinical features of normal ovarian samples and tissue samples from ovarian cancer. The aim was to explore the mechanisms underlying tumor immunotherapy resistance and to reveal the relationship between ovarian cancer's immune microenvironment and genes linked to inflammation. Various R packages were used for differential gene analysis, enrichment analysis, co-expression network construction, and prognostic model building.

**Results:** It has been found that the prognosis of ovarian cancer patients is closely associated with sets of genes involved in inflammation. The immune infiltration microenvironment, clinicopathological features, and survival rates differed significantly between two inflammatory gene expression patterns identified using cluster and immune microenvironment analyses. Further analysis revealed that the high-risk group had a higher abundance of M2-type macrophage infiltration, more active anti-tumor immune response, higher tumor stemness score, potentially worse prognosis, and lower response rates to multiple chemotherapy drugs and immune checkpoint inhibitors.

**Conclusion:** These findings provide new perspectives and potential targets for immunotherapy and prognostic evaluation of ovarian cancer and offer new strategies and directions for clinical treatment and patient management. This

study provides crucial information to further our comprehension of drug response mechanisms and tumor immunotherapy. It offers new strategies and methods for the treatment and prognostic improvement of ovarian cancer.

#### KEYWORDS

epithelial ovarian cancer, tumor immunotherapy, tumor immune microenvironment, cancer prognosis model, tumor-associated macrophages (TAM)

## 1 Introduction

In the female reproductive system, the deadliest cancerous growth is called epithelial ovarian cancer (EOC). Ovarian cancer ranks seventh among malignant tumors in women globally, accounting for over 310,000 new cases annually, according to the 2020 Global Cancer Statistics (Lee et al., 2022; Konstantinopoulos and Matulonis, 2023). Every year, ovarian cancer claims the lives of about 210,000 people. In 2020, ovarian cancer was diagnosed in 60,000 new cases and killed 40,000 people in China (Zhao et al., 2023). Patients with advanced stage ovarian cancer have an approximately 30% 5-year survival rate. With multiple recurrences, the interval between treatments and recurrences becomes shorter, leading to decreased sensitivity to platinum-based drugs and eventually developing into platinum resistance. The treatment is highly challenging, and the prognosis is often poor (Marchetti et al., 2021; Porter and Matulonis, 2023). Overcoming chemotherapy resistance in ovarian cancer is an urgent and important clinical issue.

Inflammation reactions are mainly divided into acute and chronic types. Acute inflammation occurs mainly in physical, chemical, or acute infection conditions as the body's early defense mechanism, and it usually resolves quickly on its own (Yang et al., 2023). Chronic inflammation, on the other hand, occurs in chronic infections or autoimmune diseases, where the body's normal feedback regulation cannot stop the inflammation, leading to chronic inflammation (Liu et al., 2022). Statistics show that chronic inflammation contributes to about 20% of malignant tumors worldwide (Kennel et al., 2023; Venkateshaiah and Kumar, 2021; Haas et al., 2021). Non-steroidal anti-inflammatory drugs clinically reduce the incidence and metastasis of various solid tumors and decrease tumor-induced mortality. Chronic inflammation is thought to significantly influence the initiation, growth, and progression of cancers.

The mechanisms through which chronic inflammation initiates tumor occurrence, and development are diverse but often involve the microenvironment provided by inflammation for tumors. As a crucial part of the cancer stroma, cancer-associated fibroblasts (CAFs) are intimately associated with inflammation and the tumor immune microenvironment (TME) (Chen et al., 2021). CAFs interact with various signaling pathways such as NF- $\kappa$ B, PI3K-Akt, IL6-JAK-STAT3, and TGF- $\beta$  to help form and maintain the TME, influencing ECM structure and generating immune therapy resistance (Mao et al., 2021; Wu F. et al., 2021). Additionally, activated CAFs promote monocyte adhesion and drive macrophages toward M2 polarization, further inhibiting immune responses in the TME (Lavie et al., 2022; Galbo et al., 2021). Therefore, analyzing the relationship between genes linked to inflammation and the tumor immune milieu can aid in

comprehending reasons for EOC immunotherapy resistance and contribute to developing innovative immunotherapy strategies.

## 2 Methods and materials

### 2.1 Data acquisition

The TCGA database (<https://portal.gdc.cancer.gov/>) included the gene transcripts and clinical details of 429 ovarian cancer tissue samples from patients with the disease. The patient's clinical features encompassed survival status, time, tumor grade, age, etc. In the meantime, the GTEx database (<https://www.gtexportal.org/home/>) was accessed to download 88 normal ovarian samples. For validation, the gene expression profiling microarray datasets for ovarian cancer tissues were acquired from the GEO database (<https://www.ncbi.nlm.nih.gov/geo/>). These datasets, GSE26712 (Zheng et al., 2019) and GSE102073 (Ye et al., 2021), each contained 153 and 84 ovarian cancer tissues, respectively. Additionally, ovarian cancer single-cell datasets EMTAB8107 (Ding et al., 2024), GSE118828 (Yu et al., 2022), GSE130000, and GSE154600 (Jiang et al., 2023) were downloaded to explore gene expression at the single-cell level.

### 2.2 Acquisition of inflammation-related gene sets

Inflammation-related gene sets were obtained from the Molecular Signatures Database (MSigDB) (Castanza et al., 2023) (<https://www.gsea-msigdb.org/gsea/msigdb/>), including BIOCARTE\_INFLAM\_PATHWAY (v2023.2.), GOBP\_CHRONIC\_INFLAMMATORY\_RESPONS (v2023.2.), HALLMARK\_INFLAMMATORY\_RESPONSE (v2023.2.), and REACTOME\_INFLAMMASOMES (v2023.2.).

### 2.3 Scoring of inflammation-related gene sets and prognostic evaluation

With the help of the GSVA (Hänzelmann et al., 2013) R package (v2.0.4), we evaluated the gathered sets of gene sets associated with inflammation using single-sample gene set enrichment analysis (ssGSEA). ssGSEA is an extension of the GSEA method, primarily designed for individual samples where GSEA is not applicable. The algorithm uses the empirical cumulative distribution function to calculate enrichment scores (ES) and rank normalized gene expression values for a given sample. The prognostic correlation between gene sets associated with

inflammation and patients with ovarian cancer was assessed simultaneously using the Cox proportional hazards model.

## 2.4 Consensus clustering based on inflammation-related gene set scores

Consensus clustering was often used in cancer subtype classification studies using the Consensus ClusterPlus R package (v4.12.6) (Wilkerson and Hayes, 2010). This study's ovarian cancer subtype classification was conducted based on the aforementioned inflammation-related gene set scores. The optimal clustering effect was determined by combining the consensus cumulative distribution function (CDF) with the Proportion of Ambiguous Clustering (PAC) score. In the CDF plot, the consensus matrix's cumulative distribution function was displayed for different values of  $k$  (represented by colors), aiding in identifying the approximate maximum CDF value, where consensus and cluster confidence are maximized, resulting in the most reliable clustering analysis. In PAC analysis, lower PAC values indicate more ideal clustering effects.

## 2.5 Kaplan-Meier (KM) survival analysis

Currently, the most widely used method for survival analysis is the Kaplan-Meier approach. The KM approach, as it is commonly called, was proposed by Kaplan and Meier. The Kaplan-Meier survival analysis compares the survival circumstances of two patient groups using a univariate analysis that integrates patients' survival times and terminal states. The Kaplan-Meier survival curve, a commonly encountered representation, visually reflects survival differences under various conditions.

## 2.6 Immune cell infiltration analysis

Based on the IOBR (Zeng et al., 2021) R package (v2.0), we employed built-in algorithms such as TIMER, CIBERSORT, MCPcounter, EPIC, and quantISEQ (Newman et al., 2015; Becht et al., 2016; Finotello et al., 2019; Racle et al., 2017; Li et al., 2016) to assess the abundance of immune cell infiltration in the tumor immune microenvironment of each ovarian cancer tissue.

## 2.7 Drug sensitivity analysis

The OncoPredict (Maeser et al., 2021) R package (v1.2) was created by Maeser et al. and was used to predict medication reactions in cancer patients. OncoPredict adapts tissue gene expression patterns to the semi-maximal inhibitory concentration (IC50) of drugs taken from cancer cell lines in the Genomics of Drug Sensitivity in Cancer (GDSC) database and the Cancer Cell Line Encyclopedia (CCLE) maintained by the Broad Institute. An unpaired  $t$ -test was used to assess the sensitivity of 198 drugs (between high-risk and low-risk groups). Set at  $p < 0.05$  was the significance level.

## 2.8 Prediction of immunotherapy sensitivity

The Cancer Immunome Atlas (TCIA) (Charoentong et al., 2017) database (<https://tcia.at/>) was used to download the Immunophenotype Scores (IPS) for CC. Subsequently, IPS were compared across different tumor groups to predict sensitivity to immunotherapy.

## 2.9 Differential gene identification

Using the limma (Ritchie et al., 2015) R package (3.60.4), differential gene expression analysis was performed on the TCGA data. This involved data preprocessing, normalization, and identifying significant differences in gene expression levels through linear modeling. Statistical thresholds were set (adj.  $P$  Val.  $< 0.01$  and  $|\log_2(FC)| > 1$ ) to screen for significantly differentially expressed genes. Finally, to decipher the biological significance of these differential genes, enrichment analysis and functional annotation were performed.

## 2.10 Enrichment analysis

The clusterProfiler (Wu T. et al., 2021) R package (v4.12.6) was used to perform enrichment analysis, which consisted of two steps: (1) Over-Representation Analysis (ORA) to investigate the functional enrichment of gene sets through Genomes (KEGG) analyses, Kyoto Encyclopedia of Genes, Gene Ontology (GO), and (2) Gene Set Enrichment Analysis (GSEA) to examine the enrichment of validated gene sets in KEGG pathways. These enrichment results revealed the gene sets' biological functions and pathway associations.

## 2.11 Weighted gene Co-Expression network construction

In systems biology, co-expression gene modules and their correlation to phenotypes are identified using Weighted Gene Co-Expression Network Analysis (WGCNA) (Langfelder and Horvath, 2008). Gene co-expression networks are constructed by calculating gene-gene correlations and then converting the correlation matrix into a weighted matrix. Gene modules are then built based on the weighted matrix, and the eigengene for each module is computed. Subsequently, the correlation between module eigengenes and phenotypic data determines the module-phenotype relationship. Ultimately, gene modules associated with phenotypes of interest are identified, revealing underlying biological pathways and mechanisms. The WGCNA method aids in uncovering key modules and gene correlations within gene regulatory networks.

## 2.12 Prognostic model construction and validation

The TCGA dataset was initially used to construct a survival prognostic model using the multiCox and Least Absolute Shrinkage and Selection Operator (LASSO) techniques. Gene features were

selected using LASSO, and multiCox was employed for multivariable Cox regression to establish the prognostic model. The model was then used for independent external validation datasets, and its ability to predict survival was evaluated using Kaplan-Meier survival analysis and time-dependent ROC curve analysis. These validation analyses verified the prognostic predictive efficacy of the model across different datasets, ensuring its reliability and generalizability.

## 2.13 mRNA Stemness Index (mRNAsi)

Derived from the PCBC database's mean-centered RNA-Seq data of PSCs (syn2701943) (Gul et al., 2023). A stem cell feature signature was found using the One-Class Logistic Regression (OCLR) machine learning approach, and it was confirmed using leave-one-out cross-validation. A Spearman correlation analysis was then used to compare the stem cell features and the normalized expression matrix of tumor samples. Finally, by scaling the Spearman correlation coefficient between 0 and 1, the mRNA Stemness Index (mRNAsi) was determined. A higher mRNAsi indicates a higher degree of tumor dedifferentiation and stronger stemness.

## 2.14 Single-cell analysis

The following methods were used to process ovarian cancer single-cell sequencing data: We first converted the scRNA-seq data into a Seurat (Hao et al., 2024) object using the Seurat R package. We performed quality control (QC) by determining the percentage of ribosomal or mitochondrial genes and eliminating low-quality cells. FindVariableFeatures was used to determine the top 2000 genes exhibiting high variability. Furthermore, dimensionality reduction techniques were used to group approximately 2000 genes using Principal Component Analysis (PCA) and Uniform Manifold Approximation and Projection (UMAP). We could identify marker genes for each cluster using the FindAllMarkers tool with  $|\text{Log2FC}|$  and min. 0.3 and 0.25 are the respective pct cutoff values. Different cell types were annotated using the SingleR (Aran et al., 2019) R package. Finally, we used the AddModuleScore function to compute the expression levels of prognostic model genes at the single-cell level.

## 2.15 Cell lines

Fenghuishengwu in China is where human ovarian surface epithelial cells (HOSE) are sourced (HOSE, CL0154). From the American Type Culture Collection, the SKOV3 cell line was acquired. *Mycoplasma* is routinely tested for in all cell lines. A complete medium, consisting of 1% double antibiotics and 10% fetal bovine serum (FBS), is used to cultivate both HOSE and SKOV3. When the cell confluence reaches 80%–90%, they are passaged.

## 2.16 Cell transfection

Similarly,  $5 \times 10^5$  cells were cultured in each well of a 6-well plate. For transfection, HOSE and SKOV3 cells were treated with 15 nM of siRNA IL-6, siRNA TGF- $\beta$ 1 and siRNA NC (P4157, GenePharma, Shanghai, China), respectively, using Lipofectamine 3000 (L3000150, Thermo, New York, Waltham, MA, United States).

## 2.17 qPCR

HOSE and SKOV3 cells were lysed to obtain total RNA using a TRIzol reagent (15,596,026, Invitrogen, New York, NY, United States). The qRT-PCR analysis was performed using the HiScript II One Step qRT-PCR SYBR Green kit (P131, Vazyme, Nanjing, China) and a Bio-Rad CFX96 PCR system (Bio-Rad, Hercules, CA, United States). RuiBiotech (Beijing, China) created and manufactured the primers used in this investigation. Glyceraldehyde-3-phosphate dehydrogenase (GAPDH) was used as the internal reference for assessing the target gene expression using the  $2^{-\Delta\Delta CT}$  method.

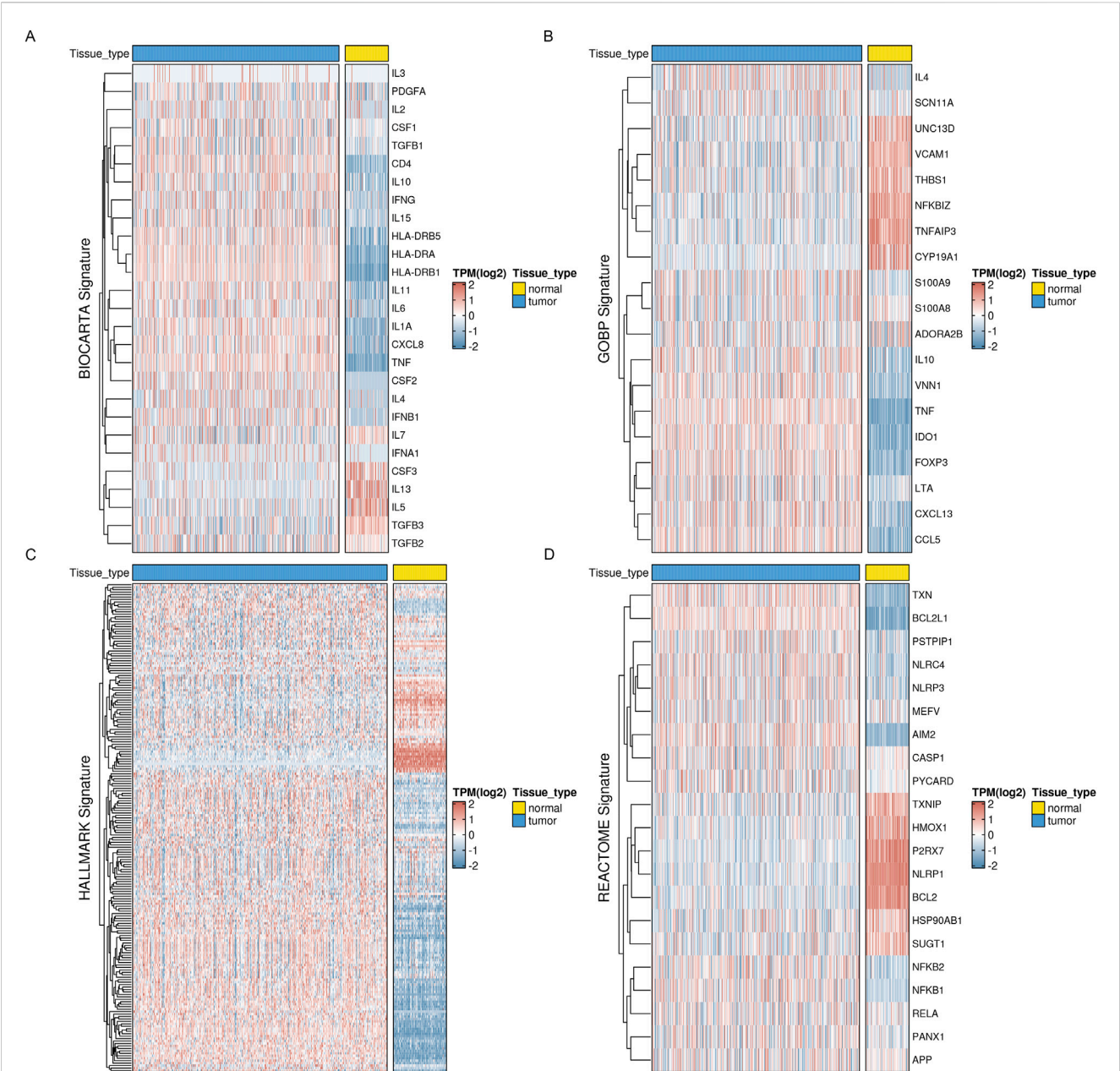
## 2.18 Western blot

The total protein was extracted using a cell lysate solution, and the proteins were separated using 10% sodium dodecyl sulfate-polyacrylamide gel electrophoresis (SDS-PAGE). PVDF membranes were then used to hold the separated proteins (03010040001, Millipore, Billerica, MA, United States). After a 30-min blocking, the membranes were subjected to adding primary antibodies and incubated at 4°C. The primary antibodies were obtained from Abcam (Abcam, United States). Secondary antibodies (BA1054, 1:5000, Boster, Wuhan, China) were added to the membranes and incubated for 2 h at room temperature after washing. The membranes were then visualized using an ECL development kit (A38554, Invitrogen, New York, NY, United States) and photographed with a GE Las-4000 (GE Healthcare, Piscataway, NJ, United States). After conducting the experiment thrice, the gray values were obtained using Media Cybernetics' ImageJ 1.8.0 program (Silver Spring, MD, United States). An internal reference was beta-actin.

## 2.19 Statistical analysis

The analysis was conducted using SPSS 26.0 and the R programming language. The measurement data was expressed using the standard deviation ( $x \pm s$ ). A one-way ANOVA was employed to compare the groups. Dunnett's multiple comparisons were performed to determine whether the variance was uneven. Measurement data with a normal distribution were displayed as mean  $\pm$  standard deviation, and t-tests were used to compare groups. The Mann-Whitney  $U$  test was performed using measurement data that was not normally distributed and displayed as the median and interquartile range to compare





groups. Count data were expressed as rates, and group comparisons were conducted using the  $\chi^2$  test.

### 3 Results

#### 3.1 Identification of inflammatory molecular subtypes in ovarian cancer based on consensus clustering

First, we obtained four inflammatory-related gene sets from the MSigDB database, including BIOCARTA\_INFLAM\_

PATHWAY, GOBP\_CHRONIC\_INFLAMMATORY\_RESPONS, HALLMARK\_INFLAMMATORY\_RESPONSE, and REACTOME\_INFLAMMASOMES. Most inflammatory-related genes had significantly different expression profiles in tumor and normal tissues, with most genes significantly elevated in tumor tissues, according to our analysis of the TCGA ovarian cancer dataset and the corresponding normal tissues from the GTEx database (Figure 1). This suggests a correlation between inflammatory phenotypes and tumor development.

Meanwhile, based on ssGSEA, we performed enrichment scoring of inflammatory-related gene sets for each ovarian cancer tissue (Figure 2A). Univariate COX regression analysis

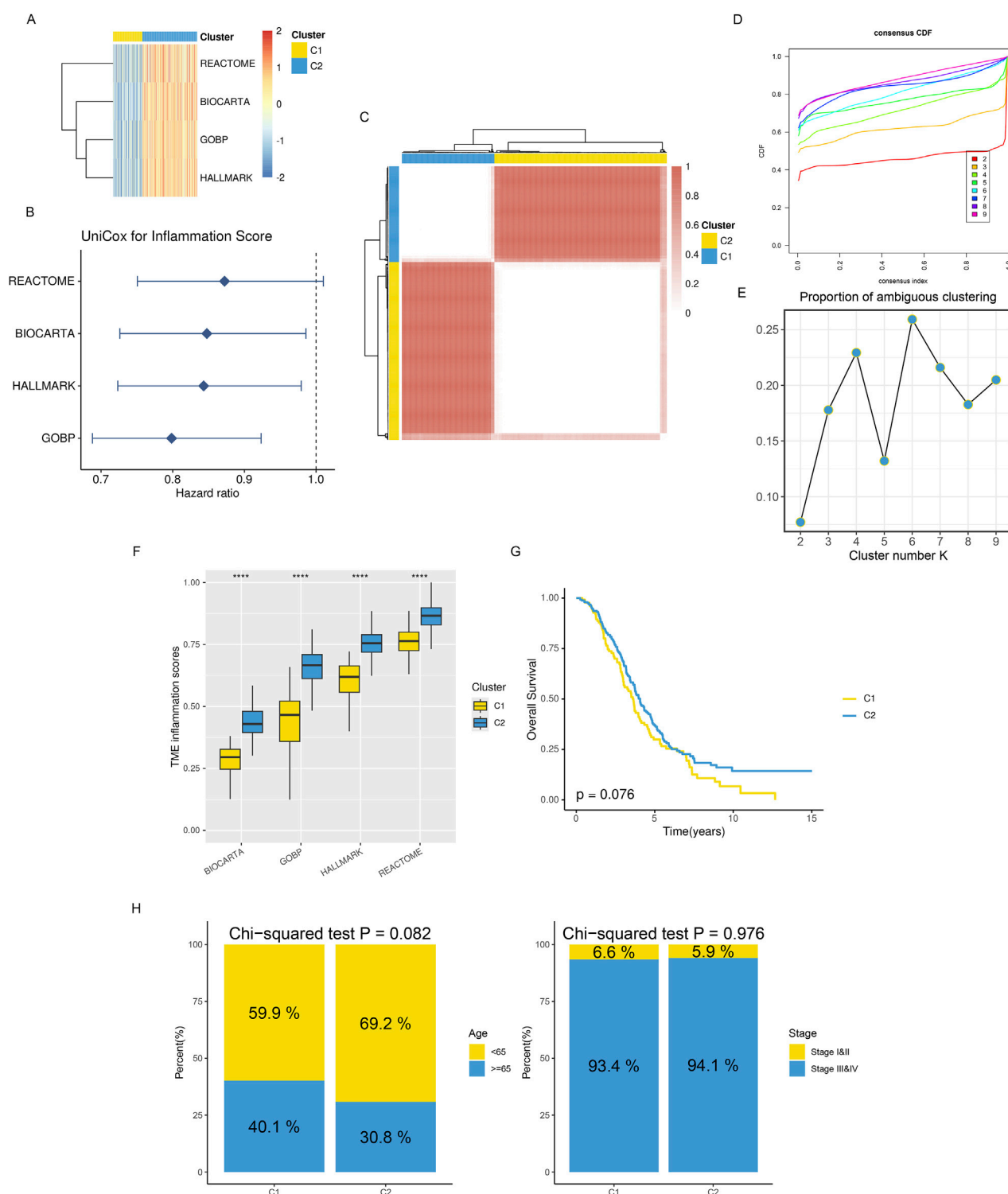
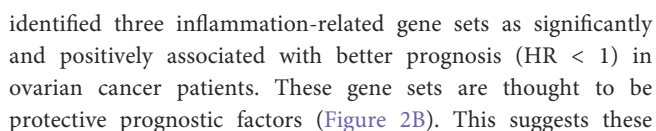
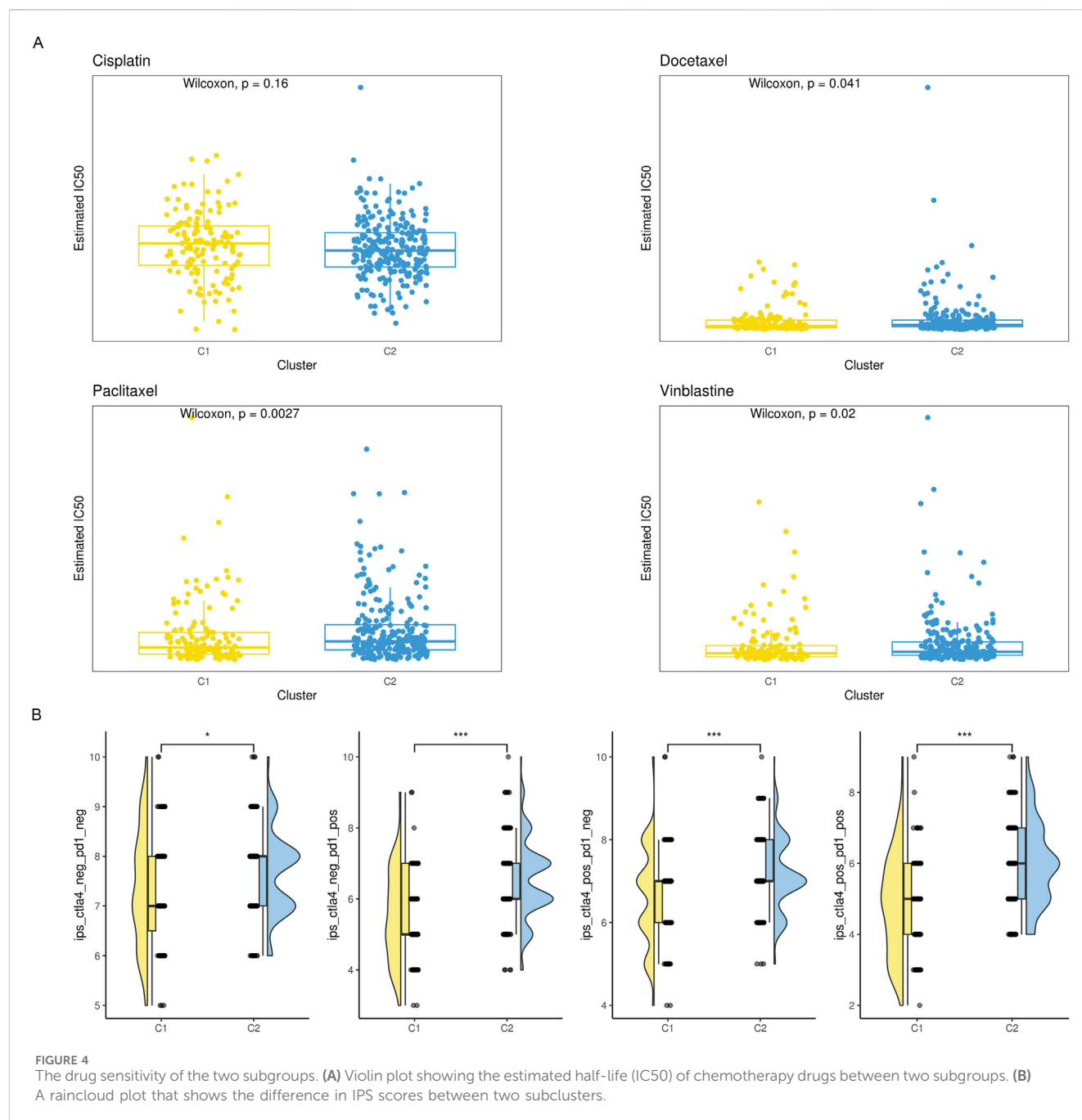


FIGURE 2

Distinct TME landscapes in OV. **(A)** The GSEA score of each signature is associated with inflammation between two subclusters. **(B)** A forest plot displaying the hazard ratio for each signature associated with inflammation was found using univariate Cox regression analysis. **(C)** The TCGA-OV consensus score matrix for the glioma sample, with  $k = 2$  clustering number. The consensus score indicates the degree of interaction between two samples. **(D, E)** The consensus matrix's PAC scores **(E)** and CDF curves **(D)** for each **(K)** **(F)** Boxplots that display the distribution of GSEA scores for every inflammatory signature between two subclusters; **(G)** Kaplan-Meier curves that analyze survival differences between two subclusters using the log-rank test. **(H)** Stacked bar graphs showing the distributions between two subclusters for age populations (left panel) and stages (right panel). Using Chi-squared testing, P values were calculated.



frontiersin.org

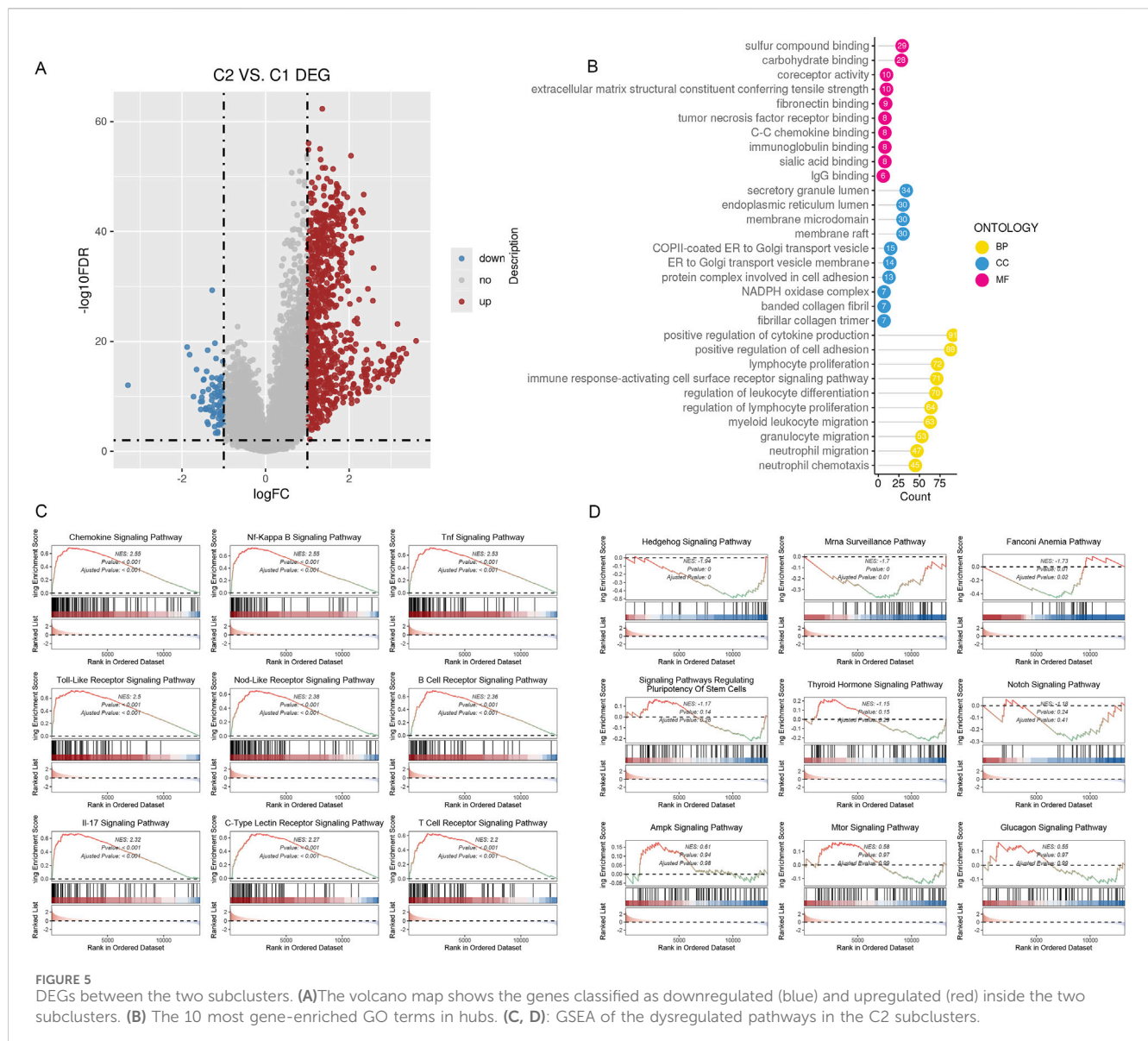


gene sets. The maximum number of clusters was set to 10, with 100 subsamples drawn, a sample proportion of 0.8, K-means as the clustering algorithm, and Euclidean distance as the metric. Ultimately, we performed nine clusters with  $k$  values ranging from 2 to 10. Through comprehensive evaluation using CDF curves and PAC analysis, we selected the ideal number of clusters as 2 (Figures 2C–E). At the same time, we found significant differences in inflammatory enrichment scores (Figure 2F) and overall survival rates (Figure 2G, log-rank  $p = 0.076$ ) among patients with different inflammatory gene expression patterns. Chi-square tests for clinicopathological features revealed differences in the age distribution (with 65 years as the cutoff) and clinicopathological grading among patients in different groups (Figure 2H).

### 3.2 Distinct immune infiltration microenvironments, responsiveness to drug treatment, and deregulated signaling pathways among subtypes

Previous studies have reported that different tissue types often have distinct immune infiltration microenvironments. Thus, we used five immune microenvironment analysis methods in this study—CIBERSORT, MCPcounter, quanTIseq, EPIC, and TIMER—for integrated evaluation and analysis of immune cell infiltration profiles to thoroughly examine the immune profiles among various subtypes. We found that the C2 subtype had much more infiltrating NK cells, B cells, macrophages, CD8<sup>+</sup>





T cells, and CD4<sup>+</sup> T cells than the C1 subtype, with consistent results across various analysis methodologies. This suggests that the C2 subtype exhibits the biological characteristics of a so-called “hot” tumor immune microenvironment (Figure 3A). In the meanwhile, we found that the C2 subtype had far higher amounts of immunomodulators and cytokines expressed than the C1 subtype, based on a list of genes encoding immunomodulators and chemokines that we downloaded from the TISIDB database (Figure 3B).

With the deepening of research on the immune tumor microenvironment, substantial evidence suggests that tumors with different levels of immune cell infiltration have distinct response rates to chemotherapy and immunotherapy. Therefore, we examined the IC50 values of vinblastine, paclitaxel, docetaxel, and cisplatin. We found that, except cisplatin, the C2 subtype’s IC50 values were considerably higher than the C1 subtype’s, indicating a noticeably lower response rate of the C2 subtype to these three drugs (Figure 4A). Simultaneously, we utilized IPS, IPS-

PD1/PD-L1/PD-L2, IPS-CTLA4, and IPS-PD1/PD-L1/PD-L2 + CTLA4 to assess differences in the response rates to immune checkpoint inhibitor therapy among different subtypes. We found that IPS, IPS-PD1/PD-L1/PD-L2 and IPS-CTLA4 were significantly higher in the C2 subtype compared to the C1 subtype (Figure 4B).

We hypothesize that the distinct immune infiltration microenvironments and responses to drug treatment among different subtypes are based on significantly different signaling pathways and biological differences. Therefore, we identified genes that were differently expressed among various subtypes using the limma R package (Figure 5A). We carried out an over-representation analysis (ORA), which included GO\_BP/CC/MF (Figure 5B), and last, we performed a GSEA analysis. The results suggested multiple signaling pathways were significantly deregulated in C2 (Figures 5C, D). In summary, subtypes based on inflammatory gene enrichment scores exhibit distinct immune infiltration microenvironments, responses to drug treatment, and deregulated signaling pathways, warranting further investigation.

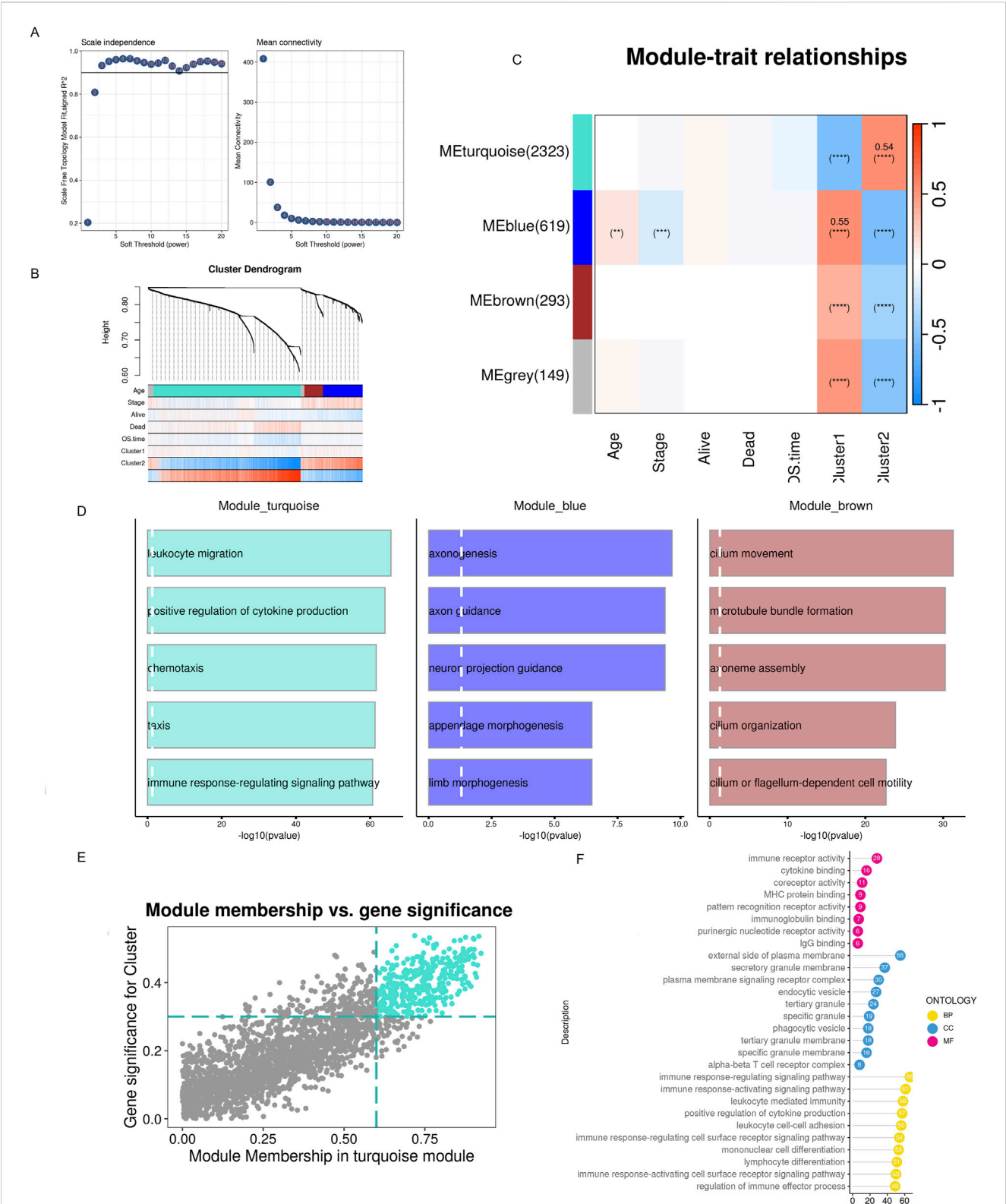


**FIGURE 6** WGCNA detects modules associated with subclusters and hub genes embedded within them. **(A)** Examination of network configuration for various soft-threshold power levels. On the scale-free topology fit index, the left panel illustrates the effect of a soft-threshold power of 3. The effect of the same criterion on the average connectivity is shown in the right panel **(B)** Cluster dendrogram of the modules exhibiting coexpression. Each color corresponds to a co-expression module. **(C)** A module-trait heatmap shows how clinical traits and module eigengenes relate. **(D)** Bar charts showing the top five enriched phrases for every module gene. The connection between gene significance and module membership in the brown modules. **(E)** Hub genes of the appropriate module were identified as dots in color with MM > 0.6 and GS > 0.3. **(F)** Top 10 enriched GO terms of hub genes.

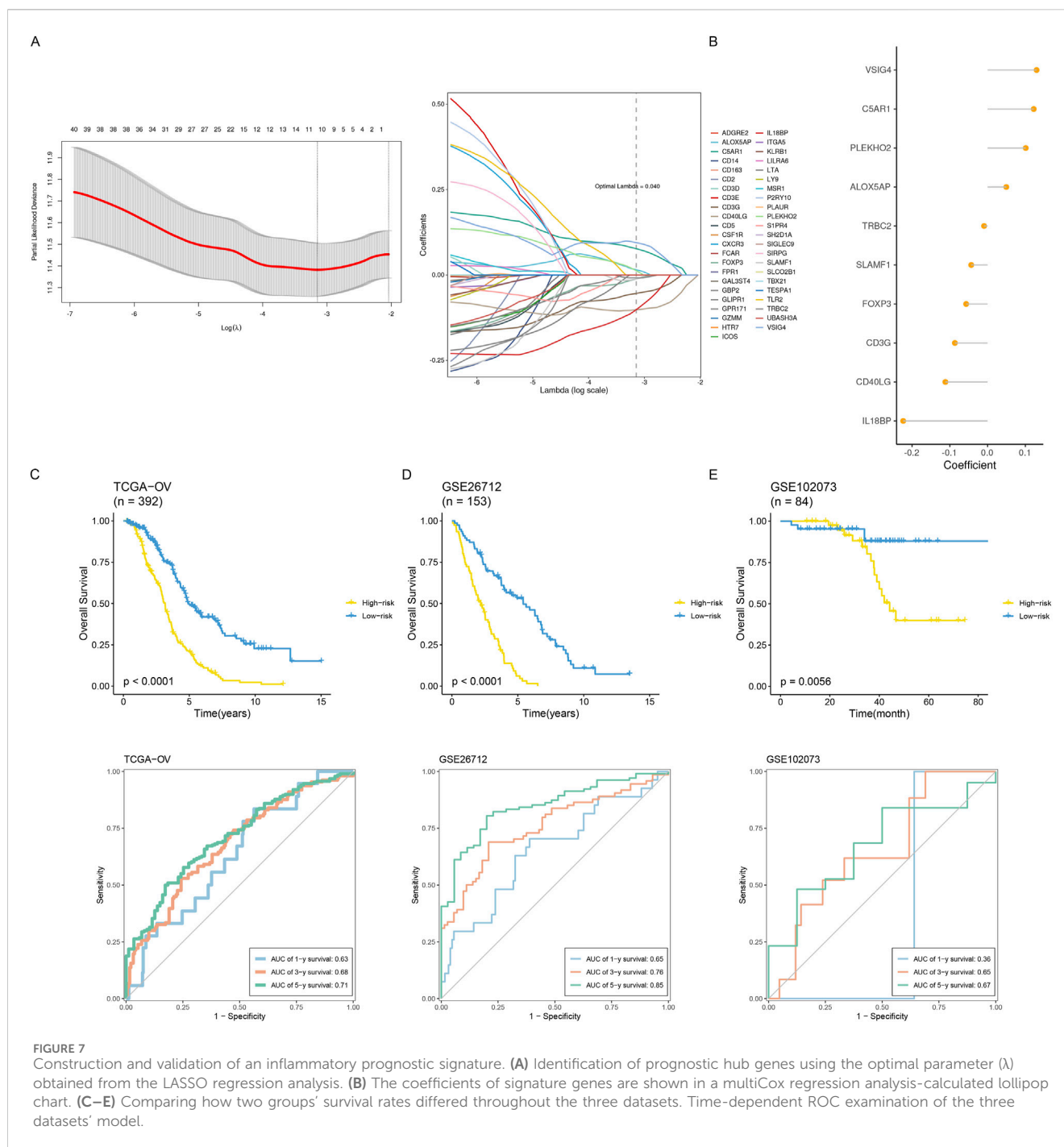


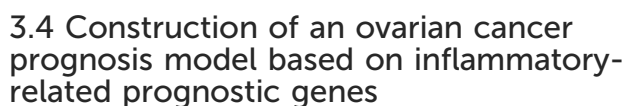
FIGURE 7

Construction and validation of an inflammatory prognostic signature. (A) Identification of prognostic hub genes using the optimal parameter ( $\lambda$ ) obtained from the LASSO regression analysis. (B) The coefficients of signature genes are shown in a multiCox regression analysis-calculated lollipop chart. (C–E) Comparing how two groups' survival rates differed throughout the three datasets. Time-dependent ROC examination of the three datasets' model.

### 3.3 Identification of biological features of different inflammatory subtypes using WGCNA gene co-expression network analysis

To conduct the WGCNA analysis, we first added the differentially expressed genes identified in the previous step. Four co-expression modules were obtained after setting the soft threshold  $\beta$  to three and the minimum number of genes in a module to 30 (Figures 6A, B). We utilized GO enrichment analysis and found that modules other than the gray module possessed distinct biological characteristics. Since previous analyses suggested that patients in the

C2 subtype had a better prognosis, responsiveness to drug treatment, and deregulated signaling pathways, we hypothesized that genes significantly associated with C2 might be involved in tumor development, invasion, and resistance to drug treatment. Based on WGCNA co-expression network analysis, we found that the C2 subtype had the strongest positive correlation with the turquoise module (Figure 6C,  $\text{Cor} = 0.54$ ), which contained 2323 genes. We could run functional enrichment analyses on these genes using thresholds ( $\text{MM} > 0.6$  and  $\text{GS} > 0.3$ ) to identify key genes inside the module (Figures 6D, E). The results showed that immune receptor activity and other biological processes were the primary roles of the module's key genes (Figure 6F).

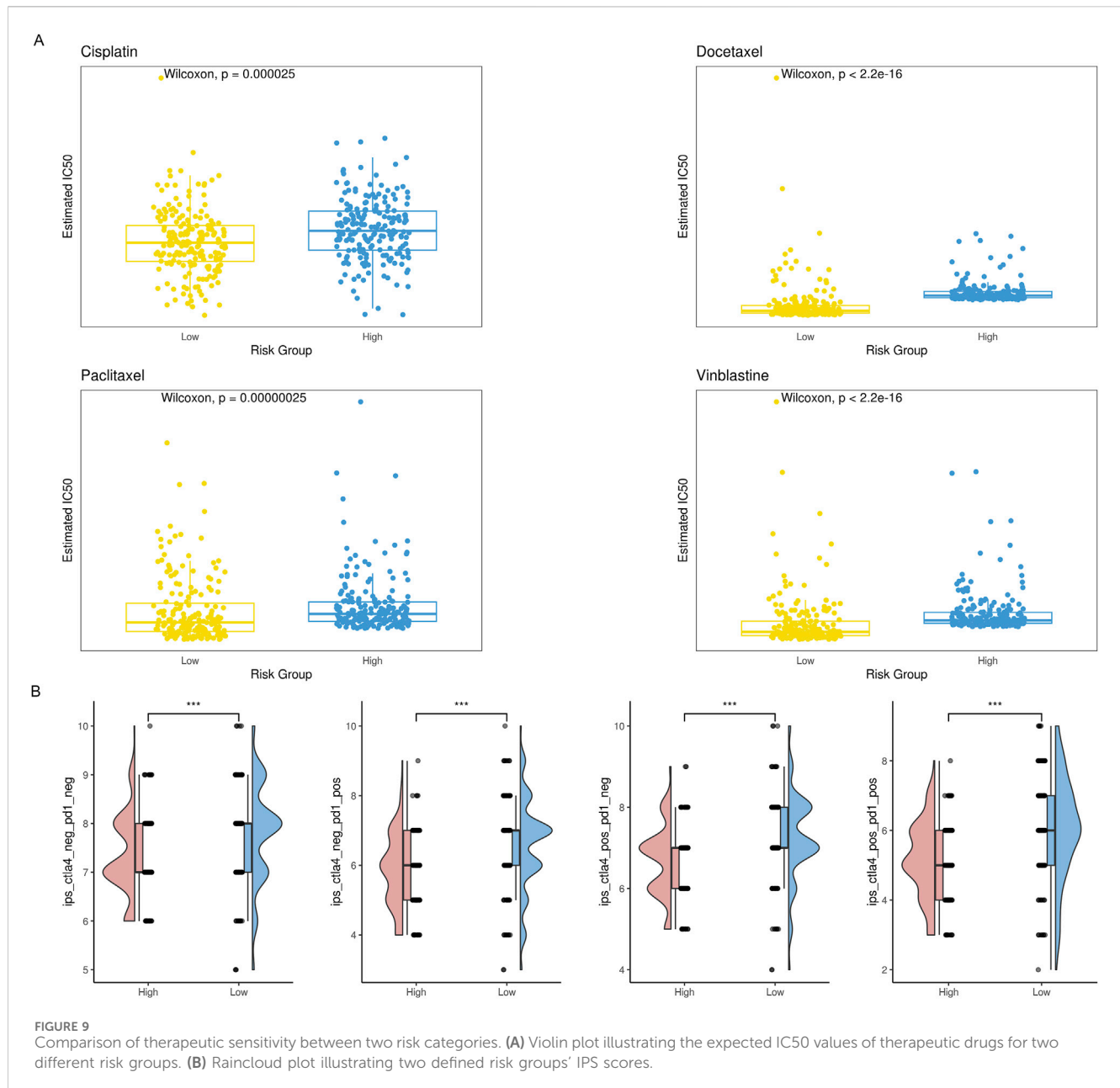


With the help of multivariate COX regression analysis, Least Absolute Shrinkage and Selector Operation (LASSO) (Figure 7A), and module key genes, we constructed a prognosis model in this study. The genes included in the model and their corresponding regression coefficients are shown (Figure 7B). Risk scores based on the prognostic model were simultaneously computed for all ovarian cancer samples in the training and validation sets. The samples were divided into low-risk and high-risk groups based on the median risk score. Our result shows the plotted Kaplan-Meier curves, which indicate substantial differences between the two groups (Figures 7C–E). Using a time-dependent ROC curve analysis, the prediction efficiency at 1, 3, and 5 years was also

### 3.5 Relationship between risk score and tumor immune microenvironment

Based on the CIBERSORT immune microenvironment analysis algorithm, we analyzed the TCGA dataset divided into high-risk and low-risk groups. We found that the low-risk group had higher M1 macrophages and CD8<sup>+</sup> T cell infiltration abundances, while the high-risk group had significantly higher abundances of M2 macrophage infiltration (Figure 8A). This suggests an active anti-tumor immune response in the tissue immunological microenvironment of the high-risk group. Further analysis of T cell exhaustion markers and M2 macrophage markers showed that the high-risk group had significantly higher expression levels than the low-risk group (Figures 8B, C). Simultaneously, analysis of cellular stemness levels also indicated higher stemness scores in the high-risk group, suggesting more pronounced tumor stemness, i.e., dedifferentiation (Figure 8D). Since cellular stemness levels





are negatively correlated with prognosis, these results imply a poorer prognosis for patients in the high-risk group.

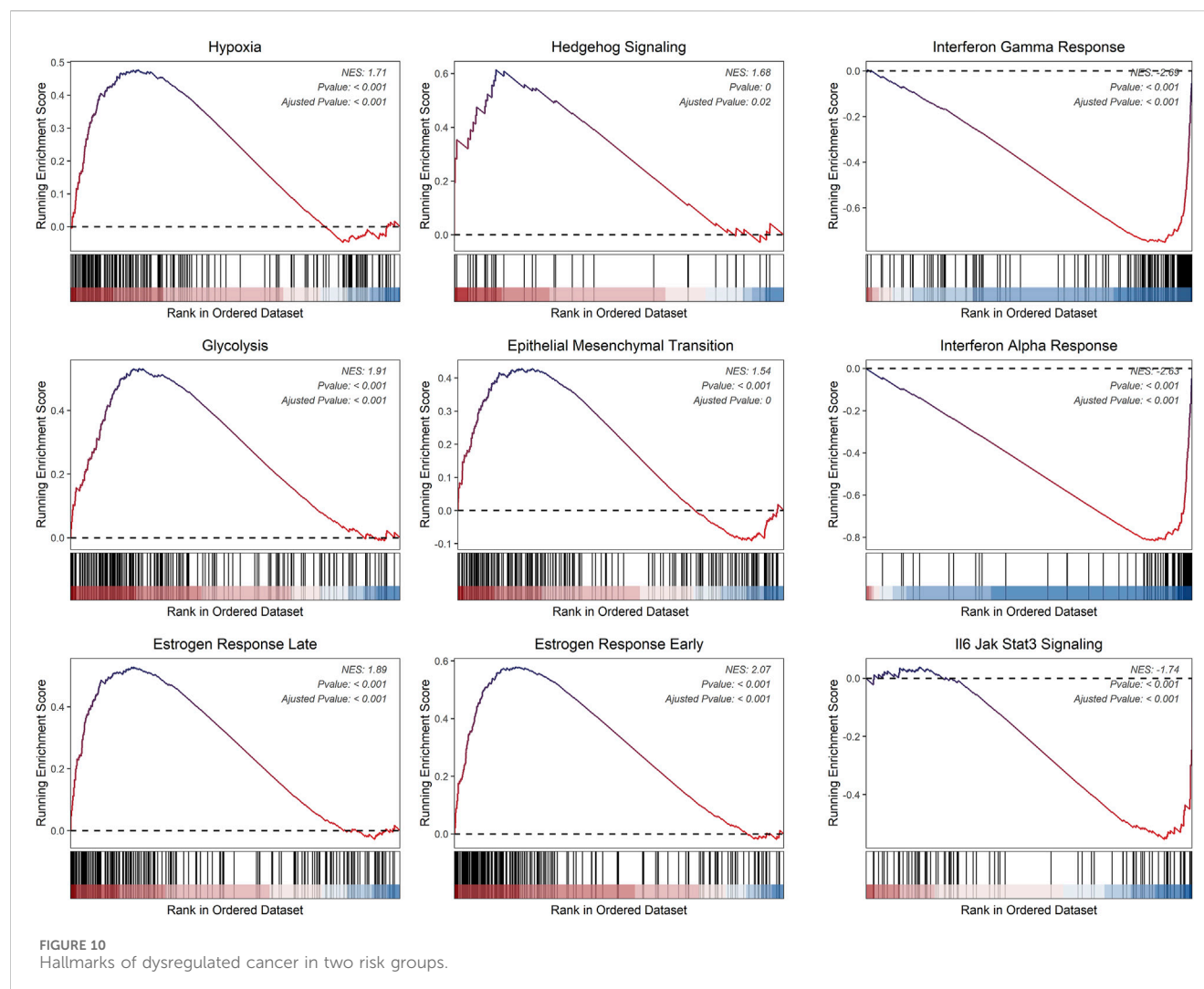
### 3.6 Relationship between risk score and responsiveness to drug treatment

The amount of immune cell infiltration substantially impacts immunotherapy and chemotherapy, according to previous studies, with the high-risk group having less anti-tumor immune cell infiltration than the low-risk group. To determine if the high-risk group responded less frequently to these four drugs, we examined the IC<sub>50</sub> values of cisplatin, vinblastine, paclitaxel, and docetaxel. Compared to the low-risk group, the IC<sub>50</sub> values of the high-risk group were much greater (Figure 9A). We employed IPS, IPS-PD1/

PD-L1/PD-L2, IPS-CTLA4, and IPS-PD1/PD-L1/PD-L2 + CTLA4 simultaneously to evaluate variations in immune checkpoint inhibitor therapy response rates across various risk groups. IPS, IPS-PD1/PD-L1/PD-L2, and IPS-CTLA4 levels were considerably lower in the high-risk group than in the low-risk group (Figure 9B).

### 3.7 Relationship between risk score and cancer hallmark signaling pathways

We hypothesize that the distinct immune infiltration microenvironments and drug responsiveness observed among risk groups are based on significantly different signaling pathways and biological differences (Zeng et al., 2021).



Consequently, we initially employed the limma R package to find genes differently expressed amongst various risk groups. Then, using cancer hallmarks as a guide, we ran a GSEA analysis on these differentially expressed genes. According to the findings, the high-risk group had significantly higher levels of several signaling pathways and significantly lower levels of others, including IL6-JAK-STAT3, hypoxia, and glycolysis. In summary, the prognostic model based on inflammatory genes exhibits distinct immune infiltration microenvironments, drug responsiveness, and deregulated signaling pathways, which has important implications for clinical decision-making (Figure 10).

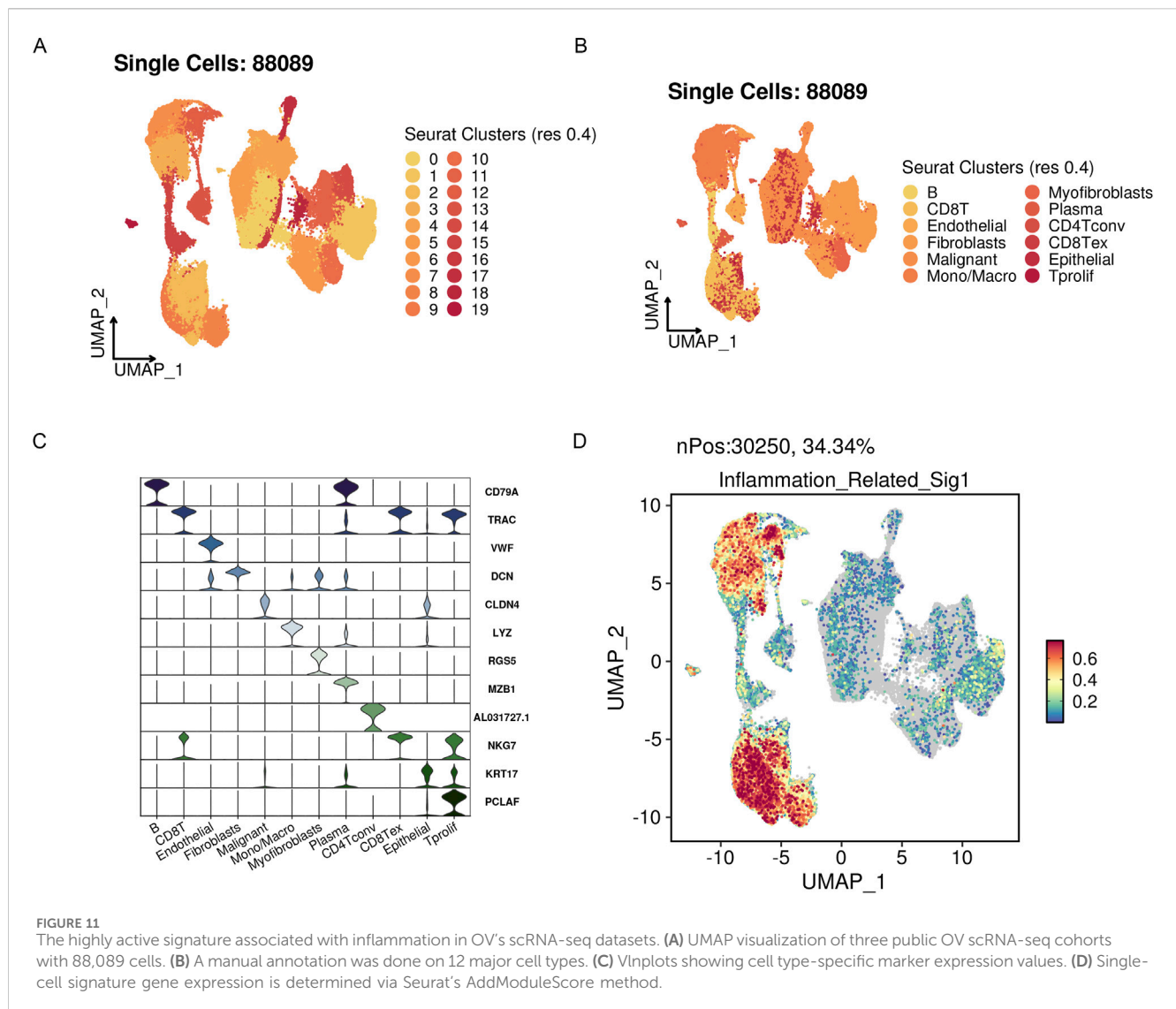
### 3.8 Single-cell level analysis of risk scores

We integrated four single-cell datasets and obtained 88,089 ovarian cancer single cells after quality control, dimensionality reduction, and clustering. With a clustering resolution set to 0.4, we identified 20 clusters (Figures 11A, B). Out of these 20 clusters, we identified 12 cell subpopulations by combining manual annotation methods with SingleR automatic annotation. We then analyzed the risk scores of these 12 cell subpopulations (Figures 11C, D). The results showed that

the prognostic model genes related to inflammation were primarily expressed in immune-related cells, further validating the findings from traditional transcriptome analysis at the single-cell level.

### 3.9 Upregulation of IL6 and TGF $\beta$ 1 in ovarian cancer cells promotes cell proliferation

Following the bioinformatics analysis, the study explored the expression levels of CCL2, IL10, IL6, and TGF $\beta$ 1 in normal ovarian epithelial cells (HOSE) and ovarian cancer cells (SKOV3). The research team used qPCR to detect the mRNA expression levels in cells. Compared with HOSE, CCL2 ( $p = 0.003$ ), IL10 ( $p = 0.003$ ), IL6 ( $p = 0.002$ ), and TGF $\beta$ 1 ( $p = 0.002$ ) were all highly expressed in SKOV3, and the differences were statistically significant (Figure 12A). Subsequently, the study used siRNA IL6 and TGF $\beta$ 1 to transfect the SKOV3 cell line. qPCR results revealed that following transfection, there was a drop in the mRNA expression levels of TGF $\beta$ 1 ( $p = 0.0002$ ) and IL6 ( $p = 0.002$ ) (Figures 12B, C). Further, CCK8 was used to evaluate the proliferation of SKOV3 after transfection. Following the knockdown of IL6 and TGF $\beta$ 1, the capacity of SKOV3 cells to



proliferate decreased in comparison to the siRNA NC group. There was a statistically significant difference ( $p < 0.0001$ ,  $p < 0.0001$ ) (Figure 12D). Finally, we used Western blot to further evaluate the protein expression levels of IL6 and TGF $\beta$ 1 in HOSE and SKOV3 cells. The SKOV3 group had higher levels of TGF $\beta$ 1 ( $p = 0.0001$ ) and IL6 ( $p = 0.004$ ) protein expression compared to HOSE, and these changes were statistically significant (Figures 12E, F).

## 4 Discussion

Chemotherapy resistance in EOC results from various processes, including reduced drug sensitivity, the influence of the tumor microenvironment (TME), changes in the metabolism of tumor cells, interactions between stromal cells and tumor cells, and immune evasion mechanisms (Veneziani et al., 2023). Among these, the TME and immune evasion mechanisms play crucial roles in chemotherapy resistance in EOC. The TME has a major impact on drug resistance,

metastasis, and tumor growth. It comprises stromal cells, immune cells, and blood vessels surrounding tumor cells (Agarwal and Kaye, 2003). In ovarian cancer, the tumor microenvironment can promote drug resistance through various mechanisms (Pujade-Lauraine et al., 2019). For example, tumor-associated macrophages (TAMs) can secrete multiple growth factors and inflammatory cytokines, promoting tumor cell proliferation and survival while reducing their sensitivity to chemotherapy drugs. Immune evasion mechanisms (Khan et al., 2021; Kim et al., 2012): Although tumor cells can employ several defence mechanisms to evade immune system attacks, which is crucial to antitumor processes. For instance, tumor cells can express immune checkpoint molecules to inhibit T-cell activity or secrete immunosuppressive factors to suppress the proliferation and function of immune cells.

Several studies have shown that inflammatory oxidative stress responses play a role in the pathogenesis of several cancers, including colon, stomach, and liver (Bast et al., 1993; Ray et al., 2023). Phagocytes and leukocytes recruited during inflammatory responses can induce DNA damage by producing peroxides and

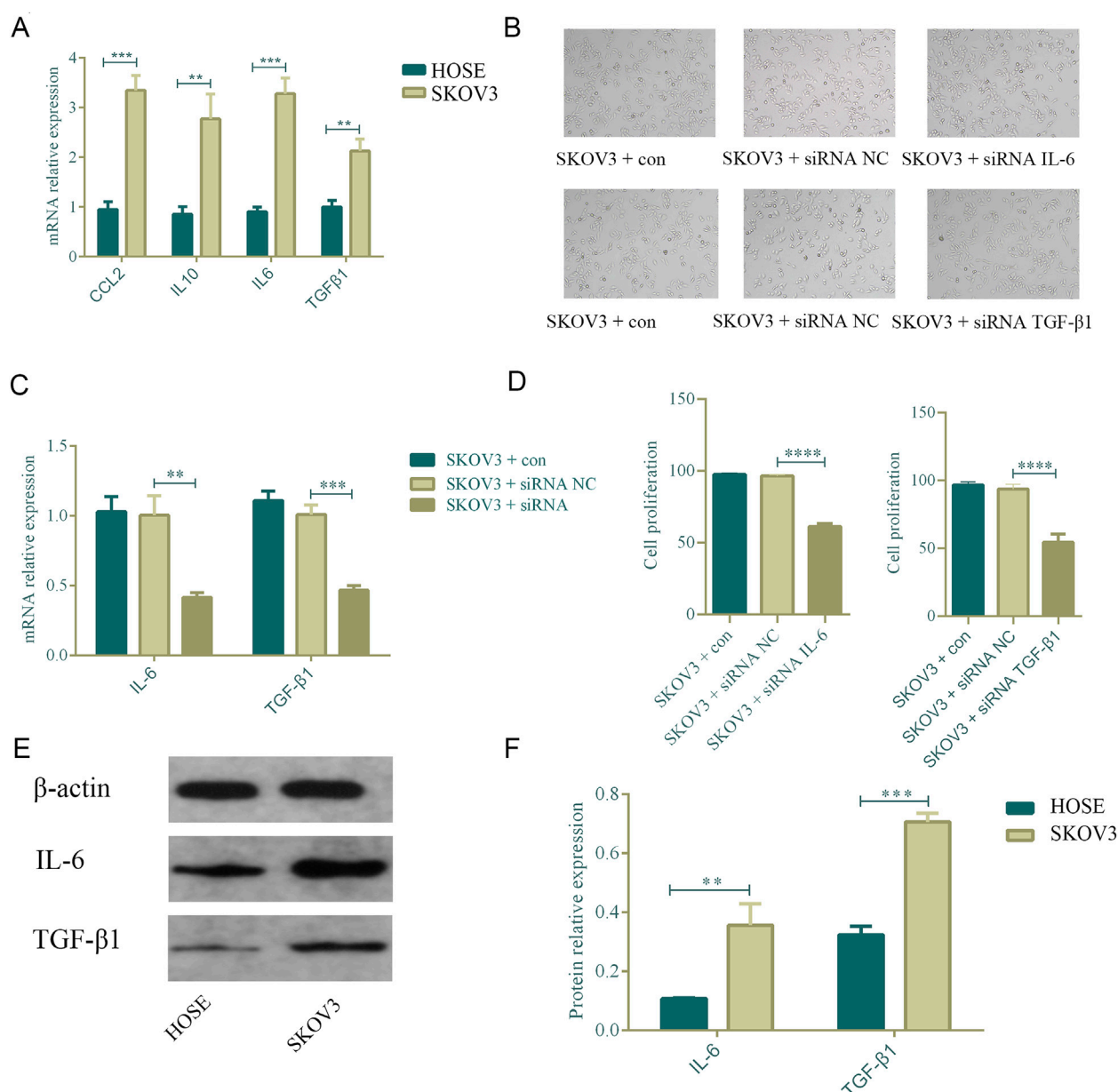


FIGURE 12

Upregulation of IL-6 and TGFβ1 in ovarian cancer cells promotes cell proliferation.  $n = 3$ . \*\* $p < 0.01$ , \* $p < 0.05$ , \*\*\*\* $p < 0.0001$ , \*\*\* $p < 0.001$ . (A) Comparison of the mRNA expression of CCL2, IL6, IL10, and TGFβ1 in normal ovarian cells and ovarian cancer cell SKOV3. (B–D) After knocking down IL6 and TGF-β1, the proliferation ability of ovarian cancer cells decreased. (E,F) Comparison of the protein expression of IL6 and TGFβ1 in normal ovarian cells and ovarian cancer cell SKOV3.

reactive nitrogen species, leading to gene mutations, deletions, and rearrangements, which in turn cause tumorigenesis. The massive secretion of pro-inflammatory factors is a hallmark of chronic inflammatory response processes and plays a vital role in the development of tumors. For example, IL-6 reduces the expression of tumor suppressor genes and DNA repair genes by inducing DNA methylation, thereby promoting tumorigenesis (Macciò and Madeddu, 2013; Torres et al., 2009). IL-6 and its downstream targets are closely related to processes such as cell proliferation and metabolism, suggesting its contribution to tumorigenesis. The expression of the proto-oncogene Kras in the pancreas activates the Stat3/Socs3 signaling pathway, which

relies on IL-6 and its downstream signaling pathways, ultimately promoting pancreatic cancer development. Inflammatory cytokines released during inflammatory responses facilitate tumor metastasis and invasion. Epithelial-mesenchymal transition (EMT) of tumor cells is a crucial process for their metastasis and invasion. TGFβ (Monavarian et al., 2022; Brewer et al., 2003; Vergara et al., 2010) has been reported to promote EMT in tumor cells, while TNFα, IL-6, and IL-1 can also promote tumor ETM by upregulating gene expression related to transcription factors such as NF-κB and STAT3. Additionally, pro-inflammatory factors upregulate chemokine receptors such as CCR1, CCR4, and CXCR7, enabling tumor cells to metastasize to



specific organs. Therefore, inflammatory cytokines and mediators in the tumor microenvironment are essential for tumor cell survival, metastasis, and development. Our research has found that in the high-risk group of EOC (Macciò and Madeddu, 2012; Browning et al., 2018), various signaling pathways, including hypoxia and glycolysis, are significantly upregulated, while pathways such as IL6-JAK-STAT3 are downregulated. These findings further confirm the significance of targeting inflammatory genes to improve drug responses in the immune microenvironment.

Moreover, in the risk model based on inflammatory gene scoring, the high-risk group exhibits higher infiltration of M2 macrophages with pronounced anti-tumor immune responses and a higher degree of dedifferentiation. Additionally, patients in the high-risk group show significantly lower response rates to IPS, IPS-PD1/PD-L1/PD-L2, and IPS-CTLA4 inhibitors compared to the low-risk group. Single-cell transcriptome sequencing data confirms this, with inflammatory prognosis model genes primarily expressed in immune-related cells. In the tumor microenvironment of ovarian cancer, the immune cells comprise innate and adaptive immune cells. B lymphocytes and T lymphocytes are components of the adaptive immune system, with T lymphocytes being particularly prevalent in ovarian tumor tissue and ascites (Fucikova et al., 2022; McMullen et al., 2021). Tumor-infiltrating lymphocytes (TILs) are T cells found in primary/metastatic tumors; tumor-associated lymphocytes (TALs) are T cells seen in ascites (Cummings et al., 2021). Through suppressing immune responses, CD4<sup>+</sup> Tregs preserve immune homeostasis and promote self-tolerance. Tregs inhibit anti-tumor responses in cancers, and their presence in the ovarian cancer tumor microenvironment has been associated with a poor prognosis. The loss of human leukocyte antigen (HLA)-I expression by tumor cells is the primary mechanism of immune evasion in T cell-mediated anti-tumor immunity (Lavoué et al., 2013; Zhang et al., 2022). There is a direct correlation between the frequency of TILs and the quantity of HLA-I-positive tumor cells in various solid tumors, including ovarian cancer. T-cell exhaustion is another method of immune evasion. Studies have revealed that TILs and TALs exhibit elevated expression levels of ICRs for PD-1, CTLA-4, TIM-3, BTLA, and LAG-3.

Tumor macrophages, in addition, comprise a very diverse and heterogeneous cell population that can be divided into type 2 (M2) and classically activated type 1 (M1) macrophages. The microenvironment of ovarian cancer tumors is rich in IL-6, IL-10, and CSF-1, which promotes M2 polarization and the accumulation of M2 macrophages (Truxova et al., 2023). An increase in the proportion of M2 macrophages often indicates a poor prognosis in ovarian cancer. These data imply that tumor macrophages may stimulate tumor growth, invasion, and metastasis via various pathways. The extracellular matrix (ECM) is another component of the immune microenvironment in addition to immune cells (Lin et al., 2022; Khatoun et al., 2022), which affects tumor growth and metastasis. Studies have shown that ECM affects cancer cells via biochemical and biophysical mechanisms in addition to acting as a physical structure and growth factor reservoir. Activating the signaling pathways for ERK, PI3K, and Rac; changing the function of cell cycle regulatory elements; regulating pro- and anti-apoptotic

regulators (Bcl-2 and NF- $\kappa$ B); influencing tumor invasion and migration through the signaling pathways for TGF $\beta$  and RhoA/Rac; influencing tumor cell stemness through the activation of STAT3 and Wnt; and activating the previously mentioned anti-apoptotic and stem cell signaling pathways, in addition to acting as a physical barrier to the delivery of anticancer drugs, which results in chemotherapy resistance (De Nola et al., 2019; Rodriguez et al., 2018; Damei et al., 2023; Majidpoor and Mortezaee, 2021).

Numerous studies have demonstrated the complex interplay between inflammation, the immune microenvironment, and the development and progression of EOC. Our findings imply that by using genes linked to inflammation, a better understanding of the characteristics of the immunological milieu in EOC patients can be achieved. This approach can facilitate the development of targeted immunotherapy drugs for different risk groups, ultimately improving patient prognosis.

Although the study comprehensively analyzed multiple data sets related to ovarian cancer, the sample size is still very limited. Patients of different races, regions, and genetic backgrounds may have different molecular characteristics and immune response mechanisms, and may not fully represent the diversity of ovarian cancer patients worldwide. In addition, bioinformatics tools play an important role in gene expression analysis, mutation detection, and pathway enrichment, but these tools themselves have limitations. Although *in vitro* experiments are an important means to verify gene function and pathway activity, the *in vitro* environment cannot fully simulate the complexity of the *in vivo* environment. Therefore, the results of *in vitro* experiments may not be directly applicable to the *in vivo* environment, and subsequent studies need to be further verified in animals and multi-center clinical samples.

## 5 Conclusion

In conclusion, the construction of an ovarian cancer prognosis model based on inflammatory-related prognostic genes can stratify EOC patients by risk. Developing corresponding drugs based on the characteristics of the immune infiltration environment, drug responsiveness, and signaling pathways of different risk groups is of great significance for clinical decision-making.

## Data availability statement

The original contributions presented in the study are included in the article/supplementary material, further inquiries can be directed to the corresponding authors.

## Author contributions

JW: Conceptualization, Data curation, Writing—original draft, Writing—review and editing. WnZ: Investigation, Methodology, Writing—original draft. XL: Formal Analysis, Writing—original draft. YuW: Data curation, Writing—original draft. WM: Software, Supervision, Writing—original draft. YaW: Methodology, Project administration, Writing—original draft. WiZ: Investigation, Writing—original draft. FW: Formal Analysis, Methodology,

Writing—original draft, WW: Data curation, Methodology, Writing—original draft, Writing—review and editing.

## Funding

The author(s) declare that financial support was received for the research, authorship, and/or publication of this article. The Shanxi Province Natural Science Foundation (grant number 201901D111364), the Shanxi Province Key National Science and Technology Cooperation Projects (project number 202104041101006), and the Natural Science Foundation of Shanxi Province (award number 20210302124591) gave funding for the study.

## References

- Agarwal, R., and Kaye, S. B. (2003). Ovarian cancer: strategies for overcoming resistance to chemotherapy. *Nat. Rev. Cancer* 3 (7), 502–516. doi:10.1038/nrc1123
- Aran, D., Looney, A. P., Liu, L., Wu, E., Fong, V., Hsu, A., et al. (2019). Reference-based analysis of lung single-cell sequencing reveals a transitional profibrotic macrophage. *Nat. Immunol.* 20 (2), 163–172. doi:10.1038/s41590-018-0276-y
- Bast, R. C., Boyer, C. M., Jacobs, I., Xu, F. J., Wu, S., Wiener, J., et al. (1993). Cell growth regulation in epithelial ovarian cancer. *Cancer* 71 (4 Suppl. 1), 1597–1601. doi:10.1002/cncr.2820710426
- Becht, E., Giraldo, N. A., Lacroix, L., Buttard, B., Elarouci, N., Petitprez, F., et al. (2016). Estimating the population abundance of tissue-infiltrating immune and stromal cell populations using gene expression. *Genome Biol.* 17 (1), 218. doi:10.1186/s13059-016-1070-5
- Brewer, M. A., Johnson, K., Follen, M., Gershenson, D., and Bast, R., Jr (2003). Prevention of ovarian cancer: intraepithelial neoplasia. *Clin. Cancer Res.* 9 (1), 20–30.
- Browning, L., Patel, M. R., Horvath, E. B., Tawara, K., and Jorczyk, C. L. (2018). IL-6 and ovarian cancer: inflammatory cytokines in promotion of metastasis. *Cancer Manag. Res.* 10, 6685–6693. doi:10.2147/CMAR.S179189
- Castanza, A. S., Recla, J. M., Eby, D., Thorvaldsdóttir, H., Bult, C. J., and Mesirov, J. P. (2023). Extending support for mouse data in the molecular signatures database (MSigDB). *Nat. Methods* 20 (11), 1619–1620. doi:10.1038/s41592-023-02014-7
- Charoentong, P., Finotello, F., Angelova, M., Mayer, C., Efremova, M., Rieder, D., et al. (2017). Pan-cancer immunogenomic analyses reveal genotype-immunophenotype relationships and predictors of response to checkpoint blockade. *Cell Rep.* 18 (1), 248–262. doi:10.1016/j.celrep.2016.12.019
- Chen, Y., McAndrews, K. M., and Kalluri, R. (2021). Clinical and therapeutic relevance of cancer-associated fibroblasts. *Nat. Rev. Clin. Oncol.* 18 (12), 792–804. doi:10.1038/s41571-021-00546-5
- Cummings, M., Freer, C., and Orsi, N. M. (2021). Targeting the tumour microenvironment in platinum-resistant ovarian cancer. *Semin. Cancer Biol.* 77, 3–28. doi:10.1016/j.semcancer.2021.02.007
- Damei, I., Trickovic, T., Mami-Chouaib, F., and Corgnac, S. (2023). Tumor-resident memory T cells as a biomarker of the response to cancer immunotherapy. *Front. Immunol.* 6 (20), 14. doi:10.3389/fimmu.2023.1205984
- De Nola, R., Menga, A., Castegna, A., Loizzi, V., Ranieri, G., Cicinelli, E., et al. (2019). The crowded crosstalk between cancer cells and stromal microenvironment in gynecological malignancies: biological pathways and therapeutic implication. *Int. J. Mol. Sci.* 20 (10), 2401. doi:10.3390/ijms20102401
- Ding, H., Hu, B., and Guo, R. (2024). Comprehensive analysis of single cell and bulk data develops a promising prognostic signature for improving immunotherapy responses in ovarian cancer. *PLoS One* 19 (2), e0298125. doi:10.1371/journal.pone.0298125
- Finotello, F., Mayer, C., Plattner, C., Laschober, G., Rieder, D., Hackl, H., et al. (2019). Molecular and pharmacological modulators of the tumor immune contexture revealed by deconvolution of RNA-seq data. *Genome Med.* 11 (1), 34. doi:10.1186/s13073-019-0638-6
- Fucikova, J., Palova-Jelinkova, L., Klapp, V., Holicek, P., Lanickova, T., Kasikova, L., et al. (2022). Immunological control of ovarian carcinoma by chemotherapy and targeted anticancer agents. *Trends Cancer* 8 (5), 426–444. doi:10.1016/j.trecan.2022.01.010
- Galbo, P. M., Zang, X., and Zheng, D. (2021). Molecular features of cancer-associated fibroblast subtypes and their implication on cancer pathogenesis, prognosis, and immunotherapy resistance. *Clin. Cancer Res.* 27 (9), 2636–2647. doi:10.1158/1078-0432.CCR-20-4226
- Gul, S., Pang, J., Yuan, H., Chen, Y., Yu, Q., Wang, H., et al. (2023). Stemness signature and targeted therapeutic drugs identification for Triple Negative Breast Cancer. *Sci. Data* 10 (1), 815. doi:10.1038/s41597-023-02709-8
- Haas, C. B., Lovász, M., Braganhol, E., Pacher, P., and Haskó, G. (2021). Ectonucleotidases in inflammation, immunity, and cancer. *J. Immunol.* 206 (9), 1983–1990. doi:10.4049/jimmunol.2001342
- Hänzelmann, S., Castelo, R., and Guinney, J. (2013). GSEA: gene set variation analysis for microarray and RNA-seq data. *BMC Bioinforma.* 14, 7. doi:10.1186/1471-2105-14-7
- Hao, Y., Stuart, T., Kowalski, M. H., Choudhary, S., Hoffman, P., Hartman, A., et al. (2024). Dictionary learning for integrative, multimodal and scalable single-cell analysis. *Nat. Biotechnol.* 42 (2), 293–304. doi:10.1038/s41587-023-01767-y
- Jiang, J., Chen, Z., Wang, H., Wang, Y., Zheng, J., Guo, Y., et al. (2023). Screening and identification of a prognostic model of ovarian cancer by combination of transcriptomic and proteomic data. *Biomolecules* 13 (4), 685. doi:10.3390/biom13040685
- Kennel, K. B., Bozlar, M., De Valk, A. F., and Greten, F. R. (2023). Cancer-associated fibroblasts in inflammation and antitumor immunity. *Clin. Cancer Res.* 29 (6), 1009–1016. doi:10.1158/1078-0432.CCR-22-1031
- Khan, M. A., Vikramdeo, K. S., Sudan, S. K., Singh, S., Wilhite, A., Dasgupta, S., et al. (2021). Platinum-resistant ovarian cancer: from drug resistance mechanisms to liquid biopsy-based biomarkers for disease management. *Semin. Cancer Biol.* 77, 99–109. doi:10.1016/j.semcancer.2021.08.005
- Khattoon, E., Parama, D., Kumar, A., Alqahtani, M. S., Abbas, M., Girisa, S., et al. (2022). Targeting PD-1/PD-L1 axis as new horizon for ovarian cancer therapy. *Life Sci.* 306, 120827. doi:10.1016/j.lfs.2022.120827
- Kim, A., Ueda, Y., Naka, T., and Enomoto, T. (2012). Therapeutic strategies in epithelial ovarian cancer. *J. Exp. Clin. Cancer Res.* 31 (1), 14. doi:10.1186/1756-9966-31-14
- Konstantinopoulos, P. A., and Matulonis, U. A. (2023). Clinical and translational advances in ovarian cancer therapy. *Nat. Cancer* 4 (9), 1239–1257. doi:10.1038/s43018-023-00617-9
- Langfelder, P., and Horvath, S. (2008). WGCNA: an R package for weighted correlation network analysis. *BMC Bioinforma.* 9, 559. doi:10.1186/1471-2105-9-559
- Lavie, D., Ben-Shmuel, A., Erez, N., and Scherz-Shouval, R. (2022). Cancer-associated fibroblasts in the single-cell era. *Nat. Cancer* 3 (7), 793–807. doi:10.1038/s43018-022-00411-z
- Lavoué, V., Thédrez, A., Levêque, J., Foucher, F., Henno, S., Jauffret, V., et al. (2013). Immunity of human epithelial ovarian carcinoma: the paradigm of immune suppression in cancer. *J. Transl. Med.* 11, 147. doi:10.1186/1479-5876-11-147
- Lee, A., Yang, X., Tyrer, J., Gentry-Maharaj, A., Ryan, A., Mavaddat, N., et al. (2022). Comprehensive epithelial tubo-ovarian cancer risk prediction model incorporating genetic and epidemiological risk factors. *J. Med. Genet.* 59 (7), 632–643. doi:10.1136/jmedgenet-2021-107904
- Li, B., Severson, E., Pignon, J. C., Zhao, H., Li, T., Novak, J., et al. (2016). Comprehensive analyses of tumor immunity: implications for cancer immunotherapy. *Genome Biol.* 17 (1), 174. doi:10.1186/s13059-016-1028-7
- Lin, Y., Zhou, X., Ni, Y., Zhao, X., and Liang, X. (2022). Metabolic reprogramming of the tumor immune microenvironment in ovarian cancer: a novel orientation for immunotherapy. *Front. Immunol.* 13, 1030831. doi:10.3389/fimmu.2022.1030831

## Conflict of interest

The authors declare that the research was conducted in the absence of any commercial or financial relationships that could be construed as a potential conflict of interest.

## Publisher's note

All claims expressed in this article are solely those of the authors and do not necessarily represent those of their affiliated organizations, or those of the publisher, the editors and the reviewers. Any product that may be evaluated in this article, or claim that may be made by its manufacturer, is not guaranteed or endorsed by the publisher.

- Liu, C., Huang, X., and Su, H. (2022). The role of the inflammasome and its related pathways in ovarian cancer. *Clin. Transl. Oncol.* 24 (8), 1470–1477. doi:10.1007/s12094-022-02805-y
- Macciò, A., and Madeddu, C. (2012). Inflammation and ovarian cancer. *Cytokine* 58 (2), 133–147. doi:10.1016/j.cyto.2012.01.015
- Macciò, A., and Madeddu, C. (2013). The role of interleukin-6 in the evolution of ovarian cancer: clinical and prognostic implications--a review. *J. Mol. Med. Berl.* 91 (12), 1355–1368. doi:10.1007/s00109-013-1080-7
- Maeser, D., Gruener, R. F., and Huang, R. S. (2021). oncoPredict: an R package for predicting *in vivo* or cancer patient drug response and biomarkers from cell line screening data. *Brief. Bioinform.* 22 (6), bbab260. doi:10.1093/bib/bbab260
- Majidpoor, J., and Mortezaee, K. (2021). The efficacy of PD-1/PD-L1 blockade in cold cancers and future perspectives. *Clin. Immunol.* 5 (226), 108707. doi:10.1016/j.clim.2021.108707
- Mao, X., Xu, J., Wang, W., Liang, C., Hua, J., Liu, J., et al. (2021). Crosstalk between cancer-associated fibroblasts and immune cells in the tumor microenvironment: new findings and future perspectives. *Mol. Cancer* 20 (1), 131. doi:10.1186/s12943-021-01428-1
- Marchetti, C., De Felice, F., Romito, A., Iacobelli, V., Sassu, C. M., Corrado, G., et al. (2021). Chemotherapy resistance in epithelial ovarian cancer: mechanisms and emerging treatments. *Semin. Cancer Biol.* 77, 144–166. doi:10.1016/j.semcancer.2021.08.011
- McMullen, M., Madariaga, A., and Lheureux, S. (2021). New approaches for targeting platinum-resistant ovarian cancer. *Semin. Cancer Biol.* 77, 167–181. doi:10.1016/j.semcancer.2020.08.013
- Monavarian, M., Elhaw, A. T., Tang, P. W., Javed, Z., Shonibare, Z., Scalise, C. B., et al. (2022). Emerging perspectives on growth factor metabolic relationships in the ovarian cancer ascites environment. *Semin. Cancer Biol.* 86 (Pt 2), 709–719. doi:10.1016/j.semcancer.2022.03.004
- Newman, A. M., Liu, C. L., Green, M. R., Gentles, A. J., Feng, W., Xu, Y., et al. (2015). Robust enumeration of cell subsets from tissue expression profiles. *Nat. Methods* 12 (5), 453–457. doi:10.1038/nmeth.3337
- Porter, R. L., and Matulonis, U. A. (2023). Mirvetuximab soravtansine for platinum-resistant epithelial ovarian cancer. *Expert Rev. Anticancer Ther.* 23 (8), 783–796. doi:10.1080/14737140.2023.2236793
- Pujade-Lauraine, E., Banerjee, S., and Pignata, S. (2019). Management of platinum-resistant, relapsed epithelial ovarian cancer and new drug perspectives. *J. Clin. Oncol.* 37 (27), 2437–2448. doi:10.1200/JCO.19.00194
- Racle, J., de Jonge, K., Baumgaertner, P., Speiser, D. E., and Gfeller, D. (2017). Simultaneous enumeration of cancer and immune cell types from bulk tumor gene expression data. *Elife* 6, e26476. doi:10.7554/eLife.26476
- Ray, I., Michael, A., Meira, L. B., and Ellis, P. E. (2023). The role of cytokines in epithelial-mesenchymal transition in gynaecological cancers: a systematic review. *Cells* 12 (3), 416. doi:10.3390/cells12030416
- Ritchie, M. E., Phipson, B., Wu, D., Hu, Y., Law, C. W., Shi, W., et al. (2015). Limma powers differential expression analyses for RNA-sequencing and microarray studies. *Nucleic Acids Res.* 43 (7), e47. doi:10.1093/nar/gkv007
- Rodriguez, G. M., Galpin, K. J. C., McCloskey, C. W., and Vanderhyden, B. C. (2018). The tumor microenvironment of epithelial ovarian cancer and its influence on response to immunotherapy. *Cancers (Basel)* 10 (8), 242. doi:10.3390/cancers10080242
- Torres, M. P., Ponnusamy, M. P., Lakshmanan, I., and Batra, S. K. (2009). Immunopathogenesis of ovarian cancer. *Minerva Med.* 100 (5), 385–400.
- Truxova, I., Cibula, D., Spisek, R., and Fucikova, J. (2023). Targeting tumor-associated macrophages for successful immunotherapy of ovarian carcinoma. *J. Immunother. Cancer* 11 (2), e005968. doi:10.1136/jitc-2022-005968
- Venakteshaiah, S. U., and Kumar, K. H. (2021). Inflammation and cancer. *Endocr. Metab. Immune Disord. Drug Targets* 21 (2), 193–194. doi:10.2174/187153032102210105105653
- Veneziani, A. C., Gonzalez-Ochoa, E., Alqaisi, H., Madariaga, A., Bhat, G., Rouzbahman, M., et al. (2023). Heterogeneity and treatment landscape of ovarian carcinoma. *Nat. Rev. Clin. Oncol.* 20 (12), 820–842. doi:10.1038/s41571-023-00819-1
- Vergara, D., Merlot, B., Lucot, J. P., Collinet, P., Vinatier, D., Fournier, I., et al. (2010). Epithelial-mesenchymal transition in ovarian cancer. *Cancer Lett.* 291 (1), 59–66. doi:10.1016/j.canlet.2009.09.017
- Wilkerson, M. D., and Hayes, D. N. (2010). ConsensusClusterPlus: a class discovery tool with confidence assessments and item tracking. *Bioinformatics* 26 (12), 1572–1573. doi:10.1093/bioinformatics/btq170
- Wu, F., Yang, J., Liu, J., Wang, Y., Mu, J., Zeng, Q., et al. (2021a). Signaling pathways in cancer-associated fibroblasts and targeted therapy for cancer. *Signal Transduct. Target Ther.* 6 (1), 218. doi:10.1038/s41392-021-00641-0
- Wu, T., Hu, E., Xu, S., Chen, M., Guo, P., Dai, Z., et al. (2021b). clusterProfiler 4.0: a universal enrichment tool for interpreting omics data. *Innov. (Camb)* 2 (3), 100141. doi:10.1016/j.xinn.2021.100141
- Yang, B., Yin, S., Zhou, Z., Huang, L., and Xi, M. (2023). Inflammation control and tumor growth inhibition of ovarian cancer by targeting adhesion molecules of E-selectin. *Cancers (Basel)*, 15(7):2136, doi:10.3390/cancers15072136
- Ye, L., Wang, X., and Li, B. (2021). Expression profile of epithelial-mesenchymal transition-related genes as a prognostic biomarker for endometrial cancer. *J. Cancer* 12 (21), 6484–6496. doi:10.7150/jca.62729
- Yu, S., Yang, R., Xu, T., Li, X., Wu, S., and Zhang, J. (2022). Cancer-associated fibroblasts-derived FMO2 as a biomarker of macrophage infiltration and prognosis in epithelial ovarian cancer. *Gynecol. Oncol.* 167 (2), 342–353. doi:10.1016/j.ygyno.2022.09.003
- Zeng, D., Ye, Z., Shen, R., Yu, G., Wu, J., Xiong, Y., et al. (2021). IOBR: multi-omics immuno-oncology biological research to decode tumor microenvironment and signatures. *Front. Immunol.* 12, 687975. doi:10.3389/fimmu.2021.687975
- Zhang, Y., Cui, Q., Xu, M., Liu, D., Yao, S., and Chen, M. (2022). Current advances in PD-1/PD-L1 blockade in recurrent epithelial ovarian cancer. *Front. Immunol.* 13, 901772. doi:10.3389/fimmu.2022.901772
- Zhao, M., Qiu, S., Wu, X., Miao, P., Jiang, Z., Zhu, T., et al. (2023). Efficacy and safety of niraparib as first-line maintenance treatment for patients with advanced ovarian cancer: real-world data from a multicenter study in China. *Target Oncol.* 18 (6), 869–883. doi:10.1007/s11523-023-00999-x
- Zheng, M. J., Li, X., Hu, Y. X., Dong, H., Gou, R., Nie, X., et al. (2019). Identification of molecular marker associated with ovarian cancer prognosis using bioinformatics analysis and experiments. *J. Cell Physiol.* 234 (7), 11023–11036. doi:10.1002/jcp.27926



## OPEN ACCESS

## EDITED BY

Jianbin Bi,  
The First Hospital of China Medical University,  
China

## REVIEWED BY

Guo Songyi,  
China Medical University, China  
Dong Wu,  
Chongqing Medical University, China  
Lei Lee,  
Wuhan University, China

## \*CORRESPONDENCE

Yanping Pang  
✉ 13916075904@163.com

RECEIVED 15 December 2024

ACCEPTED 20 January 2025

PUBLISHED 06 February 2025

## CITATION

Zhang B and Pang Y (2025) Exploring the genetic profiles linked to senescence in thyroid tumors: insights on predicting disease progression and immune responses.  
*Front. Oncol.* 15:1545656.  
doi: 10.3389/fonc.2025.1545656

## COPYRIGHT

© 2025 Zhang and Pang. This is an open-access article distributed under the terms of the [Creative Commons Attribution License \(CC BY\)](https://creativecommons.org/licenses/by/4.0/). The use, distribution or reproduction in other forums is permitted, provided the original author(s) and the copyright owner(s) are credited and that the original publication in this journal is cited, in accordance with accepted academic practice. No use, distribution or reproduction is permitted which does not comply with these terms.

# Exploring the genetic profiles linked to senescence in thyroid tumors: insights on predicting disease progression and immune responses

Baoliang Zhang<sup>1</sup> and Yanping Pang<sup>2\*</sup>

<sup>1</sup>Department of Emergency, Tongji Hospital of Tongji University, Shanghai, China, <sup>2</sup>Department of Ultrasound, Tongji Hospital of Tongji University, Shanghai, China

**Introduction:** Thyroid cancer (THCA) is the most common endocrine tumor. Research on Cell Senescence Associated Genes (CSAGs), which impact many cancers, remains limited in the THCA field.

**Methods:** In this study, we downloaded THCA sample data from several public databases and selected a set of CSAGs for subsequent analysis. Differential expression genes (DEGs) obtained through differential analysis were intersected with prognostic genes identified by Cox regression analysis to explore the correlation among these crossed genes. We constructed a prognostic model using the Least Absolute Shrinkage and Selection Operator (LASSO) algorithm and verified its efficacy. Kaplan-Meier survival curves were plotted, and Receiver Operating Characteristic (ROC) curves rigorously confirmed the accuracy of model predictions.

**Results:** To evaluate the predictive power of prognostic models across different phenotypic traits, we performed survival analysis, Gene Set Enrichment Analysis (GSEA), and immune-related differential analysis. Differences in tumor mutation burden (TMB) and treatment response between high-risk and low-risk patient groups were also analyzed. Finally, the predictive effect of our model on immunotherapy response was validated, showing promising results for THCA patients.

**Discussion:** Our study enhances the understanding of THCA cell senescence and provides new therapeutic insights. The proposed model not only accurately predicts patient survival but also reveals factors related to immunotherapy response, offering new perspectives for personalized medicine.

## KEYWORDS

thyroid cancer, cellular senescence, least absolute shrinkage and selection operator, tumor immune microenvironment, prognosis



# 1 Introduction

Accounting for 3–4% of all cancers, thyroid cancer (abbreviated as THCA or TC) holds the position of being the endocrine tumor that occurs most frequently (1). Over the past few decades, there has been a consistent rise in its incidence, with some studies suggesting this may be related to the rising incidence of differentiated thyroid cancer (DTC) (2, 3). Compared to 40 years ago, the detection rate of THCA has increased by more than 400%, with the rise in diagnoses of small, indolent papillary thyroid carcinomas (PTCs) likely contributing to the overall increase in THCA incidence (4). Globally, the incidence of THCA is influenced by geographic location, with higher rates observed in high-income countries and certain island nations (5). The origin of THCA can be traced back to either the follicular epithelial cells or the parafollicular cells, alternatively referred to as C cells, within the thyroid gland. Based on the tumor's origin and its level of differentiation, it encompasses various subtypes: PTC, which is the most prevalent, follicular thyroid carcinoma (FTC), thyroid oncocyctic carcinoma (OCA, previously termed Hürthle cell thyroid carcinoma), differentiated high-grade thyroid cancer (DHGTC), poorly differentiated thyroid carcinoma (PDTC), anaplastic thyroid cancer (ATC), and medullary thyroid carcinoma (MTC). Clinically, PTC, FTC (6), OCA, and DHGTC are collectively referred to as DTC, which accounts for more than 90% of all THCA cases, making it the most common subtype of thyroid cancer (7). MTC accounts for only 1–2% of THCA cases (5). DHGTC, PDTC, and ATC are all of follicular epithelial cell origin, while MTC originates from parafollicular cells (7). Due to the asymptomatic nature of THCA, it is difficult to detect early in clinical practice. Approximately half of cases are not suspected or detected until other diagnostic procedures or thyroid-related surgeries are performed (8). Despite the generally favorable prognosis for the majority of THCA patients, with certain studies reporting a 5-year relative survival rate surpassing 90% for those with localized disease, 10–15% of THCA patients will experience disease recurrence. Approximately 5% of patients will have distant metastasis to organs such as in the instance of the lungs and bones, and occasionally, cancer-specific mortality may occur (9). Furthermore, not all THCA patients have a good prognosis. The survival rate for patients with distant metastasis varies by pathological subtype (10). The survival rate after 10 years stands at roughly 45% for patients with metastatic DTC, whereas for those with MTC, it drops to approximately 20%. ATC has an exceptionally grim prognosis, characterized by a median survival duration of merely 3 to 6 months (11). Currently, the primary options for treating THCA include thyroid surgery, therapy with radioactive iodine, and TSH suppression. Surgery remains the preferred initial treatment when criteria for resection are met. Postoperative radioactive iodine therapy or observation as standard care is effective for most DTC patients, however, for a specific group of patients, its effectiveness is constrained. For progressive or symptomatic DTC and MTC patients, although existing targeted therapies can extend progression-free survival (PFS), they do not provide a cure (12). Conventional treatments such as radioactive iodine ablation and chemotherapy are ineffective for highly invasive and fatal ATC (9). Additionally, studies have suggested that PD-L1-targeted immunotherapy may prolong disease-free survival (DFS) and could

potentially become an effective treatment option for advanced THCA (13). In summary, early diagnosis and effective treatment of THCA remain significant challenges, necessitating continued exploration of new therapeutic targets.

Cellular senescence-associated genes (CSAG) refer to a cell state triggered by various physiological processes. Among the various factors contributing to this state are DNA damage, malfunctioning telomeres, the activation of oncogenes, mitochondrial dysfunction, as well as oxidative stress, and others (14). Senescent cells exhibit numerous characteristics, such as alterations in chromatin and secretory proteins, increased expression of senescence markers, immune evasion (15), loss of proliferative capacity, and secretion of inflammatory cytokines, chemokines, and growth factors (16). The intricate secretory proteins produced during the process are collectively referred to as the senescence-associated secretory phenotype (SASP). The International CSAG Association has proposed a consensus defining the phenotype of senescent cells based on four key features: cell cycle withdrawal, macromolecular damage, SASP, and metabolic dysregulation (17). Cell cycle inhibitors (CKIs) (14), p27KIP1 (18), p21CIP1 (CDKN1A), and Cyclin-dependent kinase inhibitor 2A (p16INK4A, CDKN2A) can participate in the CSAG process by regulating the cell cycle. For instance, upregulation of CDKN1A and CDKN2A can lead to hypophosphorylation of the retinoblastoma protein, thereby inhibiting E2F transcriptional activation and causing cell cycle arrest (19). Macromolecular damage, such as DNA, protein, and lipid damage, can also contribute to the CSAG process through activation of the tumor suppressor pathways involving p53/p21CIP1 and p16INK4A/RB (20). SASP is a complex secretory process that includes hundreds of different proteins and non-protein molecules. The full composition of SASP remains incompletely defined, but common molecules include interleukins such as IL-1 $\alpha$ , IL-1 $\beta$ , IL-6, chemokines such as CXCR2 and CCL2, and growth factors like IGFBP7 (21). Studies indicate that AMP-activated protein kinase (AMPK), a kinase activated by the ratios of AMP: ATP and ADP: ATP during the CSAG process, has a function in modulating the cellular cycle (17). The physiological processes associated with CSAG play crucial roles in normal human development and are closely related to biological processes such as cancer therapy and tissue repair (16, 22). In cancer, the SASP secreted during CSAG can alter the tumor microenvironment (TME), induce immune surveillance of precancerous cells, and suppress cancer progression (14, 23). However, the persistent DNA damage and inflammatory factors generated by the senescence process may also promote tumor development and angiogenesis (24). In THCA, studies have indicated that the B-RafV600E mutation may participate in the senescence process of PTC cells by upregulating dual-specificity phosphatases (DUSPs) (25). Nevertheless, the role of CSAG in THCA remains insufficiently explored, different subtypes of thyroid cancer may respond differently to CSAG, highlighting the need for further investigation into its specific applications and interpretations in thyroid cancer research, as well as the correlation between CSAG and gender.

In this study, we not only downloaded THCA sample data from multiple public databases, but also selected a set of cellular senescence-

associated genes (CSAGs) for subsequent analysis. Differentially expressed genes (DEGs) obtained through differential expression analysis were intersected with prognostic genes identified via Cox regression analysis, and the correlation among the intersecting genes was further investigated. Based on this, we employed the Least Absolute Shrinkage and Selection Operator (LASSO) algorithm both for finalizing the selection of model genes and for constructing the prognosis model. The precision of the predictions made by the model was rigorously confirmed using both Kaplan-Meier (KM) survival curves and Receiver Operating Characteristic (ROC) analysis. To evaluate the predictive capability of the prognostic model across different phenotypic characteristics, we subsequently conducted a thorough analysis comparing the risk groups. Besides performing survival analysis and Gene Set Enrichment Analysis (GSEA), we also carried out immune-related differential analyses that centered on the expression patterns of immune regulators, tumor-associated immune cells, and immune checkpoints. We examined variations in tumor mutational burden (TMB) and treatment responses between patient groups categorized as high- and low-risk. Additionally, we performed stratified KM survival analysis based on risk scores, giving special attention to immune checkpoints and TMB.

## 2 Material and methods

### 2.1 Data acquisition and preprocessing

Initially, we utilized the R package named “TCGAbiolinks” to obtain RNA sequencing data, comprehensive clinical details, and mutation information pertaining to THCA patients, sourced from the Cancer Genome Atlas (TCGA) database, which can be accessed at <https://portal.gdc.cancer.gov>. For the aim of facilitating better gene differential expression analysis between samples, the transcriptomic data was transformed into Transcripts Per Million (TPM) format. By employing the “GEOquery” package, we acquired transcriptomic data along with the corresponding clinical information for THCA patients (GSE84437) from the Gene Expression Omnibus (GEO) database, accessible at <http://www.ncbi.nlm.nih.gov/geo>. The cohort that underwent immunotherapy, known as IMvigor210, was downloaded through the R package “IMvigor210CoreBiologies”. The list of age-related genes used in this paper were all obtained from previous literature summary (Supplementary Table 1). In addition, we included CSAG in the list and extracted intracellular gene expression levels from TCGA samples. The open-source databases involved in this study have no restrictions on data acquisition and use, and no additional ethical approval is required. All analytical procedures in this study strictly adhere to ethical guidelines.

### 2.2 Constructing and validating the predictive model for prognosis

Differential expression analysis of CSAG between normal and tumor tissues was conducted using the “limma” package, with the results of the DEGs being graphically represented through a volcano

plot. Our criterion for DEGs selection was set as  $|\log FC| > 0.585$ , and the adjusted p value was  $< 0.05$ . Subsequently, we applied univariate Cox regression analysis to ascertain CSAGs that hold prognostic importance, and the resulting prognostic genes were displayed in a forest plot. A Venn diagram was utilized to illustrate the overlapping DEGs and prognostic genes, while an analysis was performed to investigate the relationships among these prognostic genes that were differentially expressed. Outcomes of this correlation analysis were displayed in a circular correlation plot. Afterwards, the TCGA cohort formed the training dataset, and the GSE84437 cohort was assigned for validation. LASSO is a regression analysis method, which can simplify the model and improve the prediction accuracy by introducing a penalty term to achieve both variable selection and model parameter estimation. In bioinformatics, the advantage of LASSO is that it can effectively process high-dimensional data to screen out features or genes that have a significant impact on response variables, so as to assist in disease diagnosis, drug target discovery and other studies. The parameter standard for LASSO is “cvfit\$lambda.min”. Utilizing the LASSO algorithm, a prognostic prediction model was built within the training set. The source of gene list input in LASSO model was differentially expressed prognostic genes. The model’s predictive outcomes were quantified as risk scores, which were derived by summing up the products of the levels of expression for each gene multiplied by its respective coefficient, as the formula presented below:

$$\text{Risk score} = \sum_{i=1}^n [\text{Exp}_{\text{gene}_i} * \beta_i]$$

The level of expression for each gene in the model is denoted as  $\text{Exp}_{\text{gene}_i}$ , with  $\beta_i$  representing the gene coefficient. The selection of model genes is determined by the optimal  $\lambda$  value, and the variation of coefficients across different genes with respect to  $\log(\lambda)$  is illustrated in the coefficient distribution plot. The  $\lambda$  value that yields the lowest partial likelihood deviance is taken as the optimal one. Subsequently, we perform the following analyses on both training and validation datasets, applying the same procedure to two independent cohorts. Within each cohort, using the median risk score as a benchmark, patients are grouped into high-risk and low-risk categories. The “survival” and “survminer” packages were then used for KM analysis to visually show the difference in overall survival (OS) of different risk groups over time. In order to assess the model’s predictive capabilities, the survival probabilities for 1-year, 3-year, and 5-year durations are depicted via ROC curves, and the model’s prognostic accuracy is assessed using the area under the curve (AUC) as a metric.  $\text{AUC} > 0.5$  proves that the model has good testing efficiency.

### 2.3 Prognostic and enrichment analysis for different risk groups

We standardized the expression profiles of model genes and compared them between the two groups across both datasets. A risk curve was generated by ordering individual samples in ascending order of their risk scores, and the variation in survival time as the risk

score increased was analyzed. Furthermore, within the TCGA cohort, after stratifying the patients into either Stage I-II or Stage III-IV, we performed survival analysis on them. To assess prognostic differences across various tumor stages, we utilized KM curves to compare high-risk and low-risk groups, in order to explore the impact of tumor stage on the model's predictive outcomes.

Subsequently, using pathways obtained from the MEDICUS module of the Kyoto Encyclopedia of Genes and Genomes (KEGG) database, we applied GSEA to identify functional pathways with differential distribution between the two groups and subsequently represented the findings visually. Functional pathways that exhibited an enrichment score above 0 were interpreted as having gene expression upregulated in the high-risk cohort, whereas those showing a score below 0 implied upregulation in the low-risk cohort.

## 2.4 Analysis of differential immune features

We conducted an immune regulatory expression profiling analysis, including five categories of immune regulatory molecules: chemokines, growth factors and regulators, soluble or shed receptors/ligands, and interleukins. Heatmaps were utilized to visualize the disparities in expression between the high-risk and low-risk groups. The following six algorithms utilized for TME deconvolution: CIBERSORT, CIBERSORT ABS, EPIC, MCP-counter, quanTIseq, TIMER, and xCell, were implemented using R packages. Utilizing these algorithms, we conducted a thorough examination of the relationships between the model genes and the degrees of immune cell infiltration, and then portrayed the findings of these associations through various heatmaps.

Additionally, we carried out a comprehensive examination of immune checkpoints to explore potential immune therapy targets relevant to THCA. The gene expression levels of 31 selected immune checkpoints were compared between the two patient groups. Within each group, patients were categorized into two subgroups, based on whether their expression values for the immune checkpoint molecules exceeded or fell below the median value, followed by KM survival analysis to assess the survival probability differences across the four subgroups. This procedure was performed independently for each immune checkpoint molecule, resulting in 31 survival curve plots.

## 2.5 Mutation analysis and survival analysis of TMB

By sourcing mutation data from the TCGA database, we conducted computations and comparisons of the TMB between two patient groups, and subsequently visualized the disparities through the use of box plots. To gain a deeper insight into how risk scores correlate with TMB, we carried out a Pearson correlation analysis and developed scatter plots to provide a clear visual representation of the findings. Additionally, we divided the TCGA samples into two subsets using the median TMB value as the threshold: high-TMB (H-TMB) and low-TMB (L-TMB). KM survival curves were then plotted to clearly illustrate the survival

differences between these two groups. In order to determine the joint impact of TMB and risk scores on survival outcomes, patients were divided into four distinct categories, each representing a unique combination of their TMB and risk level: the high TMB-high risk group, the high TMB-low risk group, the low TMB-high risk group, and the low TMB-low risk group. Survival differences among these four subgroups were also visualized using KM survival curves.

## 2.6 Predictive role of the model in immunotherapy response

We obtained immune phenotype score (IPS) data for TCGA samples from The Cancer Immunome Atlas (TCIA, <https://tcia.at/>). By examining patient responses to anti-CTLA-4 and anti-PD-1 antibodies, the IPS was categorized into four distinct groups: those negative for both anti-CTLA-4 and anti-PD-1 (ips\_ctla4\_neg\_pd1\_neg), negative for anti-CTLA-4 but positive for anti-PD-1 (ips\_ctla4\_neg\_pd1\_pos), positive for anti-CTLA-4 but negative for anti-PD-1 (ips\_ctla4\_pos\_pd1\_neg), and positive for both (ips\_ctla4\_pos\_pd1\_pos). Following this classification, a comparative analysis was undertaken to explore the varying responses of high-risk and low-risk groups to different immune checkpoint inhibitor treatment strategies. A violin plot was generated to visualize these results. Next, we validated the robustness of the model prognostic predictions using the IMvigor210 immunotherapy cohort using the "IMvigor210CoreBiologies" packages. After applying the prognostic model to the IMvigor210 cohort, utilizing the median risk score as a cutoff, the samples were categorized into two distinct groups: those belonging to the high-risk category and those in the low-risk category. A survival analysis was then carried out for these groups, with the results being graphically represented using KM survival curves. The outcomes of chemotherapy were classified into four categories: complete response (CR), partial response (PR), progressive disease (PD), and stable disease (SD). These categories were then simplified into two binary groups: CR/PR versus SD/PD. Within this setup, a comparison was made of the risk scores belonging to the two patient groups. Additionally, we selected 48 immune checkpoint molecules for further investigation. The IMvigor210 cohort's patients, within each risk group, were additionally subclassified into high and low subgroups, according to the expression levels exhibited by the chosen checkpoint molecules. Thus, for each immune checkpoint molecule, patients were grouped into four subgroups. To identify immune checkpoints that are significantly correlated with survival outcomes, we conducted another KM survival curve analysis to assess the prognostic differences among these subgroups.

## 2.7 Statistical analysis

Depending on the distribution of the data, we evaluated the relationships among variables by utilizing either Pearson or Spearman correlation coefficients. When continuous variables met the normality assumption, a t-test was applied to compare paired samples; otherwise, the Mann-Whitney U test was used for those that did not conform to normality. Based on the situation, either the Chi-

square test or Fisher's exact test was utilized for making comparisons among categorical variables. For the prognostic assessment of categorical variables, survival curves were generated through the KM method, and statistical significance was evaluated using the log-rank test. Statistical significance was established at a p-value below 0.05, denoted as follows: \* indicates  $p < 0.05$ , \*\* for  $p < 0.01$ , \*\*\* for  $p < 0.001$ , and \*\*\*\* for  $p < 0.0001$ . R software, specifically version 4.1.3, was utilized to carry out all statistical analyses. Unless mentioned otherwise, the "ggplot2" package was used to produce the graphs.

## 3 Results

### 3.1 Constructing and validating the predictive model for prognosis

Through differential gene expression analysis, we identified significantly upregulated (red) and downregulated (green) DEGs in tumor samples, as visualized in the volcano plot (Figure 1A). To ascertain 21 CSAGs that impact the prognosis of THCA, a univariate Cox regression analysis was executed ( $p < 0.05$ ,  $HR \neq 1$ , Figure 1B). By intersecting the 61 DEGs with the 21 prognostic genes, we identified 9 genes that were present in both gene sets (Figure 1C). These genes were: HDAC4, NDRG1, NEK1, NINJ1, PLA2R1, SNAI1, ASPH, CDKN2A, and E2F1. An analysis of the correlation network for these 9 genes showed that HDAC4, NDRG1, NEK1, NINJ1, PLA2R1, SNAI1, and ASPH exhibited predominantly positive correlations amongst themselves. Additionally, CDKN2A and E2F1 displayed a positive correlation with each other. However, the expression levels of these genes were inversely related to the majority of the other genes in the network (Figure 1D). Taking these observations into account, we refined the gene set further and developed a prognostic model employing the LASSO algorithm. The coefficient path distribution for the 9 genes showed that as  $\log(\lambda)$  increased, the coefficients of the genes gradually approached zero in a stepwise manner (Figure 1E). The optimal number of genes, determined when the cross-validation curve reached its minimum, corresponding to the lowest partial likelihood deviance, was found to be 6 genes (Figure 1F). The model equation is as follows:

$$\begin{aligned} \text{Risk score} = & \text{ASPH} \times 0.236612398528079 \\ & + \text{CDKN2A} \times 0.55903013908233 + \text{E2F1} \times (-0.429431075541726) \\ & + \text{DRG1} \times 0.455159278181108 \\ & + \text{NINJ1} \times (-0.555409521362013) \\ & + \text{SNAI1} \times 1.1381189402696 \end{aligned}$$

In comparison to the high-risk group, the TCGA cohort's low-risk patient group demonstrated a notably superior OS outcome ( $p < 0.001$ , Figure 2A). The prognostic difference between the two groups in the GEO cohort was further validated by us (Figure 2B). Furthermore, by analyzing the ROC curves associated with 1-year, 3-year, and 5-year survival rates, it was demonstrated that the model demonstrated robust diagnostic capabilities in both independent patient groups (Figures 2C, D).

### 3.2 Enrichment and prognostic analysis conducted for various risk groups

An analysis of THCA samples focusing on the expression levels of six model genes (ASPH, CDKN2A, E2F1, NDRG1, NINJ1, SNAI1) revealed that those who exhibited high expression of ASPH, CDKN2A, NDRG1, and SNAI1 were predominantly grouped into the high-risk category. In contrast, those who showed elevated expression of both E2F1 and NINJ1 were mainly classified into the low-risk group. Additionally, a higher percentage of patients in the low-risk group were found to be 5-year survivors (Figures 3A, B). Further analysis of KM survival curves for TCGA-THCA patients with tumor stages I-II revealed no statistically significant difference in survival probabilities between the two risk groups ( $p = 0.060$ , Figure 3C). For patients in stages III-IV, the risk groups showed a more distinct difference in prognosis, with the high-risk group having a significantly lower survival probability than the low-risk group ( $p = 0.003$ , Figure 3D). In addition, through GSEA analysis, it was found that genes in the high-risk group showed considerable enrichment in the pathways related to the mitochondrial electron transport chain, among which the following five pathways related to the electron transport process in the mitochondrial respiratory chain in the KEGG MEDICUS database had the highest enrichment: ENV\_FACTOR\_ARSENIC\_TO\_ELECTRON\_TRANSFER\_IN\_COMPLEX\_IV, REFERENCE\_ELECTRON\_TRANSFER\_IN\_COMPLEX\_I, REFERENCE\_ELECTRON\_TRANSFER\_IN\_COMPLEX\_IV, VARIANT\_MUTATION\_CAUSED\_ABERRANT\_SNCA\_TO\_ELECTRON\_TRANSFER\_IN\_COMPLEX\_I, VARIANT\_MUTATION\_INACTIVATED\_PINK1\_TO\_ELECTRON\_TRANSFER\_IN\_COMPLEX\_I. Conversely, the low-risk group genes exhibited significant enrichment in pathways related to cell proliferation, survival, and metabolic regulation, especially within the five most enriched pathways listed in the KEGG MEDICUS database: REFERENCE\_GF\_RTK\_PI3K\_SIGNALING\_PATHWAY, REFERENCE\_GF\_RTK\_RAS\_ERK\_SIGNALING\_PATHWAY, REFERENCE\_GF\_RTK\_RAS\_PI3K\_SIGNALING\_PATHWAY, REFERENCE\_GPCR\_PLCB\_ITPR\_SIGNALING\_PATHWAY, REFERENCE\_IL6\_FAMILY\_TO\_JAK\_STAT\_SIGNALING\_PATHWAY (Figure 4A).

### 3.3 Differential immune characteristics analysis

Upon examining the heatmap depicting the differential expression levels of immune modulators across various risk groups, it was evident that the high-risk group demonstrated heightened activity of five immune regulatory molecules ( $p < 0.05$ , Figure 4B). Our results, utilizing the CIBERSORT algorithm, revealed a positive correlation between the abundance of several immune cell types and the risk score, particularly memory B cells, M1 macrophages, monocytes, activated myeloid dendritic cells, and resting myeloid dendritic cells. Conversely, a significant negative association was observed for CD8+ T cells. Additionally, a significant negative relationship was noted between both CD8+ T cells and regulatory T cells (Tregs) and over half of the



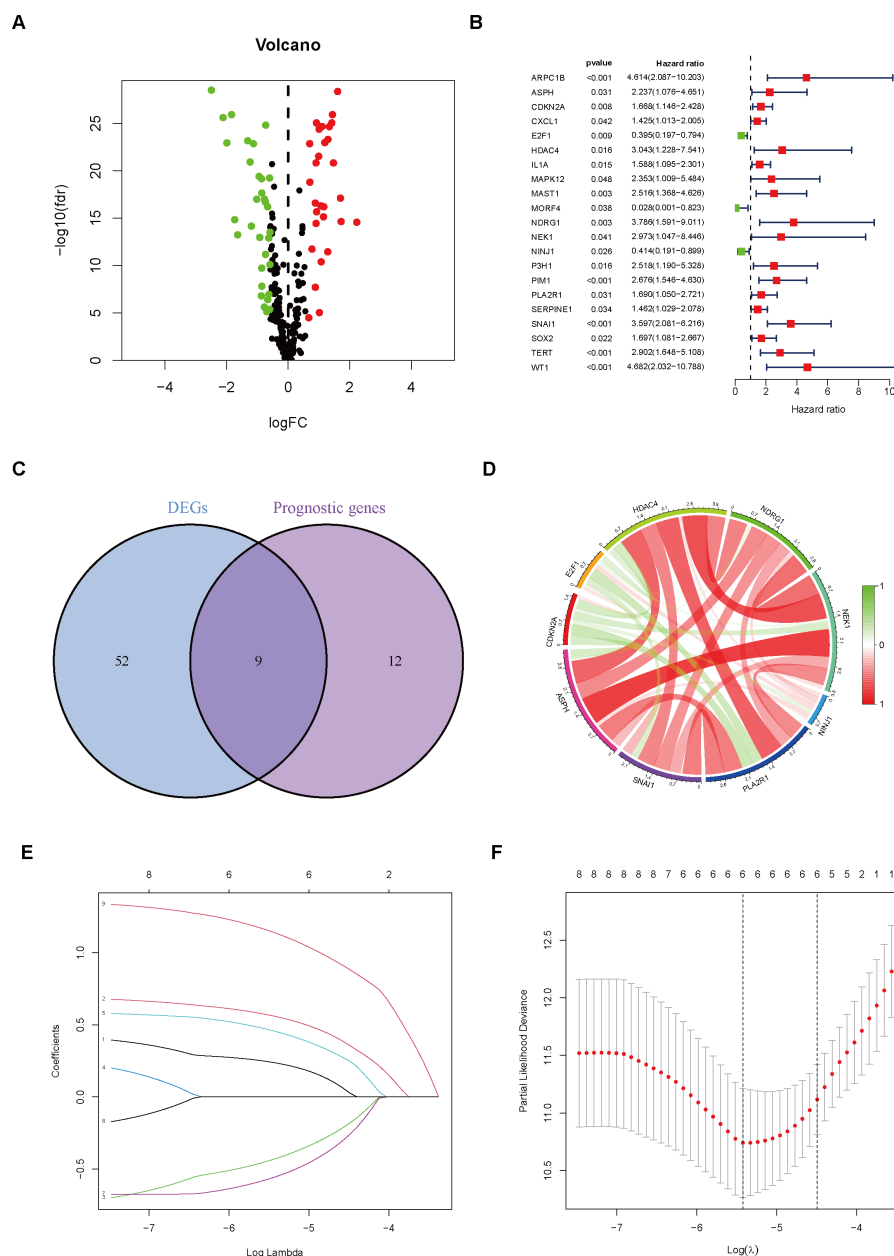


FIGURE 1

Gene Selection and Model Construction. **(A)** Differential gene analysis was performed to identify genes that differ between the normal and tumor groups. **(B)** Cox regression analysis was conducted on genes associated with cellular senescence. **(C)** The intersection of differential genes and prognostic genes was extracted. **(D)** The correlation between nine differentially expressed prognostic genes was analyzed and visualized using a correlation circle plot. **(E)** A prognostic prediction model was constructed using the LASSO algorithm. **(F)** The optimal number of variables was determined based on the  $\lambda$  value.

model's genes. Among the six model genes, ASPH, CDKN2A, and NINJ1 exhibited strong correlations with tumor-associated immune cells. In particular, the expression level of CDKN2A exhibited a positive link with the level of immune cell presence, whereas NINJ1 showed a negative correlation with immune cells at the expression level ( $p < 0.05$ , Figure 4C). Employing various algorithms yielded consistent results, suggesting that, apart from the general positive link between risk score and immune cell abundance, a substantial number of model genes exhibited notable correlations with the levels of immune cell infiltration. Notably, CDKN2A exhibited a stronger positive

correlation with immune cells compared to the other genes, while NINJ1 showed a more pronounced negative relationship with immune cells ( $p < 0.05$ , Figures 4D–I).

Furthermore, a comparison of the expression profiles of 31 immune checkpoint genes was conducted between the two risk groups. Boxplot analysis revealed that all immune checkpoint genes were significantly upregulated in the high-risk group ( $p < 0.05$ , Figure 5A), suggesting that high expression of immune checkpoints might be associated with unfavorable tumor prognosis. To further explore the impact of different immune checkpoint gene

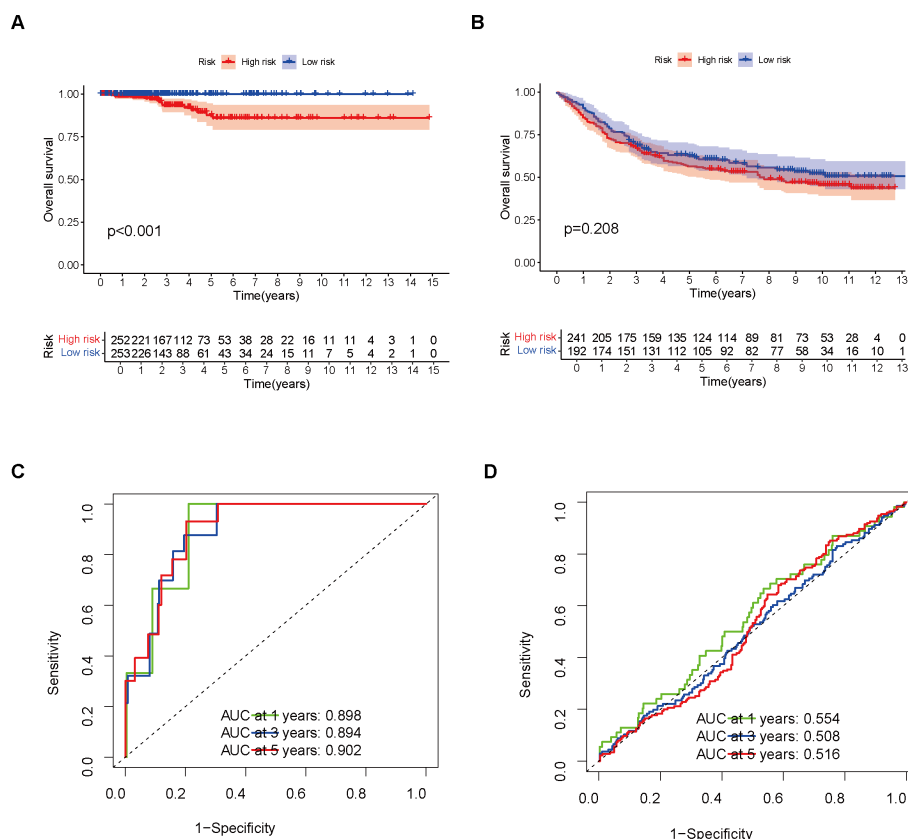


FIGURE 2

Model Validation Using Training and Validation Sets. (A) Survival analysis was performed on the training set. (B) Survival analysis was conducted on the validation set. (C) The model's performance in the training set was evaluated using a ROC curve. (D) The model's performance in the validation set was assessed using a ROC curve.

expressions on patient prognosis, we performed KM analysis. Survival curves for different subgroups indicated that, regardless of whether immune checkpoint genes were highly expressed, samples with higher risk scores consistently showed significantly lower survival probabilities compared to those with lower risk scores. The prognostic model demonstrates a strong capacity for prediction, underlining its robustness. Certain immune checkpoint genes, when upregulated in the high-risk group, showed a degree of association with improved patient prognosis. Specifically, higher expression levels of BTLA, CD28, CD48, CD70, CD86, CD160, CD200, CD200R1, CD276, CTLA4, HAVCR2, ICOS, ICOSLG, IDO1, LAIR1, LGALS9, NRP1, TIGIT, TNFRSF8, TNFRSF9, TNFSF14, TNFSF18, and VTCN1 were associated with better prognosis. Patients exhibiting high expression of ADORA2A, BTNL2, CD27, CD80, IDO2, TNFRSF4, TNFSF4, and TNFSF9 had a worse prognosis in comparison to those with low expression levels, conversely ( $p < 0.01$ , Figures 5B–J, 6A–V).

### 3.4 Mutation analysis and survival analysis of TMB

A comparison of TMB between the high-risk and low-risk groups revealed no statistically significant variation between the two ( $p =$

0.089, Figure 7A). Nevertheless, additional correlation analysis unveiled an inverse relationship between TMB and risk score, where an increase in risk score was accompanied by a decrease in TMB ( $R = -0.11$ ,  $p = 0.016$ , Figure 7B). After stratifying patients by their TMB and analyzing the survival curves of the H-TMB and L-TMB groups, we found the H-TMB group had a notably lower survival rate than the L-TMB group, which indicates that there may be a potential association between higher TMB and a poorer prognosis ( $p < 0.001$ , Figure 7C). In order to delve deeper into how both TMB and risk score collectively influence the prognosis of THCA, we performed a KM survival analysis incorporating the risk score. On one hand, high-risk scores corresponded to lower survival probabilities. Conversely, while the prognosis of low-risk patients remained relatively unaffected by TMB, high-risk patients who also had high TMB demonstrated significantly diminished survival rates in comparison to their counterparts with low TMB within the group with elevated risk ( $p < 0.001$ , Figure 7D).

### 3.5 The model's capacity to predict tumor treatment outcomes

Moreover, after conducting an analysis of the IPS across distinct risk groups, specifically *ips\_ctla4\_neg\_pd1\_neg*, *ips\_ctla4\_neg\_pd1\_pos*,

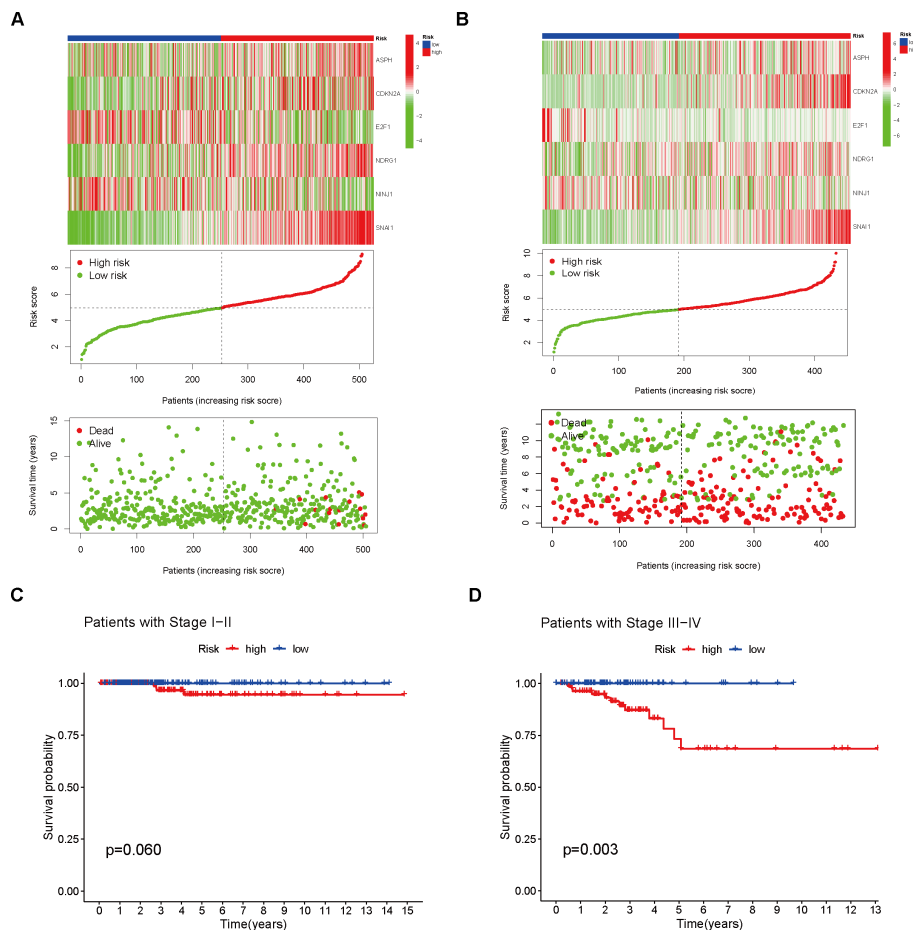


FIGURE 3

Analysis of Different Risk Groups. (A) Risk scores were calculated and the training set was divided into high- and low-risk groups. Heatmaps were used to visualize the differential model genes between the two risk groups. The cumulative risk factor plot illustrates the changes in patient survival time and status with respect to the risk score. (B) Risk scores were calculated and the validation set was divided into high- and low-risk groups. Heatmaps were used to visualize the differential model genes between the two groups. The cumulative risk factor plot illustrates the changes in patient survival time and status with respect to the risk score. (C) Survival analysis was performed on the high- and low-risk groups of stage I and II patients. (D) Survival analysis was performed on the high- and low-risk groups of stage III and IV patients.

ips\_ctla4\_pos\_pd1\_neg, and ips\_ctla4\_pos\_pd1\_pos, it became evident that the IPS within the low-risk group surpassed those in the other categories, suggesting a superior responsiveness of the low-risk group to both CTLA-4 and PD-1 inhibitors, especially in scenarios involving monotherapy with PD-1 inhibitors ( $p < 0.01$ , Figure 7E).

Finally, the IMvigor210 immunotherapy cohort was used to validate the model. The survival curves generated by the Kaplan-Meier method for the two risk groups within the IMvigor210 dataset revealed that high-risk samples exhibited a worse prognosis compared to low-risk samples, thereby reinforcing the model's capacity for generalization ( $p < 0.01$ , Figure 7F). Moreover, the predictive capability of the risk model concerning chemotherapy response was assessed, revealing that patients in the CR/PR category had notably lower risk scores compared to those in the SD/PD category ( $p = 0.0021$ , Figure 7G). Based on these findings, we propose that the risk model may serve as a reliable predictive tool for treatment response in patients with THCA. Additionally, we broadened our analysis, which was aimed at gauging the effect of the immune checkpoint co-modeling on the prognosis within the

IMvigor210 dataset. In general, irrespective of the expression levels of immune checkpoint genes, patients categorized in the low-risk group exhibited notably superior survival outcomes compared to those in the high-risk group. Specifically, the upregulation of genes including CD40, CD200, CD244, CD276, NRP1, TNFRSF14, TNFSF14, TNFSF15, and VTCN1 was associated with a significant enhancement in the survival probability of patients belonging to the low-risk group. In contrast, when genes like BTLA, CD27, CD28, CD40, CD40LG, CD80, CD244, CD274, CTLA4, HHLA2, ICOS, IDO1, IDO2, KIR3DL1, LAG3, TNFRSF8, TNFRSF18, and TNFSF15 were highly expressed, high-risk patients exhibited significantly improved prognosis ( $p < 0.01$ , Figures 8, 9).

## 4 Discussion

Human THCA stands as the most frequent endocrine tumor and ranks seventh among cancers most commonly diagnosed in women (26). Over the past few decades, there has been a consistent rise in its

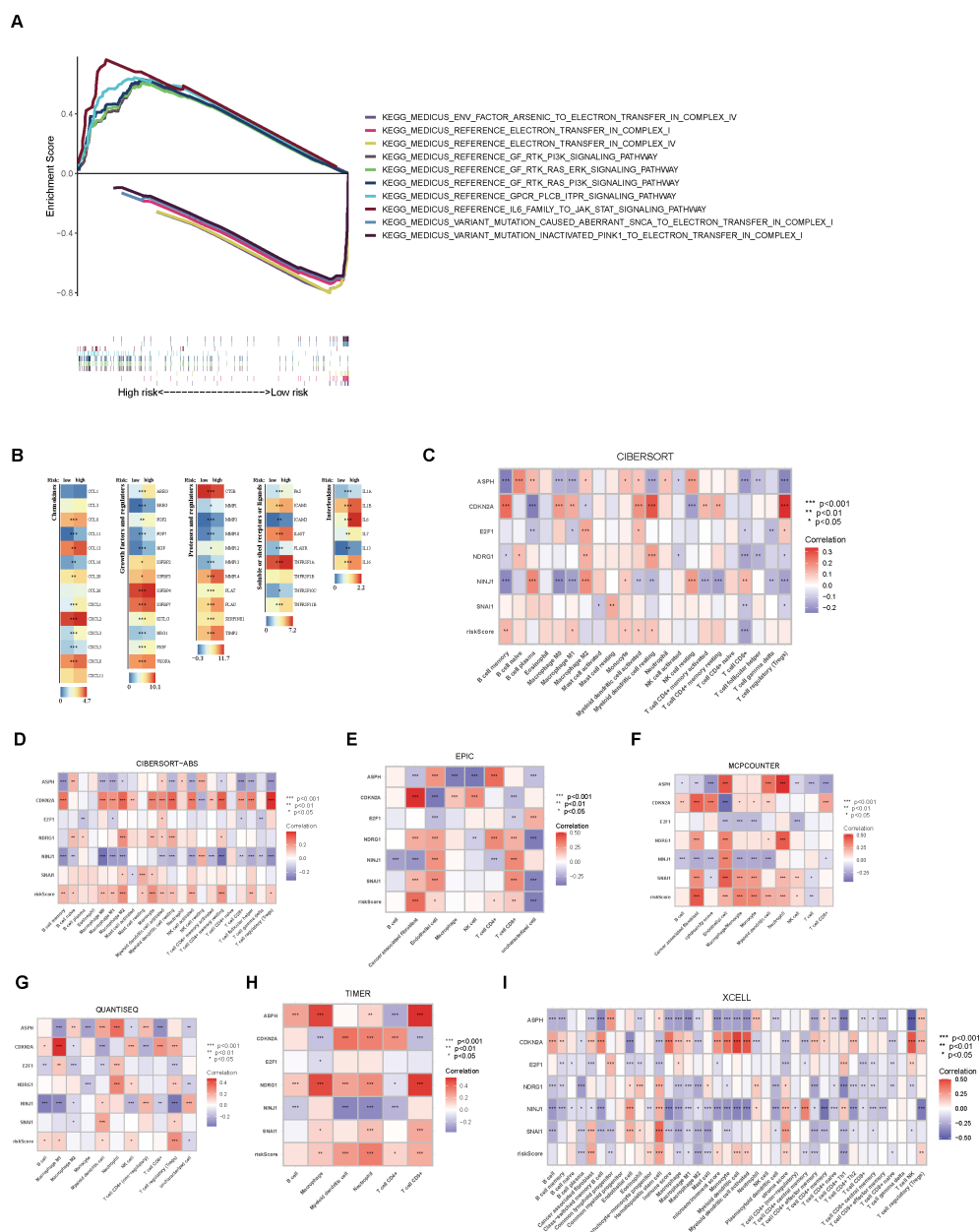


FIGURE 4

Enrichment analysis and immune characteristic differential analysis of high- and low-risk groups. **(A)** GSEA enrichment analysis of the high- and low-risk groups. **(B)** Differential expression analysis of immune regulatory genes between the two groups. **(C)** CIBERSORT analysis of the correlation between immune cell scores and model genes/risk score. **(D–I)** Analysis of immune cell scores and their correlation with model genes/risk score in the samples using CIBERSORT-ABS, EPIC, MCPOUNTER, QUANTISEQ, TIMER, and XCELL algorithms.

incidence, resulting in a current prevalence that constitutes 3–4% of all cancer cases (1). Although the prognosis for most THCA patients is favorable, early detection and diagnosis remain challenging (8). Once tumor cells metastasize to distant sites, survival rates vary significantly depending on the pathological subtype (10), with the median survival for ATC often limited to only 3–6 months (11). Worse still, the standard therapies, such as surgery and postoperative radioiodine ablation, are ineffective for ATC patients (9). Moreover, targeted therapies and immunotherapies have limited success in achieving curative outcomes for certain DTC and MTC patients (12). Therefore, the objective of this study extends beyond merely

exploring the influence of cellular senescence on THCA and its fundamental mechanisms, but also to develop a prognostic prediction model, with the goal of identifying novel and effective therapeutic targets to improve the prognosis and therapeutic outcomes for THCA patients.

Initially, a detailed examination of CSAG variations between normal and tumor tissues was carried out, resulting in the discovery of 61 DEGs. Subsequently, we conducted a Cox regression analysis of the CSAG, which yielded 21 prognostic-associated aging-related genes. By intersecting these 21 prognostic genes with the 61 DEGs, we identified 9 DEGs that were associated with prognosis. The



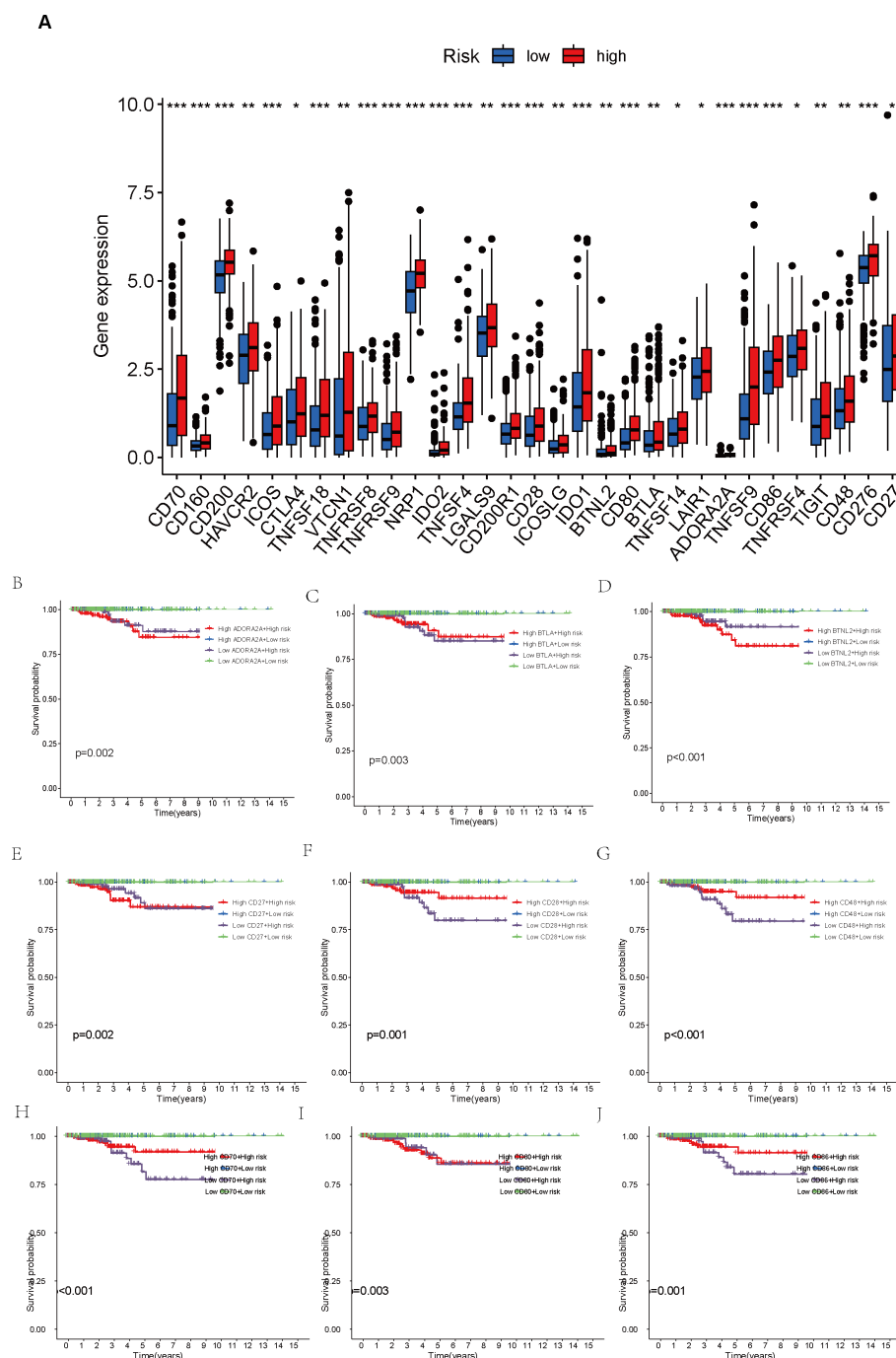


FIGURE 5

Comparison of immune checkpoint expression levels and their impact on prognosis between high- and low-risk groups. (A) Comparison of expression levels of 31 immune checkpoint genes between the high- and low-risk groups. (B–J) Survival analysis of high- and low-risk groups stratified by immune checkpoint gene expression levels. \* $p < 0.05$ ; \*\* $p < 0.01$ ; \*\*\* $p < 0.001$ .

genes that overlap may offer significant understanding of CSAG's role in predicting the outcome of THCA and might be candidates for new prognosis prediction targets and therapeutic approaches. However, Nonetheless, there is a scarcity of research investigating the connection between these genes and THCA, and the interactions between these genes remain unclear. Therefore, we analyzed the correlations among the 9 genes and found that HDAC4, NDRG1, NEK1, PLA2R1, and ASPH showed strong

positive correlations with other genes, with ASPH, HDAC4, and NEK1 demonstrating particularly strong associations. It is known that HDAC4 promotes carcinogenesis by limiting the transcription of tumor suppressor genes (27), while NEK1 is involved in DNA damage repair (28). Although CDKN2A and E2F1 are positively correlated, they show negative correlations with the expression levels of most other genes. Next, we used LASSO to perform gene selection for model construction in the training set, ultimately

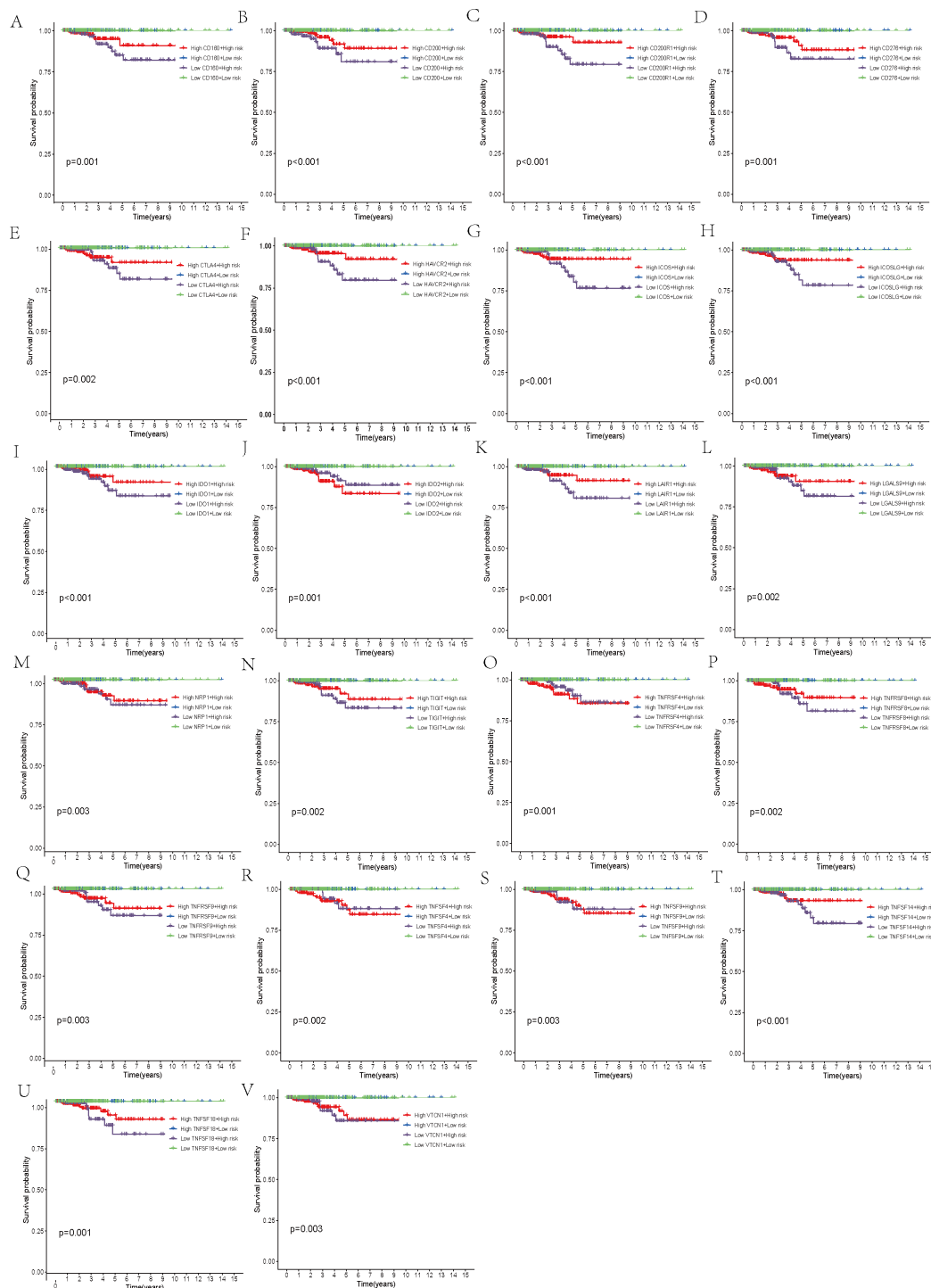


FIGURE 6

Survival analysis. (A–V) Stratification of the high- and low-risk groups based on immune checkpoint gene expression levels.

identifying six model genes: ASPH, CDKN2A, E2F1, NDRG1, NINJ1, and SNAI1. The transmembrane protein Aspartate  $\beta$ -hydroxylase (ASPH), weighing approximately 86 kDa and belonging to the highly conserved  $\alpha$ -ketoglutarate-dependent dioxygenase family, is classified as a type II protein. ASPH has been found to be overexpressed in various malignant tumors (29), and The hydroxylase activity it possesses holds a crucial function in

fostering malignant tumor characteristics, encompassing tumor growth, proliferation, invasion, and metastasis. Research has shown that ASPH not only influences the prognosis of hepatocellular carcinoma under the regulation of inositol polyphosphate-5-phosphatase F (INPP5F) (30), but also promotes tumor progression and poor prognosis by activating Notch and PI3K-dependent signaling pathways, inducing a delay in tumor cell

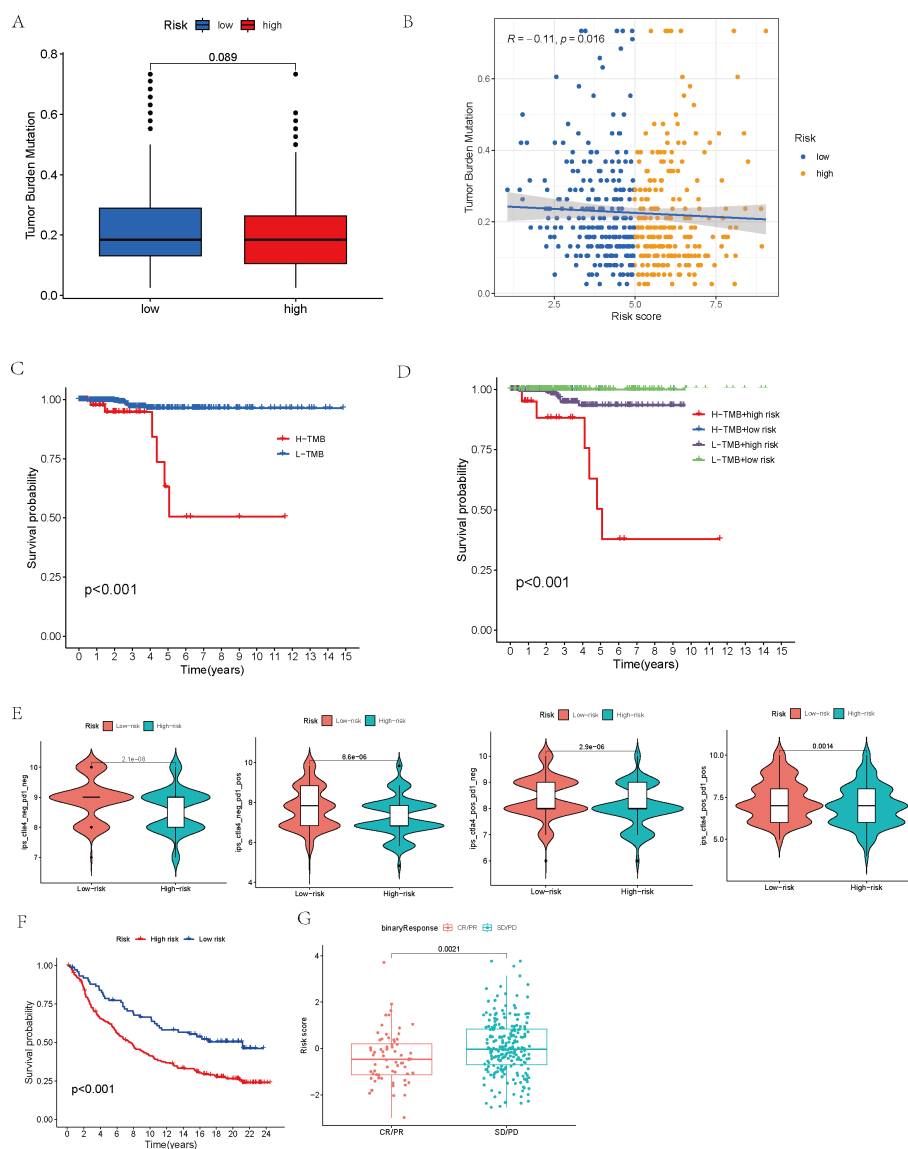


FIGURE 7

Mutation analysis and survival analysis based on TMB, and prediction of tumor treatment responses by the model. **(A)** Tumor mutation burden analysis of the high- and low-risk groups. **(B)** Analysis of the correlation between tumor mutation burden and risk score. **(C)** Survival analysis of high-TMB and low-TMB groups. **(D)** Survival analysis of high- and low-risk groups within high- and low-TMB subsets. **(E)** Analysis of immune treatment responses in high- and low-risk groups. **(F)** Survival analysis of high- and low-risk groups in the IMvigor210 immunotherapy cohort. **(G)** Analysis of risk model score differences between disease status groups in the IMvigor210 immunotherapy cohort.

senescence and impairing mitochondrial integrity (31). One of the most frequently deleted homozygous genes in human cancers is CDKN2A, situated on chromosome 9 (32). The tumor suppressors p16 and p14arf are both products of CDKN2A (33, 34). Since p16 inhibits the G1 to S phase transition and p14arf activates the tumor suppressor p53 (34, 35), the loss of CDKN2A function leads to cell cycle dysregulation and promotes tumor development. E2F transcription factor 1 (E2F1) is the archetype member of the E2F family, which includes transcriptional activators that bind to the adenoviral E2 promoter (36). In regulating the expression of a multitude of oncogenes and tumor suppressor genes, E2F1 serves as an activator. The E2F family precisely regulates the cell cycle, apoptosis, and DNA replication processes (37). E2F1 not only promotes cell migration and metastasis but also plays a critical

role in stem cell-mediated carcinogenesis and estrogen-mediated cell proliferation (38). Its non-transcriptional activities further promote DNA repair or induce autophagy and apoptosis (39). N-myc downstream regulated gene 1 (NDRG1), a gene that functions to suppress tumorigenesis, located on chromosome 8q24.3, encodes a 3.0 kb mRNA and inhibits cell proliferation, migration, invasion, and autophagy, while promoting apoptosis and differentiation, thus suppressing tumor invasive phenotypes (40). Overexpression of NDRG1 downregulates cyclin D1, a Wnt-responsive gene, and inhibits cell cycle progression (41). Although NDRG1 primarily exhibits anti-cancer and anti-metastasis functions, it has also been shown to promote cancer in certain cancers such as gastric cancer and hepatocellular carcinoma (42). Therefore, some researchers suggest that NDRG1 may exert pleiotropic effects depending on the



p53, whereby NINJ1, as a p53 target, suppresses p53 mRNA translation. Moreover, NINJ1 exerts opposite effects on cell growth, migration, and tumor development through wild-type and mutant p53 (45). Additionally, NINJ1 inhibits the IL-6 signaling pathway both *in vitro* and *in vivo*, suppressing lung cancer migration, invasion, and metastasis (46). Snail family zinc finger 1 (SNAI1) is the first and most extensively studied E-cadherin



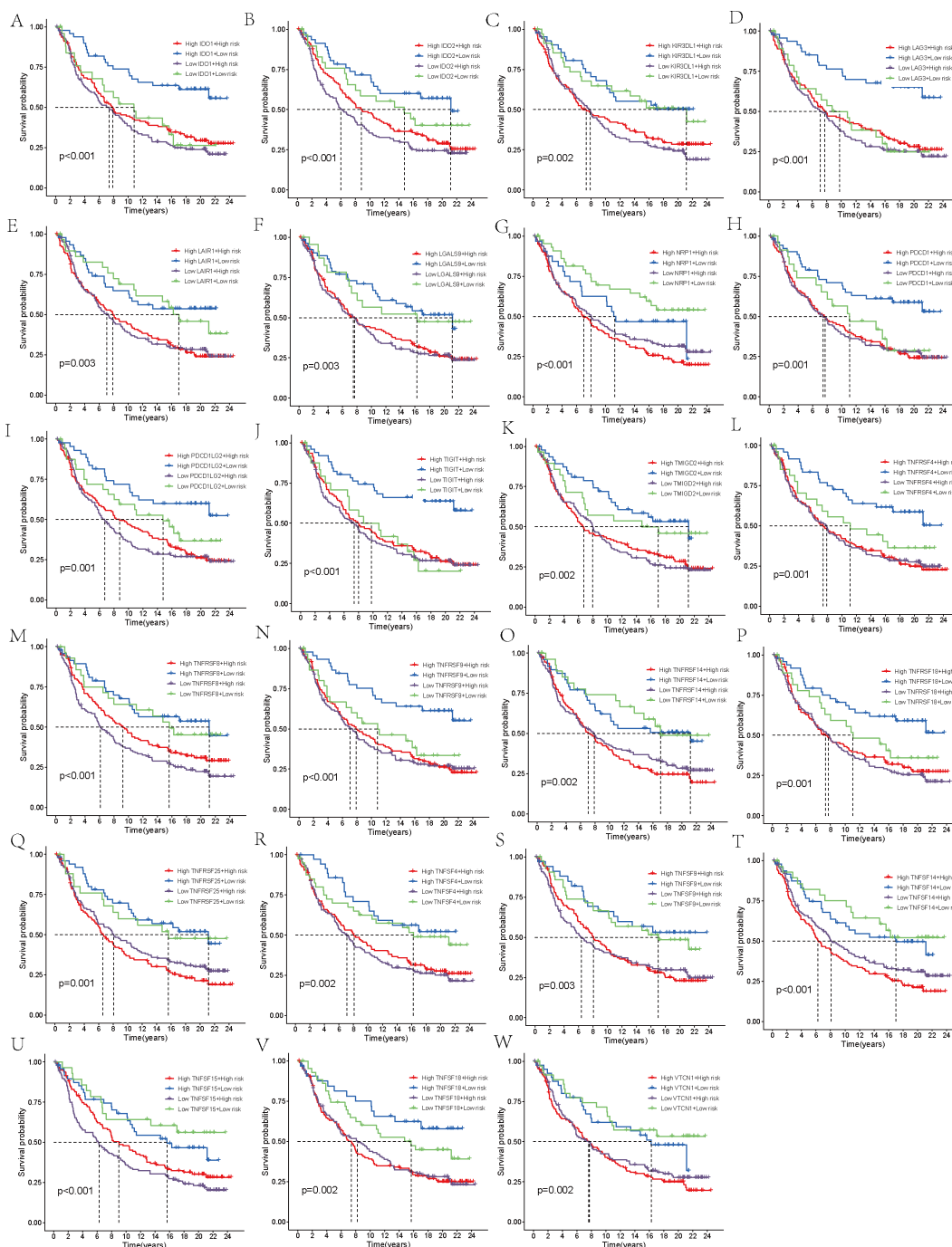


FIGURE 9

Survival analysis. (A–W) In the IMvigor210 cohort, the high-risk and low-risk groups were stratified according to the level of immune checkpoint gene expression and the difference in prognosis was compared.

transcriptional repressor, and E-cadherin, encoded by the epithelial gene CDH1, is a marker of epithelial-mesenchymal transition (EMT), a developmental process that cancer cells use to promote invasion, metastasis, and therapy resistance (47). In normal tissues, the regulation of SNAI1 expression is precise, whereas its deregulation is linked to the advancement of several types of cancer (48, 49). In addition to repressing the E-cadherin gene, the core function of SNAI1 includes the transcriptional repression of tight junction genes and fructose-1,6-bisphosphatase genes, which

regulate glycolysis rate (50). In ovarian cancer cells, SNAI1 primarily regulates intercellular and cell-matrix adhesion (51). We built a model for predicting prognosis by utilizing six model genes, and subsequently assessed the scores for patients in not only the training but also the validation datasets. Following that, the patients from both cohorts were divided into two categories – high-risk and low-risk – according to their respective risk scores. An analysis comparing the survival rates of the two groups within both cohorts unveiled that patients in the low-risk category of the TCGA

cohort exhibited a notably superior prognosis compared to those in the high-risk category. Additionally, we assessed the model's predictive power by employing ROC curves and found that it demonstrated high accuracy in both the two datasets. Given the roles of these six genes in malignant tumors, we propose that they are likely to serve as prognostic biomarkers for THCA and may influence the initiation and progression of THCA. An additional analysis was conducted across two datasets to explore the variations in the expression of model genes across the cohorts stratified as high-risk and low-risk. It is apparent that ASPH, CDKN2A, NDRG1, and SNAIL demonstrated increased expression in the high-risk group, irrespective of whether they were in the training set or the validation set. In the low-risk group, E2F1 and NINJ1 were more expressed. An analysis was conducted to compare the survival differences between the two groups, revealing that, although the high-risk group had a lower survival rate, the maximum survival duration of patients did not significantly differ from that of the low-risk group. We then conducted survival analysis for the TCGA cohort, stratifying patients into high-risk and low-risk groups based on Stage I-II and Stage III-IV, in order to investigate how tumor stage influences the predictive ability of the model. Comparable survival rates were observed between the high- and low-risk groups in Stage I-II, with no statistically significant differences emerging. However, in Stage III-IV, a notable disparity in survival rates was observed between the two groups. We interpret this as suggesting that our model holds greater predictive value in patient populations with more advanced stages. Additionally, an analysis using GSEA, focusing on the KEGG MEDICUS pathway, was conducted, revealing the enrichment of five pathways, primarily associated with cellular proliferation, differentiation, and signaling, for those at high risk. Genes in the high-risk group were highly enriched in pathways associated with the mitochondrial electron transport chain, reflecting changes in cellular energy metabolism in the high-risk group and increased apoptosis that may result from mitochondrial dysfunction. Conversely, for those at low risk, the primary association of the enriched pathways was with mitochondrial electron transport and oxidative phosphorylation processes. The results of our study introduce novel understandings into the realm of THCA treatment, implying that a customized exploration of therapeutic options for patients stratified into high- and low-risk groups may facilitate the development of more precise targeted therapies.

Following that, an analysis of the immune regulatory expression profiles was conducted for both groups, with the results showing that the high-risk group had significantly increased expression levels of five immune regulatory molecules compared to the low-risk group. This suggests that the response to immune checkpoint inhibitors or immunotherapies in THCA may differ based on the risk scores. This also indicates that the patient's immune status is strongly associated with clinical outcomes. Afterwards, various algorithms were employed under the purpose of examining the relationship existing between the abundance of immune cell infiltration and six model genes. The analysis revealed a positive association between the risk score and CDKN2A, both related to increased immune cell abundance, whereas NINJ1 displayed an inverse relationship with the expression levels of immune cells. The

indication is that CDKN2A and NINJ1 potentially impact tumor prognosis by regulating the infiltration of immune cells. We subsequently conducted an analysis to assess the variability in the expression of immune checkpoints across patient groups stratified by high and low risk. The results of our study indicated that there was an upregulation of 31 immune checkpoints among those in the high-risk category, hinting at a potentially more favorable efficacy of immune checkpoint inhibitors in this group. By utilizing the median expression levels of these 31 immune checkpoints, we further divided both high- and low-risk groups into two subgroups and conducted survival analysis for each checkpoint. Despite immune checkpoint expression having little effect on the survival of patients in the low-risk group, the high-risk group exhibited a notable correlation between immune checkpoint expression and their survival rates. Eight immune checkpoints—ADORA2A, BTNL2, CD27, CD80, IDO2, TNFRSF4, TNFSF4, and TNFSF9—were associated with poorer prognosis when highly expressed, while the high expression of most immune checkpoints was generally linked to better outcomes. This finding provides novel insights into the development of novel immunotherapy agents targeting immune checkpoints, and indicates that the level of immune checkpoint expression may serve as a marker for evaluating disease progression and prognosis, thereby laying the groundwork for tailored treatment approaches.

After computing and contrasting the TMB of the two patient groups, we observed no notable disparity, which could be attributed to the influence of potential confounding factors. The Pearson correlation analysis was conducted by us to deeply evaluate the correlation between the risk score and TMB, with the aim of bolstering the credibility of our findings. The results of our analysis revealed an inverse relationship between the risk score and TMB, implying that patients with higher risk scores had correspondingly lower TMB levels. With patients categorized into H-TMB and L-TMB groups using the median TMB value as a cutoff, we proceeded to analyze their survival rates. Our analysis revealed that patients belonging to the H-TMB group had significantly diminished survival rates in comparison to those in the L-TMB group. Subsequently, we combined TMB and risk scores to classify the patients into four subgroups for survival analysis. Our results showed that, although TMB had no substantial effect on survival among patients in the low-risk group, patients in the high-risk group with high TMB had significantly inferior survival rates compared to those with low TMB. This finding supports our previous conclusion that TMB is not an independent prognostic factor. TMB levels appear to influence the prognosis primarily in high-risk patients. Although high-risk groups generally correspond to lower TMB, patients within these groups who have higher TMB tend to experience poorer outcomes. Some studies suggest that a higher TMB reflects greater exposure to tumor antigens, and thus TMB could potentially serve as a marker for the response to therapy utilizing immune checkpoint inhibitors (52). A deeper exploration into the function of TMB in THCA is necessary, as it could potentially present a new method for therapeutic intervention and prognosis assessment in THCA.

Finally, we conducted an immunotherapy analysis on the patients, separately assessing high-risk and low-risk patients' reactions to anti-CTLA-4 and anti-PD-L1 antibodies. This led to

the identification of four distinct IPS. Our results suggest that, regardless of whether patients received anti-CTLA-4 or anti-PD-L1 antibodies, those in the low-risk group responded significantly better to immune checkpoint inhibitor treatment strategies. Notably, patients receiving monotherapy with PD-1 inhibitors exhibited the most pronounced difference. Our model suggests that it can direct the choice of more precisely targeted immunotherapy strategies according to a patient's risk score, which may lead to an enhanced response to immune suppressors for high-risk patients and, consequently, a better prognosis. To further assess the predictive efficacy of the model, we used the IMvigor210 cohort for validation. After determining the risk scores for the patients, the IMvigor210 cohort was categorized into those at high risk and those at low risk, upon which survival analysis was subsequently performed. The predictive performance of the model was validated by the results as being robust. We then classified patients into two groups based on therapeutic response: complete or partial response (CR/PR) and stable or progressive disease (SD/PD), and compared their risk scores. The CR/PR group exhibited significantly decreased risk scores when compared to the SD/PD group. Subsequently, the patients' risk scores were combined with the expression levels of 48 immune checkpoint molecules, leading to the classification of patients into four subgroups, each characterized by the expression pattern of a particular immune checkpoint molecule. The analysis of survival outcomes showed that, when compared to patients in the high-risk group, those in the low-risk group exhibited a remarkably better prognosis. Within the low-risk group, there was an upregulation of specific immune checkpoint genes, such as CD40, CD200, CD244, CD276, NRP1, TNFRSF14, TNFSF14, TNFSF15, and VTCN1, was linked to a notable elevation in the likelihood of survival, suggesting that these genes may serve as promising therapeutic targets for low-risk patients. Other studies have also linked these genes to thyroid cancer (53, 54). When it comes to the group with higher risk scores, over one-third of the immune checkpoint genes studied were identified as having a positive correlation with a better prognosis. Genes like CD40, CD244, and TNFSF15 were found to be beneficial for the prognosis of both groups. These findings open up new possibilities for targeted therapies in THCA.

While our study established a prognostic model for THCA and uncovered the role of CSAGs, limitations exist. First, using public database data may introduce sample bias. Additionally, findings are primarily data-driven, lacking experimental validation. Lastly, analysis of immune checkpoints and TMB was limited to risk stratification, requiring further investigation into their mechanisms.

## 5 Conclusion

In this study, we used bioinformatics to explore cellular senescence's impact on THCA prognosis. By integrating public database data and focusing on CSAGs, we developed a robust prognostic model validated by KM and ROC curves. By stratifying patients into high- and low-risk groups, the model uncovered notable disparities in prognosis, immune activity, and treatment response. Risk-stratified analysis provided insights into immune checkpoints

and TMB. Our findings deepen understanding of cellular senescence in THCA and suggest new therapeutic targets.

## Data availability statement

The original contributions presented in the study are included in the article/[Supplementary Material](#). Further inquiries can be directed to the corresponding author.

## Author contributions

BZ: Conceptualization, Data curation, Formal analysis, Investigation, Methodology, Resources, Software, Validation, Visualization, Writing – original draft, Writing – review & editing. YP: Conceptualization, Data curation, Formal analysis, Investigation, Methodology, Project administration, Resources, Software, Supervision, Validation, Visualization, Writing – original draft, Writing – review & editing.

## Funding

The author(s) declare that no financial support was received for the research, authorship, and/or publication of this article.

## Conflict of interest

The authors declare that the research was conducted in the absence of any commercial or financial relationships that could be construed as a potential conflict of interest.

## Generative AI statement

The author(s) declare that no Generative AI was used in the creation of this manuscript.

## Publisher's note

All claims expressed in this article are solely those of the authors and do not necessarily represent those of their affiliated organizations, or those of the publisher, the editors and the reviewers. Any product that may be evaluated in this article, or claim that may be made by its manufacturer, is not guaranteed or endorsed by the publisher.

## Supplementary material

The Supplementary Material for this article can be found online at: <https://www.frontiersin.org/articles/10.3389/fonc.2025.1545656/full#supplementary-material>

## References

- Romei C, Elisei R. A narrative review of genetic alterations in primary thyroid epithelial cancer. *Int J Mol Sci.* (2021) 22(4). doi: 10.3390/ijms22041726
- Reinecke MJ, Ahlers G, Burchert A, Eilsberger F, Flux GD, Marlowe RJ, et al. Second primary Malignancies induced by radioactive iodine treatment of differentiated thyroid carcinoma - a critical review and evaluation of the existing evidence. *Eur J Nucl Med Mol Imaging.* (2022) 49:3247–56. doi: 10.1007/s00259-022-05762-4
- Mao Y, Xing M. Recent incidences and differential trends of thyroid cancer in the USA. *Endocr Relat Cancer.* (2016) 23:313–22. doi: 10.1530/ERC-15-0445
- Lubitz CC, Sadow PM, Daniels GH, Wirth LJ. Progress in treating advanced thyroid cancers in the era of targeted therapy. *Thyroid.* (2021) 31:1451–62. doi: 10.1089/thy.2020.0962
- Kitahara CM, Schneider AB. Epidemiology of thyroid cancer. *Cancer Epidemiol Biomarkers Prev.* (2022) 31:1284–97. doi: 10.1158/1055-9965.EPI-21-1440
- Houten PV, Netea-Maier RT, Smit JW. Differentiated thyroid carcinoma: An update. *Best Pract Res Clin Endocrinol Metab.* (2023) 37:101687. doi: 10.1016/j.beem.2022.101687
- Ibrahimipasic T, Ghossein R, Shah JP, Ganly I. Poorly differentiated carcinoma of the thyroid gland: current status and future prospects. *Thyroid.* (2019) 29:311–21. doi: 10.1089/thy.2018.0509
- Tuttle RM, Ball DW, Byrd D, Dilawari RA, Doherty GM, Duh QY, et al. Thyroid carcinoma. *J Natl Compr Canc Netw.* (2010) 8:1228–74. doi: 10.6004/jnccn.2010.0093
- Laha D, Nilubol N, Boufraqueh M. New therapies for advanced thyroid cancer. *Front Endocrinol (Lausanne).* (2020) 11:82. doi: 10.3389/fendo.2020.00082
- Banerjee M, Muenz DG, Worden FP, Wong SL, Haymart MR. Conditional survival in patients with thyroid cancer. *Thyroid.* (2014) 24:1784–9. doi: 10.1089/thy.2014.0264
- Porter A, Wong DJ. Perspectives on the treatment of advanced thyroid cancer: approved therapies, resistance mechanisms, and future directions. *Front Oncol.* (2020) 10:592202. doi: 10.3389/fonc.2020.592202
- Cabanillas ME, McFadden DG, Durante C. Thyroid cancer. *Lancet.* (2016) 388:2783–95. doi: 10.1016/S0140-6736(16)30172-6
- Massari F, Santoni M, Ciccarese C, Santini D, Alfieri S, Martignoni G, et al. PD-1 blockade therapy in renal cell carcinoma: current studies and future promises. *Cancer Treat Rev.* (2015) 41:114–21. doi: 10.1016/j.ctrv.2014.12.013
- Ou HL, Hoffmann R, González-López C, Doherty GJ, Korkola JE, Muñoz-Espin D. Cellular senescence in cancer: from mechanisms to detection. *Mol Oncol.* (2021) 15:2634–71. doi: 10.1002/1878-0261.12807
- Tchkonia T, Zhu Y, van Deursen J, Campisi J, Kirkland JL. Cellular senescence and the senescent secretory phenotype: therapeutic opportunities. *J Clin Invest.* (2013) 123:966–72. doi: 10.1172/JCI64098
- Hao X, Wang C, Zhang R. Chromatin basis of the senescence-associated secretory phenotype. *Trends Cell Biol.* (2022) 32:513–26. doi: 10.1016/j.tcb.2021.12.003
- Gorgoulis V, Adams PD, Alimonti A, Bennett DC, Bischof O, Bishop C, et al. Cellular senescence: defining a path forward. *Cell.* (2019) 179:813–27. doi: 10.1016/j.cell.2019.10.005
- Toyoshima H, Hunter T. p27, a novel inhibitor of G1 cyclin-Cdk protein kinase activity, is related to p21. *Cell.* (1994) 78:67–74. doi: 10.1016/0092-8674(94)90573-8
- Salama R, Sadaie M, Hoare M, Narita M. Cellular senescence and its effector programs. *Genes Dev.* (2014) 28:99–114. doi: 10.1101/gad.235184.113
- McHugh D, Gil J. Senescence and aging: Causes, consequences, and therapeutic avenues. *J Cell Biol.* (2018) 217:65–77. doi: 10.1083/jcb.201708092
- Herbststein F, Sapochnik M, Attorresi A, Pollak C, Senin S, Gonilski-Pacin D, et al. The SASP factor IL-6 sustains cell-autonomous senescent cells via a cGAS-STING-NFkB intracrine senescent noncanonical pathway. *Aging Cell.* (2024) 23:e14258. doi: 10.1111/accel.v23.10
- Di Micco R, Krizhanovsky V, Baker D, d'Adda di Fagnana F. Cellular senescence in ageing: from mechanisms to therapeutic opportunities. *Nat Rev Mol Cell Biol.* (2021) 22:75–95. doi: 10.1038/s41580-020-00314-w
- Demaria M, O'Leary MN, Chang J, Shao L, Liu S, Alimirah F, et al. Cellular senescence promotes adverse effects of chemotherapy and cancer relapse. *Cancer Discov.* (2017) 7:165–76. doi: 10.1158/2159-8290.CD-16-0241
- Pribluda A, Elyada E, Wiener Z, Hamza H, Goldstein RE, Biton M, et al. A senescence-inflammatory switch from cancer-inhibitory to cancer-promoting mechanism. *Cancer Cell.* (2013) 24:242–56. doi: 10.1016/j.ccr.2013.06.005
- Kim YH, Choi YW, Han JH, Lee J, Soh EY, Park SH, et al. TSH signaling overcomes B-RafV600E-induced senescence in papillary thyroid carcinogenesis through regulation of DUSP6. *Neoplasia.* (2014) 16:1107–20. doi: 10.1016/j.neo.2014.10.005
- Siegel RL, Miller KD, Fuchs HE, Jemal A. Cancer statistics, 2021. *CA Cancer J Clin.* (2021) 71:7–33. doi: 10.3322/caac.21654
- Neta G, Brenner AV, Sturgis EM, Pfeiffer RM, Hutchinson AA, Aschebrook-Kilfoy B, et al. Common genetic variants related to genomic integrity and risk of papillary thyroid cancer. *Carcinogenesis.* (2011) 32:1231–7. doi: 10.1093/carcin/bgr100
- Liu S, Ho CK, Ouyang J, Zou L. Nek1 kinase associates with ATR-ATRIP and primes ATR for efficient DNA damage signaling. *Proc Natl Acad Sci USA.* (2013) 110:2175–80. doi: 10.1073/pnas.1217781110
- Hou G, Xu B, Bi Y, Wu C, Ru B, Sun B, et al. Recent advances in research on aspartate  $\beta$ -hydroxylase (ASPH) in pancreatic cancer: A brief update. *Bosn J Basic Med Sci.* (2018) 18:297–304. doi: 10.17305/bjbm.2018.3539
- Zhou Q, Lin J, Yan Y, Meng S, Liao H, Chen R, et al. INPP5F translocates into cytoplasm and interacts with ASPH to promote tumor growth in hepatocellular carcinoma. *J Exp Clin Cancer Res.* (2022) 41:13. doi: 10.1186/s13046-021-02216-x
- Zheng W, Wang X, Hu J, Bai B, Zhu H. Diverse molecular functions of aspartate  $\beta$ -hydroxylase in cancer (Review). *Oncol Rep.* (2020) 44:2364–72. doi: 10.3892/or.2020.7792
- Mulvaney KM. Early clinical success of MTA-cooperative PRMT5 inhibitors for the treatment of CDKN2A/MTAP-deleted cancers. *Cancer Discov.* (2023) 13:2310–2. doi: 10.1158/2159-8290.CD-23-0951
- Liggett WH Jr, Sidransky D. Role of the p16 tumor suppressor gene in cancer. *J Clin Oncol.* (1998) 16:1197–206. doi: 10.1200/JCO.1998.16.3.1197
- Serra S, Chetty R. p16. *J Clin Pathol.* (2018) 71:853–8. doi: 10.1136/jclinpath-2018-205216
- Gjerset RA. DNA damage, p14ARF, nucleophosmin (NPM/B23), and cancer. *J Mol Histol.* (2006) 37:239–51. doi: 10.1007/s10735-006-9040-y
- Meng P, Ghosh R. Transcription addition: can we garner the Yin and Yang functions of E2F1 for cancer therapy? *Cell Death Dis.* (2014) 5(8):e1360. doi: 10.1038/cddis.2014.326
- Yeo HC, Beh TT, Quek JJ, Koh G, Chan KK, Lee DY. Integrated transcriptome and binding sites analysis implicates E2F in the regulation of self-renewal in human pluripotent stem cells. *PLoS One.* (2011) 6:e27231. doi: 10.1371/journal.pone.0027231
- Shah ZA, Nouroz F, Ejaz S, Tayyeb A. An insight into the role of E2F1 in breast cancer progression, drug resistance, and metastasis. *Curr Mol Med.* (2023) 23:365–76. doi: 10.2174/1566524022666220308095834
- Garcia-Garcia A, Rodriguez-Rocha H, Tseng MT, Montes-de-Oca-Luna R, Zhou HS, McMasters KM, et al. E2F-1 lacking the transcriptional activity domain induces autophagy. *Cancer Biol Ther.* (2012) 13:1091–101. doi: 10.4161/cbt.21143
- Xiao XJ, Zheng HC. NDRG1 was downregulated and worked as favorable biomarker in the development of gastric cancer. *Transl Cancer Res.* (2020) 9:210–21. doi: 10.21037/tcr.2019.12.76
- Chen Z, Zhang D, Yue F, Zheng M, Kovacevic Z, Richardson DR. The iron chelators Dp44mT and DFO inhibit TGF- $\beta$ -induced epithelial-mesenchymal transition via up-regulation of N-Myc downstream-regulated gene 1 (NDRG1). *J Biol Chem.* (2012) 287:17016–28. doi: 10.1074/jbc.M112.350470
- Joshi V, Lakhani SR, McCart Reed AE. NDRG1 in cancer: A suppressor, promoter, or both? *Cancers (Basel).* (2022) 14(23). doi: 10.3390/cancers14235739
- Park KC, Paluncic J, Kovacevic Z, Richardson DR. Pharmacological targeting and the diverse functions of the metastasis suppressor, NDRG1, in cancer. *Free Radic Biol Med.* (2020) 157:154–75. doi: 10.1016/j.freeradbiomed.2019.05.020
- Araki T, Milbrandt J. Ninjurin, a novel adhesion molecule, is induced by nerve injury and promotes axonal growth. *Neuron.* (1996) 17:353–61. doi: 10.1016/S0896-6273(00)80166-X
- Yang HJ, Zhang J, Yan W, Cho SJ, Lucchesi C, Chen M, et al. Ninjurin 1 has two opposing functions in tumorigenesis in a p53-dependent manner. *Proc Natl Acad Sci U S A.* (2017) 114:11500–5. doi: 10.1073/pnas.1711814114
- Jang YS, Kang JH, Woo JK, Kim HM, Hwang JI, Lee SJ, et al. Ninjurin1 suppresses metastatic property of lung cancer cells through inhibition of interleukin 6 signaling pathway. *Int J Cancer.* (2016) 139:383–95. doi: 10.1002/ijc.v139.2
- Dong B, Wu Y. Epigenetic regulation and post-translational modifications of SNAI1 in cancer metastasis. *Int J Mol Sci.* (2021) 22(20). doi: 10.3390/ijms222011062
- Suzuki T, Conant A, Curow C, Alexander A, Ioffe Y, Untchaeher JJ. Role of epithelial-mesenchymal transition factor SNAI1 and its targets in ovarian cancer aggressiveness. *J Cancer Metastasis Treat.* (2023) 9. doi: 10.20517/2394-4722.2023.34
- Li B, Li R. SNAI1: a key modulator of survival in lung squamous cell carcinoma and its association with metastasis. *J Cardiothorac Surg.* (2024) 19:531. doi: 10.1186/s13019-024-03044-8
- Dong C, Yuan T, Wu Y, Wang Y, Fan TW, Miriyala S, et al. Loss of FBPI by Snail-mediated repression provides metabolic advantages in basal-like breast cancer. *Cancer Cell.* (2013) 23:316–31. doi: 10.1016/j.ccr.2013.01.022
- Haraguchi M, Sato M, Ozawa M. CRISPR/cas9n-mediated deletion of the snail 1Gene (SNAI1) reveals its role in regulating cell morphology, cell-cell interactions, and gene expression in ovarian cancer (RMG-1) cells. *PLoS One.* (2015) 10:e0132260. doi: 10.1371/journal.pone.0132260
- Nandakumar V, Mills JR. The now and beyond of tumor mutational burden as a predictor of response to immune checkpoint inhibitors. *Clin Chem.* (2019) 65:357. doi: 10.1373/clinchem.2018.295097
- Smith TJ, Sciaky D, Phipps RP, Jennings TA. CD40 expression in human thyroid tissue: evidence for involvement of multiple cell types in autoimmune and neoplastic diseases. *Thyroid.* (1999) 9:749–55. doi: 10.1089/thy.1999.9.749
- Shin SP, Goh AR, Kang HG, Kim SJ, Kim JK, Kim KT, et al. CD200 induces epithelial-to-mesenchymal transition in head and neck squamous cell carcinoma via  $\beta$ -catenin-mediated nuclear translocation. *Cancers (Basel).* (2019) 11(10). doi: 10.3390/cancers11101583



# Frontiers in Pharmacology

Explores the interactions between chemicals and living beings

The most cited journal in its field, which advances access to pharmacological discoveries to prevent and treat human disease.

## Discover the latest Research Topics

[See more →](#)

### Frontiers

Avenue du Tribunal-Fédéral 34  
1005 Lausanne, Switzerland  
[frontiersin.org](https://frontiersin.org)

### Contact us

+41 (0)21 510 17 00  
[frontiersin.org/about/contact](https://frontiersin.org/about/contact)



### Frontiers in Pharmacology

